Přírodovědecká fakulta
Faculty of Science
Jihočeská univerzita v Českých Budějovicích
University of South Bohemia in České Budějovice

Functional biology of wood: from structure to function

Habilitation thesis

RNDr. Lenka Plavcová Ph.D.

Hradec Králové 2023

Abstrakt v češtině: Tato habilitační práce má za cíl přispět k lepšímu porozumění vztahů mezi strukturou a funkcí xylému dřevin. Zahrnuty jsou dvě oblasti výzkumu. První oblast se věnuje funkční anatomii radiálního (paprsčitého) a axiálního parenchymu. Studuje, jak se frakce radiálního a axiálního parenchymu liší mezi dřevinami na klimatickém gradientu a jak tato frakce souvisí s koncentrací nestrukturálních sacharidů. Studována je i ultrastruktura teček spojujících parenchymatické buňky s cévami. Analyzován je trede-off vztah mezi transportní, zásobní a mechanickou funkcí v xylému dřevin. Diskutován je fakt, že zásobní funkci v xylému mohou u mnohých druhů dřevin vykonávat místo parenchymu živá xylémová vlákna. Druhou oblastí zájmu této habilitační práce je biologie dřeva ovocných stromů. Konkrétně se zaměřuji na lepší porozumění mechanismů kontrolujících vigorositu růstu stromů na různých podnožích, které souvisejí s vodním a uhlíkovým režimem dřevin. Zahrnuta je i studie o vlivu závlahy na vodní režim jabloní.

Abstract in english: This habilitation thesis aims at gaining a better understanding of relationships between structure and function in wood of trees. The thesis covers two areas of research focus. The first area is devoted to the functional anatomy of ray and axial parenchyma. It investigates how the fraction of ray and axial parenchyma differs among trees along a climate gradient and how the fraction relates to the concentration of non-structural carbohydrates. I also examines the ultrastructure of the pits connecting parenchyma cells with vessels. Analysis of trade-offs between transport, storage and mechanical function is also included. I also discuss that storage function in many tree species is facilitated by living fibers instead of axial parenchyma. The second area of research covered in this habilitation thesis is the functional biology of wood in fruit trees. More specifically, I focus on gaining a better understanding of rootstock-induced mechanisms of growth vigour control, which is linked to water and carbon relations of trees. Included is also a study on the effect of irrigation on water relations of apple trees.

Poděkování:

Děkuji svým spolupracovníkům, kteří se podíleli na přípravě publikací, jmenovitě především Dr. Radek Jupa, Dr. Martin Mészáros, Prof. Steven Jansen and Dr. Hugh Morris. Cením si finanční podpory od Humbodtovy nadace, Grantové agentury České republiky (projekt 18-19722Y) a ministerstva zemědělství České republiky (projekt QK1910165).

Ráda bych na tomto místě poděkovala také své rodině (Jeníkovi, Julince, Aličce a Ladušce) za trpělivost a podporu v mých vědeckých aktivitách. Děkuji také svým rodičům za toleranci a četné hlídání dětí, které mi umožnilo pokračovat v bádání.

Table of contents:

1. List of publications:

Publication 1: Plavcová L, Jansen S (2015) The Role of Xylem Parenchyma in the Storage and Utilization of Nonstructural Carbohydrates. In: Hacke U (ed) Functional and Ecological Xylem Anatomy. Springer International Publishing, Cham, pp 209–234.

Publication 2: Morris H*, Plavcová L*, Cvecko P, Fichtler E, Gillingham MAF, Martínez-Cabrera HI, McGlinn DJ, Wheeler E, Zheng J, Ziemińska K, Jansen S (2016) A global analysis of parenchyma tissue fractions in secondary xylem of seed plants. New Phytol 209:1553–1565.
**contributed equally and are both considered the first authors*

Publication 3: Plavcová L, Hoch G, Morris H, Ghiasi S, Jansen S (2016) The amount of parenchyma and living fibers affects storage of nonstructural carbohydrates in young stems and roots of temperate trees. American Journal of Botany 103:603–612.

Publication 4: Morris H, Plavcová L, Gorai M, Klepsch MM, Kotowska M, Jochen Schenk H, Jansen S (2018) Vessel-associated cells in angiosperm xylem: Highly specialized living cells at the symplast–apoplast boundary. Am J Bot 105:151–160.

Publication 5: Plavcová L, Gallenmüller F, Morris H, Khatamirad M, Jansen S, Speck T (2019) Mechanical properties and structure–function trade-offs in secondary xylem of young roots and stems. Journal of Experimental Botany 70:3679–3691.

Publication 6: Plavcová L, Olson ME, Jandová V, Doležal J (2023) Parenchyma is not the sole site of storage: storage in living fibres. IAWA J:1–12.

Publication 7: Jupa R, Mészáros M, Plavcová L (2021) Linking wood anatomy with growth vigour and susceptibility to alternate bearing in composite apple and pear trees. Plant Biol J 23:172–183.

Publication 8: Jupa R, Mészáros M, Hoch G, Plavcová L (2022) Trunk radial growth, water and carbon relations of mature apple trees on two size-controlling rootstocks during severe summer drought Tognetti R (ed). Tree Physiology 42:289–303.

Publication 9: Plavcová L, Mészáros M, Šilhán K, Jupa R (2022) Relationships between trunk radial growth and fruit yield in apple and pear trees on size-controlling rootstocks. Annals of Botany 130:477–489.

Publication 10: Plavcová L, Jupa R, Mészáros M, Hoch G (2023) Whole-tree storage of non-structural carbohydrates in apple and pear trees on size-controlling rootstocks. *Accepted to* Journal of Plant Growth Regulation

Publication 11: Plavcová L, Mészáros M, Jupa R, Scháňková K, Kovalíková Z, Náměstek J, Mahrová A (2023) Yield and water relations of two apple cultivars under irrigation. *Accepted to* Irrigation Science

2. Main goals and significance

This habilitation thesis is focused on exploring structure-functional relationships in wood in two main contexts. First, the thesis examines ray and axial parenchyma (six publications on this topic) which is a wood component that has not been widely studied up to recently. In fact, our global meta-analysis of ray and axial parenchyma fractions (Morris *et al.* 2016) and the follow up studies (Plavcová *et al.* 2016; Jupa *et al.* 2016; Morris *et al.* 2018) have been important contributions in this respect. Second, we utilized methods of functional wood anatomy and plant physiology to better understand growth performance of fruit trees on size-controlling rootstocks (four publications on this topic) and we also used these methods to evaluate fruit tree performance under irrigation (one publications on this topic). The thesis contains seven first author publications, one with shared first co-authorship and two publications as a senior author (i.e., eleven publications in total). Overall, the research presented in this thesis fells in the realm of plant ecophysiology, focusing mainly on water and carbon relations of trees.

3. Introduction

3.1 Anatomical structure of wood

Wood is a secondary xylem produced by secondary meristem, the cambium. Bulk wood consists mostly of dead cells (vessel elements and imperforated tracheary elements). Vessel elements are wide cells which underwent rapid cell expansion in the cambial zone and have perforated end walls (hence, they are sometimes termed perforate tracheary elements). Vessel elements align to each other vertically, ultimately forming a hollow tube – the vessel. When viewed on a transversal section, vessels can be solitary or grouped. Across tree species they differ in their diameter ranging typically from 10 to 130 μm (Hacke *et al.* 2017). Imperforate tracheary elements (ITEs) are a group of axially elongated spindle-shaped cells that include tracheids, fiber-tracheids and libriform fibers (Olson 2023). ITEs typically represent the majority of wood volume and hence are referred to as background tissue. ITEs (and libriform fibers specifically) often have thick lignified secondary cell wall and are an important determinant of wood density.

Sapwood of trees also contains living cells which are arranged in two subsystems - ray (radial) and axial parenchyma. Rays consists of parenchyma cells that are radially oriented spanning from the xylem through the cambium to the phloem. Rays can be unicellular or multicellular if they are formed by one or more radial rows of cells. Based on the shape of individual ray cells, rays can be distinguished between homogeneous and heterogeneous. While homogenous rays are composed of only procumbent (i.e., radially elongated) cells, heterogeneous rays contain procumbent, square (i.e., isodiametric) and upright (i.e., axially elongated) cells (Kribs 1935). Axial parenchyma consists of axially elongated rectangular parenchyma cells, which are often joined to form a vertically running strand. Axial parenchyma often surrounds the vessels and such arrangements are termed paratracheal. In contrast, arrangements without a direct association to vessels are referred to as apotracheal. Within paratracheal arrangements, we can distinguish several subcategories. Thus, paratracheal arrangements can be subdivided into scanty, vasicentric, aliform and confluent reflecting the gradient of increasing axial parenchyma abundance and tangential connectivity. Apotracheal parenchyma can be diffuse, diffuse with aggregates or form tangential bands.

A great anatomical diversity of wood arises as species modulate the relative fraction of the different cell types, vary the spatial arrangement of these cells and change the cell size and

cell wall thickness. Wood of conifers is simpler than angiosperm wood as it typically consists of only two cell types – tracheids and ray parenchyma. In contrast to the conifers, the wood of angiosperms typically consists of four principal cell types – vessel elements, fibers, ray and axial parenchyma, but it may also contain tracheids and fiber-tracheids. In this thesis, I will explore the structure and function of angiosperm wood in an ecophysiological context.

3.2 Ecophysiological function of wood

Wood is a multifunctional tissue. The main functions of wood are the long-distance water transport, mechanical support and storage of carbohydrates and other nutrients. These functions are seemingly divided among individual cell types. Vessel elements comprise water conduction pathway, fibers provide mechanical support and radial and axial parenchyma are mainly involved in the storage and radial transport of water, carbohydrate and nutrients (Van Bel 1990; Plavcová *et al.* 2016; Jupa *et al.* 2016; Kotowska *et al.* 2020). Due to spatial constraints (i.e., finite wood volume), the division of labour between individual cell types should result in trade-off relationships such as the trade-off between water conduction and storage, storage and mechanical support and water conduction and mechanical support (Pratt and Jacobsen 2017; Pratt *et al.* 2021). However, in reality the three functions are not entirely separated, but rather interlinked. For instance, some ITEs (tracheids) are involved not only in mechanical support but also in water transport and can serve as subsidiary water conduction pathway in addition to vessels (Carlquist 1985; Cai *et al.* 2014). Also, it has been recognized that hydraulic function depends on mechanical strength of wood to prevent conduit collapse under negative pressure and to stabilize mechanically weak pitted endwalls of vessels (Hacke *et al.* 2001; Jacobsen *et al.* 2005). Radial parenchyma does not act only in radial conduction and storage but also in mechanical strength (Burgert and Eckstein 2001; Burgert *et al.* 2001). From these examples it should be clear that the structure-function relationships in wood are highly complex.

The primary function of xylem is the long-distance water conduction from roots to leaves. In terrestrial plants, the water transport occurs under tension as explained by the cohesion-tension theory of sap ascent (Dixon 1914; Steudle 2001). The force uplifting the water is generated at the evaporative sites in the leaf mesophyll. Pores in the mesophyll cell wall are tiny and hence, a great suction force is generated that pulls the water column up. Due to the adhesive and cohesive forces in water, the suction is translated via the xylem all the way to the root tips, ultimately sucking up water from the soil. Xylem water is therefore under tension, which is a metastable condition. As xylem tension increases with increasing drought, the transport in vessels can be interrupted by cavitation. Cavitation is an abrupt transition from liquid to gas phase and occurs when air is sucked into the conduit via a pore in the pit membrane. Pits are small opening in the cell wall of vessels and some ITEs. Pits have peculiar structure consisting of pit membrane that is positioned centrally within a pit chamber delineated by an overarching secondary cell wall (referred to as a pit boarder). The pit membrane is composed of enzymatically modified primary cell wall and consists of a mesh of cellulose, hemicellulose and likely also pectins, although some studies found pectins restricted only around the outer edge of the membrane (Plavcová and Hacke 2011). The size of the pore (D_p) causing the cavitation depends on the xylem tension according to the following formula:

$$\Delta P = \frac{4T cos\alpha}{D_p}$$

where ΔP is a difference between atmospheric and xylem pressure, T is surface tension of xylem sap and α is the contact angle between sap and pore wall, which is typically assumed to be zero (i.e., complete wetting). Thus, xylem pressure that causes cavitation is inversely related to the diameter of the largest pit membrane pore (D_p) per vessel (Plavcová *et al.* 2011) and this mechanism is known as the rare pit hypothesis. More recently, this traditional view on the mechanism of drought-induced cavitation has been challenged, highlighting the complex 3D organization of pit membrane pores (Kaack *et al.* 2021) and the presence of lipid-coated nanobubbles in the transpiration stream (Schenk *et al.* 2021), which might be a more likely source of gas than the air-seeding via a pit pore (Lens *et al.* 2022).

Cavitation can be caused by drought, but also as a result of freeze-thaw events (Pittermann and Sperry 2006; Mayr and Sperry 2010; Charra-Vaskou *et al.* 2016). Because air is less soluble in ice than in liquid water, gas bubbles are formed in the frozen sap. These bubbles can then expand when the sap melts and evaporation occurs. The size of the undissolved bubble is tightly related to the size of the conduit with bigger and more easily expanding bubbles being formed in wider conduits (Pittermann and Sperry 2006). Drought- or freeze-induced cavitation leads to embolism, a situation when vessels are blocked by air bubbles instead of forming a continuous water column. Xylem pressure at 50% loss of conductivity (P50) is a common variable describing the vulnerability of plants to drought-induced cavitation.

Xylem transport efficiency is another important property of xylem and is typically measured as xylem-area specific hydraulic conductivity (K_S). K_S depends strongly on vessel diameter with the relationship being modelled by Hagen-Poiseuille equation for a laminar flow:

$$K_{th} = \frac{\pi D^4}{128\eta}$$

where K_{th} is a theoretical hydraulic conductivity, D is the conduit diameter, and η is the dynamic viscosity of water (1.002×10^{-9} MPa s at 20°C). Thus, according to this equation, hydraulic conductivity depends on conduit diameter to the fourth power. In other words, small increase in conduit diameter brings about large increase in hydraulic conductivity. The real hydraulic conductivity is lower than K_{th} because of the resistance of pitted endwalls, perforation plates and imperfections of vessel inner walls.

Plant transpiration (E) is closely related to soil-plant hydraulic conductivity ($K_{s\text{-}p}$) and pressure difference between soil and the plant ($\Delta\Psi$) according to the following equation:

$$E = K_{S-P}\Delta\Psi$$

Across longer timescales, whole-tree water loss is affected by changes in leaf area due to new leaves emergence or leaf shedding (Wolfe *et al.* 2016; Nadal-Sala *et al.* 2021). Across shorter timescales, transpiration rate is regulated by stomatal closure to maintain xylem pressure above the cavitation threshold (Sperry 2000; Rodriguez-Dominguez *et al.* 2016). Nevertheless, environmental conditions sometimes cause the plants to cross the critical threshold and cavitate, which leads to severe damage to the plant hydraulic integrity or even a plant death (Anderegg *et al.* 2013). This process has important implications for trees performance and survival under drought and have been implicated as a major factor of global tree mortality (McDowell *et al.* 2008; Hartmann *et al.* 2018).

Stomatal closure also provides a link between plant water relations, photosynthesis and carbon balance (Meinzer *et al.* 2009; Sala *et al.* 2012). If stomates are closed (e.g., due to drought), carbon dioxide (CO_2), the main substrate for photosynthesis, cannot diffuse into the

leaf and to the sites of carboxylation. The plant than uses its internal carbon reserves stored in the form of non-structural carbohydrates (NSC) that are further divided into insoluble starch and soluble sugars (mainly sucrose, glucose, fructose). Thus, the plant under prolonged drought stress is facing a dilemma whether to die of desiccation or carbon starvation (McDowell *et al.* 2008).

Due to its large biomass, sapwood provides a large storage pool for NSC with the NSC being deposited mainly in ray and axial parenchyma (RAP) (Plavcová *et al.* 2016). Branch wood is typically the most dynamic NSC storage pool because of its close proximity to the source leaves (Hoch *et al.* 2003; Furze *et al.* 2019). Trunk wood is less dynamic and there is a decreasing gradient in NSC concentration with increasing sapwood depth (Furze *et al.* 2020). Great proportion of NSC is stored in roots that typically have more ray and axial parenchyma compared to the aboveground organs (Loescher *et al.* 1990; Plavcová *et al.* 2016). Besides NSC, wood stores also inorganic nutrients with the fraction of parenchyma in sapwood being correlated with sapwood nitrogen concentration but not with the concentration of other inorganic nutrients (Kotowska *et al.* 2020). Wood can also store large amount of water (Jupa *et al.* 2016; Ziemińska *et al.* 2020), which may be released into the transpiration stream at time of high water demands and when soil water uptake is not sufficient (Borchert and Pockman 2005). Water can be stored in capillary spaces such as narrow fiber tips, as elastic stores in living parenchyma cells (i.e., wood and bark parenchyma) or in vessels from which water can be released by cavitation (Tyree and Yang 1990; Hölttä *et al.* 2009; Jupa *et al.* 2016; Ziemińska *et al.* 2020).

Wood is also a strong carbon sink and wood growth is an important process at a plant as well as an ecosystem level (Chambers *et al.* 2001; Falster and Westoby 2005). High mechanical strength of wood allows for the development of tall tree bodies, which provide advantage in the competition for light. Mechanical properties of wood are also of practical meaning in wood processing industry (Panshin and de Zeeuw 1980). Wood growth and mechanical properties are closely linked to wood density with lower growth rates and mechanically stronger wood having higher wood density (Niklas 1993; Chave *et al.* 2009; Niklas and Spatz 2010). On the other hand, dense wood represents high construction costs for the tree (Eller *et al.* 2018).

Taken together, wood fulfils several important functions in plants. Its role in long-distance water transport is presumably the most prominent one and also the one that received the most attention by researchers. However, additional functions such as storage of carbohydrates, water and nutrients also have important consequences for tree's growth and survival and should be studied in association with the corresponding structural features.

4. Main results

4.1 Structure and function of ray and axial parenchyma

Most studies on xylem structure and function so far have focused on dead xylem conduits and their role in long-distance water transport (e.g., Hacke and Sperry 2001). In these studies, wider vessel diameter has been linked to a higher xylem-specific hydraulic conductivity as a measure of hydraulic efficiency. Similarly, the structural variation of inter-vessel pit membranes has been related to the xylem vulnerability to embolism (Choat *et al.* 2008). Much less attention has been given to the structure and function of ray and axial parenchyma, despite their great anatomical variation across species. Thus, our research has addressed the following questions:

1) *What is the current state of knowledge of the role of xylem parenchyma in the storage and utilization of carbohydrates?*
2) *What is the range of ray and axial parenchyma fractions across species and do the fractions differ across a climatic gradient?*
3) *Do the fractions of ray and axial parenchyma directly influence the concentrations of non-structural carbohydrates in woody organs?*
4) *What are the distinct anatomical features of vessel-associated parenchyma cells?*
5) *Do fractions of ray and axial parenchyma affect wood mechanical strength? Are there trade-offs among the hydraulic, mechanical and storage functions?*
6) *Is parenchyma the sole site of storage in wood?*

(1) What is the current state of knowledge of the role of xylem parenchyma in the storage and utilization of carbohydrates?

To answer this question, we conducted a thorough literature review (**Publication 1**). We concluded that ray and axial parenchyma of temperate trees often contain large amount of starch particularly at the onset of winter dormancy. In tropical trees, the starch granules in wood parenchyma are less abundant as species contain carbohydrates in the form of soluble sugars. From the whole plant perspective, wood NSC represent an important storage pool because of the large wood biomass. Terminal branches of trees typically have higher NSC concentrations compared to the trunk sapwood, and their NSC concentrations are also more dynamic over the growing season. The seasonal dynamics has been most widely studied in temperate trees. In these trees, the concentration of NSC is lowest during or shortly after budbreak when NSC stores are mobilized to support leaf flushing. Then, the concentration of starch increases during the vegetation season to reach the highest values in fall. In winter, starch can be hydrolysed to soluble sugars to protect the symplast of living cells against a freeze-induced damage. The mobilization of starch reserves into soluble sugars is facilitated by a large array of carbohydrate-modifying enzymes (e.g., amylases, glucosidases, phosphotransferases, sucrose synthase). The movement of sugars between cells is facilitated by various transporters that have been localized in the plasma membrane adjacent to the parenchyma-conduit pits. Between parenchyma cells the sugars and other compounds can move via plasmodesmata that penetrate the pit membrane. The dynamics of carbohydrates has important implications for the whole plant processes (Figure 1) such as for the long-term storage, refilling of embolised conduits, osmotic adjustment, freezing protection, defence against pathogen and wound response.

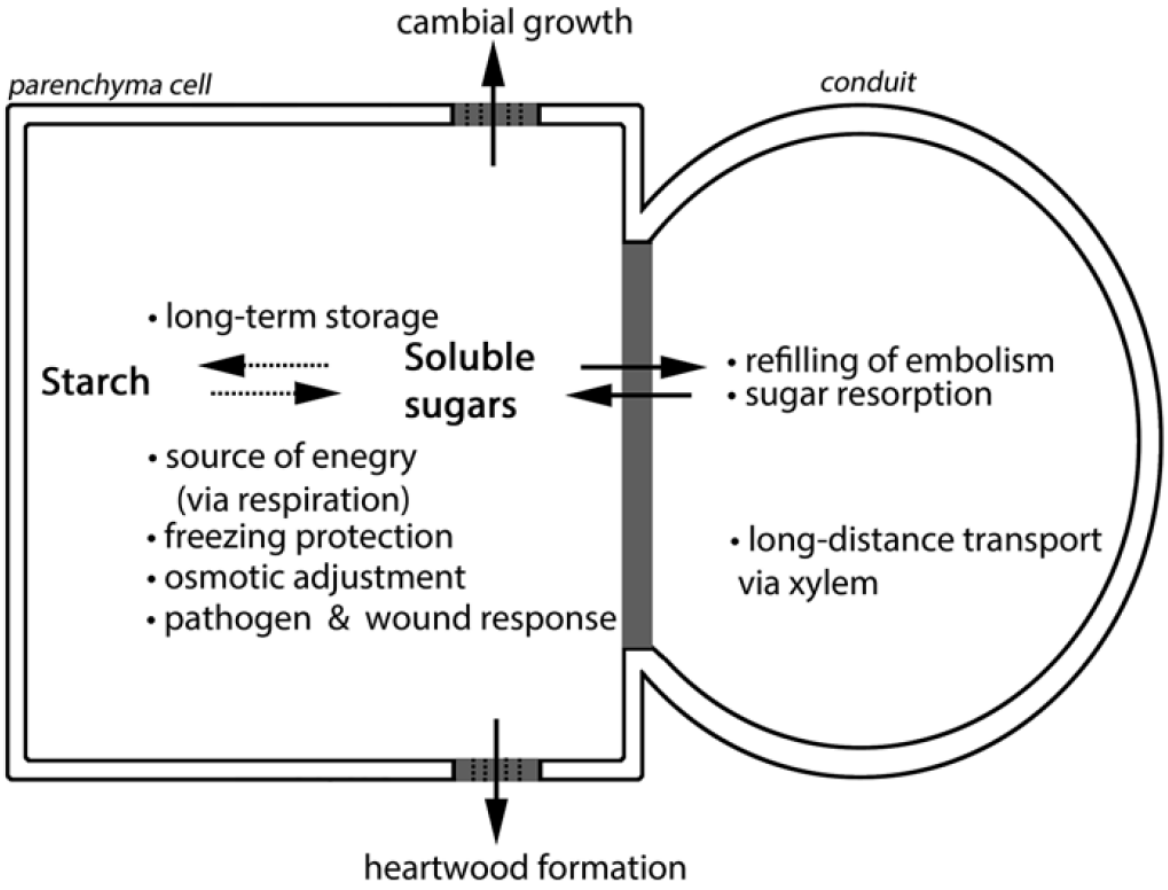

Figure 1: Schematic representation of various functions that starch and soluble sugars fulfill in sapwood.

(2) What is the range of ray and axial parenchyma fractions across species and do the fractions differ across a climatic gradient?

To answer this question, we gathered data on ray and axial parenchyma fractions from more than 30 literature sources in addition to our own measurements (**Publication 2**). In total, data for more than 1200 plant species were acquired and analysed. We documented 29-fold variation in ray and axial parenchyma fractions across species. First, we compared ray and axial parenchyma fractions among woody plant groups and growth form categories (gymnosperm tree, angiosperm tree, climber, succulent). We found that the highest ray and axial parenchyma fractions were found in succulents (~60%) followed by climbers (~60%). The lowest fractions were in gymnosperms (~10%). In angiosperm trees, tropical trees had significantly higher ray and axial parenchyma fractions than temperate and subtropical species. These results were paralleled by the relationships of ray and axial parenchyma fractions with two main climate parameters - the mean annual temperature and the mean annual precipitation (Figure 2). The results are discussed in relation to various potential functions of ray and axial parenchyma in storage of water, carbohydrates and nutrients, defence against pathogens, embolism refilling. However, it remains to be resolved which function takes precedence in any given situation.

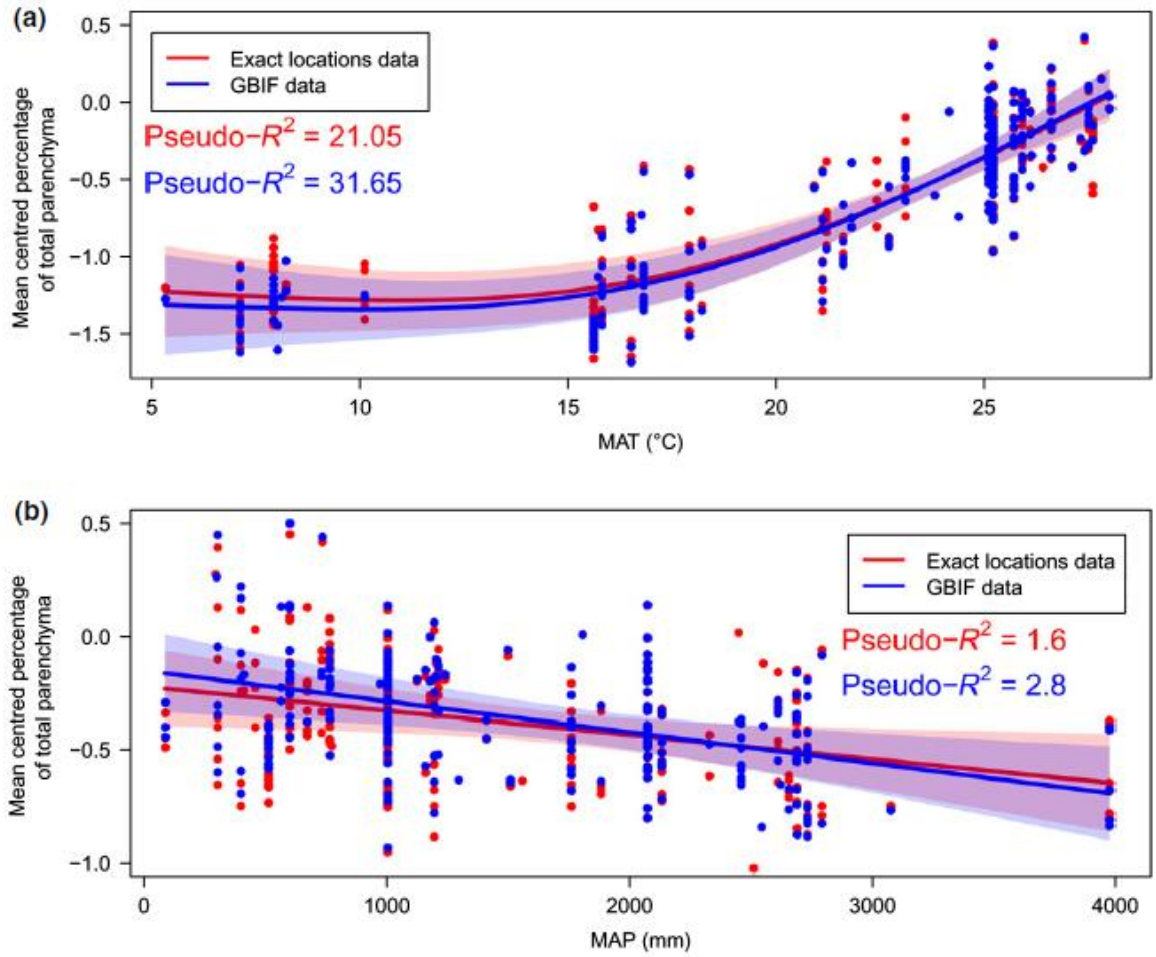

Figure 2: The effect of (a) mean annual temperature (MAT) and (b) mean annual precipitation (MAP) and the fractions or ray and axial parenchyma in angiosperm wood based on a general additive model with a binomial distribution.

(3) *Do the fractions of ray and axial parenchyma directly influence the concentrations of non-structural carbohydrates in woody organs?*

To answer this question, we sampled roots and shoots of twelve temperate and four tropical tree species and measured ray and axial parenchyma fractions together with the concentration of NSC at the onset of winter dormancy (**Publication 3**). Across species, we found significantly higher concentrations of NSC in roots compared to stems, highlighting the importance of belowground woody organs for the overall NSC storage pool. The roots typically also had higher ray and axial parenchyma fractions than stems. Wood of two species (*Clematis vitalba* and *Acer pseudoplatanus*) contained large fractions of living fibers. The topical tree species had relatively high ray and axial parenchyma fractions, but low concentrations of NSC. Overall, there was a close correlation between ray and axial parenchyma fractions and concentration of NSC across the twelve temperate species and two organs (Figure 3). These findings suggest that the fraction of parenchyma is a good proxy for the maximal NSC storage capacity and expand the number of identified structure-functional relationships in wood.

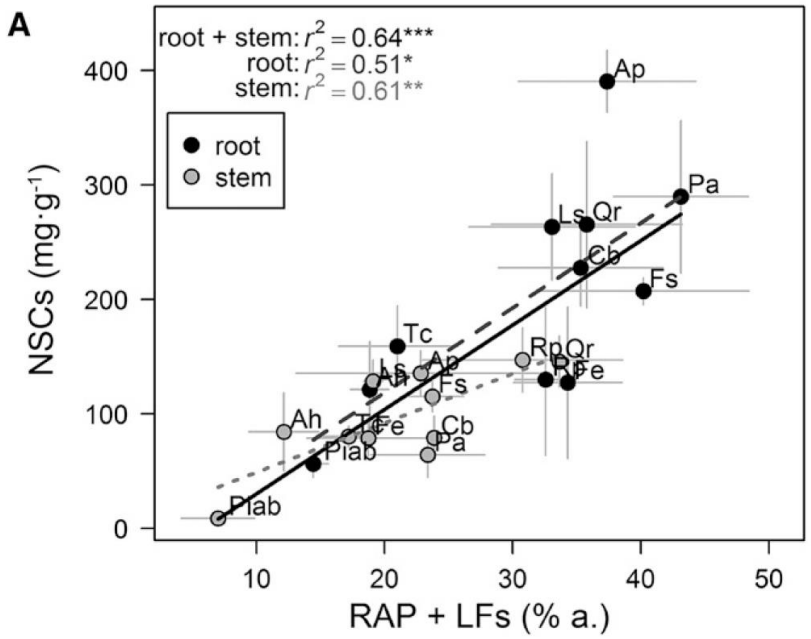

Figure 3: Close correlation between the fraction of ray and axial parenchyma (RAP) including living fibers (LF) and the concentration of non-structural carbohydrates (NSCs) in roots and stems or twelve temperate tree species.

(4) *What are the distinct anatomical features of vessel-associated parenchyma cells?*

To answer this question, we reviewed our current understanding of vessel-associated cells (VACs) focusing primarily on their unique structural features. Furthermore, we complemented the review with our own microphotographs of VACs (**publication 4**). VACs are parenchyma cells in a direct contact with vessels. These cells have a number of highly specialized traits that distinguish them from vessel-distant parenchyma cells and imply highly specialized functions due to their unique position as the boundary between the symplast and the apoplast (Figure 4). In contrast to vessel-distant cells, VACs are small with large nuclei, plentiful mitochondria, dense cytoplasm, many ribosomes, typically small vacuoles, and a well-developed endoplasmic reticulum. They typically contain less starch granules than the vessel-distant cells. VACs show hight H^+-ATPase activity and abundant aquaporins are localized within their palsma membrane and the tonoplast. A specialized pecto-cellulosic layer called the amorphous (or protective) layer lies between the plasma membrane and the lignified secondary wall. This layer represents a non-lignified extension of the apoplast and likely functions as a buffer of hydrostatic pressures generated from within the vessels. Pits interconnecting VACs and vessels are typically half-bordered and rich in pectins. On the vessel lumen side, the pit membrane is often covered with an electron dense material called the black cap. These structural features of VACs suggest high metabolic and transport activity of these cells and indicate that an intensive trafficking of various substances (e.g., water, sugars, ions) occurs between VACs and vessels facilitating numerous physiological functions.

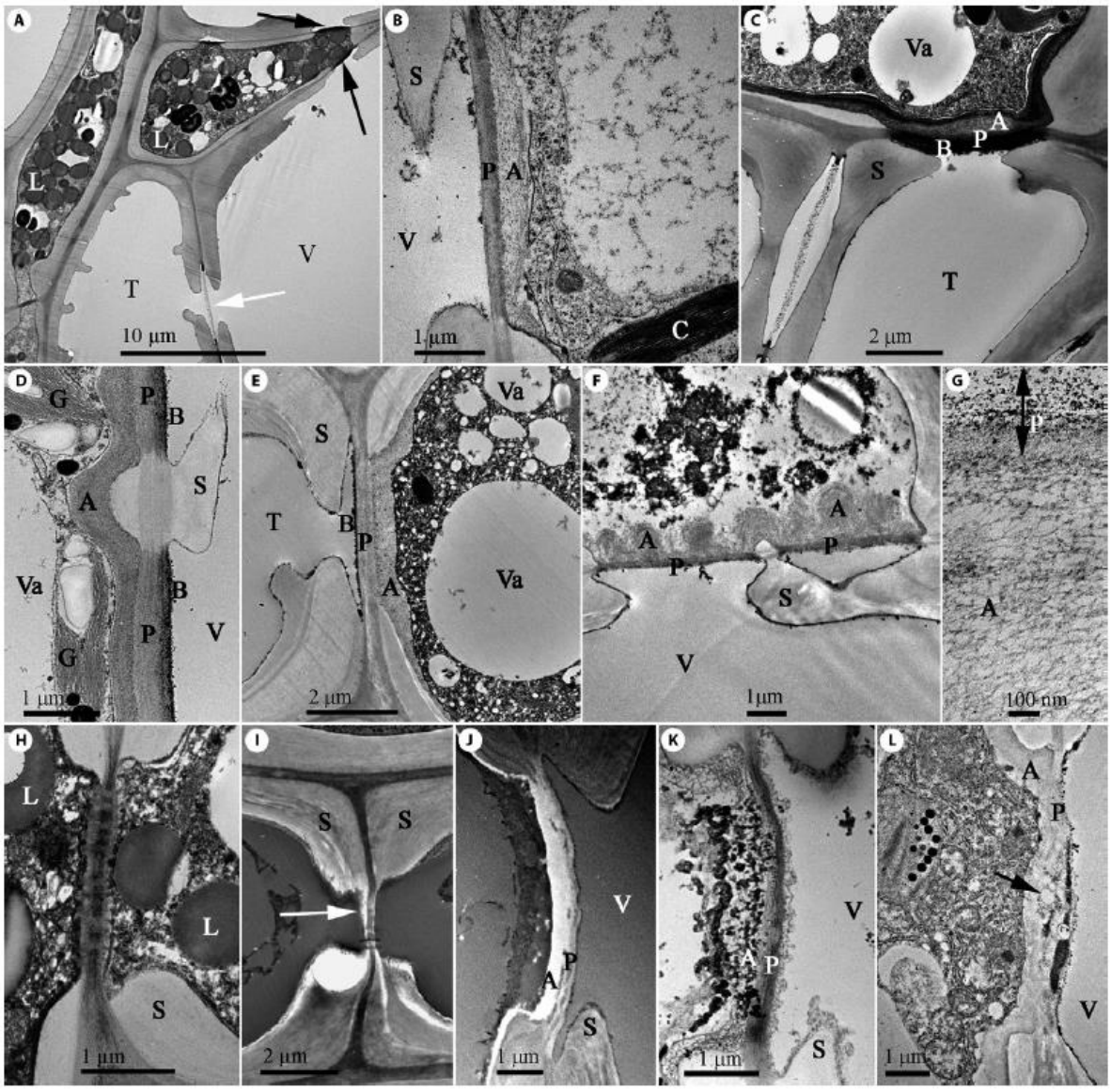

Figure 4: Transmission electron micrographs of vessel-associated parenchyma cells and their half-bordered vessel parenchyma pit membranes in stem xylem (A, C–L) and petiole xylem (B).

(5) *Do fractions of ray and axial parenchyma affect wood mechanical strength? Are there trade-offs among the hydraulic, mechanical and storage functions?*

To answer this question, we measured bending and torsional stiffness of woody roots and shoots of nine angiosperm species and analysed the mutual coordination of structural and functional xylem traits (**publication 5**). We observed that roots had five times greater flexibility in bending and two times greater flexibility in torsion than stems. Lower values of structural bending and structural torsional moduli of roots compared with stems were linked with the presence of thicker bark and a greater size of xylem cells. Higher fractions of parenchyma were not associated with a lower wood density and reduced mechanical stiffness in spite of parenchyma cells having thinner cell walls compared with fibres. The only liana species studied *Clematis vitalba* had wide partially non-lignified rays which likely contributed to its high flexibility in bending and torsion. Taken together, our findings show that higher demands for mechanical function in self-supporting stems put a major constraint

on xylem structure, whereas root xylem can be designed with a greater emphasis on both storage and hydraulic functions (Figure 5).

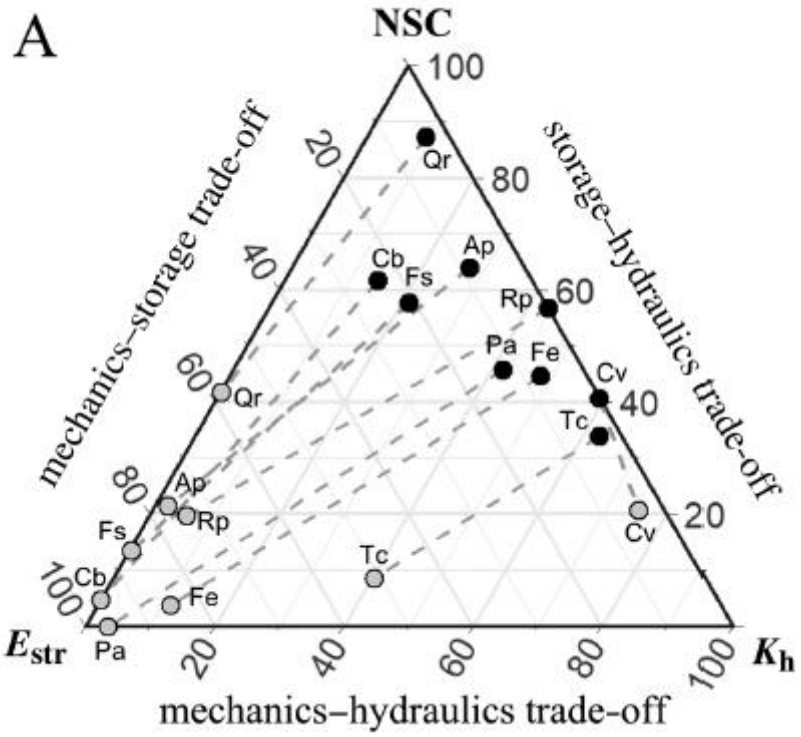

Figure 5: Trade-off triangle showing the relative division of xylem function between mechanical stiffness (E_{str}), carbohydrate storage capacity (NSC), and hydraulic conductivity (K_h) for roots and stems of nine woody angiosperm species.

(6) *Is parenchyma the sole site of storage in wood?*

To answer this question, we focused our attention on living fibers in the wood of angiosperm species (**publication 6**). Living fibers are axially oriented cells that contain nuclei and starch granules. These cells are surprisingly common in the wood of angiosperms, despite very few wood ecologists and physiologists are aware of them. Living fibers are often compartmentalized by septa made of the primary cell wall. As such, they may be incorrectly regarded as axial parenchyma by the unexperienced researchers. Thus, we rise awareness of these cells and conclude that living fibers can fulfil storage function in many (especially tropical and subtropical) species (Figure 6), although little is known about the functional implications. It seems likely that the presence of living fibers enhances the size of the storage pool in wood. However, the stored reserves may be less rapidly mobilized because of the more limited pit connections.

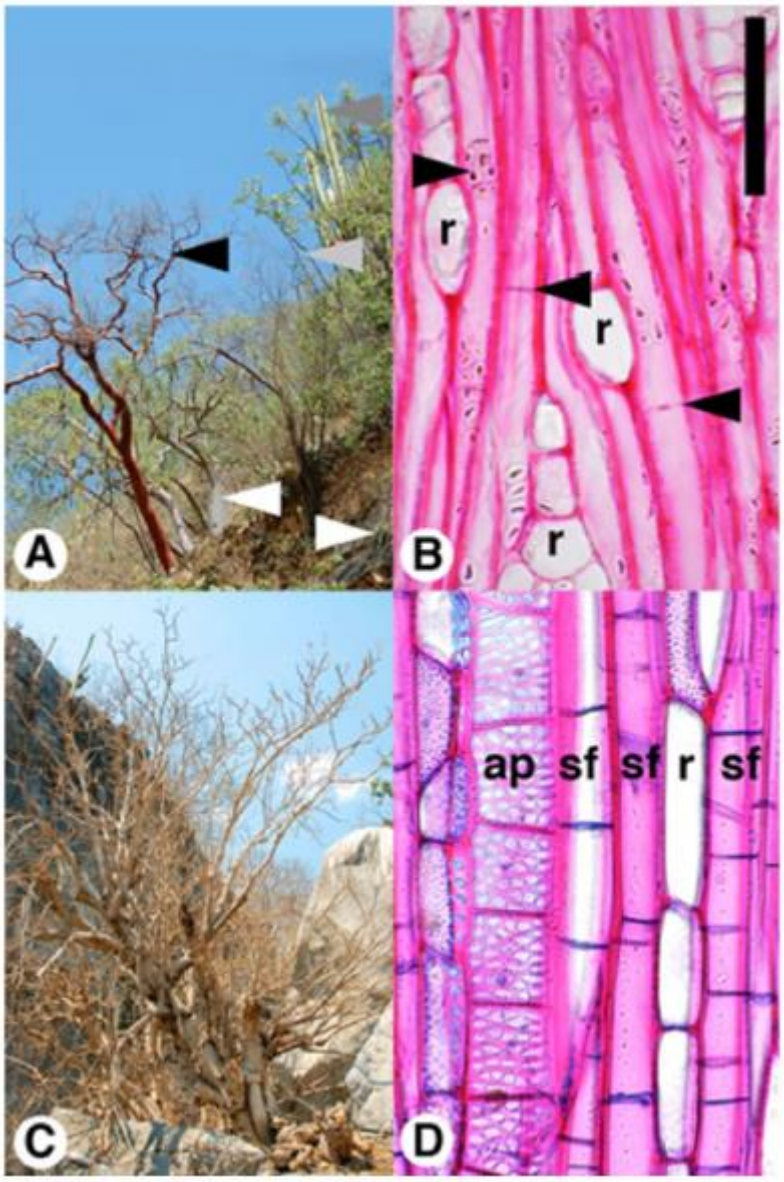

Figure 6: The presence of living fibers in water-storing trunks of (A,B) *Bursera longipes* (Burseraceae) and (C, D) *Louteridium koelzii* (Acanthaceae).

4.2 Wood biology and water and carbon relations of fruit trees

The structure and function of wood has important implications for the water and carbon relations of fruit trees. One example are the mechanisms of rootstock-induced growth vigour control. Size-controlling rootstocks have been one of the major innovations of high-efficiency fruit production; however, the exact biological mechanisms responsible for the growth vigour control remain unclear (Basile and DeJong 2018). Several hypotheses have been proposed including that the perturbation of tree water status and carbon relations are responsible for the size-controlling effect. Thus, our research has used apple and pear trees grown in a rootstock field trial to shed more light on some of those hypotheses. Understanding of xylem function and tree water relations is also important for efficient irrigation of fruit trees. Therefore, we also studied xylem hydraulics and tree water status in two apple cultivars under irrigation. Our research has addressed the following specific questions:

1) *Is there a systematic difference in vessel and wood parenchyma traits across the rootstocks of different size-controlling potential?*
2) *Do dwarfed apple trees show signs of greater drought stress and more limited trunk radial growth compared to invigorated trees?*
3) *Is there a stronger negative covariation between trunk radial growth and fruit yield in apple trees on dwarfing rootstocks than on invigorating ones?*
4) *Do trees on dwarfing rootstocks have lower NSC reserves and/or reduced capacity to mobilize NSC compared to trees on invigorating rootstocks?*
5) *Does irrigation perturb xylem hydraulic traits and plant water status in two apple tree cultivars?*

(1) Is there a systematic difference in vessel and wood parenchyma traits across the rootstocks of different size-controlling potential?

To answer this question, we sampled roots and shoots of fifteen scion/rootstock combinations of apple and pear trees growing in the field trial (**publication 7**). We prepared xylem cross-sections and measured wood anatomical traits, namely the vessel size, vessel density and the fractions of ray and axial parenchyma. We also evaluated the relative fraction of bark to xylem. The obtained anatomical parameters were correlated with shoot growth vigour and a susceptibility to alternate bearing. We found that mean vessel diameter of roots was positively correlated with annual shoot length (Figure 7a). In contrast, total parenchyma fraction (i.e., bark + ray and axial parenchyma) was negatively related to the alternate bearing index (Figure 7b). Thus, our findings suggest that a higher xylem hydraulic efficiency might underpin more vigorous growth, while greater carbohydrate storage capacity might be associated with less severe alternate bearing behaviour. We also found that the roots of pear trees were more hydraulically efficient, while the apple tree roots were more specialized in storage.

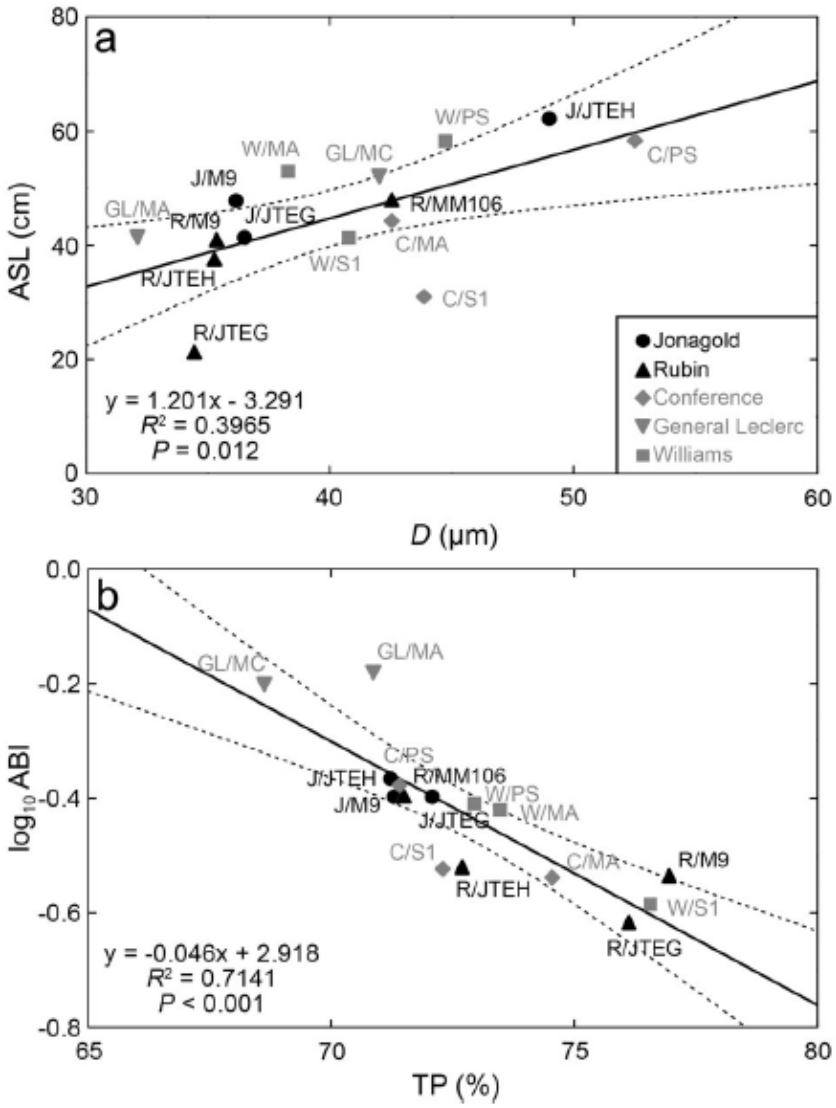

Figure 7: Correlations between (a) the root mean vessel diameter (D) and annual shoot length (ASL) and between (b) the fraction of total parenchyma and alternate bearing index (ABI) across fifteen scion/rootstock combinations.

(2) Do dwarfed apple trees show signs of greater drought stress and more limited trunk radial growth compared to invigorated trees?

To answer this question, we installed dendrometers on dwarfed and invigorated apple trees and monitored trunk radial variation during one vegetation season (**publication 8**). Additionally, we measured midday stem water potential, leaf gas exchange and concentrations of NSC in branches and roots. We found that smaller annual trunk radial growth was mainly due to an earlier cessation of trunk secondary growth. Dwarfed trees had fewer days with positive interdiurnal trunk circumference change especially during hot summer months. The trunk of dwarfed trees showed less pronounced diurnal variation of trunk circumference and the maximal daily shrinkage was only weakly responsive to the vapour pressure deficit (Figure 8). These findings suggest that dwarfed trees might have had lower turgidity in their cambial zone, which might have limited the trunk radial growth particularly during hot and dry summer days. Dwarfed trees also maintained lower midday stem water potential and stomatal conductance compared to invigorated trees and these

parameters declined in parallel during the drought progression. The concentrations on NSC were similar in both dwarfed and invigorated trees. Taken together, our results support the prominent role of water relations in rootstock-induced size-controlling mechanisms.

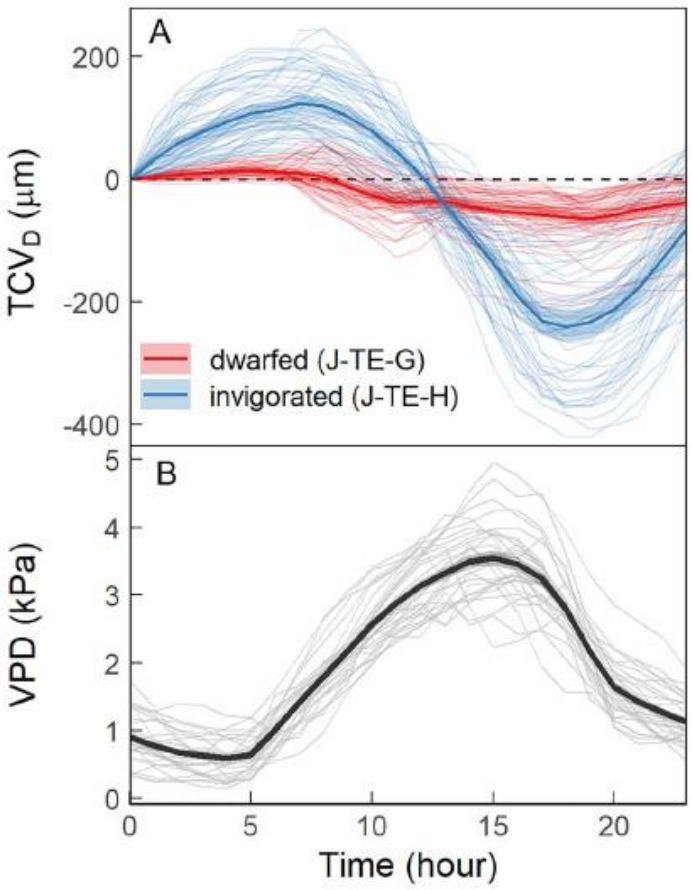

Figure 8: (A) Daily trunk circumference variation (TCV_D) in dwarfed (J-TE-G) and invigorated (J-TE-H) rootstock combinations and (B) diurnal time course of the VPD

(3) Is there a stronger negative covariation between trunk radial growth and fruit yield in apple trees on dwarfing rootstocks than on invigorating ones?

To answer this question, we used four scions (two for apple trees and two for pear trees) to evaluate the relationship between the annual fruit yield and ring width in trunks, branches and roots (**publication 9**). We found that there was a negative relationship between ring width and annual yield when data were plotted in absolute term (Figure 9a) or as detrended and normalized indices (Figure 9c). The relationship was stronger in low vigour scion/rootstock combinations but only for the indices data. In contrast, when trunk radial growth was expressed as basal area increment, the negative relationship disappeared (Figure 9b). This finding suggests that the relationship between trunk radial growth and fruit yield might not be a true trade-off arising due to the competition between the two sinks. The effect of low yield was associated with increased secondary growth not only in trunks but also in branches and roots. In trunks, we observed that overcropping was associated with reduced secondary growth in a subsequent year, possibly due to the depletion of reserves. Taken together, our results showed that variation in annual fruit yield due to tree ageing, weather cueing and inherent alternate bearing behaviour was reflected in the magnitude of secondary growth. We found little support for the competition/architecture theory of rootstock-induced growth

vigour control. More broadly, our study aimed at bridging the gap between forest ecology and horticulture because dendrochronological approach is not commonly used in horticulture.

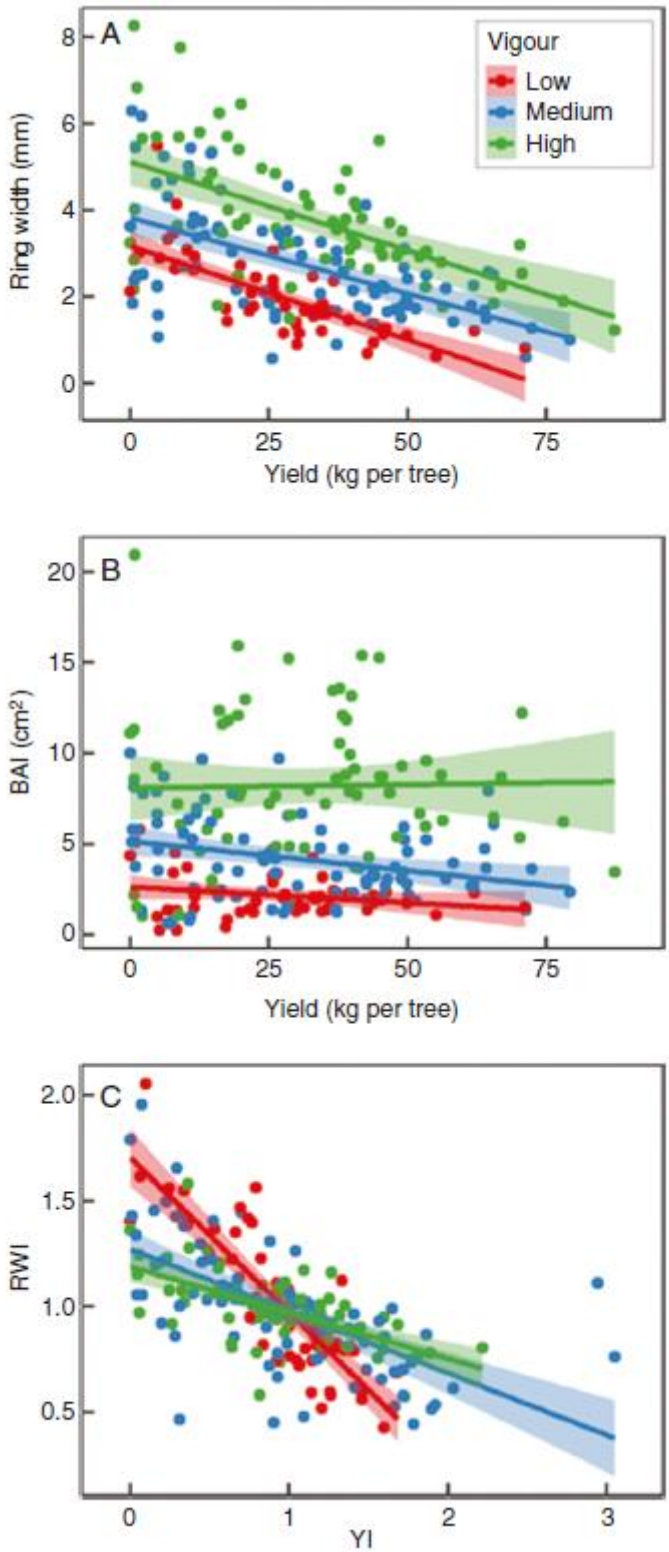

Figure 9: Relationships between annual yield and trunk radial growth separated for tree vigour categories. The data are plotted (A) in absolute terms, (B) as annual yield vs. basal area increment (BAI), (C) as detrended and normalized yield or ring width indices (YI, RWI)

(4) Do trees on dwarfing rootstocks have lower NSC reserves and/or reduced capacity to mobilize NSC compared to trees on invigorating rootstocks?

To answer this question, we measured NSC concentrations in roots, trunks, branches and leaves of dwarfed and invigorated apple and pear trees (**publication 10**). These concentrations were then scaled up to the whole-organ and whole-tree storage pools using the data on organ's biomass. We found that NSC pools scaled tightly with the overall tree biomass with vigorous trees having greater absolute storage pools compared to dwarfing trees (Figure 10a). In absolute terms, the seasonal fluctuations in NSC pools were also higher in vigorously growing trees (Figure 10b) but in relative terms and also when scaled by the tree's biomass the differences between the low and high vigour trees became negligible (Figure 10c), suggesting that the low and high vigour trees rely on their NSC reserves to a similar extent during their annual growth cycle. Thus, our results provide no support that the observed differences in growth vigour are driven by the availability of carbohydrate reserves.

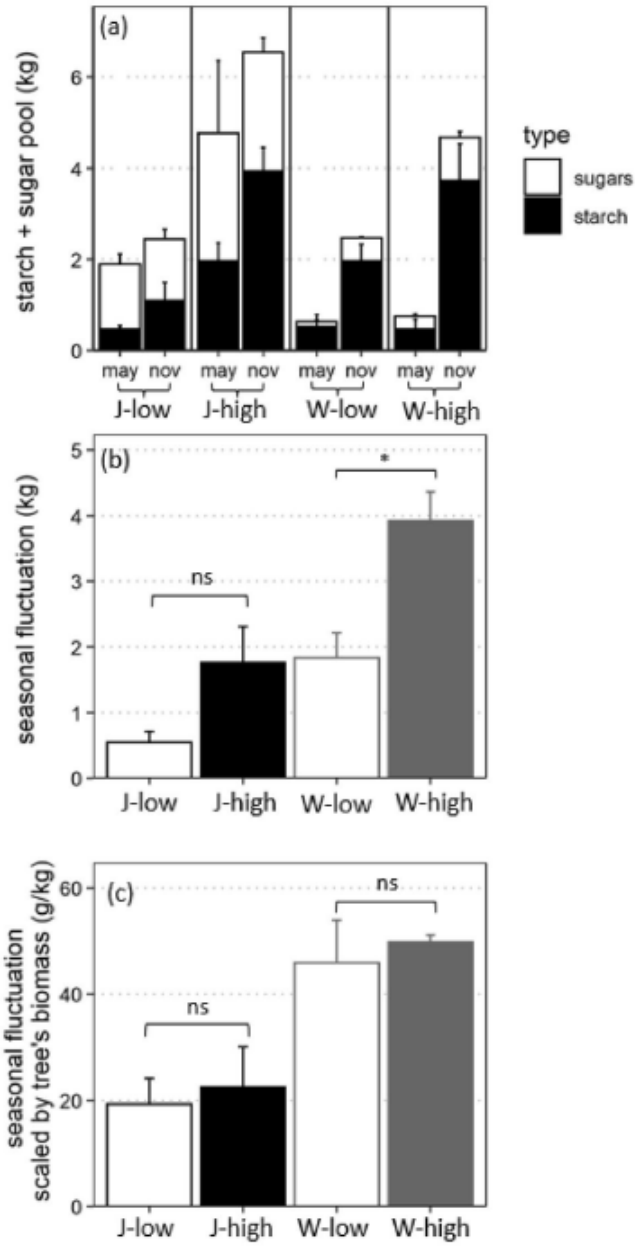

Figure 10: (a) Mean estimated pool sizes of starch and soluble sugars in May (during spring flush) and November (during the onset of winter dormancy) in the whole trees of apple tree var. 'Jonagold' (J) and pear tree var. 'Williams' (W) grafted onto rootstocks inducing low or high growth vigour. (b) Difference in the estimated pool sizes between November and May in the four studied scion/rootstock combinations. (c) Difference in the estimated pool sizes scaled by the tree's biomass. The data are means ±SE (n = 3).

(5) Does irrigation perturb plant hydraulic traits and water status in two apple tree cultivars?

To answer this question, we monitored midday stem water potential and measured xylem vulnerability to cavitation, turgor loss point, concentrations of organic osmolytes and the mutual coordination of xylem and leaf areas in two apple cultivars ('Red Jonaprince' and 'Gala Brookfield') with and without irrigation. We found that the midday stem water potential did not drop below -1.6MPa during three consecutive seasons, which is well above the turgor loss point and roughly at the onset of xylem cavitation. Non-irrigated trees had lower values of midday stem water potential compared to their irrigated counterparts. The irrigated and non-irrigated trees had similar yields and there was a tendency for smaller fruits in non-irrigated trees in 'Gala Brookfield'. The triploid cultivar 'Red Jonaprince' had typically more negative midday stem water potential than the diploid cultivar 'Gala Brookfield', but 'Gala Brookfield' exhibited higher limitations in fruit growth during drought and shoot growth during wet periods. In 'Gala Brookfield', leaf area scaled with xylem area, while no coordination of leaf and xylem areas was found in 'Red Jonaprince'. Overall, our results suggest that 'Red Jonaprince' favours hydraulic efficiency against safety, while 'Gala Brookfield' adopts a more conservative growth strategy.

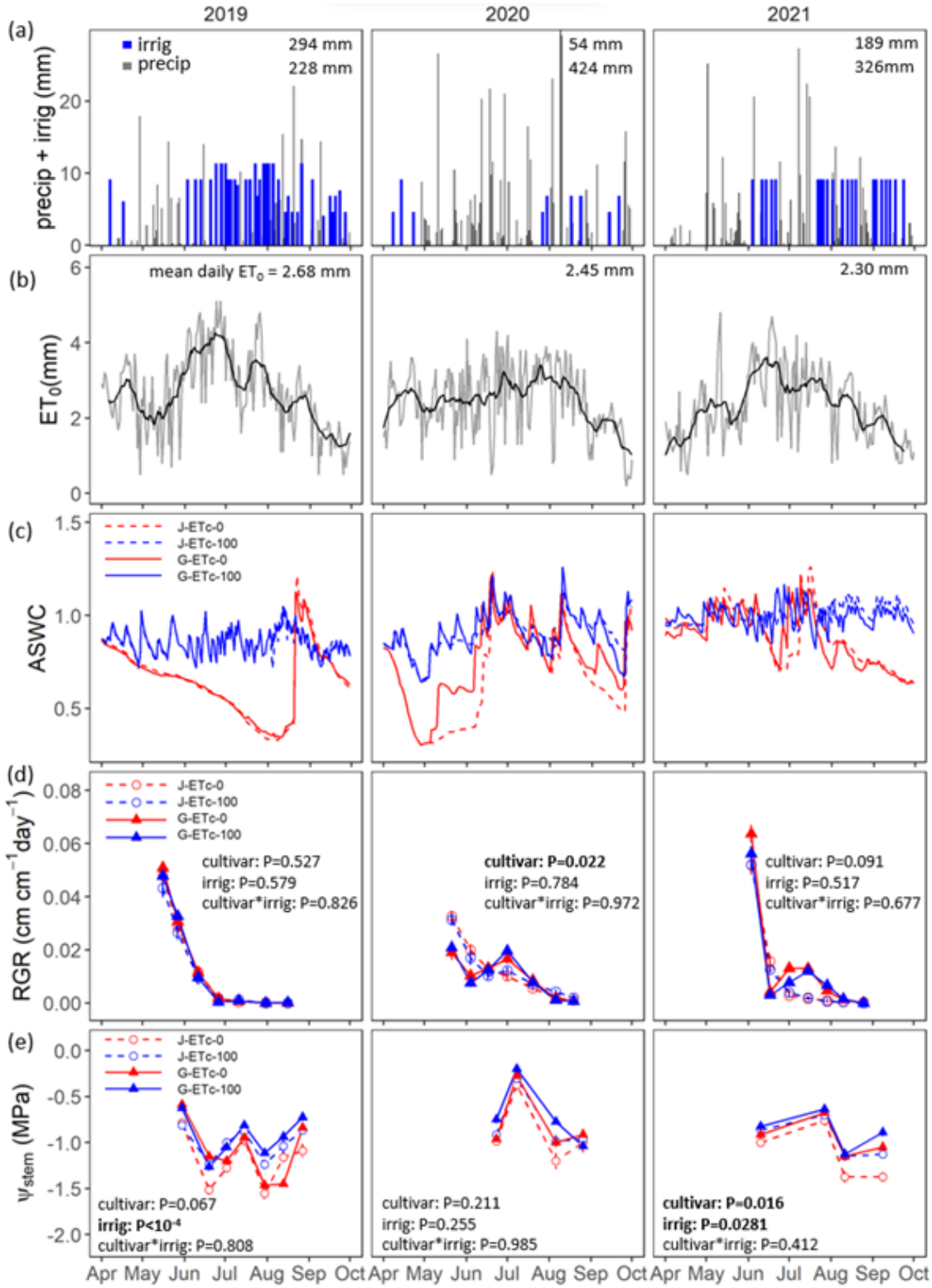

Figure 11: (a) Daily precipitation and irrigation, (b) reference evapotranspiration (ET0) and (c) available soil water capacity (ASWC) under non-irrigated (ETc-0) and irrigated (ETc-100) apple trees of 'Red Jonaprince' (J) and 'Gala Brookfield' (G) cultivars in years 2019, 2020 and 2021. (d) Relative extension growth rates of shoots (RGR) and (e) midday stem water potential (Ψ_{stem}) for non-irrigated (ETc-0) and irrigated (ETc-100) trees of each cultivar are shown. Points and error bars represent means ± standard error; n = 16-20 for shoot RGR; n = 4 for Ψ_{stem}

5. Conclusions

This habilitation thesis expands our knowledge of functional wood biology in two main areas. First, it provides seminal papers on the structure and function of ray and axial parenchyma. We showed that ray and axial parenchyma fractions are highest in tropical trees as the ray and axial parenchyma fraction increases with mean annual temperature. We provided a detailed review of parenchyma role in storage and utilization of non-structural carbohydrates and showed that parenchyma fractions are directly proportional to the concentration of non-structural carbohydrates. We looked at the ultrastructure of pits interconnecting parenchyma cells and vessels. The trade-offs between xylem cell types and their corresponding functions have been examined. Finally, we highlight that storage function can be facilitated not only by parenchyma but also by living fibers. Taken together, our papers provided one of the first detailed accounts on the structure and function of ray and axial parenchyma and have inspired more research in this field.

The second topic that is presented in this habilitation thesis is the wood biology and its implications for water and carbon relations in fruit trees. More specifically, several hypotheses regarding the mechanism of rootstock-induced growth vigour were examined in apple and pear trees grafted on size-controlling rootstocks. Size-controlling rootstocks are one of the important innovations in high density orchards, but the mechanisms of how they influence growth vigour has been poorly understood. Our findings support the role of perturbed water relations in growth vigour control mechanisms, while they do not support that it is due to the difference in the carbohydrate content, mobilization rate or allocation. A good knowledge of xylem biology and water relations is also useful for efficient irrigation. Stem water potential and stomatal conductance are frequently used plant-based indicators for irrigation scheduling and hence a better knowledge of these parameters can help improve irrigation scheduling. We observed slightly different hydraulic parameters between diploid and triploid apple tree cultivars, suggesting a different needs for irrigation.

6. Future perspectives

The field of functional wood biology combines knowledge and approaches of plant anatomy, physiology and ecology. As such it provides numerous opportunities for future research. While our publications on ray and axial parenchyma revealed great anatomical variation across species, the understating of the functional significance is just at its beginning. More research is needed from the physiological site to substantiate the role of ray and axial parenchyma in the storage and utilization of carbohydrates. For instance, studied can focus on measuring activities of various carbohydrate-modifying enzymes, localizing carbohydrate transporters or measuring the activity of genes responsible for carbohydrate metabolism. From the ecological site, investigating ray and axial parenchyma fractions along well-defined environmental gradients (e.g., temperature, precipitation, nutrients) or in phylogenetically related taxa (e.g., comparing parenchyma fractions in tropical vs. temperate Fabaceae) or between ecologically distinct species (e.g., sprouters vs. seeders; deciduous vs. evergreen) can shed more light on the functional significance of the anatomical variation.

In horticultural setting, there are also immense possibilities for the functional wood biology to tackle more applied questions as illustrated by our studies on rootstock-induced growth vigour control mechanism and irrigation. From the practical point of view, the field of horticulture would benefit from the use of continuously measuring sensors (such as dendrometers, water potential psychrometers) and remote sensing technologies (e.g.,

multispectral imaging). However, those novel approaches, which can be more easily upscaled to large, cultivated orchard areas, should be first calibrated against the traditional methods (e.g., water potential measurements using Scholander-type pressure chamber, leaf gas exchange measurements). Also, a good knowledge of water and carbon relations of individual cultivars can help to optimize cultivar selection and management in the field.

7. References:

Anderegg WRL, Plavcová L, Anderegg LDL, Hacke UG, Berry JA, Field CB. **2013**. Drought's legacy: multiyear hydraulic deterioration underlies widespread aspen forest die-off and portends increased future risk. *Global Change Biology* **19**: 1188–1196.

Basile B, DeJong TM. **2018**. Control of Fruit Tree Vigor Induced by Dwarfing Rootstocks In: Warrington I, ed. *Horticultural Reviews*. Hoboken, NJ, USA: John Wiley & Sons, Inc., 39–97.

Borchert R, Pockman WT. **2005**. Water storage capacitance and xylem tension in isolated branches of temperate and tropical trees. *Tree Physiology* **25**: 457–466.

Burgert I, Bernasconi A, Niklas KJ, Eckstein D. **2001**. The Influence of Rays on the Transverse Elastic Anisotropy in Green Wood of Deciduous Trees. *Holzforschung* **55**: 449–454.

Burgert I, Eckstein D. **2001**. The tensile strength of isolated wood rays of beech (Fagus sylvatica L.) and its significance for the biomechanics of living trees. *Trees* **15**: 168–170.

Cai J, Li S, Zhang H, Zhang S, Tyree MT. **2014**. Recalcitrant vulnerability curves: methods of analysis and the concept of fibre bridges for enhanced cavitation resistance: Recalcitrant vulnerability curves. *Plant, Cell & Environment* **37**: 35–44.

Carlquist S. **1985**. Vasicentric Tracheids as a Drought Survival Mechanism in the Woody Flora of Southern California and Similar Regions; Review of Vasicentric Tracheids. *Aliso* **11**: 37–68.

Chambers JQ, Higuchi N, Tribuzy ES, Trumbore SE. **2001**. Carbon sink for a century. *Nature* **410**: 429–429.

Charra-Vaskou K, Badel E, Charrier G, *et al.* 2016. Cavitation and water fluxes driven by ice water potential in *Juglans regia* during freeze–thaw cycles. *Journal of Experimental Botany* **67**: 739–750.

Chave J, Coomes D, Jansen S, Lewis SL, Swenson NG, Zanne AE. **2009**. Towards a worldwide wood economics spectrum. *Ecology Letters* **12**: 351–366.

Choat B, Cobb AR, Jansen S. **2008**. Structure and function of bordered pits: new discoveries and impacts on whole-plant hydraulic function. *New Phytologist* **177**: 608–626.

Dixon HH. **1914**. *Transpiration and the ascent of sap in plants*. London: MacMillan.

Eller CB, Barros FV, Bittencourt PRL, Rowland, Mencuccini M, Oliveira RS. **2018**. Xylem hydraulic safety and construction costs determine tropical tree growth. *Plant, Cell & Environment* **41**: 548–562.

Falster DS, Westoby M. **2005**. Alternative height strategies among 45 dicot rain forest species from tropical Queensland, Australia. *Journal of Ecology* **93**: 521–535.

Furze ME, Huggett BA, Aubrecht DM, Stolz CD, Carbone MS, Richardson AD. **2019**. Whole-tree nonstructural carbohydrate storage and seasonal dynamics in five temperate species. *New Phytologist* **221**: 1466–1477.

Furze ME, Huggett BA, Chamberlain CJ, *et al.* 2020. Seasonal fluctuation of nonstructural carbohydrates reveals the metabolic availability of stemwood reserves in temperate trees with contrasting wood anatomy (L Cernusak, Ed.). *Tree Physiology* **40**: 1355–1365.

Hacke UG, Sperry JS. **2001**. Functional and ecological xylem anatomy. *Perspectives in Plant Ecology, Evolution and Systematics.* **4**: 97–115.

Hacke UG, Sperry JS, Pockman WT, Davis SD, McCulloh KA. **2001**. Trends in wood density and structure are linked to prevention of xylem implosion by negative pressure. *Oecologia* **126**: 457–461.

Hacke UG, Spicer R, Schreiber SG, Plavcová L. **2017**. An ecophysiological and developmental perspective on variation in vessel diameter: Variation in xylem vessel diameter. *Plant, Cell & Environment* **40**: 831–845.

Hartmann H, Moura CF, Anderegg WRL, *et al.* 2018. Research frontiers for improving our understanding of drought-induced tree and forest mortality. *New Phytologist* **218**: 15–28.

Hoch G, Richter A, Körner Ch. **2003**. Non-structural carbon compounds in temperate forest trees: Non-structural carbon compounds in temperate forest trees. *Plant, Cell & Environment* **26**: 1067–1081.

Hölttä T, Cochard H, Nikinmaa E, Mencuccini M. **2009**. Capacitive effect of cavitation in xylem conduits: results from a dynamic model. *Plant, Cell & Environment* **32**: 10–21.

Jacobsen AL, Ewers FW, Pratt RB, Paddock WA, Davis SD. **2005**. Do Xylem Fibers Affect Vessel Cavitation Resistance? *Plant Physiology* **139**: 546–556.

Jupa R, Plavcová L, Gloser V, Jansen S. **2016**. Linking xylem water storage with anatomical parameters in five temperate tree species (F Meinzer, Ed.). *Tree Physiology* **36**: 756–769.

Kaack L, Weber M, Isasa E, *et al.* 2021. Pore constrictions in intervessel pit membranes provide a mechanistic explanation for xylem embolism resistance in angiosperms. *New Phytologist* **230**: 1829–1843.

Kotowska MM, Wright IJ, Westoby M. **2020**. Parenchyma Abundance in Wood of Evergreen Trees Varies Independently of Nutrients. *Frontiers in Plant Science* **11**: 86.

Kribs DA. **1935**. Salient Lines of Structural Specialization in the Wood Rays of Dicotyledons. *Botanical Gazette* **96**: 547–557.

Lens F, Gleason SM, Bortolami G, Brodersen C, Delzon S, Jansen S. **2022**. Functional xylem characteristics associated with drought-induced embolism in angiosperms. *New Phytologist* **236**: 2019–2036.

Loescher WH, McCamant T, Keller JD. **1990**. Carbohydrate Reserves, Translocation, and Storage in Woody Plant Roots. *HortScience* **25**: 274–281.

Mayr S, Sperry JS. **2010**. Freeze–thaw-induced embolism in Pinus contorta: centrifuge experiments validate the 'thaw-expansion hypothesis' but conflict with ultrasonic emission data. *New Phytologist* **185**: 1016–1024.

McDowell N, Pockman WT, Allen CD, *et al.* 2008. Mechanisms of plant survival and mortality during drought: why do some plants survive while others succumb to drought? *New Phytologist* **178**: 719–739.

Meinzer FC, Johnson DM, Lachenbruch B, McCulloh KA, Woodruff DR. **2009**. Xylem hydraulic safety margins in woody plants: coordination of stomatal control of xylem tension with hydraulic capacitance. *Functional Ecology* **23**: 922–930.

Morris H, Plavcová L, Cvecko P, *et al.* 2016. A global analysis of parenchyma tissue fractions in secondary xylem of seed plants. *New Phytologist* **209**: 1553–1565.

Morris H, Plavcová L, Gorai M, *et al.* 2018. Vessel-associated cells in angiosperm xylem: Highly specialized living cells at the symplast–apoplast boundary. *American Journal of Botany* **105**: 151–160.

Nadal-Sala D, Grote R, Birami B, *et al.* 2021. Leaf Shedding and Non-Stomatal Limitations of Photosynthesis Mitigate Hydraulic Conductance Losses in Scots Pine Saplings During Severe Drought Stress. *Frontiers in Plant Science* **12**.

Niklas KJ. **1993**. Influence of tissue density-specific mechanical properties on teh scaling of plant height. *Annals of Botany* **72**: 173–179.

Niklas KJ, Spatz H-C. **2010**. Worldwide correlations of mechanical properties and green wood density. *American Journal of Botany* **97**: 1587–1594.

Olson ME. **2023**. Imperforate tracheary element classification for studies of xylem structure-function relations. *IAWA Journal*: 1–26.

Panshin AJ, de Zeeuw C. **1980**. *Textbook of wood technology: Structure, indentification, properties, and uses of the commercial woods of the United States and Canada*. New York: McGraw-Hill.

Pittermann J, Sperry JS. **2006**. Analysis of Freeze-Thaw Embolism in Conifers. The Interaction between Cavitation Pressure and Tracheid Size. *Plant Physiology* **140**: 374–382.

Plavcová L, Hacke UG. **2011**. Heterogeneous distribution of pectin epitopes and calcium in different pit types of four angiosperm species. *New Phytologist* **192**: 885–897.

Plavcová L, Hacke UG, Sperry JS. **2011**. Linking irradiance-induced changes in pit membrane ultrastructure with xylem vulnerability to cavitation: Irradiance-induced changes in pit structure. *Plant, Cell & Environment* **34**: 501–513.

Plavcová L, Hoch G, Morris H, Ghiasi S, Jansen S. **2016**. The amount of parenchyma and living fibers affects storage of nonstructural carbohydrates in young stems and roots of temperate trees. *American Journal of Botany* **103**: 603–612.

Pratt RB, Jacobsen AL. **2017**. Conflicting demands on angiosperm xylem: Tradeoffs among storage, transport and biomechanics: Tradeoffs in xylem function. *Plant, Cell & Environment* **40**: 897–913.

Pratt RB, Jacobsen AL, Percolla MI, De Guzman ME, Traugh CA, Tobin MF. **2021**. Trade-offs among transport, support, and storage in xylem from shrubs in a semiarid chaparral environment tested with structural equation modeling. *Proceedings of the National Academy of Sciences* **118**: e2104336118.

Rodriguez-Dominguez CM, Buckley TN, Egea G, *et al.* 2016. Most stomatal closure in woody species under moderate drought can be explained by stomatal responses to leaf turgor. *Plant, Cell & Environment* **39**: 2014–2026.

Sala A, Woodruff DR, Meinzer FC. **2012**. Carbon dynamics in trees: feast or famine? *Tree Physiology* **32**: 764–775.

Schenk HJ, Michaud JM, Mocko K, *et al.* 2021. Lipids in xylem sap of woody plants across the angiosperm phylogeny. *The Plant Journal* **105**: 1477–1494.

Sperry JS. **2000**. Hydraulic constraints on plant gas exchange. *Agricultural and Forest Meteorology* **104**: 13–23.

Steudle E. **2001**. The cohesion-tension mechanism and the acquisition of water by plant roots. *Annual Review of Plant Physiology and Plant Molecular Biology* **52**: 847–875.

Tyree MT, Yang S. **1990**. Water-storage capacity of Thuja, Tsuga and Acer stems measured by dehydration isotherms: The contribution of capillary water and cavitation. *Planta* **182**: 420–426.

Van Bel AJE. **1990**. Xylem-Phloem Exchange Via the Rays: The Undervalued Route of Transport. *Journal of Experimental Botany* **41**: 631–644.

Wolfe BT, Sperry JS, Kursar TA. **2016**. Does leaf shedding protect stems from cavitation during seasonal droughts? A test of the hydraulic fuse hypothesis. *New Phytologist* **212**: 1007–1018.

Ziemińska K, Rosa E, Gleason SM, Holbrook NM. **2020**. Wood day capacitance is related to water content, wood density, and anatomy across 30 temperate tree species. *Plant, Cell & Environment* **43**: 3048–3067.

Chapter 8
The Role of Xylem Parenchyma in the Storage and Utilization of Nonstructural Carbohydrates

Lenka Plavcová and Steven Jansen

1 The Structure, Abundance, and Function of Ray and Axial Parenchyma in Wood

1.1 The Structure of Ray and Axial Parenchyma in Wood

The fact that most of the cells present in mature wood are dead is often highlighted. Indeed, all xylem conduits (vessels and tracheids) found in the functional sapwood undergo cell autolysis, forming hollow tubes made of lignified secondary cell wall. However, cells with a protoplasm are also present in secondary xylem. These cells are referred to as wood parenchyma because their cell wall is often much thinner than that of fibers. Depending on their arrangement and orientation with respect to the main stem axis, parenchyma cells can be divided into two distinct types—radial (ray) and axial parenchyma.

Ray parenchyma consists of ribbon-like aggregates of cells that are produced by ray initials, extending radially from the cambial zone in the xylem and phloem. Xylem rays can be classified depending on their width as uniseriate (Fig. 8.1a–d), biseriate (Fig. 8.1e), and multiseriate, referring to rays that are one-, two-, or more cells wide. Rays can also be subdivided according to the dimensions of individual cells viewed in a radial section. While most of the ray parenchyma cells have their longest axis oriented radially (procumbent cells), vertically elongated (upright) or isodiametric (square) cells also occur. Rays comprised exclusively of procumbent cells are called homocellular, while rays made of more than one parenchyma cell type are termed heterocellular (Carlquist 2001; Evert 2006). The entire ray system can consist of a single ray type, but a combination of different ray types commonly

L. Plavcová (✉) • S. Jansen
Institute for Systematic Botany and Ecology, Ulm University,
Albert-Einstein-Allee 11, Ulm 89081, Germany
e-mail: lenka.plavcova@gmail.com

U. Hacke (ed.), *Functional and Ecological Xylem Anatomy*,
DOI 10.1007/978-3-319-15783-2_8

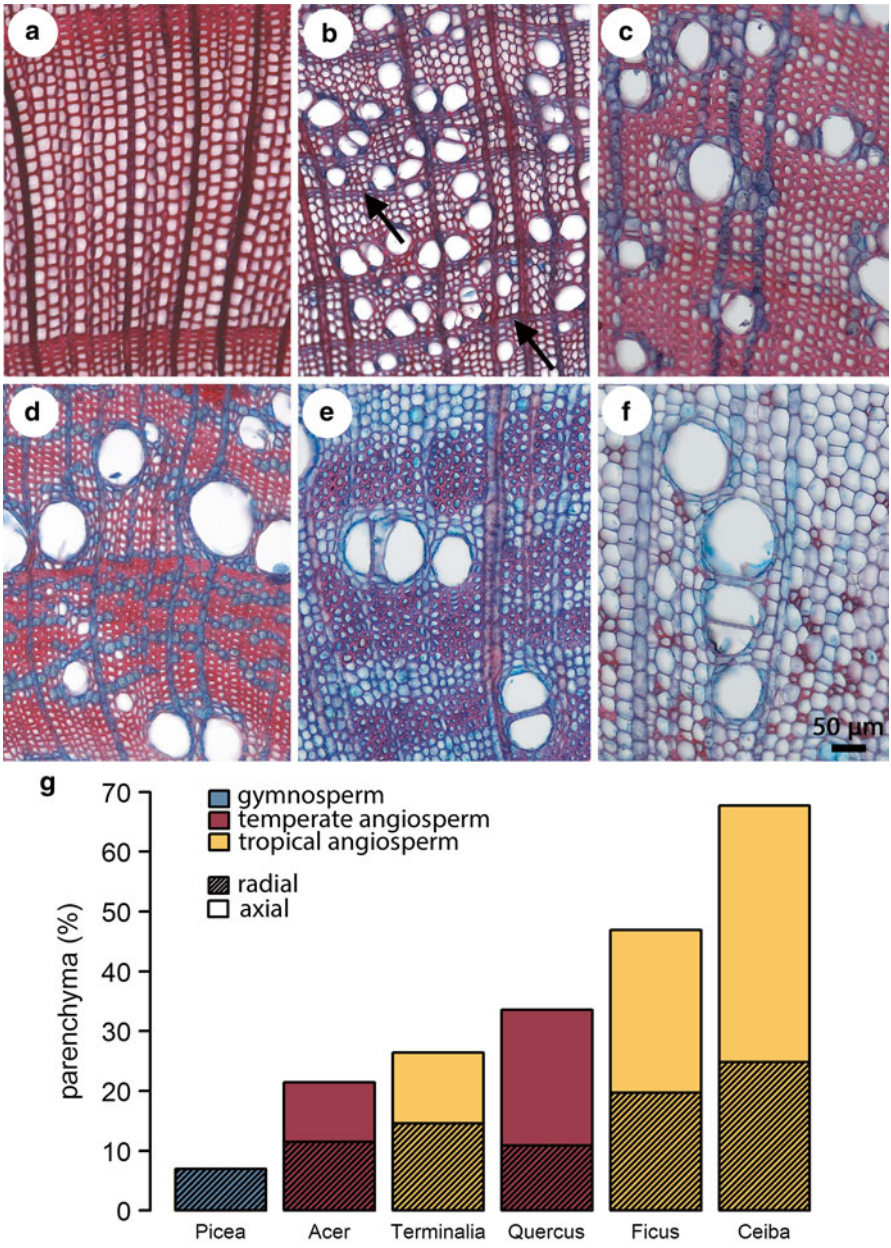

Fig. 8.1 Diversity in ray and axial parenchyma patterns as viewed in transverse wood sections stained with *safranin* and *alcian blue*. Thick lignified secondary cell walls of fibers and vessels stain *pink*, while protoplasts and less extensively lignified cell walls of parenchyma cells appear *blue*. All images were taken at the same magnification; a scale bar is shown in (**f**). (**a**) A conifer species (*Picea abies*) showing the lowest proportion of parenchyma; rays are uniseriate, axial parenchyma is absent, (**b**) a temperate, diffuse-porous tree (*Acer pseudoplatanus*)

occurs. In addition to the ray types described above, other specialized ray systems such as aggregated and interconnected rays have been identified. Interestingly, a temporal or permanent absence of rays occurs in the wood of several species (Barghoorn 1941; Carlquist 1970). Nevertheless, the complete absence of rays is a rarity restricted to small plants, in which woodiness is not pronounced and has evolved secondarily (Carlquist 1970).

Axial parenchyma is produced by fusiform cambial initials that undergo transverse divisions, resulting in a parenchyma strand or axial series of two or more parenchyma cells. In some species, axial parenchyma is absent or sparse. This condition is characteristic of conifers (Fig. 8.1a); however, it can be found in many angiosperms as well. For instance, sparse axial parenchyma occurs in *Populus*, *Aesculus*, *Berberis*, *Magnolia*, and *Eucalyptus*, to name a few examples. If present, axial parenchyma can be arranged in different patterns as distinguished in transverse sections (Carlquist 2001; Kribs 1937). Traditionally, axial parenchyma is classified as apotracheal if it appears distributed without a direct connection to vessels (Fig. 8.1d), and paratracheal if it is strongly associated with xylem vessels (Fig. 8.1b, c). These two basic categories can be further subdivided. For instance, parenchyma cells can be randomly scattered within the vessels and fibers (diffuse apotracheal parenchyma), be in contact with vessels but not ensheathing them completely (scanty paratracheal parenchyma, Fig. 8.1b), form a complete sheath surrounding vessels (vasicentric paratracheal parenchyma, Fig. 8.1c), or be arranged in distinct tangential bands (banded parenchyma, Fig. 8.1d, e). In addition, an increased occurrence of parenchyma cells at the tree ring boundary is often found in temperate species and referred to as marginal parenchyma (Fig. 8.1b). Last but not least, wood of some trees such as *Adansonia* (Chapotin et al. 2006) or *Ceiba* (Fig. 8.1f) is extremely parenchymatous, with axial parenchyma comprising most of the matrix between vessels and rays. The categorization outline above is useful, but to a certain extent arbitrary. Thus, intermediary patterns and co-occurrence of more than one type of axial parenchyma are frequently observed. Besides thin-walled parenchyma cells, some thick-walled axially oriented cells, which could be hence termed fibers, also retain living protoplasts (Fahn and Leshem 1963). Axial cells that can be classified as living fibers rather than parenchyma occur, for instance, in *Acer* (Fig. 8.1b),

Fig. 8.1 (continued) and biseriate rays, axial cells that can be, due to their thick secondary cell wall, classified as living fibers are in a scanty paratracheal and marginal arrangement (*arrows*), (**c**) a tropical dry-deciduous tree (*Terminalia catappa*) with uniseriate rays and paratracheal vasicentric parenchyma, (**d**) a ring-porous temperate species (*Quercus robur*) with apotracheal axial parenchyma arranged in narrow bands and scanty paratracheal parenchyma contacting the vessels, rays are uniseriate (but multiseriate, up to 30-cells wide rays are common in older stems of this species), (**e**) a tropical evergreen tree (*Ficus rubiginosa*) with uniseriate and biseriate rays and axial parenchyma arranged in wide bands, (**f**) a tropical dry-deciduous tree (*Ceiba aesculifolia*) showing highly parenchymatous wood composed of multiseriate rays and thin-walled axial parenchyma cells. (**g**) The relative proportion of ray and axial parenchyma cells measured using transverse sections for all six species shown above

Robinia pseudoacacia (Yamada et al. 2011), or *Cactaceae* (Mauseth and Plemons-Rodriguez 1997), although the distinction between these two cell types has often been neglected. When these cell types are distinguished, it has been hypothesized that living fibers substitute for, or complement, the function of axial parenchyma cells (Carlquist 2001; Yamada et al. 2011; Wheeler et al. 2007).

1.2 How Much Ray and Axial Parenchyma Occurs in Wood?

Ray and axial parenchyma cells make up a substantial proportion of all wood cells (Fig. 8.1g). The volumetric content is hard to measure directly; however, the proportion of parenchyma cells can be estimated from the area measurements taken on a transversal or tangential section. In gymnosperms, the total parenchyma proportions are commonly between 5 and 10 % and compose mainly of radial parenchyma (Fig. 8.1a). In angiosperms, the total amount or parenchyma ranges typically between 20 and 40 % (Fig. 8.1b–d); however, values between 40 and 60 % are not uncommon among tropical angiosperms (Fig. 8.1e). The proportion of ray parenchyma is typically around 10–20 %, while the axial parenchyma proportions between 1 and 30 % are common in angiosperms. The aforementioned numbers represent values typically encountered in wood (Fig. 8.1g) (Von Frey-Wyssling and Aeberli 1942; Wagenführ 2007; Ruelle et al. 2006; Zieminska et al. 2013); however, more extreme values also occur. For example, very low ray proportions of around 7 % were reported for two *Acacia* species (Zieminska et al. 2013), while very high axial parenchyma proportions of 67 % were measured in *Ceiba aesculifolia* (Fig. 8.1f) and several species of the genus *Adenia* (Hearn 2009).

1.3 The Function of Ray and Axial Parenchyma in the Storage of Nonstructural Carbohydrates

The function of wood parenchyma in storage is often highlighted and put in contrast with the main role of vessels in facilitating water conduction and the role of fibers in providing the mechanical support. Nonstructural carbohydrates (NSC) represent the most abundant reserves stored in wood parenchyma. The importance of NSC storage for tree growth and functioning has been known for many decades (Kozlowski 1992; Kramer and Kozlowski 1979). Recently, this topic has received renewed attention because the size and the dynamics of the NSC pool might represent factors potentially limiting tree growth (Palacio et al. 2014) and affecting tree survival under drought stress (McDowell et al. 2008).

The total volume of ray and axial parenchyma can be viewed as a finite compartment potentially available for storage. Given the large volume of woody trunks, the size of this storage pool is substantial from the whole plant perspective. For instance,

Würth et al. (2005) calculated that the carbon stored in the above ground woody biomass accounts for 80 % of the total carbon pool present in a seasonally dry tropical forest and that this amount would be sufficient to completely regrow the entire canopy. However, the storage capacity provided by wood parenchyma is not always completely filled up. Instead, the NSC levels fluctuate, reflecting the dynamic balance between carbohydrate production and utilization.

Besides the total amount of NSCs, their partitioning into starch and soluble sugar fraction is of importance. Out of these two components, starch can be considered as the primary long-term storage form of NSCs. Its molecules are large and cannot move freely between cells; however, they can be readily hydrolyzed to produce soluble sugars. Soluble sugars constitute a plethora of mono- and oligosaccharides that are mobile and fulfill more active physiological roles.

As ray and axial parenchyma are the main sites of NSC accumulation in wood, the NSC status of these cells should be directly mirrored in the NSC content and composition measured in the bulk sapwood. The sapwood NSCs have been analyzed in a number of ecological studies (Hoch et al. 2003; Sauter and Wellenkamp 1998; Ashworth et al. 1993; Palacio et al. 2007; Carbone et al. 2013), providing insights into the size and dynamics of the wood parenchyma carbohydrate pool. In the following sections, we will review the NSC accumulation patterns observed in different tree species and different woody organs and discuss changes in NSC concentration and composition that occur throughout the growing season. These aspects of sapwood NSC dynamics will be linked to the anatomy and physiology of ray and axial parenchyma cells.

2 Patterns in NSC Accumulation Across Different Woody Species, Organs, and Time

2.1 Variation in NSC Across Different Tree Species

As already mentioned, a positive relationship between the NSC content and the proportion of ray and axial parenchyma in wood can be expected. To the best of our knowledge, this assumption has not been confirmed empirically, except for the notion that conifer wood tends to have lower NSC concentrations than the wood of angiosperms, which is in agreement with the lower proportion of parenchyma found in conifer wood (Johnson et al. 2012). Considering the large differences in wood parenchyma content across angiosperms, as illustrated by the more than threefold variation shown by the five angiosperms in Fig.8.1a–g, it would be interesting to see if the tendency for a higher NSC content with increasing volume of parenchyma holds true also within this group. While the meta-analysis of published data can provide useful insights (Johnson et al. 2012), the finer-scale patterns are likely to be confounded by the different sampling schemes employed by different authors and the high variation in NSC concentration found across different woody organs and

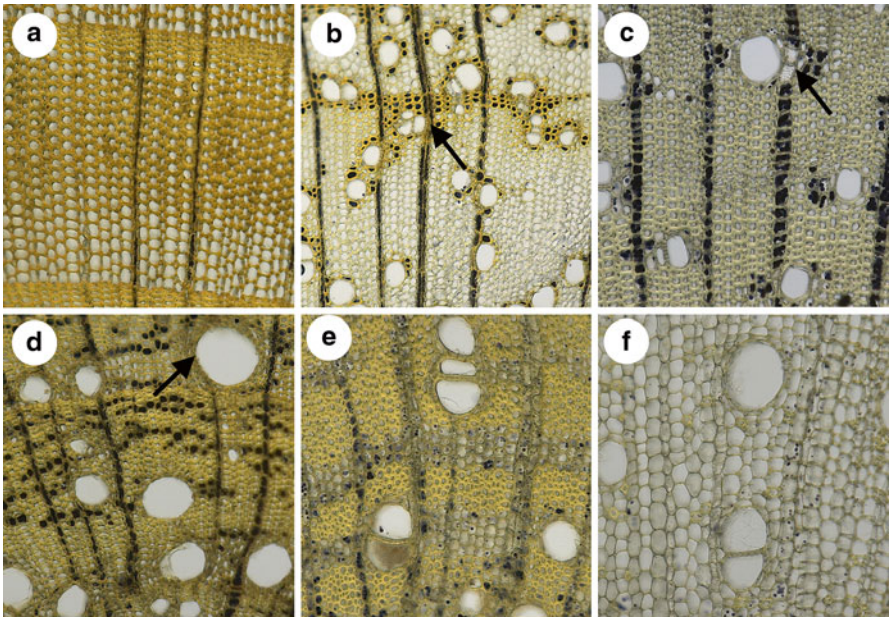

Fig. 8.2 Distribution of starch in wood parenchyma cells in the same species as shown in Fig. 8.1. The wood samples of the temperate species *Picea abies* (**a**), *Acer pseudoplatanus* (**b**), and *Quercus robur* (**d**) were collected at the Ulm University campus in October. In these species, most of the wood parenchyma cells appear densely packed with starch grains. The samples of the tropical plants *Terminalia catappa* (**c**), *Ficus rubiginosa* (**e**), and *Ceiba aesculifolia* (**f**) were obtained from the living collections of the botanical garden of Ulm University in early June. Despite growing under the same conditions of a tropical greenhouse, these species show marked differences in starch deposition. While *Terminalia* accumulates large amounts of starch in xylem parenchyma cells (**c**), the wood parenchyma in *Ficus* (**e**) and in particular in *Ceiba* (**f**) show much lower starch content. Note the absence of starch in contact cells in *Acer*, *Terminalia,* and *Quercus* (*arrows*)

seasons. In addition, the sapwood NSC content is usually expressed as a mass-based concentration, and therefore depends on wood density, which varies substantially between different species (Chave et al. 2009) and to some extent also within a single tree (Domec and Gartner 2002; McCulloh et al. 2012). This problem could be solved by expressing the NSC concentration on a wood volume rather than a wood mass basis. Unfortunately, the studies looking at the sapwood NSC content do not usually report wood density values to allow this conversion. Thus, additional research is required to demonstrate conclusively whether the proportion of ray and axial parenchyma is an important driver of the amount of NSC stored in wood. Here, we will provide some initial hints on answering this question.

Using the same species as shown in Fig. 8.1a–g, we visualized the starch deposition by staining with Lugol's solution (Fig. 8.2a–f). The iodine test revealed obvious differences in starch accumulation in these species that differ greatly in the amount of wood parenchyma. The parenchyma was packed with starch in all three temperate

species sampled at the end of the growing season (Fig. 8.2a, b, d). In contrast, the tropical plants showed varying patterns in starch accumulation, despite growing under the same conditions in a tropical greenhouse (Fig. 8.2c, e, f). The starch abundance was highest in *Terminalia* in which almost all parenchyma cells were filled with starch grains (Fig. 8.2c). The amount of starch was much lower in *Ficus* (Fig. 8.2e). In this species, the starch grains were sparse and almost absent in the regions closer to the cambium. The lowest starch accumulation was observed in the highly parenchymatous wood of *Ceiba aesculifolia* (Fig. 8.2f). Based on this simple iodine test, we cannot say whether most of the NSC were present in the form of soluble sugars in the wood of *Ficus* and *Ceiba*, or whether the total levels of NSC were low in spite of the high parenchyma content found in these two species. More than threefold differences in wood NSC concentration have recently been reported in a study encompassing 17 tropical trees from 10 different families (Würth et al. 2005). It would be interesting to see if this variability is at least partially explained by the amount of wood parenchyma. Marked differences in NSC concentration were observed not only between species but also between different tree parts. Thus, we will continue this review by comparing the patterns in NSC content found between woody branches, trunks, and roots.

2.2 Variation in NSC Across Different Woody Organs

Most studies monitoring the NSC levels in more than one woody organ report values for the main trunk and small terminal branches. Three times higher NSC concentrations in branch wood than in trunk wood were observed in eleven temperate trees (Hoch et al. 2003; Sala and Hoch 2009); however, such trend was much less pronounced in a tropical environment (Würth et al. 2005; Newell et al. 2002). The proportion of parenchyma does not differ greatly between branches and trunks (Bhat et al. 1985; Koch 1985); therefore, any differences in NSC concentrations between these two tissues are likely caused by physiological rather than anatomical drivers. Alternatively, it is possible that the branch wood NSC values are overestimated because of the inclusion of pith in the samples used for branch wood NSC measurements. Besides affecting the total branch biomass, medullary (i.e., pith) tissue is known to accumulate starch (Essiamah and Eschrich 1985). Both of these phenomena could bias the NSC concentrations toward higher values.

Nevertheless, the branch wood NSC pool consistently appears to be more dynamic than the trunk wood pool. This was manifested by a more dramatic seasonal change (Würth et al. 2005; Hoch et al. 2003; Newell et al. 2002), a higher proportion of the soluble sugar fraction (Sala and Hoch 2009), and a steeper increase in NSC levels with increasing tree height (Sala and Hoch 2009; Woodruff and Meinzer 2011) in branches as compared to trunks. The aforementioned differences between branches and trunks are consistent with the more proximal position of branches to the source of photoassimilates and developing buds and fruits that act as strong carbon sinks. Therefore, it can be suggested that branch wood parenchyma helps to buffer against a short-term imbalance between carbon supply and demand.

In contrast, the trunk wood parenchyma might be more specialized for long-term storage. This idea is supported by a recent study showing surprisingly long residence times of NSC extracted from the outermost 2 cm of sapwood in red maple and eastern hemlock. Using radiocarbon dating, the mean age of sapwood NSC has been estimated to be about a decade, although a substantial fraction of carbon seemed to have much faster turnover (Richardson et al. 2013). This faster fraction likely represents carbohydrates used to support parenchyma metabolism and cambial growth (Carbone et al. 2013; Hill et al. 1995).

In older trunks, the NSC concentration is known to decline radially with increasing distance from the cambium (Würth et al. 2005; Hoch et al. 2003). This decline is likely linked with parenchyma cell death and transition to heartwood. While low values of NSC concentrations are typically reached at the depth of 15–20 cm in trunks that showed a stem diameter of 30–100 cm, the radial patterns show interesting interspecific differences and variation with tree age (Würth et al. 2005; Hoch et al. 2003; Barbaroux and Bréda 2002). More specifically, the decrease in NSC concentration with increasing sapwood depth was particularly sharp in ring-porous oak, while diffuse porous trees exhibited a more gradual decline (Hoch et al. 2003; Barbaroux and Bréda 2002). The tropical tree, *Luehea seemanii*, exhibited remarkably constant NSC content throughout the entire 12-cm-thick sapwood (Würth et al. 2005).

Besides above-ground xylem biomass, woody roots also accumulate large amounts of NSC (Würth et al. 2005; Palacio et al. 2007; Loescher et al. 1990; Pate et al. 1990). High NSC storage capacity of belowground woody tissue is in accordance with a higher proportion of ray and axial parenchyma typically found in small woody roots compared to branches (Lens et al. 2000; Pratt et al. 2007). However, in coarser roots, the relative proportion of wood parenchyma might not be significantly different from stems due to an increase in inter-ray distance with increasing root diameter (Koch 1985; Wargo 1976).

The below-ground storage pool is particularly important when coping with disturbances that destroy a substantial portion of the above-ground plant biomass. A greater dependence on below-ground storage is characteristic for plants resprouting after disturbance, as opposed to plants that regenerate from seeds. In agreement, a higher proportion of wood parenchyma, paralleled by a greater amount of starch reserves, have been observed in resprouters than seeders growing in fire-prone habitats of Western Australia and South Africa (Pate et al. 1990; Verdaguer and Ojeda 2002). Interestingly, however, the overall starch tissue content was more strongly driven by the starch packing density than the amount of parenchyma tissue (Pate et al. 1990). Furthermore, not all the plants under study, including some of the resprouters, accumulated starch in ray and axial parenchyma cells. While some species accumulated starch only in their root cortex, other plants deposited starch in both or only one of the wood parenchyma subsystems. Yet other species had starch grains distributed in all three tissues. Unfortunately, it is not known if the same patterns occurred consistently throughout the season and what the levels of soluble sugars in the roots of these plants were.

Taken together, the comparison between species and woody organs suggests that the amount of parenchyma is important for the overall capacity to store carbohydrates;

however, the differences in starch accumulation patterns, possibly tied to the concentration of soluble sugars, provide another layer of complexity.

2.3 Seasonal Variation in NSC

The NSC content and its partitioning between starch and soluble sugars is also known to vary seasonally. The seasonal dynamics of wood NSC is most widely studied in temperate winter-deciduous trees (Kozlowski 1992; Ashworth et al. 1993; Sauter and van Cleve 1994), providing the following general picture. The total NSC concentration usually peaks at the end of the growing season and declines throughout winter, reaching its minimum during or shortly after bud break. Importantly, starch is often almost completely hydrolyzed during winter months in response to low temperatures, resulting in an increased concentration of soluble sugars (Fig. 8.3a) (Sauter and Wellenkamp 1998; Schoonmaker 2013). At the end of winter, the starch is transiently resynthesized, only to be hydrolyzed again shortly before bud break (Essiamah and Eschrich 1985; Sauter and van Cleve 1994). Starch and the total NSC levels then recover over the growing season. In contrast to deciduous trees, the peak in NSC concentration commonly occurs before bud break and remains low throughout the growing season in both temperate and boreal conifers (Hoch et al. 2003; Schoonmaker 2013). The aforementioned patterns make intuitive sense in terms of the typical progression of photosynthetic activity and growth and likely hold true on a large scale. However, recent studies indicate that this view might be an oversimplification and that various modifications of this general pattern can be found across different woody tissues, species, sites, and seasons (Hoch et al. 2003; Richardson et al. 2013). For instance, Hoch et al. (2003) did not observe a considerable reduction of NSC concentration during bud break in most of the angiosperm species studied. In some years, Richardson et al. (2013) even found higher NSC concentrations in March than in November in maple and oak, suggesting that a redistribution of NSC took place during the dormant season.

The patterns in carbohydrate concentration appear even more variable in a seasonally dry tropical forest. In a study on four trees differing in their leaf phenology (Newell et al. 2002), the branch wood of a truly drought-deciduous species (*Cecropia longipes*) exhibited a fourfold higher NSC concentration during the dry season, which was driven by a large increase in starch concentration (Fig. 8.3b). In contrast, the brevi-deciduous trees such as *Anacardium excelsum* showed much smaller seasonal variation in their NSC levels and a slight increase in soluble sugar fraction during the dry season (Fig. 8.3c). The tendency for higher levels of NSC in branch wood during the dry season was confirmed by a follow-up study encompassing 17 species (Würth et al. 2005). However, the seasonal effect was relatively weak in comparison with a striking interspecific variability.

The seasonal changes in sapwood NSC reflect the balance between carbon supply by photosynthesis and carbon utilization for various physiological needs such as growth, reproduction, or stress mitigation. The structure of ray and axial parenchyma

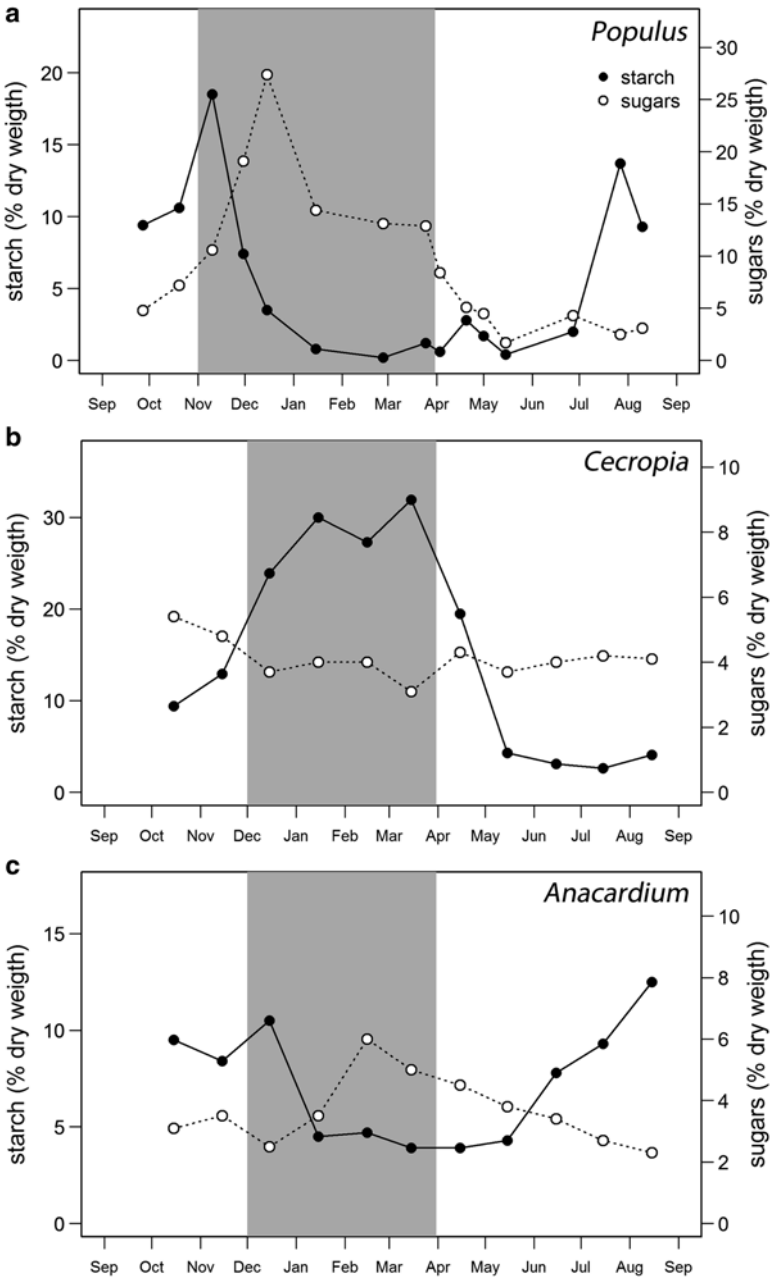

Fig. 8.3 Seasonal course of starch and soluble sugar concentrations in branch wood of winter-deciduous *Populus*×*canadensis* (**a**), drought-deciduous *Cecropia longipes* (**b**), and brevi-deciduous *Anacardium excelsum* (**c**). The shaded area in each graph indicates the period with unfavorable growing conditions (i.e., the winter in case of *Populus* and the dry season in the case of *Anacardium* and *Cecropia*). Data redrawn from Sauter and van Cleve (1994) (**a**) and Newell et al. (2002) (**b**, **c**)

and their biochemical machinery likely have a great influence on the NSC dynamics described above. The total parenchyma volume should be the parameter most closely related to the seasonal maximum in NSC content, assuming that the storage capacity of parenchyma cells is fully used during this period. In contrast, the dynamics of NSC is driven by physiological activity of ray and axial parenchyma cells and surrounding source and sink tissues (e.g., leaves, flushing buds, developing fruits, the cambium). Furthermore, the spatial proximity and connectivity between wood parenchyma and these sinks and sources is important for facilitating the NSC translocation within the plant body. While mechanisms underlying the buildup of NSC stores remain poorly understood, several studies have focused on processes involved in the mobilization and utilization of starch stored in wood parenchyma cells. The underlying cellular processes will be discussed in the following section.

3 Metabolic Activity of Wood Parenchyma Underlying the Dynamics of Sapwood NSC

3.1 Starch Mobilization and Metabolism of Soluble Sugars

The mobilization of starch reserves is initiated by the depolymerization of its molecules (Fig. 8.4). In plants, starch breakdown can be catalyzed by various enzymes such as amylases, glucosidases, and glucanohydrolases (Zeeman et al. 2010). To the best of our knowledge, only one study has looked at the starch hydrolyzing machinery acting in wood parenchyma (Witt et al. 1995). In this study, numerous enzymes with a potential amylolytic activity have been investigated in the ray parenchyma of *Populus*×*canadensis* and the main effect on starch degradation has been attributed to α-amylase and it has been hypothesized that the high temperature sensitivity of this enzyme underlies the mid-winter starch degradation and its resynthesis in early spring.

Simple sugars originating from starch hydrolysis are metabolized in a myriad of ways. Typically, the sugar molecules need to be phosphorylated before they can participate in further biochemical reactions. The phosphorylation of sugars is catalyzed by phosphotransferases. One of these enzymes is a plant hexokinase catalyzing the phosphorylation of hexoses, most importantly glucose. In addition, hexokinase also plays a prominent role in sugar-mediated signaling (Jang et al. 1997). While we are not aware of any studies on hexokinase activity in wood parenchyma, a gene encoding for this enzyme has recently been shown to exhibit a xylem parenchyma-specific expression in leaf petioles of tobacco (Giese et al. 2005).

Phosphorylation of glucose is the first step of glycolysis that can be followed by aerobic respiration. Respiration represents the key process through which the chemical energy contained in nutrients is released and made available for fueling the cellular metabolism. Respiration of wood parenchyma has been studied in a series of interesting experiments (Spicer and Holbrook 2005, 2007a, b). The respiration rates expressed per unit sapwood volume were between 0.4 and 1 μmol $O_2\,cm^{-3}\,h^{-1}$

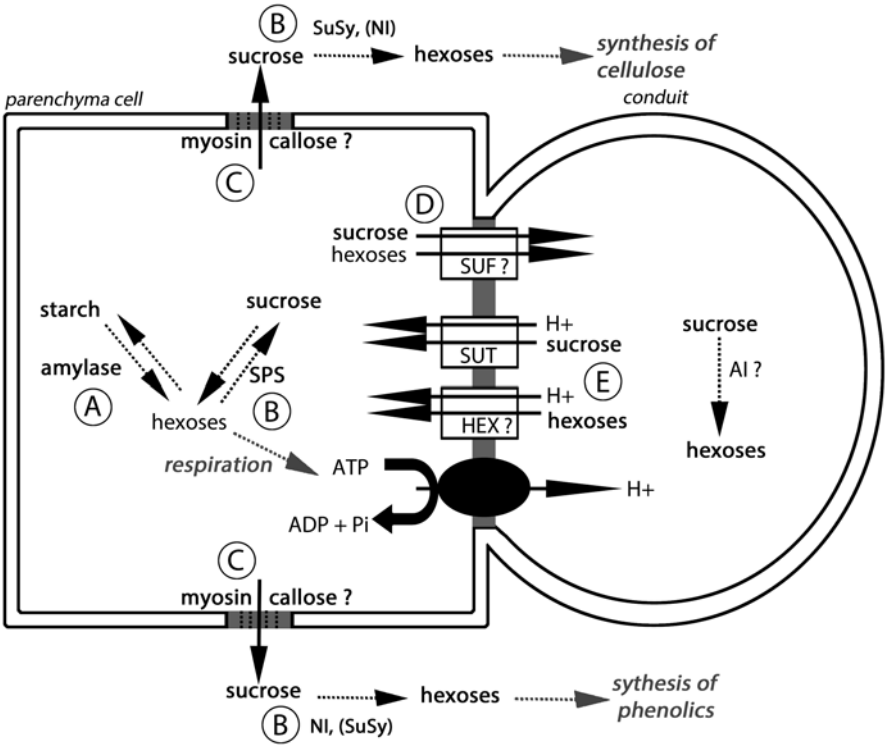

Fig. 8.4 NSC dynamics at the cellular level. Enzymes and transporters involved in the biochemical transformation and intercellular trafficking of NSC are shown. Starch hydrolysis is catalyzed by α-amylase (*A*). The synthesis of sucrose at the sites of starch mobilization is catalyzed by sucrose-6-phosphate-synthase (SPS). Sucrose breakdown at the sink sites is catalyzed by sucrose synthase (SuSy) and neutral invertase (NI) (*B*). Sucrose might also be hydrolyzed in the apoplast by acid invertase (AI). Soluble sugars are transported within the parenchyma network symplastically through pit plasmodesmata. The permeability of plasmodesmata might be affected by myosin contraction and callose deposition (*C*). Soluble sugars can move across a parenchyma-vessel pit membrane to the apoplast. The efflux of sugars to a conduit lumen is passive and driven by the concentration gradient. Putative membrane channels (SUF) likely facilitates the efflux (*D*). Soluble sugars can also be retrieved from the conduit apoplast to the parenchyma symplast by active transport via proton-sugar symporters (SUT, HEX). The electrochemical proton gradient required for the sugar uptake is generated by ATP-dependent proton pumps (*E*)

and did not differ greatly between three angiosperm and two conifer species studied. However, when expressed per living parenchyma volume, the two conifers showed one order of magnitude higher respiration than the angiosperms, with the respiration rates being around 12 and 3 μmol $O_2\,cm^{-3}\,h^{-1}$, respectively. Such respiration rates are much lower than those typically found in meristems, but considerably higher than those measured in tissues purely devoted to storage, such as tubers. This suggests that wood parenchyma cells have a more active role than just being a simple storage compartment. Based on cytochemical staining, respiratory activity appears

particularly high in parenchyma cells that are in a direct contact with xylem conduits. These so-called contact or vessel-associated cells are characterized by high mitochondrial counts, high activity of respiratory enzymes (Sauter et al. 1973; Alves et al. 2001), and reduced starch accumulation (Fig. 8.2b, c, d, Braun 1984). Interestingly, wood parenchyma cells of some species contain chloroplasts and are photosynthetically active (Langenfeld-Heyser 1989; Cocoletzi et al. 2013; Larcher et al. 1988). The carbon assimilation rates exhibited by woody stems are low and usually not sufficient to result in a net carbon uptake; nevertheless, they may be involved in the refixation of CO_2 released during parenchyma respiration, thereby reducing respiratory carbon loss (Pfanz et al. 2002).

Sucrose is usually the most abundant component of soluble sugar fraction found in wood. There are three key enzymes governing the metabolism of sucrose in plants—sucrose-6-phosphate-synthase (SPS), sucrose-synthase (SuSy), and invertase (Fig. 8.4). While SPS catalyzes the synthesis of sucrose molecules from phosphorylated monomers, the other two enzymes, SuSy and invertase, are responsible for sucrose catabolism. The difference between these two enzymes is that SuSy catalyzes the conversion of sucrose into fructose and UDP-glucose, while invertase catalyzes the hydrolysis of sucrose into nonphosphorylated monomers. In plants, several types of invertases can be distinguished based on their subcellular localization and pH optimum. While netural invertase (NI) is localized in the cytoplasm, acid invertases (AI) are found in vacuoles and cell walls (Sturm 1999).

Seasonal changes in the activity of all three enzymes, SPS, SuSy, and invertase, which play an important role in sucrose metabolism, were studied along a radial profile in the sapwood of *Robinia pseudoacacia*, providing interesting insights into the coordination of NSC mobilization and utilization (Hauch and Magel 1998). An increased activity of sucrose synthesizing SPS was indicative of starch mobilization. Thus, a high SPS activity was observed throughout the entire width of sapwood during cold winter months when starch is being hydrolyzed into soluble sugars. The high SPS activity persisted in the middle and outermost sapwood during bud break. In contrast, the activities of SuSy and neutral invertase peaked in sink tissues to which sucrose was transported and subsequently catabolized. In spring, SuSy was highly active in sapwood regions close to the cambium, producing UDP-glucose for the synthesis of cell walls of newly developing xylem cells. By contrast, NI was mostly active in the sapwood-to-heartwood transition zone during autumn, likely providing precursors for the synthesis of heartwood phenolic. Similar patterns in SPS and SuSy activity as observed in *Robinia pseudoaccacia* have also been detected in the wood of *Populus*×*canadensis* (Schrader and Sauter 2002).

3.2 Translocation of Soluble Sugars

In order to supply carbon and energy to the cambium and the sapwood-to-heartwood transition zone, sucrose and other soluble sugars arising from starch mobilization have to move radially within the stem (Fig. 8.4). Rays provide an ideal path for such a translocation (Van Bel 1990). Ray parenchyma cells are interconnected via pits

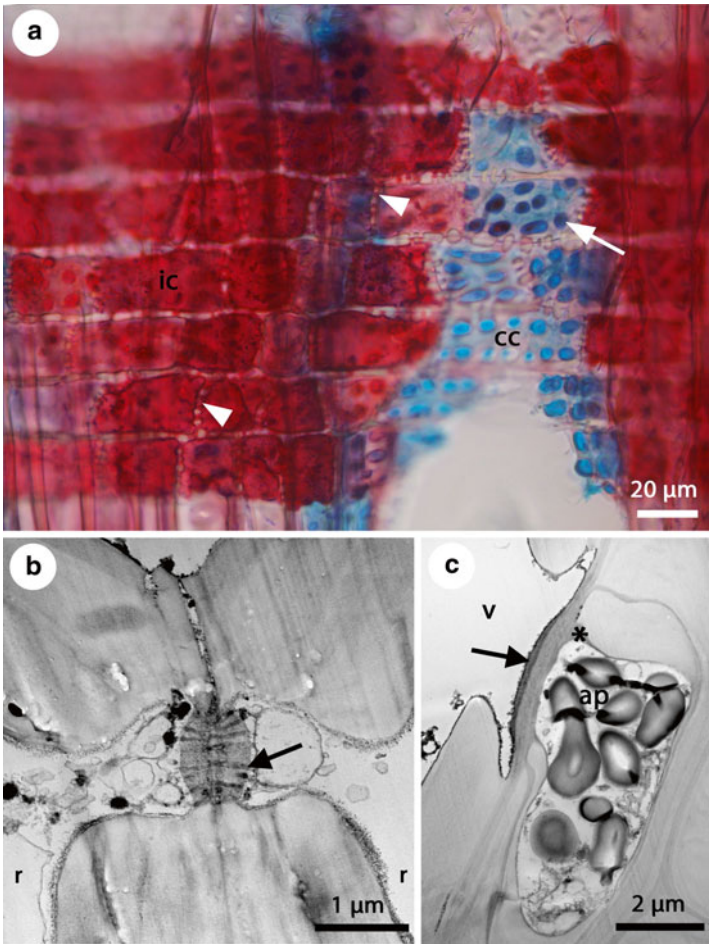

Fig. 8.5 Parenchyma–conduit and parenchyma–parenchyma cell connections in *Quercus robur*. (**a**) A radial section showing a vessel-ray interface observed with a light microscope. Numerous pit connections are apparent at the interface between the ray and vessel (*arrow*) and between the different files of ray cells (arrowheads). A clear distinction between contact (cc) and isolation cells (ic) within the ray is obvious in the picture. (**b**) A slightly bordered pit between two ray cells (r) observed with a transmission electron microscope. The pit membrane is penetrated by plasmodesmata (*arrow*). Various cytoplasmic bodies and vesicles are abundant in the pit channel, suggesting intense transport activity across the pit membrane. (**c**) Cross-section through an axial parenchyma cell (ap) connected to an adjacent vessel (v) via a half-bordered pit. The pit membrane is without plasmodesmata. The amorphous (or protective) layer between the pit membrane and the plasmalemma is thin but still apparent (*asterisk*). From the vessel lumen side, the pit membrane is covered by an electron dense plug, also known as the "black cap" (*arrow*)

perforated by numerous plasmodesmata, such that a symplastic continuum exists within the ray (Fig. 8.5a, b). This continuum can be visualized with symplastic fluorescence tracers (Sokolowska and Zagórska-Marek 2012); however, very little is known about the rate, selectivity, and regulation of this transport pathway. The rate

and direction of the bulk symplastic transport of carbohydrates are likely driven by the concentration gradient, similarly to the movement of sucrose during symplastic phloem loading. Based on the dynamics of starch deposition, Sauter and Kloth (1986) calculated a carbohydrate flow rate of 800 pmol cm^{-1} s^{-1} across the tangential ray walls of *Populus*×*canadensis* and concluded that much of this flux must have occurred via plasmodesmata.

Moreover, the presence of highly ordered microfilaments and microtubules running parallel to the longer (i.e., radial) axis of the ray cells provides possibility for active directional transport (Chaffey and Barlow 2001). Myosin, belonging to the family of ATP-dependent molecular motors, and the polysaccharide callose are localized at the plasmodesmal faces within the pit membranes. Both of these compounds are known to influence the permeability of plasmodesmata (Reichelt et al. 1999; Zavaliev et al. 2011; White and Barton 2011) and could hence facilitate an active regulation of the ray-to-ray cell conductance. Nevertheless, even if plasmodesmata are present and unblocked, the passage of molecules through pits will be associated with a certain resistance. Thus, more efficient radial conduction is expected in rays composed of procumbent rather than square or upright cells, because the number of cell-to-cell connections that need to be crossed is smaller in case of procumbent cells (Carlquist 1975).

Sugars can also move out of the parenchyma cells and enter the conduit lumen. The exchange of carbohydrates between parenchyma cells and conduits is facilitated by conduit–parenchyma pits, which exhibit a different structure than the simple or slightly bordered parenchyma–parenchyma pit pairs (Fig. 8.5a, c). When observed with a transmission electron microscope, the conduit–parenchyma pit membranes appear compact, rather electron dense and free of plasmodesmata (Fig. 8.5c). In addition, a specialized cell wall layer is deposited underneath the pit membrane, lining the entire conduit–parenchyma interface between the plasmalemma and the lignified wall. This so-called amorphous or protective layer may enlarge the actual area available for the exchange of substances (Barnett et al. 1993); however, other functions such as providing a buffer against xylem pressure oscillations were also proposed (Van Bel and Van der Schoot 1988). Both the pit membrane and the amorphous layer are rich in pectins (Wisniewski and Davis 1995; Plavcová and Hacke 2011). The amorphous layer contains also arabinogalactan-rich glycoproteins (AGPs) (Wisniewski and Davis 1995). These extracellular proteins prevent a tight alignment of pectin molecules (Lamport et al. 2006) and hence may increase the porosity and permeability of the amorphous layer. Moreover, AGPs are known to interact with the plasma membrane and act as receptors (Seifert and Roberts 2007), which points to interesting possibilities for a more active role of the amorphous layer in sensing and signaling. Another feature of conduit–parenchyma pits is the formation of an additional pectinaceous plug during winter months observed in several temperate trees (Wisniewski and Davis 1995; Wisniewski et al. 1991a). Because of its high electron density this plug is sometimes referred to as the "black cap." The exact function of the black cap is not known but it might hinder the growth of ice crystals or prevent uncontrolled loss of water and other substances from parenchyma cells during winter dormancy.

Our knowledge of molecular mechanisms involved in the sugar movement between parenchyma cells and conduits is rather limited, with most information coming from a few temperate deciduous trees. In these trees, two opposing sugar fluxes have been identified, namely the sugar efflux from and the sugar influx to the parenchyma cells (Fig. 8.4). The balance between these two fluxes drives the sugar composition of the xylem sap. High sugar concentrations, indicative of high efflux and/or low influx rates, are often found in xylem sap during winter and early spring. For instance, the spring sap concentration of sugar maple (*Acer saccharum*) reaches typically values of 2–3 % (Taylor 1956), while a concentration of about 0.6 % was measured in *Acer platanoides* (Schill et al. 1996) and *Populus*×*canadensis* (Sauter 1988). In contrast, the summer concentrations are close to 0.1 %.

The efflux of soluble sugars out of parenchyma cells (Fig. 8.4) occurs passively along a concentration gradient (Sauter 1982; Améglio et al. 2004; Münch 1930). Therefore, high efflux rates are expected when the concentration of soluble sugars in parenchyma cells is high. In agreement, high sugar efflux is observed during winter when most of the starch stored in parenchyma cells is hydrolyzed. In walnut, the sap sugar concentration was indeed highest during winter, with sucrose representing the most abundant xylem sap saccharide (Améglio et al. 2002, 2004). The dynamics of sap sugars are different in poplar. In this species, a rapid increase in sap sugar levels was observed during bud break, reaching levels more than three times higher than those measured in winter. Interestingly, hexoses comprised the major fraction of xylem sap sugars during this time, suggesting that sucrose might be hydrolyzed in the apoplast by acid invertase (Sauter 1988). The rapid increase in sap sugar levels indicates the sugar efflux is not just a mere leakage but rather an actively regulated process. The sugar efflux rates are sensitive to inhibitors, suggesting that the efflux is facilitated by membrane channels (Sauter 1982; Améglio et al. 2004). Thus, the modulation of efflux rates can be achieved by changing the abundance and activity of these hitherto uncharacterized proteins.

If sap flow occurs, sugars released into the conduit lumen can be carried via the low-resistance apoplastic pathway toward the canopy. This additional amount of carbon can be valuable to support flushing buds in spring (Bonhomme et al. 2010). However, as vascular connections are often not fully developed during the initial phase of bud reactivation (Ashworth 1982), sugars need to be reabsorbed by parenchyma cells and move to the bud tissue via extraxylary pathways.

In contrast to sugar efflux, the uptake of sugars from the xylem sap by parenchyma cells is an active process facilitated by proton-sugar symporters (Fig. 8.4). Transcript and protein levels of several of these putative transporters have been studied in walnut (Decourteix et al. 2006, 2008). While the sucrose transporter JrSUT1 was strongly up-regulated in xylem parenchyma cells during bud break, two hexose transporters, JrHT1 and JrHT2, were abundant during the period of intense radial growth. This suggests that the sugar uptake is selective and likely tailored to suit specific physiological needs. The symport of sugars is powered by the electrochemical gradient generated by ATP-dependent proton pumps also known as H^+-ATPases (Alves et al. 2007). High expression of H^+-ATPase coincides with a high activity of respiratory enzymes, indicating that the sugar retrieval is

energetically demanding but also remarkably efficient. For instance, in willow (*Salix*), the rates of sugar influx have been estimated to be more than five times higher than the rates of sugar efflux (Sauter 1983).

In this section, we described the cellular processes that underlie the dynamics of NSC in sapwood (Fig. 8.4), starting with the conversion of starch into soluble sugars, continuing with the in situ use of sugars, and finishing with their radial and axial transport into more distant sink tissues. We showed that NSC dynamics are driven by the activity of key sugar-modifying enzymes and transport systems, acting within the anatomical and physiological boundaries provided by wood parenchyma cells. In the next section, we will briefly discuss potential implications of these processes for whole plant physiology.

4 The Role of Sapwood NSC at the Whole Plant Level

Carbohydrate storage is important for a tree's ability to withstand periods of unfavorable environmental conditions and to reactivate its growth when favorable conditions are reestablished. Interestingly, the NSC reserves are rarely depleted in trees, leading to the suggestion that tree growth and survival is not limited by carbon supply (Körner 2003). Alternatively, it has recently been proposed that trees actively maintain high NSC concentration at the expense of growth in order to sustain plant functioning under environmental stress (Sala et al. 2012a; Wiley and Helliker 2012). We believe that the wide array of tightly regulated physiological processes taking place in ray and axial parenchyma cells fits well into this picture. While starch accumulation in wood parenchyma at the end of the growing season can be viewed as manifestation of a long-term storage function, the complex dynamics of soluble sugars can be perceived as a suite of active physiological processes—some are related to maintenance respiration and growth while others are mostly involved in stress mitigation (Fig. 8.6). For the sake of simplicity, we will outline these functions as consecutive events progressing over seasons typical for a temperate climate. However, we recognize that not all of these functions are relevant all the time. Instead, different functions can be more important in different tree species or under particular circumstances, resulting in different requirements on structural and physiological properties of wood parenchyma cells.

In winter, two important physiological roles of soluble sugars can be identified, namely the protection of parenchyma cells from freeze injury and reversal of freeze-induced embolism. Subzero temperatures can damage or even kill wood parenchyma cells. Therefore, two strategies for coping with freezing temperatures evolved in these cells—they either tolerate extracellular ice formation or avoid freezing by deep supercooling (Sakai et al. 1987; Kuroda et al. 2003; Burke et al. 1976). In the case of freeze tolerance, an increased concentration of soluble sugars resulting in higher osmotic potential of the cytoplasm helps to prevent cellular dehydration driven by extracellular freezing (Yuanyuan et al. 2009; Cavender-Bares 2005). In case of freeze avoidance, soluble sugars may help to inhibit the formation

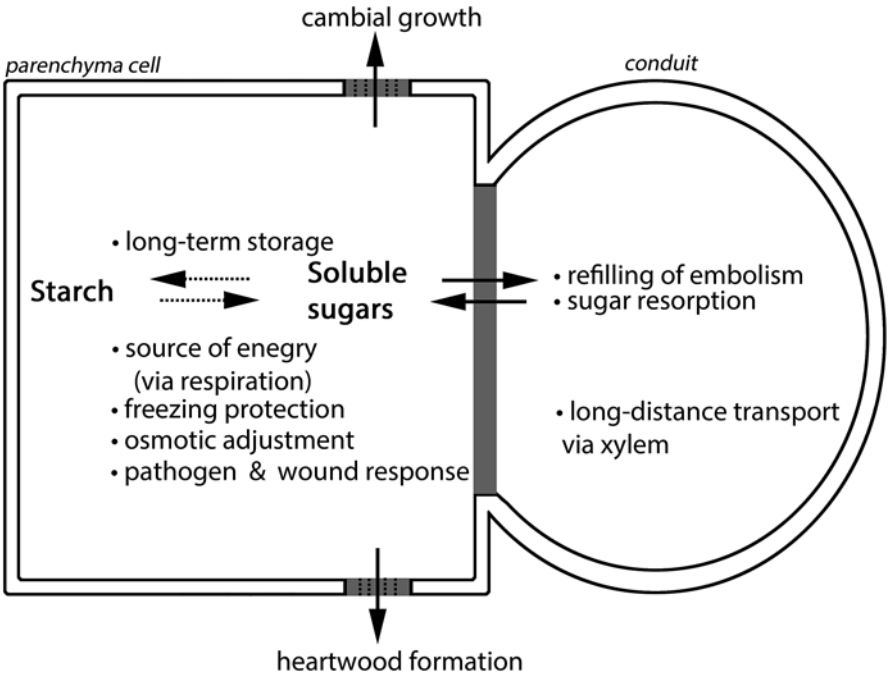

Fig. 8.6 Schematic representation of various functions that starch and soluble sugars fulfill in sapwood. Starch represents the primary form of nonstructural carbohydrates used for the long-term storage. Starch can be converted into soluble sugars that fulfill more active physiological roles. Soluble sugars are used for respiration. They are important for defense against pathogens by providing energy and material for the synthesis of defense chemicals. Increased concentration of soluble sugars in wood parenchyma cells may prevent freeze and desiccation damage. Soluble sugars can move radially via the symplastic continuum in ray parenchyma cells toward the cambium or toward the center of the stem to supply carbon and energy for the formation of new xylem or for the synthesis of heartwood extractives. Soluble sugars are also secreted into the apoplast where they can drive refilling of xylem embolism. Sugars released to the xylem sap can be carried upstream and retrieved closer to the plant apex, thereby supplying carbon to flushing buds

of ice crystals and to stabilize the plasmatic membrane. Furthermore, the integrity of the amorphous layer and its pectin composition are important for the ability of parenchyma cells to undergo supercooling (Wisniewski and Davis 1989; Wisniewski et al. 1991b).

Repeated freeze–thaw cycles are known to induce embolism of xylem conduits even under modest tensions. Ring-porous trees cope with this phenomena by producing new conduits in spring, whereas many diffuse porous species are capable of refilling embolized conduits (Hacke and Sauter 1996). Refilling can be driven by positive root or stem pressure or a combination of the two. While the accumulation of inorganic nutrients in the root apoplast seemed to underlie the development of root pressure in *Juglans*, soluble sugars released by the parenchyma cells were critical for the generation of positive stem pressure in both *Juglans* (Améglio et al. 2002, 2004;

Ewers et al. 2001) and *Acer* (Sauter et al. 1973; Hacke and Sauter 1996). Thus, in climates where freezing occurs, wood parenchyma can be important for the restoration of vascular integrity at the start of a new growing season. On the other hand, a high amount of parenchyma represents a challenge because freeze damage to the living tissue needs to be prevented.

In spring, the main function of soluble sugars is to support new growth in order to quickly reestablish photosynthetic production. Expanding buds and the active cambial zone represent the strongest sinks during this period. Both of these tissues receive carbohydrates stored in sapwood (Hill et al. 1995; Bonhomme et al. 2010; Decourteix et al. 2008). While little is known about the partitioning of reserves between these two tissues, it can be expected that it is closely related to the offset between the cambium and bud phenology. The cambium likely represents a more important sink for stored carbohydrates in ring-porous than diffuse-porous species because a large proportion of the radial stem growth occurs before the onset of photosynthetic activity in ring-porous trees (Barbaroux and Bréda 2002; Panchen et al. 2014). In species that bloom before the leaf-out, the opening flower buds draw strongly on stored reserves as indicated by a pronounced decline in branch wood NSC levels (Hoch et al. 2003). Higher allocation of NSC reserves into the cambium should put more requirements on the radial transport mechanisms via the ray symplast, while the axial transport pathway, which involves sugar exchange between wood parenchyma and xylem apoplast, should be accentuated in case of higher needs for sugar translocation into the buds.

In summer, when the canopy is fully developed and photosynthetically active, soluble sugars found in the sapwood could help to prevent and repair damage caused by environmental stress. In the more traditional sense, the importance of sapwood NSC reserves should be seen in the possibility to regrow leaves in case of severe defoliation caused by environmental stress. From the less traditional point of view, the high NSC pool may be needed for a continuous maintenance of hydraulic integrity that is constantly being perturbed. Drought and the attack of pathogens arguably represent the two most important environmental challenges frequently encountered by trees.

The importance of carbohydrates in the repair of drought-induced embolism has been widely recognized. Despite some recent concerns calling the routine occurrence of refilling under tension into question (Wheeler et al. 2013; Sperry 2013), the active release of both sugars and water into the conduit lumen by xylem parenchyma cells is believed to be at the heart of the putative mechanism that may facilitate rapid reversal of drought-induced embolism (Salleo et al. 1996; Tyree et al. 1999; Hacke and Sperry 2003; Secchi et al. 2011; Secchi and Zwieniecki 2011; Brodersen et al. 2010). Moreover, abundant wood parenchyma, as found in many tropical trees, can help to delay the onset of cavitation by providing high water storage capacity (Borchert and Pockman 2005). It is not known if excessive water loss from parenchyma cells during drought can compromise their physiological functions, although desiccation-induced damage to the protoplasm has been documented in wood parenchyma cells during cold stress (Ristic and Ashworth 1994). If the maintenance of turgor pressure is important, for instance for biomechanical reasons (Chapotin

et al. 2006), increased concentration of soluble sugars could provide means for reducing the capacitive discharge from wood parenchyma cells.

The importance of ray and axial parenchyma for wound and pathogen responses in wood is also well documented. Most importantly, parenchyma cells produce tyloses and gums that plug old or damaged xylem conduits, thereby preventing uncontrolled spread of pathogens within the xylem pipeline (Bonsen and Kucera 1990; Nicole et al. 1992). The production of these vascular occlusions involves active secretory processes (Rioux et al. 1998) and hormonal signaling (McElrone et al. 2010), and thus is likely associated with high demands for energy that can be drawn from NSC reserves. On the other hand, a higher proportion of thin-walled parenchyma cells that are rich in carbohydrates can make wood more attractive for nutrient-seeking pathogens and herbivores (Schwarze 2007; Martín et al. 2009). This could result in a faster progression of infection once the pathogen succeeds in overcoming the initial defense mechanisms.

In fall, the wood parenchyma NSC stores should be replenished and available to support the tree's physiological functions in winter and during the next growing season. However, some of the NSC can still be consumed for heartwood formation, which is known to occur predominantly during the period of early dormancy (Taylor et al. 2002). As suggested in a recent review (Spicer 2005), heartwood formation should be viewed as an active developmental program during which a conductive but vulnerable sapwood is transformed in a nonconductive but durable heartwood. This process, initiated within wood parenchyma cells, involves a suite of biochemical reactions that use, at least in part, energy and carbon from carbohydrates stored in sapwood (Hauch and Magel 1998; Magel et al. 1994).

In this section, we summarized the most important ways of how sapwood NSC are used in growth, development, and stress mitigation (Fig. 8.6) and showed the tight links to the well-known functions of ray and axial parenchyma cells. However, it is important to note that reserves other than NSC are also stored in wood parenchyma cells, with nitrogen and phosphorous representing the most important ones (Hoch et al. 2003; Langheinrich and Tischner 1991; Sauter and van Cleve 1991). Thus, it is likely that the tree performance is, at least in some occasions, more strongly limited by the availability of these nutrients than by the availability of carbon (Millard and Grelet 2010; Sala et al. 2012b). Nevertheless, we believe that our analysis of NSC dynamics provides a useful conceptual basis that can be applied to better understand the dynamics of other nutrients as well.

5 Future Perspectives

Research on xylem has a great tradition in integrating structure and function and great advances in understanding the plant water transport have been made by linking the anatomy of xylem conduits to functional hydraulic traits (Hacke et al. 2001, 2006; Jansen et al. 2009). We can envision similar progress in elucidating the functional role of parenchyma cells in carbohydrate storage and dynamics, paved by

uncovering the great diversity in ray and axial parenchyma structure and their spatial distribution. Such research would greatly benefit from integrating approaches traditionally used in studies on xylem hydraulics (e.g., perfusion experiments, analysis of pit structure) with methods used to examine phloem physiology (e.g., the application of symplastic and apoplastic tracers, radioactive labelling, molecular methods). Moreover, ecological data on sapwood NSC concentration and composition will help to upscale the processes and imply their importance for whole plant functioning.

Most research to date has been made on temperate species. However, wood structure exhibits great diversity and ray and axial parenchyma seems to be more abundant and exhibit more elaborated patterns in tropical trees. Similarly, carbohydrate metabolism in sapwood seems to be more complex, dynamic, and shifted further from the role in long-term storage in the tropics. Therefore, studies conducted on tropical trees might provide further valuable insights.

Acknowledgements L.P. was supported by a postdoctoral fellowship from the Alexander von Humboldt Foundation and research funding from Ulm University and the Ulm University Society (Ulmer Universitätsgesellschaft). J.S. acknowledges the German Research Foundation (DFG) for financial support. We gratefully acknowledge the support and facilities provided by the Botanical Garden and the Electron Microcopy Unit of Ulm University. We thank Hugh Morris for fruitful discussion and useful comments on an earlier version of this manuscript.

References

Alves G, Sauter JJ, Julien J-L, Fleurat-Lessard P, Améglio T, Guillot A et al (2001) Plasma membrane H^+-ATPase, succinate and isocitrate dehydrogenases activities of vessel-associated cells in walnut trees. J Plant Physiol 158:1263–1271

Alves G, Decourteix M, Fleurat-Lessard P, Sakr S, Bonhomme M, Améglio T et al (2007) Spatial activity and expression of plasma membrane H^+-ATPase in stem xylem of walnut during dormancy and growth resumption. Tree Physiol 27:1471–1480

Améglio T, Bodet C, Lacointe A, Cochard H (2002) Winter embolism, mechanisms of xylem hydraulic conductivity recovery and springtime growth patterns in walnut and peach trees. Tree Physiol 22:1211–1220

Améglio T, Decourteix M, Alves G, Valentin V, Sakr S, Julien J-L et al (2004) Temperature effects on xylem sap osmolarity in walnut trees: evidence for a vitalistic model of winter embolism repair. Tree Physiol 24:785–793

Ashworth EN (1982) Properties of peach flower buds which facilitate supercooling. Plant Physiol 70:1475–1479

Ashworth E, Stirm V, Volenec J (1993) Seasonal variations in soluble sugars and starch within woody stems of *Cornus sericea* L. Tree Physiol 13:379–388

Barbaroux C, Bréda N (2002) Contrasting distribution and seasonal dynamics of carbohydrate reserves in stem wood of adult ring-porous sessile oak and diffuse-porous beech trees. Tree Physiol 22:1201–1210

Barghoorn ES (1941) The ontogenetic development and phylogenetic specialization of rays in the xylem of dicotyledons-III. The elimination of rays. Bull Torrey Bot Club 68:317–325

Barnett J, Cooper P, Bonner LJ (1993) The protective layer as an extension of the apoplast. IAWA J 14:163–171

Bhat K, Bhat K, Dhamodaran T, et al. (1985) Wood and bark properties of branches of selected tree species growing in Kerala. KFRI research report, Kerala Forest Research Institute

Bonhomme M, Peuch M, Améglio T, Rageau R, Guilliot A, Decourteix M et al (2010) Carbohydrate uptake from xylem vessels and its distribution among stem tissues and buds in walnut (*Juglans regia* L.). Tree Physiol 30:89–102

Bonsen KJ, Kucera L (1990) Vessel occlusions in plants: morphological, functional and evolutionary aspects. IAWA Bull 11:393–399

Borchert R, Pockman WT (2005) Water storage capacitance and xylem tension in isolated branches of temperate and tropical trees. Tree Physiol 25:457–466

Braun H (1984) The significance of the accessory tissues of the hydrosystem for osmotic water shifting as the second principle of water ascent, with some thoughts concerning the evolution of trees. IAWA Bull 5:275–294

Brodersen CR, McElrone AJ, Choat B, Matthews MA, Shackel KA (2010) The dynamics of embolism repair in xylem: in vivo visualizations using high-resolution computed tomography. Plant Physiol 154:1088–1095

Burke M, Gusta L, Quamme H, Weiser C, Li P (1976) Freezing and injury in plants. Annu Rev Plant Physiol 27:507–528

Carbone MS, Czimczik CI, Keenan TF, Murakami PF, Pederson N, Schaberg PG et al (2013) Age, allocation and availability of nonstructural carbon in mature red maple trees. New Phytol 200:1145–1155

Carlquist S (1970) Wood anatomy of insular species of *Plantago* and the problem of raylessness. Bull Torrey Bot Club 97(6):353–361

Carlquist S (1975) Wood anatomy of Onagraceae, with notes on alternative modes of photosynthate movement in dicotyledon woods. Ann Mo Bot Gard 62:386–424

Carlquist S (2001) Comparative wood anatomy: systematic, ecological, and evolutionary aspects of dicotyledon wood. Springer, Berlin

Cavender-Bares J (2005) Impacts of freezing on long distance transport in woody plants. In: Holbrook NM, Zwieniecki MA (eds) Vascular transport in plants. Elsevier, San Diego, pp 401–424

Chaffey N, Barlow P (2001) The cytoskeleton facilitates a three-dimensional symplasmic continuum in the long-lived ray and axial parenchyma cells of angiosperm trees. Planta 213:811–823

Chapotin SM, Razanameharizaka JH, Holbrook NM (2006) A biomechanical perspective on the role of large stem volume and high water content in baobab trees (*Adansonia* spp.; Bombacaceae). Am J Bot 93:1251–1264

Chave J, Coomes D, Jansen S, Lewis SL, Swenson NG, Zanne AE (2009) Towards a worldwide wood economics spectrum. Ecol Lett 12:351–366

Cocoletzi E, Angeles G, Sosa V, Patron A (2013) The chloroplasts and unlignified parenchyma of two tropical pioneer forest tree species (Urticaceae). Bot Sci 91:251–260

Decourteix M, Alves G, Brunel N, Améglio T, Guilliot A, Lemoine R et al (2006) JrSUT1, a putative xylem sucrose transporter, could mediate sucrose influx into xylem parenchyma cells and be up-regulated by freeze-thaw cycles over the autumn-winter period in walnut tree (*Juglans regia* L.). Plant Cell Environ 29:36–47

Decourteix M, Alves G, Bonhomme M, Peuch M, Baaziz KB, Brunel N et al (2008) Sucrose (JrSUT1) and hexose (JrHT1 and JrHT2) transporters in walnut xylem parenchyma cells: their potential role in early events of growth resumption. Tree Physiol 28:215–224

Domec J-C, Gartner B (2002) Age-and position-related changes in hydraulic versus mechanical dysfunction of xylem: inferring the design criteria for Douglas-fir wood structure. Tree Physiol 22:91–104

Essiamah S, Eschrich W (1985) Changes of starch content in the storage tissues of deciduous trees during winter and spring. IAWA Bull 6:97–106

Evert RF (2006) Esau's Plant anatomy: meristems, cells, and tissues of the plant body: their structure, function, and development, 3rd edn. Wiley, Hoboken

Ewers FW, Améglio T, Cochard H, Beaujard F, Martignac M, Vandame M et al (2001) Seasonal variation in xylem pressure of walnut trees: root and stem pressures. Tree Physiol 21:1123–1132

Fahn A, Leshem B (1963) Wood fibres with living protoplasts. New Phytol 62:91–98
Giese J-O, Herbers K, Hoffmann M, Klösgen RB, Sonnewald U (2005) Isolation and functional characterization of a novel plastidic hexokinase from *Nicotiana tabacum*. FEBS Lett 579:827–831
Hacke U, Sauter J (1996) Xylem dysfunction during winter and recovery of hydraulic conductivity in diffuse-porous and ring-porous trees. Oecologia 105:435–439
Hacke U, Sperry J (2003) Limits to xylem refilling under negative pressure in *Laurus nobilis* and *Acer negundo*. Plant Cell Environ 26:303–311
Hacke UG, Sperry JS, Pockman WT, Davis SD, McCulloh KA (2001) Trends in wood density and structure are linked to prevention of xylem implosion by negative pressure. Oecologia 126:457–461
Hacke UG, Sperry JS, Wheeler JK, Castro L (2006) Scaling of angiosperm xylem structure with safety and efficiency. Tree Physiol 26:689–701
Hauch S, Magel E (1998) Extractable activities and protein content of sucrose-phosphate synthase, sucrose synthase and neutral invertase in trunk tissues of *Robinia pseudoacacia* L. are related to cambial wood production and heartwood formation. Planta 207:266–274
Hearn DJ (2009) Descriptive anatomy and evolutionary patterns of anatomical diversification in *Adenia* (Passifloraceae). Aliso J Syst Evol Bot 27:13–38
Hill S, Waterhouse J, Field E, Switsur V, Ap RT (1995) Rapid recycling of triose phosphates in oak stem tissue. Plant Cell Environ 18:931–936
Hoch G, Richter A, Körner C (2003) Non-structural carbon compounds in temperate forest trees. Plant Cell Environ 26:1067–1081
Jang J-C, León P, Zhou L, Sheen J (1997) Hexokinase as a sugar sensor in higher plants. Plant Cell 9:5–19
Jansen S, Choat B, Pletsers A (2009) Morphological variation of intervessel pit membranes and implications to xylem function in angiosperms. Am J Bot 96:409–419
Johnson DM, McCulloh KA, Woodruff DR, Meinzer FC (2012) Hydraulic safety margins and embolism reversal in stems and leaves: why are conifers and angiosperms so different? Plant Sci 195:48–53
Koch P (1985) Utilization of hardwoods growing on southern pine sites. U.S. Dept. of Agriculture, Forest Service, Washington, DC
Körner C (2003) Carbon limitation in trees. J Ecol 91:4–17
Kozlowski T (1992) Carbohydrate sources and sinks in woody plants. Bot Rev 58:107–222
Kramer PJ, Kozlowski TT (1979) Physiology of woody plants. Academic, New York
Kribs DA (1937) Salient lines of structural specialization in the wood parenchyma of dicotyledons. Bull Torrey Bot Club 64:177–187
Kuroda K, Kasuga J, Arakawa K, Fujikawa S (2003) Xylem ray parenchyma cells in boreal hardwood species respond to subfreezing temperatures by deep supercooling that is accompanied by incomplete desiccation. Plant Physiol 131:736–744
Lamport DT, Kieliszewski MJ, Showalter AM (2006) Salt stress upregulates periplasmic arabinogalactan proteins: using salt stress to analyse AGP function. New Phytol 169:479–492
Langenfeld-Heyser R (1989) CO_2 fixation in stem slices of *Picea abies* (L.) Karst: microautoradiographic studies. Trees 3:24–32
Langheinrich U, Tischner R (1991) Vegetative storage proteins in poplar induction and characterization of a 32-and a 36-kilodalton polypeptide. Plant Physiol 97:1017–1025
Larcher W, Lütz C, Nagele M, Bodner M (1988) Photosynthetic functioning and ultrastructure of chloroplasts in stem tissues of *Fagus sylvatica*. J Plant Physiol 132:731–737
Lens F, Jansen S, Robbrecht E, Smets E (2000) Wood anatomy of the Vanguerieae (Ixoroideae-Rubiaceae), with special emphasis on some geofrutices. IAWA J 21:443–455
Loescher WH, McCamant T, Keller JD (1990) Carbohydrate reserves, translocation, and storage in woody plant roots. Hortscience 25:274–281
Magel E, Jay-Allemand C, Ziegler H (1994) Formation of heartwood substances in the stemwood of *Robinia pseudoacacia* L. II. Distribution of nonstructural carbohydrates and wood extractives across the trunk. Trees 8:165–171

Martín JA, Solla A, Esteban LG, de Palacios P, Gil L (2009) Bordered pit and ray morphology involvement in elm resistance to *Ophiostoma novo-ulmi*. Can J For Res 39:420–429

Mauseth J, Plemons-Rodriguez B (1997) Presence of paratracheal water storage tissue does not alter vessel characters in cactus wood. Am J Bot 84:815

McCulloh KA, Johnson DM, Meinzer FC, Voelker SL, Lachenbruch B, Domec J-C (2012) Hydraulic architecture of two species differing in wood density: opposing strategies in co-occurring tropical pioneer trees. Plant Cell Environ 35:116–125

McDowell N, Pockman WT, Allen CD, Breshears DD, Cobb N, Kolb T et al (2008) Mechanisms of plant survival and mortality during drought: why do some plants survive while others succumb to drought? New Phytol 178:719–739

McElrone AJ, Grant JA, Kluepfel DA (2010) The role of tyloses in crown hydraulic failure of mature walnut trees afflicted by apoplexy disorder. Tree Physiol 30:761–772

Millard P, Grelet G (2010) Nitrogen storage and remobilization by trees: ecophysiological relevance in a changing world. Tree Physiol 30:1083–1095

Münch E (1930) Die Stoffbewegungen in der Pflanze. Gustav Fischer, Jena

Newell EA, Mulkey SS, Wright JS (2002) Seasonal patterns of carbohydrate storage in four tropical tree species. Oecologia 131:333–342

Nicole M, Geiger J, Nandris D (1992) Defense of angiosperm roots against fungal invasion. In: Timell TE (ed) Defense mechanisms of woody plants against fungi. Springer, Berlin, pp 181–206

Palacio S, Maestro M, Montserrat-Martí G (2007) Seasonal dynamics of non-structural carbohydrates in two species of Mediterranean sub-shrubs with different leaf phenology. Environ Exp Bot 59:34–42

Palacio S, Hoch G, Sala A, Körner C, Millard P (2014) Does carbon storage limit tree growth? New Phytol 201:1096–1100

Panchen ZA, Primack RB, Nordt B, Ellwood ER, Stevens A-D, Renner SS et al (2014) Leaf out times of temperate woody plants are related to phylogeny, deciduousness, growth habit and wood anatomy. New Phytol 203(4):1208–1219

Pate JS, Froend RH, Bowen BJ, Hansen A, Kuo J (1990) Seedling growth and storage characteristics of seeder and resprouter species of Mediterranean-type ecosystems of SW Australia. Ann Bot 65:585–601

Pfanz H, Aschan G, Langenfeld-Heyser R, Wittmann C, Loose M (2002) Ecology and ecophysiology of tree stems: corticular and wood photosynthesis. Naturwissenschaften 89:147–162

Plavcová L, Hacke UG (2011) Heterogeneous distribution of pectin epitopes and calcium in different pit types of four angiosperm species. New Phytol 192:885–897

Pratt R, Jacobsen A, Ewers F, Davis S (2007) Relationships among xylem transport, biomechanics and storage in stems and roots of nine Rhamnaceae species of the California chaparral. New Phytol 174:787–798

Reichelt S, Knight AE, Hodge TP, Baluska F, Samaj J, Volkmann D et al (1999) Characterization of the unconventional myosin VIII in plant cells and its localization at the post-cytokinetic cell wall. Plant J 19:555–567

Richardson AD, Carbone MS, Keenan TF, Czimczik CI, Hollinger DY, Murakami P et al (2013) Seasonal dynamics and age of stemwood nonstructural carbohydrates in temperate forest trees. New Phytol 197:850–861

Rioux D, Nicole M, Simard M, Ouellette G (1998) Immunocytochemical evidence that secretion of pectin occurs during gel (gum) and tylosis formation in trees. Phytopathology 88:494–505

Ristic Z, Ashworth EN (1994) Response of xylem ray parenchyma cells of red osier dogwood (*Cornus sericea* L.) to freezing stress. Plant Physiol 104:737–746

Ruelle J, Clair B, Beauchêne J, Prévost M-F, Fournier M et al (2006) Tension wood and opposite wood in 21 tropical rain forest species. 2. Comparison of some anatomical and ultrastructural criteria. IAWA J 27:341–376

Sakai A, Larcher W et al (1987) Frost survival of plants. Responses and adaptation to freezing stress. Springer, Berlin

Sala A, Hoch G (2009) Height-related growth declines in ponderosa pine are not due to carbon limitation. Plant Cell Environ 32:22–30

Sala A, Woodruff DR, Meinzer FC (2012a) Carbon dynamics in trees: feast or famine? Tree Physiol 32:764–775

Sala A, Hopping K, McIntire EJ, Delzon S, Crone EE (2012b) Masting in whitebark pine (*Pinus albicaulis*) depletes stored nutrients. New Phytol 196:189–199

Salleo S, Lo Gullo M, De Paoli D, Zippo M (1996) Xylem recovery from cavitation-induced embolism in young plants of *Laurus nobilis*: a possible mechanism. New Phytol 132:47–56

Sauter JJ (1982) Efflux and reabsorption of sugars in the xylem I. Seasonal changes in sucrose efflux in *Salix*. Z Pflanzenphysiol 106:325–336

Sauter JJ (1983) Efflux and reabsorption of sugars in the xylem II. Seasonal changes in sucrose uptake in *Salix*. Z Pflanzenphysiol 111:429–440

Sauter JJ (1988) Seasonal changes in the efflux of sugars from parenchyma cells into the apoplast in poplar stems (*Populus*×*canadensis* "robusta"). Trees 2:242–249

Sauter JJ, Kloth S (1986) Plasmodesmatal frequency and radial translocation rates in ray cells of poplar (*Populus*×*canadensis* Moench "robusta"). Planta 168:377–380

Sauter JJ, van Cleve B (1991) Biochemical, immunochemical, and ultrastructural studies of protein storage in poplar (*Populus*×*canadensis* "robusta") wood. Planta 183:92–100

Sauter JJ, van Cleve B (1994) Storage, mobilization and interrelations of starch, sugars, protein and fat in the ray storage tissue of poplar trees. Trees 8:297–304

Sauter JJ, Wellenkamp S (1998) Seasonal changes in content of starch, protein and sugars in the twig wood of *Salix caprea* L. Holzforschung 52:255–262

Sauter JJ, Iten W, Zimmermann MH (1973) Studies on the release of sugar into the vessels of sugar maple (*Acer saccharum*). Can J Bot 51:1–8

Schill V, Hartung W, Orthen B, Weisenseel MH (1996) The xylem sap of maple (*Acer platanoides*) trees—sap obtained by a novel method shows changes with season and height. J Exp Bot 47:123–133

Schoonmaker AL (2013) Resource allocation, water relations and crown architecture examined at the tree and stand-level in northern conifers. PhD thesis, University of Alberta, Edmonton

Schrader S, Sauter JJ (2002) Seasonal changes of sucrose-phosphate synthase and sucrose synthase activities in poplar wood (*Populus*×*canadensis* Moench 'robusta') and their possible role in carbohydrate metabolism. J Plant Physiol 159:833–843

Schwarze FW (2007) Wood decay under the microscope. Fungal Biol Rev 21:133–170

Secchi F, Zwieniecki MA (2011) Sensing embolism in xylem vessels: the role of sucrose as a trigger for refilling. Plant Cell Environ 34:514–524

Secchi F, Gilbert ME, Zwieniecki MA (2011) Transcriptome response to embolism formation in stems of *Populus trichocarpa* provides insight into signaling and the biology of refilling. Plant Physiol 157:1419–1429

Seifert GJ, Roberts K (2007) The biology of arabinogalactan proteins. Annu Rev Plant Biol 58:137–161

Sokolowska K, Zagórska-Marek B (2012) Symplasmic, long-distance transport in xylem and cambial regions in branches of *Acer pseudoplatanus* (Aceraceae) and *Populus tremula*×*P. tremuloides* (Salicaceae). Am J Bot 99:1745–1755

Sperry J (2013) Cutting-edge research or cutting-edge artefact? An overdue control experiment complicates the xylem refilling story. Plant Cell Environ 36:1916–1918

Spicer R (2005) Senescence in secondary xylem: heartwood formation as an active developmental program. In: Holbrook NM, Zwieniecki MA (eds) Vascular transport in plants. Elsevier, San Diego, pp 457–475

Spicer R, Holbrook NM (2005) Within-stem oxygen concentration and sap flow in four temperate tree species: does long-lived xylem parenchyma experience hypoxia? Plant Cell Environ 28:192–201

Spicer R, Holbrook NM (2007a) Effects of carbon dioxide and oxygen on sapwood respiration in five temperate tree species. J Exp Bot 58:1313–1320

Spicer R, Holbrook NM (2007b) Parenchyma cell respiration and survival in secondary xylem: does metabolic activity decline with cell age? Plant Cell Environ 30:934–943

Sturm A (1999) Invertases. Primary structures, functions, and roles in plant development and sucrose partitioning. Plant Physiol 121:1–8
Taylor FH (1956) Variation in sugar content of maple sap. Univ Vermont State Agric College Bull 587:1–39
Taylor AM, Gartner BL, Morrell JJ (2002) Heartwood formation and natural durability—a review. Wood Fiber Sci 34:587–611
Tyree MT, Salleo S, Nardini A, Gullo MAL, Mosca R (1999) Refilling of embolized vessels in young stems of laurel. Do we need a new paradigm? Plant Physiol 120:11–22
Van Bel AJ (1990) Xylem-phloem exchange via the rays: the undervalued route of transport. J Exp Bot 41:631–644
Van Bel AJ, Van der Schoot C (1988) Primary function of the protective layer in contact cells. Buffer against oscillations in hydrostatic pressure in the vessels. IAWA Bull 9:285–288
Verdaguer D, Ojeda F (2002) Root starch storage and allocation patterns in seeder and resprouter seedlings of two Cape Erica (Ericaceae) species. Am J Bot 89:1189–1196
Von Frey-Wyssling A, Aeberli H (1942) Der Anteil von Fasern, Gefäßen und Parenchym verschiedener Holzarten in Dreiecksdarstellung. Holz als Roh-und Werkstoff 5:265–268
Wagenführ R (2007) Holzatlas. VEB Fachbuchverlag, Munich
Wargo PM (1976) Variation of starch content among and within roots of red and white oak trees. For Sci 22:468–471
Wheeler E, Baas P, Rodgers S (2007) Variations in dicot wood anatomy: a global analysis based on the Inside Wood database. IAWA J 28:229
Wheeler JK, Huggett BA, Tofte AN, Rockwell FE, Holbrook NM (2013) Cutting xylem under tension or supersaturated with gas can generate PLC and the appearance of rapid recovery from embolism. Plant Cell Environ 36:1938–1949
White RG, Barton DA (2011) The cytoskeleton in plasmodesmata: a role in intercellular transport? J Exp Bot 62:5249–5266
Wiley E, Helliker B (2012) A re-evaluation of carbon storage in trees lends greater support for carbon limitation to growth. New Phytol 195:285–289
Wisniewski M, Davis G (1989) Evidence for the involvement of a specific cell wall layer in regulation of deep supercooling of xylem parenchyma. Plant Physiol 91:151–156
Wisniewski M, Davis G (1995) Immunogold localization of pectins and glycoproteins in tissues of peach with reference to deep supercooling. Trees 9:253–260
Wisniewski M, Davis G, Schafter K (1991a) Mediation of deep supercooling of peach and dogwood by enzymatic modifications in cell-wall structure. Planta 184:254–260
Wisniewski M, Davis G, Arora R (1991b) Effect of macerase, oxalic acid, and EGTA on deep supercooling and pit membrane structure of xylem parenchyma of peach. Plant Physiol 96:1354–1359
Witt W, Buchholz A, Sauter JJ (1995) Binding of endoamylase to native starch grains from poplar wood. J Exp Bot 46:1761–1769
Woodruff DR, Meinzer FC (2011) Water stress, shoot growth and storage of non-structural carbohydrates along a tree height gradient in a tall conifer. Plant Cell Environ 34:1920–1930
Würth MK, Pelaez-Riedl S, Wright SJ, Körner C (2005) Non-structural carbohydrate pools in a tropical forest. Oecologia 143:11–24
Yamada Y, Awano T, Fujita M, Takabe K (2011) Living wood fibers act as large-capacity "single-use" starch storage in black locust (*Robinia pseudoacacia*). Trees 25:607–616
Yuanyuan M, Yali Z, Jiang L, Hongbo S (2009) Roles of plant soluble sugars and their responses to plant cold stress. Afr J Biotechnol 8:2004–2010
Zavaliev R, Ueki S, Epel BL, Citovsky V (2011) Biology of callose (β-1,3-glucan) turnover at plasmodesmata. Protoplasma 248:117–130
Zeeman SC, Kossmann J, Smith AM (2010) Starch: its metabolism, evolution, and biotechnological modification in plants. Annu Rev Plant Biol 61:209–234
Zieminska K, Butler DW, Gleason SM, Wright IJ, Westoby M (2013) Fibre wall and lumen fractions drive wood density variation across 24 Australian angiosperms. AoB Plants 5:plt046

New Phytologist

Research

A global analysis of parenchyma tissue fractions in secondary xylem of seed plants

Hugh Morris[1]*, Lenka Plavcová[1]*, Patrick Cvecko[2], Esther Fichtler[3], Mark A. F. Gillingham[2], Hugo I. Martínez-Cabrera[4], Daniel J. McGlinn[5], Elisabeth Wheeler[6], Jingming Zheng[7], Kasia Ziemińska[8] and Steven Jansen[1]

[1]Institute of Systematic Botany and Ecology, Ulm University, Albert-Einstein-Allee 11, D-89081 Ulm, Germany; [2]Institute of Evolutionary Ecology and Conservation Genomics, Ulm University, Albert-Einstein-Allee 11, D-89069 Ulm, Germany; [3]Institute of Agronomy in the Tropics, University of Göttingen, Grisebachstrasse 6, 37077 Göttingen, Germany; [4]Département des Sciences Biologiques, Université du Québec à Montréal, UQÁM, CP 8888, Succ. Centre Ville Montréal, Montréal, QC H3C 3P8, Canada; [5]Department of Biology, College of Charleston, Charleston, SC 29424, USA; [6]Department of Forest Biomaterials, NC State University Raleigh, Raleigh, NC 27695-8005, USA; [7]Key Laboratory for Silviculture and Conservation of the Ministry of Education, Beijing Forestry University, Beijing 100083, China; [8]Department of Biological Sciences, Macquarie University, Sydney, NSW 2109, Australia

Author for correspondence:
Steven Jansen
Tel: +49 (0)731 50 23302
Email: steven.jansen@uni-ulm.de

Received: *27 March 2015*
Accepted: *28 September 2015*

New Phytologist (2016) **209:** 1553–1565
doi: 10.1111/nph.13737

Key words: angiosperms, axial parenchyma, conifers, growth form, mean annual precipitation, mean annual temperature, ray parenchyma, secondary xylem.

Summary

• Parenchyma is an important tissue in secondary xylem of seed plants, with functions ranging from storage to defence and with effects on the physical and mechanical properties of wood. Currently, we lack a large-scale quantitative analysis of ray parenchyma (RP) and axial parenchyma (AP) tissue fractions.

• Here, we use data from the literature on AP and RP fractions to investigate the potential relationships of climate and growth form with total ray and axial parenchyma fractions (RAP).

• We found a 29-fold variation in RAP fraction, which was more strongly related to temperature than with precipitation. Stem succulents had the highest RAP values (mean ± SD: 70.2 ± 22.0%), followed by lianas (50.1 ± 16.3%), angiosperm trees and shrubs (26.3 ± 12.4%), and conifers (7.6 ± 2.6%). Differences in RAP fraction between temperate and tropical angiosperm trees (21.1 ± 7.9% vs 36.2 ± 13.4%, respectively) are due to differences in the AP fraction, which is typically three times higher in tropical than in temperate trees, but not in RP fraction.

• Our results illustrate that both temperature and growth form are important drivers of RAP fractions. These findings should help pave the way to better understand the various functions of RAP in plants.

Introduction

Parenchyma tissue in secondary xylem is composed of living cells variable in their morphology and physiology, which usually have thin walls and are rectangular or square in shape. They are produced by fusiform and ray initials of the vascular cambium, which develop into axial parenchyma (AP) strands and ray parenchyma (RP), respectively, and run perpendicular to each other (Fig. 1). Besides the occurrence of so-called living fibres (Wolkinger, 1970, 1971), ray and axial parenchyma (RAP) tissue represents the bulk of living cells in wood. Parenchyma plays multiple functions, as seen in Fig. 2 (green boxes). These functions range from storage and transport of nonstructural carbohydrates (NSCs) (Hoch *et al.*, 2003; Salleo *et al.*, 2004; O'Brien *et al.*, 2014; Plavcová & Jansen, 2015) to defence against pathogens (Shigo, 1984; Biggs, 1987; Schmitt & Liese, 1993; Deflorio *et al.*, 2008), water storage and xylem hydraulic capacitance (Holbrook, 1995; Borchert & Pockman, 2005), storage of mineral inclusions, the transition of functional sapwood to heartwood (Pinto *et al.*, 2004; Spicer, 2005; Nawrot *et al.*, 2008), and mechanical contributions, particularly by RP (Burgert *et al.*, 1999; Burgert & Eckstein, 2001; Reiterer *et al.*, 2002). Two additional functions of RAP speculated to be involved in long-distance water transport are poorly understood, the first being embolism repair (Clearwater & Goldstein, 2005; Salleo *et al.*, 2009; Brodersen *et al.*, 2010), with the second involving the ion-mediated enhancement of xylem hydraulic conductance via the release of inorganic compounds such as K^+ and Ca^{2+} into the transpiration stream (Zwieniecki *et al.*, 2001; Jansen *et al.*, 2011; Nardini *et al.*, 2011; Santiago *et al.*, 2013). Radial transport via RAP also needs more exploration. Rays provide means for interactions between phloem and xylem (van Bel, 1990; Spicer & Holbrook, 2007; Hearn *et al.*, 2013; Pfautsch *et al.*, 2015), as they stretch from the inner bark across the cambium and into the xylem.

RAP shows a large variability in its quantitative and qualitative anatomical characteristics across species (Kribs, 1935, 1937; Barghoorn, 1940, 1941; Normand & Chatelet, 1951; Braun & Wolkinger, 1970; Panshin & de Zeeuw, 1980; Braun, 1984;

*These authors contributed equally to this work.

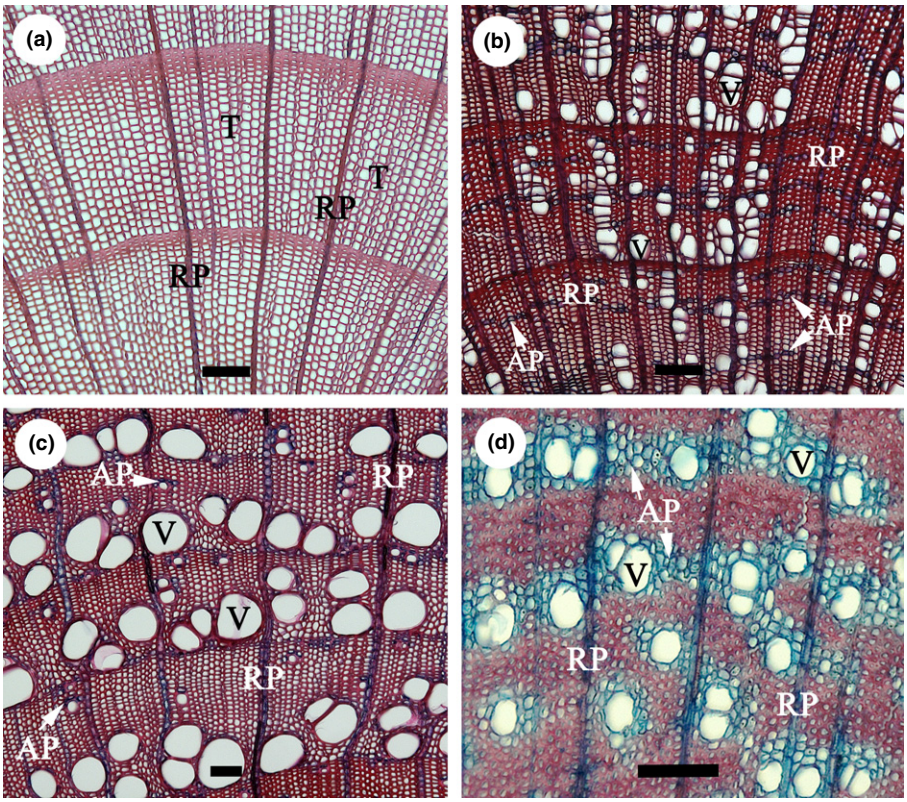

Fig. 1 Light microscopy images of transverse sections of conifer and angiosperm stem wood with different parenchyma fractions and spatial distribution, showing a gradient from low to high ray and axial parenchyma percentages. (a) *Picea abies*, a conifer species with no axial parenchyma (AP) present; (b) *Carpinus betulus*, a diffuse-porous species with narrow bands of AP (white arrows); (c) *Fraxinus excelsior*, a ring-porous species with both scanty paratracheal AP (white arrows) and marginal bands; and (d) *Crescentia cujeje,* a tropical diffuse-porous species with aliform and confluent bands of AP (white arrows). The sections were stained with a combination of safranin and alcian blue, resulting in a red colour for strongly lignified cell walls (tracheids (T), vessels (V), and fibres) and a blue to purple colour for both AP and RP (radial parenchyma). All bars, 100 μm.

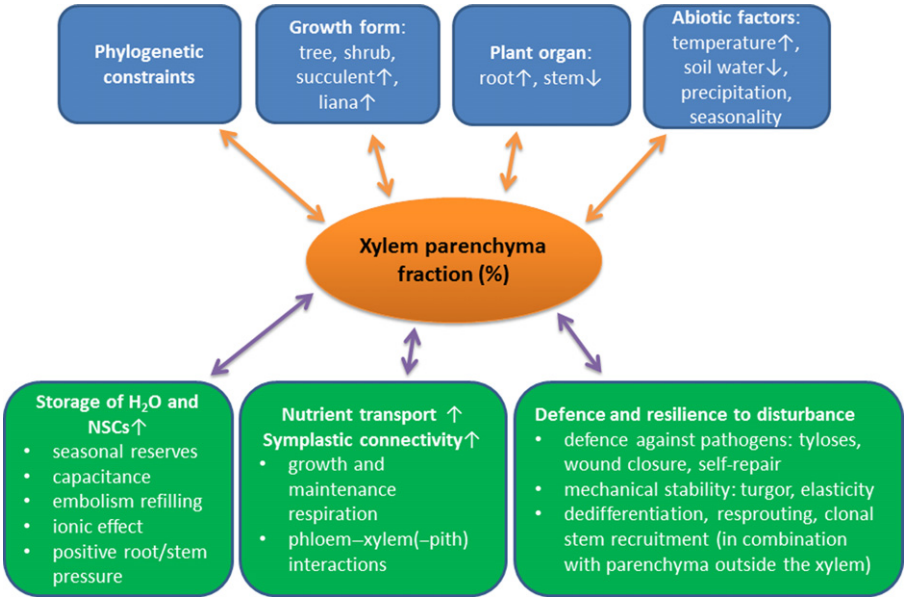

Fig. 2 Diagram of variables (in blue) hypothesised to affect xylem parenchyma (including ray and axial parenchyma) tissue fractions in wood and the functions (in green) hypothesised to be related to parenchyma fractions. Arrows pointing upwards or downwards indicate whether or not particular causes may lead to a speculative increase or decrease of parenchyma fraction, or that a functional process is either positively or negatively scaled with parenchyma fraction. Potential variations in parenchyma quantity due to developmental changes and patterns of spatial distribution within the xylem tissue are omitted in this framework. NSC, nonstructural carbohydrates.

Koch, 1985). In fact, this variability has been used for wood identification and systematic purposes (IAWA Committee, 1989, 2004; Wagenführ, 2007); however, we lack a thorough understanding of the functional meaning of this variability. Recent advances in image acquisition and analysis techniques have made possible a more accurate and thorough examination of tissue percentages along with the design of studies investigating patterns of variation in total parenchyma fraction (Martínez-Cabrera *et al.*, 2009; Zheng & Martínez-Cabrera, 2013; Ziemińska *et al.*, 2013, 2015).

RAP amount responds to both phylogenetic and environmental factors (Fig. 2). Also, RAP, with the exclusion of rayless species (Carlquist, 2001), is typically higher in angiosperm than in conifer wood for both RP (15–20% compared to 4–8%) and AP (≤1% to ≥30% compared to ≤1%), respectively (Koch, 1985; Spicer, 2014). The level of RAP also depends on growth

forms, with a surprisingly high level occurring in woody succulents and lianas (Hearn, 2009). RAP abundance might also change with climate, showing a trend for higher RAP fractions in tropical than in temperate species (Baas, 1982; Wheeler & Baas, 1991). Interestingly, the amount of AP seems to vary considerably between different eco-regions, both at the intra- and interspecific level (Wheeler & Baas, 1991; Segala Alves & Angyalossy-Alfonso, 2002), but no general trends have been reported for RP as a whole (Fahn *et al.*, 1986). As far as we know, there is no published literature on actual comparisons between AP and RP amounts across climatic regions. Different RP compositions may not have any functional advantages across a wide range of climates (Baas, 1982). If this is so, then substantial changes in the overall RP fraction might not be significant, as this paper aims to elucidate. However, RP in *Juniperus thurifera* has been shown to vary in size and abundance annually, suggesting that RP formation in this species is sensitive to interannual changes in precipitation and temperature (Olano *et al.*, 2013).

When considering the valuable contributions from earlier studies, major ecological trends in RAP levels remain unclear. The studies that have investigated the association between RAP and climate have either relied on qualitatively classifying species into broadly defined categories based on their RAP abundance (Baas, 1982; Wheeler *et al.*, 2007) or were designed as isolated case studies, which were limited in the number of species and sites investigated (Martínez-Cabrera *et al.*, 2009; Olano *et al.*, 2013; Ziemińska *et al.*, 2015). As far as we are aware, the largest datasets providing detailed information on both climate-related parameters and RAP levels encompass 61 species growing on eight different sites across South and North America (Martínez-Cabrera *et al.*, 2009) and 69 species collected on three sites along the east coast of Australia (Ziemińska *et al.*, 2015). In order to better understand the global variation in RAP levels, which could point to various functional consequences of low vs high RAP fraction, we assembled an extensive dataset that includes many hundreds of species from different climatic zones while using more rigorous quantitative methods to characterise potential trends in RAP fractions. Our main objective was to investigate the association between climate and RAP fraction across a broad range of species and environments. We expect there to be a strong relationship between both temperature and precipitation with RAP, and potentially higher RAP levels in tropical and subtropical species than in temperate species. Also, species that experience drought are hypothesised to show high levels of RAP because of potential correlations of RAP with drought resistance mechanisms such as xylem capacitance and refilling of embolised vessels (Brodersen & McElrone, 2013; Trifilò *et al.*, 2014).

We also aimed to elucidate the links between parenchyma fraction and growth form, and to explore differences in RAP amount between organs, namely roots, trunks and branches. We postulate that total RAP fractions are higher in lianas and succulents than in trees due to an increased demand for mechanical elasticity in climbing plants and the importance of water storage in succulents. Across different plant organs, higher RAP and especially RP levels can be expected in roots when compared to stems because of potential differences in storage capacity and mechanical properties (Gasson & Cutler, 1990; Stokke & Manwiller, 1994; Pratt *et al.*, 2007). Finally, by way of a large quantitative analysis, we aim to support previous studies (Panshin & de Zeeuw, 1980) that total RAP fraction shows a divergence between angiosperms and conifers. A more detailed phylogenetic investigation of RAP fractions at lower taxonomic levels is beyond the scope of this study and was addressed recently in a range of Chinese species (Zheng & Martínez-Cabrera, 2013).

Materials and Methods

Compilation of the global parenchyma dataset

A total of 1727 records of wood parenchyma percentages for 1439 separate species were obtained from 55 different literature sources (Supporting Information Notes S1). The majority of these records reported values for trunks and branches of trees and shrubs. However, data from small branches of woody climbers and succulents together with data from woody roots were also included. If available, the total fractions of vessels and fibres, representing the other main cell types found in wood, were also collected.

Data on ray parenchyma (RP) and axial parenchyma (AP) were available for 1268 angiosperm records, with 144 and 225 additional records for RP and total ray and axial parenchyma (RAP) (total of 1637 records), respectively. In conifers, only 14 out of a total of 90 records reported values for both AP and RP. This is because AP is sparse in conifers and therefore rarely measured. For this reason, it can be assumed that the total fraction of RP in conifers is equal to the total parenchyma content without introducing substantial bias to the total parenchyma estimate. Orthography and synonymy of species names were checked using the Plant List (v.1.1; http://www.theplantlist.org). In 14 instances we were unable to match the species name reported by the author to any recognised taxon name, and these entries were omitted. Upon pooling together data for trunks and branches reported in the same publication (see the Results section), a core dataset of 1727 entries (1439 species and 127 families) was obtained and used for our analyses. The compiled dataset and corresponding reference list is provided in Table S1, except for the nearly 800 species from Zheng & Martínez-Cabrera (2013), which are accessible via the TRY Plant Trait Database (https://www.try-db.org/TryWeb/Home.php; Kattge *et al.*, 2011).

Validation of the dataset

High data variability is inherent in large datasets compiled from different literature sources, probably due to different methods used to quantify parenchyma. For example, RAP fractions were based on thin transverse wood sections using light microscopy (Ruelle *et al.*, 2006; Martínez-Cabrera *et al.*, 2009; Ziemińska *et al.*, 2013, 2015), or on polished wood surfaces using stereomicroscopy (Poorter *et al.*, 2010; Fichtler & Worbes, 2012). The relative fraction of parenchyma tissue can be analysed by measuring the entire area covered by the tissue or by estimating this area using a grid overlay (Huber & Prütz, 1938; Smith, 1967). In

older books and wood atlases, the method used was not explicitly stated (Panshin & de Zeeuw, 1980; Koch, 1985; Wagenführ, 2007). Another complication is that it can be difficult to distinguish between AP and vasicentric tracheids or thin-walled living fibres in angiosperms.

As a check of accuracy we compared data taken from the literature to our own data, where we measured RAP fractions for 16 species, out of which 10 species and 14 genera were in our literature-based dataset. Transverse sections of woody branches 0.5–1 cm in diameter were prepared with a sliding microtome, dehydrated in an ethanol series, stained with a mixture of safranin and alcian blue and mounted in Neo Mount (Merck KGaA, Darmstadt, Germany). Digital images were taken with a stereo zoom microscope (Axio Zoom V16; Zeiss, Germany). A wedge-shaped region spanning a total area of *c.* 0.5–1.5 mm^2 from the cambium to the pith was outlined and individual areas taken up by the four principal wood tissues (RP, AP, vessels and imperforate tracheary elements, i.e. fibres and tracheids) within this region were segmented manually in Photoshop with the aid of a graphic tablet (Wacom, Cintiq Companion, model DTH-W1300; Vancouver, WA, USA). The areas were then measured with ImageJ (Rasband, 1997–2012) and converted to percentage proportions. For 12 temperate species, which were accessible on the Ulm University campus, three small branches from the same individual were measured for each species. For four tropical species, which were available in the glasshouses of the Botanical Garden of Ulm University, one branch could be harvested for measurements, and two radial transects were measured on a transverse section. In total, 16 species (two conifers, nine temperate angiosperms, four tropical angiosperms and one temperate climber) were measured. Our data were then matched to data for 10 species from the compiled dataset. Another comparison was made at the generic level for 14 genera.

Climate data

In order to investigate correlations between climate and the amount of RAP, AP and RP, we assigned the species into three broadly designated climatic zones: temperate, tropical and subtropical. We used the climatic classification system devised by Köppen (1936), where temperate includes both maritime and continental types, with subtropical ranging from permanent wet to summer dry and winter dry, and tropical including permanent wet, summer dry, winter dry, and monsoonal.

In order to complement the categorical classification, we looked up the spatial coordinates for species in our dataset to serve as proxies for species distribution. We used climate data by way of two different approaches: (1) based on exact locations from the literature, climatic data were obtained for 68 different sampling locations, including 461 different records and 411 species (including both angiosperms and conifers); and (2) where exact locations were not available from the literature, we used the Global Biodiversity Inventory Facility (GBIF), which allowed us to obtain climatic information for 619 species from 612 different locations, covering a wide range of latitudes, longitudes and altitudes (Fig. S1).

For the approach based on exact locations, climatic data for each geographical location were extracted from layers of two major climatic databases using ArcGIS (v.10.0.4.4; ESRI, CA, USA). The layers of the mean annual temperature (MAT, °C) and mean annual precipitation (MAP, mm) were sourced from Bioclim layers based on the World Clim Global Climate Database (Hijmans *et al.*, 2005) for the years 1950–2000. The potential evapotranspiration (PET) dataset for each month and the aridity index (AI, which is MAP divided by PET) and mean precipitation of the driest quarter (MPDQ, which is the sum of the average precipitation in the three driest successive months) was taken from the Consortium for Spatial Information (CGIAR CSI). For the GBIF approach, the following criteria were used: (1) the record was not a duplicate according to the spatial coordinates of the sample, (2) we applied a cut-off at a minimum of 10 records per species for calculating the median location and corresponding climatic computations, and (3) the record was not located within 50 km of the GBIF headquarters in Copenhagen (55.68°N, 12.59°E) to minimise the chance that a record was given a coordinate that corresponded to where the data were housed, but not where the plant was actually collected.

Statistical analyses

Potential trade-offs in angiosperm trees between total RAP fraction and the percentage of vessels and fibre (including tracheids) fractions were analysed by plotting these three major xylem tissue fractions on a ternary axis, including a total number of 1302 individual specimens (394 temperate, 428 tropical and 480 subtropical).

We used nonparametric tests due to the lack of data normality. In particular, AP fractions were skewed towards smaller values. The paired-sample Wilcoxon signed-rank test was used for evaluating the differences in parenchyma fractions between roots and stems (i.e. any part above soil level) within the same species. A Kruskal–Wallis and a pairwise Wilcoxon test were performed to detect differences in RAP fractions between conifers, angiosperm trees, the two specialized angiosperm growth forms (climbers and succulents), and between angiosperm trees from different climatic zones. Spearman's rank correlation coefficients were calculated to analyse the correlation between the tissue fractions of the three main xylem cell types: RAP, vessels and fibres (including tracheids).

The parenchyma data for which exact locations were known were analysed separately to the data for which only GBIF-derived climate data was known. We analysed the effect of MAT, MAP and altitude on the proportion of parenchyma using a general additive model (GAM) with a binomial distribution using the mgcv package (Wood, 2006). No further GAM analyses were carried out on PET, AI and MPDQ due to a high co-linearity between these variables with MAT and MAP (Fig. S2). Each explanatory variable was fitted with a smoother and the maximum effective degrees of freedom (edf, which determines the amount of smoothing) were limited to three partitions. All smooth terms are centred when fitting a GAM in order to ensure model identifiability (Wood, 2006). GAM models were carried

out on angiosperms only because the sample size was insufficient for conifers. All statistical analyses were performed using R (R Development Core Team, 2010).

Results

Overview of the core dataset

Within the core dataset of 1727 entries, there were 36 records for woody roots and 1691 records for woody stems. The latter can be further subdivided into 1520 records of trunks or branches of angiosperm trees, 89 records of trunks or branches of conifer trees, 32 records of stems from woody climbers and 50 records of stems from woody succulents (see Table 1 for an overview). In general, there was a 29-fold variation in RAP fractions, with total fractions varying from 3.4% in *Thuja occidentalis* (a coniferous tree) to 99% in *Adenia glauca* (a pachycaul succulent from the Passifloraceae family).

Validation of the dataset

A close agreement between the literature data and our measurements was found when comparing 10 tree species ($r^2 = 0.571$) and 14 genera ($r^2 = 0.920$) for total RAP percentages (Fig. S3). The agreement at the genus level was lower for the individual RP and AP data, but still significant ($r^2 = 0.39$, $P < 0.05$, $n = 15$, and $r^2 = 0.777$, $P < 0.0001$, $n = 12$ for RP and AP, respectively). However, no significant correlation occurred when comparing the RP and AP fraction data from our measurements with literature data for the same species ($n = 14$ and 8 for RP and AP, respectively), indicating that there were either potentially important concerns with AP or RP fractions reported in literature for any given species due to varying methodologies, intraspecific differences or interspecific variation. The latter two concerns could be due to developmental age, the organ or sampling position. AP in particular seems to be the most problematic to quantify because identifying AP on transverse sections can be difficult as a consequence of anatomical similarities with thin-walled living fibres or tracheids (Stokke & Manwiller, 1994; Carlquist, 2014). Therefore, most of our analyses focused on the more robust RAP data, whereas conclusions about the relative contribution of RP and AP should be interpreted with caution.

Table 1 Data summary of the global xylem parenchyma dataset compiled from the literature with respect to the total number of entries, literature sources, taxa (including angiosperms and gymnosperms) and parenchyma tissue fractions in wood

	RP	AP	RAP
n entries	1502	1282	1582
n resources	48	38	50
n species/ genera/ families	1265/542/119	1142/518/113	1364/596/123
Mean (%)	17.4	7.2	27.2
Median (%)	16.4	3.3	22.6
Min (%)	2.3	0	3.4
Max (%)	68.4	74	99
cv	45.4	129.8	57.9

RP, ray parenchyma; AP, axial parenchyma; RAP, ray and axial parenchyma; cv, coefficient of variation.

Differences between organs, growth forms and angiosperms vs conifers

The differences in parenchyma percentage between roots and stems (including both trunks and branches) were not profound. Slightly higher RP fractions were found in roots than in trunks and branches (paired-sample Wilcoxon signed-rank test, $V = 205$, $P = 0.04$, $n = 23$), whereas the difference in AP and total RAP was not significant ($V = 91.5$ and 292, $P > 0.05$, $n = 22$ and 31, respectively).

Data for both trunks and branches showed no significant difference in RP, AP and RAP fractions ($V = 237$–298.5, $P > 0.05$, $n = 33$–34). Therefore, trunks and branches were pooled together and their average was used for further analyses.

Significant differences in RAP fractions were detected between conifer and angiosperm trees, and between specialised growth forms (stem succulents and lianas), within the angiosperm group, using stem (i.e. trunk or branch) data only (Kruskal–Wallis test, $\chi^2 = 118.6$, $P < 0.001$, df = 3; Fig. 3). Stem succulents showed the highest values of RAP (mean ± SD: 70.2 ± 22.0%, $n = 50$), followed by lianas (50.1 ± 16.3%, $n = 28$), and angiosperm trees and shrubs (26.3 ± 12.4%, $n = 1384$), whereas conifers exhibited the lowest fraction of RAP (7.63 ± 2.6%, $n = 89$, Fig. 3a). In angiosperm trees, there were many entries with rather high RAP, for example 136 entries (118 species) showed total RAP fractions > 50%.

In addition to the total RAP percentage, the contribution of RP and AP was analysed (Fig. 3b), although these data should be interpreted with caution as mentioned above. The information on RP and AP fractions was available for stems of 14 conifer species, 1205 angiosperm tree species, 9 climbers and 32 succulents. Again, conifers showed much lower fractions of both RP and AP (RP, 8.1 ± 2.7%; AP, 1.7 ± 2.2%) than angiosperm trees (RP, 17.7 ± 6.3%; AP, 6.6 ± 8.5%, Fig. 3b). Climbers in our dataset had the highest fraction of AP (29.3 ± 10.2%), whereas RP was relatively low (12.5 ± 2.7%). Succulents showed a high fraction of both RP and AP (RP, 43.5 ± 14.3%, AP, 20.8 ± 18.1%, Fig. 3b).

Climate and RAP fractions

Differences in RAP fractions in angiosperm trees (including some shrubs) growing in various climatic zones were analysed for 399 temperate, 442 tropical and 543 subtropical specimens (Kruskal–Wallis test, $\chi^2 = 224.9$, $P < 0.001$, df = 2), with mean values of 21.1% (± 7.9), 22.2% (± 9.3 and 36.2% (± 13.4) for temperate, subtropical and tropical angiosperm specimens, respectively (Fig. 4a). The amount of AP appeared to be the main driver of

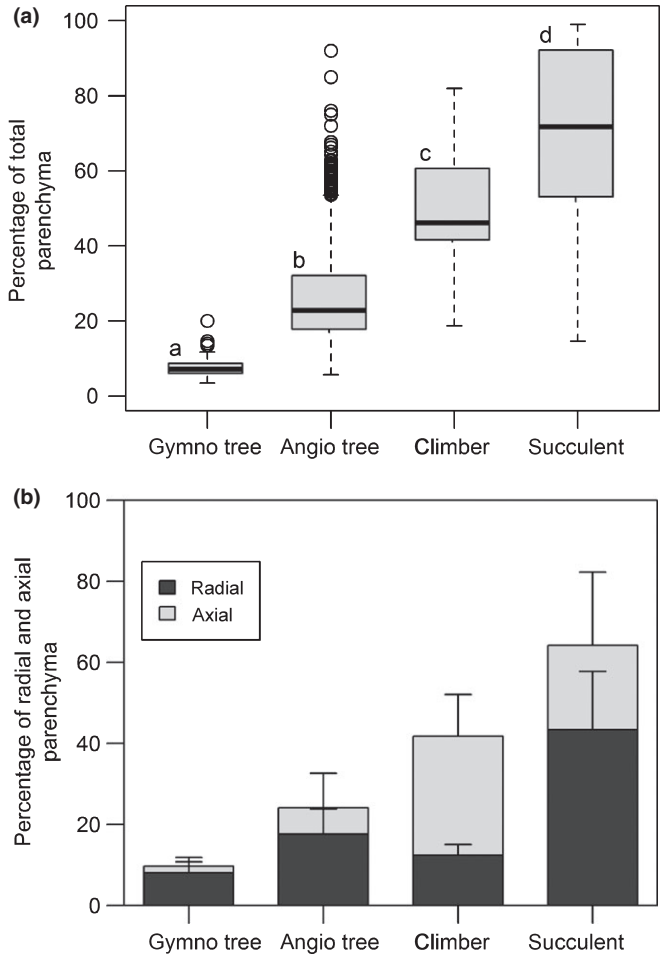

Fig. 3 Parenchyma tissue fractions (%) across different woody plant groups and growth forms. Because of inherent differences in wood anatomy between conifer and angiosperm trees, both groups are analysed separately. The lowest parenchyma fractions are found in conifers, followed by angiosperm trees (including some shrubs), climbers and succulents. The percentage of total parenchyma (including axial and ray parenchyma) is shown in (a), with the ray and axial parenchyma contribution for the same groups given in (b). The box plot in (a) shows the median, 25th and 75th percentiles, error bars demarcating 10th and 90th percentiles, and open circles showing outliers. Different letters above boxes indicate statistical significance between groups (Kruskal–Wallis test, $P \leq 0.05$). Bars in (b) represent mean values ± SD. The number of specimens for (a) (with the number of specimens for (b) between brackets) is: *n* gymno tree = 89 (14), *n* angio tree = 1384 (1205), *n* climber = 28 (9), and *n* succulent = 50 (32).

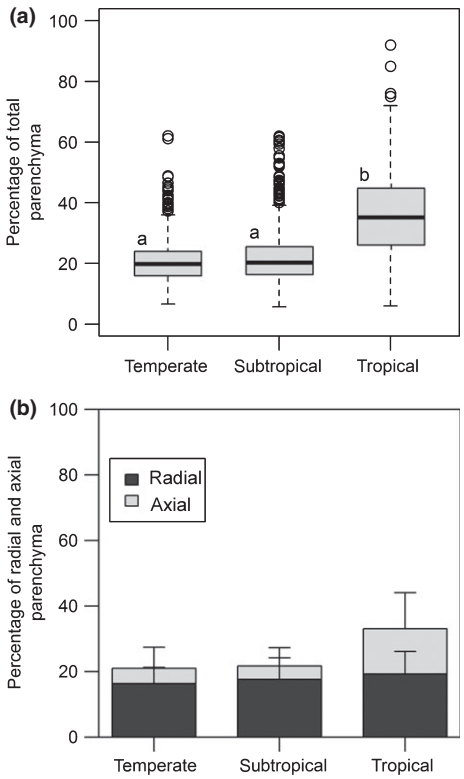

Fig. 4 Parenchyma tissue fractions (%) in angiosperm trees classified according to the temperate, subtropical and tropical biome, showing the total parenchyma fraction (a) and the individual contributions of ray and axial parenchyma (b). The box plot in (a) shows the median, 25th and 75th percentiles, error bars demarcating 10th and 90th percentiles, and open circles showing outliers. Different letters above boxes indicate statistical significance for tropical species compared to temperate and subtropical trees (Kruskal–Wallis test, $P \leq 0.05$). Bars in (b) represent mean values ± SD. The number of specimens for (a) (with the number of specimens for (b) between brackets): *n* temperate = 399 (399), *n* tropical = 442 (287), *n* climber = 28 (9), and *n* succulent = 50 (32).

this difference. The total AP fraction was 13.8% (± 11.0) in tropical trees, whereas it was between 4% and 5% in temperate and subtropical trees (see Fig. 4b). By contrast, average RP fractions spanned a narrow range from 16.4% (± 5) in temperate to 19.4% (± 6.8) in tropical trees.

The ternary axis (Fig. 5) revealed that a higher contribution of RAP occurred mainly at the expense of fibres, particularly in tropical and subtropical trees, whereas total vessel fractions were typically between 5% and 20%, and on average 14.6%. A strongly negative correlation was found between the tissue fractions for RAP and fibres (including tracheids) for all biomes, especially the tropical climate (Spearman's $r = -0.75$, $P < 0.001$ for all biomes; Table 2). Fibre tissue fractions (F) were most negatively correlated with vessel tissue fraction (V) in temperate and subtropical species ($r = -0.66$, and -0.59, respectively; $P < 0.001$), whereas a negative relationship between RAP and V was only weakly significant for temperate and tropical climates ($r = -0.21$ and -0.18, respectively; $P < 0.001$; Table 2). In some temperate trees, the relatively high vessel fractions represented ring-porous species with narrow growth rings that have a high proportion of early-wood and, therefore, many wide vessels.

There was a strong agreement between the climatic data derived from the sampling locations and those derived from the GBIF locations (Fig. S4). There was a clear difference between angiosperms and conifers, as we found only significant correlations between RAP and MAT, and between RAP and MAP for angiosperms. Moreover, due to a low sample number (90 records, 61 species) and limited number of locations, no climatic GAM analyses were performed on conifers.

The GAM models showed that MAT was the main driver for RAP in angiosperms ($F_{1.94,\ 267} = 37.21$, pseudo-$R^2 = 21.05\%$,

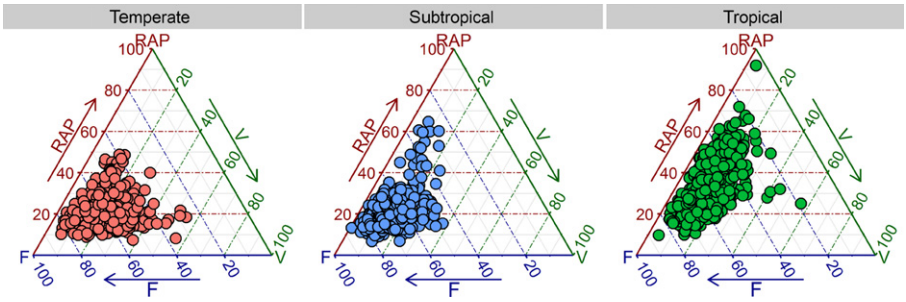

Fig. 5 Ternary plot showing the contribution of the three principal tissues in wood: the total amount of ray and axial parenchyma (RAP, %), vessels (V, %), and fibres (including tracheids) (F, %). Each dot represents a specimen. The trade-off between RAP and F tissue fractions shows a strongly negative correlation for all data and is especially clear in the tropical biome (see Table 2). Specimens are grouped according to three major climatic zones, which follow Köppen (1936).

Table 2 Spearman's rank correlation coefficients showing the trade-offs between the tissue fractions of three major xylem cell types, which were analysed for three major biomes (temperate, subtropical, tropical)

Correlation	All biomes	Temperate	Subtropical	Tropical
RAP vs F	−0.752***	−0.480***	−0.688***	−0.856***
RAP vs V	−0.153***	−0.210***	−0.066	−0.176***
F vs V	−0.427***	−0.661***	−0.591***	−0.279***

See Fig. 5 for a visual plot. RAP, ray and axial parenchyma; F, fibres (including tracheids); V, vessels. ***, $P \leq 0.001$.

P-value < 0.001; for exact locations, and $F_{1.95,\ 218} = 48.22$, pseudo-$R^2 = 31.65\%$, $P < 0.001$ for GBIF locations, Fig. 6a). However, the effect of MAT on RAP was nonlinear, with RAP fractions increasing with MAT values in hot environments (> ± 17°C), but not for species in colder environments. When analysing the effect of MAT on AP and RP fractions separately, GAM models revealed significant associations for both when controlling for altitude and precipitation (Fig S5a, S6a; Tables S2, S3).

The relationship between MAP and RAP was also significant, although the pseudo-R^2 values were very low compared to those of MAT (Fig. 6b; Tables S2, S3). Although significance was found for the relationship between MAP and RP (Fig. S6b), this was not the case for AP (Fig. S5b; Tables S2, S3). When controlling for MAP and MAT, RAP increased significantly with altitude (Fig. 6c), but these altitudinal trends were nonsignificant or significant for AP and RP, depending on whether the data were based on the exact locations or GBIF (Figs S5c, S6c).

A separate GAM model between total RAP fraction and temperature also supported a quadratic latitudinal trend (Fig. 7), for both exact locations ($F_{1.95,\ 267} = 27.01$, pseudo-$R^2 = 18\%$, $P < 0.001$) and species from the GBIF locations ($F_{1.96,\ 218} = 31.81$, pseudo-$R^2 = 24.1\%$, $P < 0.001$). The latter suggests that RAP increased significantly the closer the sampling location was to the equator for both datasets.

Discussion

The global ray and axial parenchyma (RAP) dataset compiled demonstrates that RAP tissues show a 29-fold variation in abundance, which agrees with previous reports across seed plants (Fujiwara *et al.*, 1991; Martínez-Cabrera *et al.*, 2009; Zheng & Martínez-Cabrera, 2013; Ziemińska *et al.*, 2013, 2015). A key finding is that RAP amounts in wood, especially axial parenchyma (AP), are driven by temperature (Fig. 6a). Albeit, precipitation also showed a significant relationship with RAP in the general additive model (GAM) models when controlling for altitude and mean annual temperature (MAT), although far less so than temperature (Fig. 6b; Tables S2, S3). Mean annual precipitation (MAP) showed a negative trend in the GAM models, with increasing amounts of RAP towards drier environments, which is what we expected. The temperature effect is also reflected in the latitudinal trends for RAP, especially in the northern hemisphere. However, our analyses did not support the expected difference between subtropical and temperate species (Fig. 4b). Also, no significant difference was found in the RAP tissue fraction between tropical wet environments and tropical, seasonally dry areas (data not shown).

Other drivers of RAP tissue fractions include growth forms. It is clear that lianas and succulents represent two growth forms that show higher fractions of RAP than self-supporting angiosperm trees. Within the tree and shrub growth form, tropical plants have higher levels of RAP than temperate and subtropical ones (Figs 4, 5), supporting previous studies based on qualitative (Baas, 1982; Segala Alves & Angyalossy-Alfonso, 2002; Wheeler *et al.*, 2007) and quantitative approaches (Martínez-Cabrera *et al.*, 2009). A novel finding is that RAP levels in tropical plants are mainly due to an increase in AP, whereas RP levels remain more conservative in trees across the three major biomes analysed (Fig. 4b). This finding is not as transparent in the GAM models (Figs S4, S5), as both RP and AP are highly associated with temperature. However, where RP amount gradually increases with temperate, AP remains unwavering until *c.* 17°C and then rises sharply and exponentially with temperature. This is the reason AP is so high in the tropics compared to both temperate and subtropical regions (Fig. 4b).

Explaining why some factors may drive the RAP level whereas others have little or no influence requires a more detailed understanding of RAP functions (Fig. 2), especially those related to storage capacity, resistance to drought stress, frost resistance, defence mechanisms and mechanical properties.

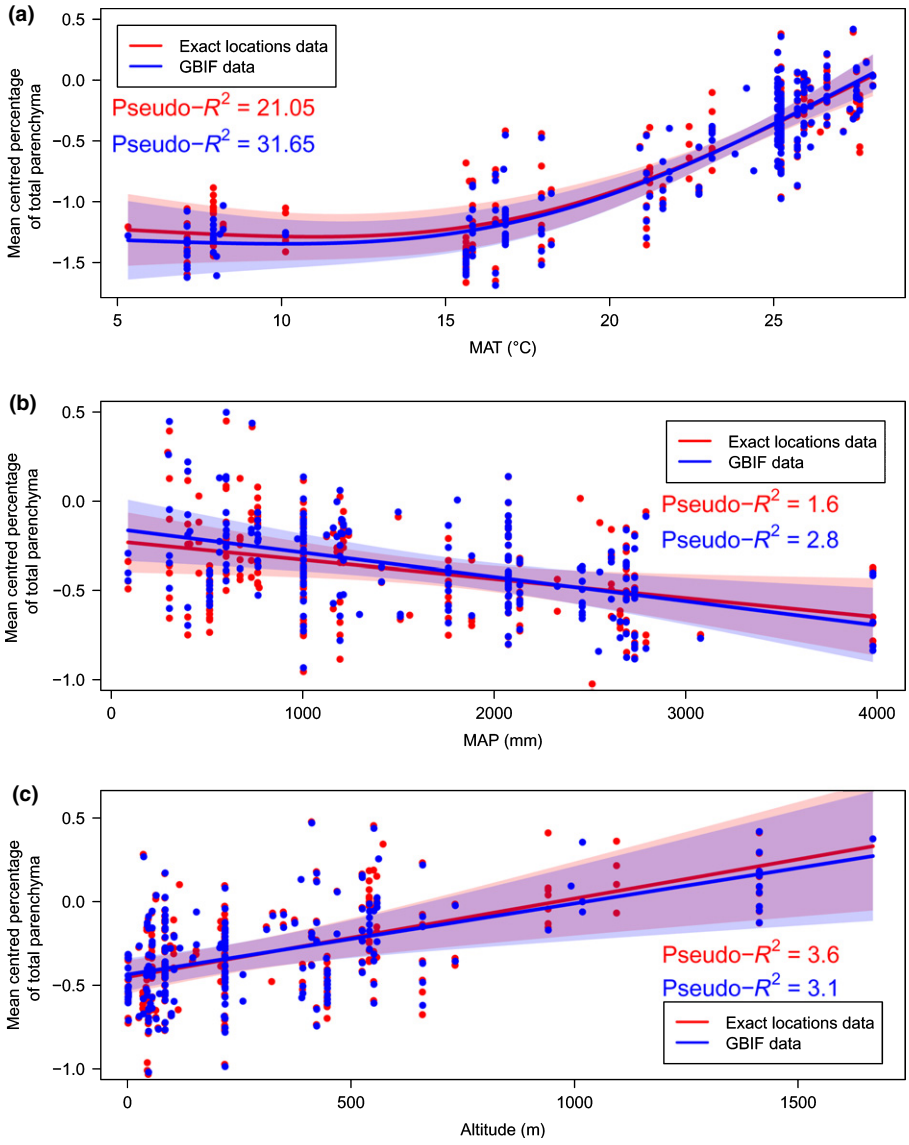

Fig. 6 The effect of (a) mean annual temperature (MAT), (b) mean annual precipitation (MAP) and (c) altitude on the proportion of ray and axial parenchyma (RAP) in angiosperm wood based on a general additive model with a binomial distribution for the exact location dataset (red) and the Global Biodiversity Inventory Facility (GBIF)-derived climate data (blue). Each climate variable was limited to three effective degrees of freedom (e.d.f.). The solid line represents the fitted smoother; 95% confidence intervals are shown as coloured tint areas. Each dot represents a specimen for which the sampling location was reported in literature, or climate data obtained from the WorldClim database. Pseudo-R^2 measures the approximate deviance explained by each explanatory variable.

RAP fractions in relation to NSC storage capacity

Storage of nonstructural carbohydrates (NSCs) is arguably one of the most widely accepted functions of RAP in wood. As far as we know, however, the hypothesis that high amounts of RAP correspond to higher storage capacity of NSCs as yet has not been tested in a direct, quantitative way. The assumption that higher amounts of RAP, and therefore a higher NSC capacity, should occur in roots when compared to stems could only partly be confirmed. We found no significant differences between stems and roots in total RAP and AP fractions, but did find higher levels of RP in root wood than in stem wood. As this finding came from a small sample set ($n = 21–30$), it is premature to make generalisations. A higher fraction of RP in roots than stems has been observed previously (Gasson & Cutler, 1990; Stokke & Manwiller, 1994; Machado *et al.*, 2007) and may be associated with a reduced need for mechanical cells such as fibres in addition to increased storage capacity of roots. Aside from RP fractions, different cell dimensions of RP have been reported in roots, especially a general increase in width of the entire ray and the individual ray cells, and a tendency towards more heterocellular rays in roots than in stems (Patel, 1965; Gasson & Cutler, 1990; Denne & Gasson, 2008).

When considering the storage capacity of RAP we would also expect to find higher RAP fractions in plants from temperate seasonal climates. However, we did not find much support for this hypothesis due to lower RAP fractions in trees from temperate compared to tropical biomes. RAP are not the only wood-tissue storing NSCs; septate or living fibres also do so (Webber, 1936; Yamada *et al.*, 2011; Carlquist, 2014).

RAP fractions and drought stress

It is possible that high RAP fractions in wood benefit plants in dry conditions by conferring high hydraulic capacitance, which could prevent embolism formation, or facilitate embolism

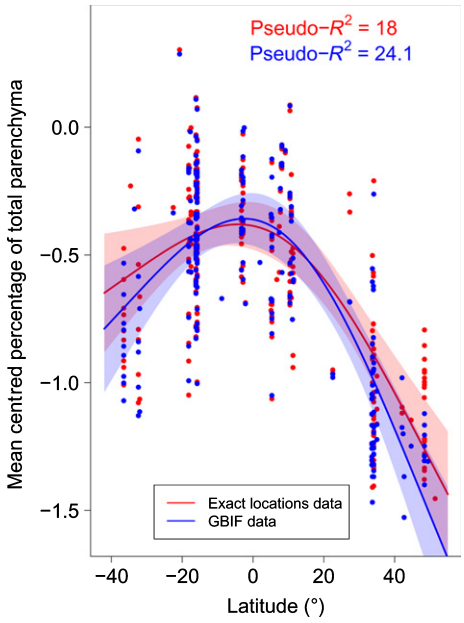

Fig. 7 The effect of latitude on the proportion of ray and axial parenchyma (RAP) in angiosperm wood based on a general additive model with a binomial distribution for the exact location dataset (red) and the Global Biodiversity Inventory Facility (GBIF) derived climate data (blue). The latitude variable was limited to three partitions. The solid line represents the fitted smoother; 95% confidence intervals are shown in colour. Each dot represents a specimen for which the sampling location was reported in literature, or climate data obtained from the WorldClim database. Pseudo-R^2 measures the approximate deviance explained by latitude.

refilling (Fig. 6b). Support for a drought related function of RAP is provided by the high levels of RAP in stem succulents. With an average of 70.3% RAP in succulents, it can be speculated that wood parenchyma not only stores a considerable amount of water, but also provides symplastic connections with bark and pith that both serve as important water reservoirs (Borchert & Pockman, 2005; Scholz *et al.*, 2007; Hearn, 2009; Hearn *et al.*, 2013; Pfautsch *et al.*, 2015). However, the large RAP variation in dry and seasonally dry environments suggests that plants have various strategies to survive these conditions, with stem succulents having large parenchyma fractions whereas other species may show comparatively few RAP. It has been suggested that vessel-associated RAP may be involved in the embolism refilling process by releasing sugars and water into embolised conduits (Bucci *et al.*, 2003; Salleo *et al.*, 2004; Brodersen *et al.*, 2010; Brodersen & McElrone, 2013). Although embolism repair remains controversial and poorly understood, refilling on a daily basis may not occur in conifers, which could be owing to their low RAP fractions (Choat *et al.*, 2014).

RAP fractions and temperature

Temperature is associated with RAP fractions in the secondary xylem, much more so than rainfall. This finding agrees with Moles *et al.* (2014), who found that 15 out of 21 plant traits are more strongly correlated with temperature than with precipitation. The high levels of RAP in tropical plants could be linked to the greater plant diversity in the tropics and the dominance of various families with high RAP levels (e.g. Fabaceae, Moraceae). Alternatively, particular functions associated with RAP (e.g. defence against pathogens, hydraulic capacitance) could be more important in tropical environments than in temperate regions. It is possible that protection against cold, including tolerance to extracellular freezing and freeze dehydration, or freeze avoidance by super-cooling, is an energy-demanding process (Quamme, 1991; Neuner, 2014), which could therefore be an important factor in reducing the RAP fraction in woody plants exposed to frost or freezing events. Also, two conifer genera growing in the tropical/subtropical mountains of the southern hemisphere (*Podocarpus* spp. and *Dacrydium* spp.) have higher RAP fractions than conifers from cool temperate regions (Braun, 1984). Similarly, *Pinus canariensis* from the warm islands of Tenerife and La Palma have RAP averages of 14.5%, with AP values accounting for 3% of this (Climent *et al.*, 1998).

RAP fractions as a defence system

RAP fractions might also play a large role in defence against the spread of decay via pathogenic fungi, viruses and bacteria. The presence of RP may prevent the lateral spread of fungi, whereas AP does the same for axial movement (Boddy & Rayner, 1983; Shigo, 1984; Biggs, 1986). Because both RP and AP may accumulate anti-microbial compounds such as phytoalexins, phenolic compounds and suberin, which all act to inhibit fungal spread (Biggs, 1987), trees with high RAP fractions might be more resistant to brown rot fungi and therefore be better overall compartmentalisers of decay than trees with lower RAP fractions (Schwarze *et al.*, 2003).

In agreement with the defence role, the amount of RAP is higher in the sapwood of trees that have recovered from pathogenesis (Tippett & Shigo, 1981; Schmitt & Liese, 1990; Arbellay *et al.*, 2010, 2012). Interestingly, another study across seven tree species from the Amazon found that high parenchyma abundance and wide dilating rays were associated with poor compartmentalisation of decay, but this was offset by fast wound closure (Romero & Bolker, 2008). Although in angiosperms, parenchyma cells in contact with vessels can seal off conduits by way of tyloses or gum deposits to avoid the spread of decay (Biggs, 1987; Bonsen & Kučera, 1990; Schmitt & Liese, 1992; Sun *et al.*, 2007), defence in gymnosperms mainly lies in the occlusion of tracheids via aspiration of the torus-margo bordered pits (Fuhr *et al.*, 2013), and the production of abundant polyphenolic compounds and traumatic resin ducts in Pinaceae and Cupressaceae (Phillips, 1948; Hudgins *et al.*, 2004). Such a strategy is therefore consistent with a lower RAP fraction in conifers. By contrast, a higher fraction of RAP in the tropics might be driven by a greater incidence of biotic stress when compared to temperate environments (Bagchi *et al.*, 2014). The evolutionary 'arms race' with pathogens and insect herbivores may require the deployment of more RAP or the synthesis of a more diverse suite of secondary compounds by RAP in order to enhance tree defence abilities. However, the trade-off between RAP and fibre tissue fractions (Fig. 5) may also suggest that high RAP fractions could equally decrease the defence capacity.

RAP and mechanical properties

Because the amount of RAP occurs mainly at the expense of fibres, one would also expect important effects on wood mechanical properties. It has long been assumed that parenchyma cells often have larger lumina and thinner cell walls than fibres, so high RAP levels should theoretically result in lower wood density together with a reduced stiffness, but retain a higher elasticity. However, rays in *Liquidambar* were found to have a higher specific gravity than surrounding tissues because the ratio of cell wall to lumen was relatively high (Taylor, 1969). Moreover, in a study of 69 angiosperm species it was found that the main driver of the modulus of elasticity (defined as the ratio of tensile stress to tensile strain) was fibre wall fraction rather than RAP fraction (Ziemińska *et al.*, 2015). However, that study only looked at species within a small wood density range and the results should be treated with caution.

Several authors have suggested that wide rays, which are common in lianas, allow vessel-bearing segments to twist without rupturing, which may also explain the occurrence of nonlignified or less lignified ray parenchyma cells in climbing plants (Schenck, 1893; Haberlandt, 1914; Sieber & Kučera, 1980; Gartner, 1991; Putz & Holbrook, 1991). Additional explanations for the high amount of RAP in lianas can be linked with dedifferentiation of parenchyma, allowing rapid recovery from injury, especially after tree fall (Dobbins & Fisher, 1986; Fisher & Ewers, 1991; Busch *et al.*, 2010), and their ability to clone readily when detached from the parent plant (Putz, 1984; Yorke *et al.*, 2013). A mechanical role of RAP dependent on their turgor pressure has also been suggested in *Adansonia* (Chapotin *et al.*, 2006), with RAP in this species occupying as much as 90%.

General conclusion

The 29-fold variation in the parenchyma fraction is associated with temperature-driven differences between tropical, subtropical and temperate woody plants, as well as with different growth forms such as succulents and lianas. The ecological trends discussed suggest ways for further research into how RAP plays a role in woody plant function in the storage of NSCs and water, defence against pathogens and resilience to damage. Various functions of RAP in wood have been suggested and it is generally not clear which function takes precedence in a given situation. Based on the available evidence, this may depend on climate, plant organ, and the potential partitioning in the functional roles of RP and AP (Zheng & Martínez-Cabrera, 2013). Also, the total RAP percentage does not reflect the spatial, three-dimensional arrangement of the parenchyma network and its connectivity to other xylem tissues. More research is also needed to test the within tree variation of RAP %, which would involve labour-intensive studies with careful and well-planned sampling. Further research based on observational evidence is needed to investigate the role of parenchyma in more detail, such as the spatial patterns of parenchyma networks and, along with this, to test the hypotheses presented in this paper.

Acknowledgements

H.M. and S.J. acknowledge financial support from the German Research Foundation (DFG, project no. 2174). L.P. was supported by a Postdoctoral Fellowship from the Alexander von Humboldt Foundation and acknowledges funding from the Ulm University and Ulm University Society (Ulmer Universitätsgesellschaft). Funding to J.Z. was available through a Special Fund for Forest Scientific Research in the Public Welfare, China (no. 201404303). We also wish to thank the Botanical garden of Ulm University for supplying plant material, Amy Zanne (George Washington University), and anonymous reviewers for valid comments on an earlier version of this paper.

Author contributions

H.M., L.P. and S.J. led the initial data compilation and coordinated the writing. H.M., L.P., S.J., E.F., H.I.M-C., J.Z. and K.Z. contributed data and ideas. L.P. and M.A.F.G. analysed data. K.Z. and E.W. assisted with writing the final manuscript. H.M., P.C. and D.J.M. extracted GBIF locations and climate data.

References

Arbellay E, Fonti P, Stoffel M. 2012. Duration and extension of anatomical changes in wood structure after cambial injury. *Journal of Experimental Botany* **63**: 3271–3277.

Arbellay E, Stoffel M, Bollschweiler M. 2010. Wood anatomical analysis of *Alnus incana* and *Betula pendula* injured by a debris–flow event. *Tree Physiology* **30**: 1290–1298.

Baas P. 1982. Systematic, phylogenetic and ecological wood anatomy – history and perspectives. In: Baas P, ed. *New perspectives in wood anatomy*. The Hague, the Netherlands: Nijhoff/Junk, 23–58.

Bagchi R, Gallery RE, Gripenberg S, Gurr SJ, Narayan L, Addis CE, Freckleton RP, Lewis OT. 2014. Pathogens and insect herbivores drive rainforest plant diversity and composition. *Nature* **506**: 85–88.

Barghoorn ES. 1940. The ontogenetic and phylogenetic specialisation of rays in the xylem of dicotyledons. I. The primitive ray structure. *American Journal of Botany* **27**: 918–928.

Barghoorn ES. 1941. The ontogenetic development and phylogenetic specialization of rays in the xylem of dicotyledons. II. Modification of the multiseriate and uniseriate rays. *American Journal of Botany* **28**: 273–282.

van Bel AJE. 1990. Xylem-phloem exchange via the rays: the undervalued route of transport. *Journal of Experimental Botany* **41**: 631–644.

Biggs AR. 1986. Comparative anatomy of host response of two peach cultivars inoculated with *Leucostoma cincta* and *L. personii*. *Phytopathology* **76**: 905–912.

Biggs AR. 1987. Occurrence and location of suberin in wound reaction zones in xylem of 17 tree species. *Phytopathology* **77**: 718–725.

Boddy L, Rayner ADM. 1983. Origins of decay in living deciduous trees: the role of moisture content and a re-appraisal of the expanded concept of tree decay. *New Phytologist* **94**: 623–641.

Bonsen KJM, Kučera LJ. 1990. Vessel occlusion in plants: morphological, functional, and evolutionary aspects. *International Association of Wood Anatomists Bulletin* **11**: 393–399.

Borchert R, Pockman WT. 2005. Water storage capacitance and xylem tension in isolated branches of temperate and tropical trees. *Tree Physiology* **25**: 457–466.

Braun HJ. 1984. The significance of the accessory tissues of the hydrosystem for osmotic water shifting as the second principle of water ascent, with some thoughts concerning the evolution of trees. *International Association of Wood Anatomists Bulletin* **5**: 275–294.

Braun HJ, Wolkinger F. 1970. Zur funktionellen Anatomie des axialen Holzparenchyms und Vorschlage zur Reform seiner Terminologie. *Holzforschung* **24**: 19–26.

Brodersen CR, McElrone AJ. 2013. Maintenance of xylem network transport capacity: a review of embolism repair in vascular plants. *Frontiers in Plant Science* **4**: 1–11, article 108.

Brodersen CR, McElrone A, Choat B, Matthews M, Shackel K. 2010. Dynamics of embolism repair in grapevine: *in vivo* visualisations using HRCT. *Plant Physiology* **154**: 1088–1095.

Bucci SJ, Scholz FG, Goldstein G, Meinzer FC, Sternberg LDL. 2003. Dynamic changes in hydraulic conductivity in petioles of two savanna tree species: factors and mechanisms contributing to the refilling of embolized vessels. *Plant, Cell & Environment* **26**: 1633–1645.

Burgert I, Bernasconi A, Eckstein D. 1999. Evidence for the strength function of rays in living trees. *Holz als Roh- und Werkstoff* **57**: 397–399.

Burgert I, Eckstein D. 2001. The tensile strength of isolated wood rays of beech (*Fagus sylvatica* L.) and its significance for the biomechanics of living trees. *Trees – Structure and Function* **15**: 168–170.

Busch S, Seidel R, Speck O, Speck T. 2010. Morphological aspects of self-repair of lesions caused by internal growth stresses in stems of *Aristolochia macrophylla* and *Aristolochia ringens*. *Proceedings of the Royal Society B* **277**: 2113–2120.

Carlquist S. 2001. *Comparative wood anatomy. Systematic, ecological, and evolutionary aspects of dicotyledon wood, 2nd edn*. Berlin, Germany: Springer.

Carlquist S. 2014. Fibre dimorphism: cell type diversification as an evolutionary strategy in angiosperm woods. *Botanical Journal of the Linnean Society* **174**: 44–67.

Chapotin SM, Razanomeharizaka JH, Holbrook NM. 2006. A biomechanical perspective on the role of large stem volume and high water content in baobab trees (*Adansonia* spp.; Bombacaceae). *American Journal of Botany* **93**: 1251–1264.

Choat B, Brodersen CR, McElrone AJ. 2014. Synchrotron X-ray microtomography of xylem embolism in *Sequoia sempervirens* saplings during cycles of drought and recovery. *New Phytologist* **205**: 1095–1105.

Clearwater MJ, Goldstein G. 2005. Embolism repair and long distance water transport. In: Holbrook NM, Zwieniecki MA, eds. *Vascular transport in plants*. Burlington, MA, USA: Elsevier Academic Press, 375–399.

Climent J, Gil L, Pardos JA. 1998. Xylem anatomical traits related to resinous heartwood formation in *Pinus canariensis* Sm. *Trees – Structure and Function* **123**: 139–145.

Deflorio G, Johnson C, Fink S, Schwarze FMWR. 2008. Decay development in living sapwood of coniferous and deciduous trees inoculated with six wood decay fungi. *Forest Ecology and Management* **255**: 2373–2383.

Denne P, Gasson P. 2008. Ray structure in root- and stem-wood of *Larix decidua*: implications for root identification and function. *International Association of Wood Anatomists Journal* **29**: 17–23.

Dobbins D, Fisher J. 1986. Wound response of girdled stems of lianas. *Botanical Gazette* **147**: 278–289.

Fahn A, Werker E, Baas P. 1986. *Wood anatomy and identification of trees and shrubs from Israel and adjacent regions*. Jerusalem, Israel: The Israel Academy of Sciences and Humanities.

Fichtler E, Worbes M. 2012. Wood anatomical variables in tropical trees and their relation to site conditions and individual tree morphology. *International Association of Wood Anatomists Journal* **33**: 19–40.

Fisher JB, Ewers FW. 1991. Structural responses to stem injury in vines. In: Putz FE, Mooney HA, eds. *The biology of vines*. Cambridge, UK: Cambridge University Press, 99–124.

Fuhr MJ, Schbert M, Stührk C, Schwarze FWMR, Herrmann HJ. 2013. Penetration capacity of the wood-decay fungus *Physisporinus vitreus*. Complex adaptive systems modelling. *Springer Open Journal* **1**: 6.

Fujiwara S, Sameshima K, Kuroda K, Takamura N. 1991. Anatomy and properties of Japanese hardwoods. I. Variation of fibre dimensions and tissue proportions and their relation to basic density. *International Association of Wood Anatomists Bulletin New Series* **12**: 419–424.

Gartner GL. 1991. Stem hydraulic properties of vines vs. shrubs of western poison oak, *Toxicodendron diversilobum*. *Ecologia* **87**: 180–189.

Gasson PE, Cutler DF. 1990. Root anatomy of 17 genera growing in the British Isles. *International Association of Wood Anatomists Bulletin New Series* **11**: 3–46.

Haberlandt G. 1914. *Physiological plant anatomy*. (Translated from the 4th German edition by M. Drummond). London, UK: MacMillan & Co.

Hearn DJ. 2009. Developmental patterns in anatomy are shared among separate evolutionary origins of stem succulent and storage root-bearing growth habits in *Adenia* (Passifloraceae). *American Journal of Botany* **96**: 1941–1956.

Hearn DJ, Poulsen T, Spicer R. 2013. The evolution of growth forms with expanded root and shoot parenchymatous storage is correlated across the eudicots. *International Journal of Plant Sciences* **174**: 1049–1061.

Hijmans RJ, Cameron SE, Parra JL, Jones PG, Jarvis A. 2005. Very high resolution interpolated climate surfaces for global land areas. *International Journal of Climatology* **25**: 1965–1978.

Hoch G, Richter A, Korner CH. 2003. Non-structural carbon compounds in temperate forest trees. *Plant, Cell & Environment* **26**: 1067–1081.

Holbrook NM. 1995. Stem water storage. In: Gartner BL, ed. *Stems and trunks in plant form and function*. San Diego, CA, USA: Academic Press, 151–174.

Huber B, Prütz G. 1938. Über den Anteil von Fasern, Gefässen und Parenchym am Aufbau verschiedener hölzer. *Holz als Roh-und Werkstoff* **10**: 377–381.

Hudgins JW, Christiansen E, Franceschi V. 2004. Induction of anatomically based defence responses in stems of diverse conifers by methyl jasmonate: a phylogenetic perspective. *Tree Physiology* **24**: 251–264.

IAWA Committee. 1989. IAWA list of microscopic features for hardwood identification. *International Association of Wood Anatomists Bulletin New Series* **10**: 219–332.

IAWA Committee. 2004. IAWA list of microscopic features for softwood identification. *International Association of Wood Anatomists Journal* **25**: 1–70.

Jansen S, Gortan E, Lens F, Lo Gullo MA, Salleo S, Scholz A, Stein A, Trifilò P, Nardini A. 2011. Do quantitative vessel and pit characters account for ion-mediated changes in the hydraulic conductance of angiosperm xylem? *New Phytologist* **189**: 218–228.

Kattge J, Díaz S, Lavorel S, Prentice IC, Leadley P, Bönisch G, Garnier E, Westoby M, Reich PB, Wright IJ *et al.* 2011. TRY – a global database of plant traits. *Global Change Biology* **17**: 2905–2935.

Koch P. 1985. *Utilization of hardwoods growing on southern pine sites*. Asheville, NC, USA: USDA-Forest Service.

Köppen W. 1936. Das geographische System der Klimate. In: Köppen W, Geiger R, eds. *Handbuch der Klimatologie*. Berlin, Germany: Gebrüder Borntraeger, 1–44.

Kribs DA. 1935. Salient lines of structural specialisation in the wood rays of dicotyledons. *Botanical Gazette* **96**: 547–557.

Kribs DA. 1937. Salient lines of structural specialization in the wood parenchyma of dicotyledons. *Bulletin of the Torrey Botanical Club* **64**: 177–186.

Machado SR, Rodella RA, Angyalossy V, Marcati CR. 2007. Structural variations in root and stemwood of *Styrax* (*Styracaceae*) from Brazilian forest and cerrado. *IAWA Journal* **28**: 173–188.

Martínez-Cabrera HI, Jones CS, Espino S, Schenk HJ. 2009. Wood anatomy and wood density in shrubs: responses to varying aridity along transcontinental transects. *American Journal of Botany* **96**: 1388–1398.

Moles AT, Perkins SE, Laffan SW, Flores-Moreno H, Awasthy M, Tindall ML, Sack L, Pitman A, Kattge J, Aarssen LW *et al.* 2014. Which is a better predictor of plant traits: temperature or precipitation? *Journal of Vegetation Science* **25**: 1167–1180.

Nardini A, Salleo S, Jansen S. 2011. More than just a vulnerable pipeline: xylem physiology in the light of ion-mediated regulation of plant water transport. *Journal of Experimental Botany* **62**: 4701–4718.

Nawrot M, Pazdrowski W, Szymanski M. 2008. Dynamics of heart-wood formation and axial and radial distribution of sapwood and heartwood in stems of European larch (*Larix decidua* Mill.). *Journal of Forest Science.* **54**: 409–417.

Neuner G. 2014. Frost resistance in alpine woody plants. *Frontiers in Plant Science* **5**: 1–13, article 654.

Normand D, Chatelet R. 1951. Observations taxonomiques et xylologiques sur le genre *Pinacopodium* Exell et Mendoça. *Bulletin Jardin Botanique É tat, Bruxelles* **21**: 451–463.

O'Brien MJ, Leuzinger S, Philipson CD, Tay J, Hector A. 2014. Drought survival of tropical tree seedlings enhanced by non-structural carbohydrate levels. *Nature Climate Change* **4**: 710–714.

Olano JM, Arzac A, García-Cervigón AI, von Arx G, Rozas V. 2013. New star on the stage: amount of ray parenchyma in tree rings shows a link to climate. *New Phytologist* **198**: 486–495.

Panshin AJ, de Zeeuw C. 1980. *Textbook of wood technology. Structure, identification and uses of the commercial woods of the United States and Canada.* New York, NY, USA: McGraw-Hill Book Company.

Patel RN. 1965. A comparison of the anatomy of the secondary xylem in roots and stems. *Holzforschung* **19**: 72–79.

Pfautsch S, Renard J, Tjoelker MG, Salih A. 2015. Phloem as capacitor: radial transfer of water into xylem of tree stems occurs via symplastic transport in ray parenchyma. *Plant Physiology* **167**: 963–971.

Phillips EWJ. 1948. Identification of softwoods by their microscopic structure. *Forest Products Research Bulletin* **22**: 1–56.

Pinto I, Pereira H, Usenius A. 2004. Heartwood and sapwood development within maritime pine (*Pinus pinaster* Ait.) stems. *Trees – Structure and Function* **18**: 284–294.

Plavcová L, Jansen S. 2015. The role of xylem parenchyma in the storage and utilization of non-structural carbohydrates. In: Hacke UG, ed. *Functional and ecological xylem anatomy*. Heidelberg, Germany: Springer International, 209–234.

Poorter L, McDonald I, Alarcon A, Fichtler E, Licona JC, Pena-Claros M, Sterck F, Villegas Z, Sass-Klaassen U. 2010. The importance of wood traits and hydraulic conductance for the performance and life history strategies of 42 rainforest tree species. *New Phytologist* **185**: 481–492.

Pratt RB, Jacobsen AL, Ewers FW, Davis SD. 2007. Relationships among xylem transport, biomechanics and storage in stems and roots of nine Rhamnaceae species of the California chaparral. *New Phytologist* **174**: 787–798.

Putz FE. 1984. The natural history of lianas on Barro Colorado Island, Panama. *Ecology* **65**: 1713–1724.

Putz FE, Holbrook NM. 1991. Biomechanical studies of vines. In: Putz FE, Mooney HA, eds. *The biology of vines*. Cambridge, UK: Cambridge University Press, 73–98.

Quamme HA. 1991. Application of thermal analysis to breeding fruit crops for increased cold hardiness. *HortScience* **26**: 513–517.

R Development Core Team. 2010. *R: a language and environment for statistical computing*. Vienna, Austria: R Foundation for Statistical Computing. [WWW document] URL http://www.r-project.org/ [accessed 7 July 2014].

Rasband WS. 1997–2012. *ImageJ*. Bethesda, MD, USA: US National Institutes of Health. [WWW document] URL http://imagej.nih.gov/ij/ [accessed 27 Aug 2014].

Reiterer A, Burgert I, Sinn G, Tschegg S. 2002. The radial reinforcement of the wood structure and its implication on mechanical and fracture mechanical properties – a comparison between two tree species. *Journal of Materials Science* **37**: 935–940.

Romero C, Bolker BM. 2008. Effects of stem anatomical and structural traits on responses to stem damage: an experimental study in the Bolivian Amazon. *Canadian Journal of Forest Research* **38**: 611–618.

Ruelle J, Clair B, Beauchêne J, Prévost MF, Fournier M. 2006. Tension wood and opposite wood in 21 tropical rain forest species. 2. Comparison of some anatomical and ultrastructural criteria. *International Association of Wood Anatomists Journal* **27**: 341–376.

Salleo S, Lo Gullo MA, Trifilo P, Nardini A. 2004. New evidence for a role of vessel-associated cells and phloem in the rapid xylem refilling of cavitated stems of *Laurus nobilis* L. *Plant, Cell & Environment* **27**: 1065–1076.

Salleo S, Trifilo P, Esposito S, Nardini A, Lo Gullo MA. 2009. Starch-to-sugar conversion in wood parenchyma of field-growing *Laurus nobilis* plants: a component of the signal pathway for embolism repair? *Functional Plant Biology* **36**: 815–825.

Santiago M, Pagay V, Strook AD. 2013. Impact of electroviscosity on the hydraulic conductance of the bordered pit membrane: a theoretical investigation. *Plant Physiology* **163**: 999–1011.

Schenck H. 1893. Beitrage zur Biologie und Anatomie der Lianen, im besonderen der in Brasilien einheimischen Arten, II. Beitrage zur Anatomie der Lianen. In: Schimper AFW, ed. *Botanische Mitteilungen aus den Tropen*. Jena, Germany: Verlag von Gustav Fischer, 1–271.

Schmitt U, Liese W. 1990. Wound reaction of the parenchyma in *Betula*. *International Association of Wood Anatomists Bulletin* **11**: 413–420.

Schmitt U, Liese W. 1992. Seasonal influences on early wound reactions in *Betula* and *Tilia*. *Wood Science and Technology* **26**: 405–412.

Schmitt U, Liese W. 1993. Response of xylem parenchyma to suberisation in some hardwoods after mechanical injury. *Trees – Structure and Function* **8**: 23–30.

Scholz FG, Bucci SJ, Goldstein G, Meinzer FC, Franco AC, Miralles-Wilhelm F. 2007. Biophysical properties and functional significance of stem water storage tissues in Neotropical savannah trees. *Plant, Cell & Environment* **30**: 236–248.

Schwarze FWMR, Fink S, Deflorio G. 2003. Resistance of parenchyma cells in wood to degradation by brown rot fungi. *Mycological Progress* **2**: 267–274.

Segala Alves E, Angyalossy-Alfonso V. 2002. Ecological trends in the wood anatomy of some Brazilian species. 2. Axial parenchyma, rays and fibres. *International Association of Wood Anatomists Journal* **23**: 391–418.

Shigo AL. 1984. Compartmentalisation: a conceptual framework for understanding how trees grow and defend themselves. *Annual Review Phytopathology* **22**: 189–214.

Sieber M, Kučera LJ. 1980. On the stem anatomy of *Clematis vitalba* L. *International Association of Wood Anatomists Bulletin* **1**: 49–54.

Smith DM. 1967. *Microscopic methods for determining cross-sectional cell dimensions*. US Forest Service Research Paper FPL 79, October 1967. Madison, WI, USA: US Department of Agriculture, Forest Service, Forest Products Laboratory.

Spicer R. 2005. Senescence in secondary xylem: heartwood formation as an active development programme. In: Holbrook N, Zwieniecki M, eds. *Vascular transport in plants*. Burlington, MA, USA: Elsevier Academic Press, 457–475.

Spicer R. 2014. Symplastic networks in secondary vascular tissues: parenchyma distribution and activity supporting long-distance transport. *Journal of Experimental Botany* **65**: 1829–1848.

Spicer R, Holbrook NM. 2007. Parenchyma cell respiration and survival in secondary xylem: does metabolic activity decline with cell age? *Plant, Cell & Environment* **30**: 934–943.

Stokke DD, Manwiller FG. 1994. Proportions of wood elements in stem, branch, and root wood of Black Oak (*Quercus velutina*). *International Association of Wood Anatomists Journal* **15**: 301–310.

Sun Q, Rost TL, Reid MS, Matthews MA. 2007. Ethylene and not embolism is required for wound-induced tyloses development in stems of grapevines. *Plant Physiology* **145**: 1629–1636.

Taylor FW. 1969. The effect of ray tissue on the specific gravity of wood. *Wood & Fiber Science* **2**: 142–145.

Tippett JT, Shigo AL. 1981. Barrier zone formation: a mechanism of the tree defence against vascular pathogens. *International Association of Wood Anatomists Bulletin* **2**: 163–168.

Trifilò P, Barbera PM, Raimondo F, Nardini A, Lo Gullo MA. 2014. Coping with drought-induced xylem cavitation: coordination of embolism repair and ionic effects in three Mediterranean evergreens. *Tree Physiology* **34**: 109–122.

Wagenführ R. 2007. *Holzatlas*. Leipzig, Germany: Carl Hanser Verlag.

Webber IE. 1936. Systematic anatomy of the woods of the Simarubaceae. *American Journal of Botany* **23**: 577–587.

Wheeler EA, Baas P. 1991. A survey of the fossil record for dicotyledonous wood and its significance for evolutionary and ecological wood anatomy. *International Association of Wood Anatomists Journal* **12**: 275–332.

Wheeler EA, Baas P, Rodgers S. 2007. Variations in dicot wood anatomy: a global analysis based on the Insidewood database. *International Association of Wood Anatomists Journal* **28**: 229–258.

Wolkinger F. 1970. Das Vorkommen der lebenden Holzfasern in Sträuchern und Bäumen. *Phyton* **14**: 55–67.

Wolkinger F. 1971. Morphologie und systematische Verbreitung lebenden Holzfasern bei Sträuchern und Bäumen. III. Systematische Verbreitung. *Holzforschung* **25**: 29–39.

Wood SN. 2006. *Generalized additive models: an introduction with R*. London, UK: Chapman and Hall.

Yamada Y, Awano T, Fujita M, Takabe K. 2011. Living wood fibers act as large-capacity "single-use" starch storage in black locust (*Robinia pseudoacacia*). *Trees – Structure and Function* **25**: 607–616.

Yorke SR, Schnitzer SA, Mascaro J, Letcher S, Carson WP. 2013. Increasing liana abundance and basal area in a tropical forest: the contribution of long-distance clonal colonization. *Biotropica* **45**: 317–324.

Zheng J, Martínez-Cabrera HI. 2013. Wood anatomical correlates with theoretical conductivity and wood density across China: evolutionary evidence of the functional differentiation of axial and radial parenchyma. *Annals of Botany* **112**: 927–935.

Ziemińska K, Butler DW, Gleason SM, Wright IJ, Westoby M. 2013. Fibre wall and lumen fractions drive wood density variation across 24 Australian angiosperms. *AoB PLANTS* **5**: plt046.

Ziemińska K, Wright IJ, Westoby M. 2015. Broad anatomical variation within a narrow wood density range – a study of twig wood across 69 Australian angiosperms. *PLoS ONE* **10**: e0124892.

Zwieniecki MA, Melcher PJ, Holbrook NM. 2001. Hydrogel control of xylem hydraulic resistance in plants. *Science* **291**: 1059–1062.

Supporting Information

Additional supporting information may be found in the online version of this article.

Fig. S1 Distribution map of the species for which parenchyma fraction values were compiled.

Fig. S2 Poly-co-linearity matrix for the parameters analysed in relation to wood anatomy, plant organ, geography and climate.

Fig. S3 Comparison of total parenchyma fractions in wood based on our own measurements and literature.

Fig. S4 Comparison of mean annual temperature and mean annual precipitation for species for which both sampling locations and GBIF locations were available.

Fig. S5 The effect of MAT, MAP and altitude on the proportion of axial parenchyma in angiosperms.

Fig. S6 The effect of MAT, MAP and altitude on the proportion of ray parenchyma in angiosperms.

Table S1 The Global Wood Parenchyma Database

Table S2 Summary of statistics for the general additive models (GAM) based on the exact locations dataset

Table S3 Summary of statistics for the general additive models (GAM) based on the GBIF locations dataset

Notes S1 Published references from which data were extracted for analyses.

Please note: Wiley Blackwell are not responsible for the content or functionality of any supporting information supplied by the authors. Any queries (other than missing material) should be directed to the *New Phytologist* Central Office.

RESEARCH ARTICLE

AMERICAN JOURNAL OF BOTANY

The amount of parenchyma and living fibers affects storage of nonstructural carbohydrates in young stems and roots of temperate trees[1]

Lenka Plavcová[2,4], Günter Hoch[3], Hugh Morris[2], Sara Ghiasi[2], and Steven Jansen[2]

PREMISE OF THE STUDY: Concentrations of nonstructural carbohydrates (NSCs) are used as proxies for the net carbon balance of trees and as indicators of carbon starvation resulting from environmental stress. Woody organs are the largest NSC-storing compartments in forest ecosystems; therefore, it is essential to understand the factors that affect the size of this important storage pool. In wood, NSC are predominantly deposited in ray and axial parenchyma (RAP); however, direct links between nutrient storage and RAP anatomy have not yet been established. Here, we tested whether the NSC storage capacity of wood is influenced by the amount of RAP.

METHODS: We measured NSC concentrations and RAP fractions in root and stem sapwood of 12 temperate species sampled at the onset of winter dormancy and in stem sapwood of four tropical trees growing in an evergreen lowland rainforest. The patterns of starch distribution were visualized by staining with Lugol's solution.

KEY RESULTS: The concentration of NSCs in sapwood of temperate trees scales tightly with the amount of RAP and living fibers (LFs), with almost all RAP and LFs being densely packed with starch grains. In contrast, the tropical species had lower NSC concentrations despite their higher RAP and LFs fraction and had considerable interspecific differences in starch distribution.

CONCLUSIONS: The differences in RAP and LFs abundance affect the ability of sapwood to store NSC in temperate trees, whereas a more diverse set of functions of RAP might be pronounced in species growing in a tropical environment with little seasonality.

KEY WORDS axial parenchyma; carbohydrates; living fibers; rays; starch; storage; wood; xylem

Nonstructural carbohydrates (NSCs, including mono-, di-, oligo-, and polysaccharides) are the direct products of plant photosynthesis that can be stored in various plant tissues and used as substrate for growth and various metabolic processes. The amount of NSCs available in a plant is considered an important indicator of the net carbon balance in woody plants, although the functional role and the active or passive regulation of NSC storage are not fully understood (Kozlowski, 1992; Hoch, 2015). Nonstructural carbohydrate levels have traditionally been studied with respect to seasonal cycles of growth and dormancy (Drossopoulos and Niavis, 1988; Saranpää and Höll, 1989; Sauter and van Cleve, 1994). More recently, they have been investigated in relation to growth limitation (Körner, 2003; Sala and Hoch, 2009; Wiley and Helliker, 2012), altitudinal boundaries for forests (Hoch et al., 2002), plant survival under limited resource conditions, increased atmospheric CO_2 levels, and drought-induced tree mortality (McDowell et al., 2008; Anderegg et al., 2012; Galvez et al., 2013). Although developmental shifts are likely between seedlings and mature trees, wood provides the largest NSC-storing compartment among all tree tissues (Hoch et al., 2003; Würth et al., 2005), with an additional role for parenchyma cells in the pith and bark (Essiamah and Eschrich, 1985).

In wood, NSCs are predominantly deposited in ray and axial parenchyma (RAP). Ray parenchyma (RP) represents a series of procumbent, square, or upright cells produced by ray initials that extend radially from the cambium. Besides storage, RP facilitates radial conduction of NSCs, water, and other substances and enables

[1] Manuscript received 17 November 2015; revision accepted 3 February 2016.

[2] Institute for Systematic Botany and Ecology, Ulm University, Albert-Einstein-Allee 11, D-89081 Ulm, Germany; and

[3] Department of Environmental Sciences–Botany, University of Basel, Schönbeinstrasse 6, CH-4056 Basel, Switzerland

[4] Author for correspondence (e-mail: lenka.plavcova@gmail.com); present address: University of Hradec Králové, Faculty of Science, Rokitanského 62, 500 03 Hradec Králové, the Czech Republic

doi:10.3732/ajb.1500489

their exchange between phloem and xylem, although the mechanisms of this trafficking remain poorly understood (Van Bel, 1990; Sokolowska and Zagórska-Marek, 2012; Pfautsch et al., 2015). Axial parenchyma (AP) is made up of axially elongated cells, which are often organized in strands. The AP has been suggested to be involved in NSC storage and transport, similar to the RP (Braun and Wolkinger, 1970; Baas, 1982; Braun, 1984; Carlquist, 2001). Abundant AP may not only increase the physical space available for storage but could also enhance connectivity between RP and AP.

While NSC storage and dynamics appear tightly coupled to RAP anatomy and physiology (reviewed by Plavcová and Jansen, 2015), direct links between structural and functional RAP traits have not yet been established. Elucidating firm connections between structural and functional traits has a long tradition in the field of functional and ecological wood anatomy. While most research to date focuses on the functional anatomy of xylem conduits, providing us with a better understanding of xylem water transport (Baas, 1982; Carlquist, 1984; Hacke and Sperry, 2001; Jansen et al., 2009), the current study used a similar approach to shed more light on the role of RAP in NSC storage. More specifically, we tested whether the amount of RAP found in wood is a structural proxy for the NSC storage capacity of wood.

As most of the wood biomass consists of dead, protoplasm-free fibers and conduits, the total volume of RAP should place a limitation on the amount of NSC that can be stored. The proportion of RAP in wood, usually expressed as the percentage area of RAP relative to the total wood cross-sectional area, varies greatly across species. In gymnosperms, the RAP area fractions are commonly between 5 and 10% (Panshin and de Zeeuw, 1980), while in angiosperms, the RAP proportions are higher, typically between 20 and 50% (Martínez-Cabrera et al., 2009; Fichtler and Worbes, 2012; Zheng and Martínez-Cabrera, 2013; Ziemińska et al., 2013). Fractions higher than 80% have also been observed in some woody succulents and climbers (Mauseth and Plemons-Rodriguez, 1997; Hearn, 2009). Interestingly, RAP fractions tend to be higher in tropical than temperate angiosperm trees (Morris et al., 2016). The higher RAP fractions of tropical species might be surprising at first sight when considering that the storage function is likely to be less active in tropical environments with a weak seasonality. However, RAP has multiple functions beyond storage of NSCs, such as storage of water (capacitance), embolism refilling, symplastic connectivity, and various functions related to defense and resilience to disturbance (for an overview, see fig. 2 of Morris et al., 2016). Moreover, the storage capacity provided by RAP may not always be fully used. For instance, it is well known that NSC content of wood fluctuates seasonally in both temperate (Sauter and van Cleve, 1994; Barbaroux et al., 2003) and tropical environments (Newell et al., 2002; Würth et al., 2005). Besides seasonal variation, there can be differences in NSC distribution between vessel-associated RAP cells and the RAP cells that are not in direct contact with vessels (Braun and Wolkinger, 1970; Czaninski, 1977; Braun, 1984).

In many species, living fibers (LFs) accumulate starch and hence contribute to NSC storage in addition to RAP. LFs, defined as fibers that retain living protoplasts, are either septate or nonseptate, and vary interspecifically in their lumen diameter to wall thickness ratio (Fahn and Leshem, 1963; Wolkinger, 1970; Carlquist, 2014). The occurrence of LFs is, however, poorly documented in woody plants, and their anatomical and functional distinction can be difficult to make due to a structure–function continuum with AP (Carlquist, 2014). A storage function has been suggested for septate fibers (Carlquist, 2001), which are twice as common in tropical as in temperate trees (Wheeler et al., 2007). Similar to AP, septate fibers often have thin secondary walls that distinguish them from thick-walled living and nonliving fibers. In contrast, nonseptate LFs, which are found, for instance, in maples, often have thick secondary walls (Carlquist, 2001, 2014). Providing that the thicker cell wall occurs at the expense of cell lumen volume, it is reasonable to expect that thick-walled LFs are less efficient in storage than septate fibers or AP.

The main goal of this study was to test whether the amount of NSCs stored in wood is linked with RAP and LF abundance, and to quantify the relative contribution of RP, AP, and LFs to storage function. To achieve this goal, we measured NSC concentration in root and stem sapwood of 12 temperate species, including 10 angiosperm trees, one conifer tree and one woody climber. Samples were collected at the onset of winter dormancy when the NSC concentration is expected to be at its maximum. We measured the area fractions of RP, AP, and LFs and visualized starch in situ. We expected that species with a relatively high amount of RAP, such as pedunculate oak (*Quercus robur*) and black locust (*Robinia pseudoacacia*), would show higher concentrations of NSC in wood than species with a low RAP fraction, for example, in horse chestnut (*Aesculus hippocastanum*) and Norway spruce (*Picea abies*). We also hypothesized that more NSC would be stored in woody roots than stems and that this pattern will be paralleled by a higher RAP abundance in the roots (Pate et al., 1990). Complementing the data obtained for temperate trees, NSC content, the presence of starch, together with RAP fractions, were measured in the stems of four tropical tree species growing in a lowland rainforest in Costa Rica. We expected to find higher RAP proportions in tropical species (Morris et al., 2016), but with NSC levels not necessarily as high as those of temperate species because tropical species are always actively growing, whereas the temperate were sampled at the onset of winter dormancy. Nevertheless, we anticipated a positive correlation between the amount of NSCs and the amount of RAP across the four tropical species.

MATERIALS AND METHODS

Plant material—Young woody roots and stems of 12 temperate species (Table 1) were collected from mature trees (more than 3 m tall) growing in a forested area surrounding the Ulm University campus, which included the arboretum of the Botanical Garden of Ulm University (48°25′N, 9°58′E), and a forest strip along the Iller River, 2 km south of Ulm (48°22′N, 9°60′E). These areas experience a temperate climate with a mean annual temperature of 8.9°C and mean annual precipitation of 726 mm (climate-data.org). The roots were collected from a depth of 10–50 cm at 1 to 2 m from the root collar. The stem samples were removed from the end regions of subcanopy lateral branches cut at a height of 2 to 3 m with the aid of a telescopic pruning pole. All roots and stems were between 0.5 and 1.5 cm in diameter, which corresponded to a root or stem age of 3 to 8 yr. All samples consisted of juvenile sapwood with no heartwood formation apparent on the cross-section after visual inspection. By avoiding heartwood, we were sure that all RAP cells in our samples were living, and therefore capable of storing NSC. During the last week of October 2014, six root and stem samples from three separate individuals of each species were collected and prepared for NSC analyses. Samples for wood anatomy and wood

TABLE 1. Temperate and tropical species studied.

Species	Family	Abbreviation
Temperate		
Aesculus hippocastanum L.	Sapindaceae	Ah
Acer pseudoplatanus L.	Sapindaceae	Ap
Carpinus betulus L.	Betulaceae	Cb
Clematis vitalba L.	Ranunculaceae	Cv
Fraxinus excelsior L.	Oleaceae	Fe
Fagus sylvatica L.	Fagaceae	Fs
Liquidambar styraciflua L.	Altingiaceae	Ls
Prunus avium (L.) L.	Rosaceae	Pa
Quercus robur L.	Fagaceae	Qr
Robinia pseudoacacia L.	Fabaceae	Rp
Tilia cordata Mill.	Malvaceae	Tc
Picea abies (L.) H.Karst.	Pinaceae	Piab
Tropical		
Brosimum sp.	Moraceae	Bros
Ceiba pentandra (L.) Gaertn.	Malvaceae	Cepe
Pentaclethra macroloba (Willd.) Kuntze	Fabaceae	Pecl
Warszewiczia coccinea (Vahl) Klotzsch	Rubiaceae	Waco

density measurements were collected from the same population of trees, were of a similar size, and came from the same position on the tree as those used for the NSC analyses. For logistical reasons, the material for anatomical and wood density measurements was sampled ad hoc throughout the year 2014, which has no effect on the structural variables measured. Anatomical measurements were carried out on three different root and stem samples per species, while wood density measurements were made on six different root and stem samples collected from three individuals of each species.

Stem samples from four tropical species (Table 1) were collected in the vicinity of the Reserva Biológica Tirimbina, Heredia Province, Costa Rica (10°24′N, 84°6′W) using the same protocol as described for the temperate trees. The climate of Tirimbina is described as wet tropical showing little seasonality, with a mean annual temperature of 25.3°C and mean annual precipitation of 3777 mm (Lapinski and Tschapka, 2013). All samples of tropical trees were collected on 12 September 2014.

NSC analyses—Root and stem samples prepared for NSC analyses (n = 6 roots and 6 stems for each species) were taken to the laboratory where they were then processed immediately or kept on ice and processed later on the same day. In the laboratory, the root and stem samples were cut into 3-cm-long segments, and their bark and pith were carefully removed. The wood samples were heated in a microwave oven at 600 W for 40 s to deactivate the NSC-modifying enzymes (Popp et al., 1996). They were then dried to a constant mass at 80°C for 2 d and sent to the Plant Ecophysiology Laboratory at the University of Basel for NSC content analyses. NSCs, defined here as the sum of starch together with the three most abundant low molecular weight sugars (i.e., sucrose, glucose, and fructose), were analyzed photometrically following a slightly modified protocol described by Hoch et al. (2002). While various protocols can be used for NSC concentration measurements, the method of Hoch et al. (2002) is well established and broadly agrees with other methods based on a recent comparison among 29 different laboratories (Quentin et al., 2015). Approximately 10 mg of plant powder was extracted with 2 mL distilled water at 100°C for 30 min. A sample of the extract was used for the determination of low molecular carbohydrates after enzymatic conversion of fructose and sucrose to glucose. The concentration of total free glucose was then determined photometrically after enzymatic conversion of glucose to gluconate-6-phosphate using a glucose hexokinase (GHK) assay reagent (G3292, Sigma-Aldrich, St. Louis, Missouri, USA). Following the degradation of starch to glucose with amyloglucosidase at 49°C overnight, the NSCs were determined in a separate analysis. The concentration of starch was calculated as NSC minus the free low molecular carbohydrates. Tissue concentrations were given as percentage dry matter.

The gravimetrically based concentrations (in $mg \cdot g^{-1}$) were also converted to volume-based values (in $mg \cdot cm^{-3}$) using data on wood density. Wood density was measured by the water displacement method. Root or stem segments about 3 cm in length (n = 6 roots and 6 stems per species) were cut and debarked. Stem segments were additionally split in half, and the pith was removed. Each segment was then immersed, with the aid of a dissecting needle, into a water-filled beaker resting on an electronic balance, where upon the mass of the displaced water was recorded. All segments were then oven-dried at 80°C to a constant mass, and wood density was calculated by dividing the wood dry mass by the volume of the water displaced.

Wood anatomy and starch distribution—Root and stem segments (n = 3 roots and 3 stems for each species) collected in the field were cut into 1-cm-long pieces and stored in 70% ethanol at 4°C until sectioned for anatomical observations. Upon rehydration in distilled water, transverse sections about 40 μm thick were prepared with a sliding microtome. The sections were immersed in a mixture of 0.35% w/v safranin (in 50% ethanol) and 0.65% w/v alcian blue

TABLE 2. Fixed effects estimates (means ±SE) for organ (root and stem) and climate (temperate and tropical) on concentrations of total nonstructural carbohydrates (NSCs), starch, and soluble sugars and on the amount of ray and axial parenchyma (RP + AP = RAP) and living fibers (LFs). Statistical significance was tested by comparing full and reduced models using the likelihood ratio test. Test statistics (L), degrees of freedom (df), and corresponding *P* values are shown. Statistically significant results ($P \leq 0.05$) are indicated in bold. To corroborate the results of the likelihood ratio tests, ΔAIC values were calculated, which represent the difference in Akaike information criterion values between the reduced and full model.

	Organ (stem relative to root)					Climate (tropical relative to temperate)				
Variable	Mean ± SE	L	df	*P* value	ΔAIC	Mean ± SE.	L	df	*P* value	ΔAIC
NSC	−10.5 ± 2.2	13.1	1	**<10⁻³**	11.1	−6.3 ± 1.7	10.0	1	**0.002**	4
Starch	−9.8 ± 2.1	12.2	1	**<10⁻³**	10.2	−6.7 ± 1.7	10.5	1	**0.001**	4.9
Sugars	−0.7 ± 0.2	12	1	**<10⁻³**	10.0	0.4 ± 0.4	0.7	1	0.391	−1.2
RAP + LFs	−11.1 ± 1.8	17.2	1	**0.007**	15.2	9.5 ± 6.7	2.0	1	0.158	0.3
RAP	−8.9 ± 1.8	13.8	1	**<10⁻³**	11.8	12.9 ± 5.2	5.4	1	**0.020**	3.8
RP	−5.0 ± 0.9	24.9	1	**<10⁻³**	22.9	3.8 ± 2.5	2.2	1	0.136	2.0
AP	−3.9 ± 1.9	3.6	1	0.058	1.6	9.1 ± 5.6	2.6	1	0.110	0.6

(in distilled water) for 2 min, thoroughly washed with distilled water, then gradually dehydrated through an ethanol series before being mounted on a slide in Neo-Mount (Merck Millipore, Darmstadt, Germany). Digital images were captured at a 150× magnification using an Axio Zoom V16 microscope (Zeiss Microscopy GmbH, Jena, Germany). The relative proportions of ray and axial parenchyma (RP + AP = RAP) and living fibers (LFs) were measured on wedge-shaped transects from the root or stem center to the cambium. Axially oriented thick-walled cells with apparent cellular content were typically considered LFs, while axial cells with a protoplasm and a thin secondary wall were always identified as AP. To aid with distinguishing between LFs and thick-walled AP, we also inspected radial sections of wood to assess whether the axial cells have a spindle-shaped morphology typical for fibers or are rectangular and arranged in strands as typical for AP. The different cell types were outlined manually with the aid of a graphical tablet (Cintiq Companion, Wacom Co., Kazo, Japan) in Photoshop Elements (v12.1, Adobe Systems, San Jose, California, USA) and their area proportions were measured in the program Fiji/ImageJ (Schindelin et al., 2012). For obtaining the relative proportions of RAP and LFs, the total surface area occupied by each cell type was divided by the total surface area of the entire transect measured, which typically was about 1 mm^2.

For visualizing the distribution of starch, wood sections were incubated in a drop of 5% w/v aqueous Lugol's iodine for 2 min. The samples were then briefly washed in distilled water, mounted in glycerol, and observed immediately with the Axio Zoom V16 microscope.

Statistical analyses—Mean differences in NSCs and RAP between organs (roots and stems) and between climate (temperate or tropical) were tested using linear mixed effects models, where organ and climate represented the fixed factors and species were treated as a random factor. The models were constructed in R using the lme function available in the *nlme* package (Pinheiro et al., 2015). The maximal likelihood method was used to fit the models. Statistical significance of fixed factors was assessed using the likelihood ratio tests by comparing the full models to reduced models from which the fixed factors were eliminated. The validity of the models was checked by visual inspection of residual plots. The Akaike information criterion for the full and reduced models was also calculated to confirm the appropriateness of the model selection. Relationships between RAP + LFs and NSCs were analyzed by ordinary least squares regression on species- and organ-level means. All analyses were conducted in R (R Core Team, 2013). Results were considered statistically significant at $P \leq 0.05$.

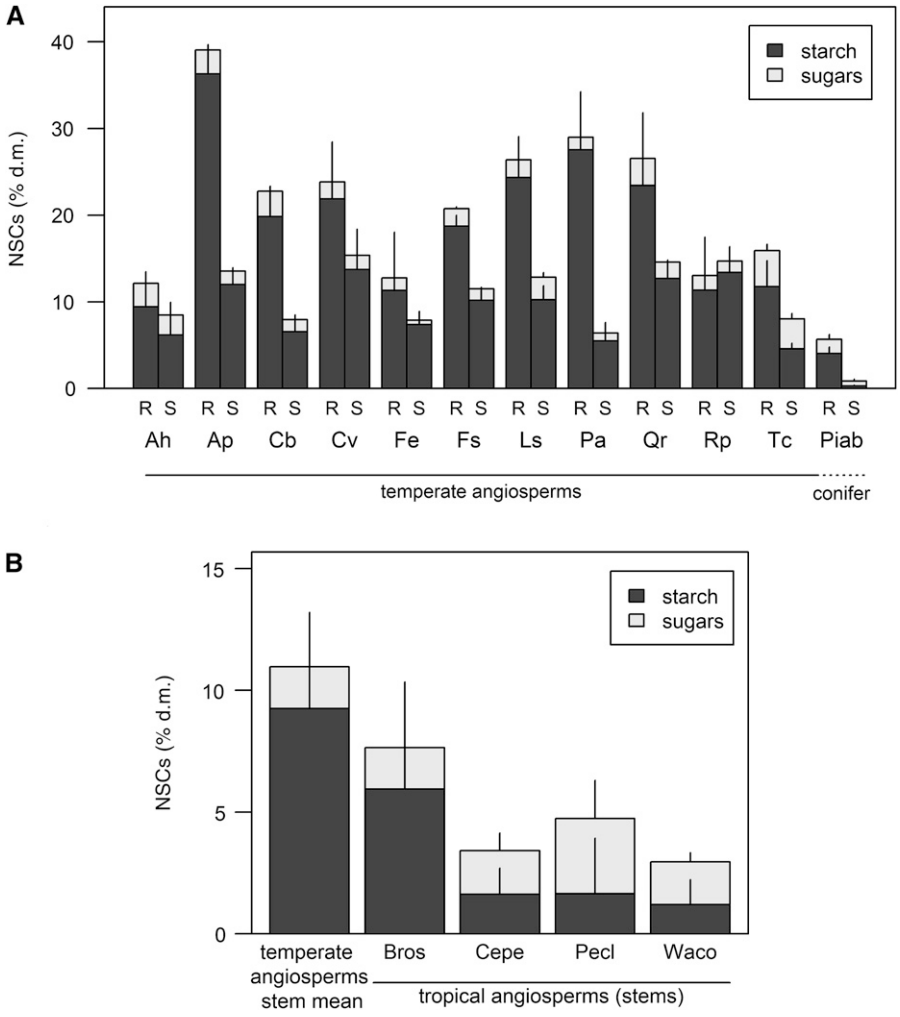

FIGURE 1 Concentration of nonstructural carbohydrates (NSCs) and their division between starch (dark bars) and soluble sugar (lighter bars) fractions in the root (R) and stem (S) sapwood of 12 temperate tree species (A) and in the stems sapwood of four tropical species (B). Mean concentrations (±SD; $n = 6$) are expressed as percentage dry matter (% d.m.). Abbreviations for species are defined in Table 1.

RESULTS

NSC concentrations—The concentrations of NSCs and their two main fractions (i.e., starch and soluble sugars) were significantly higher in roots than stems (Table 2, Fig. 1A). Overall, the highest NSC concentration of 39.1 ± 2.7% (mean ± SD) was measured in the roots of *Acer pseudoplatanus*, while the lowest concentration (0.9 ± 0.1%) was found in the stems of *Picea abies*. In all species and organs, NSC were present mainly in the form of starch, whereas the soluble sugar fraction was less abundant, typically falling between 1 and 3%. The NSC and starch concentrations were not significantly linearly correlated between roots and stems of the same species, largely because of the relatively low NSC and starch concentrations in *Robinia pseudoacacia* roots (Fig. 2A). In contrast, there was a significant correlation between the concentrations of soluble sugars in both organs, which was principally driven by the high soluble sugar fraction found in *Tilia cordata* (Fig. 2B).

Stems of tropical trees had on average less than half the amount of NSC than stems of temperate angiosperms (Table 2, Fig. 1B). The difference in NSC concentrations was driven

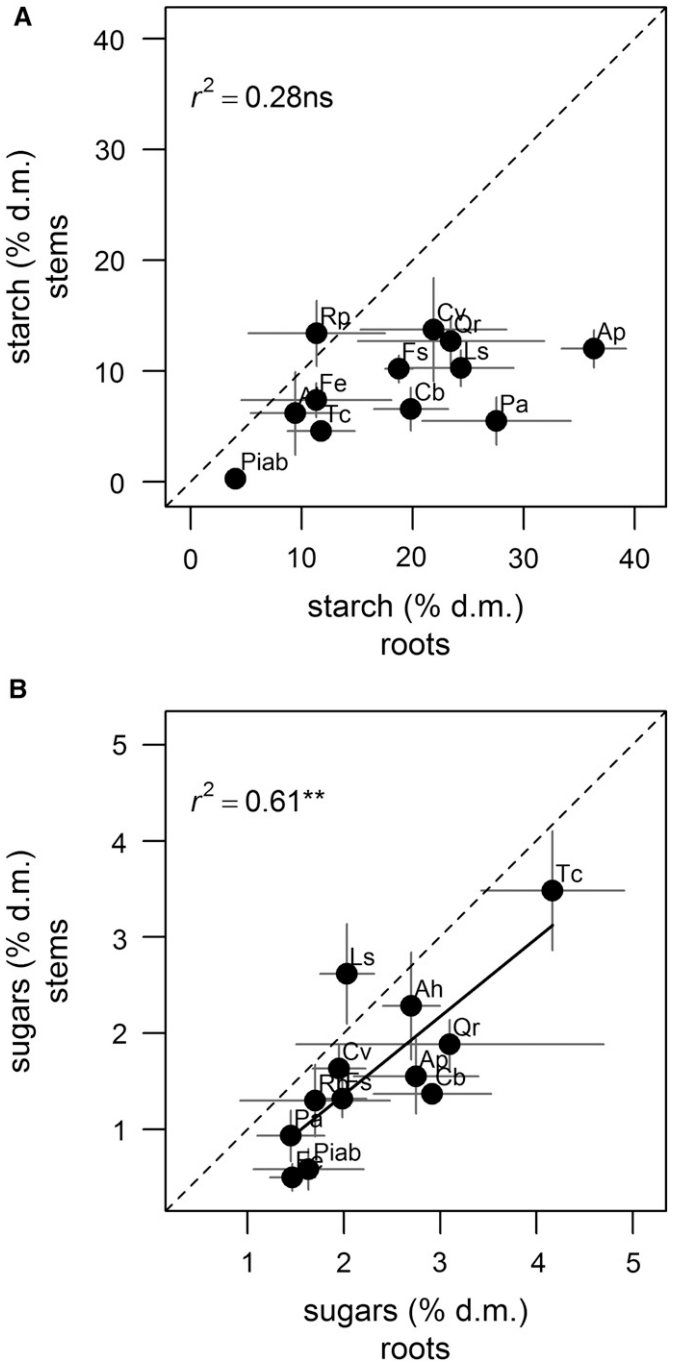

FIGURE 2 Correlation between mean (±SD) root and stem concentrations of (A) starch and (B) soluble sugars in 12 temperate species. Abbreviations of species names are defined in Table 1. ns = nonsignificant relationship ($P > 0.05$), **significant relationship with $P \geq 0.01$; $n = 6$. Reference lines showing a theoretical 1:1 relationship are plotted as dashed lines; solid line represents the linear regression.

by lower starch levels, while the soluble sugar fractions were not significantly different between temperate and tropical trees (Table 2). However, NSC concentrations varied markedly among the four tropical species studied. *Brosimum* sp. showed a NSC concentration of 7.7 ± 3.7%, which is comparable to the lower-end concentrations in the stems of temperate angiosperms. In contrast, *Ceiba pentandra*, *Pentaclethra macroloba*, and *Warszewiczia coccinea* had lower NSC concentrations than any of the temperate angiosperm species (Fig. 1B).

RAP and LFs anatomy—RP was present in all species investigated with a mean area fraction of 15.9 ± 5.4%. AP was found in all specimens (mean area fraction 10.0 ± 9.0%) except in the stems of *Picea abies* and *Warszewiczia coccinea*. Nonseptate LFs occurred in *Clematis vitalba* and *Acer pseudoplatanus*, while septate LFs were found in *Warszewiczia coccinea*. In all three species, sparse simple pitting was observed on the walls of LFs. Overall, roots of temperate species exhibited significantly higher fractions of storage cells (i.e., RAP + LFs) than stems (34.9 ± 14.8% vs. 23.8 ± 11.9%, Table 2) with the exception of *Robinia pseudoacacia* and *Quercus robur* where the amount of RAP was comparable between roots and stems, averaging around 33% (Fig. 3A). In most species, both types of wood parenchyma (i.e., RP and AP) were higher in roots than in stems (Table 2). However, two ring-porous species, *Quercus robur* and *Robinia pseudoacacia*, exhibited lower AP area fractions in roots compared with stems, and *Clematis vitalba* and *Fraxinus excelsior* showed an increase in AP only (Fig. 3A). RP represented the dominant fraction of the total RAP, with the contribution of AP being approximately one-third of the total RAP. On average, the relative contribution of AP to the total RAP was about 5% higher in roots than stems. The presence of LFs was particularly noticeable in *Clematis vitalba,* resulting in very high LFs area fractions of 49.1% and 34.4% in roots and stems, respectively, and virtually all fibers were alive and filled with starch (Fig. 4A, E).

The amount of living cells (RAP + LFs) tended to be higher in tropical than in temperate trees (means 34.9 vs. 25.4%, Table 2), although the difference was not statistically significant, presumably due to the high LFs fraction in *Clematis vitalba*. Nevertheless, the four tropical species had significantly higher fractions of RAP compared with the stems of temperate angiosperms (mean difference ± SE: 12.9 ± 5.2, Table 2). *Ceiba pentandra* had the highest amount of RAP reported in this study. The RAP area fraction for the latter reached 56 ± 8.6% and was driven mainly by a high AP content (AP fraction of 38.4 ± 5.3%; Fig. 3B). In contrast, *Warszewiczia coccinea* had a particularly high RP fraction of 25.9 ± 1.8% (Fig. 3B). This value is almost twice as high as the mean RP fraction of all other stems measured in this study.

Starch localization—Staining with Lugol's solution was used to visualize the starch distribution in RP, AP, and LFs (Fig. 4). In temperate species, almost all RAP + LFs cells were filled with starch that completely occupied the cell lumen with tightly packed grains (Fig. 4A–C, E–G). *Tilia cordata* and *Picea abies* (Fig. 4D, H) were two exceptions to this pattern, with starch grains being packed more loosely. In most species, starch grains were present in both vessel-associated RAP cells and the cells that were not in contact with vessels, although a tendency for lower starch accumulation in vessel-associated RAP cells was sometimes apparent (Appendix S1, see Supplemental Data with online version of this article). In the case of *Clematis vitalba*, staining was found in the lumina of all fibers, leaving vessels and tracheids as the only cell types void of starch (Fig. 4A, E, Appendix S1). Besides RAP and LFs, starch grains were also abundant in parenchyma cells of the perimedullary region (i.e., the region surrounding the pith) and in some species (*Quercus robur*, *Carpinus betulus*, and *Liquidambar styraciflua*) were in the pith. In these species, the amount of starch found in the pith tended to decline as the branch age increased. In roots, the central region with

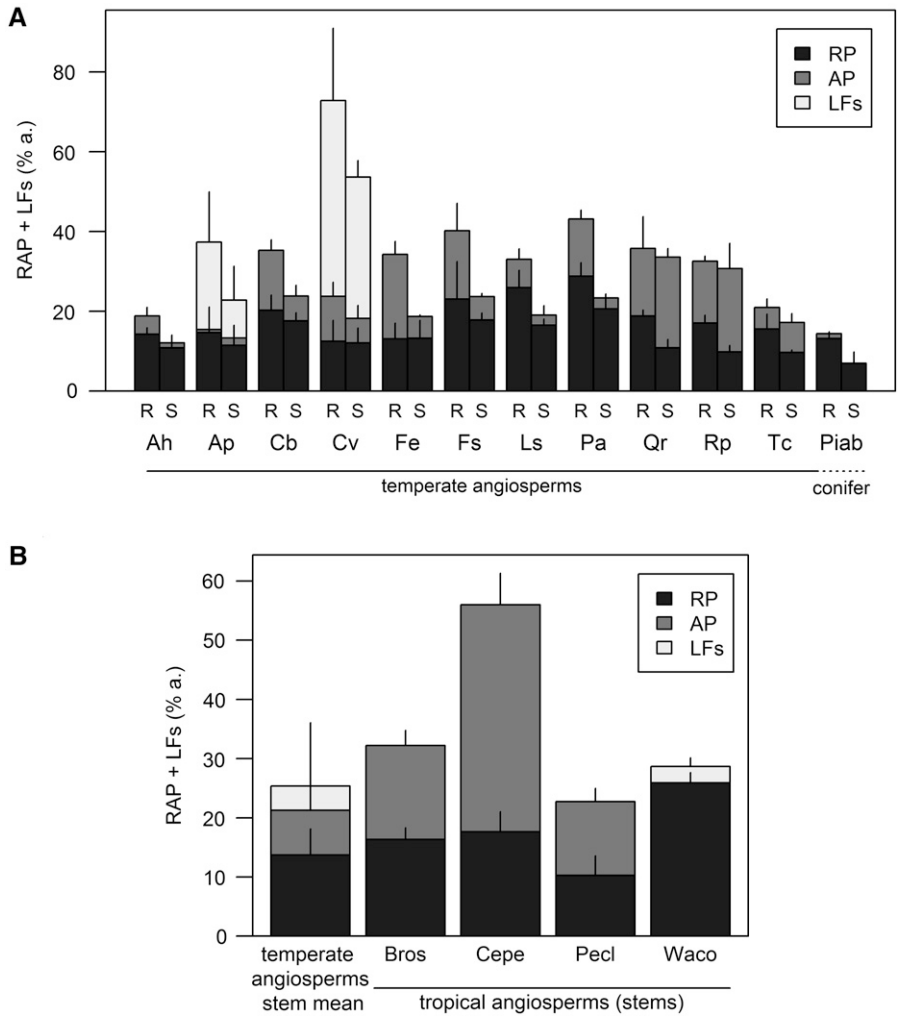

FIGURE 3 Percentage area (% a.) of ray and axial parenchyma (RP + AP = RAP) and living fibers (LFs) in root (R) and stem (S) wood of twelve temperate tree species (A) and in stem wood of four tropical species (B). Means ± SDs (n = 3) are shown. Abbreviations for species are defined in Table 1.

primary xylem appeared sometimes enriched in starch (e.g., *Carpinus betulus*, *Aesculus hippocastanum*). In *Picea abies*, starch was also present in the epithelial cells associated with the resin ducts (Fig. 4D). While starch was generally less abundant in tropical (Fig. 4I–L) than temperate trees (Fig. 4E–H), interspecific differences in starch distribution were observed among the tropical species. In *Ceiba pentandra*, starch grains were present predominantly in RP (Fig. 4I), which was in contrast to *Pentaclethra macroloba* where they were mostly present in the AP (Fig. 4K). Starch grains were also present in the LFs of *Warszewiczia coccinea* (Fig. 4L), while in *Brosimum* sp. they appeared abundant in both RP and AP, similar to that of temperate species (Fig. 4J).

Relationship between NSCs and RAP—There was a strong positive correlation ($P < 0.001$, $r^2 = 0.64$) between the NSC concentration and the RAP + LFs fraction in temperate species when the data for *Clematis vitalba* were excluded (Fig. 5A). The contrasting relationship between NSCs and RAP + LFs in *C. vitalba* compared with the temperate trees was likely due to the lower storage capacity of thick-walled LFs that were particularly prominent in *C. vitalba* (Fig. 5C). The relationship between NSCs and RAP + LFs was significant with $r^2 > 0.5$ when either the data for roots and stems were analyzed together or when analyzed separately (Fig. 5A). This relationship became even stronger when the NSC concentrations were expressed per unit wood volume rather than on a gravimetric basis, i.e., when the differences in wood density between species and organs were taken into account (Fig. 5B). In contrast to temperate trees, NSC concentrations in the stems of the four tropical species were independent of the respective RAP + LFs content (Fig. 5C, white squares).

DISCUSSION

In this study, we showed that the differences in NSC concentrations between the young roots and stems of temperate species at the onset of winter dormancy were strongly related to the abundance of RAP (Fig. 5), with LFs contributing to storage in *Clematis vitalba* and *Acer pseudoplatanus*. Thus, our data provide evidence that the amount of RAP can serve as a suitable proxy for the capacity of wood to store NSC. In this regard, our results expand on the list of apparent structure–function relationships identified in xylem, which help us to better understand the vast diversity in wood anatomical traits that evolved in plants.

The visual assessment of starch distribution revealed that virtually all RAP and LFs of temperate trees were filled with starch (Fig. 4A–H), indicating that the entire space available for storage in wood was used at the onset of winter dormancy. Contrary to earlier observations (Braun and Wolkinger, 1970; Braun, 1984), there was no clear distinction in starch accumulation between vessel-associated RAP cells and the RAP cells that are not in direct contact with vessels (Appendix S1). Our results also showed that both types of interconnected wood parenchyma, i.e., ray (RP) and axial parenchyma (AP) as a whole, contribute greatly to NSC storage. While RP represented the dominant part of the total RAP in most of the temperate species investigated in this study, abundant AP resulted in a substantial increase in the total RAP of some species, for example, in *Quercus robur* and *Robinia pseudoacacia*. AP fractions, often accounting for more than 40% of the total RAP, were higher in the roots than in the stems of the temperate species (Fig. 3A). It is possible that an increased need for mechanical support requires a strong fiber matrix that may limit the occurrence of thin-walled AP in self-supporting stems.

Alternatively, thick-walled LFs could take on the storage function without compromising wood mechanical strength (Carlquist, 2014, 2015). Among temperate species included in this study, *Clematis vitalba* showed particularly high (up to 50% of the total cross-sectional area) proportions of LFs in both roots and stems (Figs. 3A, 4A, 4E; Appendix S1). Considering its high RAP + LFs fraction, the NSC levels measured in *Clematis vitalba* were relatively low (Fig. 5C). The lower NSC storage efficiency (defined as the NSC concentration per

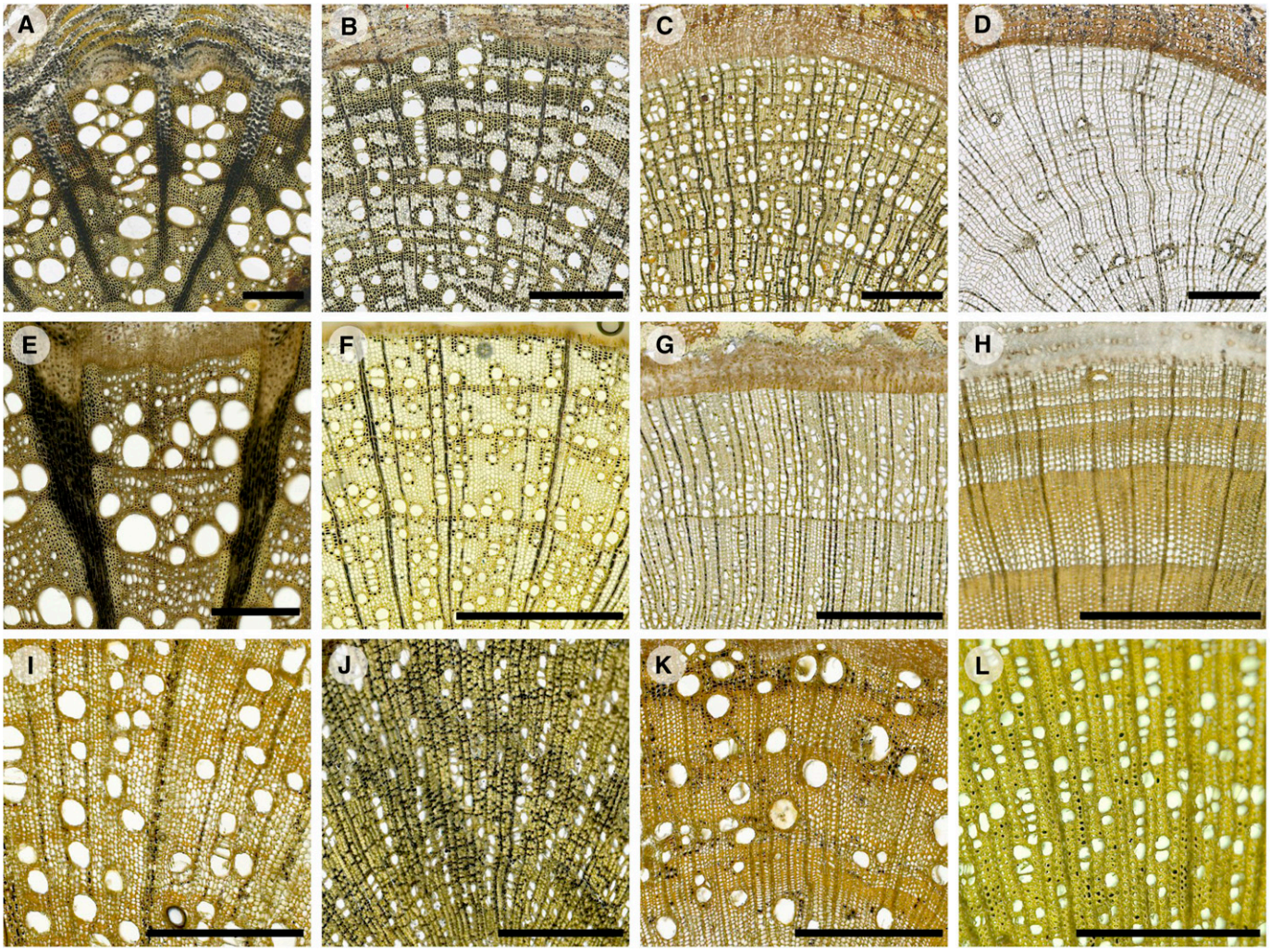

FIGURE 4 Transverse sections of (A–D) roots and (E–L) stems stained with Lugol's solution showing the spatial distribution of starch in wood (stained black) in temperate species (A, E) *Clematis vitalba*, (B, F) *Acer pseudoplatanus*, (C, G) *Aesculus hippocastanum*, and (D, H) *Picea abies* and in tropical species (I) *Ceiba pentandra*, (J) *Brosimum* sp., (K) *Pentaclethra macroloba*, and (L) *Warszewiczia coccinea*. Starch was present in ray and axial parenchyma of all species, although the staining intensity varied from high (A, B, E, F, J) to low (D, G, H, I, K, L). In some species, starch was also present in living fibers (A, B, E, F, L). Scale bars = 500 µm.

unit RAP + LFs area) in this species might be attributed to a lower ratio between cell lumen and cell wall fractions in storage tissue composed of LFs instead of AP. On the other hand, the storage capacity of LFs in *Acer pseudoplatanus* appeared to be in line with that of the other temperate species relying solely on parenchyma (Fig. 5). Whether LFs may provide a storage potential comparable to AP should be tested for a larger number of species. There is evidently a continuum in the dimensions and wall-to-lumen ratios of AP and LFs across species (Carlquist, 2014), and the anatomical variability of these cells, including their pit dimensions (especially pit size and density), should be more thoroughly documented to better understand its influence on the storage and mechanical properties of wood. Investments in thicker cell walls together with the occurrence of less extensive pitting in LFs, thus resulting in a lower storage capacity and lower accessibility and mobility of stored nutrients, might be factors that favor the occurrence of the typically thin-walled AP.

Due to the higher RAP fraction, roots were able to store more NSC than stems were (Fig. 1A, Table 2), with the difference being about 2.5-fold on average and 6.5-fold at maximum. This finding highlights the important contribution of belowground biomass to the overall NSC storage pool. The NSC concentrations of roots and stems of the same species were only partially correlated (Fig. 2), showing that the division of NSC reserves between below- and aboveground woody biomass is variable across species. The variation observed might relate to species- and organ-specific differences in phenology and subsequent growth dynamics. While little is known about the coordination between root and shoot phenology (Steinaker et al., 2009), large intraspecific variation in the timing and rates of root growth has recently been observed in a dozen temperate trees (McCormack et al., 2014). It is possible that the availability of NSC reserves could play a major role in driving these differences in root growth.

In this study, we focused on NSC storage in young woody organs that consist of juvenile sapwood located in close proximity to the apical meristems. Mature wood in tree trunks also represents important sites of NSC storage, and it can be assumed that the NSC

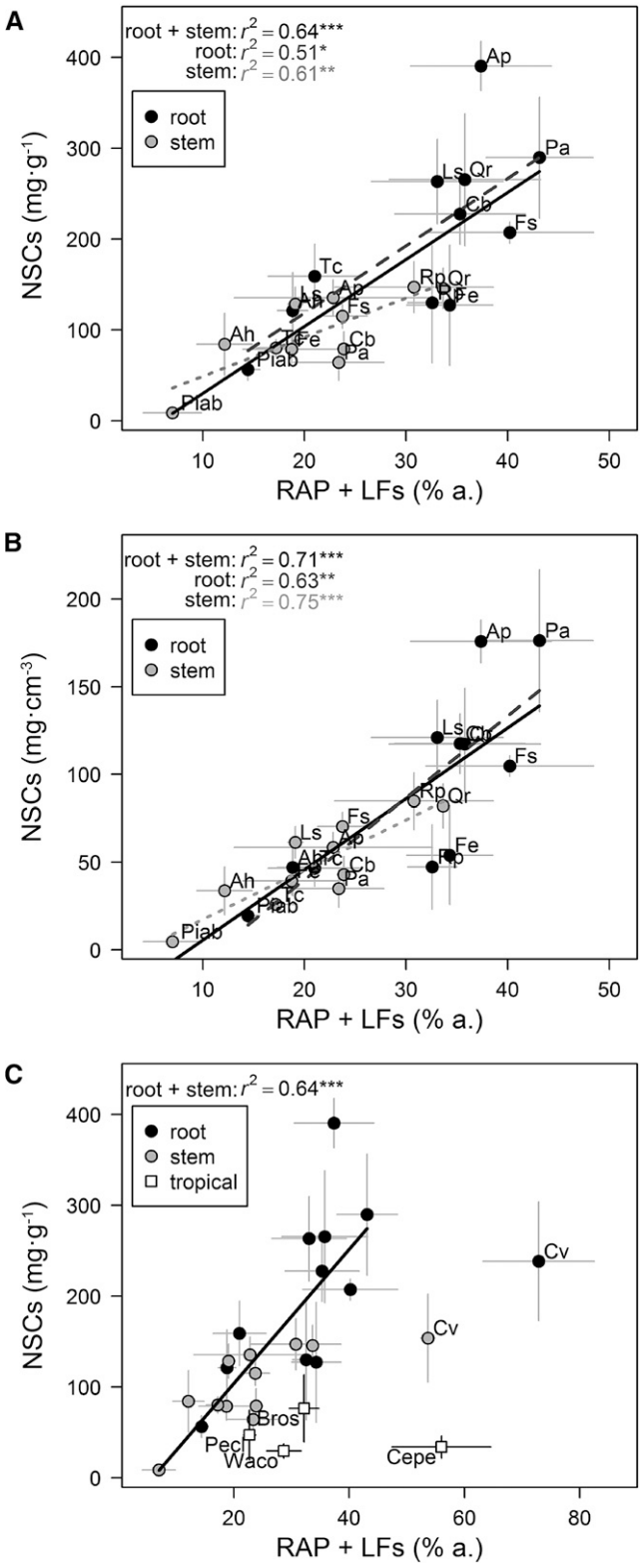

FIGURE 5 Relationship between the amount of wood parenchyma (RAP) and living fibers (LFs) and nonstructural carbohydrate (NSC) concentrations in sapwood of roots (black circles) and stems (gray circles) of temperate trees (A, B). Sapwood NSC concentrations were expressed on a (A) gravimetric or a (B) volumetric basis. Means ± SDs (n = 3–6) are shown. Linear regression lines through all (solid black line), root (dashed dark gray line), and stem (dotted light gray line) data and the corresponding regression coefficients (r^2) are indicated; significance of linear relationship: *$P \leq 0.05$, **$P \leq 0.01$, ***$P \leq 0.001$. Abbreviations of species are defined in Table 1. The same data as in (A) are presented in (C) with the data for the temperate liana *Clematis vitalba* (Cv) and four tropical species (white squares). Both *Clematis vitalba* and the tropical species were excluded from the correlation because they had lower NSC concentrations than in the temperate trees in spite of their high amount of RAP and LFs.

stored in trunks provide the primary source of energy and material for the resumption of cambial activity at the beginning of the growing season (Hill et al., 1995). In tree trunks, not only the RAP content determines the total NSC storage potential, but so does the amount of sapwood, as the death of RAP cells associated with heartwood formation makes these cells unavailable for NSC storage (Magel et al., 1994). The RAP fractions in mature wood from tree trunks may also differ from that in juvenile wood in branches, although no significant differences were found in AP, RP, and RAP between trunks and branches of 34 tree species (Morris et al., 2016).

Compared with levels in temperate trees, the NSC levels of the four tropical species included in this study were significantly lower (Fig. 1B) in spite of their on average higher RAP + LFs content (Fig. 3B). This finding is not surprising considering that the wood tissue of the tropical trees used for NSC analyses was collected during active growth in the case of tropical trees, whereas the samples of the temperate trees were taken at the onset of winter dormancy. In fact, the tropical trees studied here never experience dormancy in their native habitat and thus may not require large reserves for the resumption of growth.

The finding that NSC and RAP data were not correlated in the tropical trees (Fig. 5C) may indicate that, in some cases, RAP plays a less important role in NSC accumulation, but might have various alternative functions. Interestingly, the abundant AP in *Ceiba pentandra* was essentially void of starch grains (Fig. 4I), and the soluble sugar fraction was not noticeably higher either (Fig. 1B). This finding suggests that the accumulation of NSC is not the primary function of AP in *C. pentandra*. It is possible that AP serves as an important water-storage reservoir in this fast-growing tropical pioneer that often colonizes forest gaps and copes with increased evaporative demands. In support of this idea, the role of RAP in stem water storage has already been proposed (Borchert and Pockman, 2005), and a high sapwood hydraulic capacitance was recently measured in another representative of the same genus (*C. speciosa*; Carrasco et al., 2015). Besides storing water, RAP is also known to play a part in defense against pathogens (Schwarze, 2007), which is a function that might be particularly important in diverse tropical ecosystems (Bagchi et al., 2014). An additional explanation for the higher levels of RAP in tropical compared with temperate species may be that the tropical trees do not need to protect their living cells from cold-induced damage. Since protection against cold is energetically costly, it may limit the RAP abundance in environments where frost frequently occurs (Morris et al., 2016). However, more research across a broader selection of tropical species is needed to establish firm links between NSC accumulation, functional traits of RAP and plant ecological strategies.

In conclusion, the results of this study demonstrate that the amount of RAP and LFs is strongly related to the NSC storage capacity in the wood of temperate-deciduous trees. Because virtually all RAP and LFs of temperate trees were filled with starch, the

values of NSC concentrations measured here at the onset of winter dormancy provide estimates of the seasonal maxima. In contrast to the RAP in temperate trees, the RAP in species growing in a tropical environment with little or no seasonality may have a more diverse set of functions. Future research should move beyond a static approach of studying NSC and focus on the functional questions related to NSC transport, conversion, and use (Richardson et al., 2013, 2015; Klein and Hoch, 2015). It can be expected that these processes are tightly coupled to RAP connectivity and the activity of various carbohydrate-modifying enzymes and transporters within the RAP cells (Sauter et al., 1973; Decourteix et al., 2006, 2008).

ACKNOWLEDGEMENTS

The authors thank the Botanical Garden of Ulm University and Reserva Biológica Tirimbina in Costa Rica for access to plant material. The authors also wish to thank Jan Plavec and Hana Plavcová for help with fieldwork and Gaby Wiest-Danner, Mohammad Khatamirad, and Sandra Schmid for technical assistance in the laboratory. L.P. was supported by a Postdoctoral Fellowship from the Alexander von Humboldt Foundation and acknowledges funding from the Ulm University and Ulm University Society (Ulmer Universitätsgesellschaft). H.M. and S.J. acknowledge financial support from the German Research Foundation (DFG, project number 2174).

LITERATURE CITED

Anderegg, W. R. L., J. A. Berry, D. D. Smith, J. S. Sperry, L. D. L. Anderegg, and C. B. Field. 2012. The roles of hydraulic and carbon stress in a widespread climate-induced forest die-off. *Proceedings of the National Academy of Sciences* 109: 233–237.

Baas, P. 1982. Systematic, phylogenetic, and ecological wood anatomy—History and perspectives. *In* P. Baas [ed.], New perspectives in wood anatomy, 23–58. Springer, Dordrecht, Netherlands.

Bagchi, R., R. E. Gallery, S. Gripenberg, S. J. Gurr, L. Narayan, C. E. Addis, R. P. Freckleton, and O. T. Lewis. 2014. Pathogens and insect herbivores drive rainforest plant diversity and composition. *Nature* 506: 85–88.

Barbaroux, C., N. Bréda, and E. Dufrêne. 2003. Distribution of above-ground and below-ground carbohydrate reserves in adult trees of two contrasting broad-leaved species (*Quercus petraea* and *Fagus sylvatica*). *New Phytologist* 157: 605–615.

Borchert, R., and W. T. Pockman. 2005. Water storage capacitance and xylem tension in isolated branches of temperate and tropical trees. *Tree Physiology* 25: 457–466.

Braun, H. 1984. The significance of the accessory tissues of the hydrosystem for osmotic water shifting as the second principle of water ascent, with some thoughts concerning the evolution of trees. *IAWA Bulletin* 5: 275–294.

Braun, H., and F. Wolkinger. 1970. Zur funktionellen Anatomie des axialen Holzparenchyms und Vorschläge zur Reform seiner Terminologie. *Holzforschung-International Journal of the Biology, Chemistry, Physics and Technology of Wood* 24: 19–26.

Carlquist, S. 2001. Comparative wood anatomy: Systematic, ecological, and evolutionary aspects of dicotyledon wood. Springer Science & Business Media, Berlin, Germany.

Carlquist, S. 2014. Fibre dimorphism: Cell type diversification as an evolutionary strategy in angiosperm woods. *Botanical Journal of the Linnean Society* 174: 44–67.

Carlquist, S. 2015. Living cells in wood. 1. Absence, scarcity and histology of axial parenchyma as keys to function. *Botanical Journal of the Linnean Society* 177: 291–321.

Carlquist, S. 1984. Vessel grouping in dicotyledon wood: Significance and relationship to imperforate tracheary elements. *Aliso: A Journal of Systematic and Evolutionary Botany* 10: 505–525.

Carrasco, L. O., S. J. Bucci, D. Di Francescantonio, O. A. Lezcano, P. I. Campanello, F. G. Scholz, S. Rodríguez, et al. 2015. Water storage dynamics in the main stem of subtropical tree species differing in wood density, growth rate and life history traits. *Tree Physiology* 35: 354–365.

Czaninski, Y. 1977. Vessel-associated cells. *IAWA Bulletin* 3: 51–55.

Decourteix, M., G. Alves, M. Bonhomme, M. Peuch, K. B. Baaziz, N. Brunel, A. Guilliot, et al. 2008. Sucrose (JrSUT1) and hexose (JrHT1 and JrHT2) transporters in walnut xylem parenchyma cells: Their potential role in early events of growth resumption. *Tree Physiology* 28: 215–224.

Decourteix, M., G. Alves, N. Brunel, T. Améglio, A. Guilliot, R. Lemoine, G. Petel, and S. Sakr. 2006. JrSUT1, a putative xylem sucrose transporter, could mediate sucrose influx into xylem parenchyma cells and be up-regulated by freeze–thaw cycles over the autumn–winter period in walnut tree (*Juglans regia* L.). *Plant, Cell & Environment* 29: 36–47.

Drossopoulos, J., and C. Niavis. 1988. Seasonal changes of the metabolites in the leaves, bark and xylem tissues of olive tree (*Olea europaea* L.) II. Carbohydrates. *Annals of Botany* 62: 321–327.

Essiamah, S., and W. Eschrich. 1985. Changes of starch content in the storage tissues of deciduous trees during winter and spring. *IAWA Bulletin* 6: 97–106.

Fahn, A., and B. Leshem. 1963. Wood fibres with living protoplasts. *New Phytologist* 62: 91–98.

Fichtler, E., and M. Worbes. 2012. Wood anatomical variables in tropical trees and their relation to site conditions and individual tree morphology. *IAWA Journal* 33: 119–140.

Galvez, D. A., S. Landhäusser, and M. T. Tyree. 2013. Low root reserve accumulation during drought may lead to winter mortality in poplar seedlings. *New Phytologist* 198: 139–148.

Hacke, U. G., and J. S. Sperry. 2001. Functional and ecological xylem anatomy. *Perspectives in Plant Ecology, Evolution and Systematics* 4: 97–115.

Hearn, D.J. 2009. Descriptive anatomy and evolutionary patterns of anatomical diversification in *Adenia* (Passifloraceae). *Aliso: A Journal of Systematic and Evolutionary Botany* 27: 13–38.

Hill, S., J. Waterhouse, E. Field, V. Switsur, and T. Ap Rees. 1995. Rapid recycling of triose phosphates in oak stem tissue. *Plant, Cell & Environment* 18: 931–936.

Hoch, G. 2015. Carbon reserves as indicators for carbon limitation in trees. *In* U. Lüttge and W. Beyschlag [eds.], Progress in botany, 321–346. Springer, Cham, Switzerland.

Hoch, G., M. Popp, and C. Körner. 2002. Altitudinal increase of mobile carbon pools in *Pinus cembra* suggests sink limitation of growth at the Swiss treeline. *Oikos* 98: 361–374.

Hoch, G., A. Richter, and C. Körner. 2003. Non-structural carbon compounds in temperate forest trees. *Plant, Cell & Environment* 26: 1067–1081.

Jansen, S., B. Choat, and A. Pletsers. 2009. Morphological variation of intervessel pit membranes and implications to xylem function in angiosperms. *American Journal of Botany* 96: 409–419.

Klein, T., and G. Hoch. 2015. Tree carbon allocation dynamics determined using a carbon mass balance approach. *New Phytologist* 205: 147–159.

Kozlowski, T. 1992. Carbohydrate sources and sinks in woody plants. *Botanical Review* 58: 107–222.

Körner, C. 2003. Carbon limitation in trees. *Journal of Ecology* 91: 4–17.

Lapinski, W., and M. Tschapka. 2013. Habitat use in an assemblage of Central American wandering spiders. *Journal of Arachnology* 41: 151–159.

Magel, E., C. Jay-Allemand, and H. Ziegler. 1994. Formation of heartwood substances in the stemwood of *Robinia pseudoacacia* L. II. Distribution of nonstructural carbohydrates and wood extractives across the trunk. *Trees (Berlin)* 8: 165–171.

Martínez-Cabrera, H. I., C. S. Jones, S. Espino, and H. J. Schenk. 2009. Wood anatomy and wood density in shrubs: Responses to varying aridity along transcontinental transects. *American Journal of Botany* 96: 1388–1398.

Mauseth, J., and B. Plemons-Rodriguez. 1997. Presence of paratracheal water storage tissue does not alter vessel characters in cactus wood. *American Journal of Botany* 84: 815–822.

McCormack, M. L., T. S. Adams, E. A. Smithwick, and D. M. Eissenstat. 2014. Variability in root production, phenology, and turnover rate among 12 temperate tree species. *Ecology* 95: 2224–2235.

McDowell, N., W. T. Pockman, C. D. Allen, D. D. Breshears, N. Cobb, T. Kolb, J. Plaut, et al. 2008. Mechanisms of plant survival and mortality during drought: Why do some plants survive while others succumb to drought? *New Phytologist* 178: 719–739.

Morris, H., L. Plavcová, P. Cvecko, E. Fichtler, M. A. F. Gillingham, H. I. Martínez-Cabrera, D. J. McGlinn, et al. 2016. A global analysis of parenchyma tissue fractions in secondary xylem of seed plants. *New Phytologist* 209: 1553–1565.

Newell, E. A., S. S. Mulkey, and J. S. Wright. 2002. Seasonal patterns of carbohydrate storage in four tropical tree species. *Oecologia* 131: 333–342.

Panshin, A. J., and C. de Zeeuw. 1980. Textbook of wood technology: structure, identification, properties and uses of the commercial woods of the United States and Canada. McGraw-Hill College, Blacklick, Ohio, USA.

Pate, J. S., R. H. Froend, B. J. Bowen, A. Hansen, and J. Kuo. 1990. Seedling growth and storage characteristics of seeder and resprouter species of mediterranean-type ecosystems of SW Australia. *Annals of Botany* 65: 585–601.

Pfautsch, S., J. Renard, M. Tjoelker, and A. Salih. 2015. Phloem as capacitor: Radial transfer of water into xylem of tree stems seems to occur via symplastic transport in ray parenchyma. *Plant Physiology* 167: 963–971.

Pinheiro, J., D. Bates, S. Debroy, D. Sarkar, and R Core Team. 2015. *nlme*: Linear and nonlinear mixed effects models. R package version 3.1-119. Available at http://CRAN.R-project.org/package=nlme.

Plavcová, L., and S. Jansen. 2015. The role of xylem parenchyma in the storage and utilization of non-structural carbohydrates. *In* U. G. Hacke [ed.], Functional and ecological xylem anatomy, 209–234. Springer International Publishing, Cham, Switzerland.

Popp, M., W. Lied, A. J. Meyer, A. Richter, P. Schiller, and H. Schwitte. 1996. Sample preservation for determination of organic compounds: Microwave versus freeze-drying. *Journal of Experimental Botany* 47: 1469–1473.

Quentin, A. G., E. A. Pinkard, M. G. Ryan, D. T. Tissue, L. S. Baggett, H. D. Adams, P. Maillard, et al. 2015. Non-structural carbohydrates in woody plants compared among laboratories. *Tree Physiology* 35: 1146–1165.

R Core Team. 2013. R: A language and environment for statistical computing. R Foundation for Statistical Computing, Vienna, Austria. Available at http://www.R-project.org/.

Richardson, A. D., M. S. Carbone, B. A. Huggett, M. E. Furze, C. I. Czimczik, J. C. Walker, X. Xu, et al. 2015. Distribution and mixing of old and new nonstructural carbon in two temperate trees. *New Phytologist* 206: 590–597.

Richardson, A. D., M. S. Carbone, T. F. Keenan, C. I. Czimczik, D. Y. Hollinger, P. Murakami, P. G. Schaberg, and X. Xu. 2013. Seasonal dynamics and age of stemwood nonstructural carbohydrates in temperate forest trees. *New Phytologist* 197: 850–861.

Sala, A., and G. Hoch. 2009. Height-related growth declines in ponderosa pine are not due to carbon limitation. *Plant, Cell & Environment* 32: 22–30.

Saranpää, P., and W. Höll. 1989. Soluble carbohydrates of *Pinus sylvestris* L. sapwood and heartwood. *Trees (Berlin)* 3: 138–143.

Sauter, J. J., and B. van Cleve. 1994. Storage, mobilization and interrelations of starch, sugars, protein and fat in the ray storage tissue of poplar trees. *Trees (Berlin)* 8: 297–304.

Sauter, J. J., W. Iten, and M. H. Zimmermann. 1973. Studies on the release of sugar into the vessels of sugar maple (*Acer saccharum*). *Canadian Journal of Botany* 51: 1–8.

Schindelin, J., I. Arganda-Carreras, E. Frise, V. Kaynig, M. Longair, T. Pietzsch, S. Preibisch, et al. 2012. Fiji: An open-source platform for biological-image analysis. *Nature Methods* 9: 676–682.

Schwarze, F. W. 2007. Wood decay under the microscope. *Fungal Biology Reviews* 21: 133–170.

Sokolowska, K., and B. Zagórska-Marek. 2012. Symplasmic, long-distance transport in xylem and cambial regions in branches of *Acer pseudoplatanus* (Aceraceae) and *Populus tremula* × *P. tremuloides* (Salicaceae). *American Journal of Botany* 99: 1745–1755.

Steinaker, D. F., S. D. Wilson, and D. A. Peltzer. 2009. Asynchronicity in root and shoot phenology in grasses and woody plants. *Global Change Biology* 16: 2241–2251.

Van Bel, A. J. 1990. Xylem–phloem exchange via the rays: The undervalued route of transport. *Journal of Experimental Botany* 41: 631–644.

Wheeler, E., P. Baas, and S. Rodgers. 2007. Variations in dicot wood anatomy: A global analysis based on the InsideWood database. *IAWA Journal* 28: 229–258.

Wiley, E., and B. Helliker. 2012. A re-evaluation of carbon storage in trees lends greater support for carbon limitation to growth. *New Phytologist* 195: 285–289.

Wolkinger, F. 1970. Das Vorkommen lebender Holzfasern in Sträuchern und Bäumen. *Phyton* 14: 55–67.

Würth, M. K., S. Pelaez-Riedl, S. J. Wright, and C. Körner. 2005. Non-structural carbohydrate pools in a tropical forest. *Oecologia* 143: 11–24.

Zheng, J., and H. I. Martínez-Cabrera. 2013. Wood anatomical correlates with theoretical conductivity and wood density across China: Evolutionary evidence of the functional differentiation of axial and radial parenchyma. *Annals of Botany* 112: 927–935.

Ziemińska, K., D. W. Butler, S. M. Gleason, I. J. Wright, and M. Westoby. 2013. Fibre wall and lumen fractions drive wood density variation across 24 Australian angiosperms. *AoB Plants* 5: plt046.

American Journal of Botany

RESEARCH ARTICLE

INVITED SPECIAL ARTICLE
For the Special Section: The Biology of Wood

Vessel-associated cells in angiosperm xylem: Highly specialized living cells at the symplast–apoplast boundary

Hugh Morris[1,2,7], Lenka Plavcová[3], Mustapha Gorai[4], Matthias M. Klepsch[1], Martyna Kotowska[1,5], H. Jochen Schenk[6], and Steven Jansen[1]

Manuscript received 10 July 2017; revision accepted 13 November 2017.

[1] Ulm University, Institute of Systematic Botany and Ecology, Albert-Einstein-Allee 11, 89081, Ulm, Germany

[2] Laboratory for Applied Wood Materials, Empa-Swiss Federal Laboratories for Materials Testing and Research, St. Gallen, Switzerland

[3] University of Hradec Králové, Department of Biology, Faculty of Science, Rokitanského 62, 500 03, Hradec Králové, Czech Republic

[4] University of Gabes, Higher Institute of Applied Biology of Medenine, Medenine, 4119, Tunisia

[5] Macquarie University, Department of Biological Sciences, North Ryde, NSW 2109, Australia

[6] California State University Fullerton, Department of Biological Science, 800 N. State College Blvd., Fullerton, CA 92831-3599, USA

[7] Author for correspondence (e-mail: hugh.morris@empa.ch)

Citation: Morris, H., L. Plavcová, M. Gorai, M. M. Klepsch, M. Kotowska, H. J. Schenk, and S. Jansen. 2018. Vessel-associated cells in angiosperm xylem: Highly specialized living cells at the symplast–apoplast boundary. *American Journal of Botany* 105(2): 1–10.

doi:10.1002/ajb2.1030

BACKGROUND: Vessel-associated cells (VACs) are highly specialized, living parenchyma cells that are in direct contact with water-conducting, dead vessels. The contact may be sparse or in large tight groups of parenchyma that completely surrounds vessels. VACs differ from vessel distant parenchyma in physiology, anatomy, and function and have half-bordered pits at the vessel-parenchyma juncture. The distinct anatomy of VACs is related to the exchange of substances to and from the water-transport system, with the cells long thought to be involved in water transport in woody angiosperms, but where direct experimental evidence is lacking.

SCOPE: This review focuses on our current knowledge of VACs regarding anatomy and function, including hydraulic capacitance, storage of nonstructural carbohydrates, symplastic and apoplastic interactions, defense against pathogens and frost, osmoregulation, and the novel hypothesis of surfactant production. Based on microscopy, we visually represent how VACs vary in dimensions and general appearance between species, with special attention to the protoplast, amorphous layer, and the vessel-parenchyma pit membrane.

CONCLUSIONS: An understanding of the relationship between VACs and vessels is crucial to tackling questions related to how water is transported over long distances in xylem, as well as defense against pathogens. New avenues of research show how parenchyma-vessel contact is related to vessel diameter and a new hypothesis may explain how surfactants arising from VAC can allow water to travel under negative pressure. We also reinforce the message of connectivity between VAC and other cells between xylem and phloem.

KEY WORDS amorphous layer; aquaporin; axial parenchyma; black cap; deep supercooling; half-bordered pit; pit membrane; ray parenchyma; water transport; xylem.

Xylem is often described as a "dead tissue" where water movement through hollow pipes is governed by physical forces. Yet, all flowering plants with vessels are quite often surrounded by a sleeve of highly specialized living parenchyma cells. Parenchyma cells in direct contact with vessels are called vessel-associated cells (VACs), a term coined by Czaninski (1964) and still in broad use today (Salleo et al., 2004; Morris et al., 2018; Schenk et al., 2017; Secchi et al., 2017). VACs have a number of highly specialized traits that distinguish them from other parenchyma cells and imply highly specialized functions due to their unique position as the boundary between symplast and apoplast.

VACs differ both anatomically and functionally from vessel-distant parenchyma cells (Fig. 1A–D; Czaninski, 1964, 1977, 1987) and have been described in a large range of herbaceous and woody plants (Foster, 1967; Fujita et al., 1975; Catesson et al., 1982). In contrast to VACs, vessel-distant cells lack direct contact with tracheary elements: they can be ray parenchyma cells positioned between the outer layers in multiseriate rays or can be axial parenchyma cells in various paratracheal arrangements around vessels (Fig. 1B, 1D). In paratracheal arrangements of axial parenchyma, VACs completely surround the vessels in most cases while the vessel-distant axial parenchyma forms multiple

layers beyond the VAC (e.g., *Prosopsis chilensis*, Fig. 1D), often extending to link up with other vessels and ray parenchyma in the secondary xylem (Metcalfe and Chalk, 1983; Braun, 1970, 1984; IAWA Committee, 1989; Morris and Jansen, 2016). The result is a highly interconnected three-dimensional ray and axial parenchyma lattice (Spicer, 2014) connecting beyond the cambium to the phloem (Sokołowska, 2013). In plants that do not have vessels, the term contact cell is used to describe parenchyma in direct association with tracheary elements (Sauter, 1966; Sauter et al., 1973; Zhang et al., 2017).

Our understanding of the unique ultrastructure of cell wall layers of VACs (Fujii et al., 1980) exceeds our knowledge of their function, little of which has direct experimental support. In this review, we focus primarily on six principal features of VACs that separate them in anatomy and function from vessel distant cells: the protoplast, the plasma membrane, the amorphous layer, the vessel-parenchyma pit membrane, the black cap, and the pit connections to other living cells. The ultrastructure is discussed first and followed by functional aspects, which are also summarized in Table 1.

THE ULTRASTRUCTURE OF VESSEL-ASSOCIATED CELLS

The protoplast

In contrast to vessel-distant cells (Gunning et al., 1968; Gunning and Pate, 1974), VACs are small with large nuclei, plentiful mitochondria, dense cytoplasm, many ribosomes, typically small vacuoles, and a well-developed endoplasmic reticulum (Figs. 2A, B, D, E, L; Czaninski and Catesson, 1969; Czaninski, 1977; Fromard et al., 1995; Alves et al., 2001, 2007; Lalonde et al., 2001). VACs also have plastids that are fewer or/and smaller than in more typical parenchyma cells (Fromard et al., 1995). Starch located in amyloplasts can be stored in the VACs of ray and axial parenchyma, but in much smaller quantities and for shorter storage periods than the larger vessel-distant cells (Sauter, 1966; Essiamah and Eschrich, 1985; Fromard et al., 1995; Plavcová and Jansen, 2015; Plavcová et al., 2016). Chloroplasts in the VACs closer to the bark where light can still penetrate have been observed in a range of mangrove species (Schmitz et al., 2012), in *Cucurbita maxima* (Buvat, 1989), and in xylem of a leaf petiole in *Acer pseudoplatanus*, with typically one

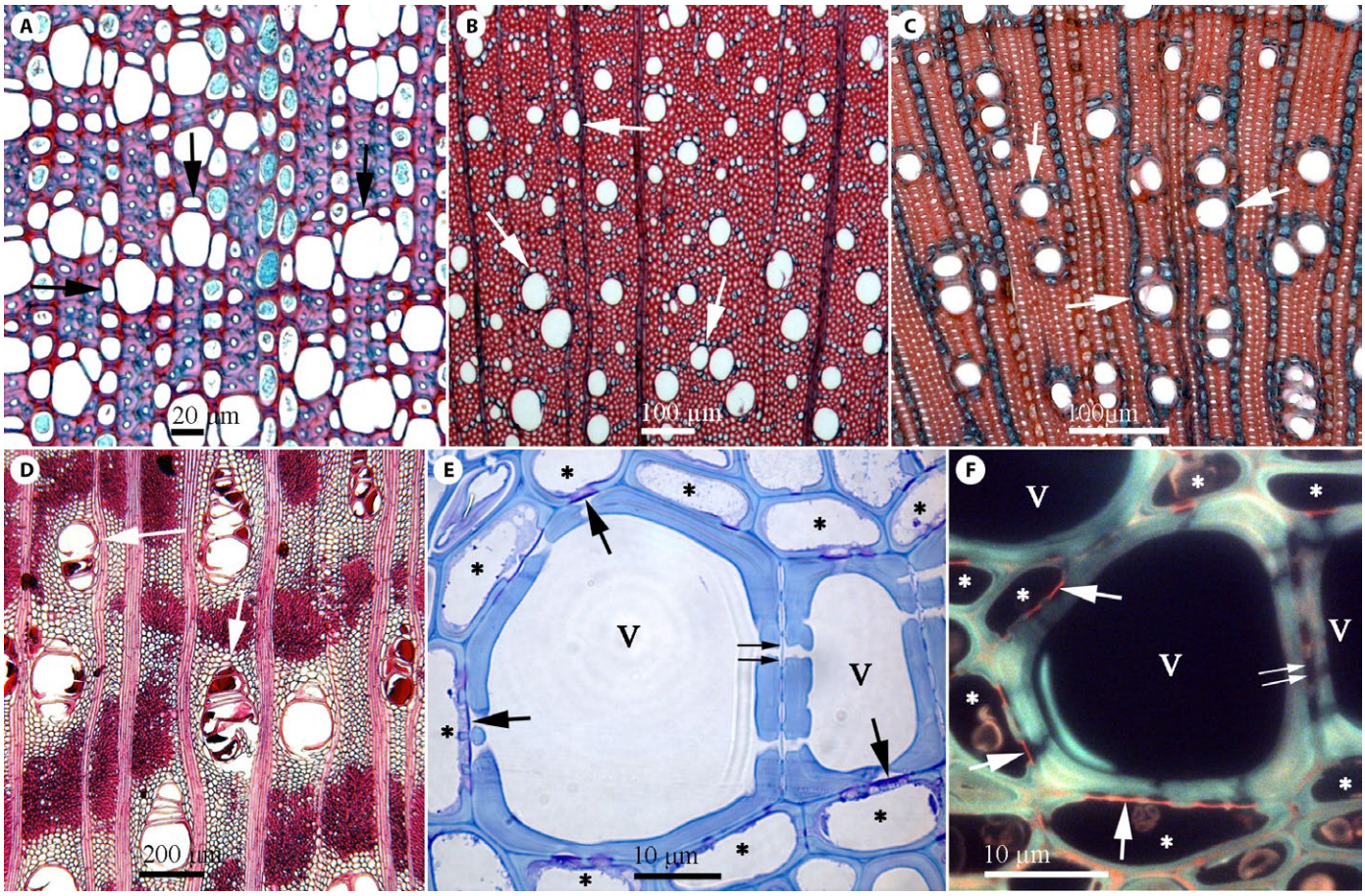

FIGURE 1. Light micrographs of transverse wood sections stained with safranin and alcian blue showing different patterns of vessel-associated parenchyma cells (arrows in A–D) defined as ray and axial parenchyma cells that are directly connected to vessels. (A) *Abelia serrata* (Dipsaceae). (B) *Cercocarpus ledifolius* (Rosaceae). (C) *Ziziphus jujuba* (Rhamnaceae). (D) *Prosopis chilensis* (Fabaceae). (E) *Triadica sebiferum* (Euphorbiaceae) stained with toluidine blue O; vessel-parenchyma pit membranes (large arrows) between vessel-associated cells (indicated by *) and vessels stain purple intervessel pit membranes (small arrows) stain light blue. (F) *Geijera parviflora* (Rutaceae), fluorescence image after staining with coriphosphine O; pectins associated with vessel-parenchyma pits (large arrows) and primary cell walls stained red; no pectins were found in intervessel pit membranes (small arrows). V = vessel, * = vessel-associated cell.

TABLE 1. Overview of the major functions of vessel-associated parenchyma cells in angiosperm xylem.

Function	Potential significance and key references
Storage	Hydraulic capacitance (Meinzer et al., 2003); embolism avoidance and/or refilling (Clearwater and Goldstein, 2005); storage of nonstructural carbohydrates (Plavcová et al., 2016)
Water transport	Aquaporins (Sakr et al., 2003; Secchi et al., 2016); symplastic and apoplastic xylem–phloem interactions (van Bel, 1990; Pfautsch et al., 2015)
Defense and resilience	Formation of tyloses and gels (Bonsen and Kučera, 1990; Rioux et al., 1998); formation of suberin (Biggs, 1987); supercooling (Wisniewski et al., 1987a, b, 1991a, b, 1993); heartwood formation (Chattaway, 1949); compartmentalization (Schmitt and Liese, 1990; Liese et al., 1995; Morris et al., 2016a)
Osmoregulation	Hydraulic equilibrium with xylem sap; changing the ionic composition and pH of xylem sap (Fromard et al., 1995; Secchi and Zwieniecki, 2016)
Surfactants	Black cap formation, production of xylem sap surfactants (Schenk et al., 2015, 2017)

chloroplast per cell (Fig. 2B). Chloroplasts are presumably found in any parenchyma cell where there is sufficient light.

The plasma membrane

The plasma membrane of VACs have some unique structural features. The amount of some key proteins of the plasma membrane is considered high based on measured activity. For instance, using immunolabeling techniques, VACs show high H^+-ATPase activity along the plasma membrane compared to vessel-distant cells during spring (Fromard et al., 1995; Alves et al., 2001, 2004, 2007; Arend et al., 2002), and parallel levels only shared by the companion cells of the phloem (Bouché-Pillon et al., 1994).

In woody angiosperms, aquaporins (water channel proteins) are present at a high frequency in VACs (Sakr et al., 2003; Almeida-Rodriguez and Hacke, 2012; Secchi et al., 2017). Aquaporins can be found not only in the plasma membrane, but also in the tonoplast of the vacuole. Of the various families of aquaporins known in the plant kingdom (Maurel et al., 2015), PIP1 and PIP2 are the most studied in woody plants, partly due to their role in regulating apoplastic water movement (Secchi et al., 2017). Although aquaporin proteins were present in all vessel-distant cells within xylem and across to the phloem in *Juglans regia*, Sakr et al. (2003) found, using localized immunostaining techniques, that PIP2 aquaporin transcripts were highest in the VACs, possibly related to thaw-induced embolism recovery.

The amorphous layer

Cell walls of VACs are always lignified, and the VACs are connected to other parenchyma cells via simple pits with numerous plasmodesmata traversing a pit membrane (Czaninski 1977, 1979). Between the plasma membrane and the secondary cell wall lies a pecto-cellulosic layer called the amorphous layer (also known as the protective layer; Fig. 2B, D–G, J–L). The amorphous layer forms as adjoining vessels die, and its development possibly involves activity of multivesicular bodies derived from large Golgi vesicles abundant in VACs (Fig. 2B, D, E, L; Halperin and Jensen, 1967; Robards, 1968; Chafe, 1974). The amorphous layer represents an nonlignified extension of the apoplast made up of loose fibrillar cross-linking polysaccharides (Fig. 2G; Fujii et al., 1981), highly esterified pectin, and arabinogalactan proteins (Wisniewski and Davis, 1995; Plavcová and Hacke, 2011; Klepsch et al., 2016).

The amorphous layer varies in length and thickness among species (Fig. 2B–G). It is always present at the pit contact region with the vessel, but often extends along the entire circumference of the secondary wall of the VAC (Wisniewski et al., 1987a, b; Barnett et al., 1993). The structure is commonly thickest at the contact region, as shown in a range of temperate species (Mueller and Beckman, 1984; Barnett et al., 1993; Fig. 2B, E, J); an irregular and extremely thick (>2 μm) amorphous layer was found in the subtropical species *Ziziphus spina-christi* (Fig. 2F, G). The narrowing of the amorphous layer with increased distance from the vessel-parenchyma contact region can be abrupt (Fig. 2B) or gradual (Fig. 2E). Due to its pectocellulosic constituents (Fig. 1F), the amorphous layer is likely highly elastic, possibly allowing it to withstand hydrostatic pressures generated from within vessels (van Bel and van der Schoot, 1988). This layer is also porous, as demonstrated by various traceable apoplastic dyes and forms tyloses that can block or impede the spread of pathogens in the vessels (Wisniewski et al., 1987a, b; Barnett et al., 1993; Rioux et al., 1995, 1998).

The parenchyma-vessel pit membrane

Half-bordered vessel-parenchyma pits are typically larger than simple or indistinctly bordered parenchyma-parenchyma pits (Braun, 1967; van der Schoot and van Bel, 1989; van Bel, 1990). In woody angiosperms, ray cells bordering vessels were found to be particularly large compared to vessel distant rays cells (i.e., isolation cells; Braun, 1967).

The ratio of the contact fraction between the VACs of ray and axial parenchyma varies greatly between species. For instance, axial parenchyma VACs and vessels had greater surface area contact than ray parenchyma VACs and vessels in sugar maple (*Acer saccharum*) (Gregory, 1978). These contact fractions, which represent direct physical contact, depend largely on the amount of axial parenchyma, where more axial parenchyma results in increased connectivity with vessels (Morris et al., 2018). More axial parenchyma in secondary xylem suggests divergence in functions of ray and axial parenchyma, supporting recent findings that a higher axial parenchyma fraction coupled with a tightly packed spatial arrangement around vessels is related to larger vessel sizes, which is hypothesized to be associated with hydraulic maintenance (Fig. 1D; Morris et al., 2018); possible specialization between ray and axial parenchyma poses an interesting question that cannot be answered yet.

Regarding the presence of pectins, strong immunolabeling for low and high methyl-esterified homogalacturonans was evident in ray parenchyma-vessel pit membrane, especially in the amorphous layer, but not in intervessel pit membranes (Plavcová and Hacke, 2011; Kim and Daniel, 2013). Evidence of pectins in the amorphous layer and parenchyma-vessel pit membranes has been confirmed in a range of angiosperm species using several antibodies (Fig. 1F; Rioux et al., 1998; Kim and Daniel, 2013; Herbette et al. 2015;

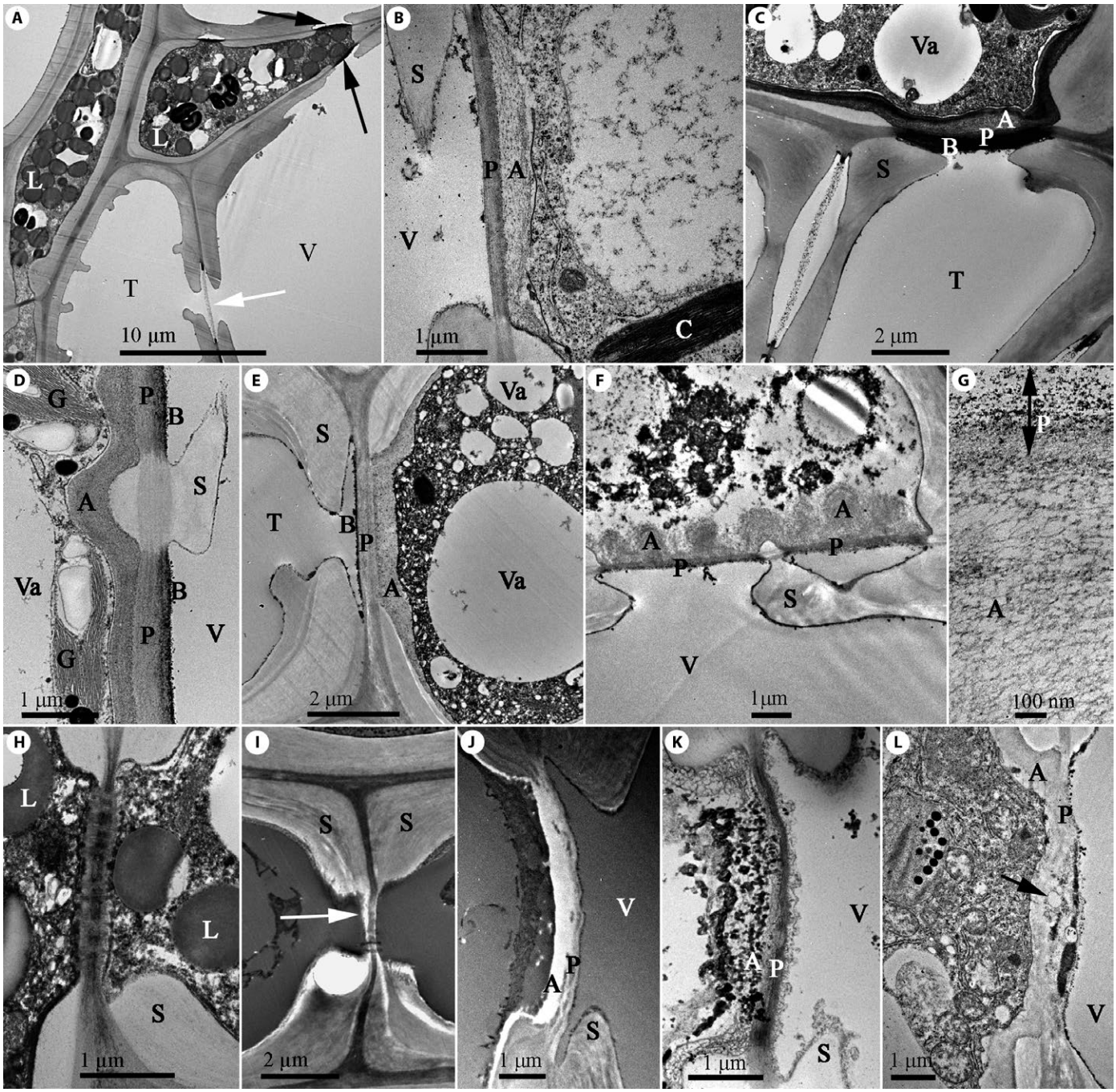

FIGURE 2. Transmission electron micrographs of vessel-associated parenchyma cells and their half-bordered vessel-parenchyma pit membranes in stem xylem (A, C–L) and petiole xylem (B). (A) *Tilia cordata* (Malvaceae), a ray cell (left) and axial parenchyma cell (upper right) near a tracheid and vessel, with vessel-parenchyma pits (black arrows) and a vessel-tracheid pit (white arrow). (B) *Acer pseudoplatanus* (Sapindaceae), vessel-parenchyma pit membrane with amorphous layer, endoplasmatic reticulum, mitochondrion, and chloroplast, but without black cap. (C) *A. pseudoplatanus*, a tracheid-parenchyma pit membrane with a distinct black cap and a tracheid-tracheid bordered pit (bottom left). (D) *A. pseudoplatanus*, detail of two vessel-parenchyma pit membranes and parenchyma protoplast with a well-developed Golgi apparatus. (E) *Acer platanoides*, a tracheid-parenchyma pit membrane with a black cap and amorphous layer. (F) *Ziziphus spina-christi* (Rhamnaceae), vessel-parenchyma pit membrane with a thick, irregular and wavy amorphous layer. (G) *Z. spina-christi*, detail of the vessel-parenchyma pit membrane and amorphous layer with a filamentous, loosely arranged structure. (H) *Tilia cordata*, simple pit between two parenchyma cells with plasmodesmata. (I) *Encelia farinosa* (Asteraceae), simple pit between two parenchyma cells after staining with $KMnO_4$, suggesting lignification of the pit membrane (arrow). (J–L) *Triadica sebiferum* (Euphorbiaceae), vessel-parenchyma pit membrane after (J) fixation with glutaraldehyde only, showing a white, electron transparent amorphous layer; (K) fixation with glutaraldehyde and postfixation with uranyl acetate and staining with lead citrate, showing many electron-dense vesicles within the amorphous layer and a darker pit membrane; and (L) fixation with glutaraldehyde and postfixation with OsO_4, showing a protoplast with endoplasmatic reticulum, mitochondria, and vesicles in the vessel-parenchyma pit membrane (arrow). A = amorphous layer, B = black cap, C = chloroplast, G = Golgi apparatus, L = lipids, P = pit membrane, S = secondary wall, T = tracheid, V = vessel, Va = vacuole.

Klepsch et al., 2016). The presence of pectins in the parenchyma-vessel pits may result from pectins secreted from the abutting parenchyma cell through the amorphous layer, while hydrolytic enzymes remove all noncellulosic compounds in the pit membrane area closest to the vessel lumen during the latest stages of vessel element differentiation (Kim and Daniel, 2013; Herbette et al., 2015). Moreover, similar to intervessel pit membranes (Schmid and Machado, 1968; Wheeler, 1981), parenchyma-vessel pit membranes may undergo seasonal lignificaion as the wood ages, making it more rigid and less permeable, which may have implications for a number of hypothesized functions, such as supercooling (Czaninski, 1973; Chafe, 1974; Fujii et al., 1980; Wisniewski et al., 1991a).

The black cap

On the vessel lumen side of the pit membrane is an electron-dense material called the black cap (Shaffer and Wisniewski, 1989; Plavcová and Jansen, 2015; Schenk et al., 2017) because of its appearance in TEM (Fig. 2C–E). Likely composed of lipids, which also line the inner wall of the conduits and pit border, the black cap is rendered visible only after osmium tetroxide (OsO_4) staining, but not after glutaraldehyde fixation (Fig. 2J) or post-staining with uranyl acetate and lead citrate (Fig. 2K). OsO_4 reacts mainly with the double carbon bonds in unsaturated fatty acid chains of lipids, but also some proteins and lipoprotein complexes, and because osmium is a heavy metal, it is electron dense in TEM (Fineran, 1997; Westhoff et al., 2008; Schenk et al., 2017).

A constituent of the pit membrane, the black cap is found in many angiosperm species (Fig. 2C, D, E), including vesselless angiosperms (Zhang et al., 2017), but can be weakly formed or completely absent in some cases (Fig. 2B), which might be due to seasonal influence. After treatment with ethylene glycol aminoethyl ether (EGTA; egtazic acid), the black cap was shown to be completely separated without having any effect on other pit membrane constituents, indicating that the black cap may be a structure unto itself (Wisniewski et al., 1991a). If lipids in the black cap originate from the protoplasm of the VAC, lipid transport through the amorphous layer and pit membrane could involve nonspecific lipid transfer proteins capable of transporting lipids across cell walls (Li et al., 2016; Misra, 2016). More research is required to understand where lipids are manufactured and the transport mechanism and functional significance behind lipid deposition in the black cap (Schenk et al., 2017).

VAC parenchyma pits

Simple pits or indistinctly bordered pits typically connect VAC to adjacent parenchyma cells (Carlquist, 2007; Plavcová and Jansen, 2015). Pit membranes between VACs and other parenchyma cells are suggested to be lignified (e.g., Fig. 2I; Czaninski 1977, 1979) and crossed by numerous plasmodesmata (Fig. 2H; Czaninski 1977, 1979), indicating that symplastic water movement between neigboring parenchyma cells can occur via plasmodesmata.

STRUCTURE–FUNCTION RELATIONSHIPS OF VACS

Functions of the protoplast and plasma membrane in VACs

High protein activity in the plasma membrane of VACs is hypothesized to be related to the refilling of embolized vessels (Secchi and Zwieniecki, 2016) and presumably to buffer xylem negative pressures through capacitance of living cells around the vessel (i.e., absolute amounts of water released into the vessel per unit decline in water potential; Meinzer et al., 2003).

Besides generating the proton-motive force across the plasma membrane, H^+-ATPase in VAC is involved in the regulation of xylem sap pH, inducing the acidification of the sap (Fromard et al., 1995). In addition, the high activity of metal ions generated by H^+-ATPase and the lower apoplastic pH may result in the release of inorganic ions into the transpiration stream that are thought to regulate xylem hydraulic conductance via the so-called ionic effect (Gascó et al., 2006; Nardini et al., 2011; Secchi and Zwieniecki, 2012, 2016). Along with H^+-ATPase, sucrose and hexose sugar transport proteins (JrHT1 and JrHT2) were found along the plasma membrane of VAC in *Juglans*, which were particularly active before bud break (Decourteix et al., 2006, 2008). Since this discovery, sugar transporters have also been located in the plasma membrane of VACs in *Populus* (PtSUC2.1 and PtSUT2b) (Secchi et al., 2011; Secchi and Zwieniecki, 2010, 2011).

All substances exuded through the plasma membrane, including ions and sugars, have to pass the amorphous layer, which may provide some resistance to passage before the pit membrane and before their eventual exit into the vessel. This system would seem to be ineffective for moving osmotica into vessels, and in fact, no studies to date have observed solute concentrations in vessels that would be large enough to move water via an osmotic gradient from living cells into vessels (Tyree et al., 1999; Enns et al., 2000; Vesala et al., 2003; Clearwater and Goldstein, 2005). Moreover, since the amorphous layer often extends alongside the plasma membrane around the entire circumference of the protoplast, it likely enhances plasma membrane transport and helps channel substances to the vessel-parenchyma pits along the inside of the lignified secondary wall (Barnett et al., 1993). To summarize the Barnett hypothesis, if no protective layer were present, the plasma membrane over most of the protoplast surface would no longer be in contact with the apoplastic system in the way that it is when the wall is nonlignified and porous.

Aquaporins undergo what is termed gating, which makes the plasma membrane impervious to water flow by sealing the protein pores in response to stress-induced changes (Törnroth-Horsedield et al., 2006; Maurel et al., 2016; Groszmann et al., 2017). However, the mechanism of symplastic–apoplastic water movement across membranes/structures in VACs remains poorly understood.

Functions of the amorphous layer

Five key functions of the amorphous layer have been proposed: (1) a protective role to prevent the digestion of protoplasm from autolytic enzymes arising from the vessels (Schmid, 1965; O Brien, 1970), (2) tylosis and/or gel production (Foster, 1967; Murmanis, 1975), (3) deep supercooling to avoid frost damage (Wisniewski and Davis, 1989; Wisniewski et al., 1991b), (4) buffering against oscillations in hydrostatic pressure from within the vessels (van Bel and van der Schoot, 1988), and (5) increase of the surface area at the symplast–apoplast interface, thus allowing for increased exchange across the plasma membrane (Barnett et al., 1993).

The first proposed function gave rise to the term protective layer, a term used as frequently as the amorphous layer. However,

hydrolysis of a pit membrane generally stops more or less at the middle lamella (Evert, 2006; fig. 4B of Schenk et al., 2017). Hence, the protective hypothesis generally lacks support (Czaninski, 1973; Chafe, 1974; Barnett et al., 1993).

A general consensus accepts that the amorphous layer plays a role in tylosis production, where cytoplasm-filled balloon-like sacs from VACs of both ray and axial parenchyma enter the vessels through the half-bordered pit membranes, resulting in partial or full vessel occlusion. In fact, Czaninski (1977) coined the term vessel-associated cells with the function of tyloses or gel secretion in mind (Catesson and Moreau, 1985; De Micco et al., 2016; Morris and Jansen, 2016). Tyloses maintain symplastic continuity with the VACs, where the primary wall of the tylosis is actually an extension of the amorphous layer, which, due to its high porosity, can allow the movement of pectins and other materials from the tylosis into the remaining vessel lumen space (Rioux et al., 1998). However, although an amorphous layer is present in every VAC, tyloses do not occur in all species and were found in ca. 22% of the 172 species studied by Zürcher et al. (1985). Also, there is a higher frequency of tyloses in ray parenchyma than in axial parenchyma (Chattaway, 1949). The latter, however, is likely due to the overall percentage ray and axial parenchyma share within the xylem. Given that ray parenchyma has a relatively consistent xylem cross-sectional fraction (between 5–20% across species), the contact fraction around vessels would largely relate to the high variability of axial parenchyma (between 0 and 60% across species; Morris et al., 2016a, b). Tyloses are also reported to be more common in angiosperms with parenchyma-vessel pit membranes larger than >8 μm in diameter (Zürcher et al., 1985).

Many species exhibit the ability to avoid the lethal effects of freezing in xylem parenchyma through what is termed deep supercooling (Quamme, 1991; Kasuga et al., 2007, 2008), with the colder the region, the greater the levels of resistance (Sakai and Larcher, 1987). Supercooling can be described as the cooling of a liquid below freezing point without becoming solid, while deep supercooling occurs in woody plants that experience severe cold periods, an adaptation that prevents ice propagation, otherwise lethal to the plant (Wisniewski et al., 2004; Neuner, 2014). zThe function of the amorphous layer in preventing the formation of damaging ice crystals purports a role in protection, thus allowing VAC to supercool (Wisniewski and Davis, 1989). The hypothesis proposing the prevention of damaging ice crystals may be the case in temperate species where freezing conditions occur; however, it does not explain the structure's function in tropical species. Moreover, this hypothesis relies on the presence of pectin in the amorphous layer where pectin works as a hydrogel to prevent desiccation of the VAC. Tyloses and gels were found to depend on pectin in the amorphous layer of the species investigated (Rioux et al., 1998). Pectic polysaccharides have been observed in the amorphous layer of a range of angiosperm species (Fig. 1F; Fujii et al., 1981; Mueller and Beckman, 1984; Wisniewski and Davis, 1995; Plavcová and Hacke, 2011; Herbette et al., 2015; Klepsch et al., 2016). However, the amount of pectic polysaccharides varies between species and likely depends on the time of the year in seasonal climates and during the development of the tylosis. Immunolabeling for pectin is greater in the amorphous layer during tylosis development (Rioux et al., 1998). The hypothesis that the amorphous layer may function to protect the VAC against diurnal oscillations of hydrostatic pressure from within the transpiration stream is also plausible, but protection would only be needed at the parenchyma-vessel connection sites, whilst the amorphous layer may completely surround the parenchyma cell protoplasm (Spicer, 2014). Rather than functioning in protection, the hypothesis offered by Barnett (1993), in which the amorphous layer expands the area of exchange between parenchyma and vessels, is the most persuasive, given that it is a consistent feature among species. However, the amorphous layer likely has various functions, depending on the species, the climate type, and the time of year in temperate and seasonal tropical species. More ultrastructural work, coupled with physiological and biochemical measurements, are clearly needed to build on our existing knowledge of this structure.

Functions of the vessel-parenchyma pit membrane

The structure of the vessel-parenchyma pit membrane may have a key role in tylosis formation (Bonsen and Kuĉera, 1990; Rioux et al., 1998), in deep supercooling (Wisniewski et al., 1987a, b, 1991a, b; Wisniewski and Davis, 1995), and in defense against vascular pathogens (Schmitt and Liese, 1990; Liese et al., 1995). The presence of pectin has been hypothesized to be linked to deep supercooling with pectin levels found to be highest in winter and lowest in spring, where, in the latter, pectin is enzymatically removed, coinciding with reduced ability to deep supercool (Wisniewski et al., 1991a). Wisniewski and Davis (1995) hypothesized that pectin acts by forming a barrier during winter months in temperate regions, thus making the pit membrane less permeable to water movement and the propagation of ice crystals, which would otherwise be deleterious to the plant. However, in older wood where rigidity increases due to lignification of the pit region, deep supercooling may not be as effective because lignification decreases permeability.

Rioux et al. (1998) found a close relationship between the presence of pectin in the pit chamber and the adjoining amorphous layer, with tylosis and gel development extending from the VACs into the neighboring vessels to block the pathway to pathogen spread. An important protective trait of intervessel pit membranes is pore size. Small pores in pit membranes between vessels act as a barrier to spores of pathogenic fungi and bacteria in the tracheary elements (Jarbeau et al., 1995; Choat et al., 2003, Choat et al., 2004, 2008; Yadeta and Thomma, 2013). For example, pore sizes were found to be between 5 and 20 nm in diameter in a range of species using colloidal gold particles (Choat et al., 2003; Zhang et al., 2017), while spore sizes of *Xylella fastidiosa* (a bacterium) and *Verticillium* spp. (a fungus) ranged between 0.25 and 2.2 μm, respectively (Mollenhauer and Hopkins, 1974; Qin et al., 2008). We assume that pore size should be similar between intervessel pit membranes and vessel-parenchyma pit membranes, acting as an important barrier to vascular pathogens attempting to gain entry into the VAC. Aside from pore size, substances secreted from VAC in birch modified the vessel-parenchyma pit structure, preventing bacterial degradation of the pits (Liese et al., 1995). Moreover, callose and various antimicrobial proteins in VACs accumulate along the cell walls and the pit membranes abutting infected conduits, which have thickened secondary walls, resulting in a decrease in the size of the parenchyma-vessel pit border and aperture, thus limiting the spread of pathogens (Benhamou, 1995; Hilaire et al., 2001).

Functions of the black cap

The function(s) of the black cap remains relatively unknown. Schaffer and Wisniewski (1989) named the structure and referred to it as a torus-like layer. Recently, the black cap of a phylogenetically

wide range of angiosperm species has been proposed to be composed of amphiphilic, insoluble lipids deriving from xylem sap (Schenk et al., 2017; Zhang et al., 2017). More observational and experimental work is required on xylem sap surfactants and their role in long-distance water transport in plants under negative pressure (Jansen and Schenk, 2015; Schenk et al., 2015, 2017).

Functions of VAC-parenchyma pit connections

VAC-parenchyma pit membranes are likely lignified (Fig. 2I; Czaninski, 1977, 1979), which presumably would inhibit apoplastic water flow between VACs and other living cells. Thus, water flow between VAC and other parenchyma cells may be entirely symplastic through plasmodesmata (Fig. 2L) and may therefore be under some degree of control by the living cells (Sauter and Kloth, 1986; Pfautsch et al., 2015). Also, plasmodesmata have been found to close in response to turgor pressure differences between cells that exceed 200 kPa (Oparka and Prior, 1992). Thus, a sudden increase or decrease of turgor pressure in a VAC could potentially trigger closure of plasmodesmata, which would hydraulically isolate the VAC from its neighbors at least temporarily. Such a mechanism could play a role in refilling of embolized vessels and/or in buffering pressure fluctuations in the xylem.

STORAGE, MOVEMENT, AND CONNECTIVITY OF VACS

VACs, like the companion cells of the phloem, could be viewed as a kind of control center (or a "sorting office"), regulating movement of substances into and out of the vessels. VACs are generally not considered to have the capacity for storage as evidenced by the lack of cell storage compartments, such as a large vacuole. Although starch and other compounds can be present in VACs (e.g., Plavcová et al., 2016), such compounds are probably not stored in large quantities or for very long in the VACs. By contrast, vessel-distant cells (including the isolation cells of the ray system) have been referred to as "storage cells" by Czaninski (1977), a slightly biased functional description given that a morphological continuum exists across the entire symplastic network of the xylem through to the phloem. The term "storage cell" perhaps wrongly implies something sedentary or static, when movement of water and metabolites is continuous throughout the growing season (van Bel, 1990; Salleo et al., 2004, 2009; Pfautsch et al., 2015). However, vessel-distant cells do accumulate tannins, oxalate crystals, proteins, large quantities of starch, and lipids in some species, a trend not observed to the same level in VACs (Buvat, 1989; Sauter and van Cleve, 1994). In contrast, acid phosphatases, peroxidases, and dehydrogenases are higher in VACs than in vessel-distant cells (Sauter, 1972; Sauter et al., 1973; Alves et al., 2001).

Although clear differences exist between VACs and the vessel-distant cells of ray and axial parenchyma, both form part of an elaborate three-dimensional trafficking and communication network that extends from the xylem to the phloem, where there exists a physiological nexus between the two adjacent transport systems (Hölttä et al., 2009; Sevanto et al., 2011, 2014; Pfautsch et al., 2015). Along this pathway, hormones, solutes, and metabolites pass from cell to cell, where substances are either stored long-term or moved along, depending on the level of enzymatic activity in the VACs of the xylem and in the companion cells of the phloem. On both sides of the cambium, inward and outward solute fluxes are managed at the level of the plasma membrane (van Bel, 1990; Evert, 2006). Using a fluorescein dye to study water transport between phloem and xylem, Pfautsch et al. (2015) showed that movement occurred over a water potential gradient along the ray symplastic pathway, with no evidence of apoplastic movement. Water is likely transported through the symplast in two ways: (1) through plasmodesmata (Höll, 1975) and (2) across cellular membranes, likely aided by aquaporins (Sevanto et al., 2011; Afzal et al., 2016). The VACs trigger the movement of water from the phloem as evidenced by the contraction of bark owing to phloem tissue hydraulic capacitance (Mencuccini et al., 2013), a process driven by changes in water potentials across the transport system. High mRNA transcript levels for three specific aquaporin genes in the cambium, phloem, and ray parenchyma demonstrate hydraulic coupling between the phloem and xylem (Almeida-Rodriguez et al., 2012). Although active transport is known to facilitate phloem uploading and movement between ray parenchyma cells from phloem to xylem occurs symplastically, the mechanism behind the exchange of substances between the VACs and the dead tracheary elements has long been debated (Münch, 1930; Zeigler, 1975; Sauter, 1982; Salleo et al., 2004; Zwieniecki and Holbrook, 2009; Secchi and Zwieniecki, 2016).

CONCLUSIONS

The association between VACs and vessels is not exclusive, but part of a large symplastic three-dimensional connectivity with vessel-distant cells of ray and axial parenchyma, which extends through the rays and into the phloem via plasmodesmata. Future research is required to address three-dimensional reconstructions within the xylem along with quantitative measurements to help underpin structure–function relationships between parenchyma, fibers, and conduits. Additional questions to be tackled include the contribution of aquaporins for symplastic–apoplastic transport, the potential production of lipids and/or other substances by VACs, and how these could be transported and deposited either in the black cap or directly into the water transport system. Aquaporin expression and the ultrastructure of the amorphous layer, pit membrane, and black cap could vary either independently of each other or together as an entity due to seasonal changes in temperate species.

ACKNOWLEDGEMENTS

H.M. and S.J. acknowledge financial support from the German Research Foundation (DFG, project no. JA 2174/3-1). Technical support for anatomical observations was provided by the Electron Microscopy Section of Ulm University. H.J.S. and S.J. acknowledge support from the National Science Foundation (NSF, project IOS-1146993). The authors thank the Botanical Garden of Ulm University for providing plant material. They also thank the reviewers and associate editor for helpful and critical comments on the manuscript.

LITERATURE CITED

Afzal, Z., T. Howton, Y. Sun, and M. Mukhtar. 2016. The roles of aquaporins in plant stress responses. *Journal of Developmental Biology* 4: 9.

Almeida-Rodriguez, A. M., and U. G. Hacke. 2012. Cellular localization of aquaporin mRNA in hybrid poplar stems. *American Journal of Botany* 99: 1249–1254.

Alves, G., T. Améglio, A. Guilliot, P. Fleurat-Lessard, A. Lacointe, S. Sakr, G. Pétel, and J. L. Julien. 2004. Winter variation of xylem sap pH in walnut trees: involvement of plasma membrane H^+-ATPase of vessel-associated cells. *Tree Physiology* 24: 99–105.

Alves, G., M. Decourteix, P. Fleurat-Lessard, S. Sakr, M. Bonhomme, T. Améglio, A. Lacointe, et al. 2007. Spatial activity and expression of plasma membrane H^+-ATPase in stem xylem of walnut during dormancy and growth resumption. *Tree Physiology* 27: 1471–1480.

Alves, G., J. J. Sauter, J. L. Julien, P. Fleurat-Lessard, T. Améglio, A. Guillot, G. Pétel, et al. 2001. Plasma membrane H^+-ATPase, succinate and isocitrate dehydrogenases activities of vessel-associated cells in walnut trees. *Journal of Plant Physiology* 158: 1263–1271.

Arend, M., M. H. Weisenseel, M. Brummer, W. Osswald, and J. H. Fromm. 2002. Seasonal changes of plasma membrane H^+-ATPase and endogenous ion current during cambial growth in poplar plants. *Plant Physiology* 129: 1651–1663.

Barnett, J. R., P. Cooper, and L. J. Bonner. 1993. The protective layer as an extension of the apoplast. *International Association of Wood Anatomists Bulletin* 14: 163–171.

Benhamou, N. 1995. Ultrastructural and cytochemical aspects of the response of eggplant parenchyma cells in direct contact with *Verticillium*-infected xylem vessels. *Physiological and Molecular Plant Pathology* 46: 321–338.

Biggs, A. R. 1987. Occurrence and location of suberin in wound reaction zones in xylem of 17 tree species. *Phytopathology* 77: 718–725.

Bonsen, K. J. M., and L. J. Kučera. 1990. Vessel occlusion in plants: morphological, functional, and evolutionary aspects. *International Association of Wood Anatomists Bulletin* 11: 393–399.

Bouché-Pillon, S., P. Fleurat-Lessard, J. C. Fromont, R. Serrano, and J. L. Bonnemain. 1994. Immunolocalization of the plasma membrane H^+-ATPase in minor veins of *Vicia faba* in relation to phloem loading. *Plant Physiology* 105: 691–697.

Braun, H. J. 1967. Entwicklung und Bau der Holzstrahlen unter dem Aspekt der Kontakt-Isolations-Differenzierung gegenuber dem Hydrosystem. I. Das Prinzip der Kontakt-Isolations DifTerenzierung. *Holzforschung* 21: 33–7.

Braun, H. J. 1970. Funktionelle Histologie der Sekundären Sprossachse I. Das Holz. Encyclopedia of plant anatomy IC, part 1. Borntraeger, Berlin, Germany.

Braun, H. J. 1984. The significance of the accessory tissues of the hydrosystem for osmotic water shifting as the second principle of water ascent, with some thoughts concerning the evolution of trees. *International Association of Wood Anatomists Bulletin, new series* 5: 275–294.

Buvat, R. 1989. Ontogeny, cell differentiation, and structure of vascular plants. Springer-Verlag, Berlin, Germany.

Carlquist, S. 2007. Bordered pits in ray cells and axial parenchyma: the histology of conduction, storage, and strength in living wood cells. *Botanical Journal of the Linnean Society* 153: 157–168.

Catesson, A. M., and M. Moreau. 1985. Secretory activity in vessel contact cells. *Israel Journal of Botany* 34: 157–165.

Catesson, A. M., M. Moreau, and J. C. Duval. 1982. Réponse des cellules contigues aux vaisseaux selon la nature de l'agression. *International Association of Wood Anatomists Journal* 3: 11–14.

Chafe, S. C. 1974. Cell wall formation and "protective layer" development in the xylem parenchyma of trembling aspen. *Protoplasma* 80: 335–354.

Chattaway, M. M. 1949. The development of tyloses and secretion of gum in heartwood formation. *Australian Journal of Scientific Research, B, Biological Sciences* 2: 227–240.

Choat, B., M. Ball, J. Luly, and J. Holtum. 2003. Pit membrane porosity and water stress-induced cavitation in four co-existing dry rainforest tree species. *Plant Physiology* 131: 41–48.

Choat, B., S. Jansen, M. A. Zwieniecki, E. Smets, and N. M. Holbrook. 2004. Changes in pit membrane porosity due to deflection and stretching: the role of vestured pits. *Journal of Experimental Botany* 55: 1569–1575.

Choat, B., A. R. Cobb, and S. Jansen. 2008. Structure and function of bordered pits: new discoveries and impacts on whole-plant hydraulic function. *New Phytologist* 177: 608–625.

Clearwater, M. J., and G. Goldstein. 2005. Embolism repair and long distance water transport. *In* N. M. Holbrook and M. A. Zwieniecki [eds.], Vascular transport in plants, 375–399. Elsevier Academic Press, Amsterdam, Netherlands.

Czaninski, Y. 1964. Variations saisonnières du chondriome dans les cellules du parenchyme ligneux vertical de *Robinia pseudoacacia*. *Comptes Rendus de l'Académie des Sciences* 258: 697–682.

Czaninski, Y. 1973. Observations sur une nouvelle couche pariétale dans les cellules associées aux vaisseaux du Robinier et du Sycomore. *Protoplasma* 77: 211–219.

Czaninski, Y. 1977. Vessel-associated cells. *International Association of Wood Anatomists Bulletin* 3: 51–55.

Czaninski, Y. 1979. Cytochimie ultrastructurale des parois du xylème secondaire. *Biologie Cellulaire* 35: 97–102.

Czaninski, Y. 1987. Généralité et diversité des cellules associées aux éléments conducteurs (cellules de contact sensu lato). *Bulletin de la Société botanique de France* 134: 19–26.

Czaninski, Y., and A. M. Catesson. 1969. Localisation ultrastructurale d'activities peroxydasiques dans les tissus conducteurs vegetaux au cours du cycle. *Annuel Journal de Microscopie* 8: 875–888.

De Micco, V., A. Balzano, E. A. Wheeler, and P. Baas. 2016. Tyloses and gums: a review of structure, function and occurrence of vessel occlusions. *International Association of Wood Anatomists Journal* 37: 186–205.

Decourteix, M., G. Alves, M. Bonhomme, M. Peuch, K. B. Baaziz, N. Brunel, et al. 2008. Sucrose (JrSUT1) and hexose (JrHT1 and JrHT2) transporters in walnut xylem parenchyma cells: their potential role in early events of growth resumption. *Tree Physiology* 28: 215–224.

Decourteix, M., G. Alves, N. Brunel, T. Améglio, A. Guilliot, R. Lemoine, G. Pétel, and S. Sakr. 2006. JrSUT1, a putative xylem sucrose transporter, could mediate sucrose influx into xylem parenchyma cells and be upregulated by freeze–thaw cycles over the autumn–winter period in walnut tree (*Juglans regia* L.). *Plant, Cell & Environment* 29: 36–48.

Enns, L. C., M. J. Canny, and M. E. McCully. 2000. An investigation of the role of solutes in the xylem sap and in the xylem parenchyma as the source of root pressure. *Protoplasma* 211: 183–197.

Essiamah, S., and W. Eschrich. 1985. Changes of starch content in the storage tissues of deciduous trees during winter and spring. *International Association of Wood Anatomists Bulletin New Series* 6: 97–106.

Evert, R. F. 2006. Esau's plant anatomy: meristems, cells, and tissues of the plant body: their structure, function and development. Wiley, Hoboken, NJ, USA.

Fineran, B. A. 1997. Cyto- and histochemical demonstration of lignins in plant cell walls: an evaluation of the chlorine water ethanolamine silver nitrate method of Coppick and Fowler. *Protoplasma* 198: 186–201.

Foster, R. C. 1967. Fine structure of tyloses in three species of the Myrtaceae. *Australian Journal of Botany* 15: 25–34.

Fromard, L., V. Babin, P. Fleurat-Lessard, J. C. Fromont, R. Serrano, and J. L. Bonnemain. 1995. Control of vascular sap pH by the vessel-associated cells in woody species. *Plant Physiology* 108: 913–918.

Fujii, T., H. Harada, and H. Saiki. 1980. The layered structure of secondary walls in axial parenchyma of the wood of 51 Japanese angiosperm species. *Mokuzai Gakkaishi* 26: 373–380.

Fujii, T., H. Harada, and H. Saiki. 1981. Ultrastructure of 'amorphous layer' in xylem parenchyma cell wall of angiosperm species. *Mokuzai Gakkaishi* 27: 149–156.

Fujita, M., M. Kato, H. Saiki, and H. Harada. 1975. Changes in parenchyma cell structure followed by incubated tylosis development in *Quercus serrata* Thumb. *Bulletin of the Kyoto Prefectural University Forests* 50: 183–190.

Gascó, A., A. Nardini, E. Gortan, and S. Salleo. 2006. Ion-mediated increase in the hydraulic conductivity of laurel stems: role of pits and consequences for the impact of cavitation on water transport. *Plant, Cell & Environment* 29: 1946–1955.

Gregory, R. A. 1978. Living elements of the conducting secondary xylem of sugar maple (*Acer saccharum* Marsh.). *International Association of Wood Anatomists Bulletin* 4: 65–69.

Groszmann, M., H. L. Osborn, and J. R. Evans. 2017. Carbon dioxide and water transport through plant aquaporins. *Plant, Cell & Environment* 40: 938–961.

Gunning, B. E. S., and J. S. Pate. 1974. Transfer cells. *In* A. W. Robards [ed.], Dynamic aspects of plant ultrastructure, 441–479. McGraw-Hill, London, UK.

Gunning, B. E. S., J. S. Pate, and L. G. Briarty. 1968. Specialized "transfer cells" in minor veins of leaves and their possible significance in phloem translocation. *Journal of Cell Biology* 37: 7–12.

Halperin, W., and W. A. Jensen. 1967. Ultrastructural changes during growth and embryogenesis in carrot cell cultures. *Journal of Ultrastructure Research* 18: 428–443.

Herbette, S., B. Bouchet, N. Brunel, E. Bonnin, H. Cochard, and F. Guillon. 2015. Immunolabelling of intervessel pits for polysaccharides and lignin helps in understanding their hydraulic properties in Populus tremula × alba. *Annals of Botany* 115: 187–199.

Hilaire, E., S. A. Young, L. H. Willard, J. D. Mcgee, T. Sweat, J. M. Chittoor, J. A. Guikema, et al. 2001. Vascular defense responses in rice: peroxidase accumulation in xylem parenchyma cells and xylem wall thickening. *Molecular Plant Microbe Interactions* 14: 1411–1419.

Höll, W. 1975. Radial transport in rays. *In* M. H. Zimmermann and J. A. Milburn, [eds.], Transport in plants I. Phloem transport, 432–450. Springer-Verlag, Berlin, Germany.

Hölttä, T., M. Mencuccini, and E. Nikinmaa 2009. Linking phloem function to structure: analysis with a coupled xylem–phloem transport model. *Journal of Theoretical Biology* 259: 325–337.

IAWA Committee. 1989. IAWA list of microscopic features for hardwood identification. *International Association of Wood Anatomists Bulletin, new series* 10: 219–332.

Jansen, S., and H. J. Schenk. 2015. On the ascent of sap in the presence of bubbles. *American Journal of Botany* 102: 1–3.

Jarbeau, J. A., F. W. Ewers, and S. D. Davis. 1995. The mechanism of water-stress-induced embolism in two species of chaparral shrubs. *Plant Cell & Environment* 18: 189–196.

Kasuga, J., K. Arakawa, and S. Fujikawa. 2007. High accumulation of soluble sugars in deep supercooling Japanese white birch xylem parenchyma cells. *New Phytologist* 174: 569–579.

Kasuga, J., Y. Hashidoko, A. Nishioka, M. Yoshiba, K. Arakawa, and S. Fujikawa. 2008. Deep supercooling xylem parenchyma cells of katsura tree (*Cercidiphyllum japonicum*) contain flavonol glycosides exhibiting high antiice nucleation activity. *Plant, Cell & Environment* 31: 1335–1348.

Kim, J. S., and G. Daniel. 2013. Developmental localization of homogalacturonan and xyloglucan epitopes in pit membranes varies between pit types in two poplar species. *International Association of Wood Anatomists Journal* 34: 245–262.

Klepsch, M. M., M. Schmitt, J. P. Knox, and S. Jansen. 2016. The chemical identity of intervessel pit membranes in *Acer* challenges hydrogel control of xylem hydraulic conductivity. *AOB Plants* 8: plw052.

Lalonde, S., V. R. Franceschi, and W. B. Frommer. 2001. Companion cells. John Wiley, Chichester, UK.

Li, N., C. Xu, Y. Li-Beisson, and K. Philippar. 2016. Fatty acid and lipid transport in plant cells. *Trends in Plant Science* 21: 145–158.

Liese, W., O. Schmidt, and U. Schmitt. 1995. On the behaviour of hardwood pits towards bacteria during water storage. *Holzforschung* 49: 389–393.

Maurel, C., Y. Boursiac, D. T. Luu, V. Santoni, Z. Shahzad, and L. Verdoucq. 2015. Aquaporins in plants. *Physiological Reviews* 95: 1321–1358.

Maurel, C., L. Verdoucq, and O. Rodrigues. 2016. Aquaporins and plant transpiration. *Plant, Cell & Environment* 39: 2580–2587.

Meinzer, F. C., S. A. James, G. Goldstein, and D. Woodruff. 2003. Whole-tree water transport scales with sapwood capacitance on tropical forest canopy trees. *Plant, Cell & Environment* 26: 1147–1155.

Mencuccini, M., T. Hölttä, S. Sevanto, and E. Nikinmaa. 2013. Concurrent measurements of change in the bark and xylem diameters of trees reveal a phloem-generated turgor signal. *New Phytologist* 198: 1143–1154.

Metcalfe, C. R., and L. Chalk. 1983. Anatomy of the dicotyledons, 2nd ed., vol. II, Wood structure and conclusion of the general introduction. Clarendon Press, Oxford, UK.

Misra, B. B. 2016. The black-box of plant apoplast lipidomes. *Frontiers in Plant Science* 7: 323.

Mollenhauer, H. H., and D. L. Hopkins. 1974. Ultrastructural study of Pierce's disease bacterium in grape xylem tissue. *Journal of Bacteriology* 119: 612–618.

Morris, H., C. R. Brodersen, F. W. M. R. Schwarze, and S. Jansen. 2016a. The parenchyma of secondary xylem and its critical role in tree defense against fungal decay in relation to the CODIT model. *Frontiers in Plant Science* 7: 1665.

Morris, H., M. A. F. Gillingham, L. Plavcová, S. M. Gleason, M. E. Olson, D. A. Coomes, E. Fichtler, et al. 2018. The amount and spatial arrangement of axial parenchyma is related to vessel diameter in woody angiosperms. *Plant, Cell & Environment* 44: 245–260.

Morris, H., and S. Jansen. 2016. Secondary xylem parenchyma—from classical terminology to functional traits. *International Association of Wood Anatomists Journal* 37: 1–13.

Morris, H., L. Plavcová, P. Cvecko, E. Fichtler, M. A. F. Gillingham, H. I. Martínez-Cabrera, D. McGlinn, et al. 2016b. A global analysis of parenchyma tissue fractions in secondary xylem of seed plants. *New Phytologist* 206: 1553–1565.

Mueller, W. C., and C. H. Beckman. 1984. Ultrastructure of the cell wall of vessel contact cells in the xylem of tomato stems. *Annals of Botany* 53: 107–114.

Münch, E. 1930. Die Stoffbewegungen in Pflanze. Fischer, Jena, Germany.

Murmanis, L. 1975. Formation of tyloses in felled *Quercus rubra* L. *Wood, Science and Technology* 9: 3–14.

Nardini, A., M. A. Lo Gullo, and S. Salleo. 2011. Refilling embolized xylem conduits: Is it a matter of phloem unloading? *Plant Science* 180: 604–611.

Neuner, G. 2014. Frost resistance in alpine woody plants. *Frontiers in Plant Science* 5: 1–13, 654.

O'Brien, T. P. 1970. Further observations on hydrolysis of the cell wall in the xylem. *Protoplasma* 69: 1–14.

Oparka, K. J., and D. A. M. Prior. 1992. Direct evidence for pressure-generated closure of plasmodesmata. *Plant Journal* 2: 741–750.

Pfautsch, S., J. Renard, M. J. Tjoelker, and A. Salih. 2015. Phloem as capacitor: radial transfer of water into xylem of tree stems occurs via symplastic transport in ray parenchyma. *Plant Physiology* 167: 963–971.

Plavcová, L., and U. G. Hacke. 2011. Heterogeneous distribution of pectin epitopes and calcium in different pit types of four angiosperm species. *New Phytologist* 192: 885–897.

Plavcová, L., G. Hoch, H. Morris, S. Ghiasi, and S. Jansen. 2016. The amount of parenchyma and living fibers affects storage of nonstructural carbohydrates in young stems and roots of temperate trees. *American Journal of Botany* 113: 603–612.

Plavcová, L., and S. Jansen. 2015. The role of xylem parenchyma in the storage and utilization of non-structural carbohydrates. *In* U. G. Hacke [ed.], Functional and ecological xylem anatomy, 209–234. Springer International Publishing, Cham, Switzerland.

Qin, Q. M., G. E. Vallad, and K. V. Subbarao. 2008. Characterization of *Verticillium dahliae* and *V. tricorpus* isolates from lettuce and artichoke. *Plant Disease* 92: 69–77.

Quamme, H. A. 1991. Application of thermal analysis to breeding fruit crops for increased cold hardiness. *HortScience* 26: 513–517.

Rioux, D., H. Chamberland, M. Simard, and G. B. Ouellette. 1995. Suberized tyloses in trees: an ultrastructural and cytochemical study. *Planta* 196: 125–140.

Rioux, D., M. Nicole, M. Simard, and G. B. Ouellette. 1998. Immunocytochemical evidence that secretion of pectin occurs during gel (gum) and tylosis formation in trees. *Phytopathology* 88: 494–505.

Robards, A. W. 1968. On the ultrastructure of differentiating secondary xylem in willow. *Protoplasma* 65: 449–464.

Sakai, A., and W. Larcher. 1987. Frost survival of plants: responses and adaptation to freezing stress. Springer-Verlag, Berlin, Germany.

Sakr, S., G. Alves, R. Morillon, K. Maurel, M. Decourteix, A. Guilliot, P. Fleurat-Lessard, et al. 2003. Plasma membrane aquaporins are involved in winter embolism recovery in walnut tree. *Plant Physiology* 133: 630–641.

Salleo, S., M. A. Lo Gullo, P. Trifilo, and A. Nardini. 2004. New evidence for a role of vessel-associated cells and phloem in the rapid xylem refilling of cavitated stems of *Laurus nobilis* L. *Plant, Cell & Environment* 27: 1065–1076.

Salleo, S., P. Trifilo, S. Esposito, A. Nardini, and M. A. Lo Gullo. 2009. Starch-to-sugar conversion in wood parenchyma of field-growing *Laurus nobilis* plants: a component of the signal pathway for embolism repair? *Functional Plant Biology* 36: 815–825.

Sauter, J. J. 1966. Untersuchungen zur Physiologie der Pappelholzstrahlen. I. Jahresperiodischer Verlauf der Starkespeicherung im Holzstrahlparenchym. *Zeitschrift für Pflanzenphysiologie* 55: 246–258.

Sauter, J. J. 1972. Respiratory and phosphatase activities in contact cells of wood rays and their possible role in sugar secretion. *Zeitschrift für Pflanzenphysiologie* 67: 135–145.

Sauter, J. J. 1982. Transport in Markstrahlen. *Berichte der Deutschen Botanischen Gesellschaft* 95: 593–618.

Sauter, J. J., W. Iten, and W. H. Zimmermann. 1973. Studies on the release of sugar into the vessels of sugar maple (*Acer saccharum*). *Canadian Journal of Botany* 51: 1–8.

Sauter, J. J., and S. Kloth. 1986. Plasmodesmatal frequency and radial translocation rates in ray cells of poplar (*Populus* × *canadensis* Moench 'Robusta'). *Planta* 168: 377–380.

Sauter, J. J., and B. van Cleve. 1994. Storage, mobilization and interrelations of starch, sugars, protein and fat in the ray storage tissue of poplar trees. *Trees* 8: 297–304.

Schaffer, K., and M. Wisniewski. 1989. Development of the amorphous layer (protective layer) in xylem parenchyma of cv. Golden Delicious apple, cv. Loring peach, and willow. *American Journal of Botany* 76: 1569–1582.

Schenk, H. J., S. Espino, D. M. Romo, N. Nima, A. Y. T. Do, J. M. Michaud, B. Papahadjopoulos-Sternberg, et al. 2017. Xylem surfactants introduce a new element to the cohesion-tension theory. *Plant Physiology* 173: 1177–1196.

Schenk, J. H., K. Steppe, and S. Jansen. 2015. Nanobubbles: a new paradigm for air-seeding in xylem. *Trends in Plant Science* 20: 199–205.

Schmid, R. 1965. The fine structure of pits in hardwoods. *In* W. A. Côté [ed.], Cellular ultrastructure of woody plants, 291–304. Syracuse University Press, Syracuse, New York, USA.

Schmid, R., and R. Machado. 1968. Pit membranes in hardwoods—fine structure and development. *Protoplasma* 66: 185–204.

Schmitz, N., L. Egerton, C. Lovelock, and M. Ball. 2012. Light-dependent maintenance of hydraulic function in mangrove branches: Do xylary chloroplasts play a role in embolism repair? *New Phytologist* 195: 40–46.

Schmitt, U., and W. Liese. 1990. Wound reaction of the parenchyma in *Betula*. *International Association of Wood Anatomists Bulletin, new series* 11: 413–420.

Secchi, F., M. E. Gilbert, and M. A. Zwieniecki. 2011. Transcriptome response to embolism formation in stems of *Populus trichocarpa* provides insight into signaling and biology of refilling. *Plant Physiology* 157: 1419–1429.

Secchi, F., C. Pagliarani, and M. A. Zwieniecki. 2017. The functional role of xylem parenchyma cells and aquaporins during recovery from severe water stress. *Plant, Cell & Environment* 40: 858–871.

Secchi, F., and M. A. Zwieniecki. 2010. Patterns of PIP gene expression in *Populus trichocarpa* during recovery from xylem embolism suggest a major role for the PIP1 aquaporin subfamily as moderators of refilling process. *Plant, Cell & Environment* 33: 1285–1297.

Secchi, F., and M. A. Zwieniecki. 2011. Sensing embolism in xylem vessels: the role of sucrose as a trigger for refilling. *Plant, Cell & Environment* 34: 514–524.

Secchi, F., and M. A. Zwieniecki. 2012. Analysis of xylem sap from functional (nonembolized) and nonfunctional (embolized) vessels of *Populus nigra*: chemistry of refilling. *Plant Physiology* 160: 955–964.

Secchi, F., and M. A. Zwieniecki. 2016. Accumulation of sugars in the xylem apoplast observed under water stress conditions is controlled by xylem pH. *Plant, Cell & Environment* 39: 2350–2360.

Sevanto, S., T. Hölttä T, and N. M. Holbrook. 2011. Effects of the hydraulic coupling between xylem and phloem on diurnal phloem diameter variation. *Plant, Cell & Environment* 34: 690–703.

Sevanto, S., N. G. McDowell, L. T. Dickman, R. Pangle, and W. T. Pockman. 2014. How do trees die? A test of the hydraulic failure and carbon starvation hypotheses. *Plant, Cell & Environment* 37: 153–161.

Sokołowska, K. 2013. Symplasmic transport in wood: the importance of living xylem cells. *In* K. Sokołowska and P. Sowiński [eds.], Symplastic transport in vascular plants, 101–132. Springer, New York, NY, USA.

Spicer, R. 2014. Symplastic networks in secondary vascular tissues: parenchyma distribution and activity supporting long-distance transport. *Journal of Experimental Botany* 65: 1829–1848.

Törnroth-Horsefield, S., Y. Wang, K. Hedfalk, U. Johanson, M. Karlsson, E. Tajkhorshid, R. Neutze, et al. 2006. Structural mechanism of plant aquaporin gating. *Nature* 439: 688–694.

Tyree, M. T., S. Salleo, A. Nardini, M. A. Lo Gullo, and R. Mosca. 1999. Refilling of embolized vessels in young stems of laurel. Do we need a new paradigm? *Plant Physiology* 120: 11–21.

van Bel, A. J. E. 1990. Xylem–phloem exchange via the rays: the undervalued route of transport. *Journal of Experimental Botany* 41: 631–644.

van Bel, A. J. E., and C. van der Schoot. 1988. Primary function of the protective layer in contact cells: buffer against oscillations in hydrostatic pressure in the vessels? *International Association of Wood Anatomists Bulletin* 9: 285–288.

van der Schoot, C., and A. J. E. van Bel. 1989. Architecture of the internodal xylem of tomato (*Solanum lycopersicum*) with reference to longitudinal and lateral transfer. *American Journal Botany* 76: 487–503.

Vesala, T., T. Hölttä, M. Perämäki, and E. Nikinmaa. 2003. Refilling of a hydraulically isolated embolised vessel: Model calculations. *Annals of Botany* 91: 419–428.

Westhoff, M., H. Schneider, D. Zimmermann, S. Mimietz, A. Stinzing, L. H. Wegner, W. Kaiser, et al. 2008. The mechanisms of refilling of xylem conduits and bleeding of tall birch during spring. *Plant Biology* 10: 604–623.

Wheeler, E. A. 1981. Intervascular pitting in *Fraxinus americana* L. *International Association of Wood Anatomists Bulletin* 2: 169–174.

Wisniewski, W., E. Ashworth, and K. Schaffer. 1987a. Use of lanthanum to characterize cell wall permeability to deep supercooling and extracellular freezing in woody plants. I. Intergeneric comparisons between *Prunus*, *Cornus*, and *Salix*. *Protoplasma* 139: 105–116.

Wisniewski, W. E., E. Ashworth, and K. Schaffer. 1987b. The use of lanthanum to characterize cell wall permeability in relation to deep supercooling and extracellular freezing in woody plants. II. Intrageneric comparisons between *Betula lenta* and *Betula papyrifera*. *Protoplasma* 141: 160–168.

Wisniewski, M., and G. Davis. 1989. Evidence for the involvement of a specific cell wall layer in regulation of deep supercooling of xylem parenchyma. *Plant Physiology* 91: 151–156.

Wisniewski, M., and G. Davis. 1995. Immunogold localization of pectins and glycoproteins in tissues of peach with reference to deep supercooling. *Trees* 9: 253–260.

Wisniewski, M., G. Davis, and R. Arora. 1991a. Effect of macerase, oxalic acid, and EGTA on deep supercooling and pit membrane structure of xylem parenchyma of peach. *Plant Physiology* 96: 1354–1359.

Wisniewski, M., G. Davis, and K. Schaffer. 1991b. Mediation of deep supercooling of peach and dogwood by enzymatic modifications in cell-wall structure. *Planta* 184: 254–260.

Wisniewski, M., M. Fuller, J. Palta, J. Carter, and R. Arora. 2004. Ice nucleation, propagation, and deep supercooling in woody plants. *Journal of Crop Improvement* 10: 5–15.

Yadeta, K. A., and B. P. H. J. Thomma. 2013. The xylem as battleground for plant hosts and vascular wilt pathogens. *Frontiers in Plant Science* 4: 97.

Zhang, Y., M. Klepsch, and S. Jansen 2017. Bordered pits in xylem of vesselless angiosperms and their possible misinterpretation as perforation plates. *Plant, Cell & Environment* 40: 2133–2146.

Ziegler, H. 1975. Nature of transported substances *In* A. Pirson and M. H. Zimmermann [eds.], Encyclopedia of plant physiology; M. H. Zimmerman and S. A. Milburn [eds.], vol. 1, Transport in plants: Phloem transport, 59–100. Springer-Verlag, Berlin, Germany.

Zürcher, E., L. J. Kucera, and H. H. Bosshard. 1985. Bildung und Morphologie der Thyllen. Eine Lieteraturübersicht. *Vierteljahrsschrift der Naturforschenden Gesellschaft in Zürich* 130: 311–333.

Zwieniecki, M. A., and N. M. Holbrook. 2009. Confronting Maxwell's demon: biophysics of xylem embolism repair. *Trends in Plant Science* 14: 530–534.

Journal of Experimental Botany, Vol. 70, No. 14 pp. 3679–3691, 2019
doi:10.1093/jxb/erz286 Advance Access Publication 13 July, 2019

RESEARCH PAPER

Mechanical properties and structure–function trade-offs in secondary xylem of young roots and stems

Lenka Plavcová[1,*], Friederike Gallenmüller[2], Hugh Morris[3], Mohammad Khatamirad[4], Steven Jansen[4] and Thomas Speck[2,5]

[1] University of Hradec Králové, Department of Biology, Faculty of Science, Rokitanského 62, 500 03 Hradec Králové, Czech Republic
[2] Plant Biomechanics Group Freiburg, Botanic Garden of the Albert-Ludwigs-University of Freiburg, Faculty of Biology, Schänzlestrasse 1, 79104 Freiburg, Germany
[3] Laboratory for Applied Wood Materials, Empa – Swiss Federal Laboratories for Materials Testing and Research, St Gallen, Switzerland
[4] Institute of Systematic Botany and Ecology, Ulm University, Albert-Einstein-Allee 11, D-89081 Ulm, Germany
[5] Cluster of Excellence livMatS @ FIT – Freiburg Center for Interactive Materials and Bioinspired Technologies, Georges-Köhler-Allee 105, 79110 Freiburg, Germany

* Correspondence: lenka.plavcova@gmail.com

Received 14 December 2018; Editorial decision 3 June 2019; Accepted 27 June 2019

Editor: Anja Geitmann, McGill University, Canada

Abstract

Bending and torsional properties of young roots and stems were measured in nine woody angiosperms. The variation in mechanical parameters was correlated to wood anatomical traits and analysed with respect to the other two competing functions of xylem (namely storage and hydraulics). Compared with stems, roots exhibited five times greater flexibility in bending and two times greater flexibility in torsion. Lower values of structural bending and structural torsional moduli (E_{str} and G_{str}, respectively) of roots compared with stems were associated with the presence of thicker bark and a greater size of xylem cells. Across species, E_{str} and G_{str} were correlated with wood density, which was mainly driven by the wall thickness to lumen area ratio of fibres. Higher fractions of parenchyma did not translate directly into a lower wood density and reduced mechanical stiffness in spite of parenchyma cells having thinner, and in some cases less lignified, cell walls than fibres. The presence of wide, partially non-lignified rays contributed to low values of E_{str} and G_{str} in *Clematis vitalba*. Overall, our results demonstrate that higher demands for mechanical stability in self-supporting stems put a major constraint on xylem structure, whereas root xylem can be designed with a greater emphasis on both storage and hydraulic functions.

Keywords: Axial parenchyma, fibres, mechanical function, rays, structural bending modulus, structural torsional modulus, trade-off, wood.

Introduction

Wood fulfils several biophysical functions, including the facilitation of long-distance transport of water and nutrients (Tyree and Ewers, 1991), mechanical support (Badel *et al.*, 2015), and storage of water (Tyree and Yang, 1990), nutrients (Plavcová *et al.*, 2016) and secondary compounds (Morris *et al.*, 2016*a*). In most angiosperms, these functions are seemingly divided between different cell types.Vessels and tracheids are specialised in the hydraulic function, fibres are devoted to mechanical support, whereas ray and axial parenchyma act as the main sites for storage and movement of non-structural carbohydrates.

However, this view is to a certain degree oversimplified because the different cell types and the functions commonly attributed to them are in fact tightly interwoven and linked in a complex manner. The interaction between mechanical and hydraulic function arises because structural support from fibres helps to prevent hydraulic dysfunction (Jacobsen *et al*., 2005; Lens *et al*., 2016) and bridges made out of pitted fibre–tracheids hydraulically connect isolated vessels thereby serving as a safer auxiliary pathway for water transport (Cai *et al*., 2014). Similarly, parenchyma cells, which are primarily devoted to nutrient storage, may interact with hydraulic function by facilitating embolism reversal (Brodersen *et al*., 2010) and by providing hydraulic capacitance (Pfautsch *et al*., 2015). The storage and mechanical function is also interlinked as ray parenchyma affects wood mechanical strength (Burgert *et al*., 2001) and living fibres are involved in storage of non-structural carbohydrates in some species (Yamada *et al*., 2011). Thus, determining to what degree multiple functions overlap in wood and deciphering the key anatomical drivers associated with physiological traits remains a challenge.

When analysing relationships in xylem structure and function, ecologists have frequently viewed traits as being along contrasting spectra of trade-offs (Baas *et al*., 2004; Pratt and Jacobsen, 2017). Several structural–functional trade-offs have already been described in wood, although the continuum and multi-functionality of xylem tissue is unlikely to be simplified to strictly opposing categories. The covariation between hydraulic safety versus efficiency is one of the most frequently studied relationships, although this apparent trade-off remains fairly weak and poorly understood (Lens *et al*., 2011; Bittencourt *et al*., 2016; Gleason *et al*., 2016). Also, the strength of the trade-off may vary between different growth forms (van der Sande *et al*., 2019). A trade-off between hydraulic and mechanical function is another example of structure–function relationships, which has been documented at cellular and tissue levels. The existence of a trade-off between hydraulics and mechanics is more self-evident in conifers because tracheids fulfil both of these functions. Across a wide range of conifer species, higher mechanical reinforcement of tracheids was associated with increased hydraulic resistance (Pittermann *et al*., 2006). The trade-off arose from cell reinforcement primarily achieved by narrowing of cell diameters rather than through increase in the thickness of the secondary wall. In angiosperms, hydraulic and mechanical functions can be more easily decoupled because of the distinct roles of vessels and fibres. Thus, hydraulic conductivity can theoretically remain unchanged in mechanically stronger wood if the increased mechanical strength is achieved by modifying fibre properties. In agreement, no significant relationship between mechanical strength and hydraulic conductivity was observed across five *Acer* species in which higher mechanical strength was due to the presence of narrower fibre lumen diameters (Woodrum *et al*., 2003). However, a strong negative correlation between specific hydraulic conductivity and the modulus of elasticity was reported along the root axial length in six tropical tree species (Christensen-Dalsgaard *et al*., 2007*a*,*b*). In this case, changes in wood density corresponded with a strong gradient in the size and frequency of vessels. Thus, while there is evidence for the negative coupling between hydraulics and mechanics in both gymnosperms and at least some angiosperm species, a trade-off between mechanical and storage functions has rarely been considered beyond the observation of a negative correlation between fibre and parenchyma fractions (Pratt *et al*., 2007; Zieminńska *et al*., 2015; Morris *et al*., 2016*b*).

The evolution of secondary growth and production of secondary xylem (i.e. wood) can be considered one of the strategies increasing the mechanical stability of plants, allowing for larger and taller plant bodies. Resistance of woody organs to mechanical loads can be correlated to complex morpho-anatomical structures at different hierarchical levels (Speck and Burgert, 2011; Lachenbruch and McCulloh, 2014). The character and intensity of the dominant stresses and strains change along the plant body. Therefore, mechanical properties of wood vary considerably within one individual and also along one individual root or stem (Niklas, 1999*b*, Christensen-Dalsgaard *et al*., 2007*a*). High mechanical stiffness of wood has been repeatedly linked to high wood density (Jacobsen *et al*., 2007; Niklas and Spatz, 2010). However, it is often less clear which finer-scale anatomical properties are the main drivers of this integrative trait (Ziemińska *et al*., 2013). While fibre properties certainly exert strong control over wood density and wood mechanical properties (Fujiwara *et al*., 1991; Jacobsen *et al*., 2007), considerable influence of ray and axial parenchyma has also been reported across a diverse range of species (Fujiwara, 1992; Zheng and Martínez-Cabrera, 2013; Ziemińska *et al*., 2015). A high proportion of thin-walled parenchyma cells occurring at the expense of thick-walled fibres is expected to lead to a reduction in wood mechanical stiffness. However, the mechanical effects are hypothesised to differ between ray and axial parenchyma, partly owing to their orientation in radial and axial directions (Zheng and Martínez-Cabrera, 2013). Due to the perpendicular orientation of rays to the wood grain, a high proportion of them were found to enhance the mechanical stiffness of wood, particularly in the radial direction (Burgert *et al*., 2001; Woodrum *et al*., 2003). Contrarily, it has been suggested that the presence of wide rays underpins a high torsional and flexural flexibility of liana stems (Gartner, 1991; Putz and Holbrook, 1991; Carlquist, 2001). In comparison to ray parenchyma, axial wood parenchyma cells are grouped in strands that have a similar shape and longitudinal orientation to fibres. Therefore, a higher proportion of axial parenchyma should directly reduce the stiffness of the fibre matrix. However, several questions have not been fully addressed yet, such as (i) to what extent the amount of parenchyma can have an appreciable effect on wood stiffness, and (ii) whether the relative differences in wall reinforcement between axial wood parenchyma and fibres are similar across species and organs.

In the current study, we measured bending and torsional moduli and conducted detailed observations of wood anatomy of young stems and roots in nine angiosperm species. The main objectives of our study were (i) to evaluate the effect of ray and axial parenchyma on mechanical properties and (ii) to better understand the trade-offs in xylem structure–function. Young stems and roots provide a convenient study system for this purpose as these organs are designed with a different adaptive emphasis on mechanical, storage, and hydraulic functions. We

expected self-supporting stems to be mechanically stronger than roots, but the question arose as to whether hydraulics or storage or both of these functions are consequently increased in roots. Furthermore, we anticipated morphological and anatomical features that presumably underlie a higher mechanical stiffness (e.g. less abundant axial wood parenchyma, narrower rays, and thicker cell walls) to be more prominent in stems as opposed to roots.

Materials and methods

Plant material

Young roots and stems were collected from nine different angiosperm species, including eight common temperate forest trees, and one temperate woody liana (Table 1). The latter was included in our comparative study, to get some first results on differences in functional trade-offs between self-supporting angiosperm trees and non-self-supporting lianas. All samples were collected from a minimum of three mature individuals per species during June to August 2014. The sampling was done in a forested area of the Ulm University campus (48° 25′N, 9° 58′E), from a forest strip along the Iller river 2 km south of Ulm (48° 22′N, 9° 60'E), and in a forested area located 4 km southeast of Freiburg, Germany (47° 59′N, 7° 53′E). The root segments were excavated from 10–50 cm depth in a distance of approx. 1 m from the root collar. The stem segments were cut from lateral branches at a height of 2–3 m with the aid of a telescopic pruning pole. The diameters of the segments ranged between 0.5 to 1.5 cm and their ages were between 3 and 8 years. All segments had already undergone substantial secondary thickening but still can be classified as juvenile in relation to the age of the plant specimens they were collected from. Thus, the sampled segments had morphological and anatomical characteristics typical of root and stem organs and could be considered, based on their age and position in the entire plant body, as being in the medium advance in their specialisation process towards mechanical, hydraulic, and storage demands. Upon collection, the samples were put into a dark plastic bag with a moist paper towel and transported to the laboratory where they were stored at 4 °C until used for mechanical measurements. All samples were measured within 3 days of collection.

Table 1. *List of abbreviations*

Abbreviation	
Species	
Ap	*Acer pseudoplatanus* L.
Cb	*Carpinus betulus* L.
Fe	*Fraxinus excelsior* L.
Fs	*Fagus sylvatica* L.
Pa	*Prunus avium* (L.) L.
Qr	*Quercus robur* L.
Rp	*Robinia pseudoacacia* L.
Tc	*Tilia cordata* Mill.
Cv	*Clematis vitalba* L.
Organs	
R	Roots
S	Stems
Mechanical parameters	
EI	Bending stiffness (N m^2)
GI	Torsional stiffness (N m^2)
E_{str}	Structural bending modulus (MN m^{-2})
G_{str}	Structural torsional modulus (MN m^{-2})
I_{ax}	Axial second moment of area (m^4)
I_{pol}	Polar second moment of area (m^4)
$I_{rel,tissue}$	Relative contribution of tissue (wood, bark, or pith) to I_{ax} or I_{pol}

Flexural and torsional stiffness

Mechanical measurements were performed on stem and root segments with a length of 10–25 cm. Care was taken to select straight segments with a low degree of taper, avoiding side branches, knots, and obvious structural damage. Flexural stiffness was measured in four-point-bending tests using a manual bending apparatus. The segments were placed on two cylindrical holders 5–12 cm apart from each other, depending on the length and the bending resistance of the tested segment. The bending force was applied via a suspended holder, which was attached to the tested sample at two points, and placed equidistant and outside of the cylindrical supports. The bending force was then gradually increased by adding up to six weights of 50, 100, or 200 g onto the metal holder. The resulting upward deflection of the segment was monitored with an eyepiece graticule on a dissecting microscope. The cumulative deflection values were plotted against the applied force and fitted with a linear equation. Only measurements with a coefficient of determination higher than 0.97 were accepted. The flexural stiffness (EI) was then calculated as

$$EI = \frac{l_1^2 \times \frac{1}{2}(l_2 - l_1)}{16 \times a} \quad (1)$$

where l_1 is the distance of the sample holders (i.e. support span, in m), l_2 is the span of the weight holder attachment (i.e. load span, in m) and a is the slope of the linear regression line of the deflection versus applied force data (in N m^{-1}). For a detailed description of the bending tests and formulas see Niklas (1992), Speck (1994), Rowe and Speck (1996), and Rowe *et al.* (2006).

The flexural stiffness is determined by the dimensions of a sample (described by the axial second moment of area, I_{ax}) and its material properties (described by the structural bending modulus, E_{str}), according to the following formula:

$$EI = E_{str} I_{ax} \quad (2)$$

In engineering, the term bending modulus is defined as a property of a homogeneous and isotropic material. As plant stems and roots are heterogeneous, anisotropic composite structures, we use the term *structural* bending modulus E_{str} (Rowe and Speck, 1996; Speck *et al.*, 1996). The higher the resistance to bending or tension of a sample, the higher is its structural modulus of elasticity, independent of its geometrical dimensions (Niklas, 1992). Following Eq. 2, the structural bending modulus E_{str} was obtained by dividing the flexural stiffness EI by I_{ax}, with I_{ax} being calculated according to the following formula:

$$I_{ax} = \frac{\pi}{64} D^4 \quad (3)$$

where D is the root or stem diameter (in m). The diameter was obtained from the measured mean cross-sectional area of the tested root or stem when assuming a circular geometry. Due to the fact that the stems and roots segments tested in our study showed almost perfectly circular cross-sections and small deviations were developed only intermittently and never along the whole segment, we decided that the use of a circular model represents the best approximation.

Immediately after the bending test, which was limited to the elastic range of the samples, torsional stiffness was assessed on the same root or stem segment. The torsional stiffness was measured using a range of custom-made spring-loaded cylinders that could apply a range of torques according to the thickness and resistance of the samples tested. The torsion cylinders consist of a central spindle and a clamp that can rotate freely against a spring. The cylinder was gradually rotated in 10–20° steps against the spring. The resulting root or stem deflection was measured relative to the torsional force applied. Torque was calculated by multiplying the rotational angle with the stiffness of the spring inside the cylinder determined from a calibration curve. Torsional stiffness (GI) was then calculated by dividing the length of the tested segment (l, in m) by the slope of the regression line fitted to the data of deflection angles plotted against the applied torque (b, in rad N^{-1} m^{-1}), according to the following formula:

$$GI = \frac{l}{b} \quad (4)$$

The structural torsional modulus was calculated using the formula:

$$G_{str} = \frac{GI}{I_{pol}} \quad (5)$$

where I_{pol} is the polar second moment of area of the tested segment calculated as:

$$I_{pol} = \frac{\pi}{32} D^4 \quad (6)$$

where D represents the mean root or stem diameter (i.e. assuming circular geometry of the tested segments, same as for I_{ax}). For a detailed description of the torsional tests see Gallenmüller *et al.* (2001).

Tissue proportions and their contribution to I_{ax} and I_{pol}

Roots and stems are highly inhomogeneous and anisotropic structures composed of different tissues, namely wood and bark in the case of roots, and pith, wood, and bark in the case of stems. To gain insights into the relative importance of these three tissues for the overall mechanical stiffness, their relative contributions to I_{ax} and I_{pol} were assessed. To calculate the relative contribution of each tissue to I_{ax} and I_{pol} ($I_{rel,tissue}$), the cross-sectional areas of pith, wood, and bark were measured from surface images of stem cross-sections obtained with a stereo zoom microscope (Axio Zoom V16, Zeiss, Germany). In roots, which do not have pith tissue, only the relative contribution of wood and bark was considered. The tissue cross-sectional areas were then converted to diameters and the partial second moments of area ($I_{ax,tissue}$ and $I_{pol,tissue}$) of each tissue were calculated assuming circular tissue outlines and a symmetrical distribution. The standard formulas for filled cylinders (Eqs 5, 6) were used to calculate the partial second moment of area of wood in roots and pith in young stems, whereas the partial second moment of area of bark in both stems and roots and of wood in stems was derived using standard formulas for hollow cylinders:

$$I_{ax,\ tissue} = \frac{\pi}{64}\left(D_j^4 - D_i^4\right)$$

, and correspondingly

$$I_{pol,\ tissue} = \frac{\pi}{32}\left(D_j^4 - D_i^4\right)$$

where D_j and D_i are outer and inner diameters of the tissue outlines. The relative contribution of each tissue to I_{ax} and I_{pol} ($I_{rel,tissue}$) was finally calculated by dividing $I_{ax,tissue}$ ($I_{pol,tissue}$) by I_{ax} (I_{pol}). As the relative contributions of the different tissues are equal for I_{ax} and I_{pol}, the $I_{rel,tissue}$ values are not reported separately for axial and polar moments of area.

Wood traits

Wood density (in g cm^{-3}) was measured using the water displacement method. Root and stem segments, about 3 cm in length, were cut and debarked. Stem segments were additionally split in half and the pith carefully removed. The wood pieces were soaked in water for at least 30 min to ensure they were well hydrated. Each segment was then immersed into a water-filled beaker placed on an electronic balance with the aid of a dissecting needle and the weight of the displaced water was recorded. All segments were then dried at 80 °C for 24 h to a constant weight, and wood density was calculated by dividing the wood dry weight by the volume of displaced water.

For wood anatomical measurements, transverse sections about 40 µm thick were prepared with a sliding microtome. The sections were stained in a mixture of 0.35% safranin and 0.65% alcian blue, dehydrated through an ethanol series, and mounted in Neo-Mount (Merck Millipore, Germany). The relative proportions of various cell types in wood, i.e. vessels, fibres (including tracheids), and ray and axial parenchyma, were measured with an Axio Zoom V16 microscope on wedge-shaped transects spanning from the root or stem centre to the cambium at ×150 magnification. Image analysis involved manual tissue segmentation in Photoshop followed by area proportion measurements using Fiji/ImageJ (Schindelin *et al.*, 2012). To obtain the relative proportions of different cell types, the total surface area taken up by each cell type was divided by the total surface area of the entire transect measured. The axial and ray parenchyma proportions were already published in Plavcová *et al.* (2016).

In addition to cell type proportions, finer scale anatomical parameters were analysed. Vessel lumen area was measured on the same xylem wedges as the cell type proportions. The lumen areas were converted to vessel diameters assuming circular vessel geometry. Ray density was measured by counting the number of rays per quarter-circle-shaped root or stem wedge imaged at ×100 magnification. Ray width was assessed on images taken at ×200 magnification. The double wall thickness (DWT) and the lumen area of fibres and axial parenchyma cells were measured on transverse sections. These measurements were done at ×1000 magnifications using a light microscope equipped with an oil immersion objective (Leitz DMRB, Leica, Germany). At least 150 individual cells were measured for each species and organ. The lumen area was converted to lumen diameter (D_L) assuming a circular cell shape and the cell cross-sectional area (CSA), including the cell lumen and secondary wall, was calculated as $\pi(D_L/2+DWT/2)^2$. In addition, the thickness to span ratio of fibre and axial parenchyma was calculated by dividing DWT by D_L, and used as a measure of cell reinforcement (Pittermann *et al.*, 2006). The DWT and CSA values for four out of the nine species shown here were already published in Jupa *et al.* (2016).

Wood density and wood anatomy measurements were carried out on a different set of samples from those used for the mechanical testing. However, the samples were collected from the same population of trees following the same sampling scheme. Wood density was measured for six root and stem samples from at least three different individuals per species. Wood anatomy was measured on three root and stem samples from three different individuals.

Carbohydrate storage capacity and hydraulic conductivity of wood

In addition to data on mechanical properties, we obtained estimates of wood storage capacity and hydraulic conductivity in order to analyse potential trade-offs among the three competing functions. Concentrations of non-structural carbohydrates (NSC) in root wood and stem wood (in mg g^{-1}) measured for the same population of trees were taken from Plavcová *et al.* (2016), and used as a measure of wood storage capacity. Theoretical hydraulic conductivity was calculated from the measured vessel radius (r) using the Hagen–Poiseuille equation ($K_h=(\pi r^4)/8\mu$) and normalized by a corresponding xylem wedge area (McCulloh *et al.*, 2010). All three functional parameters (E_{str}, NSC, and K_h) were then converted to a common scale from 0 to 100 and plotted on ternary axes using the ggtern R package (Hamilton and Ferry, 2018).

Statistical analyses

The differences in structural and functional parameters between roots and stems were analysed using linear mixed-effect models. The models were fitted with organ (root or stem) being considered as a fixed factor and species identity as a random factor. To analyse differences in cell wall thickness of fibres and axial parenchyma, cell type was implemented as an additional fixed effect factor. Prior to the modelling, the normality and homogeneity of variance of the data were checked using the Shapiro–Wilk and Bartlett's tests, respectively. When the assumptions were not met, the data were log transformed. The analyses were conducted on species-level means. The models were fitted using the lme function from the nlme R package (Pinheiro *et al.*, 2013). The mixed effect models described above were designed to test for the overall difference between the two organs across all species. In addition, we analysed differences between roots and stems within each species using the Welch two-sample *t*-test. The interspecific differences in mechanical parameters within each organ were evaluated using Tukey-adjusted multiple mean comparisons. All data analyses were completed using R statistical software (R Core Team, 2016).

Results

Mechanical properties

On average, roots were about five times more flexible in bending and two times more flexible in torsion than stems.

The total axial second moment of area (I_{ax}) fell in a relatively narrow range of between 100 and 250 mm^4 for most of the samples measured as care was taken to collect samples of similar diameter. Correspondingly, the total polar second moment of area (I_{pol}) values ranged between 150 and 550 mm^4. Slightly larger stems and roots, corresponding to I_{ax} and I_{pol} values of ca. 500 mm^4 and 1000 mm^4, respectively, were collected for the woody climber *Clematis vitalba*. When structural bending and structural torsional moduli (E_{str} and $G_{str,}$) were calculated, neither of them correlated significantly with I_{ax} and I_{pol} (P>0.05). Thus, we assume that the variation of E_{str} and G_{str} occurring during ontogeny can be neglected in good approximation within the range of sample size tested in this study.

E_{str} and G_{str} values varied substantially among species and organs, with E_{str} ranging from 558 to 2913 MN m^{-2} and from 1220 to 12 681 MN m^{-2} (Fig. 1A) and G_{str} spanning from 48 to 254 MN m^{-2} and from 50 to 532 MN m^{-2} (Fig. 1B) for roots and stems, respectively. *Carpinus betulus* showed the highest E_{str} and G_{str} measured among all roots, while the roots of *Robinia pseudoacacia* were found to be the most flexible. Among stems, *Robinia pseudoacacia*, *Carpinus betulus*, *Acer pseudoplatanus*, *Fraxinus excelsior*, and *Fagus sylvatica* exhibited high values of both E_{str} and G_{str}, whereas the stems of *Clematis vitalba*, *Tilia cordata*, and *Quercus robur* showed relatively low resistance to deformation in both bending and twisting (Fig. 1). Neither E_{str} nor G_{str} showed a significant linear correlation between roots and stems (P>0.05), indicating that the mechanical properties of roots and stems within the same species are rather independent of each other. Contrasting mechanical properties of roots and stems were most apparent in *Robinia pseudoacacia*. Furthermore, all samples measured were consistently stiffer in bending than in torsion, as shown by their twist to bend ratios (EI/GI) higher than 1. Roots had significantly lower bend to twist ratios than stems (Fig. 1C). Overall, E_{str} and G_{str} values were closely correlated across species and organs (Fig. 2A, r^2=0.77, P<10^{-4} and r^2=0.86, P<10^{-4} for roots and stems, respectively).

Relative tissue contributions to axial and polar second moment of area

The mean relative contribution of pith to I_{ax} or I_{pol} ($I_{rel,pith}$) was very small in all stems measured, with $I_{rel,pith}$ typically less than 0.01 and never over 0.05. The mean relative contribution of wood to I_{ax} or I_{pol} ($I_{rel,wood}$) was 0.36 in roots and 0.48 in stems. Thus, the relative contribution of bark ($I_{rel,bark}$) was 12% higher in roots than in stems. Substantial differences in $I_{rel,wood}$ and $I_{rel,bark}$ also existed across the species investigated. The stems of *Carpinus betulus*, *Fagus sylvatica*, *Robinia pseudoacacia*, and *Acer pseudoplatanus* showed $I_{rel,wood}$ higher than 0.5, whereas $I_{rel,wood}$ values lower than 0.4 were observed in the stems of *Clematis vitalba* and *Tilia cordata*. Due to the presence of a thick bark, $I_{rel,wood}$ was also relatively low (i.e. less than 25%) in *Robinia pseudoacacia* and *Fraxinus excelsior* roots. In contrast, the roots of *Fagus sylvatica* had a very thin bark and hence $I_{rel,wood}$ was as high as 59%. In both organs, a higher proportion of wood was associated with higher mechanical stiffness, as indicated by significant positive correlations between $I_{rel,wood}$ and both E_{str} (Fig. 2B, r^2=0.62, P<0.05 and r^2 =0.81, P<10^{-4} for roots and stems, respectively) and G_{str} (r^2=0.65, P<0.01 and r^2 =0.91, P<10^{-4} for roots and stems, respectively).

Xylem anatomical traits in relation to mechanical properties

Wood density was significantly correlated with both E_{str} (r^2= 0.27, P<0.05) and G_{str} (r^2=0.33, P<0.05) when data from the two organs were pooled. When the organs were considered separately, a significant correlation was found only between wood density and E_{str} in roots (r^2=0.48, P=0.04, Fig. 2C). Fibre properties appeared to be the main driver of wood density as evidenced by a significant positive correlation with fibre double wall thickness to lumen diameter ratio (referred to as fibre thickness to span ratio hereafter, Fig. 2D). The tissue fractions of ray and axial wood parenchyma did not correlate significantly with the mechanical parameters and were not directly associated with wood density (P>0.05). The cell walls of both axial parenchyma and fibres were lignified as evidenced by staining with safranin. However, compared with fibres, axial wood parenchyma showed similar cross-sectional areas (Fig. 3A) and narrower cell walls than fibres (Fig. 3B), leading to a lower thickness to span ratio in axial wood parenchyma of both roots and stems (Fig. 3C). On the contrary, comparison of cell lumen and cell wall dimensions between organs revealed significantly higher mean cross-sectional areas in roots than in stems (Fig. 3A), but a similar mean cell wall thickness in both axial wood parenchyma and fibres (Fig. 3B). However, the resulting tendency to lower thickness to span ratios in roots compared with stems was not statistically significant (Fig. 3C). Across species, the thickness to span ratios of axial parenchyma cells were more homogeneous, ranging from 0.13 to 0.24 in roots and from 0.16 to 0.37 in stems, while the thickness to span ratios of fibres were much more variable, ranging from 0.15 to 1.09 in roots and from 0.17 to 0.79 in stems (Fig. 4). The interspecific variation in the thickness to span ratio was primarily determined by the wall thickness rather than the cell diameter as evidenced by approximately two times higher coefficients of covariation between thickness to span ratio and wall thickness.

Roots had wider rays (P=0.01) and higher overall fractions of radial parenchyma (P=0.004) compared with stems. However, wide rays were not universally associated with greater mechanical flexibility. For instance, wide multiseriate rays were found in both stems and roots of *Fagus sylvatica* (Fig. 5A, B, E, F), although these organs belonged to the mechanically stiffest specimens. In most species, ray cell walls were as thick as fibre walls and appeared lignified as indicated by a positive staining reaction with safranin. *Clematis vitalba* represented the only notable exception from this general pattern. In this species, the outermost portions of rays in both roots and stems were non-lignified as evidenced by intensive staining with alcian blue (Fig. 5H).

Association between traits and trade-off analysis

A principal component analysis (PCA) clearly separated roots and stems, summarized correlations between multiple traits,

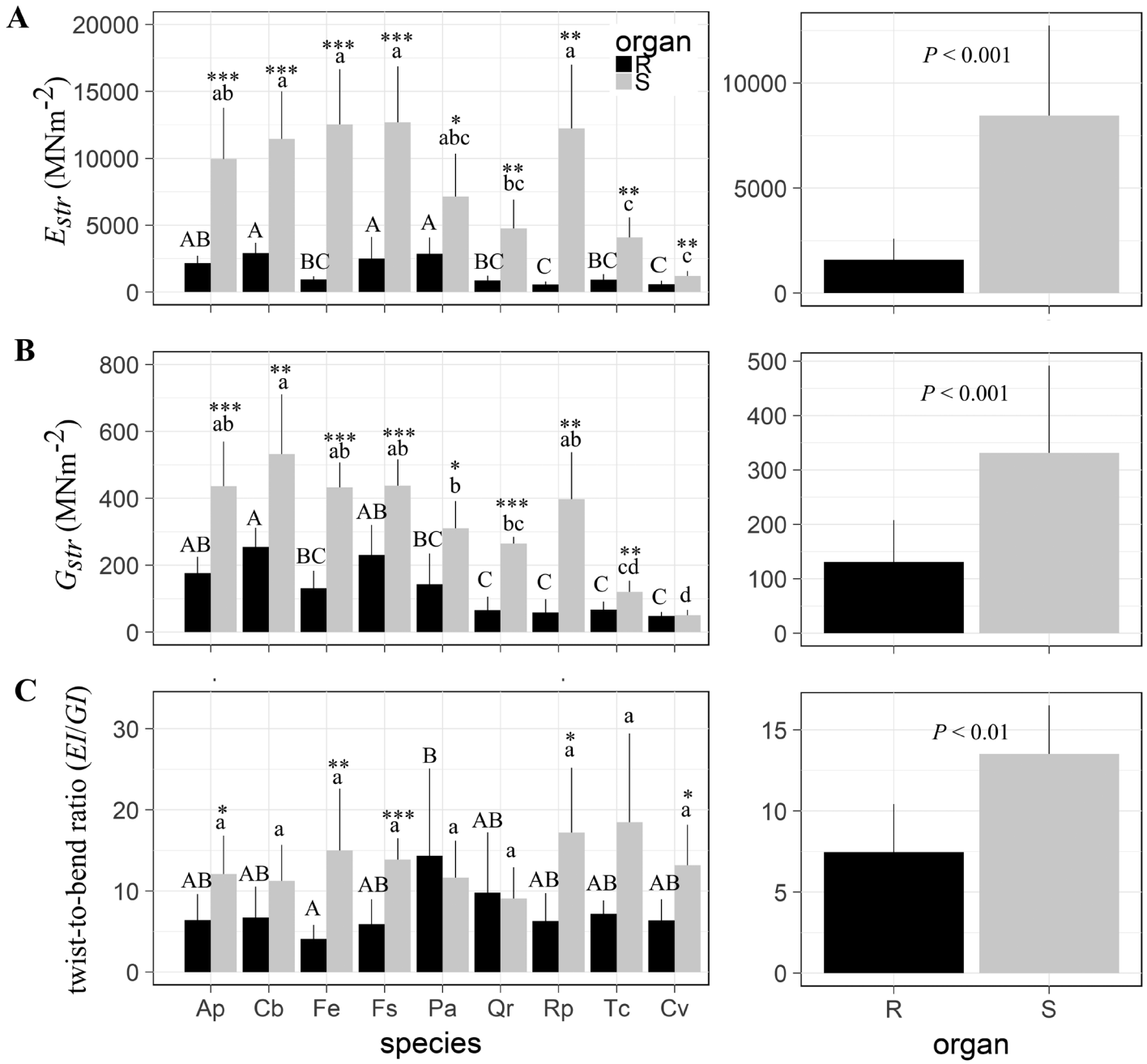

Fig. 1. Mechanical properties of young woody roots and stems. Structural bending moduli (E_{str}) (A), structural torsional moduli (G_{str}) (B) and ratios between bending and torsional stiffness (*EI*/*GI*) (C) in roots (R) and stems (S) of nine woody angiosperms. Bars represent species-level means ±SD (left-hand graph panels, *n*=6–8 samples) and root- and stem-level means ±SD calculated from the species-level means (right-hand panels, *n*=9 species). Roots and stems are depicted in black and grey, respectively. For abbreviation of species names see Table 1. Asterisks above bars indicate significant differences between root and stems within each species (Welch two sample *t*-test) at $P<0.05$ (*), $P<0.01$ (**) and $P<0.001$ (***). Significant differences between species within each organ are indicated by different letters (Tukey's adjusted multiple mean comparisons); uppercase letters are for roots, lowercase letters are for stems. *P*-values in the right-hand panels correspond to significance levels of the fixed effect 'organ' (mixed effect models with random effect of species).

and provided insights into trade-offs and their structural underpinnings (Fig. 6). The first component explained 45% of the variation of the dataset and showed strong positive loadings with E_{str}, G_{str}, $I_{xyl.rel}$, and wood density, and negative loadings with lumen area of parenchyma cells and vessel diameter. The first component can therefore be interpreted as a trade-off between mechanical function, which is prominent in stems, and storage and hydraulic functions that are both more emphasized in roots. The second component, which explained 22% of the variation, was most strongly related to fibre and parenchyma tissue fractions, which co-vary in the opposite direction.

The overall coordination between mechanical stiffness, storage capacity, and hydraulic conductivity was also visualized in ternary diagrams. The diagrams provide evidence for structure–functional trade-offs that differ across and within organs (Fig. 7). A strong trade-off between mechanical

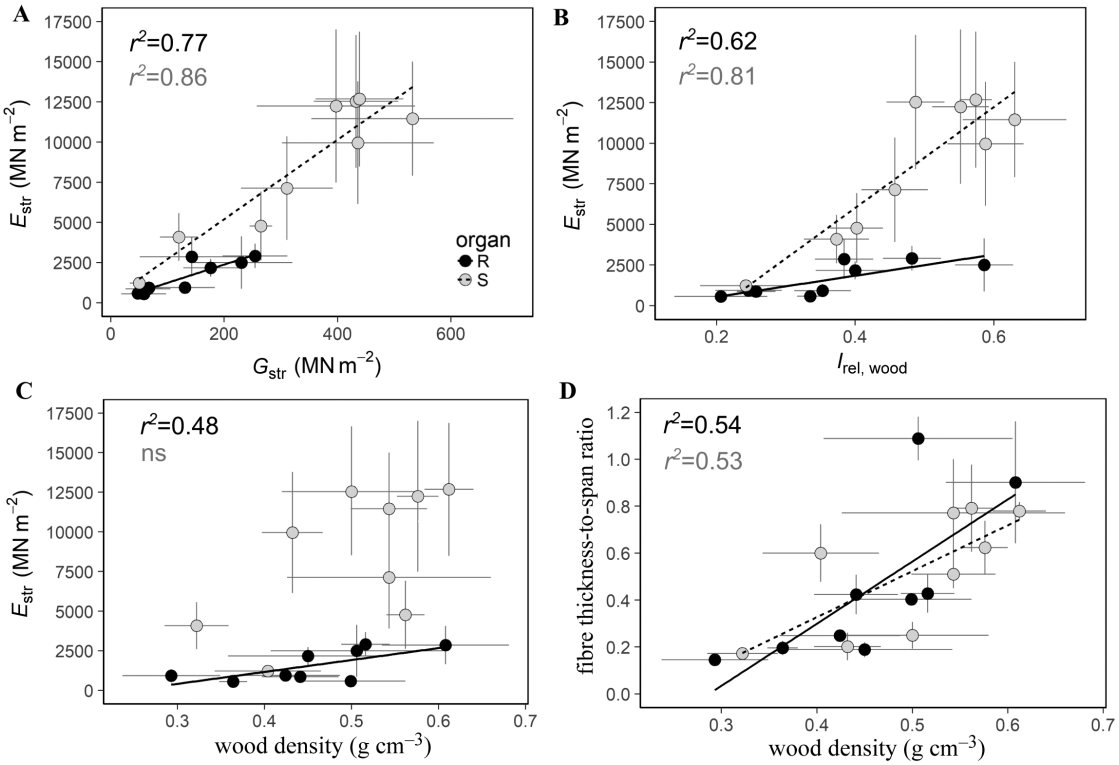

Fig. 2. Correlations between mechanical and structural properties. Correlation between (A) structural bending modulus (E_{str}) and structural torsional modulus (G_{str}), (B) between the contribution of wood to the axial second moment of area ($I_{rel,wood}$) and structural bending modulus (E_{str}), (C) between wood density and structural bending modulus (E_{str}), and (D) between wood density and fibre double wall thickness to lumen diameter ratio. The symbols represent mean values and SD of roots (black) and stems (grey).

stiffness and storage capacity is clearly apparent between roots and self-supporting stems (Fig. 7A). The stems of the non-self-supporting liana *Clematis vitalba* exhibited low mechanical stiffness and high hydraulic conductivity, and hence clustered with roots (Figs 6, 7A). The stems of *Tilia cordata* were positioned in the centre of the ternary plot (Fig. 7A), exhibiting the strongest compromise between all three functions. When the data for *Clematis vitalba* were excluded and the data for self-supporting trees were plotted separately for roots (Fig. 7B) and stems (Fig. 7C), the within organ variation became more apparent. The root data (Fig. 7B) separated more homogeneously across the functional triangle compared with stems (Fig. 7C), in which the data were mostly positioned along the mechanics–storage trade-off. Within roots (Fig. 7B), hydraulics was the dominant function in *Robinia pseudoaccacia*, *Fraxinus excelsior*, and *Tilia cordata*, while mechanics was dominant in *Carpinus betulus* and *Fagus sylvatica*, with storage being dominant in *Quercus robur*. All three functions were most strongly compromised in the roots of *Acer pseudoplatanus* and *Prunus avium*. Within stems (Fig. 7C), the mechanical function was most pronounced in *Carpinus betulus* and *Prunus avium*, while the storage function was most dominant in *Quercus robur*, with hydraulics being most prominent in *Tilia cordata*. The stems of *Fraxiunus excelsior* compromised mainly between the mechanical and hydraulic function, while *Fagus sylvatica*, *Robinia pseudoaccacia*, and *Acer pseudoplatanus* were found to be compromised between storage and mechanical functions.

Discussion

In agreement with our hypothesis, roots showed lower resistance to both bending and twisting forces than self-supporting stems (Fig. 1A, B). From the two mechanical parameters, a greater difference was observed in E_{str} than in G_{str}, resulting in lower twist to bend ratios (EI/GI) of roots (Fig. 1C). The higher mechanical stiffness of self-supporting stems allows them to grow outward and support leaves for efficient light acquisition. Contrarily, the greater mechanical flexibility of roots helps them to avoid overcritical bending and torsional loads caused by the movement of soil components in relation to the Mohr–Coulomb law (Mattheck and Breloer, 1994), and allows roots to navigate their surroundings with less resistance. Mechanical properties of woody roots were less frequently quantified than those of stems, despite their importance in anchoring trees to their substrate (Niklas, 1999*b*; Karrenberg *et al.*, 2003), penetrating compacted soil (Day *et al.*, 1995), and stabilising and reinforcing slopes (Schwarz *et al.*, 2010). Thus, our data may be useful to parameterise models for these kinds of applications. However, it has to be taken into account that we did not investigate the variation of mechanical properties along the stems and roots depending on their position within the plant and their stage of ontogeny. Fine roots are likely to be exposed to tensile forces and show a high tensile rigidity, whereas older root segments close to the stem base show a high resistance to bending and compression (Ennos, 2000). In order to allow for a comparison between species we sampled all root segments at approximately 1 m from the root collar. It

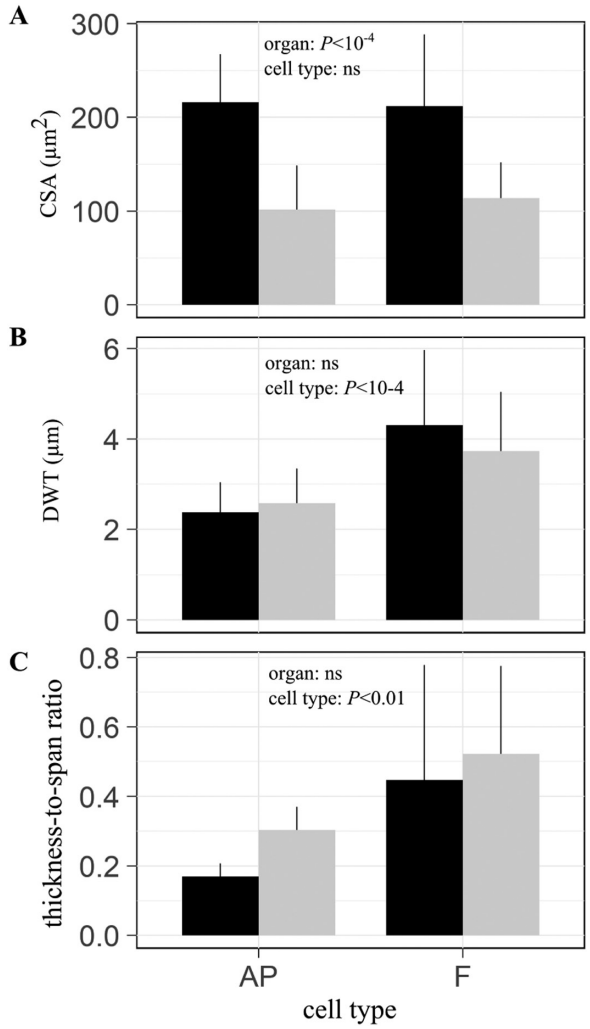

Fig. 3. Comparison of axial wood parenchyma and fibre cell structure in roots and stems of nine angiosperm species. Mean values and SD of (A) cell cross-sectional area (CSA), (B) double wall thickness (DWT), and (C) thickness to span ratio of axial wood parenchyma (AP) and fibre (F) cells. Roots and stems are depicted in black and grey, respectively. Significance levels for the fixed effect factors organ and cell type are given (mixed effect models with random effect of species).

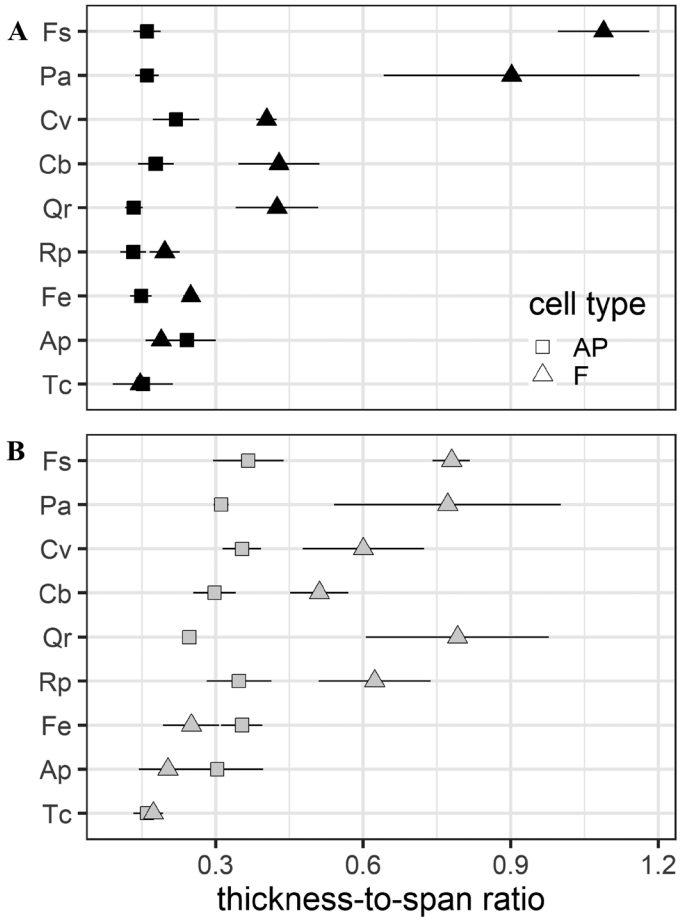

Fig. 4. Variation in thickness to span ratio (i.e. the ratio between double wall thickness and cell lumen diameter) of axial wood parenchyma cells (AP, black) and fibres (F, grey) in roots (A) and stems (B) of nine woody angiosperm species. For abbreviation of species names see Table 1.

is likely that segments farther away from the stem show different mechanical properties, in particular in tension, which we have not studied here. Young stems (or the young tips of stems) are also known to be more flexible in bending than older stems (or the older bases of stems) and are therefore able to avoid critical stresses by streamlining parallel to mechanical forces (e.g. when submitted to wind loads), whereas older stems have a considerably higher bending resistance (Speck, 1994; Speck *et al.*, 1996; Rowe and Speck, 2004).

The structural underpinnings of mechanical properties can be linked to multiple morpho-anatomical characteristics of woody organs (Figs 2, 6). In both woody organs, E_{str} and the G_{str} were positively correlated to a greater proportion of wood relative to bark. While wood represents the stronger of the two tissues, the importance of bark for whole organ mechanics originates mainly from its position far from the neutral axis (Niklas, 1999*a*; Karrenberg *et al.*, 2003). The overall lower $I_{rel,wood}$ and the relatively weaker correlation of $I_{rel,wood}$ with both structural moduli in roots compared with stems (Fig. 2B) indicates that the relative contribution of bark to the mechanical properties was greater in roots. These results are consistent with Pratt *et al.* (2007), who reported an important contribution of bark to root mechanics for nine chaparral species. In our study, higher values of $I_{rel,bark}$ were typically found in organs with low wood density (e.g. in the roots of *Robinia pseudoacacia*, *Fraxinus excelsior*, and *Quercus robur*, and in the stems of *Tilia cordata*) suggesting that a thick bark, sometimes strengthened by the presence of lignified fibres (Fig. 5C), partially compensates for a mechanically weak wood and may even have additional functions for controlling tree posture (Clair *et al.*, 2019). An additional structural role of bark may be in the protection from abrasion caused by soil particles and stones when roots are mechanically loaded. However, other functions, unrelated to mechanical properties, such as defence against pathogens, storage, and phloem transport towards the root apical meristems, are also correlated with bark thickness (Rosell *et al.*, 2014).

Although there was no significant difference in wood density between the tested young roots and stems, wood density was positively related to E_{str} and G_{str} across species (Fig. 2C). A close association of wood density and mechanical properties has also been evidenced in a number of previous studies (Jacobsen *et al.*,

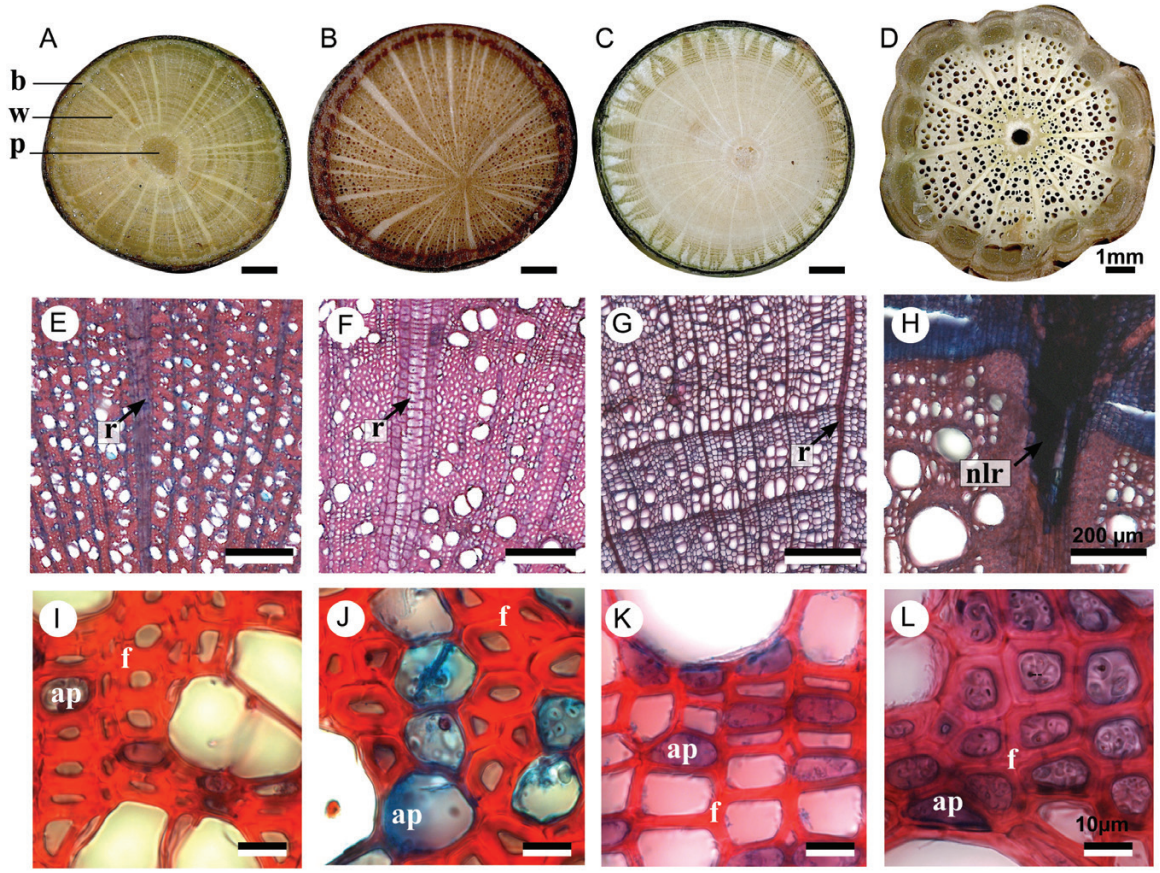

Fig. 5. Anatomy of young woody roots and stems at three different magnifications. Anatomical characteristics of roots of *Fagus sylvatica* (A, E, I) and stems of *Fagus sylvatica* (B, F, J), stems of *Tilia cordata* (C, G, K) and stems of *Clematis vitalba* (D, H, L) photographed at increasing magnification. Thicker bark (A versus B), wider rays (E versus F) and greater size of xylem cells (I versus J) are typical of roots compared with stems. Stems of *Tilia cordata* have a thick bark strengthened by strands of lignified fibres (C), wood of low density (G) and fibre and axial parenchyma with narrow cell walls (K). Specialized anatomy of lianescent stem of *Clematis vitalba* showing lobbed wood–bark boundary (D), wide multiseriate rays that have a non-lignified outermost portion (nlr-r) (H) and living fibres large in diameter and with a thick secondary wall (L). Abbreviations: ap, axial parenchyma; b, bark; f, fibre; nlr, non-lignified ray; p, pith; r, ray; w, wood.

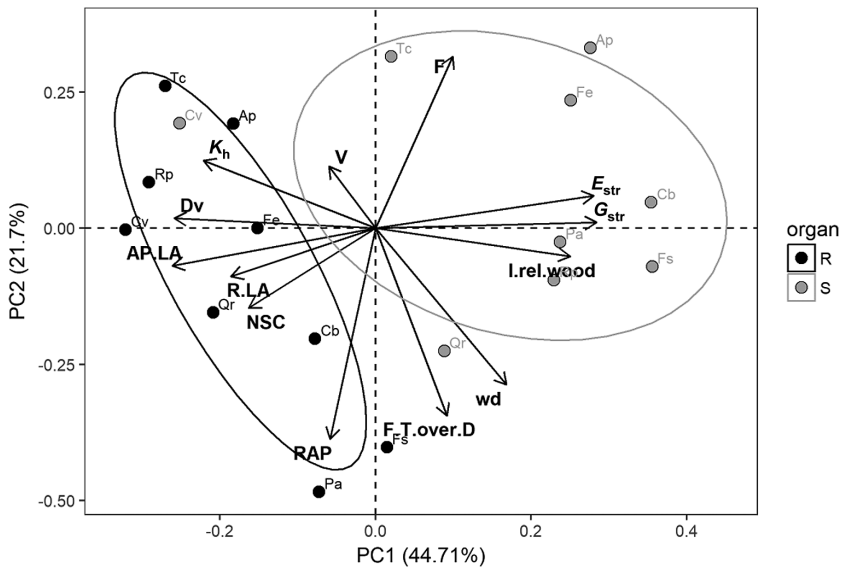

Fig. 6. Principal component analysis (PCA) biplot showing the overall coordination of xylem structural traits in roots (black) and stems (grey). Structural traits are lumen area of axial and ray parenchyma (AP.LA, R.LA), vessel diameter (Dv), thickness to span ratio of fibres (F.T.over.D), fibres tissue fraction (F), ray and axial parenchyma tissue fraction (RAP), vessel tissue fractions (V), theoretical hydraulic conductivity (K_h), concentration of non-structural carbohydrates (NSC), bending structural modulus (E_{str}), torsional structural moduls (G_{str}) and wood density (wd). Roots and stems are depicted in black and grey symbols, respectively. For abbreviation of species names see Table 1.

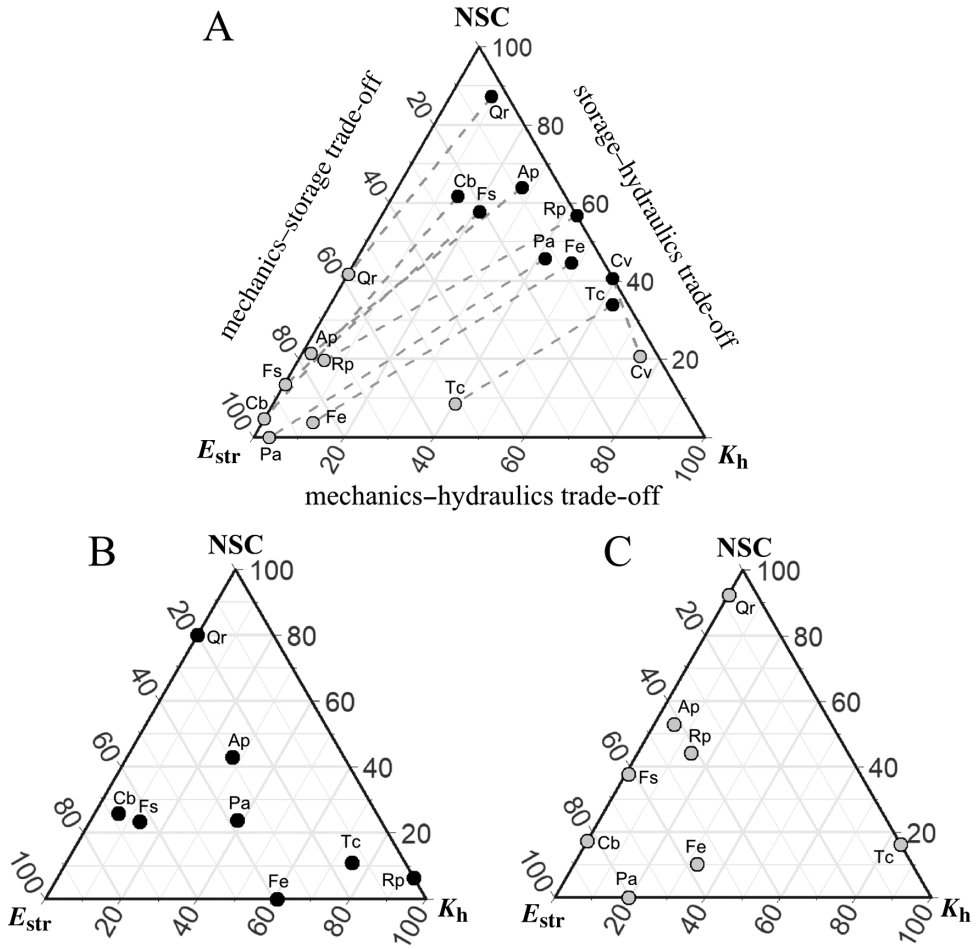

Fig. 7. Trade-off triangle showing the relative division of xylem function between mechanical stiffness, carbohydrate storage capacity, and hydraulic conductivity for roots and stems of nine woody angiosperm species. Data from both organs are plotted together (A), or for roots (B) and stems (C) separately. The data for non-self-supporting *Clematis vitalba* are not included in (B, C). Mechanical properties are represented by the structural bending modulus (E_{str}), storage capacity is represented by the concentration of non-structural carbohydrates measured at the onset of winter dormancy (NSC), and hydraulic conductivity is represented by the theoretical hydraulic conductivity (K_h). Species abbreviations follow Table 1. Roots and stems are shown in black and grey symbols, respectively.

2007; Chave *et al.*, 2009; Niklas and Spatz, 2010). From all anatomical parameters measured, wood density was most strongly correlated with the wall thickness to span ratio of fibres (Fig. 2D). Mechanically stiffer stems also had higher area fractions of fibres and lower fractions of ray and axial parenchyma compared with roots (Table 2). However, the higher fractions of parenchyma did not translate directly into reduced mechanical stiffness despite parenchyma cells having lower thickness to span ratios than fibres (Fig. 3C). The finding that fibre reinforcement rather than fibre proportions exerts major control over wood density and mechanical performance is in line with the findings on 24 Australian tree and shrub species from three climate zones (Ziemińska *et al.*, 2013).

Parenchyma and fibre cells were on average larger in diameter in roots than in stems, while the wall thickness did not differ significantly between organs (Fig. 3A, B). Consequently, the larger cell size resulted in lower thickness to span ratio of root fibres and axial wood parenchyma cells, which is in line with lower mechanical demands and greater storage capacity of roots. While the presence of narrower cell walls constitutes an important criterion in the formal anatomical definition of axial wood parenchyma cells (Wheeler *et al.*, 1989; Carlquist, 2001), our results demonstrate that the morphological dichotomy between fibres and axial parenchyma cells is highly variable across species (Figs 4, 5I–L). The dichotomy was large in *Fagus sylvatica* and *Prunus avium*, and low in *Acer pseudoplatanus*, *Fraxinus excelsior*, and *Tilia cordata*. The difference was mainly driven by fibre wall thickness, while the lumen size and wall thickness of axial parenchyma cells were rather uniform across species.

Due to its radial orientation, the effect of ray parenchyma on mechanical stiffness is complex and will differ depending on the direction of mechanical loading. In our study, a higher fraction of ray parenchyma associated with the presence of wider rays (Table 2) could contribute to a greater mechanical flexibility of roots compared with stems. Wide multiseriate rays were found in the roots of *Clematis vitalba*, *Fagus sylvatica* (Fig. 5A, E), and *Prunus avium*, and also in the stems of *Fagus sylvatica* (Fig. 5B, F). Ray cells in most of the tested species appeared fully lignified as suggested by a positive staining reaction with safranin, and the thickness of their walls was comparable to those of fibres. Only the rays of *Clematis vitalba* were partially non-lignified (Fig. 5H). In this climbing species, wide non-lignified

Table 2. *Anatomical parameters of ray and axial parenchyma for roots and stems of nine woody angiosperm species*

Species	RP (%)	AP (%)	RAP (%)	Ray density (count per 90° wedge)	Ray width (μm)	AP DWT (μm)	AP D_L (μm)
Roots							
All	18.2±5.2a	13.0±6.3a	31.3±9.2a	24.4±11.1a	32.8±26.2a	2.4±0.7a	14.1±1.4a
Ap	14.7±6.4	0.7±0.3	15.4±6.6	22.3±7	17.3±3.3	3.4±0.3	14.3±2.5
Cb	20.3±3.8	15±2.6	35.3±6.4	36.3±3.5	30.3±6.4	2.6±0.6	14.3±0.8
Fe	13.2±3.9	21.1±3.3	34.3±4.2	20±4	19.5±6.2	2.2±0.3	14.9±1
Fs	23.1±9.5	17.1±6.9	40.2±8.2	21±1.7	43.2±2.1	2.1±0.4	13.1±0.4
Pa	28.8±3.5	14.3±2.3	43.1±5.2	33±5.6	35.7±11	2±0.1	12.5±1.5
Qr	18.9±1.5	16.9±8	35.7±7.5	39.7±13.1	15.9±1.9	1.8±0.1	13.9±1.5
Rp	17.1±2	15.5±1.3	32.6±2.5	28.3±7.1	16±0.2	2±0.4	15.4±0.3
Tc	15.6±3.8	5.4±2.1	21±4.5	13.7±3.8	19.6±5.3	1.8±0.5	12±1.6
Cv	12.5±5.3	11.3±3.6	23.8±8.6	5±1	97.5±2.8	3.6±0.3	16.6±2.1
Stems							
All	13.7±4.0b	8.8±7.6a	22.5±6.5b	30.7±12.2b	26.6±34.1a	2.6±0.8a	8.6±1.7b
Ap	11.5±5.1	1.8±0.6	13.4±5.7	30.3±2.1	10.2±1	2.5±0.5	8.6±1.2
Cb	17.6±2	6.2±2.7	23.8±0.8	49.3±9	11.2±1.1	2.7±0.4	9.1±0.3
Fe	13.3±4.5	5.4±0.4	18.7±4.8	25.3±4.9	13±1.4	2.7±0.3	7.5±0.2
Fs	16.4±0.4	30.7±5.3	47.1±5.7	20.7±1.2	21.1±2.9	1.6±0.2	21.1±1.9
Pa	20.7±3.5	2.7±1	23.4±4.5	41±3.6	13±1.7	2.1±0.2	6.6±0.4
Qr	10.9±2.1	22.7±2.1	33.6±0.1	35.3±4	9.9±1.4	2.2±0.2	9±1
Rp	9.9±1.6	20.9±6.3	30.8±7.8	30.3±6.7	11.1±2	2.7±0.4	7.9±0.5
Tc	9.7±0.7	7.5±2.3	17.2±2	27±5.3	11.3±1.3	1.5±0.4	9.4±0.9
Cv	12.1±3.7	6.1±3.3	18.3±3.4	5±1	111.3±8.5	4.3±0.3	12.4±1.7

Values represent means ±SD. Different letters indicate significant difference between roots and stems (mixed effect models with random effect of species). AP, area fraction of axial parenchyma; AP D_L, mean lumen diameter of axial parenchyma cells; AP DWT, mean double wall thickness of axial parenchyma cells; RAP, area fraction of ray and axial parenchyma; RP, area fraction of ray parenchyma.

portions of rays were present in the outermost region, close to the vascular cambium, thereby forming wedge-shaped incisions in the otherwise lignified secondary xylem. Due to their position far from the neutral axis, the incompletely lignified ray cells likely result in a substantial mechanical weakening and represent one of the structural features causing the high mechanical flexibility found in *Clematis vitalba* roots and stems (Isnard *et al.*, 2003). Similarly, non-lignified or partially lignified rays have also been observed in other climbers such as *Aristolochia malacophylla* (Wagner *et al.*, 2012). The high proportion of large-diameter vessels typical of lianescent wood and some roots can be considered as an additional factor contributing to the low mechanical stiffness in stems of climbing species (Gasson and Dobbins, 1991; Rowe and Speck, 1996, 2014; Gallenmüller *et al.*, 2001).

The overall structure–function trade-offs differ for between- and within-organ comparisons (Fig. 7). Our results demonstrate that it is rare for xylem to compromise all three functions equally. Instead, one of the three functions is usually more pronounced, while the remaining two functions may or may not co-vary. In self-supporting stems, the higher demands for mechanical stability clearly represent a major constraint. The isolated position of the stems of the liana *Clematis vitalba* in the trade-off triangle (Fig. 7) represents a further proof of the different mechanical and hydraulic properties of non-self-supporting plants (Rowe and Speck, 2004, 2014). In roots with fewer mechanical demands, xylem can be designed with a greater emphasis on either storage (e.g. *Quercus robur*) or hydraulic function (e.g. *Tilia cordata*, *Robina pseudoaccacia*; Fig. 7B).

The functional trade-offs primarily originate from a division of labour between different cell types. Besides cell type fractions, finer scale anatomical properties of different xylem cells, such as the lumen size and cell wall thickness, affect these relationships. From a functional perspective, the secondary wall thickness is critical in fibres, the lumen area in parenchyma cells and conduits (including vessels and tracheids). Our data show that, at least in juvenile wood, fibre wall thickness is highly variable across species and organs, while wall thickness of axial parenchyma is much less variable (Fig. 4). The main source of functional diversity in axial parenchyma across species is due to variation in their tissue fraction (Morris *et al.*, 2016*b*; Plavcová *et al.*, 2016), arrangement (Morris *et al.*, 2018), and biochemical properties (Plavcová and Jansen, 2015), rather than in the lumen size of individual cells. In contrast to axial parenchyma cells, vessel diameter is greatly variable across species and organs (Hacke *et al.*, 2017). Greater plasticity of vessel diameter may represent a selective advantage because hydraulic function is more sensitive to increases in vessel diameter. In accordance with the Hagen–Poiseuille equation, even a small increase in vessel diameter results in a large increase in conductivity, depending on the vessel diameter by the power of four (Tyree and Ewers, 1991). However, in self-supporting species the xylem structure is not severely altered by conduit width because larger conduits are less numerous, and the overall conduit lumen fraction remains fairly similar at around 15–20% (Zanne *et al.*, 2010; Morris *et al.*, 2016*b*).

In summary, our results demonstrate that higher demands for mechanical stability in self-supporting stems put a major

constraint on xylem structure, whereas root xylem can be designed with a greater emphasis on both storage and hydraulic functions. The interplay between mechanical stiffness, nutrient storage, and hydraulic conductivity in young woody roots and stems is driven by differences in cell type relative fractions, cell size, and secondary wall reinforcement of these cells.

Acknowledgements

LP was initially supported by a Postdoctoral Fellowship from the Alexander von Humboldt Foundation and research funding granted by Ulm University and Ulm University Society (Ulmer Universitätsgesellschaft). SJ acknowledges the German Research Foundation (DFG, project no. JA 2174/3-1) for financial support. We wish to thank the Botanical Garden of the University of Freiburg for access to plant material. We also thank Jan Plavec and Aneta Bulíčková for technical assistance and Dr Stephanie Stuart for useful discussions.

References

Baas P, Ewers FW, Davis SD, Wheeler EA. 2004. Evolution of xylem physiology. In: Hemsley AR, Poole I, eds. The evolution of plant physiology. London: Elsevier Academic Press, 273–295.

Badel E, Ewers FW, Cochard H, Telewski FW. 2015. Acclimation of mechanical and hydraulic functions in trees: impact of the thigmomorphogenetic process. Frontiers in Plant Science **6**, 266.

Bittencourt PR, Pereira L, Oliveira RS. 2016. On xylem hydraulic efficiencies, wood space-use and the safety-efficiency tradeoff: comment on Gleason *et al*. (2016) 'Weak tradeoff between xylem safety and xylem-specific hydraulic efficiency across the world's woody plant species'. New Phytologist **211**, 1152–1155.

Brodersen CR, McElrone AJ, Choat B, Matthews MA, Shackel KA. 2010. The dynamics of embolism repair in xylem: in vivo visualizations using high-resolution computed tomography. Plant Physiology **154**, 1088–1095.

Burgert I, Bernasconi A, Niklas K, Eckstein D. 2001. The influence of rays on the transverse elastic anisotropy in green wood of deciduous trees. Holzforschung **55**, 449–454.

Cai J, Li S, Zhang H, Zhang S, Tyree MT. 2014. Recalcitrant vulnerability curves: methods of analysis and the concept of fibre bridges for enhanced cavitation resistance. Plant, Cell & Environment **37**, 35–44.

Carlquist S. 2001. Comparative wood anatomy: systematic, ecological, and evolutionary aspects of dicotyledon wood. Berlin, Heidelberg: Springer-Verlag.

Chave J, Coomes D, Jansen S, Lewis SL, Swenson NG, Zanne AE. 2009. Towards a worldwide wood economics spectrum. Ecology Letters **12**, 351–366.

Christensen-Dalsgaard KK, Ennos AR, Fournier M. 2007*a*. Changes in hydraulic conductivity, mechanical properties, and density reflecting the fall in strain along the lateral roots of two species of tropical trees. Journal of Experimental Botany **58**, 4095–4105.

Christensen-Dalsgaard KK, Fournier M, Ennos AR, Barfod AS. 2007*b*. Changes in vessel anatomy in response to mechanical loading in six species of tropical trees. New Phytologist **176**, 610–622.

Clair B, Ghislain B, Prunier J, Lehnebach R, Beauchêne J, Alméras T. 2019. Mechanical contribution of secondary phloem to postural control in trees: the bark side of the force. New Phytologist **221**, 209–217.

Day S, Bassuk N, Van Es H. 1995. Effects of four compaction remediation methods for landscape trees on soil aeration, mechanical impedance and tree establishment. Journal of Environmental Horticulture **13**, 64–64.

Ennos, AR. 2000. The mechanics of root anchorage. Advances in Botanical Research **33**, 133–157.

Fujiwara S. 1992. Anatomy and properties of Japanese hardwoods II. Variation of dimensions of ray cells and their relation to basic density. IAWA Bulletin **13**, 397–402.

Fujiwara S, Sameshima K, Kuroda K, Takamura N. 1991. Anatomy and properties of Japanese hardwoods. I. Variation of fibre dimensions and tissue proportions and their relation to basic density. IAWA Bulletin **12**, 419–424.

Gallenmüller F, Müller U, Rowe N, Speck T. 2001. The growth form of *Croton pullei* (Euphorbiaceae) – functional morphology and biomechanics of a neotropical liana. Plant Biology **3**, 50–61.

Gartner BL. 1991. Stem hydraulic properties of vines vs. shrubs of western poison oak, *Toxicodendron diversilobum*. Oecologia **87**, 180–189.

Gasson P, Dobbins DR. 1991. Wood anatomy of the Bignoniaceae, with a comparison of trees and lianas. IAWA Bulletin **12**, 389–417.

Gleason SM, Westoby M, Jansen S, *et al*. 2016. Weak tradeoff between xylem safety and xylem-specific hydraulic efficiency across the world's woody plant species. New Phytologist **209**, 123–136.

Hacke UG, Spicer R, Schreiber SG, Plavcová L. 2017. An ecophysiological and developmental perspective on variation in vessel diameter. Plant, Cell & Environment **40**, 831–845.

Hamilton NE, Ferry M. 2018. *ggtern*: ternary diagrams using ggplot2. Journal of Statistical Software, Code Snippets **87**, 1–17.

Isnard S, Speck T, Rowe N. 2003. Mechanical architecture and development in *Clematis*: implications for canalised evolution of growth forms. New Phytologist **158**, 543–559.

Jacobsen AL, Agenbag L, Esler KJ, Pratt RB, Ewers FW, Davis SD. 2007. Xylem density, biomechanics and anatomical traits correlate with water stress in 17 evergreen shrub species of the Mediterranean-type climate region of South Africa. Journal of Ecology **95**, 171–183.

Jacobsen AL, Ewers FW, Pratt RB, Paddock WA 3rd, Davis SD. 2005. Do xylem fibers affect vessel cavitation resistance? Plant Physiology **139**, 546–556.

Jupa R, Plavcová L, Gloser V, Jansen S. 2016. Linking xylem water storage with anatomical parameters in five temperate tree species. Tree Physiology **36**, 756–769.

Karrenberg S, Blaser S, Kollmann J, Speck T, Edwards P. 2003. Root anchorage of saplings and cuttings of woody pioneer species in a riparian environment. Functional Ecology **17**, 170–177.

Lachenbruch B, McCulloh KA. 2014. Traits, properties, and performance: how woody plants combine hydraulic and mechanical functions in a cell, tissue, or whole plant. New Phytologist **204**, 747–764.

Lens F, Picon-Cochard C, Delmas CE, *et al*. 2016. Herbaceous angiosperms are not more vulnerable to drought-induced embolism than Angiosperm trees. Plant Physiology **172**, 661–667.

Lens F, Sperry JS, Christman MA, Choat B, Rabaey D, Jansen S. 2011. Testing hypotheses that link wood anatomy to cavitation resistance and hydraulic conductivity in the genus *Acer*. New Phytologist **190**, 709–723.

Mattheck C, Breloer H. 1994. The body language of trees: a handbook for failure analysis [Edited by David Lonsdale from a translation by Robert Strouts]. London: H. M. Stationery Office.

McCulloh K, Sperry JS, Lachenbruch B, Meinzer FC, Reich PB, Voelker S. 2010. Moving water well: comparing hydraulic efficiency in twigs and trunks of coniferous, ring-porous, and diffuse-porous saplings from temperate and tropical forests. New Phytologist **186**, 439–450.

Morris H, Brodersen C, Schwarze FW, Jansen S. 2016*a*. The parenchyma of secondary xylem and its critical role in tree defense against fungal decay in relation to the CODIT model. Frontiers in Plant Science **7**, 1665.

Morris H, Gillingham MAF, Plavcová L, *et al*. 2018. Vessel diameter is related to amount and spatial arrangement of axial parenchyma in woody angiosperms. Plant, Cell & Environment **41**, 245–260.

Morris H, Plavcová L, Cvecko P, *et al*. 2016*b*. A global analysis of parenchyma tissue fractions in secondary xylem of seed plants. New Phytologist **209**, 1553–1565.

Niklas KJ. 1992. Plant biomechanics: an engineering approach to plant form and function. Chicago: University of Chicago Press.

Niklas KJ. 1999*a*. The mechanical role of bark. American Journal of Botany **86**, 465–469.

Niklas KJ. 1999*b*. Variations of the mechanical properties of *Acer saccharum* roots. Journal of Experimental Botany **50**, 193–200.

Niklas KJ, Spatz H-C. 2010. Worldwide correlations of mechanical properties and green wood density. American Journal of Botany **97**, 1587–1594.

Pfautsch S, Hölttä T, Mencuccini M. 2015. Hydraulic functioning of tree stems—fusing ray anatomy, radial transfer and capacitance. Tree Physiology, **35**, 706–722.

Pinheiro J, Bates D, DebRoy S, Sarkar D, **The R Development Core Team**. 2013. nlme: linear and nonlinear mixed effects models. R package version 3.1-108.

Pittermann J, Sperry JS, Wheeler JK, Hacke UG, Sikkema EH. 2006. Mechanical reinforcement of tracheids compromises the hydraulic efficiency of conifer xylem. Plant, Cell & Environment **29**, 1618–1628.

Plavcová L, Hoch G, Morris H, Ghiasi S, Jansen S. 2016. The amount of parenchyma and living fibers affects storage of nonstructural carbohydrates in young stems and roots of temperate trees. American Journal of Botany **103**, 603–612.

Plavcová L, Jansen S. 2015. The role of xylem parenchyma in the storage and utilization of nonstructural carbohydrates. In: Hacke UG, ed. Functional and ecological xylem anatomy. Cham: Springer International Publishing, 209–234.

Pratt RB, Jacobsen AL. 2017. Conflicting demands on angiosperm xylem: Tradeoffs among storage, transport and biomechanics. Plant, Cell & Environment **40**, 897–913.

Pratt RB, Jacobsen AL, Ewers FW, Davis SD. 2007. Relationships among xylem transport, biomechanics and storage in stems and roots of nine Rhamnaceae species of the California chaparral. New Phytologist **174**, 787–798.

Putz FE, Holbrook NM. 1991. Biomechanical studies of vines. In Putz FE, Mooney HA, eds. The biology of vines. Cambridge: Cambridge University Press, 73–98.

R Core Team. 2016. R: a language and environment for statistical computing. Vienna, Austria: R Foundation for Statistical Computing. https://www.R-project.org/.

Rosell JA, Gleason S, Méndez-Alonzo R, Chang Y, Westoby M. 2014. Bark functional ecology: evidence for tradeoffs, functional coordination, and environment producing bark diversity. New Phytologist **201**, 486–497.

Rowe NP, Isnard S, Gallenmüller F, Speck T. 2006. Diversity of mechanical architectures in climbing plants: an ecological perspective. In: Herrel A, Speck T, Rowe NP, eds. Ecology and biomechanics: a mechanical approach to the ecology of animals and plants. Boca Raton, FL, USA: Taylor & Francis, 35–59.

Rowe NP, Speck T. 1996. Biomechanical characteristics of the ontogeny and growth habit of the tropical liana *Condylocarpon guianense* (Apocynaceae). International Journal of Plant Sciences **157**, 406–417.

Rowe N, Speck T. 2004. Hydraulics and mechanics of plants: novelty, innovation and evolution. In: Hamsley AR, Poole I, eds. The evolution of plant physiology. London: Elsevier Academic Press, 297–325.

Rowe NP, Speck T. 2014. Stem biomechanics, strength of attachment, and developmental plasticity of vines and lianas. In: Schnitzer S, Bongers F, Burnham, R, Putz F, eds. Ecology of lianas. Chichester: Wiley-Blackwell, 323–341.

Schindelin J, Arganda-Carreras I, Frise E, *et al*. 2012. Fiji: an open-source platform for biological-image analysis. Nature Methods **9**, 676–682.

Schwarz M, Cohen D, Or D. 2010. Root-soil mechanical interactions during pullout and failure of root bundles. Journal of Geophysical Research: Earth Surface **115**, F04035.

Speck T. 1994. Bending stability of plant stems: ontogenetical, ecological, and phylogenetical aspects. Biomimetics **2**, 109–128.

Speck T, Burgert I. 2011. Plant stems: functional design and mechanics. Annual Review of Materials Research **41**, 169–193.

Speck T, Rowe NP, Bruechert F, Haberer W, Gallenmüller F, Spatz H-C. 1996. How plants adjust the'material properties' of their stems according to differing mechanical constraints during growth: an example of smart design in nature. In: The 3rd Biennial Joint Conference on Engineering Systems Design and Analysis, ESDA. Part 5, 233–241.

Tyree MT, Ewers FW. 1991. The hydraulic architecture of trees and other woody plants. New Phytologist **119**, 345–360.

Tyree MT, Yang S. 1990. Water-storage capacity of *Thuja*, *Tsuga* and *Acer* stems measured by dehydration isotherms: the contribution of capillary water and cavitation. Planta **182**, 420–426.

van der Sande MT, Poorter L, Schnitzer SA, Engelbrecht BMJ, Markesteijn L. 2019. The hydraulic efficiency-safety trade-off differs between lianas and trees. Ecology **100**, e02666.

Wagner ST, Isnard S, Rowe NP, Samain MS, Neinhuis C, Wanke S. 2012. Escaping the lianoid habit: evolution of shrub-like growth forms in *Aristolochia* subgenus *Isotrema* (Aristolochiaceae). American Journal of Botany **99**, 1609–1629.

Wheeler EA, Baas P, Gasson PE. 1989. IAWA list of microscopic features for hardwood identification. IAWA Bulletin **10**, 219–332.

Woodrum CL, Ewers FW, Telewski FW. 2003. Hydraulic, biomechanical, and anatomical interactions of xylem from five species of *Acer* (Aceraceae). American Journal of Botany **90**, 693–699.

Yamada Y, Awano T, Fujita M, Takabe K. 2011. Living wood fibers act as large-capacity "single-use" starch storage in black locust (*Robinia pseudoacacia*). Trees **25**, 607–616.

Zanne AE, Westoby M, Falster DS, Ackerly DD, Loarie SR, Arnold SE, Coomes DA. 2010. Angiosperm wood structure: global patterns in vessel anatomy and their relation to wood density and potential conductivity. American Journal of Botany **97**, 207–215.

Zheng J, Martínez-Cabrera HI. 2013. Wood anatomical correlates with theoretical conductivity and wood density across China: evolutionary evidence of the functional differentiation of axial and radial parenchyma. Annals of Botany **112**, 927–935.

Ziemińska K, Butler DW, Gleason SM, Wright IJ, Westoby M. 2013. Fibre wall and lumen fractions drive wood density variation across 24 Australian angiosperms. AoB Plants **5**, plt046.

Ziemińska K, Westoby M, Wright IJ. 2015. Correction: broad anatomical variation within a narrow wood density range-a study of twig wood across 69 Australian angiosperms. PLoS ONE **10**, e0139496.

BRILL

IAWA Journal 0 (0), 2023: 1-12

iawa

Parenchyma is not the sole site of storage: storage in living fibres

Lenka Plavcová [1,*], Mark E. Olson [2], Veronika Jandová [3,4] and Jiří Doležal [3,4]

[1] *Department of Biology, Faculty of Science, University of Hradec Králové, Rokitanského 62, Hradec Králové 500 03, Czech Republic*
[2] *Instituto de Biología, Universidad Nacional Autónoma de México, Tercer Circuito sn de Ciudad Universitaria, Ciudad de México 04510, Mexico*
[3] *Institute of Botany, The Czech Academy of Sciences, Průhonice, Czech Republic*
[4] *Department of Botany, Faculty of Science, University of South Bohemia, České Budějovice, Czech Republic*
**Corresponding author; email: lenka.plavcova@uhk.cz*
ORCID iD: Plavcová: 0000-0002-3395-4463

Accepted for publication: 16 January 2023; published online: 30 January 2023

Summary – Storage of nutrients and water are important functions of secondary xylem that have received much attention lately. In most of these studies, the storage role has been attributed to the fraction and arrangement of ray and axial parenchyma. However, in the current article, we show that in many species, especially those from tropical and subtropical regions (where most of the world's plant species are found), nutrient and water storage is carried out by living imperforate tracheary elements (ITEs), colloquially termed "living fibres". The occurrence of living fibres has been long recognized by anatomists, and especially emphasized in the work of Sherwin Carlquist. In spite of this, living fibres have remained largely unacknowledged by most plant physiologists and ecologists. To raise awareness about the existence of living fibres and to celebrate the illuminating work of Sherwin Carlquist, we summarize our current understanding of the structure, function, and occurrence of living fibres and emphasize that they should receive more attention when studying storage in wood.

Keywords – axial parenchyma, capacitance, carbohydrates, rays, trade off, tropics, wood.

Introduction

Sherwin would be pleased with the recent upsurge of interest in the storage of water and non-structural carbohydrates in the secondary xylem (Jupa *et al.* 2016; Morris *et al.* 2016a; Plavcová *et al.* 2016, 2019; Secchi *et al.* 2017; Klein *et al.* 2018; Kiorapostolou *et al.* 2019; Pratt *et al.* 2021a, b). Most of these studies emphasize the role of ray and axial parenchyma in storage, which is consistent with the traditional view of the division of labor between different cell types in wood (Pratt & Jacobsen 2017; Pratt *et al.* 2021a, b; Fig. 1). However, it is very important to note that axial parenchyma is often not the only or even the main storage site in the axial system (Carlquist 1988, 2012, 2015a; Plavcová *et al.* 2016). Sherwin was by far the anatomist who emphasized most strongly that in many, possibly even most, species with libriform fibres, these cells are living at maturity, as evidenced by nuclei, septa, or starch. Based on his detailed observations and excellent knowledge of species biology (e.g., their ecological preference, habitat, and reproductive biology), he formulated hypotheses and tested them by the comparative method. In his attempt to understand how natural selection shapes plant water and nutrient storage, Carlquist focused on species lacking parenchyma as well as those with conspicuous types of parenchyma (such as wide parenchyma bands, diamond-shaped paratracheal arrangements, or regular reticulate parenchyma meshes). In his work, he pointed out that there

DOI 10.1163/22941932-bja10112

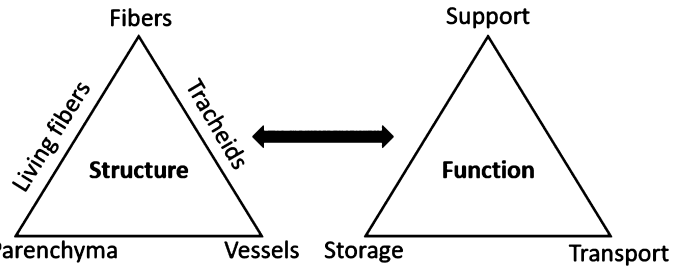

Fig. 1. Division of functions (mechanical support, storage of water and nutrients, transport of water) among major cell types in wood. Redrawn from Pratt & Jacobsen (2017).

are many cases where axial parenchyma is very scarce or even absent, even in species that store large amounts of carbohydrates or water in the axial cells (Carlquist 2015a).

Given the widespread occurrence of living fibres and that, when present, they are invariably involved in storage, it is crucial that the expanding field of xylem storage studies be built on a proper foundation in which living fibres are explicitly included and that the parenchyma is not considered as dependably being the main living fraction and storage site (as do, e.g., Kotowska *et al.* 2020). To help guide the emerging and much-welcomed interest in secondary xylem storage, we emphasize various Carlquistian points. We explain why xylem biologists cannot assume that storage is occurring only in the parenchyma. In doing so, we explain the distinction between axial parenchyma and living fibres. We summarize the typical features that anatomists use to diagnose living non-parenchyma cells, and touch on the need to study fresh or liquid-preserved, and not dried, wood samples, a topic Sherwin highlighted repeatedly throughout his work. To illustrate our point that storage can occur in sites other than parenchyma, we give examples of massive storage in species that have very little or even entirely lack axial parenchyma. We also touch on the relationship between ray and axial parenchyma before summarizing some important research priorities that urgently require attention with regard to the sites of storage in the secondary xylem.

Anatomical features of axial parenchyma and living fibres

Thorough knowledge of structure is an essential prerequisite for understanding function. In the following, we highlight the anatomical features that help distinguish axial parenchyma from living fibres. While angiosperm wood consists of only four principal cell types (i.e., vessel elements, axial parenchyma, ray parenchyma, and imperforate tracheary elements (ITEs)), their distinction is often not straightforward due to the high variability of their anatomical features (e.g., cell size, wall thickness, pit abundance and structure) as well as their complex integration into the three-dimensional structure of wood (Kedrov 2012; Morris *et al.* 2016a).

The cells in secondary xylem can be thought of as two "systems," axial and radial. The ray initials give rise to the radial system — the ray cells — which in larger woody stems have the long axes of their cells oriented radially. The axial cell types are produced by fusiform cambial initials rather than ray initials. The cells produced by the fusiform cambial initials have their long axes oriented parallel to the stem or axis, hence they are called "axial" cells. The axial cells include vessel elements, axial parenchyma, and various types of ITEs. In Sherwin's classification, the main ITEs were of three types, tracheids (which are water conductive), plus libriform fibres and fibre-tracheids, which are non-conductive (Carlquist 1986; Rosell *et al.* 2007; Olson *et al.* 2020). Throughout the article we follow this more inclusive definition of ITEs as proposed by Carlquist (1986) and limit our discussion to flowering plants. "Imperforate" is a useful qualifier because it indicates that, unlike vessel elements, imperforate tracheary elements lack perforations, communicating with adjacent cells via pits and the primary membranes that surround each cell. "Tracheary" refers to both vessel elements and ITEs. In contrast to the helpful "imperforate,", "tracheary" is a little more unfortunate qualifier because it references air movement in animal tracheas, harkening back to a time when vessels were thought

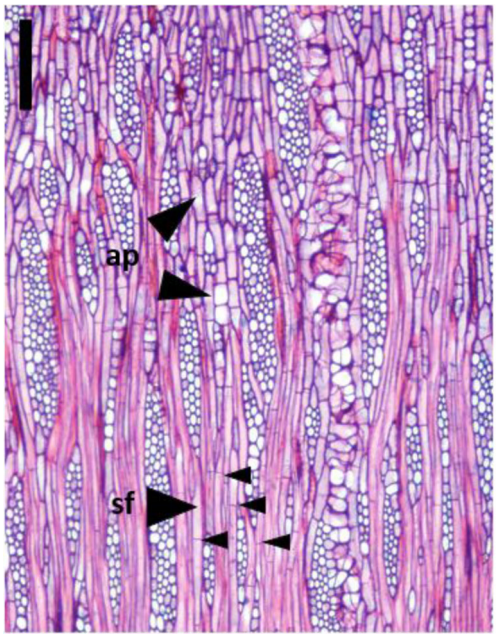

Fig. 2. Distinction between septate fibres and axial parenchyma in a specimen of *Ilex mitis* (Aquifoliaceae). The axial parenchyma cells (ap) are divided into strands about the same lengths as the vessel elements they are adjacent to, and each cell in a strand is surrounded by a secondary cell wall. In contrast, the septate fibres (sf) are single cells divided into compartments by one or more septa (small arrowheads), primary walls traversing the cell lumen perpendicularly. Scale = 200 μm.

to conduct air (Malpighi 1675; Grew 1682). Moreover, "tracheary" is confusing because not all tracheary elements conduct, as in libriform fibres and fibre-tracheids. Whether conducting or not, the tracheary elements are united in that they are all the axial cells that are not axial parenchyma. Tracheids are dead at maturity, whereas fibre-tracheids and libriform fibres are often living and participate with, and often instead of, the axial parenchyma in storage of photosynthates and their loading into vessels (Carlquist 1988, 2007, 2015). Similar to Carlquist, Wolkinger (1969) observed the presence of living fibres in many species of trees and shrubs. Based on morphological and histological features, Wolkinger (1969) distinguished three types of fibres: dead libriform fibres, living non-septate fibres, and living septate fibres. He also noted that the living wood fibres were usually shorter than the dead libriform fibres and the septate fibres were shorter than the non-septate ones. Variation in living fibre length was accompanied by a difference in the shape of the nuclei, which were oval in the longer fibres and round in the shorter ones. Septa consist of primary cell wall material and therefore contrast with the lignified secondary wall when stained e.g., with a mixture of safranin-Alcian blue.

In most species, ITEs and axial parenchyma cells are quite distinct developmentally, but across, and sometimes within species, it is possible to find a developmental and functional continuum between them (Figs 2 and 3B). Examining this morphological and functional continuum helps to understand why axial parenchyma and ITEs regions can trade off functionally across species. When distinguishing ITEs from axial parenchyma, ITEs almost always elongate via intrusive growth beyond the lengths of the fusiform cambial initials from which they are derived (Majda *et al.* 2021). Axial parenchyma cells, on the other hand, do not elongate during maturation and typically divide into "strands" of two or more cells by transverse division of the derivatives of fusiform cambial initials. However, in some cases, the products of fusiform cambial initials do not elongate and do not divide into strands, which means that they are, with regard to length and transverse division or lack thereof, morphologically intermediate between ITEs and axial parenchyma cells. Another feature that distinguishes ITEs and axial parenchyma is the deposition of lignified

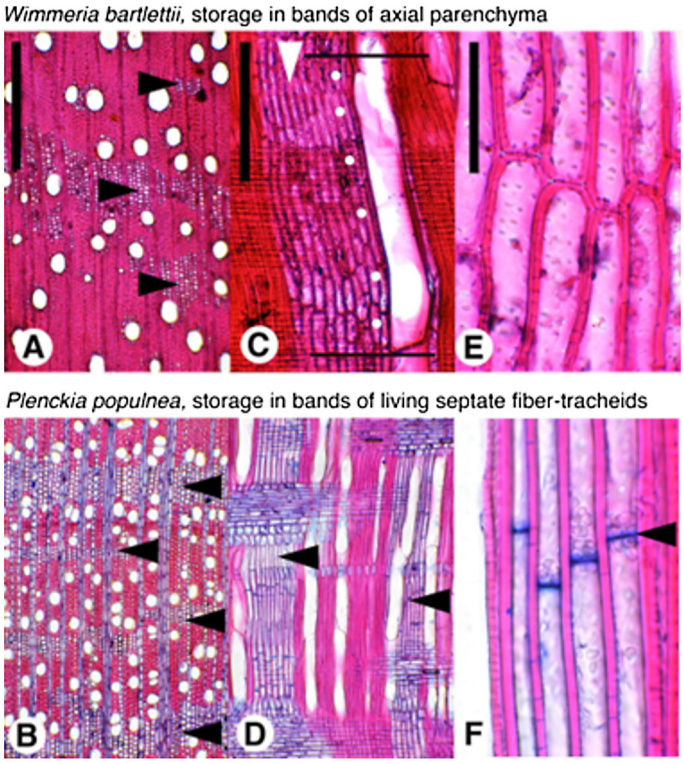

Fig. 3. Similar patterns of water and starch storage can be carried by either axial parenchyma or living imperforate tracheary elements, an example from Celastraceae. In transection, both *Wimmeria bartlettii* (Olson 4831), a rainforest tree (A), and *Plenckia populnea* (Olson 5613), a savannah tree (B), have tangential bands of living, starch-filled storage cells (arrows) traversing backgrounds of true tracheids, which are dead, water conductive imperforate tracheary elements. In this respect, both *W. bartlettii* and *P. populnea* look very similar in the basic organization of their wood, with conductive background imperforate tracheary elements with mostly solitary vessels embedded in them, and largely vessel-free bands of storage cells. Closer inspection reveals that the storage cells are different in these species. C. In *W. bartlettii*, the storage cells are axial parenchyma, as can be seen in this radial section (the white arrow highlights a band of axial parenchyma), but in *P. populnea* (D), the storage cells are septate fibre-tracheids (black arrows). (E) In a strand of axial parenchyma, each storage cell is surrounded by its own secondary wall. (F) In contrast, in septate fibres or fibre-tracheids, a single cell is divided into two or more living compartments by a primary membrane that traverses the imperforate tracheary element lumen. One septum of a fibre-tracheid is indicated here with a black arrow. In developing into axial parenchyma, a cell produced by division of a fusiform cambial initial usually divides into "strands." In forming a strand, the product of a fusiform initial division divides transversely one or more times. In *Wimmeria*, the strands are quite long (C), in this case 5–10 cells long. The cells of one strand are identified with white dots. Fusiform cambial initial length is estimated from the lengths of vessel elements; the length of one element is delimited with black bars. The strand of axial parenchyma is the number of cells falling between these bars and thus presumably derived from a fusiform initial of about that length; because the strand is very close to the vessel element in this radial section, it is possible that the strand of axial parenchyma and the vessel element were produced from the same initial. Scale: A, B, D = 500 μm; C = 300 μm; E, F = 50 μm.

secondary cell wall, which is usually (but not always, see Carlquist 2014) thicker in ITEs compared to axial parenchyma (Plavcová *et al.* 2019). When distinguishing septate ITEs from axial parenchyma strands, one must carefully examine whether the secondary cell wall surrounds the entire outline of each cell in the strand (denoting axial parenchyma) or whether the secondary wall is present only on the longitudinal walls while the transversal wall is formed as a thin septum formed only by the primary wall (indicating septate fibres) (Figs 3 and 4). Taken together, a morphological continuum from libriform fibres to non-septate and septate fibres to axial parenchyma makes developmental sense

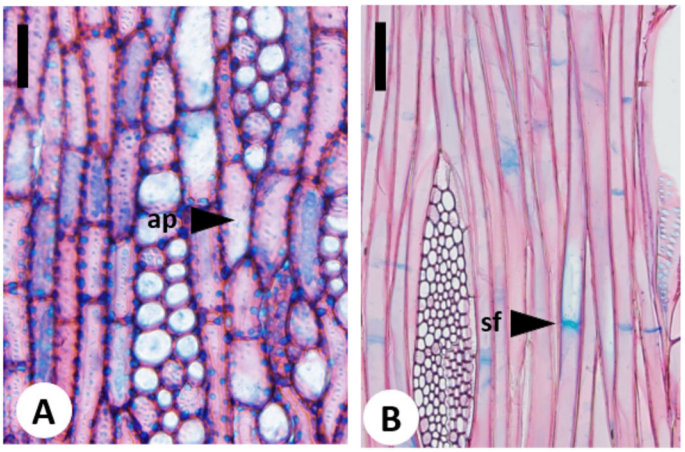

Fig. 4. (A) Axial parenchyma (ap) in *Ilex mitis* (Aquifoliaceae) with the secondary cell wall and ample pitting on both lateral and transversal walls. (B) Septate fibre (sf) in *Schefflera abyssinica* (Araliaceae) with septum made of primary cell wall material. Scale: A = 50 μm; B = 100 μm.

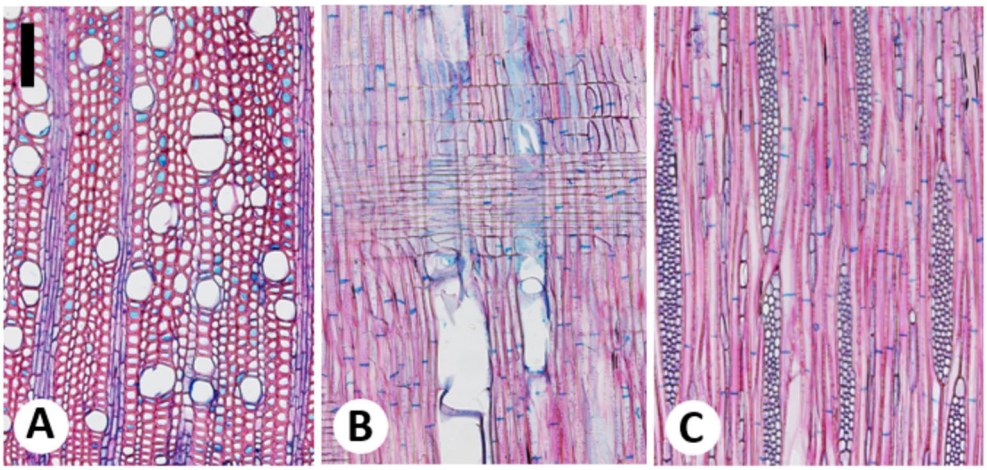

Fig. 5. The appearance of septate libriform fibres on a transversal (A), radial (B) and tangential (C) section in *Nuxia congesta* (Stilbaceae). (A) in transverse section, the plane of sectioning passing through a fibre occasionally includes a septum. In this image, septa can be seen as blue-staining membranes traversing the fibre lumen. In radial (B) and tangential (C) sections, septa can be seen as blue bands running perpendicular to the libriform fibre lumina. Most fibres have a single septum but some have two or three. Unlike axial parenchyma strands, which are the same lengths as the vessel elements they accompany, here it is easy to see that libriform fibres are longer than vessel elements thanks to the intrusive growth they experience.

because all these cell types can be produced by altering the timing and intensity of cell division, cell death, cell intrusive elongation, and cell wall deposition. It also follows that the correct distinction between these cell types can only be made by consulting transverse, radial, and tangential sections (Figs 3 and 5) along with macerations and then making an educated guess as to what can be seen in transection. As a result, in interpreting any given transection, it will often be the case that the identity of some cells cannot be determined with certainty.

In addition to axial parenchyma, another main fraction of parenchyma in secondary xylem is ray parenchyma. The rays appear to be key cell types that translocate water and photosynthates, potentially across a pressure gradient (Carlquist 2007). In small stems, ray cells are oriented vertically and probably participate in the movement of

photosynthates axially. As stems expand in girth, ray cells become oriented radially and likely engage in radial movement (Olson 2020). Because the rays of larger stems run radially, they provide little axial connectivity. Living axial cells, such as the axial parenchyma, provide such axial connectivity. They do so because, when they come into contact with a ray, they advance in concatenated axial strands traversing ray-free areas, to contact rays again. In this way, the ray and axial parenchyma cells in wood can form an interconnected three-dimensional network (Kedrov 2012; Morris *et al.* 2016a). In species that lack axial parenchyma, the ITEs are apparently always living, often, apparently always septate (Carlquist 2015a). This suggests that axial connectivity is essential in wood and that natural selection never favours configurations that lack some kind of axial connectivity between rays, whether in living ITEs or in axial parenchyma. It is, therefore, possible to observe woods with both ray and axial parenchyma plus living or dead ITEs. However, there appear to be no cases of species with dead ITEs that lack axial parenchyma entirely. Moreover, the species that lack rays either have axial parenchyma or living ITEs (Carlquist 2015b). Again, apparently, natural selection never favors a situation where there are no living cells in the secondary xylem.

The usefulness of Sherwin's ITE classification system for studying storage in wood

Currently, there are two main systems for classifying ITEs, and these systems have different objectives. Sherwin's is a tool to explore relationships between xylem structure and function and its categories can be considered hypotheses for testing and potential rejection and refinement (Carlquist 1986). The other is the IAWA wood identification classification (Wheeler *et al.* 1989). This classification is a set of conventions intended to be stable over time, facilitating communication and the construction of wood identification tools. In the IAWA scheme, all ITEs are lumped together as "fibres," almost certainly masking important parenchyma-ITE covariation patterns that the Carlquistian classification helps to highlight. For example, Carlquist notes that tracheids are dead at maturity and so all storage must take place in the axial and ray parenchyma or in non-conductive ITEs. To our knowledge, there are no rayless species or species lacking axial parenchyma that have tracheids as the only ITE type; such species would have nowhere to store water and photosynthates in the axial system. Because the axial system provides essential axial interconnectivity between rays, it is unlikely that natural selection would ever favour a wood that entirely lacks some sort of axial system storage. In contrast, species with libriform fibres can indeed lack axial parenchyma or even be rayless, but there are no species with only tracheids that are rayless (Carlquist 1970, 1985, 2015b). Species with tracheids might have more rays and axial parenchyma than species with non-conductive ITEs, and almost certainly those with living ITEs. This expectation remains to be tested empirically. Only species with living fibres or fibre-tracheids can, presumably, lack axial parenchyma entirely. Moreover, there can be a diversity of ITEs in the samples of the same specimen, with some functioning more in support and others more in storage (Carlquist 2014, 2015a), so careful examination of ITEs morphology and histology within species is necessary. Thus, careful anatomical work is required to begin to obtain quantitative data that are informative regarding the covariation or lack thereof, between ITEs and axial and ray parenchyma.

Different cell types can carry out similar functions in xylem tissue

Secondary xylem (wood) is not only the primary water-transporting tissue but also an important site storing water, carbohydrates, and nutrients. Due to the high stiffness and rigidity of lignified cell walls, wood also provides excellent mechanical support, allowing for the remarkable height growth of trees as compared to species with little accumulation of secondary xylem. In most angiosperms, water conduction occurs via dead hollow tubes formed by stacked vessel elements, the storage function has traditionally been attributed to living ray and axial parenchyma cells, and mechanical support is facilitated by libriform fibres (Fig. 1). This division of labour between cell types presents a traditional view included in most textbooks on xylem anatomy and physiology. However, the reality is

fuzzier, and the same cell type often fulfills multiple functions, or in another view, multiple cell types work together in carrying out the same elemental function. For instance, wood rays are involved in radial transport, and storage (Van Bel 1990), and also contribute significantly to the high radial strength of wood (Burgert *et al.* 2001; Burgert & Eckstein 2001). Similarly, long-distance transport of water occurs mainly in vessels, but tracheids can serve as auxiliary water-conducting pathways or a bypass route around the cavitated vessels (Sano *et al.* 2011; Cai *et al.* 2014). Likewise, fibres help to sustain conduction by bearing the mechanical loads imposed by negative pressures within vessels (Jacobsen *et al.* 2005).

Involvement in functions in addition to mechanical strength is common in the case of ITEs, perhaps because they represent the most abundant cell type in wood. As already mentioned, based on their involvement in water conduction versus mechanical support, ITEs have been distinguished into tracheids, fibre-tracheids, and libriform fibres, with the first type being water conductive and the two later types being non-conductive (Carlquist 1986; Sano *et al.* 2011; Carlquist 2014). Although these categories are useful, it has been emphasized that these cell types might form a morphological continuum rather than discrete categories (Sano *et al.* 2011; Echeverría *et al.* 2022). However sharp the morphological and functional boundaries between these categories might be, tracheids have been reliably shown to be involved in water conduction in many species (Sano *et al.* 2011). Due to their narrow lumina, they are not very hydraulically efficient compared to vessels, but they probably serve as an auxiliary water-conducting pathway (Kedrov 2012). Thus, tracheids may provide the conductivity of residual water after embolization of wide vessels (Sano *et al.* 2011; Pratt *et al.* 2023), may serve as efficient hydraulic bridges that connect solitary vessels (Cai *et al.* 2014; Pan & Tyree 2019), or contribute to wood capacitance (Jupa *et al.* 2016; Ziemińska *et al.* 2020). Detailed structure-function observations provide further insight into the functioning of ITEs. For instance, tracheids occurring in latewood rather than earlywood have more pits, and the pit membranes are sheet-like without large holes that would permit air entry (Sano *et al.* 2011).

Background tissue ITEs may also serve in storage because both libriform fibres and fibre-tracheids can be living at maturity (Carlquist 2001, 2015b). The presence of nuclei, septa, and starch grains are common features of living fibres that distinguish them from dead ones. The lifespan of living fibres varies among species. In early observations, Wolkinger (1970b) found that living fibres remain alive for many years in diffuse-porous species, while their occurrence is restricted to only a few outermost tree rings in ring-porous trees. In agreement, Yamada et al. (2011) found that the living fibres were involved in starch storage for only a single growing season in ring-porous *Robinia pseudoacacia*, although they did not assess whether the fibres remained alive or died after starch dissolution. In *Tamarix aphylla*, starch grains were present in the outermost six to twelve growth rings but viable protoplasts remained up to 21 years (Fahn & Arnon 1963), suggesting that starch dissolution precedes the breakdown of the cell nucleus. Lifespans of living fibres have been estimated between 10 and 40 years for four tropical species without annual rings (Herrera-Ramírez *et al.* 2021). In species with very low wood density, it is likely that living fibres are very short-lived and quickly replaced (Castorena *et al.* 2022). Taken together, it appears that the lifespan of living fibres can vary from one season to several decades, similar to the lifespan of ray and axial parenchyma (Fahn & Arnon 1963).

The functional implications of storage in living fibres have not been widely studied. An important exception is a recent study that linked the presence of living fibres vs. axial parenchyma with the growth and survival of eight tropical species (Herrera-Ramírez *et al.* 2021). In this study, species that stored NSC in living fibres had greater total NSC pools, slower growth rates, and higher survival rates, showing that living versus dead fibres is an important component of variation in plant life history strategies. Since ITEs are typically the most abundant cell type in wood, storage in them provides a great opportunity to substantially increase the overall storage capacity. Along these lines, Carlquist (2015a) discussed the roles that storage in living fibres might have in growth, flowering, and fruiting in the small African tree *Halleria lucida* L. or in the members of Araliaceae. However, compared to storage in axial parenchyma, storage in living fibres may be associated with slower remobilization rates due to less efficient connections between cells (Herrera-Ramírez *et al.* 2021). On the other hand, if living fibres are present, the ray parenchyma can remain free of starch and become more efficient in active radial transport because the radial

symplastic pathway is not blocked by densely packed starch grains (Yamada *et al.* 2011). It is also possible that the freed parenchyma volume can be utilized to store other specialized compounds such as secondary metabolites or lipids (Herrera-Ramírez *et al.* 2021). A disadvantage of having living fibres is a reduction in the mechanical strength of the wood due to their typically lower wall thickness-to-span ratio compared to dead libriform fibres, although the required trunk stiffness can also be achieved via a high trunk moment of inertia as in thick stems of conspicuously water-storing trees (Chapotin *et al.* 2006). It might be thought that living ITEs increase base respiration and maintenance costs, which would be particularly high in subzero environments where frost protection is needed (e.g., synthesis of anti-freeze compounds, reversal or freeze-induced embolism). However, it seems likely that low-density woods, such as those with abundant living ITEs, probably have very low stem metabolic rates (Castorena et al. 2022), perhaps contributing to explaining their global ecological distribution. Clearly, more studies are needed to elucidate the functional aspects associated with the presence of living fibres.

Occurrence of living fibres and the need for surveys of living imperforate tracheary elements based on liquid-preserved material

Although rarely considered in studies of NSC storage, the occurrence of living fibres is widespread. For instance, Wolkinger (1970a) documented the presence of living fibres in more than 400 species of temperate trees and shrubs. The lack of axial parenchyma, and thus the presence of living fibres, can even be found in some species of "pachycaul" (conspicuously fat-trunked) trees of tropical dry regions, which store large amounts of water in their massive trunks, and this storage often occurs in living libriform fibres (Fig. 6). By contrast, in some species, especially those with highly dense wood, and/or water conductive ITEs as the background cell type (i.e., true tracheids; see Rosell *et al.* 2007; Olson 2020; Olson *et al.* 2020), the ITEs are dead and the living cells available for storage are indeed parenchyma cells, or, alternatively, situations in which there is, in addition to tracheids, an additional type of living ITE (Fig. 6). Tracheids are water conductive cells and are thus dead at maturity. Thus, in species with only tracheids as the ITE type, the only cells available for storage are parenchyma cells or living fibres (Carlquist 1988, 2014b). However, in many species, including some with very low wood density, axial parenchyma is scant or even absent, and water and starch are stored in living fibres exclusively. Striking examples are the tropical dryland genera *Bursera* and *Commiphora* (Fig. 6), which with over 300 species often dominate the warm drylands of the northern Neotropics and the vast dryland arc stretching from southwestern Africa through the Horn of Africa to Arabia and India. They are succulent trees or shrubs with stout trunks and brittle branches, which epitomize water storage, and yet they completely or almost completely lack axial parenchyma. Studying the way storage and mechanical support trade-off, therefore, requires expert anatomical work to identify which cells and traits actually contribute to these functions.

Throughout his work, Sherwin repeatedly mentioned the need to study liquid-preserved and not just dried wood samples. Many of his publications made a special effort to emphasize when he had available liquid-preserved material (which he usually collected himself). In this context, the question of the main storage site in the axial xylem highlights another remarkably fundamental knowledge gap. The proportion of species with living fibre-tracheids and libriform fibres is unknown. Most wood anatomy has been conducted on dried xylarium specimens. When wood is slowly dried, starch, which often helps diagnose living cells, is rapidly broken down by bacterial activity and is usually absent from xylarium specimens. Similarly, bacterial activity often degrades other signs of living status, such as nuclei. Treatments with strong oxidizing agents can degrade these fine features as well. If Olson *et al.* (2020) reflect global percentages, then about 75% of woody species have fibre-tracheids or libriform fibres. Given the importance of the issue, few surveys have attempted to document the proportion of libriform fibres and fibre-tracheids that are living (Wolkinger 1970a, 1971; Wheeler *et al.* 2007; Carlquist 2015a; Plavcová *et al.* 2016). It is a remarkably fundamental knowledge gap that there is no global estimate of the proportion of these species that have living fibres, or even, for that matter, solid estimates of the percentages of species with tracheids, libriform fibres, or fibre-tracheids. Priority for future

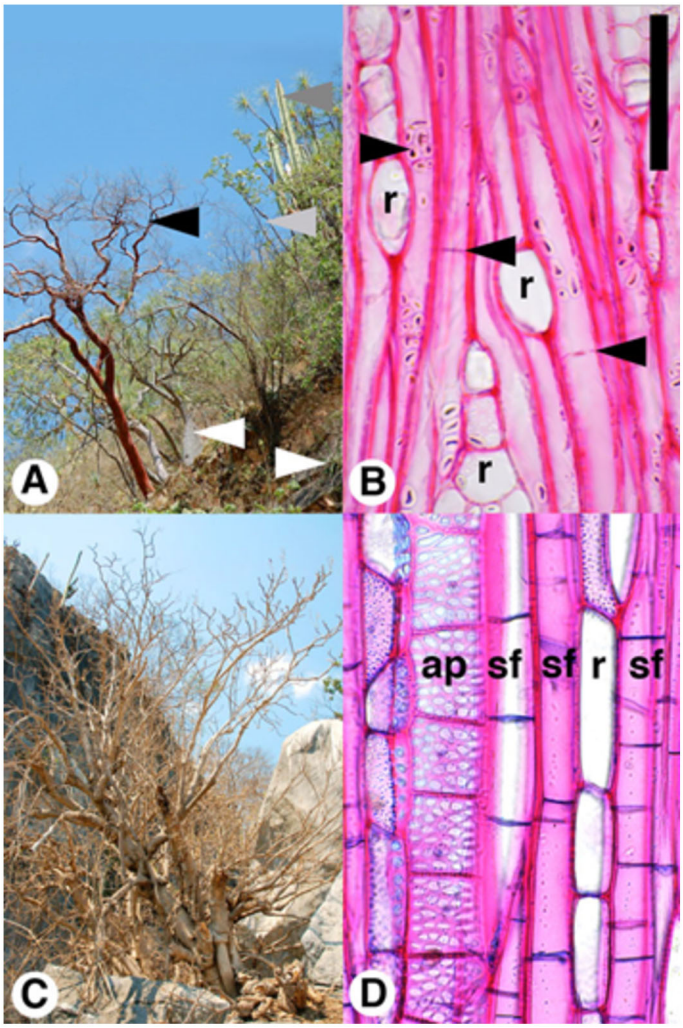

Fig. 6. Even conspicuously water-storing trees can lack or almost entirely lack axial parenchyma. Lowland warm tropical and subtropical seasonally dry plant communities usually support species with very low wood density, which store water in conspicuously swollen trunks, e.g., baobabs (*Adansonia*). These species epitomize water storage, but it cannot be assumed that the storage in the axial system in these species is occurring in axial parenchyma. In the dry tropics of Mexico, Africa, Madagascar, Arabia, to India, species of *Bursera* or *Commiphora* (Burseraceae) are very common water-storing trees. (A) With its swollen red trunk, *Bursera longipes* (Olson 1029) (black arrow) is a conspicuous element of central Mexican tropical dry forests, growing here with other water-storing plants, such as *Agave marmorata* (right-pointing arrow), *Beaucarnea olsonii* (left-pointing white arrow), *Plumeria rubra* (light gray arrow), and *Isolaterocereus dumortieri* (dark gray arrow). *Bursera longipes* is leafless for much of the 8-month dry season, but flowers, fruits, and leafs out in anticipation of the rains, drawing on stored water and starch. (B) *Bursera longipes* almost entirely lacks axial parenchyma, and the great bulk of its secondary xylem is made up of living septate libriform fibres (left-pointing arrows indicate two septa). These living septate libriform fibres store abundant starch (right-pointing arrow). (C) Similarly, *Louteridium koelzii* (Acanthaceae) (Olson 6707) is a conspicuously fat-trunked small tree with very fragile stems. It grows on dry limestone boulder fields in lowland tropical dry forest. (D) Like *B. longipes*, although *L. koelzii* stores massive amounts of water and starch, most storage in the axial system occurs not in axial parenchyma but in living septate libriform fibres. Axial parenchyma occurs sparsely around vessels. In species such as *L. koelzii*, storage occurs in axial parenchyma, imperforate tracheary elements, and ray cells. Distinguishing the different types of storage cells in such species requires careful anatomical work. ap, axial parenchyma; sf, septate libriform fibre; r, ray cells. Scale: B, D = 100 µm.

anatomical work will need to be based on liquid-preserved material, in which diagnosis of living status can be made more reliably than from slowly dried material.

Conclusion

We hope we have helped to show why the assumption that "fibres are dead and for support and parenchyma is living and for storage" cannot be assumed to hold in any given case. Instead, this situation is just one subset of a large universe of possible trait combinations. Future work on nutrient and water storage in wood should pay more attention to the presence of living fibres, explore their occurrence across species, life forms and environments, and elucidate the functional consequences of their presence.

Acknowledgements

LP acknowledges financial support from the Czech Science Foundation (18-19722Y). MEO acknowledges Consejo Nacional de Ciencia y Tecnología project A1-S-26934. JD and VL were supported by the MŠMT INTER-EXCELLENCE project (LTAUSA18007).

References

Burgert I, Eckstein D. 2001. The tensile strength of isolated wood rays of beech (*Fagus sylvatica* L.) and its significance for the biomechanics of living trees. *Trees* 15(3): 168–170. DOI: 10.1007/s004680000086.

Burgert I, Bernasconi A, Niklas KJ, Eckstein D. 2001. The influence of rays on the transverse elastic anisotropy in green wood of deciduous trees. *Holzforschung* 55(5): 449–454. DOI: 10.1515/HF.2001.074.

Cai J, Li S, Zhang H, Zhang S, Tyree MT. 2014. Recalcitrant vulnerability curves: methods of analysis and the concept of fibre bridges for enhanced cavitation resistance. *Plant Cell Environ.* 37(1): 35–44. DOI: 10.1111/pce.12120.

Carlquist S. 1970. Wood anatomy of insular species of *Plantago* and the problem of raylessness. *Bull. Torrey Bot. Club* 97(6): 353–361. DOI: 10.2307/2483855.

Carlquist S. 1985. Wood anatomy of Begoniaceae, with comments on raylessness, paedomorphosis, relationships, vessel diameter, and ecology. *Bull. Torrey Bot. Club* 112(1): 59–69. DOI: 10.2307/2996105.

Carlquist S. 1986. Terminology of imperforate tracheary elements. *IAWA J.* 7(1): 75–81. DOI: 10.1163/22941932-90000445.

Carlquist S. 1988. Tracheid dimorphism: a new pathway in evolution of imperforate tracheary elements. *Aliso* 12(1): 103–118. DOI: 10.5642/aliso.19881201.12.

Carlquist S. 2001. *Comparative wood anatomy: systematic, ecological, and evolutionary aspects of dicotyledon wood*. Springer, Berlin.

Carlquist S. 2007. Bordered pits in ray cells and axial parenchyma: the histology of conduction, storage, and strength in living wood cells. *Bot. J. Linn. Soc.* 153(2): 157–168. DOI: 10.1111/j.1095-8339.2006.00608.x.

Carlquist S. 2012. How wood evolves: a new synthesis. *Botany* 90(10): 901–940. DOI: 10.1139/b2012-048.

Carlquist S. 2014. Fibre dimorphism: cell type diversification as an evolutionary strategy in angiosperm woods: fibre dimorphism in angiosperm wood. *Bot. J. Linn. Soc.* 174(1): 44–67. DOI: 10.1111/boj.12107.

Carlquist S. 2015a. Living cells in wood. 1. Absence, scarcity and histology of axial parenchyma as keys to function: axial parenchyma and wood function. *Bot. J. Linn. Soc.* 177(3): 291–321. DOI: 10.1111/boj.12247.

Carlquist S. 2015b. Living cells in wood. 2. Raylessness: histology and evolutionary significance: significance of raylessness in wood. *Bot. J. Linn. Soc.* 178(4): 529–555. DOI: 10.1111/boj.12291.

Castorena M, Olson ME, Enquist BJ, Fajardo A. 2022. Toward a general theory of plant carbon economics. *Trends Ecol. Evol.* 37(10): 829–837. DOI: 10.1016/j.tree.2022.05.007.

Echeverría A, Petrone-Mendoza E, Segovia-Rivas A, Figueroa-Abundiz VA, Olson ME. 2022. The vessel wall thickness–vessel diameter relationship across woody angiosperms. *Am. J. Bot.* 109(6): 856–873. DOI: 10.1002/ajb2.1854.

Fahn A, Arnon N. 1963. The living wood fibres of *Tamarix aphylla* and the changes occurring in them in transition from sapwood to heartwood. *New Phytol.* 62(1): 99–104. DOI: 10.1111/j.1469-8137.1963.tb06318.x.

Grew N. 1682. *The anatomy of plants*. W. Rawlins, London.

Herrera-Ramírez D, Sierra CA, Römermann C, Muhr J, Trumbore S, Silvério D, Brando PM, Hartmann H. 2021. Starch and lipid storage strategies in tropical trees relate to growth and mortality. *New Phytol.* 230(1): 139–154. DOI: 10.1111/nph.17239.

Jacobsen AL, Ewers FW, Pratt RB, Paddock WA, Davis SD. 2005. Do xylem fibres affect vessel cavitation resistance? *Plant Physiol.* 139(1): 546–556. DOI: 10.1104/pp.104.058404.

Jupa R, Plavcová L, Gloser V, Jansen S. 2016. Linking xylem water storage with anatomical parameters in five temperate tree species. *Tree Physiol.* 36(6): 756–769. DOI: 10.1093/treephys/tpw020.

Kedrov GB. 2012. Functioning wood. *Wulfenia* 19: 57–95.

Kiorapostolou N, Da Sois L, Petruzzellis F, Savi T, Trifilò P, Nardini A, Petit G. 2019. Vulnerability to xylem embolism correlates to wood parenchyma fraction in angiosperms but not in gymnosperms. *Tree Physiol.* 39(10): 1675–1684. DOI: 10.1093/treephys/tpz068.

Klein T, Zeppel MJB, Anderegg WRL, Bloemen J, De Kauwe MG, Hudson P, Ruehr NK, Powell TL, von Arx G, Nardini A. 2018. Xylem embolism refilling and resilience against drought-induced mortality in woody plants: processes and trade-offs. *Ecol. Res.* 33(5): 839–855. DOI: 10.1007/s11284-018-1588-y.

Kotowska MM, Wright IJ, Westoby M. 2020. Parenchyma abundance in wood of evergreen trees varies independently of nutrients. *Front. Plant Sci.* 11: 86. DOI: 10.3389/fpls.2020.00086.

Majda M, Kozlova L, Banasiak A, Derba-Maceluch M, Iashchishyn IA, Morozova-Roche LA, Smith RS, Gorshkova T, Mellerowicz EJ. 2021. Elongation of wood fibers combines features of diffuse and tip growth. *New Phytol.* 232(2): 673–691. DOI: 10.1111/nph.17468.

Malpighi M. 1675. *Anatome plantarum*. Johannis Martyn, London.

Morris H, Brodersen C, Schwarze FWMR, Jansen S. 2016a. The Parenchyma of secondary xylem and its critical role in tree defense against fungal decay in relation to the CODIT model. *Front. Plant Sci.* 7: 1665. DOI: 10.3389/fpls.2016.01665.

Morris H, Plavcová L, Cvecko P, Fichtler E, Gillingham MAF, Martínez-Cabrera HI, McGlinn DJ, Wheeler E, Zheng J, Ziemińska K, Jansen S. 2016b. A global analysis of parenchyma tissue fractions in secondary xylem of seed plants. *New Phytol.* 209(4): 1553–1565. DOI: 10.1111/nph.13737.

Olson ME. 2020. From Carlquist's ecological wood anatomy to Carlquist's law: why comparative anatomy is crucial for functional xylem biology. *Am. J. Bot.* 107(10): 1328–1341. DOI: 10.1002/ajb2.1552.

Olson ME, Rosell JA, Martínez-Pérez C, León-Gómez C, Fajardo A, *et al.* 2020. Xylem vessel diameter-shoot length scaling: ecological significance of porosity types and other traits. *Ecol. Monogr.* 90(3): e01410. DOI: 10.1002/ecm.1410.

Pan R, Tyree MT. 2019. How does water flow from vessel to vessel? Further investigation of the tracheid bridge concept. *Tree Physiol.* 39(6): 1019–1031. DOI: 10.1093/treephys/tpz015.

Plavcová L, Hoch G, Morris H, Ghiasi S, Jansen S. 2016. The amount of parenchyma and living fibers affects storage of nonstructural carbohydrates in young stems and roots of temperate trees. *Am. J. Bot.* 103(4): 603–612. DOI: 10.3732/ajb.1500489.

Plavcová L, Gallenmüller F, Morris H, Khatamirad M, Jansen S, Speck T. 2019. Mechanical properties and structure–function trade-offs in secondary xylem of young roots and stems. *J. Exp. Bot.* 70(14): 3679–3691. DOI: 10.1093/jxb/erz286.

Pratt RB, Jacobsen AL. 2017. Conflicting demands on angiosperm xylem: tradeoffs among storage, transport and biomechanics. *Plant Cell Environ.* 40(6): 897–913. DOI: 10.1111/pce.12862.

Pratt RB, Jacobsen AL, Percolla MI, De Guzman ME, Traugh CA, Tobin MF. 2021a. Trade-offs among transport, support, and storage in xylem from shrubs in a semiarid chaparral environment tested with structural equation modeling. *Proc. Natl. Acad. Sci. USA* 118(33): e2104336118. DOI: 10.1073/pnas.2104336118.

Pratt RB, Tobin MF, Jacobsen AL, Traugh CA, De Guzman ME, Hayes CC, Toschi HS, MacKinnon ED, Percolla MI, Clem ME, Smith PT. 2021b. Starch storage capacity of sapwood is related to dehydration avoidance during drought. *Am. J. Bot.* 108(1): 91–101. DOI: 10.1002/ajb2.1586.

Pratt RB, Castro V, Jacobsen AL. 2023. The functional significance of tracheids co-occurring with vessels within xylem of eudicots suggests role in embolism tolerance. *IAWA J.* 44: in press (IAWA 2228).

Rosell JA, Olson ME, Aguirre-Hernández R, Carlquist S. 2007. Logistic regression in comparative wood anatomy: tracheid types, wood anatomical terminology, and new inferences from the Carlquist and Hoekman southern Californian data set. *Bot. J. Linn. Soc.* 154(3): 331–351. DOI: 10.1111/j.1095-8339.2007.00667.x.

Sano Y, Morris H, Shimada H, Ronse De Craene LP, Jansen S. 2011. Anatomical features associated with water transport in imperforate tracheary elements of vessel-bearing angiosperms. *Ann. Bot.* 107(6): 953–964. DOI: 10.1093/aob/mcr042.

Secchi F, Pagliarani C, Zwieniecki MA. 2017. The functional role of xylem parenchyma cells and aquaporins during recovery from severe water stress: response of xylem parenchyma cells to embolism. *Plant Cell Environ.* 40(6): 858–871. DOI: 10.1111/pce.12831.

Van Bel AJE. 1990. Xylem-phloem exchange via the rays: the undervalued route of transport. *J. Exp. Bot.* 41(6): 631–644. DOI: 10.1093/jxb/41.6.631.

Wheeler EA, Baas P, Gasson PE. 1989. IAWA list of microscopic features for hardwood identification. *IAWA J.* 10(3): 219–332. DOI: 10.1163/22941932-90000496.

Wheeler EA, Baas P, Rodgers S. 2007. Variations in dicot wood anatomy: a global analysis based on the InsideWood database. *IAWA J.* 28(3): 229–258. DOI: 10.1163/22941932-90001638.

Wolkinger F. 1969. Morphologie und systematische Verbreitung der lebenden Holzfasern bei Sträuchern und Bäumen. I. Zur Morphologie und Zytologie. *Holzforschung* 23(4): 135–144. DOI: 10.1515/hfsg.1969.23.4.135.

Wolkinger F. 1970a. Das Vorkommen lebender Holzfasern in Sträuchern und Bäumen. *Phyton* 14(1–2): 55–67.

Wolkinger F. 1970b. Morphologie und systematische Verbreitung der lebenden Holzfasern bei Sträuchern und Bäumen. II. Zur Histologie. *Holzforschung* 24(5): 141–151. DOI: 10.1515/hfsg.1970.24.5.141.

Wolkinger F. 1971. Morphologie und systematische Verbreitung der lebenden Holzfasern bei Sträuchern und Bäumen. III. Systematische Verbreitung. *Holzforschung* 25(1): 29–30. DOI: 10.1515/hfsg.1971.25.1.29.

Yamada Y, Awano T, Fujita M, Takabe K. 2011. Living wood fibers act as large-capacity "single-use" starch storage in black locust (*Robinia pseudoacacia*). *Trees* 25(4): 607–616. DOI: 10.1007/s00468-010-0537-3.

Ziemińska K, Rosa E, Gleason SM, Holbrook NM. 2020. Wood day capacitance is related to water content, wood density, and anatomy across 30 temperate tree species. *Plant Cell Environ.* 43(12): 3048–3067.

Edited by Marcelo R. Pace

plant biology

Plant Biology ISSN 1435-8603

RESEARCH PAPER

Linking wood anatomy with growth vigour and susceptibility to alternate bearing in composite apple and pear trees

R. Jupa[1], M. Mészáros[2] & L. Plavcová[1]

1 Department of Biology, Faculty of Science, University of Hradec Králové, Hradec Králové, Czech Republic

2 Research and Breeding Institute of Pomology, Hořice, Czech Republic

Keywords
fruit tree; parenchyma; rootstock; scion; vessel; water potential; xylem.

Correspondence
Radek Jupa, Department of Biology, Faculty of Science, University of Hradec Králové, Rokitanského 62, CZ-500 03, Hradec Králové, Czech Republic.
E-mail: r.jupa@mail.muni.cz

Editor
S. Pfautsch

Received: 9 July 2020; Accepted: 27 August 2020

doi:10.1111/plb.13182

ABSTRACT

- Excess vegetative growth and irregular fruit-bearing are often undesirable in horticultural practice. However, the biological mechanisms underlying these traits in fruit trees are not fully understood. Here, we tested if growth vigour and susceptibility of apple and pear trees to alternate fruit-bearing are associated with vascular anatomy.
- We examined anatomical traits related to water transport and nutrient storage in young woody shoots and roots of 15 different scion/rootstock cultivars of apple and pear trees. In addition, soil and leaf water potentials were measured across a drought period.
- We found a positive correlation between the mean vessel diameter of roots and the annual shoot length. Vigorously growing trees also maintained less negative midday leaf water potential during drought. Furthermore, we observed a close negative correlation between the proportions of total parenchyma in the shoots and the alternate bearing index.
- Based on anatomical proxies, our results suggest that xylem transport efficiency of rootstocks is linked to growth vigour of both apple and pear trees, while limited carbohydrate storage capacity of scions may be associated with increased susceptibility to alternate bearing. These findings can be useful for the breeding of new cultivars of commercially important fruit trees.

INTRODUCTION

Apple (*Malus domestica* Borkh.) and pear (*Pyrus communis* L.) trees are two highly important temperate fruit trees producing 85 and 25 million tonnes of fruit worldwide and 15 and 3 million tonnes of fruit in Europe, respectively (data for fruit production in 2017; FAO 2019). Both apple and pear trees are members of the *Rosaceae* family and have similar growth demands (Jackson 2003). In commercial orchards, apple and pear trees are grown as composite trees, in which two different genotypes are combined into an individual tree by means of grafting. In composite trees, the aboveground scion is usually selected for its production properties and is grafted onto a rootstock that influences the growth vigour and resistance to both biotic and abiotic stresses (Jackson 2003). In the grafting process, desired properties of various scions and rootstocks can be combined to optimize fruit tree performance according to a grower's demands (Mészáros *et al.* 2019).

Trees with suppressed vegetative growth are often favoured in pomiculture to reduce costs associated with pruning and to maximize fruit production per orchard unit area through an increased density of trees per hectare. Furthermore, trees with suppressed vegetative growth also frequently produce fruit earlier during their lifespan (*i.e.* precocity) (Reighard & Loreti 2008; Muleo *et al.* 2011; Fazio *et al.* 2014; Mészáros *et al.* 2015). The use of dwarfing rootstocks is a primary means to control the vegetative growth of commercial fruit trees, although the final vigour of the trees is a combined effect of the scion and rootstock vigour. While there is currently a wide selection of rootstocks with known potential to control scion vigour, the biological mechanisms of how this is achieved are not fully understood.

Differences in hydraulic performance have been suggested as one of the prominent mechanisms of how a rootstock may control tree growth vigour (Atkinson *et al.* 2003; Basile *et al.* 2003a). Maintenance of a high water potential in aboveground organs is necessary to sustain vegetative growth (Berman & DeJong 1997; Weibel *et al.* 2003; Basile *et al.* 2003a; Solari *et al.* 2006a), as it is essential for meristematic activity (Sacks *et al.* 1997), cell expansion (Guerriero *et al.* 2014) and unimpeded carbon uptake *via* open stomata (Comstock & Mencuccini 1998). High hydraulic conductivity of the transport pathway enables plants to maintain high water potentials and consequently delay stomatal closure during decreasing soil water potentials (Goncalves *et al.* 2005; Solari *et al.* 2006a). The low hydraulic conductivity of roots has been implicated in slower shoot growth and limited secondary thickening (Tyree & Sperry 1988; Tyree *et al.* 1998; Comas *et al.* 2002; Martínez-Alcántara *et al.* 2013). Dwarf trees often exhibit poorer hydraulic performance and are also less resistant to abiotic stress, pests and diseases compared to vigorously growing trees (Atkinson *et al.* 1999; Trifilo *et al.* 2007; Bauerle *et al.* 2011; Hajagos & Végvári 2013; Albacete *et al.* 2015).

Regular fruit-bearing in successive fruiting seasons is another desirable trait in fruit trees. However, many fruit trees, including the apple and pear trees, are prone to irregular bearing. In

an extreme case, fruit trees can give very high fruit yields in one year (*i.e.* 'on' year) and very low fruit yields (or no fruits at all) in the next year (*i.e.* 'off' year). Such alternate bearing often results in considerable economic loss to the growers. Alternate fruit-bearing is triggered and controlled by a combination of exogenous (*e.g.* late frost, dry summer) and endogenous (hormones, nutrients) factors (Goldschmidt 2005). It is well-known that some fruit tree species and some cultivars are more prone to alternate bearing than others, due to their different susceptibility to environmental factors (Monselise & Goldschmidt 1982) or the different branching and bearing patterns associated with their growth habits (Lauri *et al.* 1995, 2014). Although the physiological basis of these differences remains insufficiently understood, cycling of stored non-structural carbohydrates (*e.g.* starch, glucose, fructose, sucrose) and other reserve nutrients appears to be one of the factors that can drive susceptibility of fruit trees to alternate bearing (Goldschmidt 2013). Specifically, the depletion of carbohydrate reserves due to high production of fruits and/or long-lasting exposure to stress conditions throughout one year can lead to low production of fruits in the following season during which the carbohydrate levels are replenished (Baninasab & Rahemi 2006). As developing fruits represent a strong carbohydrate sink (Monselise & Goldschmidt 1982; Martínez-Alcántara *et al.* 2015; Capelli *et al.* 2016), the alternation of cropping presumably allows trees to maintain a balance between vegetative growth and reproduction under nutrient-limited conditions (Goldschmidt 2013).

The properties of secondary xylem (*i.e.* wood) affect long-distance water transport as well as storage of carbohydrates. Therefore, differences in the xylem structure and related functional properties may significantly affect both the vegetative growth of fruit trees and their susceptibility to alternate bearing. The xylem of apple and pear trees consists of three morphologically and functionally distinct cell types: (i) vessel elements, (ii) parenchyma cells (axial and ray parenchyma) and (iii) libriform fibres. Vessel elements are longitudinally elongated dead cells conducting water and dissolved compounds over long distances in the direction from roots to leaves. The dimensions and density of the vessels drive the maximum transport capacity of the xylem. According to the Hagen–Poiseuille law describing laminar flow in a capillary, hydraulic conductivity of a vessel increases with the fourth power of its diameter (Tyree & Zimmermann 2002). Positive correlations between vessel dimensions, hydraulic efficiency and tree growth have been reported in natural stands (Gleason *et al.* 2012) and managed plantation trees (Fichot *et al.* 2011). Wider vessels have also been observed in vigorously growing rootstocks compared to dwarfing rootstocks in a wide range of fruit tree species (Olmstead *et al.* 2006; Goncalves *et al.* 2007; Tombesi *et al.* 2010a, b; Tombesi *et al.* 2011; Martínez-Alcántara *et al.* 2013; Bruckner & DeJong 2014; Chen *et al.* 2015).

Compared to vessel characteristics, the anatomy of ray and axial parenchyma is less frequently studied, in spite of their importance in nutrient storage and transport (Sauter & van Cleve 1992; Pfautsch *et al.* 2015; Plavcová *et al.* 2016). Living parenchyma cells mediate short distance symplastic transport (Pfautsch *et al.* 2015) and serve as storage sites for water (Tyree & Zimmermann 2002; Jupa *et al.* 2016), carbohydrates (Plavcová *et al.* 2016) and other nutrients (Sauter & van Cleve 1992). Ray parenchyma provides a direct radial connection between the tree bark, wood and pith (Sokolowska & Zagórska-Marek 2012), while the axial parenchyma facilitates a higher contact fraction with the vessels (Morris *et al.* 2018; Słupianek *et al.* 2019). Compared to vessels, the links between tree growth and parenchyma anatomy are less understood, although several studies had reported larger proportions of rays and bark in dwarfing rootstocks of fruit trees (Beakbane & Thompson 1940; Chen *et al.* 2015). Angiosperm species with larger proportions of parenchyma cells in xylem usually contain more carbohydrate reserves (Plavcová *et al.* 2016; Pratt & Jacobsen 2017), but this might make them more susceptible to hydraulic failure through drought-induced embolism, consistent with the involvement of parenchyma cells in embolism repair (Kiorapostolou *et al.* 2019; Chen *et al.* 2020). Given the important roles of the parenchyma cells in storage and translocation of carbohydrates and other reserve compounds, differences in the parenchyma proportions may be related to susceptibility to alternate bearing. However, to the best of our knowledge, this hypothesis has not been tested.

In this study, we analysed the anatomical differences in 15 scion/rootstock combinations of apple and pear trees and tested whether the structural properties of xylem in the shoots and roots are linked to the growth vigour and susceptibility to alternate bearing. We expect that trees with high growth vigour will have larger xylem cross-sectional area and wider vessels (translating into higher hydraulic capacity) and lower proportions of bark and ray parenchyma. We also hypothesized that low parenchyma fractions might be associated with high susceptibility of trees to irregular bearing. The anatomical observations were complemented with measurements of leaf water potential during summer drought in order to examine whether expected differences in xylem anatomy are reflected in tree water status.

MATERIAL AND METHODS

Plant material

Samples for anatomical observations were collected from approx. 25-year-old apple (*Malus domestica* Borkh.) and pear (*Pyrus communis* L.) trees that were part of the scion/rootstock field trial established by the Research and Breeding Institute of Pomology in Holovousy, Czech Republic. This site (50.37 N, 15.57 E; 283 m a.s.l.) experiences a temperate climate, with mean annual temperature of 8.4 °C and mean annual precipitation of 664 mm. The trees were planted in 1990 and 1992 with spacing of 4.5 × 2.3 m for apple trees and 5.0 × 3.0 m for pear trees. The trees were trained as free-growing hedges with a short stem height and the central leader being removed in the fifth year. Plant protection followed standard integrated pest management practices and fertilization based on local recommendations for commercial orchards. The orchard was established on a loamy brown soil with neutral pH and medium fertility, without irrigation. There was no hand or chemical thinning of the fruits. The weed control in 1.5-m wide strips was maintained using herbicides and grass growing in interrows was periodically mowed.

The full field trial consisted of 36 different scion/rootstock combinations of apple and pear trees. The trial focused on two scions of apple tree ('Jonagold' and 'Rubin') and three scions of pear tree ('Conference', 'Williams' and 'General Leclerc').

The scions were grafted onto eight and nine different rootstocks for apple and pear trees, respectively. The field trial was not planted in a completely factorial design but rather included scion/rootstock combinations that were of interest to local farmers at the time of planting.

The scion/rootstock combinations were expected to show differences in growth and bearing behaviour; therefore, the trunk cross-sectional area (TCSA; cm^2) and annual fruit yield ($kg \cdot tree^{-1}$) of these trees were measured periodically from 1996 to 2011. To obtain TCSA, trunk circumference (C) of each tree was measured with a measuring tape at the end of the growing season and converted to TCSA according to the following equation:

$$\mathrm{TCSA} = \frac{C^2}{4\pi} \quad (1)$$

The measurements were done at an approximate height of 40 cm above the root collar. This point was well below the point of the first lateral branching, and no graft-related trunk swelling was evident at this height.

Annual fruit yield of each tree (in $kg \cdot tree^{-1}$) was measured at harvest using a portable balance with a 0.1 kg precision. The time-series of mean annual yields for each scion/rootstock combination were then used to calculate the alternate bearing index (ABI) over the period 1996–2011 according to the following equation:

$$\mathrm{ABI} = \frac{\sum_{i=2}^{n}(|y_i - y_{i-1}|)/(y_i + y_{i-1})}{n-1} \quad (2)$$

where y_i and y_{i-1} represent fruit yields in two successive years and n represents the number of years in the time series. ABI is a measure of susceptibility to alternate bearing, where ABI = 0 indicates no alternate bearing behaviour and ABI = 1 indicates strict biennial bearing (Hoblyn *et al.* 1936; Monselise & Goldschmidt 1982). Between four and eight individual trees were used for TCSA and ABI measurements for each scion/rootstock combination.

Selection of target scion/rootstock combinations

The measurements described above provided us with useful background information that guided our selection of scion/rootstock combinations for anatomical observations. Within each species, the scion/rootstock combinations were sorted according to their accumulated trunk growth (*i.e.* TCSA recorded in 2011). The trees were then divided into three vigour classes, hereafter referred to as low, medium and high, with each class corresponding to one third of the span between the maximum and minimum TCSA (Figure S1). Similarly, the scion/rootstock combinations were sorted according to their ABI and divided into trees with low (ABI $\leq$ 0.3), medium (ABI between 0.3 and 0.6) and high (ABI $\geq$ 0.6) susceptibility to irregular bearing (Figure S2). These visualizations showed that the differences in TCSA were mainly driven by the rootstock identity in apple trees, while both scion and rootstock identity affected TCSA in pear trees. Susceptibility to alternate bearing was mainly associated with scion identity in both fruit tree species. Based on these findings, we selected 15 scion/rootstock combinations that cover the whole gradient of growth vigour and susceptibility to alternate bearing, while aiming at factorial combinations of individual scions and rootstocks when possible. Following these criteria, our final selection included 'Jonagold' and 'Rubin' scions of apple trees grafted onto three size-controlling rootstocks (J-TE-G < M.9 < J-TE-H). Similarly, 'Conference' and 'Williams' scions grafted onto three size-controlling rootstocks (S1 < MA < PS) were selected in pear trees. Additionally, we decided to include 'Rubin' grafted onto MM.106 rootstock because it showed the largest TCSA of all available scion/rootstock combinations. All trees of 'General Leclerc' scion showed medium growth vigour and high susceptibility to alternate bearing. As neither S1 nor PS rootstocks were available, we included MA and MC grafts of this scion. All 15 selected scion/rootstock combinations and their growth and yield characteristics are listed in Table 1. Their relative position within the spectrum of growth vigour and susceptibility to alternate bearing among all available scion/rootstock combinations can be seen in Figures S1 and S2.

Growth vigour in 2018

Additional measurements of growth vigour were conducted for the 15 selected scion/rootstock combinations in 2018. TCSA was measured following the same procedure as described above. Trunks of four to nine individual trees were measured for each scion/rootstock combination. The numbers of replicates differ among scion/rootstock combinations because some individuals, which were originally planted in the field trial, have died back since the time of planting. As an alternative measure of growth vigour, annual shoot length (ASL) was measured at the end of August 2018 after the cessation of shoot elongation. The measurements were done on proleptic shoots that did not bear any fruit. Between 15 and 27 shoots from three to four individuals were measured for each scion/rootstock combination.

Anatomical measurements

Samples for anatomical observations were instead of was collected in April 2018 during bud break. One-year-old proleptic shoots (3–6-mm diameter, 30–60-cm long) and coarse woody roots (3–9-mm diameter, 10–20-cm long) were sampled. The shoots were excised from an unshaded part of the canopy at a height of approx. 1.5 m above the ground. The roots were excavated from 20–50 cm depth and at a distance of 30–70 cm from the root collar. Two samples from three different individuals (n = 6) were taken for each organ and scion/rootstock combination. Shoot and root samples were collected at the opposite sides of the tree. Excised samples were immediately wrapped in a black plastic bag containing a wet paper towel to prevent desiccation during transport to the laboratory. The samples were stored in a refrigerator and processed within 5 days.

Cross-sections of approx. 50-μm thick were prepared from the middle regions of the shoot and root samples using a GSL1 sledge microtome (Swiss Federal Research Institute WSL, Birmensdorf, Switzerland). The sections were stained with a mixture of 0.35% Safranin (dissolved in 50% ethanol; w/v) and 0.65% Alcian blue (dissolved in water; w/v) for 3 min and thoroughly washed in distilled water. The staining

Table 1. Fifteen scion/rootstock (S/R) combinations of apple and pear trees used for anatomical observations. S/R combinations were selected to span a gradient of growth vigour and susceptibility to alternate bearing. Abbreviated names for each S/R combination as well as full names of individual scions and rootstocks are included. S/R combinations within each species are listed alphabetically by scion. The rootstocks within each scion are then sorted in ascending order with respect to their trunk cross-sectional area measured in 2011 (TCSA). The absolute values of TCSA in cm^2 as well as the percentage of maximum TCSA calculated separately for each species are shown. Susceptibility to alternate bearing was evaluated based on the alternate bearing index (ABI) calculated from mean annual yields for the period from 1996 to 2011. The growth vigour and susceptibility to alternate bearing categories (low, medium, high) were assigned based on the relative comparison across 36 S/R combinations available in the field trial (Figures S1, S2).

	S/R	scion	rootstock	TCSA (cm^2)	growth vigour	ABI	susceptibility to alternate bearing
Apple tree	J/JTEG	'Jonagold'	Apple J-TE-G	78.1 (24%)	Low	0.40	Medium
	J/M9	'Jonagold'	Apple M.9	167.1 (50%)	Medium	0.40	Medium
	J/JTEH	'Jonagold'	Apple J-TE-H	249.1 (75%)	High	0.43	Medium
	R/JTEG	'Rubin'	Apple J-TE-G	95.6 (29%)	Low	0.24	Low
	R/M9	'Rubin'	Apple M.9	193.8 (58%)	Medium	0.29	Low
	R/JTEH	'Rubin'	Apple J-TE-H	254.7 (77%)	High	0.30	Low
	R/MM106	'Rubin'	Apple MM.106	331.3 (100%)	High	0.40	Medium
Pear tree	C/S1	'Conference'	Quince S1	161.5 (50%)	Medium	0.30	Low
	C/MA	'Conference'	Quince A	212.9 (66%)	High	0.29	Low
	C/PS	'Conference'	Pear seedling	320.4 (100%)	High	0.42	Medium
	GL/MA	'General Leclerc'	Quince A	224.1 (70%)	Medium	0.66	High
	GL/MC	'General Leclerc'	Quince C	216.3 (68%)	Medium	0.63	High
	W/S1	'Williams'	Quince S1	110.1 (34%)	Low	0.26	Low
	W/MA	'Williams'	Quince A	143.6 (45%)	Low	0.38	Medium
	W/PS	'Williams'	Pear seedling	200.0 (62%)	Medium	0.39	Medium

differentiates the lignified cell walls of vessels and fibres (stained pink to red) from the parenchyma cells (stained blue to purple). Finally, the sections were mounted in distilled water and observed in a bright field using an Olympus BX50 microscope (Olympus, Tokyo, Japan) equipped with an SLT-A35 digital camera (Sony, Tokyo, Japan).

The cross-sections were photographed at 10× objective magnification and the total area of pith, xylem and bark within each cross-section was manually outlined using Adobe Photoshop CS6 (Adobe Systems, Mountain View, CA, USA). The areas of individual tissues were measured with ImageJ software and converted to relative proportions. A representative wedge of xylem was then photographed at 40× objective magnification and the relative proportions of vessels (*V*), axial parenchyma (AP), ray parenchyma (RP) and fibres (*F*) determined using the gridline method (Ziemińska *et al.* 2015). For this purpose, the wedge was overlaid with a grid containing at least 300 intersections. Individual cell types were identified at each intersection, the intersections were colour coded and the relative proportions of individual xylem cell types were calculated as the number of points belonging to a given cell type divided by the total number of analysed points (Figure S3). We also calculated the sum of the relative proportions of pith, total xylem parenchyma (RP + AP = RAP) and bark parenchyma (*i.e.* proportions of bark excluding rhytidome, phellem and regions with lignified sclereids and fibres) and refer to this compound parenchyma fraction as the relative proportion of total organ parenchyma (TP). As such, TP provides an estimate of the maximum cross-sectional area of each organ available for carbohydrate storage.

Furthermore, the diameters of all vessels within each 45° wedge were measured. The lumina of all vessels were carefully outlined, their areas were measured in ImageJ and converted into diameters assuming circular shape of vessels. The mean vessel lumen diameter (*D*; μm) of each sample was calculated. Vessel density (VD; $n \cdot mm^{-2}$) was determined as the ratio of the number of vessels to xylem cross-sectional area in the 45° wedge.

Furthermore, we estimated the theoretical hydraulic conductivity (K_h; kg m $MPa^{-1} \cdot s^{-1}$) of each sample by extrapolating conductivity calculated for the subset of vessels present in the 45° wedge (XA_{wedge}) to the total xylem area (XA_{tot}) of each sample:

$$K_h = \left(\sum \frac{\pi \rho d^4}{128\eta} \right) \frac{XA_{tot}}{XA_{wedge}} \quad (3)$$

where d is the vessel lumen diameter, ρ is the density of water at 20 °C (998.2 $kg \cdot m^{-3}$) and η is the dynamic viscosity of water at 20 °C (1.002×10^{-9} MPa s). Thus, K_h integrates the effect of vessel diameters, vessel numbers and the size of xylem cross-sectional area.

Leaf water potential and climate conditions

To complement the anatomical proxies of plant water transport, midday leaf water potential (Ψ_{MD}) was monitored during the summer 2018 in trees with contrasting growth vigour. Due to time constraints, the measurements of Ψ_{MD} were restricted to J/J-TE-G, J/M.9 and J/J-TE-H combinations of apple trees and W/S1, W/MA and W/PS combinations of pear trees. The measurements were done on fully expanded uncovered leaves between 11:00 h and 13:00 h on six different dates. The leaves were inserted into plastic bags, excised using a sharp razor blade, and Ψ_{MD} determined within 30 s using a portable Scholander pressure chamber (1505D-EXP; PMS Instrument Co., Albany, OR, USA). Two leaves from four to six different

individuals (n = 8–12) were measured for each scion/rootstock combination.

The Ψ_{MD} data were interpreted in conjunction with data on soil water potential (Ψ_S) and atmospheric water demand. The Ψ_S was continuously measured on site during the growing season using two water potential sensors (Teros 21; Meter Environment, Pullman, WA, USA) placed at depths of 5 cm and 30 cm and connected to a data logger (MicroLog SP3; EMS, Brno, Czech Republic). Based on our preliminary analyses of root vertical distribution in scion/rootstock combinations of contrasting growth vigour (J/JTEH *versus* J/JTEG; W/PS *versus* W/S1), these depths were within the zone of maximum root density, and thus maximum absorption capacity of the root system. The air temperature and air relative humidity were measured at 2 m above ground level with an HMP 35D sensor (Vaisala, Vantaa, Finland) and converted into vapour pressure deficit (VPD). The environmental data were acquired at 1-h intervals.

Statistical analysis

Because the experimental design was not full factorial, we conducted two types of analyses to evaluate the effect of individual scions and rootstocks on the growth and anatomical parameters. Mean differences between scions within each species and organ (when applicable for anatomical parameters) were tested using mixed-effect linear models, where scion was treated as a fixed factor and rootstock was included as a random factor. Within each scion, the effect of rootstock was then analysed by one-way ANOVA, with rootstock implemented as a single factor. Validation of the models was done by graphical checking of the residual plots. If the effect of rootstock was significant, the means of individual rootstocks were separated using a Tukey HSD test. Principal components analysis (PCA) was used to summarize the relationships among all the anatomical traits in the roots and shoots separately. Relationships between the anatomical parameters and growth and yield characteristics were analysed using simple linear regressions and were described using Pearson's correlation coefficients (r). Variables were transformed to meet the assumptions of normality, if necessary. Finally, a two-way ANOVA was used to evaluate the differences in Ψ_{MD} among the sampling dates and rootstocks for 'Jonagold' and 'Williams' scions separately. In the case of a significant effect of the interaction of both factors, the Tukey HSD test was used to compare the means of the rootstocks within each scion and sampling date. Prior ANOVA, normality of residuals and homogeneity of variance were tested with exact Shapiro-Wilk and Cochran-Hartley-Bartlett tests, respectively. Results were considered statistically significant at $P < 0.05$. All statistical analyses were performed using R development (R Core Team, 2010). Throughout this paper, data are presented as mean ± 1 SE.

RESULTS

Growth vigour and susceptibility to alternate bearing

Trunk cross-sectional area measurements conducted on selected 15 scion/rootstock combinations in 2018 corresponded well with the background data from 2011 (compare Tables 1 and 2), indicating that the relative differences in trunk growth vigour have not changed with the additional 7 years of age. In apple trees, 'Jonagold' showed a slightly lower TCSA than 'Rubin' (Tables 1, 2, Figure S1a). In pear trees, 'Williams' had lower TCSA than 'Conference' and 'General Leclerc' (Tables 1, 2, Figure S1b). Across rootstocks, TCSA increased in the following order: J-TE-G < M.9 < J-TE-H < MM.106 for apple trees and S1 < MA/MC < PS in pear trees (Table 2). The two measures of growth vigour, TCSA and ASL, were mutually correlated within each scion (Fig. 1). However, there were scion-specific differences in the relative magnitude of trunk *versus* shoot growth. More specifically, 'Jonagold' had longer shoots but thinner trunks than 'Rubin' (Table 2, Fig. 1a). A similar tendency was observed in 'Williams' scion compared to 'Conference' (Table 2, Fig. 1b).

The susceptibility to alternate bearing was higher in 'Jonagold' scions of apple trees compared to 'Rubin' (Table 1, Figure S2a). In pear trees, 'General Leclerc' showed higher ABI than 'Williams' and 'Conference' (Table 1, Figure S2b). Overall, there was no significant correlation between ABI and TCSA ($P = 0.250$) or ASL ($P = 0.093$); however, within each scion, more vigorous trees tended to be more susceptible to alternate bearing than trees of a low vigour (*e.g.* compare R/MM.106 *versus* R/J-TE-G, or C/S1 *versus* C/PS; Table 1, Figure S2b).

Anatomical variation

The anatomical differences between apple and pear trees, and among the scion/rootstock combinations, and the mutual relationships among the individual anatomical parameters observed in the shoots and roots are summarized using PCA (Fig. 2). The first two principal components (PCs) of PCA explained 77.08% and 79.09% of the total variability observed in shoots and roots, respectively. For both shoots and roots,

Table 2. Growth characteristics of 15 scion/rootstock (S/R) combinations of apple and pear trees. Trunk cross-sectional area (TCSA) and annual shoot length (ASL) were measured at the end of the growing season of 2018. S/R combinations are listed alphabetically by scion. Within each scion, the rootstocks are sorted in ascending order with respect to their growth vigour. See Table 1 for full names of S/R combinations. Data are mean ± 1 SE (n = 4–9 for TCSA and n = 17–27 for ASL). Lowercase letters indicate statistically significant differences among rootstocks within individual scions. Uppercase letters indicate significant differences among scions within each species. Differences were considered as significant at $P < 0.05$.

	S/R	TCSA (cm^2)		ASL (cm)	
Apple tree	J/JTEG	113.9 ± 7.2 a	A	41.4 ± 2.3 a	B
	J/M9	215.5 ± 20.1 b		47.9 ± 2.5 a	
	J/JTEH	298.8 ± 10.6 c		62.2 ± 3.4 b	
	R/JTEG	122.2 ± 21.0 a	B	21.1 ± 1.6 a	A
	R/M9	240.4 ± 22.4 b		40.8 ± 3.0 bc	
	R/JTEH	402.8 ± 23.5 c		37.4 ± 3.2 b	
	R/MM106	420.9 ± 22.1 c		47.8 ± 2.3 c	
Pear tree	C/S1	204.4 ± 7.5 a	B	30.9 ± 1.5 a	A
	C/MA	311.5 ± 10.5 b		44.3 ± 2.3 b	
	C/PS	453.1 ± 40.2 c		58.4 ± 3.4 c	
	GL/MA	308.3 ± 14.2 a	B	41.6 ± 2.0 a	A
	GL/MC	311.9 ± 34.1 a		52.2 ± 2.2 b	
	W/S1	159.5 ± 13.2 a	A	41.3 ± 2.1 a	B
	W/MA	226.3 ± 15.3 b		52.9 ± 2.2 b	
	W/PS	277.4 ± 14.3 b		58.3 ± 3.1 b	

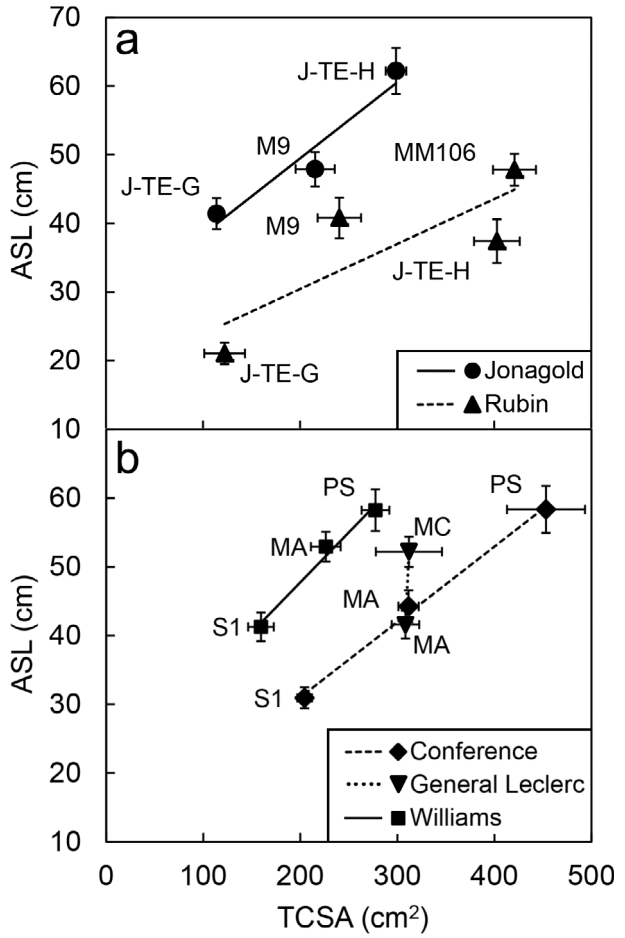

Fig. 1. Relationships between trunk cross-sectional area (TCSA) measured 40 cm above the ground and annual shoot length (ASL) for selected scion/rootstock combinations of apple (a) and pear (b) trees. Data points and error bars represent mean ± SE (n = 15–27 for ASL and 4–9 for TCSA). The data within individual scions were fitted with linear functions. Full names of the rootstocks are provided in Table 1.

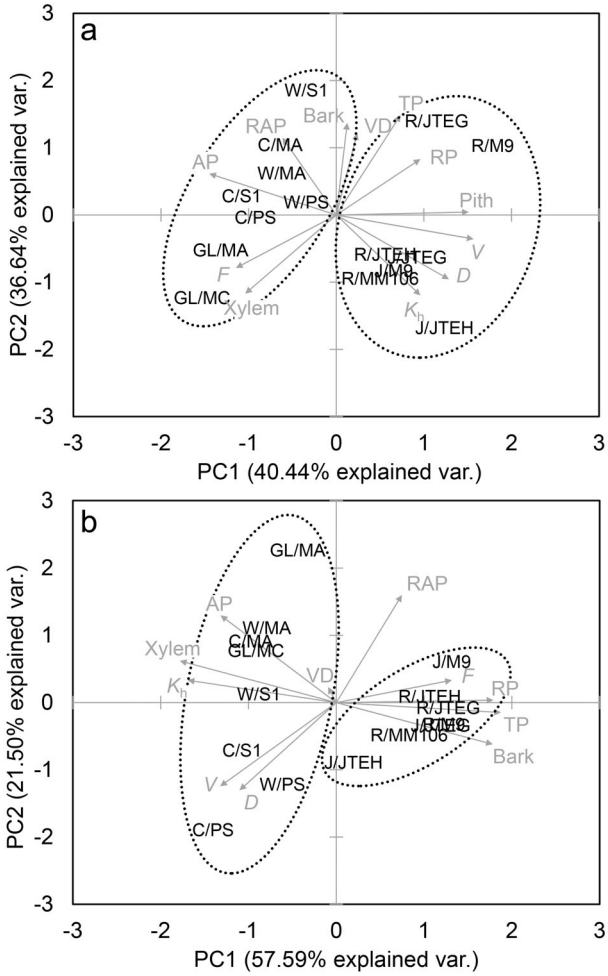

Fig. 2. Principal components analysis showing coordination among anatomical parameters in shoots (a) and roots (b) of 15 different scion/rootstock combinations of apple and pear trees. Representatives of individual species are grouped inside of dotted ellipses. Full names of the scion/rootstock combinations are provided in Table 1. Pith – proportion of pith, xylem – proportion of xylem, bark – proportion of bark, TP – proportion of total organ parenchyma, *V* – proportion of vessels, AP – proportion of axial parenchyma, RP – proportion of ray parenchyma, RAP – proportion of total xylem parenchyma, *F* – proportion of fibres, *D* – mean vessel lumen diameter, VD – vessel density, K_h – theoretical hydraulic conductivity.

groups of apple and pear trees were separated from each other by PC1 (explaining 40.44% and 57.59% of the total variability). Among notable differences, the shoots of apple trees had a larger proportion of pith and larger *D* compared to pear trees (Fig. 2a). In roots, proportions of xylem and *D* were larger in pear trees, whereas apple trees had higher proportions of bark, ray parenchyma and total organ parenchyma (Fig. 2b). These results point to contrasting functional specialization of apple and pear tree roots towards transport and storage, respectively.

The differences in anatomical parameters observed among the selected scion/rootstock combinations were rather small (Table S1; Figs 3, 4). We expected to find traits underlying higher transport capacity in more vigorously growing trees. In agreement with this hypothesis, significantly larger proportions of xylem were found in shoots and roots of 'Jonagold' compared to 'Rubin', consistent with a longer ASL of 'Jonagold' (Table S1). Higher xylem proportions were also found along the size-controlling rootstock sequence in 'Rubin' shoots and 'Jonagold' roots (Table S1). 'Jonagold' shoots had significantly wider vessels than 'Rubin', with a mean difference in *D* of 2.5 μm (Fig. 3a). A general tendency for wider vessels and higher K_h was evident along the sequence of size-controlling rootstocks for most within-scion comparisons (Fig. 3a,b). However, the differences were not always statistically significant, partly due to higher variability within the root samples.

Across all 15 scion/rootstock combinations, there was a significant positive correlation between *D* in roots and ASL (Fig. 5 a), suggesting better hydraulic efficiency of rootstocks in trees with higher shoot growth vigour. This correlation was also significant within the apple trees alone ($r = 0.83$, $P = 0.022$), but not within the pear trees (Table S2). In apple trees, the *D* in shoots was also positively correlated with ASL ($r = 0.89$, $P = 0.007$; Table S2).

Based on our literature survey, we expected to find lower proportions of parenchyma tissues in vigorously growing trees. In agreement, lower TP were observed in the shoots of 'Rubin' grafted onto the rootstocks that induced increased growth

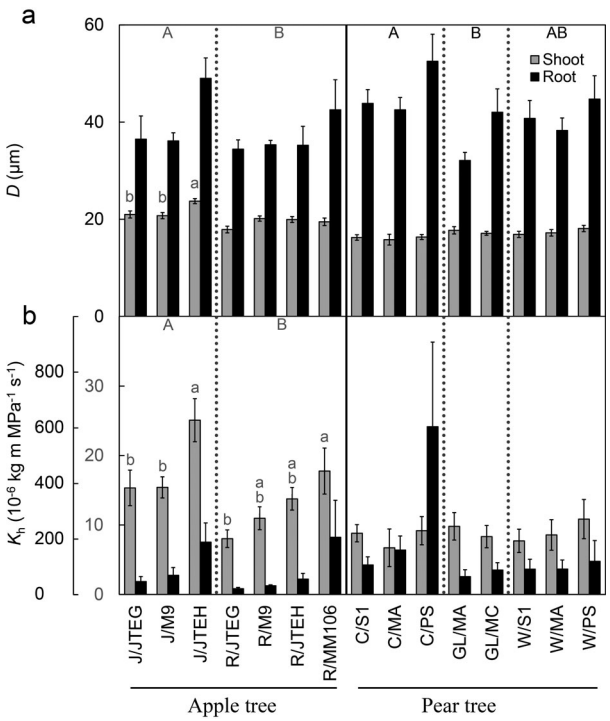

Fig. 3. Mean vessel lumen diameter (a) and theoretical hydraulic conductivity (b) in shoots and roots of 15 different scion/rootstock combinations of apple and pear trees. Scion/rootstock combinations are listed alphabetically by scion (separated by vertical dotted lines). Within each scion, the rootstocks are sorted in ascending order with respect to their growth vigour. Full names of the scion/rootstock combinations are provided in Table 1. Columns and error bars represent mean ± 1 SE (n = 5–6). Lowercase letters indicate statistically significant differences among rootstocks within individual scions. Uppercase letters in bold indicate significant differences among scions within each organ and species. Grey and black letters correspond to the differences in shoots and roots, respectively. Differences were considered as significant at $P < 0.05$. Note different scales of theoretical hydraulic conductivities for shoots (inner scale) and roots (outer scale).

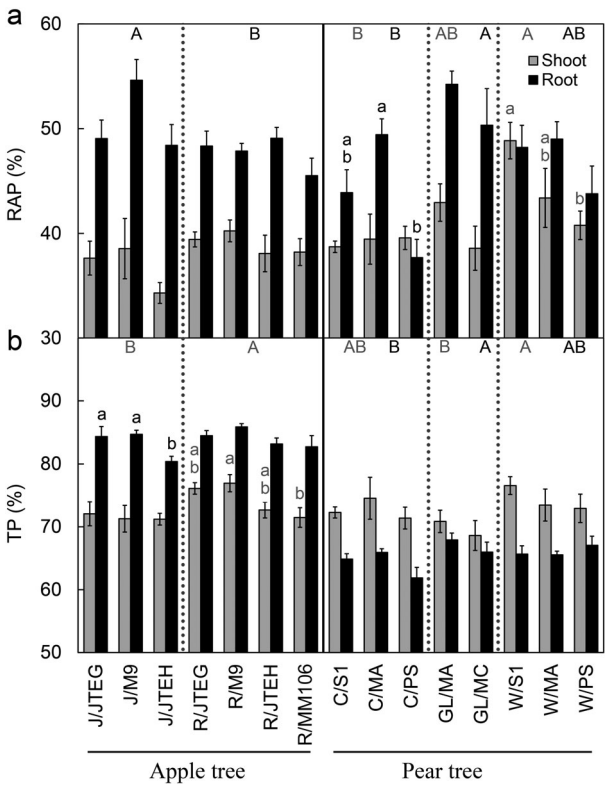

Fig. 4. Proportion of the total xylem parenchyma (a) and proportion of total organ parenchyma (b) in shoots and roots of 15 different scion/rootstock combinations of apple and pear trees. Scion/rootstock combinations are listed alphabetically by scion (separated by vertical dotted lines). Within each scion, the rootstocks are sorted in ascending order with respect to their growth vigour. Full names of the scion/rootstock combinations are provided in Table 1. Columns and error bars represent mean ± 1 SE (n = 5–6). Lowercase letters indicate statistically significant differences among rootstocks within individual scions. Uppercase letters in bold indicate significant differences among scions within each organ and species. Grey and black letters correspond to the differences in shoots and roots, respectively. Differences were considered significant at $P < 0.05$.

vigour (*i.e.* R/J-TE-H, R/MM.106; Fig. 4b). Significantly lower proportions of bark, RP and TP were also detected in the roots of the most vigorously growing rootstock combination of 'Jonagold' (*i.e.* J/J-TE-H). In pear trees, significantly lower RAP was found in the most vigorously growing rootstock combination in 'Williams' shoots (W/PS) and 'Conference' roots (C/PS; Fig. 4a). However, we also detected patterns that were inconsistent with our hypothesis, such as the significantly higher AP in roots of J/J-TE-H compared to J/J-TE-G, significantly higher proportions of bark in W/PS roots compared to W/MA, and the higher RP and RAP in less vigorously growing shoots of 'Williams' compared to 'Conference' (Table S1, Fig. 4a).

While we did not observe any clear overall relationship between proportions of parenchyma and growth vigour (Table S2), TP in shoots correlated closely with ABI (Fig. 5b). The correlation between TP and ABI was significant for both species together ($r = -0.85$, $P < 0.001$; Fig. 5b) and for apple ($r = -0.88$, $P = 0.009$) and pear ($r = -0.84$, $P = 0.009$) trees separately. This relationship was largely driven by the parenchyma in bark, as the relative proportions of bark correlated significantly with ABI ($r = -0.75$, $P = 0.001$) while the correlation between RAP and ABI was not significant (Table S2).

Midday leaf water potential during drought

Monitoring of Ψ_{MD} indicates a more balanced water status in vigorously growing trees during an extraordinarily hot and dry summer of 2018. In our site, the drought was exacerbated from mid-July to mid-August, as indicated by gradually decreasing Ψ_S and increasing VPD, reaching >3 kPa at the peak of the drought period (Fig. 6a). During this period, more vigorous scion/rootstock combinations of apple (Fig. 6b) and pear trees (Fig. 6c) maintained higher Ψ_{MD} compared to their less vigorously growing counterparts.

DISCUSSION

In this study, we investigated whether the structure of secondary xylem relates to differences in growth vigour and susceptibility to alternate bearing across 15 scion/rootstock

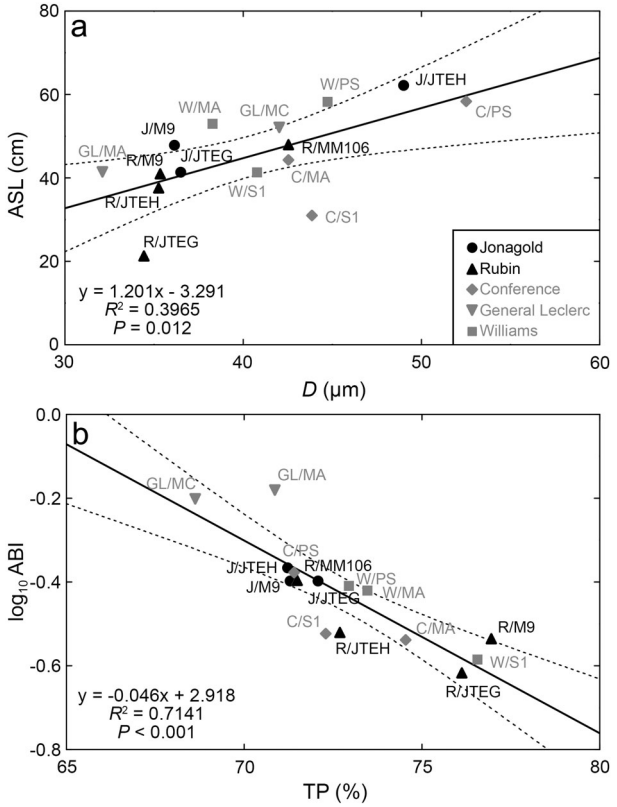

Fig. 5. Correlation between mean vessel lumen diameter in roots and annual shoot length (a; *i.e.* ASL) and correlation between the proportion of total parenchyma in annual shoots and alternate bearing index (b; *i.e.* ABI). Data points represent the mean measured for each scion/rootstock combination of apple (black symbols) and pear (grey symbols) trees. Full names of the scion/rootstock combinations are provided in Table 1. Data for both apple and pear trees were best fitted with linear functions (solid line). Dashed lines represent 0.95 confidence intervals.

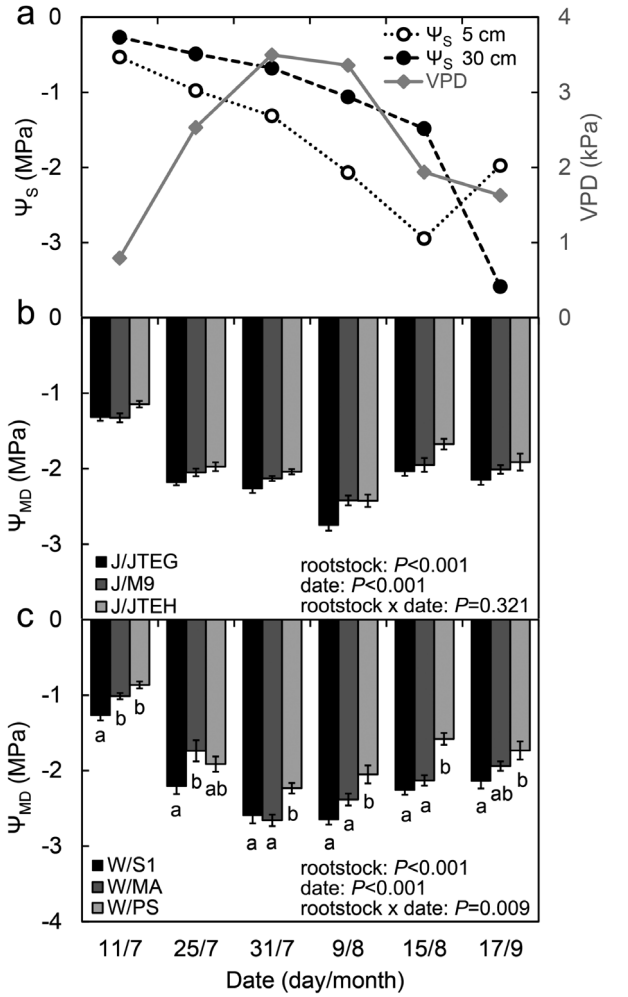

Fig. 6. Variations in climate conditions (a) and midday leaf water potentials (b, c) observed on six different dates during the summer of 2018. Vapour pressure deficit (VPD) and soil water potential measured at depths of 5 cm (Ψ_S 5 cm) and 30 cm (Ψ_S 30 cm) at midday (a) and corresponding variation in midday leaf water potential of selected scion/rootstock combinations of apple (b) and pear (c) trees are shown. Columns and error bars represent mean ± 1 SE (n = 6–16). Letters indicate statistically significant differences among scion/rootstock combinations within individual days ($P < 0.05$, Tukey's HSD test). Full names of the scions and rootstocks are provided in Table 1.

combinations of apple and pear trees (Table 1). The study encompasses four scions (namely 'Jonagold' and 'Rubin' for apple tree; 'Conference' and 'Williams' for pear tree) grafted onto a sequence of three to four size-controlling rootstocks (namely J-TE-G < M.9 < J-TE-H < MM.106 for apple tree, and S1 < MA < PS for pear tree). The scion 'General Leclerc' was included in this study because of its high susceptibility to alternate bearing. Mainly, we focused on anatomical traits related to water transport and nutrient storage capacity.

In agreement with our hypothesis, we observed wider vessels in more vigorously growing scion/rootstock combinations (Fig. 3a) and an overall positive correlation between mean vessel lumen diameter in roots and annual shoot length (Fig. 5a). Our results are consistent with several other studies that reported a strong positive association between vessel diameter and vegetative growth in natural- (Olson *et al.* 2014; Pfautsch *et al.* 2016) and plantation-grown (Fichot *et al.* 2009; Hajek *et al.* 2014) tree species, including fruit trees (Beakbane 1952; Olmstead *et al.* 2006; Goncalves *et al.* 2007; Tombesi *et al.* 2010a,b; Hajagos & Végvári, 2013). In this study, the links between vessel diameter and vigour were more prominent in apple trees than pear trees, as evident from the significant correlations between *D* and ASL found for both roots and shoots in apple but not in the pear trees (Table S2, Fig. 5a). This difference between species might be related to a less steep gradient of growth vigour (relative trunk cross-sectional area between 24–100% *versus* 34–100% for apple and pear trees, respectively; Table 1) and the fact that growth vigour was more strongly associated with scion identity in pear trees (Figure S1). Alternatively, it is possible that xylem hydraulic constraints are less important in the pear tree due to its generally higher root transport capacity (Fig. 2).

Larger xylem fractions and wider vessels likely underpin higher hydraulic conductivity of organs in vigorously growing trees. Although we did not measure the hydraulic conductivity directly, the values of theoretical hydraulic conductivity calculated based on the anatomical data (Fig. 3b) agree well with the results of Atkinson *et al.* (2003), who reported nearly six times

higher conductivity in MM.106 compared with M.9 rootstock. More efficient xylem water transport may contribute to the higher hydraulic conductance of the whole root systems that has been measured in invigorating rootstocks using a high-pressure flowmeter (Basile *et al.* 2003b; Nardini *et al.* 2006; Solari *et al.* 2006b). However, it is unlikely that the differences in root conductance are solely due to the variation in xylem anatomy. Axial transport *via* the xylem network represents only a single component of the overall hydraulic pathway, one with the highest path length but presumably with a low resistance (Cruiziat *et al.* 2002). Major hydraulic resistances are encountered in the extra-xylary tissues of roots and can be modulated through the expression of aquaporins (Laur & Hacke 2013) and deposition of apoplastic barriers (Doblas *et al.* 2017). In addition, the graft union may impose substantial resistance to water flow in some composite trees (Atkinson *et al.* 2003), although other studies found its contribution was negligible (Basile *et al.* 2003b; Nardini *et al.* 2006).

Efficient xylem water transport may affect tree vegetative growth through a combination of several mechanisms. Higher hydraulic conductivity facilitates the transport of water, dissolved nutrients (Jones 1976) and growth regulators (Webster 2004) towards meristems to stimulate their activity. Sufficient water delivery during high transpiration demand may also prevent an excessive drop in leaf water potential and sustain leaf gas exchange for a longer period of time (Sperry 2000). Focusing on 'Jonagold' and 'Williams' scions only, we found that the more vigorous rootstock combinations maintained less negative midday leaf water potentials during summer drought, suggesting a more favourable water status of high-vigour trees (Fig. 6). These observations are consistent with previous results on apple (Olien & Lakso 1986), peach (Basile *et al.* 2003b; Solari *et al.* 2006a) and cherry trees (Goncalves *et al.* 2007) and lend more support to the water relations theory of rootstock-induced control of growth vigour (Basile & DeJong 2018).

While midday leaf water potential serves as a useful indicator of plant water stress, its actual value is a result of complex interactions between water uptake, transport and loss (Sperry 2000; Rodriguez-Dominguez *et al.* 2016). Less negative water potentials in vigorously growing trees could also indicate better access to soil water. Vigorously growing rootstocks are known to produce more extensive and deeper root systems, allowing water uptake from deep soil layers (De Silva *et al.* 1999; Solari *et al.* 2006b; Ma *et al.* 2013; An *et al.* 2017). Our preliminary observations of vertical root distribution indicated effective rooting depths of around 60 and 100 cm for low and high vigour apple trees, respectively, although the majority of the fine root biomass was restricted to the topmost 40 cm of soil. The root systems of pear trees penetrated into even deeper soil layers, with effective rooting depths of more than 100 and 130 cm for W/S1 and W/PS, respectively. Thus, the differences in xylem transport efficiency of roots (Fig. 3) might be supported by a more extensive root system in vigorously growing trees, thereby improving their water status during drought.

The positive relationship between vessel size and growth observed in this as well as in the previous studies might also be related to the seemingly universal pattern of axial conduit widening along the plant's hydraulic path (Anfodillo *et al.* 2013; Olson *et al.* 2014). According to this paradigm, vessels become progressively wider with an increasing distance from the plant apex in order to compensate for the increasing hydrodynamic resistance associated with the longer conductive path (Anfodillo *et al.* 2013; Olson *et al.* 2014). As we analysed xylem anatomy in the middle of shoots of slightly variable lengths (Table 2, Fig. 1) and in root segments excavated haphazardly from a given soil depth without a direct reference to the path length, it is possible that the measured differences in vessel diameters may be biased through vessel widening patterns (Lechthaler *et al.* 2019). However, analysis of vessel packing densities (*i.e.* the ratio of vessel diameter to vessel density) did not reveal large differences across the scion/rootstock combinations (Figure S4), suggesting that vessel tapering likely had only a small effect on the analysed vessel characteristics. From a developmental point of view, the axial conduit widening is a result of endogenous regulation orchestrated from the apical bud. These patterns might be quite complex in fruit trees, in which the apical dominance has been perturbed by extensive training and pruning. On the other hand, dwarfing rootstocks are known to have lower capacity for basipetal auxin transport (Somelidou *et al.,* 1994), which would be consistent with the development of narrower vessels (Aloni 1987).

Apart from the water relations, contrasting growth vigour may be related to the carbohydrate balance. In previous studies, rootstock-induced dwarfism has been linked to starch immobilization within the root system, leading to reduced availability of soluble sugars for scion growth (Foster *et al.* 2017; Basile & DeJong 2018). Increased accumulation of starch would be consistent with the higher proportions of bark and ray parenchyma observed in dwarfing rootstocks (Beakbane & Thompson 1940; Chen *et al.* 2015). Our data, however, do not indicate consistent differences in the proportions of storage tissues between trees of low *versus* high growth vigour among the selected scion/rootstock combinations (Fig. 4). Direct measurements of non-structural carbohydrates are needed to shed more light on the role of carbohydrates and their dynamics in relation to growth vigour.

While the proportions of parenchyma were not directly related to growth vigour, we observed a close negative relationship between alternate bearing index and proportions of total organ parenchyma in shoots (Fig. 5b). Thus, larger proportions of storage tissue were associated with lower susceptibility to alternate bearing, highlighting the importance of nutritional limitation for alternate bearing behaviour. Given that TP is one of the factors underlying the maximum carbohydrate content in tree organs (Plavcová *et al.* 2016; Pratt & Jacobsen 2017), lower carbohydrate reserves in trees with lower TP may be more easily depleted during stress. In contrast, higher reserves of carbohydrates stored in TP may prolong the tree's ability to resist stress, accumulate more carbohydrate reserves for the following season and support the development of a higher number of generative buds. The difference in TP was driven by the different proportions of bark, rather than the proportions of xylem parenchyma (Table S1; Fig. 4). Bark is a multifunctional tissue with its functional roles still poorly understood (Rosell 2019). Thus, more research on the structure and function of bark in relation to alternate bearing would be desirable.

Compared to some previous studies, the variation in xylem anatomy observed here among different scion/rootstock combinations was rather small. For instance, Beakbane & Thompson (1940) reported variation in proportions of ray parenchyma between 22% and 47% (~2.1-fold variation) across ten apple tree rootstocks of different growth vigour,

while we observed values between 23% and 33% for apple trees, and between 16% and 22% in pear trees (~1.4 variation; Table S1). Similarly, Tombesi *et al.* (2010b) found mean vessel diameters of 26 μm *versus* 62 μm in peach tree rootstocks of low *versus* high growth vigour, while we observed *D* in a narrower range of 34–49 μm for apple trees, and 32–52 μm in pear trees (Fig. 3a). This difference might be because we studied trees >25 years old, while most previous studies were done with trees in their first years of growth. It is possible that there are initially larger differences in anatomical parameters at earlier stages of tree ontogeny. Such anatomical variation may lead to the development of morphological differences (*e.g.* different rooting depth, shoot-to-root ratio) that later become the dominant features driving tree performance in the field. To fully understand the controls of growth vigour in composite fruit trees, more studies at whole-plant scale and during the entire tree lifespan would be desirable.

ACKNOWLEDGEMENTS

We thank Lucy Boulton for linguistic help and three anonymous reviewers for their valuable comments. The authors acknowledge support from the Czech Science Foundation (18-19722Y). This research was also supported by the project Pomology Research Center within National Sustainable Development (LO1608) and institutional support from the Ministry of Agriculture of the Czech Republic (MZE-RO1518).

SUPPORTING INFORMATION

Additional supporting information may be found online in the Supporting Information section at the end of the article.

Table S1. Parameters related to tissue proportions and xylem anatomy measured in shoots and roots of fifteen scion/rootstock combinations of apple and pear trees.

Table S2. Pearson correlation coefficients for linear correlations between selected anatomical parameters and fruit bearing characteristics as well as between anatomical parameters and growth vigour characteristics obtained for apple and pear trees.

Figure S1. Trunk cross-sectional areas of scion/rootstock combinations of apple and pear trees measured after 20 years of growth.

Figure S2. Alternate bearing index of scion/rootstock combinations of apple and pear trees calculated from fruit yields measured between years 1996 and 2011.

Figure S3. Scheme illustrating the process of image analysis.

Figure S4. Ratio of the mean vessel lumen diameter to vessel density measured in annual shoots and roots of fifteen different scion/rootstock combinations of apple and pear trees.

REFERENCES

Albacete A., Martínez-Andújar C., Merínez-Pérez A., Thompson A.J., Dodd I.C., Pérez-Alfocea F. (2015) Unravelling rootstock×scion interactions to improve food security. *Journal of Experimental Botany*, **66**, 2211–2226.

Aloni R. (1987) Differentiation of vascular tissues. *Annual Review of Plant Physiology*, **38**, 179–204.

An H., Luo F., Wu T., Wang Y., Xu X., Zhang X., Han Z. (2017) Dwarfing effect of apple rootstocks is intimately associated with low number of fine roots. *HortScience*, **52**, 503–512.

Anfodillo T., Petit G., Crivellaro A. (2013) Axial conduit widening in woody species: a still neglected anatomical pattern. *IAWA Journal*, **34**, 352–364.

Atkinson C.J., Else M.A., Taylor L., Dover C.J. (2003) Root and stem hydraulic conductivity as determinants of growth potential in grafted trees of apple (*Malus pumila* Mill.). *Journal of Experimental Botany*, **54**, 1221–1229.

Atkinson C.J., Policarpo M., Webster A.D., Kuden A.M. (1999) Drought tolerance of apple rootstocks: Production and partitioning of dry matter. *Plant and Soil*, **206**, 223–235.

Baninasab B., Rahemi M. (2006) Possible role of nonstructural carbohydrates in alternate bearing of pistachio. *European Journal of Horticultural Science*, **71**, 277–282.

Basile B., DeJong T.M. (2018) Control of fruit tree vigor induced by dwarfing rootstocks. In: Warrington I. (Ed), *Horticultural Reviews*. John Wiley & Sons, Hoboken, NY, USA, pp 39–97.

Basile B., Marsal J., DeJong T.M. (2003a) Daily shoot extension growth of peach trees growing on rootstocks that reduce scion growth to daily dynamics of stem water potential. *Tree Physiology*, **23**, 695–704.

Basile B., Marsal J., Solari L.I., Tyree M.T., Bryla D.R., DeJong T.M. (2003b) Hydraulic conductance of peach trees grafted on rootstocks with differing size-controlling potentials. *The Journal of Horticultural Science and Biotechnology*, **78**, 768–774.

Bauerle T.L., Centinari M., Bauerle W.L. (2011) Shifts in xylem vessel diameter and embolisms in grafted apple trees of differing rootstock growth potential in response to drought. *Planta*, **234**, 1045–1054.

Beakbane A.B. (1952) Anatomical structure in relation to rootstock behaviour. In: Synge P.M. (Ed.), *Proceedings 13th International Horticultural Congress*, vol. **1**. London, UK. pp. 152–157.

Beakbane A.B., Thompson E.C. (1940) Anatomical studies of stems and roots of hardy fruit trees II. The internal structure of the roots of some vigorous and some dwarfing apple rootstocks, and the correlation of structure with vigour. *Journal of Pomology and Horticultural Science*, **17**, 141–149.

Berman M.E., DeJong T.M. (1997) Diurnal patterns of stem extension growth in peach (*Prunus persica*): temperature and fluctuations in water status determine growth rate. *Physiologia Plantarum*, **100**, 361–370.

Bruckner C.H., DeJong T.M. (2014) Proposed pre-selection method for identification of dwarfing peach rootstocks based on rapid shoot xylem vessel analysis. *Scientia Horticulturae*, **165**, 404–409.

Capelli M., Lauri P.É., Normand F. (2016) Deciphering the costs of reproduction in mango – vegetative growth matters. *Frontiers in Plant Science*, **7**, 1531.

Chen B., Wang C., Tian Y., Chu Q., Hu C. (2015) Anatomical characteristics of young stems and mature leaves of dwarf pear. *Scientia Horticulturae*, **186**, 172–179.

Chen Z., Zhu S., Zhang Y., Luan J., Li S., Sun P., Wan X., Liu S. (2020) Tradeoff between storage capacity and embolism resistance in the xylem of temperate broadleaf tree species. *Tree Physiology*, **40**, 1029–1042.

Comas L.H., Bouma T.J., Eissenstat D.M. (2002) Linking root traits to potential growth rate in six temperate tree species. *Oecologia*, **132**, 34–43.

Comstock J., Mencuccini M. (1998) Control of stomatal conductance by leaf water potential in *Hymenoclea salsola* (T. & G.), a desert subshrub. *Plant, Cell & Environment*, **21**, 1029–1038.

Cruiziat P., Cochard H., Améglio T. (2002) Hydraulic architecture of trees: main concepts and results. *Annals of Forest Science*, **59**, 723–752.

De Silva H.N., Hall A.J., Tustin D.S., Gandar P.W. (1999) Distribution of root length density of apple trees on different dwarfing rootstocks. *Annals of Botany*, **83**, 335–345.

Doblas V.G., Geldner N., Barberon M. (2017) The endodermis, a tightly controlled barrier for nutrients. *Current Opinion in Plant Biology*, **39**, 136–143.

FAO. (2019) *FAO Statistics Data 2019*. Available at http://www.fao.org/faostat/en/#data (accessed 21 May 2020).

Fazio G., Wan Y., Kviklys D., Romero L., Adams R., Strickland D., Robinson T. (2014) Dw2, a new dwarfing locus in apple rootstocks and its relationship to induction of early bearing in apple scions. *Journal of the American Society for Horticultural Science*, **139**, 87–98.

Fichot R., Chamaillard S., Depardieu C., Le Thiec D., Cochard H., Barigah T.S., Brignolas F. (2011) Hydraulic efficiency and coordination with xylem resistance to cavitation, leaf function, and growth performance among eight unrelated *Populus deltoides* × *Populus nigra* hybrids. *Journal of Experimental Botany*, **62**, 2093–2106.

Fichot R., Laurans F., Monclus R., Moreau A., Pilate G., Brignolas F. (2009) Xylem anatomy correlates with gas exchange, water-use efficiency and growth performance under contrasting water regimes: evidence from *Populus deltoides* × *Populus nigra* hybrids. *Tree Physiology*, **29**, 1537–1549.

Foster T.M., McAtee P.A., Waite C.N., Boldingh H.L., McGhie T.K. (2017) Apple dwarfing rootstocks exhibit an imbalance in carbohydrate allocation and

reduced cell growth and metabolism. *Horticulture Research*, **4**, 17009.

Gleason S.M., Butler D.W., Ziemińska K., Waryszak P., Westoby M. (2012) Stem xylem conductivity is key to plant water balance across Australian angiosperm species. *Functional Ecology*, **26**, 343–352.

Goldschmidt E.E. (2005) Regolazione dell'alternanza di produzione negli alberi da fruto (Italia). *Italus Hortus*, **12**, 11–17.

Goldschmidt E.E. (2013) The evolution of fruit tree productivity: a review. *Economic Botany*, **67**, 51–62.

Goncalves B., Correia C.M., Silva A.P., Bacelar E.A., Santos A., Ferreira H., Moutinho-Pereira J.M. (2007) Variation in xylem structure and function in roots and stems of scion–rootstock combinations of sweet cherry tree (*Prunus avium* L.). *Trees*, **21**, 121–130.

Goncalves B., Moutinho-Pereira J., Santos A., Silva A.P., Bacelar E., Correia C., Rosa E. (2005) Scion–-rootstock interaction affects the physiology and fruit quality of sweet cherry. *Tree Physiology*, **26**, 93–104.

Guerriero G., Hausman J.-F., Cai G. (2014) No stress! Relax! Mechanisms governing growth and shape in plant cells. *International Journal of Molecular Sciences*, **15**, 5094–5114.

Hajagos A., Végvári G. (2013) Investigation of tissue structure and xylem anatomy of eight rootstocks of sweet cherry (*Prunus avium* L.). *Trees*, **27**, 53–60.

Hajek P., Leuschner C., Hertel D., Delzon S., Schuldt B. (2014) Trade-offs between xylem hydraulic properties, wood anatomy and yield in *Populus*. *Tree Physiology*, **34**, 744–756.

Hoblyn T., Grubb N., Painter A., Wates B. (1936) Studies in biennial bearing - I. *Journal of Pomology and Horticultural Science*, **14**, 39–76.

Jackson J.E. (2003) *Biology of horticultural crops: Biology of apples and pears*. Cambridge University Press, Edinburgh, UK, pp 500.

Jones O.P. (1976) Effect of dwarfing interstocks on the xylem sap composition in apple trees. Effect on nitrogen, potassium, phosphorus, calcium and magnesium content. *Annals of Botany*, **40**, 1231–1235.

Jupa R., Plavcová L., Gloser V., Jansen S. (2016) Linking xylem water storage with anatomical parameters in five temperate tree species. *Tree Physiology*, **36**, 756–769.

Kiorapostolou N., Da Sois L., Petruzzellis F., Savi T., Trifilò P., Nardini A., Petit G. (2019) Vulnerability to xylem embolism correlates to wood parenchyma fraction in angiosperms but not in gymnosperms. *Tree Physiology*, **39**, 1675–1684.

Laur J., Hacke U.G. (2013) Transpirational demand affects aquaporin expression in poplar roots. *Journal of Experimental Botany*, **64**, 2283–2293.

Lauri P.E., Combe F., Brun L. (2014) Regular bearing in the apple – Architectural basis for an early diagnosis on the young tree. *Scientia Horiculturae*, **174**, 10–16.

Lauri P.E., Térouanne E., Lespinasse J.M., Regnard J.L., Kelner J.J. (1995) Genotypic differences in the axillary bud growth and fruiting pattern of apple fruit branches over several years – an approach to regulation of fruit bearing. *Scientia Horiculturae*, **64**, 265–281.

Lechthaler S., Turnbull T.L., Gelmini Y., Pirotti F., Anfodillo T., Adams M.A., Petit G. (2019) A standardization method to disentangle environmental information from axial trends of xylem anatomical traits. *Tree Physiology*, **39**, 495–502.

Ma L., Hou C.W., Zhang X.Z., Li H.L., Han D.G., Wang Y., Han Z.H. (2013) Seasonal growth and spatial distribution of apple tree roots on different rootstocks or interstems. *Journal of the American Society for Horticultural Science*, **138**, 79–87.

Martínez-Alcántara B., Iglesias D.J., Reig C., Mesejo C., Agustí M., Primo-Millo E. (2015) Carbon utilization by fruit limits shoot growth in alternate-bearing citrus trees. *Journal of Plant Physiology*, **15**, 108–117.

Martínez-Alcántara B., Rodriguez-Gamir J., Martínez-Cuenca M.R., Iglesias D.J., Primo-Millo E., Forner-Giner M.A. (2013) Relationship between hydraulic conductance and citrus dwarfing by the Flying Dragon rootstock (*Poncirus trifoliata* L. Raft var. monstruosa). *Trees*, **27**, 629–638.

Mészáros M., Kosina J., Laňar L., Náměstek J. (2015) Long-term evaluation of growth and yield of Stanley and Cacanska lepotica plum cultivars on selected rootstocks. *Horticultural Science*, **42**, 22–28.

Mészáros M., Laňar L., Kosina J., Náměstek J. (2019) Aspects influencing the rootstock – scion performance during long term evaluation in pear orchard. *Horticultural Science*, **46**, 1–8.

Monselise S.P., Goldschmidt E.E. (1982) Alternate bearing in fruit trees: a review. *Horticultural Reviews*, **4**, 128–173.

Morris H., Gillingham M.A., Plavcová L., Gleason S.M., Olson M.E., Coomes D.A., Fichtler E., Klepsch M.M., Martínez-Cabrera H.I., McGlinn D.J., Wheeler E.A., Zheng J., Zieminska K., Jansen S. (2018) Vessel diameter is related to amount and spatial arrangement of axial parenchyma in woody angiosperms. *Plant, Cell & Environment*, **41**, 245–260.

Muleo R., Intrieri M.C., Iacona C., Maggi E., Loreti F. (2011) Peach rootstocks inducing different vigour reflect genomic, physiological and morphological diversity in roots. *Acta Horticulturae*, **903**, 113–120.

Nardini A., Gasco A., Raimondo F., Gortan E., Lo Gullo M.A., Caruso T., Salleo S. (2006) Is rootstock-induced dwarfing in olive an effect of reduced plant hydraulic efficiency? *Tree Physiology*, **26**, 1137–1144.

Olien W.C., Lakso A.N. (1986) Effect of rootstock on apple (*Malus domestica*) tree water relations. *Physiologia Plantarum*, **67**, 421–430.

Olmstead M.A., Lang N.S., Ewers F., Owens S. (2006) Xylem vessel anatomy of sweet cherries (*Prunus avium* L.) grafted onto dwarfing and non-dwarfing rootstocks. *Journal of the American Society for Horticultural Science*, **131**, 577–585.

Olson M.E., Anfodillo T., Rosell J.A., Petit G., Crivellaro A., Isnard S., León-Gómez C., Alvarado-Cárdenas L.O., Castorena M. (2014) Universal hydraulics of the flowering plants: vessel diameter scales with stem length across angiosperm lineages, habits and climates. *Ecology Letters*, **19**, 240–248.

Pfautsch S., Harbusch M., Wesolowski A., Smith R., Macfarlane C., Tjoelker M.G., Reich P.B., Adams M.A. (2016) Climate determines vascular traits in the ecologically diverse genus *Eucalyptus*. *Ecology Letters*, **19**, 240–248.

Pfautsch S., Renard J., Tjoelker M., Salih A. (2015) Phloem as capacitor – radial transfer of water into xylem of tree stems seems to occur via symplastic transport in ray parenchyma. *Plant Physiology*, **167**, 963–971.

Plavcová L., Morris H., Hoch G., Ghiasi S., Jansen S. (2016) The amount of parenchyma and living fibres affects storage of non-structural carbohydrates in young stems and roots of temperate trees. *American Journal of Botany*, **103**, 603–612.

Pratt R.B., Jacobsen A.L. (2017) Conflicting demands on angiosperm xylem: Tradeoffs among storage, transport and biomechanics. *Plant, Cell & Environment*, **40**, 897–913.

R Development Core Team (2010) *R: a language and environment for statistical computing*. Vienna, Austria: R Foundation for Statistical Computing. http://www.R-project.org/

Reighard G.L., Loreti F. (2008) Rootstock development. In: Layne D. R., Bassi D. (Eds), *The peach: Botany, production and uses*. CABI, Wallingford, UK, pp 193–220.

Rodriguez-Dominguez C.M., Buckley T.N., Egea G., de Cires A., Hernandez-Santana V., Martorell S., Diaz-Espejo A. (2016) Most stomatal closure in woody species under moderate drought can be explained by stomatal responses to leaf turgor. *Plant, Cell & Environment*, **39**, 2014–2026.

Rosell J.A. (2019) Bark in woody plants: understanding the diversity of a multifunctional structure. *Integrative and Comparative Biology*, **59**, 535–547.

Sacks M.M., Silk W.K., Burman P. (1997) Effect of water stress on cortical cell division rates within the apical meristem of primary roots of maize. *Plant Physiology*, **114**, 519–527.

Sauter J.J., van Cleve B. (1992) Seasonal variation of amino acids in the xylem sap of "*Populus* × *canadensis*" and its relation to protein body mobilization. *Trees*, **7**, 26–32.

Słupianek A., Kasprowicz-Maluśki A., Myśkow E., Turzańska M., Sokołowska K. (2019) Endocytosis acts as transport pathway in wood. *New Phytologist*, **222**, 1846–1861.

Sokolowska K., Zagórska-Marek B. (2012) Symplasmic, long-distance transport in xylem and cambial regions in branches of *Acer pseudoplatanus* (Aceraceae) and *Populus tremula* × *P. tremuloides* (Salicaceae). *American Journal of Botany*, **99**, 1745–1755.

Solari L.I., Johnson S., DeJong T.M. (2006a) Relationship of water status to vegetative growth and leaf gas exchange of peach (*Prunus persica*) trees on different rootstocks. *Tree Physiology*, **26**, 1333–1341.

Solari L.I., Pernice F., DeJong T.M. (2006b) The relationship of hydraulic conductance to root system characteristics of peach (*Prunus persica*) rootstocks. *Physiologia Plantarum*, **128**, 324–333.

Somelidou K., Morris D.A., Battey N.H., Barnett J.R., John P. (1994) Auxin transport capacity in relation to the dwarfing effect of apple rootstocks. *Journal of Horticultural Science*, **69**, 719–725.

Sperry J.S. (2000) Hydraulic constraints on plant gas exchange. *Agricultural and Forest Meteorology*, **104**, 13–23.

Tombesi S., Almehdi A., DeJong T.M. (2011) Phenotyping vigour control capacity of new peach rootstocks by xylem vessel analysis. *Scientia Horiculturae*, **127**, 353–357.

Tombesi S., Johnson R.S., Day K.R., DeJong T.M. (2010a) Relationships between xylem vessel characteristics, calculated axial hydraulic conductance and size controlling capacity of peach rootstocks. *Annals of Botany*, **105**, 327–331.

Tombesi S., Johnson R.S., Day K.R., DeJong T.M. (2010b) Interactions between rootstock, inter-stem and scion xylem vessel characteristics of peach trees growing on rootstocks with contrasting size-controlling characteristics. *AoB Plants*, **10**, plq013.

Trifilo P., Lo Gullo M.A., Nardini A., Pernice F., Salleo S. (2007) Rootstock effects on xylem conduit dimensions and vulnerability to cavitation of *Olea europaea* L. *Trees*, **21**, 549–556.

Tyree M.T., Sperry J.S. (1988) Do woody plants operate near the point of catastrophic xylem dysfunction caused by dynamic water stress? *Plant Physiology*, **88**, 574–580.

Tyree M.T., Velez V., Dalling J.W. (1998) Growth dynamics of root and shoot hydraulic conductance in seedlings of five neotropical tree species: scaling to show possible adaptation to differing light regimes. *Oecologia*, **114**, 293–298.

Tyree M.T., Zimmermann M.H. (2002) *Xylem structure and ascent of sap*. Springer, Berlin, Germany, pp. 331.

Webster A.D. (2004) Vigour mechanisms in dwarfing rootstocks for temperate fruit trees. *Acta Horticulturae*, **658**, 29–41.

Weibel A., Johnson R.S., DeJong T.M. (2003) Comparative vegetative growth responses of two peach cultivars grown on size-controlling versus standard rootstocks. *Journal of the American Society for Horticultural Science*, **128**, 463–471.

Ziemińska K., Wright I.J., Westoby M. (2015) Broad anatomical variation within a narrow wood density range – a study of twig wood across 69 Australian angiosperms. *PLoS One*, **10**, e0124892.

Tree Physiology 00, 1–15
https://doi.org/10.1093/treephys/tpab111

Research paper

Trunk radial growth, water and carbon relations of mature apple trees on two size-controlling rootstocks during severe summer drought

Radek Jupa[1], Martin Mészáros[2], Günter Hoch[3] and Lenka Plavcová[1,4]

[1]Department of Biology, Faculty of Science, University of Hradec Králové, Rokitanského 62, Hradec Králové CZ-500 03, Czech Republic; [2]Department of Technology, Research and Breeding Institute of Pomology, Research and Breeding Institute of Pomology, Holovousy 129, Hořice CZ-508 01, Czech Republic; [3]Department of Environmental Sciences – Botany, University of Basel, Schönbeinstrasse 6, 4056 Basel, Switzerland; [4]Corresponding author (lenka.plavcova@uhk.cz)

Received June 4, 2021; accepted August 9, 2021; handling Editor Roberto Tognetti

The use of size-controlling rootstocks is central to modern high-density fruit production systems. While biological mechanisms responsible for vigor control are not fully understood, differences in water relations and carbohydrate storage ability have been suggested as two potential factors. To better understand the processes that control growth vigor, we analyzed the trunk radial variation at seasonal and diurnal timescales and measured the midday leaf water potential (Ψ_{MD}), leaf gas exchange and concentrations of non-structural carbohydrates (NSC) in apple trees of variety 'Jonagold' grafted on two rootstocks of contrasting growth vigor (dwarfing J-TE-G vs invigorating J-TE-H). The measurements were conducted during an exceptionally hot and dry summer. We found that smaller annual trunk radial increments in dwarfed trees were primarily due to an earlier cessation of trunk secondary growth. The interdiurnal trunk circumference changes (ΔC) were slightly lower in dwarfed trees, and these trees also had fewer days with positive ΔC values, particularly during the driest summer months. The trunks of dwarfed trees shrank gradually during the drought, showed less pronounced diurnal variation of trunk circumference and the maximum trunk daily shrinkage was only weakly responsive to the vapor pressure deficit. These results indicated that lower turgidity in the cambial region may have limited the trunk radial expansion in dwarfed trees during the hot and dry days. Dwarfed trees also maintained lower Ψ_{MD} and leaf gas exchange rates during the summer drought. These parameters decreased in parallel for both rootstock combinations, suggesting their similar drought sensitivity. Similar concentrations and seasonal dynamics of NSC in both rootstock combinations, together with their similar spring growth rates, suggest that NSC reserves were not directly limiting for growth. Our results support the prominent role of water relations in rootstock-induced size-controlling mechanisms and highlight the complexity of this topic.

Keywords: dendrometer, dwarfing rootstocks, gas exchange, *Malus domestica* Borkh., non-structural carbohydrates, turgor, vegetative growth, water potential.

Introduction

In commercial orchards, most fruit trees are traditionally propagated by means of grafting, whereby the desired scion variety is combined with a genetically different lower part (rootstock) to form a composite tree. Growers preferentially select dwarfing or semi-dwarfing rootstocks that suppress canopy growth to reduce the labor costs associated with pruning and harvest (DeJong et al. 2004) and maximize the orchards' incomes through increased planting density and the precocity of cropping (Webster and Hollands 1999). Despite the long tradition and great economic importance of size-controlling rootstocks, the biological mechanisms responsible for the reduced growth are not fully understood. This gap in our knowledge prevents the development of optimal management practices for

size-controlling rootstocks and hinders the breeding and selection of new rootstock genotypes with improved properties (Atkinson and Else 2001).

Several physiological mechanisms have been proposed to explain the size-controlling potential of different rootstocks. Among them, the role of water relations in the dwarfing mechanisms has received wide experimental support, highlighting that scions grown on dwarfing rootstocks are more likely subjected to drought stress when compared with scions grafted on invigorating rootstocks (Basile and DeJong 2018). The drought stress experienced by the scion is typically evaluated by measuring its organ water potentials. Scions on dwarfing rootstocks often have lower stem or leaf water potentials than those on invigorating ones (Olien and Lakso 1986, Solari et al. 2006*a*, Gonçalves et al. 2007, Jupa et al. 2021), although the opposite trend has also been observed (Atkinson et al. 2000, Tworkoski et al. 2016). The reasons for the inferior water status of scions on dwarfing rootstocks are often sought in the reduced hydraulic conductance, either in the rootstock (Atkinson et al. 2003, Basile et al. 2003, Nardini et al. 2006, Solari et al. 2006*b*, Jupa et al. 2021) or at the graft union (Atkinson et al. 2000, Cohen et al. 2007).

Besides the hydraulic conductance, the scion water balance is also affected by stomatal conductance to water vapor. Stomatal conductance depends on the structural properties of stomata (e.g., stomata size and density) and their physiological regulation. In general, stomata close in response to decreasing water availability to prevent a further drop in the organ water potential that could otherwise lead to a hydraulic failure (Sperry 2000). Dwarfed trees have been reported to have a lower stomatal conductance than invigorated trees in sweet cherry (Gonçalves et al. 2006), peach (Solari et al. 2006*b*) and apple trees (Schechter et al. 1991, Atkinson et al. 2000). There is also scarce evidence for a more stringent (i.e., isohydric) stomatal behavior in dwarfed compared with invigorated trees, although the stomatal response to drought was investigated only in a few studies (Atkinson et al. 2000, Tworkoski et al. 2016). Thus, it is still not clear if dwarfed trees are more susceptible or more resistant to drought stress, which is an important shortcoming, considering their extensive use in commercial orchards and predictions of increasing drought conditions as a result of climate change.

Lower stomatal conductance prevents excessive water loss but at the cost of reduced CO_2 assimilation, which might be another factor potentially contributing to the reduced growth vigor. The relative balance between carbon supply and demand is generally reflected in the tissue concentrations of non-structural carbohydrates (NSC). The NSCs are thus often used as indicators for carbon limitation of tree growth (Hoch 2015, Weber et al. 2018), although a prolonged limitation in carbon uptake can also lead to an upregulation of tissue NSC concentrations on account of other carbon-sink activities in trees (Weber et al. 2019). Lower NSC concentrations (Yano et al. 2002, Weibel et al. 2008) and slower spring shoot expansion rates have been observed in dwarfed trees (Weibel et al. 2003, Clearwater et al. 2006), supporting the hypothesis that the growth of trees on size-controlling rootstocks is carbon-limited. Besides the growth resumption in spring, similar mechanisms could also reduce the growth of dwarfed trees in response to drought. The presumably lower NSC reserves in dwarfed trees could be more easily depleted during long-term drought exposure, resulting in a tree's inability to restore water transport and growth after the drought stress is relieved (McDowell 2011).

Given the plethora of interweaving processes, the exact roles of water- and carbon-related mechanisms in rootstock-induced size-controlling mechanisms remain poorly understood and warrant further investigations (Basile and DeJong 2018). To date, the physiological controls of rootstock-induced vegetative growth have been mainly studied by measuring the short-term dynamics of shoot extension together with the presumed environmental or physiological drivers (Berman and DeJong 1997*a*, 1997*b*, Solari et al. 2006*a*). Compared with the apical shoot growth, the effect of rootstock on the dynamics of radial trunk growth is much less understood, although differences in the trunk cross-sectional area (TCSA) are frequently used to assess the efficiency of size-control conferred by various rootstocks. Due to the cumulative nature of the trunk radial growth, most TCSA-based comparisons are conducted at annual or inter-annual scales (Russo et al. 2007, Mészáros et al. 2019), while the information on finer scale growth dynamics of trunks is scarce.

Seasonal measurements of TCSA increments were done in two peach cultivars on five size-controlling rootstocks (Weibel et al. 2003). In this study, the trees on dwarfing rootstocks grew slowly but continuously during the growing season, while the trees on invigorating rootstocks grew faster initially but slowed down profoundly during the hottest summer months. The authors hypothesized that the invigorated trees suffered from greater drought stress due to excessive water loss from their large canopies. This explanation, however, contrasted the findings in shoots, in which the greatest difference in growth among the rootstock combinations was observed during the early part of the season before the onset of a major drought. While the overall shoot and trunk growth are usually tightly correlated among rootstock variants (Basile and DeJong 2018, Jupa et al. 2021), different seasonal growth patterns can be expected due to the inherent developmental constraints (Lauri et al. 2010) and different environmental sensitivities of primary versus secondary growth (Gričar et al. 2017, Peters et al. 2021).

To expand our understanding of trunk growth dynamics and to shed more light on the involvement of water- and carbon-related processes in rootstock-induced mechanisms of

growth vigor control in composite fruit trees, we examined the trunk radial growth and water and carbon relations of 'Jonagold' apple trees grafted on two rootstocks with contrasting size-controlling potential during an exceptionally dry and hot growing season. To monitor the trunk radial growth, we used automatic high-precision dendrometers. These devices provide a great opportunity to continuously monitor growth- and water-related processes in trees (Zweifel et al. 2006) and have been explored for their potential to optimize irrigation scheduling in fruit tree orchards (Fernández and Cuevas 2010). Here, we combined the dendrometer data with the measurements of leaf water potential, leaf gas exchange and NSC concentrations in branches and roots. We hypothesized that dwarfed trees are subject to greater drought stress compared with invigorated trees, which translates into lower trunk radial growth increments. We also expected that drought-induced stomatal closure in dwarfed trees will result in reduced NSC reserves and lead to slower or delayed vegetative growth, which is consistent with the carbohydrate reserve theory (Basile and DeJong 2018).

Materials and methods

Plant material and site conditions

Twenty-eight-year-old composite apple trees (*Malus domestica* Borkh.) of 'Jonagold' variety grafted on two different size-controlling rootstocks were used for this study. The selected rootstocks have previously been shown to induce either low (J-TE-G rootstock) or high (J-TE-H rootstock) vegetative vigor (Kosina 2010, Jupa et al. 2021). The studied trees were grown in the experimental orchard of the Research and Breeding Institute of Pomology in Holovousy, Czech Republic (50.37 N, 15.57 E; 283 m above sea level). The orchard was established in 1990 on loamy brown soil with a neutral pH and medium fertility. The trees were planted in hedgerows in the spacing of 4.5 × 2.3 m and were cultivated to short (70 cm) stem heights with the topmost scaffold branches at the heights of 1.5 m for all trees. After planting, pest management and fertilization practices were conducted based on local recommendations for commercial orchards. Neither irrigation nor fruit thinning was applied. In March 2018, three healthy individuals of each rootstock type were selected for measurement of their trunk circumference with a measuring tape ~50 cm above the root collar. The TCSA was then calculated assuming a circular trunk cross-section. Further, in late September 2018, the fruit yield per tree was determined using a portable scale.

Micro-meteorological conditions in the orchard were monitored throughout the growing season with a set of standard meteorological sensors placed 2 m above the ground level. Air temperature and relative humidity were measured with an HMP 35D sensor (Vaisala, Vantaa, Finland), while the precipitation was measured with a WXT531 sensor (Vaisala). The data were transmitted in 15-min intervals and were used for calculating the vapor pressure deficit (VPD; kPa). Soil water potential (Ψ_{soil}; MPa) was measured in close vicinity of the study trees, with two Teros 21 water potential sensors (Meter Environment, Pullman, WA, USA) connected to a MicroLog SP3 data logger (EMS Brno, Brno, Czech Republic). The sensors were installed between two neighboring trees in the weed-free strip of soil at depths of 5 and 30 cm. The Ψ_{soil} values were recorded at 1-h intervals.

To evaluate the year 2018 in terms of its dryness relative to the long-term climate conditions, the monthly mean temperatures and monthly precipitation sums measured in 2018 were compared with the values measured during the previous 20 years (1998–2017). For this interannual comparison, official meteorological data obtained from the weather station run by the Czech Hydrometeorological Institute at Holovousy were used (data available at: https://bit.ly/3qF6jcQ). The weather station is located within 500 m of our experimental site.

Changes in trunk circumference

Automatic band dendrometers equipped with a data logger (DRL26C; EMS Brno, Brno, Czech Republic) were installed on the trunks of two selected trees of each rootstock combination. The dendrometers were placed at a height of ~40 cm above the root collar. The circumference readings were acquired in hourly intervals during the entire growing season. The raw values were thermally corrected and expressed as cumulative circumference increments starting from zero on 1 May. The temperature correction factor (in μm °C^{-1}) was calculated separately for each dendrometer from the circumference and temperature readings obtained during November 2018 when the trees were already leafless and the detected changes in trunk circumference were thus not affected by transpiration. The dendrometer data were then analyzed using two complementary approaches focusing on the trunk circumference variation at either seasonal or diurnal timescales.

To describe the overall seasonal pattern in the trunk radial growth, the cumulative circumference increments were fitted by the Gompertz model using the following formula:

$$y = y_0 + a \times \mathbf{exp}\left[-\mathbf{exp}\left(b - c \times t\right)\right], \quad (1)$$

where y is the cumulative circumference increment, y_0 is the lower asymptote, a is the upper asymptote, b is the x-axis displacement parameter, c is the rate of growth parameter and t is the time since the measurement began (Duchesne et al. 2012). Based on the Gompertz model, the total annual trunk circumference increment (G_A; mm) was calculated as $G_A = a - y_0$. We used the fitted circumference data to estimate the daily trunk circumference growth rate (GR; μm day^{-1}) as GR = $y_t - y_{t-1}$. The circumference GR of 7 μm day^{-1} was then considered as a threshold value to determine the date of growth initiation (D_{INI}) and cessation (D_{END}). For each tree, the duration of the growing season (G_{DUR}; days) was calculated as the number of

days between D_{INI} and D_{END}. Similarly, the mean daily GR of each tree (GR_{MEAN}; μm day^{-1}) was calculated from GR values within the D_{INI}–D_{END} period. Finally, we determined the maximal seasonal GR (GR_{MAX}; μm day^{-1}) and the corresponding date of maximal growth (D_{MAX}) of each tree.

To understand the trunk radial growth and the patterns of stem shrinkage and swelling at a finer scale, the diurnal changes in the trunk circumference were analyzed. The changes in trunk circumference were transformed to start at zero at the beginning of each day (i.e., at 00:00 h). The transformation involved the subtraction of the first circumference reading from all subsequent readings within each day. The resulting values are referred to as daily trunk circumference variation (TCV_D; μm). For most days, the changes in the trunk circumference showed a characteristic sinusoidal pattern of trunk shrinking and swelling with a regular diurnal periodicity (Drew and Downes 2009). Occasionally, long cycles of intensive trunk swelling that lasted for 2–3 days occurred (Deslauriers et al. 2007). These irregular readings coincided with rain events and were excluded from the analyses, as were data recorded on the days following a major rain event (i.e., days with a precipitation sum >5 mm). From the regular diurnal readings, we then extracted two parameters. First, we calculated the interdiurnal trunk circumference change (ΔC; μm) as the difference between the daily maxima of two consecutive days (Deslauriers et al. 2007, Dolezal et al. 2019). The values of ΔC were either positive or negative. The positive ΔC values were interpreted as irreversible trunk growth, while the negative ΔC suggested no or minimal trunk growth and gradual depletion of stored water reserves (Deslauriers et al. 2007, Zweifel et al. 2016). The second parameter derived from the diurnal data was the maximum trunk daily shrinkage (MDS; μm), which was calculated as the difference between the daily maximal and minimal trunk circumference values. The MDS values reflect mainly the reversible changes in stem water storage rather than the trunk growth (Fernández and Cuevas 2010). The MDS and ΔC obtained from our dendrometer readings were compared across the rootstock variants and months and were analyzed in relation to the VPD. In the exploratory analyses, we also looked at the relationships with other potential environmental drivers (such as air temperature and Ψ_{soil}). However, these relationships were either non-significant or collinear with the VPD.

Leaf water potential and leaf gas exchange measurements

To characterize the tree water status and photosynthetic performance, the midday leaf water potential (Ψ_{MD}) and leaf gas exchange parameters were measured repeatedly during the summer drought period. The Ψ_{MD} was measured on two fully developed, unshaded leaves from each tree (n = 6) between 11:00 and 13:00 h using a portable Scholander pressure chamber (1505D-EXP, PMS Instrument Company, Albany, OR, USA). The Ψ_{MD} data were already included in another paper by the authors (Jupa et al. 2021). With the Ψ_{MD} measurements, the midday stomatal conductance (g_s; mmol H_2O m^{-2} s^{-1}) and net assimilation rates (A; μmol CO_2 m^{-2} s^{-1}) were simultaneously assessed on a neighboring leaf using the LI-6800P portable photosynthesis system (Li-COR Inc., Lincoln, NE, USA). One leaf from each tree (n = 3) was measured at each measuring date. The leaf was inserted into the chamber and was allowed to equilibrate for at least 10 min to the pre-set chamber conditions (irradiance: 1800 μmol m^{-2} s^{-1}; air temperature: ambient; chamber relative humidity: ambient; reference CO_2 concentration: 400 p.p.m.; flow rate: 300 μmol s^{-1}; fan speed: 10,000 rpm). The reference and sample infrared gas analyzer readings were matched before each measurement.

Non-structural carbohydrates analysis

To provide insights into the tree carbon balance and carbohydrate storage, the concentrations of NSC were measured in 1-year-old lateral branches and coarse woody roots of trees on both rootstocks. The sampling took place on four dates in the year 2018: in spring, during bud break (18 April); in early summer, during the period of the most active vegetative growth (5 June); in mid-summer, during the peak of the drought period (31 July); and in late autumn, after leaf fall (16 November). At each sampling date, two samples of both branches and roots were collected from the opposite sides of each tree (n = 6; eastern and western tree sides). 1-year-old proleptic shoots (10–15 mm in diameter, 15–25 cm in length) were excised from a sunlit part of the crown at a 1.5 m height, and the leaves or buds were removed. The root segments (5–10 mm in diameter, 10–20 cm in length) were collected at a soil depth of 15–50 cm and at a distance of 50 cm from the root collar. The samples were transported to the laboratory within 30 min after collection, microwaved at 600 W for 30 s to deactivate the NSC-modifying enzymes (Popp et al. 1996) and oven-dried at 80 °C for 3 days. The dried samples, composed of sapwood and bark tissues, were homogenized using a centrifugal grinding mill (ZM 100; Retsch; Haan, Germany) and were sent to the Plant Ecophysiology Laboratory at the University of Basel, Switzerland, for NSC analyses.

The NSC data were expressed as the sum of the three quantitatively most important sugars (glucose, fructose and sucrose) plus starch. The NSCs were analyzed using the enzymatic-photometric method described in Landhäusser et al. (2018). Briefly, low molecular weight sugars were extracted from the plant powder with 80% ethanol at 90 °C for 10 min, the supernatant was collected, the pellet was washed three more times with ethanol and the supernatants were mixed. After evaporation of the ethanol and resuspension of the extracts in deionized water, the total amount of glucose was determined photometrically after the enzymatic conversion of fructose and sucrose to glucose in a multiplate photometer (HR 700, Hamilton, Reno, NE, USA) at 340 nm by converting glucose-6-P

Table 1. Growth and yield characteristics of the studied apple trees grafted on dwarfing (J-TE-G) and invigorating (J-TE-H) rootstocks.

Rootstock:	Dwarfing (J-TE-G)			Invigorating (J-TE-H)		
Tree id:	1	2	3	1	2	3
Dendrometer	Yes	Yes	No	Yes	Yes	No
TCSA (cm^2)	103.1	103.1	121.0	305.9	315.8	309.9
Yield (kg)	68.2	71.8	68.0	131.9	110.2	97.4
Yield efficiency (kg cm^{-2})	0.66	0.70	0.56	0.46	0.35	0.32
D_{INI}	3 May	2 May	—	9 May	3 May	—
D_{MAX}	21 May	17 May	—	4 June	6 June	—
D_{END}	25 June	19 June	—	25 July	15 August	—
G_A	1.52	1.39	—	2.47	4.06	—
G_{DUR}	54	49	—	78	105	—
GR_{MAX}	43.8	47.0	—	46.6	64.9	—
GR_{MEAN}	26.0	28.2	—	27.5	35.2	—

The Note: TCSA was calculated from trunk circumference measured at 50 cm above the root collar. Fruit yield per tree (yield) was quantified at the end of September 2018. Yield efficiency was determined as the yield divided by TCSA. The following growth parameters were derived based on the cumulative circumference increments modeled with the Gompertz function (Figure 2C and D). D_{INI}—date of growth initiation, D_{MAX}—date of the maximum growth rate, D_{END}—date of growth cessation, G_A—annual trunk circumference increment (mm), G_{DUR}—growth duration (number of days), GR_{MAX}—maximum growth rate (μm day^{-1}), GR_{MEAN}—mean growth rate (μm day^{-1}). Estimated daily growth rate of 7 μm day^{-1} was considered as the threshold for growth initiation and cessation.

to gluconate-6-P. To break down the starch in the remaining pellet, the pellet was resuspended in deionized water and first treated with α-amylase (from *Bacillus licheniformis*) for 2 h at 85 °C. After centrifugation of the samples, an aliquot of the supernatant was treated with amyloglucosidase (from *Aspergillus niger*) at 55 °C for 2 h for complete conversion of the starch to glucose. The total amount of glucose (corresponding to the initial amount of starch) was determined photometrically as given above. To control the reproducibility of the extraction, standard plant powder (Orchard leaves, Leco, St Joseph, MI, USA) and pure starch, glucose, fructose and sucrose solutions were included in the analysis. Glucose standard (1 mg ml^{-1}) was used to calculate the glucose concentrations of the extracts. All chemicals and enzymes were purchased from Sigma Aldrich, St Louis, MO, USA. The concentration of starch and low molecular sugars are expressed as % dry mass.

Statistical analyses

General linear models (LMs) and corresponding analyses of variance (ANOVAs) or covariance (ANCOVAs) were used to evaluate the effects of the rootstock, month or VPD on MDS and ΔC values. The model residuals were graphically checked to assure assumptions of homoscedasticity and normality. To satisfy the model assumptions and to remove patterns in the residuals, the MDS response variable was log-transformed. In the case of the ΔC response variable, outliers beyond 0.1 and 0.9 quantiles were removed. Significant ANOVA and ANCOVA results were followed up by Tukey-adjusted multiple mean comparisons using *emmeans* R package (Lenth 2020). To analyze the fraction of days with positive or negative ΔC as a function of the rootstock, month or VPD and their respective interactions, the response variables were coded as binary (i.e., 1 for positive ΔC, or 0 for negative ΔC), and the relationship was modeled using the logistic regression. Two-way ANOVAs were used to evaluate the effects of the rootstock, date and their interaction on the values of physiological parameters (Ψ_{MD}, g_s, A and NSC concentrations). For all relationships modeled with LMs, we also constructed analogous linear mixed-effect models with individual tree ID included as a random factor. These analyses were implemented using the *lme4* package (Bates et al. 2015). However, since the amount of residual variability attributed to the random factor was generally low, and the results were not largely different from the LM models, we decided to use the simpler linear regression approach. All statistical analyses were performed in R (R Development Core Team 2010). Results were considered statistically significant at $P < 0.05$. Data are presented as mean ± 1 SE (number of replicates). Predicted relationships are shown surrounded by 95% confidence intervals. Graphs were produced using the R packages *ggplot2* (Wickham 2016) and *cowplot* (Wilke 2019).

Results

Tree size and yield characteristics

Dwarfed trees on J-TE-G rootstock had about one-third the TCSA of the invigorated trees on J-TE-H rootstock (109 vs 311 cm^2, Table 1). Annual fruit yield in dwarfed versus invigorated trees was 69 vs 113 kg $tree^{-1}$, respectively. Correspondingly, yield efficiencies were almost two times higher in dwarfed compared with invigorated trees (0.64 vs 0.36 kg cm^{-2}, Table 1).

Climatic conditions

The year 2018 was substantially hotter and drier than the previous 20 years (Figure 1). The mean annual temperature in 2018 was 1.6 °C higher than the long-term mean, and the total

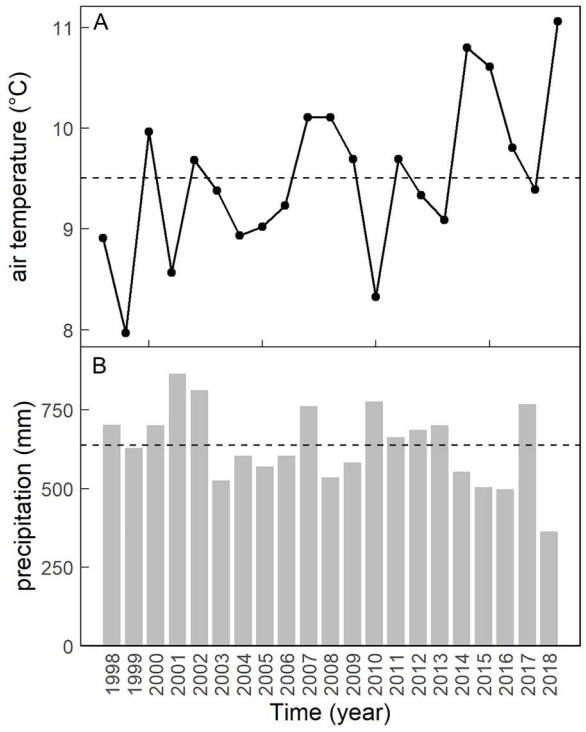

Figure 1. (A) Mean annual air temperature and (B) annual precipitation totals from 1998–2018. The dashed lines indicate the long-term averages for the depicted period. The year 2018 stands out as the hottest and driest on record.

sum of precipitation reached only 57% of the long-term mean. These differences were even more extreme when focusing on the active growing season, with the spring temperatures in April and May being >3 °C higher than the long-term mean and the precipitation in July and August being only 25% of the long-term mean sum (the daily data can be accessed at https://bit.ly/3qF6jcQ).

The seasonal time courses of VPD and Ψ_{soil} measured in the orchard indicated that the severe drought conditions culminated in July and August (Figure 2). At the peak of the drought period, the mean daily VPD values reached up to 2.5 kPa (Figure 2A) corresponding to the maximal daily VPD of around 5 kPa. The Ψ_{soil} at 5-cm soil depth declined from 0 MPa in spring to −4 MPa by the end of August and recovered only partially with the onset of cooler and wetter weather in September (Figure 2B). We acknowledge that the extremely low values of Ψ_{soil} might be artifacts resulting from the disconnection of the sensor from the soil matrix. Nevertheless, the Ψ_{soil} data provide valuable insights into the overall seasonal pattern of soil water availability.

Seasonal trunk growth pattern

Clear differences were observed in the duration and dynamics of the seasonal trunk growth of the examined rootstock combinations (Table 1, Figure 2C and D). The initiation of trunk secondary growth (D_{INI}) occurred in the first half of May in all four examined trees (Table 1, Figure 2C and D). However, dwarfed trees reached their maximum GRs ∼2 weeks earlier compared with the invigorated trees (D_{MAX} at 17 and 21 May for low vigor vs 4 and 6 June for high vigor trees, Table 1). Similarly, dwarfed trees ceased their radial growth >1 month sooner (i.e., in the second half of June) when compared with the invigorated trees (Table 1, Figure 2C and D). The substantially shorter duration of the growth period (G_{DUR}) together with slightly lower mean and maximal GRs (GR_{MEAN}, GR_{MAX}) resulted in 0.8–2.7 mm lower annual trunk circumference increments (G_A) in dwarfed when compared with invigorated trees (Table 1, Figure 2C).

The drought period between the middle of July and end of August was associated with a stagnation of the trunk radial growth in both rootstock variants (Figure 2C). During this period, the trunks of invigorated trees showed no appreciable increase in circumference, while the dwarfed trees even showed a gradual decline in their trunk circumference (Figure 2C).

Diurnal variation in trunk circumference and differences in ΔC and MDS values

Marked differences between rootstock combinations were also observed in the diurnal variation of the trunk circumference and the derived ΔC and MDS values. In invigorated trees, the trunk circumference variation showed a characteristic diurnal pattern of sinusoidal shape on most of the days, particularly on days with high VPD (Figure 3). The increase in trunk circumference (i.e., trunk swelling) occurred mainly during the night hours (from 20:00 to 06:00 h) and continued during the early morning hours when the VPD was low. The maximal daily circumference values were typically attained between 08:00 and 10:00 h. Then, the trunk circumference started to decrease (i.e., trunk shrinking), reaching its minimum typically around 18:00–19:00 h. In dwarfed trees, the diurnal pattern was less pronounced and the overall amplitude of the diurnal changes, corresponding to MDS, was much lower (Figure 3A) when compared with invigorated trees. The comparison of rootstocks across months revealed significantly lower MDS in dwarfed when compared with invigorated trees (mean ratio 0.48 ± 0.024, t-ratio = −14.817, df = 438, $P < 0.001$), with the differences being greatest in July and August (Figure 4A). The significant differences across months ($P < 0.001$) were paralleled by a strong positive association between MDS and VPD ($\beta = 0.30$, $P < 0.001$). While MDS increased with an increasing VPD in both rootstock combinations, the effect was stronger in invigorated trees (Figure 4B).

The ΔC ranged typically between −68 and + 54 µm (0.10 and 0.90 quantiles). There was a significant effect of rootstock ($P < 0.001$) and month ($P < 0.001$), while the interaction between those two factors was non-significant ($P = 0.103$). The

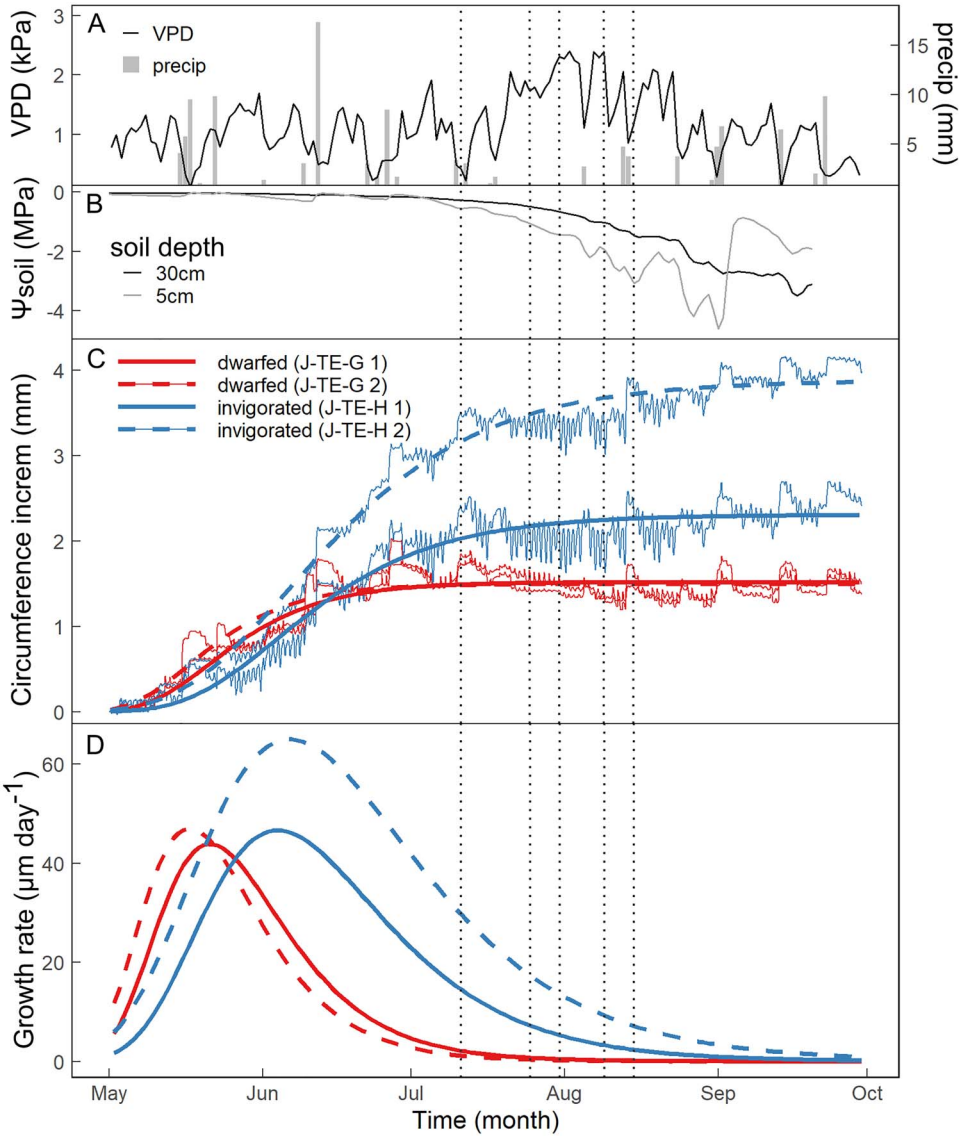

Figure 2. (A, B) Micrometeorological conditions at the orchard site and (C, D) seasonal patterns of the trunk radial growth in four individual apple trees, two dwarfed (J-TE-G) and the other two invigorated (J-TE-H). (A) Time course of the mean daily VPD, precipitation (precip) and (B) soil water potential (Ψ_{soil}) at 5- and 30-cm soil depths are shown. (C) Cumulative trunk circumference increments measured by band dendrometers (thin wiggly lines) are plotted together with seasonal growth trends modeled with the Gompertz function (thick smooth lines). (D) Changes in the estimated growth rates derived from the Gompertz fits are shown. The vertical dotted lines indicate dates when the leaf water potential and leaf gas exchange measurements (Figures 6) were conducted. The period between the first and last dotted lines corresponds roughly to the peak of the seasonal drought.

ΔC values were lower in dwarfed than invigorated trees (mean difference $-$ 12.1 $\pm$ 3.11 µm, t-ratio = -3.875, df = 342, $P < 0.001$). The ΔC values were highest in June and lowest in August. There was a tendency for decreasing ΔC with increasing VPD; however, this relationship was rather weak ($\beta = -7.09$, $P = 0.123$; Figure 4D). The values of ΔC were frequently negative in both rootstock combinations. The results of the logistic regression showed that the probability of observing a positive ΔC value was significantly lower in dwarfed than in invigorated trees (odds ratio: 0.595 $\pm$ 0.13, z-ratio = -2.34, $P = 0.012$; Figure 5A). The probability of positive ΔC was generally lower in July, August and September compared with the first 2 months of the growing season (Figure 5A). The probability of observing a positive ΔC value decreased with an increasing VPD ($\beta = -0.76$, $P = 0.017$; Figure 5B).

Leaf water potential and leaf gas exchange

During the whole drought period, dwarfed trees had significantly lower Ψ_{MD}, g_s and A than invigorated trees (Figure 6). The interaction between the rootstock and date was not significant for any of the parameters, indicating that the physiological response to drought was similar in both rootstock variants. Across the measuring dates, the values of Ψ_{MD} and g_s were linearly correlated ($R = 0.732$, $P = 0.016$) and g_s decreased as

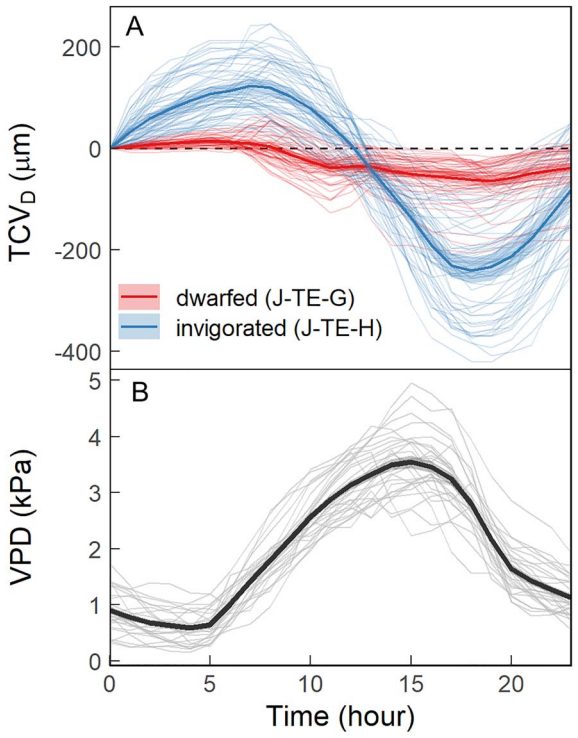

Figure 3. (A) Daily trunk circumference variation (TCV_D) in dwarfed (J-TE-G) and invigorated (J-TE-H) rootstock combinations and (B) diurnal time course of the VPD. The thin lines represent the daily trunk circumference variation for 28 individual July and August days with no rain and high evaporative demands (i.e., mean daily VPD >1.5 kPa). The thick lines show the mean surrounded by the 95% confidence interval.

Ψ_{MD} became more negative. Both variables were also correlated with VPD with the correlation being stronger for Ψ_{MD} (VPD vs Ψ_{MD}: $R = -0.907$, $P < 0.001$; VPD vs g_s: $R = -0.632$, $P = 0.050$).

Non-structural carbohydrates

The trees showed broadly similar seasonal patterns of NSC concentrations in their branches and roots, with several notable differences between the two rootstock combinations (Figure 7). The highest total NSC and starch concentrations were found during late autumn (16 November, Figure 7A and D), whereas the lowest values were observed at bud break (18 April, Figure 7A–C) or during the phase of the most intense vegetative growth in branches of invigorated trees (5 June, Figure 7A and C). The NSCs were never completely depleted as total NSC concentrations were always higher than 8% (dry weight). However, starch concentrations close to zero were observed in branches of invigorated trees on 5 June and in roots of dwarfed trees on 18 April, indicating a strong withdrawal of NSC reserves during this time. Significantly lower starch concentrations were observed in roots of dwarfed when compared with invigorated trees (Figure 7D). The lower starch concentrations of roots of dwarfed trees were, however, compensated by higher concentrations of soluble sugars (Figure 7F), resulting in similar total NSC concentrations in the roots of both rootstock combinations (Figure 7B). Both total NSC and starch concentrations decreased during the initial phase of the growing season (between 18 April and 5 June) in branches of invigorated trees, while they slowly increased in dwarfed trees. Consequently, the branches of invigorated trees had significantly lower total NSC and starch concentrations in June and July when compared with dwarfed trees.

Discussion

The analysis of the trunk circumference growth conducted at the seasonal timescale revealed marked differences in the duration and dynamics of the trunk radial growth between the two rootstock combinations. We conclude that the smaller annual trunk increments of dwarfed trees were mainly due to their shorter growing season rather than lower absolute GRs (Table 1, Figure 2). The shorter growing season was mainly driven by an earlier growth cessation, while the onset of trunk radial growth occurred around the same time in both rootstock combinations. Our initial hypothesis that the differences in trunk radial growth between dwarfed and invigorated trees are shaped by greater drought stress in low vigor trees seems plausible in the light of our results, although an unequivocal conclusion as to whether the drought stress was the decisive driver of the differences in growth vigor cannot be drawn based on our current data. In both rootstock combinations, we found very limited trunk radial growths in July and August, which were the driest months (Figure 2). While tree growth in the northern temperate climate typically peaks around the summer solstice and declines afterward (Rossi et al. 2006), such minimal growth increments during July and August, as observed here, are extreme and likely related to the exceptionally hot and dry weather in 2018 (Figures 1 and 2A and B). The summer drought of 2018 was one of the worst on record for Central Europe (Büntgen et al. 2021) and resulted in marked declines in ecosystem productivity, extensive forest diebacks and major agricultural losses (Buras et al. 2020, Schuldt et al. 2020). Thus, water limitation of tree growth at our non-irrigated orchard site was likely to occur. However, the growth cessation in dwarfed trees was initiated already before the onset of the major drought period (Figure 2C and D). This indicates that other mechanisms, unrelated to drought stress, may have affected the trunk radial growth of the study trees. For instance, it is possible that the relatively high fruit load and the differences in yield efficiencies between dwarfed and invigorated trees (Table 1) influenced the trunk radial growth due to carbon allocation trade-offs (Stevenson and Shackel 1998, Lauri et al. 2010). Similarly, differences in hormonal levels, as widely accepted mechanisms of rootstock-scion signaling (Aloni et al. 2010), could have been involved.

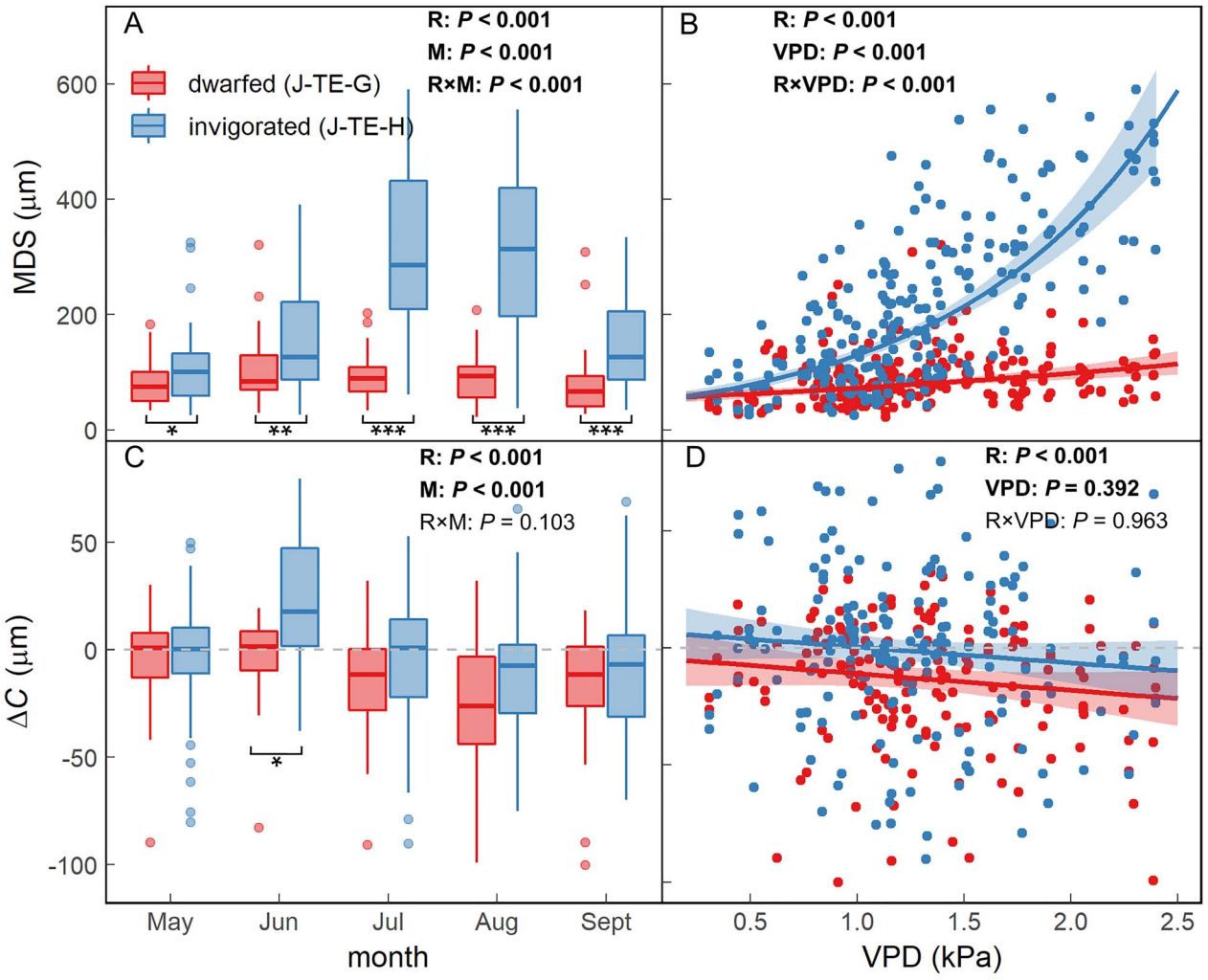

Figure 4. (A, B) The MDS (i.e., a difference between the daily maximal and minimal trunk circumference) and (C, D) interdiurnal trunk circumference change (ΔC; i.e., the difference between the daily maxima of two consecutive days) in dwarfed (J-TE-G) and invigorated (J-TE-H) rootstock combinations. The MDS and ΔC values are compared across months (A, C) and in relation to the mean daily VPD (B, D). The boxplots show the 25th and 75th percentiles (box), 10th and 90th percentiles (whiskers) and the median (line). Predictions from the general LM are shown with 95% confidence intervals (ribbon). Log-transformation was applied for MDS values, and outliers outside of 0.1 and 0.9 quantiles were removed from ΔC to satisfy the model assumptions. Results from the ANOVA- and ANCOVA-type tests evaluating the effects of rootstock (R), month (M), VPD and their respective interactions (R × M, R × VPD) are shown. Significant effects ($P < 0.05$) are highlighted in bold. The means of the two rootstock combinations within each month were separated by Tukey-adjusted pairwise comparisons and significant differences are indicated with an asterisk (*$P < 0.05$, **$P < 0.01$, ***$P < 0.001$).

The results obtained from the analyses of dendrometer data on a daily timescale corroborate the results of the seasonal modeling and provide additional support for the important role of water limitation in radial trunk growth. Wood formation in trees is known to be water-limited, although it remains to be elucidated how soil-, atmospheric- and plant-related drivers interact to limit tree growth across various species and environments (Zweifel et al. 2006, Cabon et al. 2020). From a mechanistic point of view, water limitation of radial growth hinges on the assumption that turgor is the key driver of cell division and expansion in the cambial and differentiation zones, respectively (Abe et al. 2003, Steppe et al. 2006). We observed that a positive net radial growth was less likely to occur (Figure 5), and the ΔC increments were lower (Figure 4C and D) during days with high evaporative demands. These patterns were stronger in dwarfed trees. Dwarfed trees also had less profound diurnal trunk circumference variation (Figure 3) and smaller MDS (Figure 4A and B), particularly during warm and dry summer days, suggesting that they stored and/or utilized less water reserves compared with invigorated trees. Since water storage helps to buffer the disbalance in water potential, dwarfed trees will likely experience reduced turgidity in their cambial region, which, in turn, restricted their trunk radial growth.

The limited trunk water storage dynamics in dwarfed trees can be structurally or physiologically explained. Structurally, the absolute water storage is proportional to the tree size

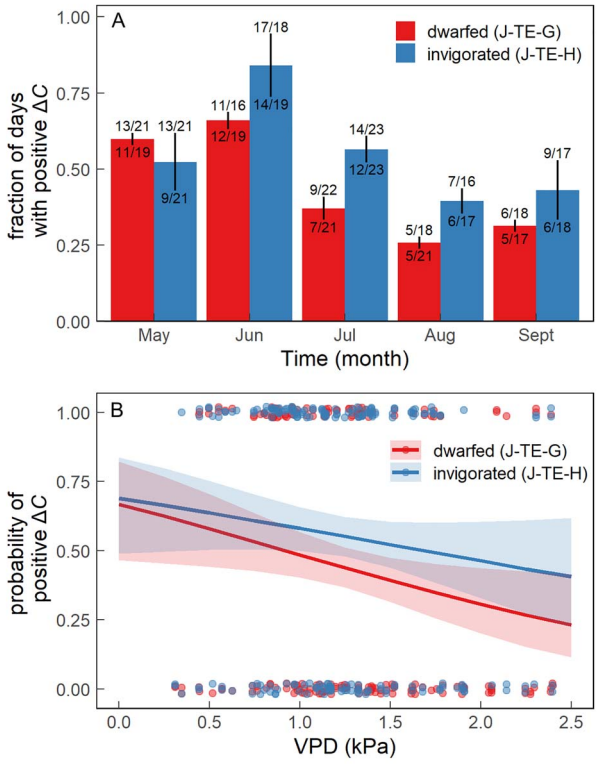

Figure 5. (A) The relative fraction of days with a positive interdiurnal trunk circumference change (ΔC) in dwarfed (J-TE-G) and invigorated (J-TE-H) rootstock combinations compared across months and (B) the probability of positive ΔC values as a function of an increasing daily VPD. (A) The columns and error bars represent the means and ranges of the two values for each rootstock combination, respectively. The number of days with positive ΔC out of the total considered days (i.e., days not affected by rain and after removing outlier ΔC outside of 0.1 and 0.9 quantiles) for the two individual trees for each rootstock combination are printed below and above the bars. (B) The observed data (points) and predicted relationships modeled using a logistic regression (lines). The shaded ribbons surrounding the prediction lines show 95% confidence intervals.

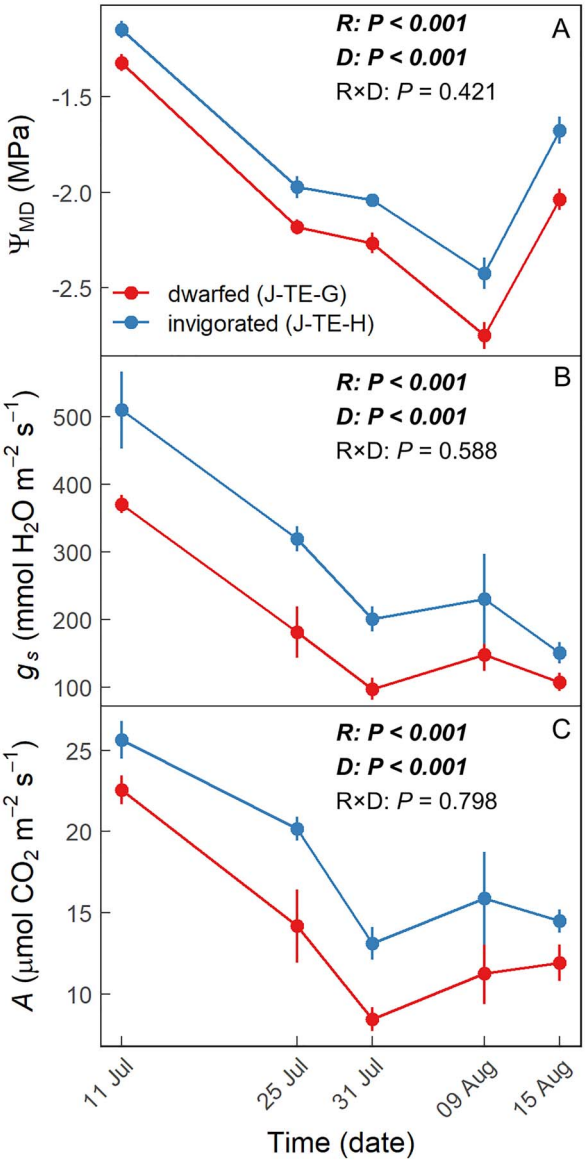

Figure 6. (A) Midday leaf water potential (Ψ_{MD}), (B) stomatal conductance (g_s) and (C) net assimilation rates (A) measured in dwarfed (J-TE-G) and invigorated (J-TE-H) rootstock combinations during the drought period. Data points and error bars represent the means and SE (n = 6 for Ψ_{MD}, n = 3 for g_s and A). Two-way ANOVA was used to evaluate the effects of rootstock (R), date (D) and their interaction (R × D). Significant effects ($P < 0.05$) are highlighted in bold.

(Olien and Lakso 1986, Goldstein et al. 1998). Thus, a lower absolute amount of water is stored in trunks of dwarfed trees, which had one-third the TCSAs compared with the invigorated trees (Table 1). Dwarfed trees also tend to have less extensive and shallower root systems (Jupa et al. 2021), which could have prevented them from accessing soil water to replenish the depleted reserves. Alternatively, physiological mechanisms related to phloem-xylem functioning might have been involved. It is generally believed that stored water is withdrawn from an elastic bark, while wood contributes less to the diurnal trunk variation (Pfautsch et al. 2015*a*). The radial exchange of water between the bark, cambium and mature xylem is facilitated by the abundant connections via rays (Van Bel 1990). Perturbed bark-to-xylem ratios, different fractions of rays (Beakbane and Thompson 1940, Chen et al. 2015, Jupa et al. 2021), as well as a lower capacity of bark for auxin transport (Kamboj et al. 1997), have been documented in dwarfing rootstocks, and these changes might lead to the disruptions of phloem-xylem coupling and reduce the ability to exchange water between these tissues and the cambial zone. Future experiments with symplastic tracers (Sokołowska and Zagórska-Marek 2012, Pfautsch et al. 2015*b*) will be useful to test this hypothesis.

Our data also provide insights into the sensitivity of leaf-level physiological processes to drought. The values of Ψ_{MD} and leaf gas exchange parameters measured in the two rootstock combinations (Figure 6) demonstrate substantial drought

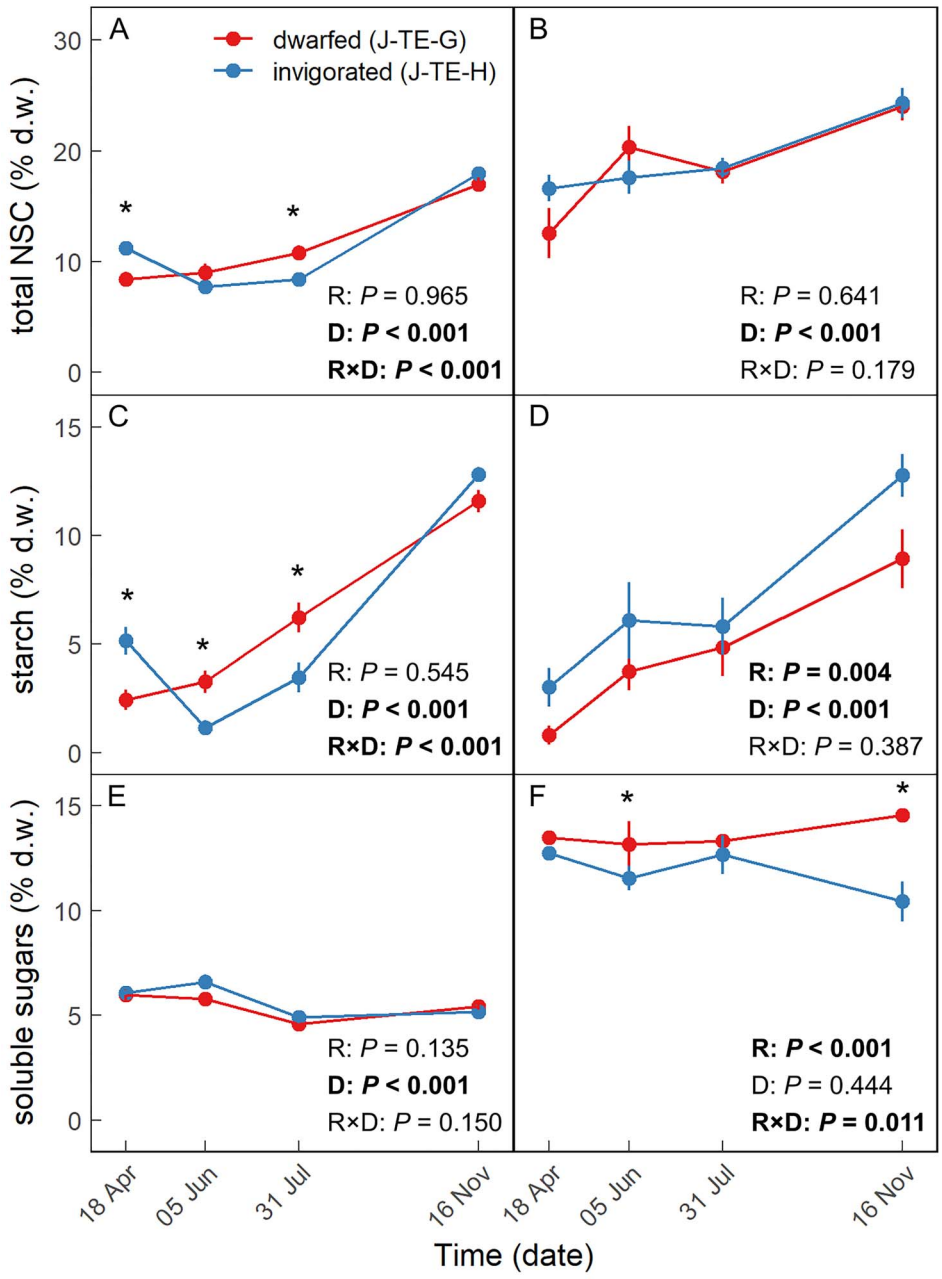

Figure 7. Concentrations of NSC measured in 1-year-old branches (A, C, E) and coarse woody roots (B, D, F) of dwarfed (J-TE-G) and invigorated (J-TE-H) rootstock combinations. The concentrations of total NSC (A, B), starch (C, D) and soluble sugars (E, F) are given as a percentage of dry weight (% d.w.). Data points and error bars represent the means and SE (n = 5–6). Two-way ANOVA was used for the statistical testing. The significant effects ($P < 0.05$) of the rootstock (R), date (D) or their interaction (R × D) are highlighted in bold. In the case of a significant interaction, the means of the two rootstock variants within each sampling date were separated by Tukey-adjusted pairwise comparisons. Significant differences ($P < 0.05$) between the rootstock means are highlighted with an asterisk (*).

stress, which resulted from a combined effect of atmospheric and soil drying, as is often the case in natural field conditions. The minimal Ψ_{MD} of −2.4 and − 2.8 MPa observed in early August in invigorated and dwarfed trees, respectively (Figure 6A), correspond roughly to the values causing turgor loss in leaves and critical embolism in the stem xylem of apple trees (Beikircher et al. 2013, 2019). While apple trees are quite drought resistant, horticultural studies report tangible impacts on the yield (mostly reduction of fruit size) at stem water potentials of around −1.5 MPa (Naor et al. 1995). The generally lower values of Ψ_{MD} and leaf gas exchange parameters in dwarfed trees (Figure 6) are likely related to the less efficient water uptake and delivery caused by their less extensive root systems and lower xylem transport efficiency (Atkinson et al. 2003, Jupa et al. 2021). The finding that leaf-level processes in dwarfed trees declined at the same rate during drought as those

in invigorated trees is surprising, considering its shallower root system and lower hydraulic conductance, and the differences in water storage dynamics (Figure 3). If water storage buffered the leaf water status, we would expect to find a less pronounced decline in Ψ_{MD} and/or g_s in invigorated trees whose water storage dynamics was apparently not disrupted (Figure 3). Nevertheless, our data are consistent with the conclusions of Olien and Lakso (1986), who examined the diurnal variation of leaf water potential in apple trees grafted on different size-controlling rootstocks and also concluded that water storage did not play a major role in controlling the bulk leaf hydration. Taken together, these results point to a more subtle role of water storage that can be manifested at a finer spatial scale, such as by sustaining cambial region turgidity as discussed above.

The similar drought sensitivity of the trees on different rootstocks contrasts with the results of some previous studies (Atkinson et al. 2000, Cohen and Naor 2002, Tworkoski et al. 2016). The diverse patterns in g_s, leaf water potential dynamics and their mutual coordination observed across various studies on size-controlling rootstocks reflect the interspecific differences, various tree age (seedlings vs mature trees), specific growing conditions (pots vs field grown) and the type of drought stress imposed (short-term vs long-term, atmospheric vs soil drought). The similar drought sensitivity of dwarfed and invigorated trees in the present study might be a result of the long-term structural acclimation throughout the tree's lifetime. The studied trees were grown without irrigation for >20 years and may have adjusted the mutual coordination of water uptake, transport and loss, allowing them to effectively operate at different physiological levels. For example, canopy water demands, as a consequence of the tree growth potential, are likely mutually coordinated with the structure of the root system and its ability to extract water from the soil within a self-regulating feedback loop (Contador et al. 2015). To substantiate this hypothesis, it would be useful to evaluate the allometric scaling between root, sapwood and leaf biomass or areas. While such measurements are laborious for large mature trees, adjustments of these parameters are known from studies using smaller trees and show that the reduction of shoot-to-root ratio may partially compensate for the lower hydraulic conductivity of dwarfed trees (Nardini et al. 2006, Solari et al. 2006*b*, Tworkoski et al. 2016).

Despite the lower photosynthetic rate in dwarfed trees (Figure 6C), the evidence for the reduced NSC levels and consequent carbon limitation of their growth is weak. Throughout the season, the NSC reserves were never completely depleted in either branches or roots, providing no support for direct carbon starvation (Figure 7). It is, however, possible that the trees prioritized the maintenance of certain NSC levels over growth, although storage is traditionally assumed to have lower sink priority (Oliveira and Priestley 1988, Wardlaw 1990). The NSC concentrations and seasonal dynamics were generally similar in dwarfed and invigorated trees, suggesting no major differences in NSC accumulation and mobilization between both rootstock combinations. This would mean that a higher proportion of newly produced carbohydrates were spent on the maintenance of NSC reserves in dwarfed trees, which also allocated more biomass to fruits (Table 1). Consequently, the lower vigor of these trees is associated with perturbations of their overall sink-source relationships.

Consistent with our expectations, dwarfed trees had slightly lower concentrations of NSC reserves in branches during the bud break (Figure 7C). However, during the growing season, invigorated trees consumed a greater proportion of the NSC reserves to support their vigorous growth (Figure 7C). Unfortunately, we have no information on the NSC concentrations and dynamics in the cambial zone, as destructive sampling in the trunk region was avoided so as not to perturb tree growth and dendrometer readings. Nevertheless, static measurements of NSC concentrations in trunks would not be sufficient to provide a definitive answer regarding the NSC reserve availability for the cambial growth because a trunk NSC storage pool appears to be divided into distinct components with contrasting turnover times and specialized functional roles (Carbone et al. 2013). If the trunk growth of dwarfed trees was limited by the low NSC reserves, the greatest differences in the growth between dwarfed and invigorated trees would be expected in spring before full canopy expansion, which was not the pattern observed here (Figure 2C and D).

In conclusion, this study focused on the seasonal and daily dynamics of the trunk radial growth, which is an aspect of vegetative growth that has not been explored so far in the context of rootstock-induced size-controlling mechanisms in composite fruit trees. Our results support the important role of tree water relations in the size-controlling mechanisms. Using high-precision band dendrometers, we showed that the trunk radial growth in both rootstock combinations was water-limited and that dwarfed trees will likely experience greater water deficit and lower turgidity in their cambial zone when compared with invigorated trees. On the other hand, we found little evidence that the reduced leaf gas exchange rates translate into lower NSC reserves in dwarfed trees. We do not exclude the possibility that other factors, such as hormonal signaling, perturbed nutritional status or competition from reproductive tissues, further shaped the vegetative growth of the studied trees. Moreover, tree size by itself is an important factor potentially affecting trees' water and carbon balance (Meinzer et al. 2003, Furze et al. 2019). Separating the physiological behavior related to the different tree sizes from the direct effect of rootstock is difficult. From this perspective, the size effect can be viewed as an indirect (or extended) component of the rootstock-mediated mechanism of growth vigor control that becomes compounded over the tree's lifetime. To truly separate the impacts of the size-related traits from the proximate influence by the rootstock

would require laborious comparisons of differences in plant biomass and monitoring of physiological responses during trees' lifespan or by studying contrasting scion/rootstock combinations of different ages growing side-by-side. Clearly, the biological mechanisms underlying the rootstock-induced control of growth vigor are complex and require further investigations to identify specific traits that can be targeted in the breeding and selection of new size-controlling rootstock genotypes.

Authors' contributions

R.J. and L.P. initiated the study, performed most of the field work, analyzed the data and wrote the first draft of the paper. M.M. contributed to the field work and advised on the horticultural aspects of the study. G.H. was responsible for the NSC analyses. All authors discussed the results and contributed to the final version of the manuscript.

Acknowledgments

We thank Svenja Förster for her assistance with the NSC analyses. We thank Karolína Bjelková and Jana Fenclová for technical assistance.

Funding

Czech Science Foundation (18-19722Y to L.P.); Ministry of Education Youth and Sports (LO1608); Ministry of Agriculture of the Czech Republic (MZE-RO1518).

Conflict of interest

None declared.

References

Abe H, Nakai T, Utsumi Y, Kagawa A (2003) Temporal water deficit and wood formation in *Cryptomeria japonica*. Tree Physiol 23:859–863.

Aloni B, Cohen R, Karni L, Aktas H, Edelstein M (2010) Hormonal signaling in rootstock–scion interactions. Sci Hortic 127:119–126.

Atkinson C, Else M (2001) Understanding how rootstocks dwarf fruit trees. 44th Annual IDFTA Conference. Compact Fruit Tree 34:46–49.

Atkinson CJ, Policarpo M, Webster AD, Kingswell G (2000) Drought tolerance of clonal *Malus* determined from measurements of stomatal conductance and leaf water potential. Tree Physiol 20:557–563.

Atkinson CJ, Else MA, Taylor L, Dover CJ (2003) Root and stem hydraulic conductivity as determinants of growth potential in grafted trees of apple (*Malus pumila* Mill.). J Exp Bot 54:1221–1229.

Basile B, DeJong TM (2018) Control of fruit tree vigor induced by dwarfing rootstocks. Hortic Rev 46:39–97.

Basile B, Marsal J, Solari LI, Tyree MT, Bryla DR, Dejong TM (2003) Hydraulic conductance of peach trees grafted on rootstocks with differing size-controlling potentials. J Hortic Sci Biotech 78:768–774.

Bates D, Mächler M, Bolker B, Walker S (2015) Fitting linear mixed-effects models using lme4. J Stat Softw 67:1–48.

Beakbane BA, Thompson EC (1940) Anatomical studies of stems and roots of hardy fruit trees. II. The internal structure of the roots of some vigorous and some dwarfing apple rootstocks, and the correlation of structure with vigour. J Pomol Hortic Sci 17:141–149.

Beikircher B, De Cesare C, Mayr S (2013) Hydraulics of high-yield orchard trees: a case study of three *Malus domestica* cultivars. Tree Physiol 33:1296–1307.

Beikircher B, Losso A, Gemassmer M, Jansen S, Mayr S (2019) Does fertilization explain the extraordinary hydraulic behaviour of apple trees? J Exp Bot 70:1915–1925.

Berman ME, DeJong TM (1997*a*) Diurnal patterns of stem extension growth in peach (*Prunus persica*): temperature and fluctuations in water status determine growth rate. Physiol Plant 100:361–370.

Berman ME, DeJong TM (1997*b*) Crop load and water stress effects on daily stem growth in peach (*Prunus persica*). Tree Physiol 17:467–472.

Büntgen U, Urban O, Krusic PJ et al. (2021) Recent European drought extremes beyond common era background variability. Nat Geosci 14:190–196.

Buras A, Rammig A, Zang CS (2020) Quantifying impacts of the 2018 drought on European ecosystems in comparison to 2003. Biogeosciences 17:1655–1672.

Cabon A, Fernández-de-Uña L, Gea-Izquierdo G, Meinzer FC, Woodruff DR, Martínez-Vilalta J, De Cáceres M (2020) Water potential control of turgor-driven tracheid enlargement in Scots pine at its xeric distribution edge. New Phytol 225:209–221.

Carbone MS, Czimczik CI, Keenan TF, Murakami PF, Pederson N, Schaberg PG, Xu X, Richardson AD (2013) Age, allocation and availability of nonstructural carbon in mature red maple trees. New Phytol 200:1145–1155.

Chen B, Wang C, Tian Y, Chu Q, Hu C (2015) Anatomical characteristics of young stems and mature leaves of dwarf pear. Sci Hortic 186:172–179.

Clearwater MJ, Seleznyova AN, Thorp TG, Blattmann P, Barnett AM, Lowe RG, Austin PT (2006) Vigor-controlling rootstocks affect early shoot growth and leaf area development of kiwifruit. Tree Physiol 26:505–515.

Cohen S, Naor A (2002) The effect of three rootstocks on water use, canopy conductance and hydraulic parameters of apple trees and predicting canopy from hydraulic conductance: apple rootstocks influence canopy and hydraulic conductance. Plant Cell Environ 25: 17–28.

Cohen S, Naor A, Bennink J, Grava A, Tyree M (2007) Hydraulic resistance components of mature apple trees on rootstocks of different vigours. J Exp Bot 58:4213–4224.

Contador ML, Comas LH, Metcalf SG, Stewart WL, Porris Gomez I, Negron C, Lampinen BD (2015) Root growth dynamics linked to above-ground growth in walnut (*Juglans regia*). Ann Bot 116:49–60.

DeJong T, Johnson R, Doyle J, Weibel A, Solari L, Marsal J, Basile B, Ramming D, Bryla D (2004) Growth, yield and physiological behaviour of size-controlling peach rootstocks developed in California. Acta Hortic 658:449–455.

Deslauriers A, Rossi S, Anfodillo T (2007) Dendrometer and intra-annual tree growth: What kind of information can be inferred? Dendrochronologia 25:113–124.

Dolezal J, Kopecky M, Dvorsky M et al. (2019) Sink limitation of plant growth determines tree line in the arid Himalayas. Funct Ecol 33:553–565.

Drew DM, Downes GM (2009) The use of precision dendrometers in research on daily stem size and wood property variation: a review. Dendrochronologia 27:159–172.

Duchesne L, Houle D, D'Orangeville L (2012) Influence of climate on seasonal patterns of stem increment of balsam fir in a boreal forest of Québec, Canada. Agric For Meteorol 162-163:108–114.

Fernández JE, Cuevas MV (2010) Irrigation scheduling from stem diameter variations: a review. Agric For Meteorol 150:135–151.

Furze ME, Huggett BA, Aubrecht DM, Stolz CD, Carbone MS, Richardson AD (2019) Whole-tree nonstructural carbohydrate storage and seasonal dynamics in five temperate species. New Phytol 221:1466–1477.

Goldstein G, Andrade JL, Meinzer FC, Holbrook NM, Cavelier J, Jackson P, Celis A (1998) Stem water storage and diurnal patterns of water use in tropical forest canopy trees. Plant Cell Environ 21:397–406.

Gonçalves B, Moutinho-Pereira J, Santos A, Paula A, Bacelar E, Correia C, Rosa E (2006) Scion–rootstock interaction affects the physiology and fruit quality of sweet cherry. Tree Physiol 26:93–104.

Gonçalves B, Correia CM, Silva AP, Bacelar EA, Santos A, Ferreira H, Moutinho-Pereira JM (2007) Variation in xylem structure and function in roots and stems of scion–rootstock combinations of sweet cherry tree (*Prunus avium* L.). Trees 21:121–130.

Gričar J, Lavrič M, Ferlan M, Vodnik D, Eler K (2017) Intra-annual leaf phenology, radial growth and structure of xylem and phloem in different tree parts of *Quercus pubescens*. Eur J For Res 136: 625–637.

Hoch G (2015) Carbon reserves as indicators for carbon limitation in trees. In: Lüttge U, Beyschlag W (eds) Progress in botany. Springer, Cham, pp 321–346.

Jupa R, Mészáros M, Plavcová L (2021) Linking wood anatomy with growth vigour and susceptibility to alternate bearing in composite apple and pear trees. Plant Biol 23:172–183.

Kamboj J, Browning G, Quinlan J, Blake P, Baker D (1997) Polar transport of [3H]-IAA in apical shoot segments of different apple rootstocks. J Hortic Sci 72:773–780.

Kosina J (2010) Effect of dwarfing and semi dwarfing apple rootstocks on growth and productivity of selected apple cultivars. Hortic Sci 37:121–126.

Landhäusser SM, Chow PS, Dickman LT et al. (2018) Standardized protocols and procedures can precisely and accurately quantify nonstructural carbohydrates. Tree Physiol 38:1764–1778.

Lauri PÉ, Kelner JJ, Trottier C, Costes E (2010) Insights into secondary growth in perennial plants: its unequal spatial and temporal dynamics in the apple (*Malus domestica*) is driven by architectural position and fruit load. Ann Bot 105:607–616.

Lenth R (2020) Emmeans: estimated marginal means, aka least-squares means. R package version 1.4.8. https://CRAN.R-project.org/package=emmeans.

McDowell NG (2011) Mechanisms linking drought, hydraulics, carbon metabolism, and vegetation mortality. Plant Physiol 155:1051–1059.

Meinzer FC, James SA, Goldstein G, Woodruff D (2003) Whole-tree water transport scales with sapwood capacitance in tropical forest canopy trees. Plant Cell Environ 26:1147–1155.

Mészáros M, Laňar L, Kosina J, Náměstek J (2019) Aspects influencing the rootstock-scion performance during long term evaluation in pear orchard. Hortic Sci 46:1–8.

Naor A, Klein I, Doron I (1995) Stem water potential and apple size. J Am Soc Hort Sci 120:577–582.

Nardini A, Gasco A, Raimondo F, Gortan E, Lo Gullo MA, Caruso T, Salleo S (2006) Is rootstock-induced dwarfing in olive an effect of reduced plant hydraulic efficiency? Tree Physiol 26:1137–1144.

Olien WC, Lakso AN (1986) Effect of rootstock on apple (*Malus domestica*) tree water relations. Physiol Plant 67:421–430.

Oliveira CM, Priestley CA (1988) Carbohydrate reserves in deciduous fruit trees. Hort Rev 10:403–430.

Peters RL, Steppe K, Cuny HE, De Pauw DJW, Frank DC, Schaub M, Rathgeber CBK, Cabon A, Fonti P (2021) Turgor – a limiting factor for radial growth in mature conifers along an elevational gradient. New Phytol 229:213–229.

Pfautsch S, Hölttä T, Mencuccini M (2015*a*) Hydraulic functioning of tree stems—fusing ray anatomy, radial transfer and capacitance. Tree Physiol 35:706–722.

Pfautsch S, Renard J, Tjoelker MG, Salih A (2015*b*) Phloem as capacitor: radial transfer of water into xylem of tree stems occurs via symplastic transport in ray parenchyma. Plant Physiol 167:963–971.

Popp M, Lied W, Meyer AJ, Richter A, Schiller P, Schwitte H (1996) Sample preservation for determination of organic compounds: microwave versus freeze-drying. J Exp Bot 47:1469–1473.

R Development Core Team. (2010) R: a language and environment for statistical computing. R Foundation for Statistical Computing, Vienna, Austria, http://www.R-project.org.

Rossi S, Deslauriers A, Anfodillo T, Morin H, Saracino A, Motta R, Borghetti M (2006) Conifers in cold environments synchronize maximum growth rate of tree-ring formation with day length. New Phytol 170:301–310.

Russo NL, Robinsion TL, Fazio G, Aldwinckle HS (2007) Field evaluation of 64 apple rootstocks for orchard performance and fire blight resistance. HortScience 42:1525–1525.

Schechter I, Elfving DC, Proctor JTA (1991) Apple tree canopy development and photosynthesis as affected by rootstock. Can J Bot 69:295–300.

Schuldt B, Buras A, Arend M et al. (2020) A first assessment of the impact of the extreme 2018 summer drought on Central European forests. Basic Appl Ecol 45:86–103.

Sokołowska K, Zagórska-Marek B (2012) Symplasmic, long-distance transport in xylem and cambial regions in branches of *Acer pseudoplatanus* (Aceraceae) and *Populus tremula* × *P . tremuloides* (Salicaceae). Am J Bot 99:1745–1755.

Solari LI, Johnson S, DeJong TM (2006*a*) Relationship of water status to vegetative growth and leaf gas exchange of peach (*Prunus persica*) trees on different rootstocks. Tree Physiol 26:1333–1341.

Solari LI, Johnson S, DeJong TM (2006*b*) Hydraulic conductance characteristics of peach (*Prunus persica*) trees on different rootstocks are related to biomass production and distribution. Tree Physiol 26:1343–1350.

Sperry JS (2000) Hydraulic constraints on plant gas exchange. Agric For Meteorol 104:13–23.

Steppe K, De Pauw DJW, Lemeur R, Vanrolleghem PA (2006) A mathematical model linking tree sap flow dynamics to daily stem diameter fluctuations and radial stem growth. Tree Physiol 26:257–273.

Stevenson MT, Shackel KL (1998) Alternate bearing in pistachio as a masting phenomenon: construction cost of reproduction versus vegetative growth and storage. J Am Soc Hort Sci 123:1069–1075.

Tworkoski T, Fazio G, Glenn DM (2016) Apple rootstock resistance to drought. Sci Hortic 204:70–78.

Van Bel AJE (1990) Xylem-phloem exchange via the rays: the undervalued route of transport. J Exp Bot 41:631–644.

Wardlaw IF (1990) The control of carbon partitioning in plants. New Phytol 116:341–381.

Weber R, Schwendener A, Schmid S, Lambert S, Wiley E, Landhäusser SM, Hartmann H, Hoch G (2018) Living on next to nothing: tree seedlings can survive weeks with very low carbohydrate concentrations. New Phytol 218:107–118.

Weber R, Gessler A, Hoch G (2019) High carbon storage in carbon-limited trees. New Phytol 222:171–182.

Webster A, Hollands MS (1999) Apple rootstock studies: comparison of Polish, Russian, USA and UK selections as rootstocks for the apple cultivar Cox's Orange Pippin (*Malus domestica* Borkh.). J Hortic Sci Biotech 74:367–374.

Weibel A, Johnson RS, DeJong TM (2003) Comparative vegetative growth responses of two peach cultivars grown on size-controlling versus standard rootstocks. J Am Soc Hort Sci 128:463–471.

Weibel A, Reighard G, Rajapakse N, DeJong T (2008) Dormant carbohydrate reserves of two peach cultivars grafted on different vigor rootstocks. ISHS Acta Hortic. 903: 815–820. https://www.actahort.org/books/903/903_113.htm.

Wickham H (2016) ggplot2: elegant graphics for data analysis. Springer, New York, NY.

Wilke CO (2019) cowplot: streamlined plot theme and plot annotations for 'ggplot2'. R package version 1.0.0. https://CRAN.R-project.org/package=cowplot.

Yano T, Inoue H, Shimizu Y, Shinkai S (2002) Dry matter partitioning and carbohydrate status of 'Kawanakajima Hakuto' peach trees grafted onto different rootstocks or with an interstock at pre-bloom period. J Jpn Soc Hortic Sci 71:164–170.

Zweifel R, Zimmermann L, Zeugin F, Newbery DM (2006) Intra-annual radial growth and water relations of trees: implications towards a growth mechanism. J Exp Bot 57:1445–1459.

Zweifel R, Haeni M, Buchmann N, Eugster W (2016) Are trees able to grow in periods of stem shrinkage? New Phytol 211:839–849.

Annals of Botany **130**: 477–489, 2022
https://doi.org/10.1093/aob/mcac089, available online at www.academic.oup.com/aob

ANNALS OF BOTANY
Founded 1887

Relationships between trunk radial growth and fruit yield in apple and pear trees on size-controlling rootstocks

Lenka Plavcová[1,*], Martin Mészáros[2], Karel Šilhán[1] and Radek Jupa[1]

[1]*Department of Biology, Faculty of Science, University of Hradec Králové, Rokitanského 62, CZ-500 03, Hradec Králové, Czech Republic and* [2]*Research and Breeding Institute of Pomology, Holovousy 129, CZ-508 01, Hořice, Czech Republic*
**For correspondence. E-mail lenka.plavcova@uhk.cz*

Received: 20 June 2022 Editorial decision: 27 June 2022 Accepted: 29 June 2022 Electronically published: 5 July 2022

• **Background and Aims** Understanding the mutual co-ordination of vegetative and reproductive growth is important in both agricultural and ecological settings. A competitive relationship between vegetative growth and fruiting is often highlighted, resulting in an apparent trade-off between structural growth and fruit production. However, our understanding of factors driving this relationship is limited.
• **Methods** We used four scions grafted onto a series of size-controlling rootstocks to evaluate the relationships between the annual fruit yield and radial growth of trunks, branches and roots. To assess tree radial growth, we measured ring widths on extracted tree cores, which is an approach not frequently used in a horticultural setting.
• **Key Results** We found that the yield and radial growth were negatively related when plotted in absolute terms or as detrended and normalized indices. The relationship was stronger in low vigour trees, but only after the age-related trend was removed. In contrast, when trunk radial growth was expressed as basal area increment, the negative relationship disappeared, suggesting that the relationship between trunk radial growth and fruit yield might not be a true trade-off related to the competition between the two sinks. The effect of low yield was associated with increased secondary growth not only in trunks but also in branches and roots. In trunks, we observed that overcropping was associated with reduced secondary growth in a subsequent year, possibly due to the depletion of reserves.
• **Conclusions** Our results show that variation in annual fruit yield due to tree ageing, weather cueing and inherent alternate bearing behaviour is reflected in the magnitude of secondary growth of fruit trees. We found little support for the competition/architecture theory of rootstock-induced growth vigour control. More broadly, our study aimed at bridging the gap between forest ecology and horticulture.

Key words: Apple, pear, *Malus* × *domestica*, *Pyrus communis*, growth, reproduction, rootstock, trade-off, tree ring, yield.

INTRODUCTION

Growth and reproduction are key components of plant fitness and performance. Identifying factors that drive these two processes and understanding their mutual interactions is therefore of paramount importance in both ecological and agricultural contexts. The trade-off relationship between vegetative growth and reproduction has often been highlighted, considering them as two sinks competing for a finite amount of assimilated carbon and nutrients (Sala *et al.*, 2012). However, reproduction also depends positively on vegetative growth because vegetative structures are necessary to acquire and transport resources from the environment and to provide structural scaffolds that display leaves, flowers and fruits (Lauri *et al.*, 2010; Lehnebach *et al.*, 2018). In this regard, the evolution of secondary growth has been important as mechanically strong wood enables the development of large plant bodies, thereby granting trees an advantage in competition for light, nutrient and water, and allowing them to carry ample and heavy fruit loads (Spicer and Groover, 2010; Poorter *et al.*, 2012).

In forest ecology, the vegetative–reproductive trade-off has been mostly studied by exploring the covariation between ring width and a measure of fruiting. Due to the large size and inaccessibility of forest trees canopies, fruiting is usually expressed on a semi-quantitative nominal scale, e.g. as a seed index or an estimated number of fruits or cones (Koenig *et al.*, 1996; Monks and Kelly, 2006; Hacket-Pain *et al.*, 2018). In addition, fruit production is often not directly referenced to an individual tree but is instead representative for an entire local population (Koenig *et al.*, 1996). Many studies report a negative effect of fruiting on secondary growth; however, the character and strength of this relationship is variable. While some studies showed a clear negative correlation between trunk radial growth and fruiting output (Hacket-Pain *et al.*, 2017), other studies found no such correlation or found that the reduction of growth was restricted only to mast years (Drobyshev *et al.*, 2010; Żywiec and Zielonka, 2013). Furthermore, the relationship is often complicated by complex delayed effects and interactions with environmental cues (Hacket-Pain *et al.*, 2018; Mund *et al.*, 2020). For instance, in European beech (*Fagus sylvatica* L.), the reduction of growth was greatest during mast years that coincided with summer drought (Hacket-Pain *et al.*, 2017). Similarly, Mund *et al.* (2020) found that radial growth

of beech was responsive to spring temperature and precipitation as well as to the amount of fruits, highlighting that a complex system of sink–source limitations governs tree growth.

The horticultural literature provides a complementary view on the interplay between vegetative growth and fruiting. Studies reporting a close proportionality between vegetative and reproductive biomass provide evidence for a resource allocation trade-off. For instance, the construction costs of perennial woody tissues during 'off' years corresponded to 64 % of the construction costs of fruits during 'on' years, while stored carbohydrate reserves accumulated during 'off' years accounted for only 8 % of fruiting costs (Stevenson and Shackel, 1998). Similarly, in two olive cultivars subjected to deflowering, Rosati *et al.* (2018*b*) observed a tight negative relationship between the dry matter of vegetative and reproductive structures, while the total biomass increment was not altered in response to fruit removal treatments.

In their seminal review, Forshey and Elfving (1989) state: 'When reduced to the simplest terms, the ultimate objective of all pomological practices is really the manipulation of the vegetative growth–fruiting relationship'. Thus, the main aim in horticulture is to shift the allocation of carbohydrates and minerals towards fruits. In contrast, excessive vegetative growth is undesirable as it competes with fruits for resources, limits planting densities and makes tree management and harvesting more labour intensive. The yield efficiency or harvest index are commonly used measures in agriculture and, in the case of crops grown for their fruits or seeds, a representation of the allocation to fruits relative to total biomass (Hay, 1995; Sinclair, 1998). For the improvement of the harvest index in fruit crops, selection of an appropriate cultivar and efficient tree pruning and training practices are desirable. Besides that, the introduction of size-controlling rootstocks has arguably been one of the major innovations that contributed to the development of high efficiency fruit orchards as dwarfing rootstocks increase yield efficiency per tree, per hectare as well as over time by a faster planting turnover (Atkinson and Else, 2003).

In trees on size-controlling rootstocks, both the total dry matter production and its partitioning between fruit and wood are altered (Webster, 1995). The biological mechanisms of growth vigour control are multifaceted, and several theories grounded on the perturbations of water, nutrient, hormonal and carbon balance have been proposed (Basile and DeJong, 2018). However, none of the theories has been conclusively supported to date. According to one of these theories, the so-called competition/architecture theory, it is possible that the precocity of cropping, which is a common feature in dwarfing trees, diverts resources from vegetative to reproductive structures and causes architectural changes that further perpetuate the reduction of vegetative growth (Basile and DeJong, 2018). The preferential allocation of resources to fruits implies that they are sinks of a high strength. This is consistent with the generally assumed hierarchy of sinks which have been ranked as follows: seed/fruits > vegetative growth > storage (Wardlaw, 1990; Fischer *et al.*, 2013). However, this view might be too simplistic, and it has been suggested that both the transition from source to sink limitation and the strength of the potentially competing sinks can change during the growing season (Lauri *et al.*, 2010; Mund *et al.*, 2020).

While horticultural studies are often focused on the co-ordination of primary growth and fruiting during one or a few seasons (Rosati *et al.*, 2018*a*, *b*), forest ecology contributes to our understanding of secondary growth and reproduction at larger spatial–temporal scales (Drobyshev *et al.*, 2010; Hacket-Pain *et al.*, 2015, 2018). Drawing inspiration from the forest ecology literature and a rare horticultural study by Stevenson and Shackel (1998), we performed the measurements of tree ring width in composite apple and pear trees of contrasting growth vigour and bearing behaviour. Using four different scions grafted onto a series of size-controlling rootstocks, we assessed the relationship between annual fruit yield and secondary growth of trunks. We expected to find a negative covariation between fruit production and radial trunk growth and we hypothesized that the trade-off would be stronger in low vigour trees because fruits have higher sink strength. For a subset of four scion–rootstock combinations (SRCs), we also looked at the radial growth of coarse woody roots and scaffold branches. More pronounced trade-offs were expected with branches due to their closer proximity to the fruit sinks (Obeso, 1997).

MATERIALS AND METHODS

Plant material

Twelve different SRCs were used in this study. These SRCs were selected to cover a gradient of growth vigour and susceptibility to alternate bearing. A more detailed description of the field trial and the rationale for the selection of the specific SRCs can be found in Jupa *et al.* (2021). The trees included two varieties of *Malus* × *domestica* Borkh. ('Rubin'; abbreviated as R and 'Jonagold'; abbreviated as J) and two varieties of *Pyrus communis* L. ('Williams'; abbreviated as W and 'General Leclerc'; abbreviated as GL) grafted onto eight different size-controlling rootstocks: J-TE-G, M.9, J-TE-H and MM.106 for *M.* × *domestica*, and S1, MA, MC, and peer seedling (abbreviated as PS) for *P. communis*. The growth vigour categories (low, medium and high) for each SRC are described in Table 1.

The trees were grown at the experimental plots of the Research and Breeding Institute of Pomology in Holovousy, Czech Republic (50°37′N, 15°57′E; 283 m a.s.l.). The site is on a loamy brown soil with a medium fertility and experiences a temperate climate with a mean annual temperature of 8.4 °C and mean annual precipitation of 664 mm. The trees were propagated in a nursery and planted in the field in 1990 (*P. communis*) and 1992 (*M.* × *domestica*) when they were 4 years old. The trees were planted at a spacing of 4.5 × 2.3 m and 5.0 × 3.0 m for *M.* × *domestica* and *P. communis*, respectively, and trained as freely growing hedgerows with a short (70 cm) stem height with the tip of the central leader being removed in the fifth year. Fertilization was applied twice a year (in April during spring flush and in June during fruit drop) and consisted of 256 kg ha^{-1} 1:1:1 NPK fertilizer for each application. Plant protection followed standard integrated pest management practices. The trees received no supplemental irrigation. They were winter pruned each year, but no hand or chemical thinning of the fruits was carried out.

Table 1. *Growth and yield characteristics of individual scion–rootstock combinations (SRCs)*

SRC	Vigour category	$TCSA_{2011}$ (cm^2)	Cumulative yield (1992–2011) (kg pe tree)	Mean annual yield (kg per tree)	Cumulative yield efficiency (1992–2011) (kg cm^{-2})	Mean flowering intensity (0–9 scale)	Yield CV	AC–1 YI
J/JTEG*	Low	78.1	396.3	20.9	5.08	6	0.739	–0.528
J/M9	Medium	167.1	590.4	31.1	3.53	5.6	0.706	–0.446
J/JTEH*	High	249.1	581.4	30.6	2.33	5.2	0.716	–0.368
R/JTEG	Low	95.6	501.9	26.4	5.25	6.8	0.579	–0.07
R/M9	Medium	193.8	595.6	31.3	3.07	6.3	0.647	–0.041
R/JTEH	High	254.7	538.2	28.3	2.11	6	0.703	–0.112
R/MM106	High	331.3	469.6	24.7	1.42	5.7	0.788	–0.103
W/S1*	Low	110.1	515.5	25.8	4.68	5.9	0.795	–0.144
W/MA	Medim	143.6	577.0	28.9	4.02	5.6	0.765	–0.362
W/PS*	High	200	605.5	30.3	3.03	5.3	0.819	–0.098
GL/MA	Medium	224.1	439.1	22	1.96	4.6	1.035	–0.653
GL/MC	Medium	216.3	413.6	20.7	1.91	4.6	1.041	–0.523

Abbreviations: AC–1 YI, yield index time series lag–1 autocorrelation; $TCSA_{2011}$, trunk cross-sectional area in 2011; yield CV, yield coefficient of variation (interannual).

SRCs for which branch and root samples were measured for ring widths are denoted with an asterisk.

Annual fruit yield, flowering intensity and trunk cross-sectional area measurements

All trees in the field trials were assessed for fruit yield, flowering intensity and trunk growth. Fruit yield (kg per tree) was measured annually from 1992 (1993) to 2011 using a portable balance with a 0.1 kg precision. The flowering intensity was rated in 1999–2011 at a semi-quantitative scale from 1 to 9 (1 = no flowers, 9 = all shoots covered by mixed buds). Trunk cross-sectional area (TCSA; cm^2) was measured from 1996 to 2011 with a 1–4 year periodicity. Some of the data were previously reported as a part of a standard horticultural assessment (Kosina, 2010; Mészáros *et al.*, 2013). Thus, we took the published data, complemented them with additional unpublished data and produced a mean chronology of annual yield spanning a period of 17 years (1993–2011). The SRC-level chronologies are based on 5–8 individual trees for each SRC. We used the mean SRC-level chronologies instead of tree-level chronologies because individual tree yields were not consistently determined. In addition to annual yield, we also accessed data on the flowering intensity and TCSA obtained during the field trial assessment.

Ring width measurements in trunks

Measurements of tree-ring widths were used as estimates of annual trunk radial growth. Trunk cores were taken from 3–4 individual trees for each of the 12 selected SRCs. We originally aimed to take cores from at least five trees per SRC; however, during coring we found out that some trunks had internal decay. This is also the reason why only two trees were cored in the case of J/JTEH. From each tree, we took 2–4 cores perpendicular to each other, resulting in 5–14 individual measurements for each SRC (Supplementary data Table S1). The cores were extracted from the trunk at the height of 40 cm above the root collar. This position was well above the graft union and well below the first branching point to minimize potential irregularities in ring growth due to graft-related swelling or branch insertion. The cores were air-dried, glued to a wooden support and gradually sanded until all tree rings were clearly observable under a stereoscope. The tree rings were counted and their widths were measured with a 0.01 mm accuracy using the dendrochronological TimeTable measuring device connected with the PAST4 software (VIAS, 2005). The increment curves from each tree were cross-dated using the skeleton plot technique and graphical and statistical tools in PAST4 to identify and correct possible false or missing rings. The cross-dating accuracy was checked using Cofecha (Holmes, 1994). Mean ring width chronology for each SRC was then calculated by averaging the measurements from all individual trees and cores.

Ring width measurements in branches and roots

Ring width measurements were also conducted in the scaffold branches and large first-order roots to evaluate if annual growth patterns are consistent across other woody parts. These destructive and labour-intense measurements were restricted to four SRCs (J/JTEG, J/JTEH, W/S1 and W/PS). For each of these SRCs, three trees were cut down and their scaffold branches were separated from the trunk with a chain saw. Tree stumps including the adjacent portions of roots were excavated to a distance of 1–1.5 m from the trunk and to a depth of 0.5–1 m using a mechanical digging machine. Discs from the basal portion of scaffold branches and coarse first-order roots were then cut using a 240 mm high quality folding saw. Two to three discs were taken from each harvested tree, resulting in 8–9 individual measurements for each SRC and organ combination. The discs were air dried and gradually sanded for ring width measurements. The tree ring width measurements and cross-dating followed the procedure described for trunks. Three

to five measurements were performed on each disc. Each measurement was cross-dated against others from the same disc, and the final increment curve was obtained by averaging of all corrected measurements per disc. The ring width data were processed as described for trunks, except that they were truncated to a common period of 2000–2011 due to the lower age of the branches and roots compared with the trunks.

Processing of the ring width and annual yield chronologies

The raw ring width and yield chronologies were truncated to 1995–2011 to match each other and to exclude the period of tree establishment after planting. Both types of chronologies exhibited a strong age-related trend. To emphasize the interannual patterns, the low frequency variation was removed by fitting a 7 year cubic spline with a frequency cut-off of 0.5. Standardized yield indices (YIs) and ring width indices (RWIs) were then calculated by dividing the raw ring width and yield data by the fitted spline (Hacket-Pain *et al.*, 2017). Raw ring width measurements were also converted to the basal area increments (BAI) using the following formula:

$$BAI_t = \pi(r_t^2 - r_{t-1}^2),$$

where r is the radius of the tree in year t (Hacket-Pain *et al.*, 2019). Thus, we obtained three measures of tree's radial growth: (1) raw ring width exhibiting a strong age-related trend; (2) BAI that accounts for the geometric effect of an increasing circumference of cambium as the trees grew larger; and (3) RWI highlighting a high frequency variation. The processing of chronologies was done using the dplR package in R (Bunn, 2008).

Climate data

Climate data for 1995–2011 were obtained from the weather station run by the Czech Hydrometeorological Institute at Holovousy located within 500 m of our experimental site. The data can be accessed at https://bit.ly/3qF6jcQ. To evaluate the potential environmental drivers of interannual yield variation, we analysed monthly mean air temperatures and monthly precipitation sums across years. We also extracted information on the occurrence of the last spring frost event. In addition to the date of the last frost and the minimum recorded temperature, we calculated cumulative growing degree days (cum GDD) on the day of the last frost as a proxy for the vegetation phenology advancement. To calculate the cum GDD, the heat sum was accumulated from 1 January and the standard temperature threshold of 5 °C was used (Vitasse *et al.*, 2018).

Data analysis

When tree-level data were available, correlation between trees/cores (RBAR), expressed population signal (EPS) and signal-to-noise ratio (SNR) was calculated within each SRC. The synchrony of YI and RWI chronologies among individual SRCs was evaluated using mean interseries correlation. Interannual variability of YI and RWI for each SRC was assessed using the coefficient of variation (CV). We classified the years as low or high yield years if the YI fell below or surpassed the long-term mean by 1 s.d. (LaMontagne and Boutin, 2009; Hacket-Pain *et al.*, 2017). The trade-off between yield and radial trunk growth was initially assessed using the Pearson's product–moment correlation. The relationship was evaluated as either yield vs. ring width, yield vs. BAI or YI vs. RWI. To test if tree vigour affects the relationship between reproductive and vegetative growth, we constructed linear models and analysed the model coefficients. First, ring widths (or RWIs) were modelled as a function of yield (or YI) and individual SRC vigour (categorical factor with three levels: low, medium and high) and corresponding interaction terms. Second, we modelled ring width (BAI or RWI) as a function of yield (or YI) separately for each SRC. 'Slope' coefficients and R^2 of these relationships were compared and correlated with TCSA measurements. The 'Slope' coefficient reflects the steepness of the relationship, while R^2 corresponds to the tightness of the relationship.

RESULTS

Variation in fruit yield

The trees started to bear fruits already in the first years after they were transplanted from the nursery. Overall, annual yield increased until the trees reached their full bearing capacity in around 2000 (i.e. 7 years after transplanting). Besides the age-related trends, yield data also showed high year to year variability and SRC-specific patterns (Fig. 1A–D). 'General Leclerc' and 'Jonagold' scions had a strong tendency for alternate bearing with a fairly regular biennial periodicity as indicated by a negative lag–1 autocorrelation, 'Williams' scions exhibited slightly less regular bearing cycles, while 'Rubin' showed the most regular bearing (see AC–1 in Table 1). Within the same scion cultivar, trees grafted on the rootstocks inducing low vigour had lower interannual variability in yields compared with medium and high vigour trees (Table 1).

Despite the high interannual variability and SRC-specific patterns, the mean SRC-level chronologies of YI were highly synchronized with each other (Fig. 1E–H; mean interseries correlation = 0.75). During the studied period (1995–2011), approximately a third of YI data points fell outside the mean ± s.d. threshold indicating substantially low or high YI (Fig. 1E–H). The years 1996, 2000, 2008 and 2009 were identified as high yield years, with the year 2009 being particularly distinct. In contrast, the years 1995, 2002, 2007 and 2011 were low yield years, with the yield in 2011 being close to zero in almost all studied SRCs. Across years (1999–2011), the yield was positively correlated with the flowering intensity ($R = 0.56$, $P < 0.047$, Supplementary data Fig. S1).

Micrometeorological conditions associated with low and high yield

Considering the relatively short length of our time series and the strong endogenous periodicity of annual yields, we focused our analysis of potential micrometeorological

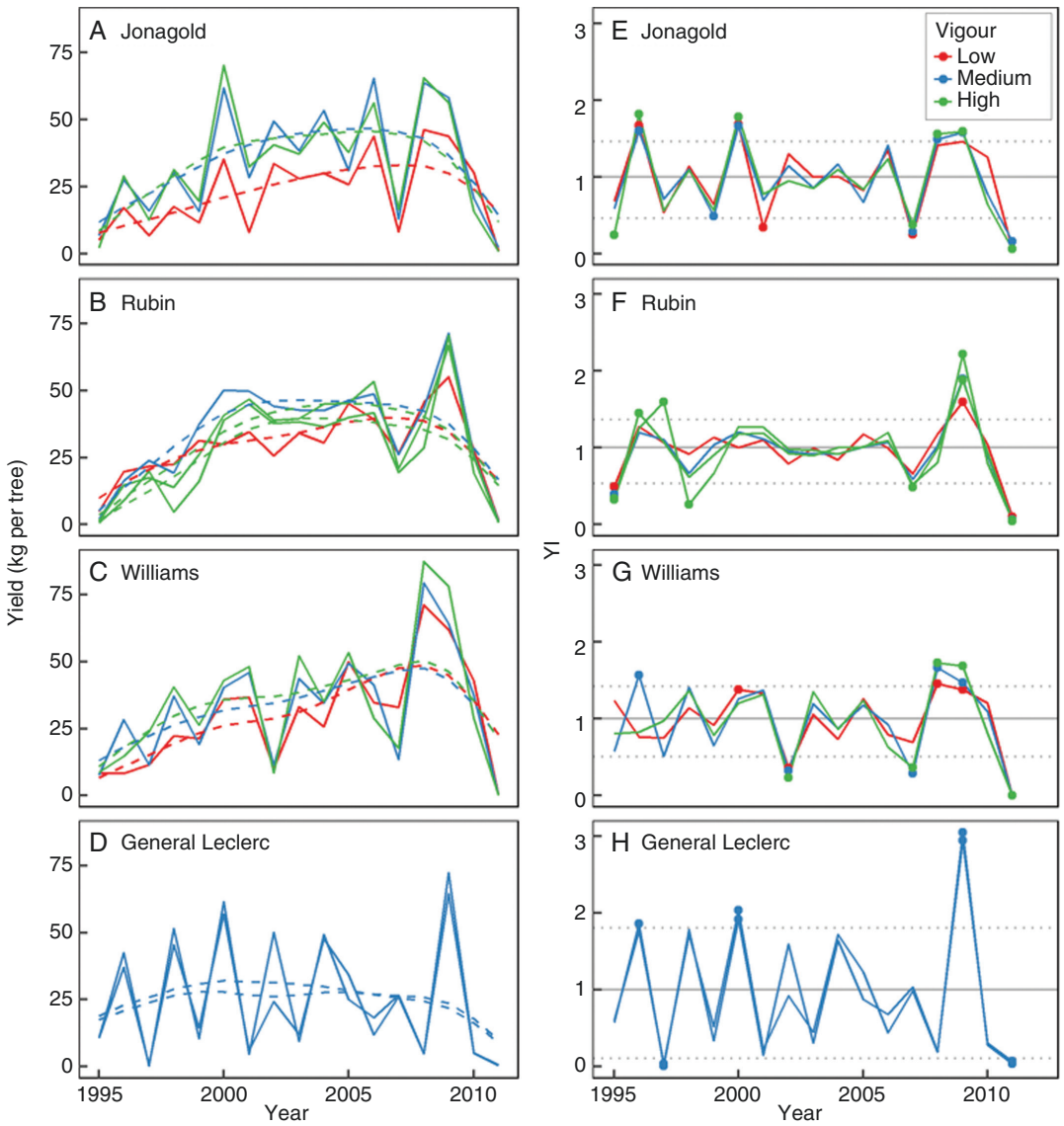

Fig. 1. Chronologies of annual fruit yield parameters in 12 scion–rootstock combinations (SRCs) of *Malus* × *domestica* and *Pyrus communis* with contrasting growth vigour. (A–D) Mean chronologies of annual yield (solid lines) are shown together with the long-term trend fitted to each chronology using the 7 year cubic spline (dashed lines). (E–H) Mean chronologies of standardized yield indices (YIs) are plotted. Horizontal solid and dotted lines correspond to the mean and s.d., respectively (averaged across SRCs within each scion). Years with standardized indices above or below this threshold are highlighted as filled points.

drivers of fruit yield variation on the years with particularly high or low yields and utilized the existing knowledge of factors commonly affecting fruit yields. We found that the year 2009, when yield was particularly high, was characterized by a warm and dry April (Fig. 2A, B). Low yields were associated with the occurrence of late spring frost in at least some of the years (Fig. 2C, D). In our conditions, *M.* × *domestica* typically starts flowering between 18 and 29 April (Blažek and Pištěková, 2017), while in *P. communis*, full bloom starts approx. 1–2 weeks earlier (Kožnarová *et al.*, 2011). Daily minimal temperatures below 0 °C were recorded on 15 May 1995 and 4 May 2011. Frost damage was also a likely cause of low yield in 2007 due to a frost event on 21 April in combination with an advanced spring phenology (cum GDD > 200).

Variation in radial growth of trunks, branches and roots

Standard descriptive statistics confirmed that the ring width chronologies of trunks met the general standards for dendrochronological analysis, with strong and common signals prevailing over the individual signal from each core as demonstrated by RBAR and EPS values (Supplementary data Table S1). Correlation between the individual chronologies within each SRC were moderate to high (mean RBAR = 0.628). The mean EPS was 0.882 and the mean SNR was 14.36. The ring width chronologies showed a strong age-related trend, with the widths decreasing as the trees became older (Fig. 3A–D). The differences in ring widths between low and high vigour trees were more pronounced during the early years of growth. Interannual CV was higher in low vigour trees at least in *M.* × *domestica* (Table 1). Based on the mean ± s.d. threshold, years 1997, 2001,

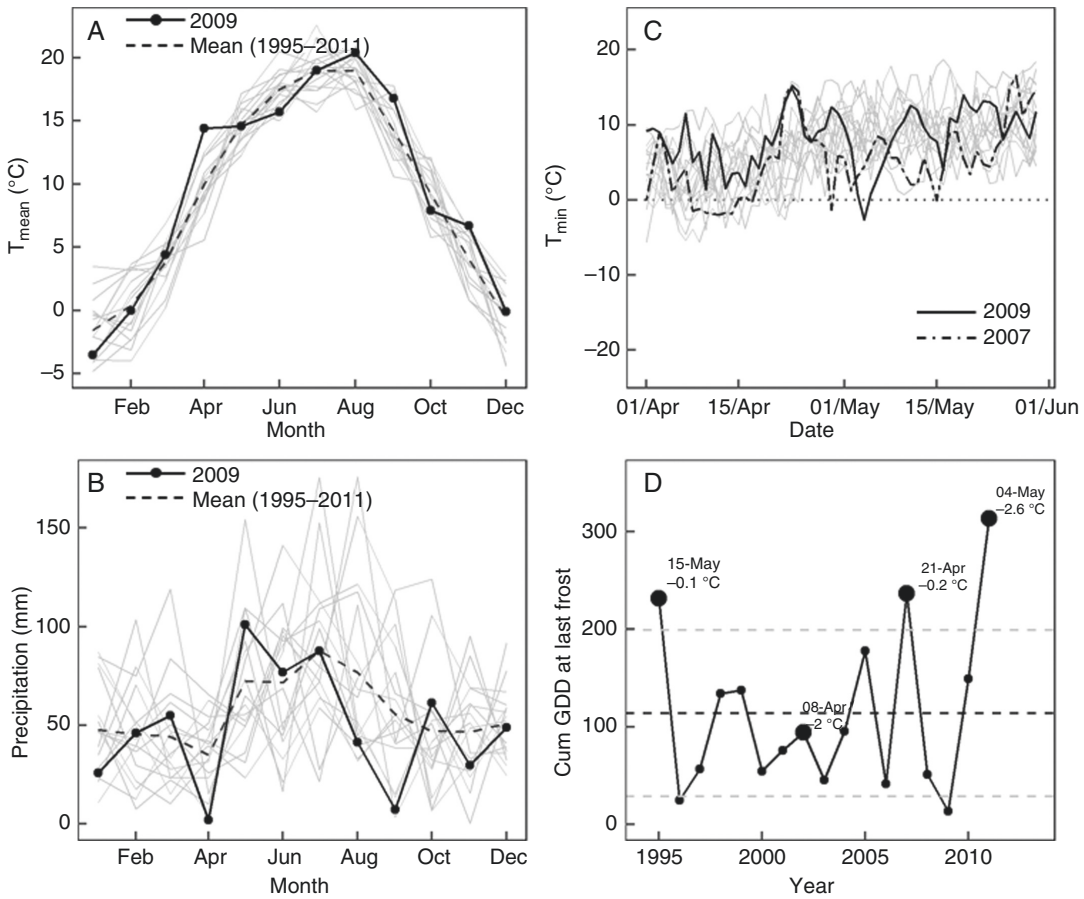

FIG. 2. Micrometeorological characteristics in years with exceptionally high and low annual yields. (A, B) Monthly mean temperature and mean precipitation in years 1995–2011 (grey lines) and the long-term (1995–2011) mean (dashed line). High yield year 2009 is highlighted by a solid black line and shows that this year was characterized by a warm and dry April. (C) The incidence of late spring frost in the second half of May was detected in years 2007 and 2011 when the annual yields were low. All individual years 1995–2011 are plotted as grey lines; years 2007 and 2011 are highlighted in black. The dotted horizontal line corresponds to the freezing point at 0 °C. (D) High values of cumulative growing degree days (cum GDD) at the date of the last frost were observed in three (i.e. 1995, 2007 and 2011) out of the four years that were classified as the low yield years. Horizontal dashed lines correspond to mean ± s.d.

2007 and 2011 were classified as high growth years, while in years 1998, 2000, 2008, 2009 and 2010 the trunk radial increments were low (Fig. 3E–H). The mean RWI chronologies were synchronized across SRCs except for both 'General Leclerc' chronologies. After excluding them, the mean interseries correlation for the remaining ten chronologies was 0.70.

The radial growth patterns of trunks were broadly coherent with those observed in branches and roots (Fig. 4; Supplementary data Fig. S2). For instance, corresponding RWI peaks in low yield years 2007 and 2011 were apparent particularly in the branches of 'Williams', to a lesser extent in the branches of 'Jonagold', and also in some individual root chronologies (Fig. 4). Nevertheless, the ring width measurements for branches and roots were quite variable, and the dendrochronological statistics indicated they did not meet the common standards for a reliable chronology reconstruction (Supplementary data Table S2).

Trade-off between fruit yield and trunk radial growth

Across all SRCs and years, fruit yield was negatively correlated with trunk radial growth, whether evaluated either as yield vs. ring width ($R = –0.48$, $P < 10^{–4}$, Table 2) or as YI vs. RWI ($R = –0.64$, $P < 10^{–4}$, Table 2). The correlation between yield vs. BAI was non-significant ($P = 0.602$, Table 2). The relationship between reproductive and vegetative growth was affected by tree vigour (Fig. 5; Table 2). For yield vs. ring width and yield vs. BAI relationships, the vigour categories had different intercepts (Fig. 5A, B; Supplementary data Fig. S3). For the YI vs. RWI relationship, the regression slope ('Slope') was steeper for low vigour trees, suggesting that a unit change in YI was associated with a greater relative change in RWI in these trees (Fig. 5C). Across SRCs, growth vigour assessed as TCSA in 2011 was closely correlated with both 'Slope' and R^2 (Fig. 6; Supplementary data Fig. S4). In all SRCs except for R/JTEG, 'Slope' was higher (i.e. less negative) than –1 (Fig. 6A), indicating that a unit change in YI generated a relatively smaller change in RWI. The YI and RWI values obtained during the years with exceptionally low and high yields had large effects on the overall shape of the trade-off relationship (Fig. 7). In 2009, which was a year with an exceptionally high yield, the two trees of 'General Leclerc' had average RWI values despite having very high YI (Fig. 7A). In the following year 2010, most SRCs showed substantially lower RWI than expected

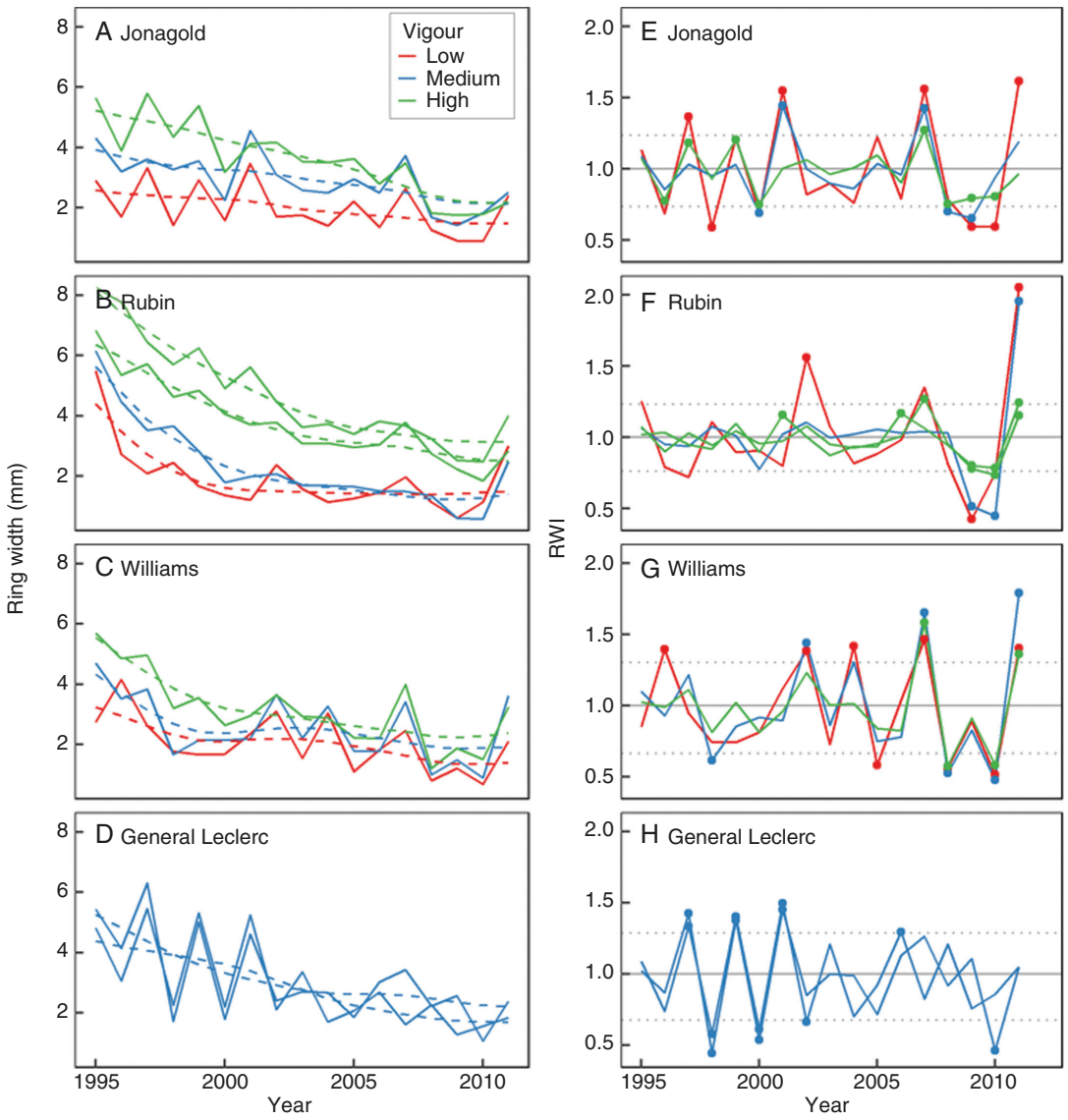

FIG. 3. Chronologies of trunk radial growth parameters in 12 scion–rootstock combinations (SRCs) of *Malus* × *domestica* and *Pyrus communis* with contrasting growth vigour. The facets are arranged vertically by scions. (A–D) Mean chronologies of ring width (solid lines) are shown together with the long-term trend fitted to each chronology using the 7 year cubic spline (dashed lines). (E–H) Mean chronologies of standardized ring width indices (RWIs) are plotted. Horizontal solid and dotted lines correspond to mean and s.d. (averaged across SRCs within each scion). Years with standardized indices above or below this threshold are highlighted as filled points.

considering their current YI, suggesting a lagged effect of overcropping on radial trunk growth (Fig. 7B). In 2011, when all SRCs had very low yields, RWI values were highest in R/JTEG and R/M9, while J/JTEH, GL/MA and GL/MC showed RWI close to the average of 1 (Fig. 7C).

DISCUSSION

In this study, we tested for a negative association between fruit yield and trunk radial growth using four different scion cultivars of apple and pear trees grafted onto a series of size-controlling rootstocks. As we expected, yield and radial growth were generally negatively related (Table 2; Figs 5 and 7; Supplementary data Figs S3 and S4). However, the parameters of these relationships and their interpretation differed depending on the measure of radial growth (ring width, BAI or RWI) and yield (annual yield or YI) used. More specifically, the effect of sink competition became apparent only after the age-related trend was removed by data detrending and normalization. In contrast to the absolute values, RWI and YI highlighted the interannual variability that was related to the endogenous cycles of alternate bearing combined with the variability caused by the extreme meteorological conditions (Fig. 2). The effect of low yield was associated with increased secondary growth not only in trunks but also in branches and roots, although the ring width measurements were more variable in these lateral woody organs (Fig. 4). In trunks, overcropping was associated with reduced secondary growth in the subsequent year, possibly due to the depletion of reserves (Fig. 7).

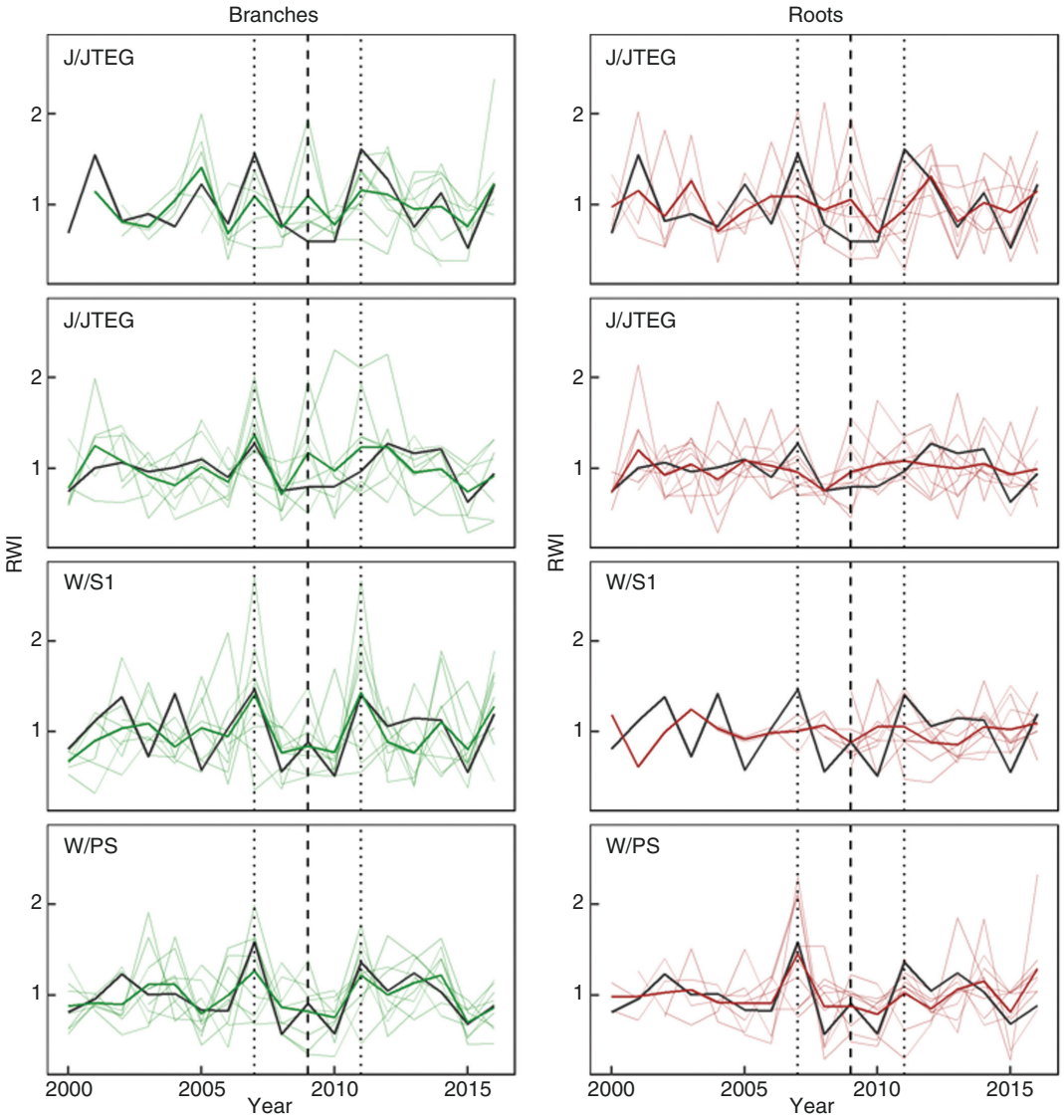

FIG. 4. Indiviudual chronologies (thin lines) and mean organ-level chronologies (thick lines) of standardized ring width indices (RWIs) in scaffold branches (green) and main lateral roots (brown) of four scion–rootstock combinations of contrasting growth vigour (J/JTEG, J/JTEH, W/S1 and W/PS). Mean chronologies for trunks (black thick line) are shown for comparison. Vertical lines indicate pointer years corresponding to the 2007 and 2011 low yield years (dotted vertical lines) and 2009 high yield year (dashed vertical line).

TABLE 2. *Pearson's product–moment correlation coefficients between various measures of yield and trunk radial growth calculated across all measured scion–rootstock combinations and within low, medium and high growth vigour categories*

Correlated variables	All data	Low vigour	Medium vigour	High vigour
Yield vs. ring width	**–0.48**	**–0.74**	**–0.57**	**–0.56**
Yield vs. BAI	–0.037	–0.23	–0.3	0.02
YI vs. RWI	**–0.64**	**–0.85**	**–0.61**	**–0.61**

Significant correlations are highlighted in bold.

The yield chronologies showed large interannual variation (Table 1; Fig. 1) that arose for several reasons. The first layer of variation in yield was an age-related trend, with gradual increases in yield as trees approached their full bearing capacity. The second layer of variation was expressed as an alternate bearing behaviour. The exact nature of this endogenous cycling was scion specific, with some scions or scion/rootstock combinations being more susceptible than others (Table 1; see also Mészáros *et al.*, 2019). The correlation between yield and flower intensity (Supplementary data Fig. S1) indicated that it was the reduction in flower initiation, rather than the variation in fruit set and fruit growth, that was the basis of alternation as is typical in apple trees (Krasniqi *et al.*, 2017). The third layer of yield variation that we explored in this study represents the occurrence of extreme years during which the yield was extraordinarily low or high. We attributed the incidence of such years to meteorological cues. The low yield years were associated with the occurrence of late spring frost (Fig. 2C, D), a condition that presents a major threat

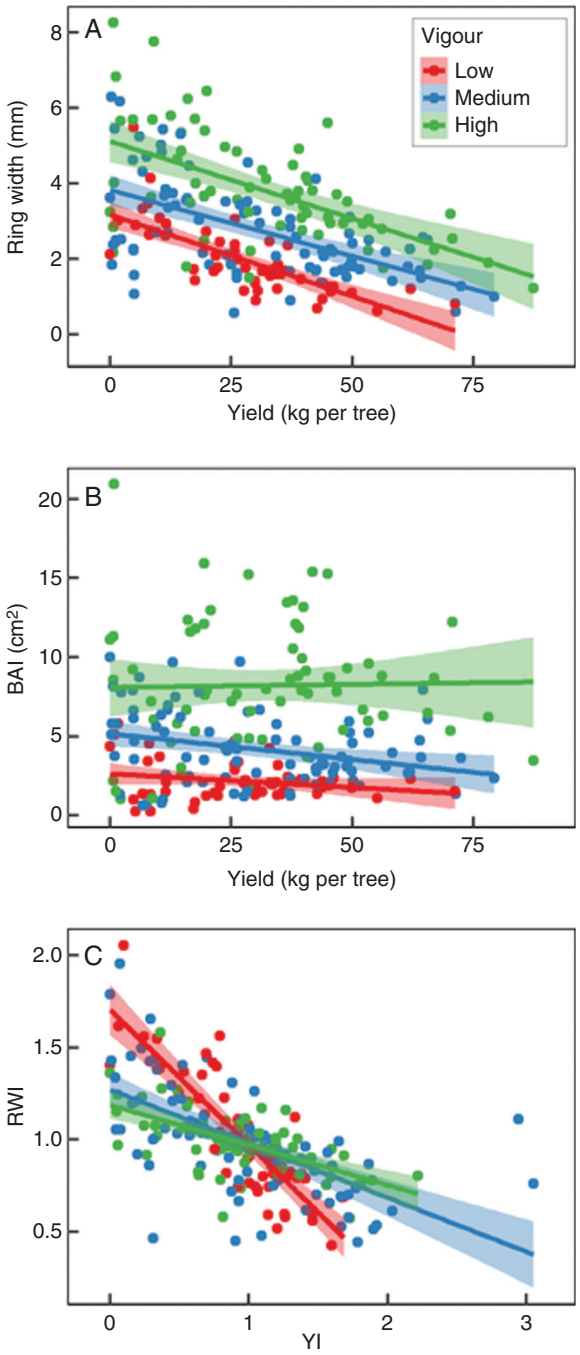

FIG. 5. Relationships between annual yield and trunk radial growth separated for tree vigour categories. Linear regression lines were fitted to (A) yield vs. ring width, (B) yield vs. basal area index (BAI) and (C) YI vs. RWI for low (red), medium (blue) and high (green) vigour trees. Ribbons indicate 95 % confidence intervals.

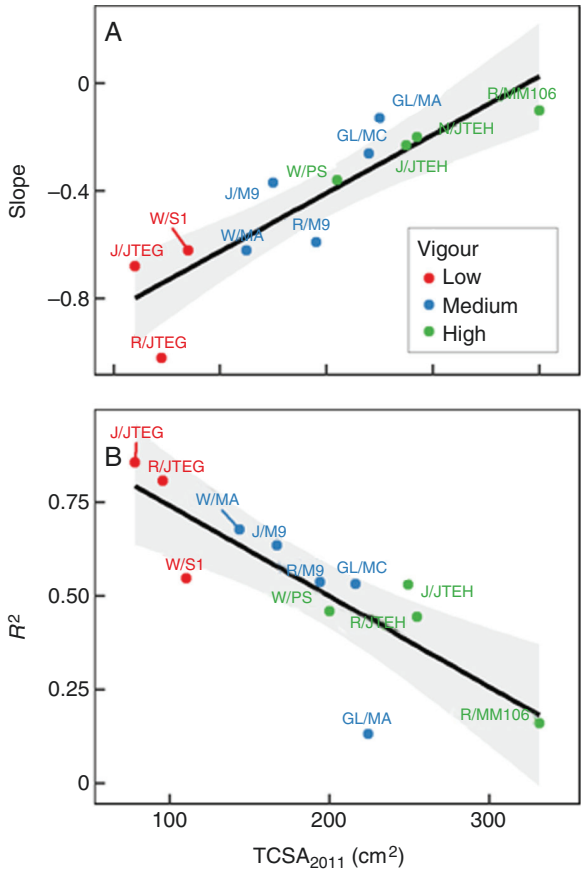

FIG. 6. Correlation between tree growth vigour assessed as trunk cross-sectional area in 2011 ($TCSA_{2011}$) and (A) the slope coefficient (Slope) or (B) the coefficient of determination (R_2) of the linear regressions between YI and RWI fitted to each scion–rootstock combination (SRC). The data points are labelled by scion/rootstock identity and colour coded for vigour category. The solid lines represent linear fits; the shaded areas correspond to 95 % confidence intervals.

to horticultural production in the temperate regions (Rodrigo, 2000). In contrast, the extraordinarily high yield in 2009 was probably related to warm and dry April weather (Fig. 2A, B), which is favourable for pollination and fertilization. Similar patterns, indicating that a warm and dry spring promotes ample fruiting, have been reported for wind-pollinated oaks (Koenig *et al.*, 1996).

Like yield chronologies, tree ring chronologies also showed high interannual variation and strong age-related trends (Fig. 3). When ring width and annual yield values were plotted, the regression lines for low, medium and high vigour trees were all negative and parallel with each other (Fig. 5A). These relationships were dominated by age-related trends and reflected the co-ordination of vegetative and reproductive growth as trees age (Forshey and Elfving, 1989; Costes and Guédon, 2012). The widest rings were produced at young ages because trees first established a sufficient vegetative scaffold to bear and support fruits. The differences in growth vigour between the trees on different size-controlling rootstocks were apparent in their different intercepts, while the slopes were similar (Fig. 5A). This suggests that the developmental co-ordination of vegetative and reproductive growth was not affected by the overall growth vigour, as sometimes may happen during the tree ontogeny (Mészáros *et al.*, 2015). When BAI values were used as a measure of trunk radial growth, the relationships with annual yield appeared as flat lines with minimal slopes (particularly for the high vigour trees). In other words, the BAIs were constant or slowly declining throughout a tree's ontogeny. Compared with ring width, BAI should be more representative of the total biomass investment into the trunk growth. The fact that BAIs were

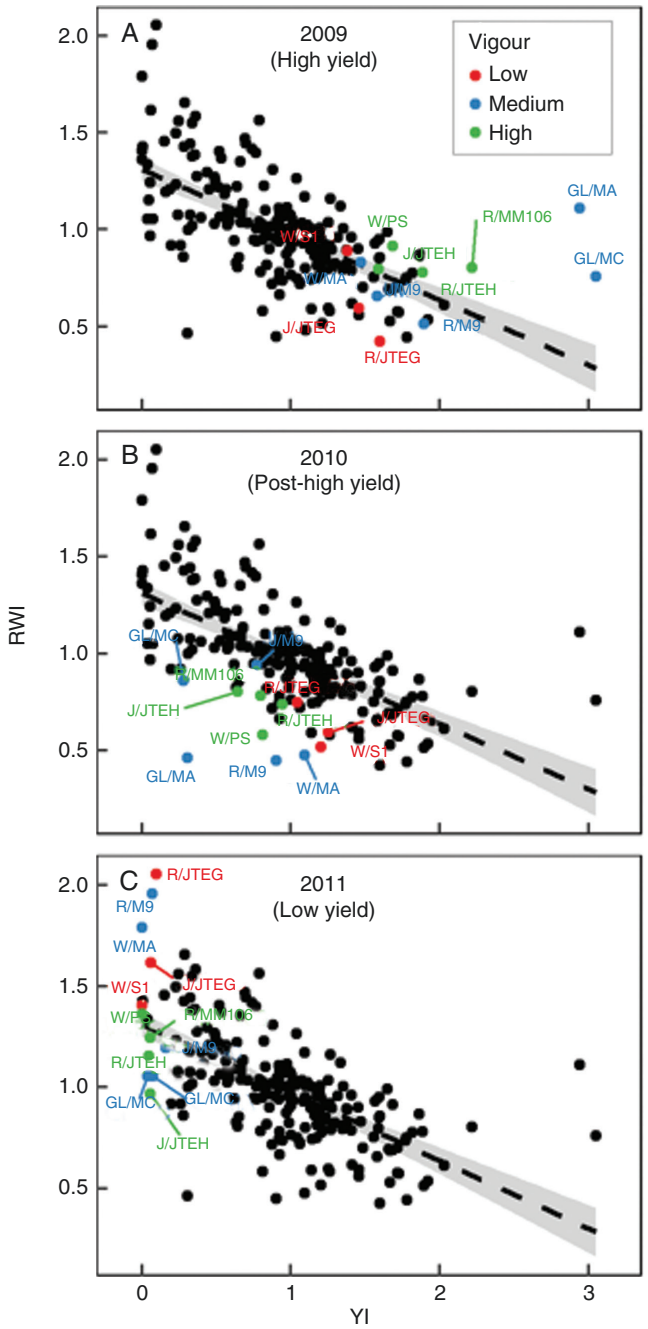

FIG. 7. The overall negative relationships between YI and RWI across all years. Data points corresponding to (A) the high yield year 2009, (B) the post-high yield year 2010 (B) and the low yield year 2011 (C) are highlighted in corresponding panels, colour coded for vigour category and labelled by scion/rootstock identity. The dashed lines represent linear fits; the shaded areas correspond to 95 % confidence intervals.

constant or declined only slowly with tree age suggests that the negative relationship between ring width and yield might not be a true trade-off related to the competition for resources between the two sinks. The observed pattern also suggests that it was the rate of cambial division and/or cell expansion (which affects the number of radial files or the size of the cells) rather than the total cambial production (which affects the overall area/volume of wood produced) that was changed throughout tree ontogeny. This might be indicative of hormonal signalling between reproductive and vegetative organs.

The development of vegetative and generative organs is a very complex process that involves mutual interaction of various hormones, peptides and other growth regulators. Auxins, cytokinins and gibberellins are currently understood as the foremost hormones involved in the endogenous regulation of cambial activity and subsequent expansion and differentiation of cambial derivatives (Milhinhos and Miguel, 2013; Fischer *et al.*, 2019). Other participating hormones, such as abscisic acid (ABA) and ethylene, and their mutual interactions, typically facilitate the developmental responses of vascular tissue to exogenous cues (Liu *et al.*, 2005). All these hormones, and several others, also contribute to fruit development, and their involvement and mutual interactions change during tree ontogeny (Campos-Rivero *et al.*, 2017; Fenn and Giovannoni, 2021; Kou *et al.*, 2021). Specifically, auxin–gibberellin interference appears to be critical during the fruit set and initial development of fruits, while ethylene–ABA cross-talk orchestrates later maturation phases and is decisive for the ripening of climacteric fruits such as apples and pears (Fenn and Giovannoni, 2021; Kou *et al.*, 2021). Thus, auxin–gibberellin and ethylene–ABA interactions would be the most promising candidates for the key signalling mechanisms involved in the co-ordination of vegetative and reproductive growth. Future research could therefore utilize mutants in hormone synthesis and signalling pathways or involve conducting manipulative experiments with exogenous hormone application to shed more light on the mutual co-ordination of fruiting and secondary growth.

In forest ecology literature, the normalized and detrended values of ring width (RWI) are the most commonly used measures of trunk radial growth (e.g. Żywiec and Zielonka, 2013; Hacket-Pain *et al.*, 2017). When we plotted YI and RWI values against each other, low vigour trees had a significantly higher slope than the other two vigour classes (Fig. 5C). The relationships were tighter and stronger than those reported from forest ecology literature. The amount of variation explained by YI was 41 %, which is substantially higher than in European beech (Hacket-Pain *et al.*, 2017) or Norway spruce (Hacket-Pain *et al.*, 2019). Across the 12 SRCs, there was a close correlation between tree vigour expressed as TCSA and both 'Slope' and R^2 of the YI to RWI relationship (Fig. 6). This result agrees with our expectations and suggests that the negative coupling between vegetative and reproductive growth was stronger and tighter in trees on the dwarfing rootstocks. Fruit represents a stronger sink in dwarfed trees compared with invigorated trees, as also indicated by their higher yield efficiencies (Table 1; Massai *et al.*, 2008). If the fruit sinks are missing due to the crop failure (e.g. due to frost damage), then resources could be diverted to wood growth. The analysis of YI and RWI relationships also revealed a potential carry-over effect from 2009 to 2010 (Fig. 7). It is likely that overcropping in 2009 depleted reserves of trees, leading to lower trunk radial growth in the following year. Alternatively, it is possible that other factors such as drought negatively affected trunk radial growth beyond the effect of cropping (Jupa *et al.*, 2022).

To test if wood growth also responds to yield variation in woody organs other than trunks, we measured ring widths in coarse woody branches and roots. In theory, the response to heavy fruiting should be greatest in branches because they

are closer to strong fruit sinks and are considered to be rather autonomous with regards to their carbon needs (Sprugel *et al.*, 1991; Obeso, 1997). Reduction in growth could also be expected in the radial growth of woody roots as those organs are involved in storage, which has been ranked as a sink with low priority (Wardlaw, 1990). In branches and roots, we found high RWI in the low yield years 2007 and 2011 (Fig. 4; Supplementary data Fig. S2). This result would again point to the competition between fruit and wood growth and to the fact that this competition occurs in all perennial woody organs of the tree. In contrast to crop failure, overcropping in 2009 was not associated with a particularly strong reduction in secondary growth (Fig. 4). Thus, it seems that secondary growth was maintained in those organs to support fruits with water and nutrients. However, these conclusions should be viewed with caution considering the great variability of the ring width chronologies among the individual branches and roots (Fig. 4; Supplementary data Table S2). The greater variability is likely to be associated with the different architectural position and mechanical loading of the branches, variable environmental conditions within the canopy, and the effect of pruning or the alternations in bearing among branches (Forshey and Elfving, 1989; Negrón *et al.*, 2014*a*, *b*).

The results of this study are also relevant for our understanding of rootstock-induced size-controlling mechanisms. It has been proposed that the perturbation of competition for carbon between vegetative and reproductive organs could be one mechanism contributing to the size-controlling mechanism of rootstocks (Basile and DeJong, 2018). Dwarfing rootstocks are known to exhibit precocious bearing (Webster, 1995; Knäbel *et al.*, 2015). Because fruits are strong sinks, the resources are preferentially diverted to fruits, which results in decreased overall vegetative growth which can be further perpetuated by associated changes in tree architecture, e.g. reduced number of axes per tree, more spurs per shoot length or higher floral bud density (Costes and García-Villanueva, 2007; Seleznyova *et al.*, 2008). Trees on dwarfing rootstocks have also been shown to accumulate relatively more biomass compared with their counterparts grown on invigorated rootstocks following fruit or flower bud removal treatments (Avery, 1970). In our trees, we did not observe differences in the precocity of cropping among trees on different rootstocks (Fig. 1). The cumulative fruit production was higher in high vigour trees due to their greater size, but the yield efficiency was greater in low vigour trees (Table 1). The developmental co-ordination of vegetative and reproductive growth was similar across vigour classes (Fig. 5A, B). We found that high fruit crop was associated with a greater reduction in trunk radial growth in low vigour trees; however, this reduction was compensated by the increased growth during low crop years (Fig. 5C). Taken together, our results indicate that fruits are generally stronger sinks in low vigour trees but the relative partitioning between fruit and trunk growth remains constant over the tree's lifetime, possibly because co-ordinated changes in canopy size and/or photosynthetic performance modulate resource availability to match growth demands. The mechanistic basis of the greater sink strength of fruits on dwarfing rootstocks remains to be elucidated.

Our study provides an unconventional perspective on the relationship between the reproductive and vegetative growth in commercially important fruit trees and bridges the gap between forest ecology and horticultural literature. The smaller tree stature and easier accessibility of fruits in horticultural plantings allowed for a more precise assessment of fruit output. We demonstrated that the use of tree ring chronologies is feasible in fruit trees and provides useful insights into the long-term growth dynamics and developmental co-ordination of vegetative and reproductive growth. On the other hand, our chronologies were relatively short compared with the time series commonly collected from the forest trees, which made, for example, correlations with climate variables difficult. In future studies, it would be interesting to count and weigh fruits at the individual tree level, to evaluate the developmental step that limits the final fruit crop (e.g. if it is determined at the stage of flower initiation, fruit set or fruit growth) and to monitor the canopy size and architecture as trees grow older. In addition, it would be advisable to perform experimental manipulations such as defruiting, defoliation, girdling or application of growth regulators, and to utilize various cultivars and mutants of known genetic background to provide a more detailed assessment of physiological mechanisms of growth co-ordination and sink–source relationships. We hope that our study will stimulate further cross-fertilization of ideas and approaches between horticulture and forest ecology as also advocated for in a recent commentary by Ryan *et al.* (2018) and demonstrated in a recent study by Garcia *et al.* (2021).

SUPPLEMENTARY DATA

Supplementary data are available online at https://academic.oup.com/aob and consist of the following. Table S1: ring width chronology statistics for individual scion–rootstock combinations. Table S2: ring width chronology statistics for branches, roots and trunks in four selected scion–rootstock combinations. Figure S1: correlation between flowering intensity and mean annual fruit yield avearged across all scion–rootsock combinations. Figure S2: correlations of ring width indices among trunk, scaffold branches and roots. Figure S3: relationships between yield and basal area increment fitted individually for each scion–rootstock combination. Figure S4: relationships between YI and RWI fitted individually for each scion–rootstock combination.

ACKNOWLEDGEMENTS

We thank J. Toman, M. Nalezinková and J. Fenclová for field and laboratory assistance. We thank four anonymous reviewers for their thoughtful suggestions that improved the manuscript.

FUNDING

This work was supported by Czech Science Foundation, Grant/Award no. 18-19722Y and Institutional support by the Ministry of Agriculture of the Czech Republic (MZE-RO1518).

LITERATURE CITED

Atkinson CJ, **Else MA. 2003**. Enhancing harvest index in temperate fruit tree crops through the use of dwarfing rootstocks. Proceedings of the International workshop on Cocoa Breeding for Improved Production Systems, 118–131.

Avery DJ. 1970. Effects of fruiting on the growth of apple trees on four rootstock varieties. *New Phytologist* **69**: 19–30. doi: 10.1111/j.1469-8137.1970.tb04045.x

Basile B, **DeJong TM. 2018**. Control of fruit tree vigor induced by dwarfing rootstocks. *Horticultural Reviews* **46**: 39–97.

Blažek J, **Pištěková I. 2017**. Prediction of the harvesting time for four apple cultivars on the basis of beginning of flowering and attaining of T-stage of fruitlets and dependence of diameter of fruitlets at T-stage and fruits at ripening stage. *Journal of Horticultural Research* **25**: 55–59.

Bunn AG. 2008. A dendrochronology program library in R (dplR). *Dendrochronologia* **26**: 115–124. doi: 10.1016/j.dendro.2008.01.002

Campos-Rivero G, **Osorio-Montalvo P**, **Sánchez-Borges R**, ***et al.* 2017**. Plant hormone signaling in flowering: an epigenetic point of view. *Journal of Plant Physiology* **214**: 16–27. doi: 10.1016/j.jplph.2017.03.018

Costes E, **García-Villanueva E. 2007**. Clarifying the effects of dwarfing rootstock on vegetative and reproductive growth during tree development: a study on apple trees. *Annals of Botany* **100**: 347–357.

Costes E, **Guédon Y. 2012**. Deciphering the ontogeny of a sympodial tree. *Trees* **26**: 865–879.

Drobyshev I, **Övergaard R**, **Saygin I**, ***et al.* 2010**. Masting behaviour and dendrochronology of European beech (*Fagus sylvatica* L.) in southern Sweden. *Forest Ecology and Management* **259**: 2160–2171.

Fenn MA, **Giovannoni JJ. 2021**. Phytohormones in fruit development and maturation. *The Plant Journal* **105**: 446–458.

Fischer G, **Almanza-Merchán PJ**, **Ramírez F. 2013**. Source–sink relationships in fruit species: a review. *Revista Colombiana de Ciencias Hortícolas* **6**: 238–253.

Fischer U, **Kucukoglu M**, **Helariutta Y**, **Bhalerao R. 2019**. The dynamics of cambial stem cell activity. *Annual Review of Plant Biology* **70**: 293–319.

Forshey CG, **Elfving DC. 1989**. The relationship between vegetative growth and fruiting in apple trees. *Horticultural Reviews* **11**: 229–287.

Garcia H, **Re B**, **Orians C**, **Crone E. 2021**. By wind or wing: pollination syndromes and alternate bearing in horticultural systems. *Philosophical Transactions of Royal Society B: Biological Sciences* **376**: 20200371.

Hacket-Pain AJ, **Friend AD**, **Lageard JGA**, **Thomas PA. 2015**. The influence of masting phenomenon on growth–climate relationships in trees: explaining the influence of previous summers' climate on ring width. *Tree Physiology* **35**: 319–330.

Hacket-Pain AJ, **Lageard JGA**, **Thomas PA. 2017**. Drought and reproductive effort interact to control growth of a temperate broadleaved tree species (*Fagus sylvatica*). *Tree Physiology* **37**: 744–754.

Hacket-Pain AJ, **Ascoli D**, **Vacchiano G**, ***et al.* 2018**. Climatically controlled reproduction drives interannual growth variability in a temperate tree species. *Ecology Letters* **21**: 1833–1844.

Hacket-Pain AJ, **Ascoli D**, **Berretti R**, ***et al.* 2019**. Temperature and masting control Norway spruce growth, but with high individual tree variability. *Forest Ecology and Management* **438**: 142–150.

Hay R. 1995. Harvest index: a review of its use in plant breeding and crop physiology. *Annals of Applied Biology* **126**: 197–216.

Holmes R. 1994. *Dendrochronology Program Library – user manual*. Tucson, AZ: Laboratory of Tree-Ring Research.

Jupa R, **Mészáros M**, **Plavcová L. 2021**. Linking wood anatomy with growth vigour and susceptibility to alternate bearing in composite apple and pear trees. *Plant Biology* **23**: 172–183.

Jupa R, **Mészáros M**, **Hoch G**, **Plavcová L. 2022**. Trunk radial growth, water and carbon relations of mature apple trees on size-controlling rootstocks during severe summer drought. *Tree Physiology* **42**: 289–303.Ju

Knäbel M, **Friend AP**, **Palmer JW**, ***et al.* 2015**. Genetic control of pear rootstock-induced dwarfing and precocity is linked to a chromosomal region syntenic to the apple Dw1 loci. *BMC Plant Biology* **15**: 1–16.

Koenig W, **Knops J**, **Carmen W**, **Stanback M**, **Mumme R. 1996**. Acorn production by oaks in central coastal California: influence of weather at three levels. *Canadian Journal of Forest Research* **26**: 1677–1683.

Kosina J. 2010. Effect of dwarfing and semi dwarfing apple rootstocks on growth and productivity of selected apple cultivars. *Horticultural Science* **37**: 121–126.

Kou X, **Feng Y**, **Yuan S**, ***et al.* 2021**. Different regulatory mechanisms of plant hormones in the ripening of climacteric and non-climacteric fruits: a review. *Plant Molecular Biology* **107**: 477–497.

Kožnarová V, **Sulovská S**, **Hájková L. 2011**. Časová variabilita nástupu fenofází ovocných dřevin sledovaných ve fenologické síti ČHMÚ za období 1991–2010 ve vztahu k synoptickým situacím. *Úroda* **59**: 285–295. .

Krasniqi A, **Blanke M**, **Kunz A**, **Damerow L**, **Lakso A**, **Meland M. 2017**. Alternate bearing in fruit tree crops: past, present and future. *Acta Horticulturae* **1177**: 241–248.

LaMontagne JM, **Boutin S. 2009**. Quantitative methods for defining mast-seeding years across species and studies. *Journal of Vegetation Science* **20**: 745–753.

Lauri PÉ, **Kelner JJ**, **Trottier C**, **Costes E. 2010**. Insights into secondary growth in perennial plants: its unequal spatial and temporal dynamics in the apple (*Malus domestica*) is driven by architectural position and fruit load. *Annals of Botany* **105**: 607–616.

Lehnebach R, **Beyer R**, **Letort V**, **Heuret P. 2018**. The pipe model theory half a century on: a review. *Annals of Botany* **121**: 773–795.

Liu F, **Jensen CR**, **Andersen MN. 2005**. A review of drought adaptation in crop plants: changes in vegetative and reproductive physiology induced by ABA-based chemical signals. *Australian Journal of Agricultural Research* **56**: 1245–1252.

Massai R, **Loreti F**, **Fei C. 2008**. Growth and yield of 'Conference' pears grafted on quince and pear rootstocks. *Acta Horticulturae*orticultuae **800**: 617–624.

Mészáros M, **Kosina J**, **Laňar L**, **Náměstek J. 2013**. Hodnocení pěstitelských vlastností čtyř odrůd hrušní na vybraných podnožích. *Vědecké práce ovocnářské* **23**: 179–188.

Mészáros M, **Kosina J**, **Laňar L**, **Náměstek J. 2015**. Long-term evaluation of growth and yield of Stanley and Cacanska lepotica plum cultivars on selected rootstocks. *Horticultural Science* **42**: 22–28.

Mészáros M, **Laňar L**, **Kosina J**, **Náměstek J. 2019**. Aspects influencing the rootstock–scion performance during long term evaluation in pear orchard. *Horticultural Science* **46**: 1–8.

Milhinhos A, **Miguel CM. 2013**. Hormone interactions in xylem development: a matter of signals. *Plant Cell Reports* **32**: 867–883.

Monks A, **Kelly D. 2006**. Testing the resource-matching hypothesis in the mast seeding tree *Nothofagus truncata* (Fagaceae). *Austral Ecology* **31**: 366–375.

Mund M, **Herbst M**, **Knohl A**, ***et al.* 2020**. It is not just a 'trade-off': indications for sink- and source-limitation to vegetative and re-generative growth in an old-growth beech forest. *New Phytologist* **226**:111–125.

Negrón C, **Contador L**, **Lampinen BD**, ***et al.* 2014a**. Differences in proleptic and epicormic shoot structures in relation to water deficit and growth rate in almond trees (*Prunus dulcis*). *Annals of Botany* **113**: 545–554.

Negrón C, **Contador L**, **Lampinen BD**, ***et al.* 2014b**. How different pruning severities alter shoot structure: a modelling approach in young 'Nonpareil' almond trees. *Functional Plant Biology* **42**: 325–335.

Obeso JR. 1997. Costs of reproduction in *Ilex aquifolium*: effects at tree, branch and leaf levels. *Journal of Ecology* **85**, 159–166.

Poorter H, **Niklas KJ**, **Reich PB**, **Oleksyn J**, **Poot P**, **Mommer L. 2012**. Biomass allocation to leaves, stems and roots: meta-analyses of interspecific variation and environmental control: Tansley review. *New Phytologist* **193**: 30–50.

Rodrigo J. 2000. Spring frosts in deciduous fruit trees – morphological damage and flower hardiness. *Scientia Horticulturae* **85**: 155–173.

Rosati A, **Paoletti A**, **Al Hariri R**, **Famiani F. 2018a**. Fruit production and branching density affect shoot and whole-tree wood to leaf biomass ratio in olive. *Tree Physiology* **38**: 1278–1285.

Rosati A, **Paoletti A**, **Al Hariri R**, **Morelli A**, **Famiani F. 2018b**. Resource investments in reproductive growth proportionately limit investments in whole-tree vegetative growth in young olive trees with varying crop loads. *Tree Physiology* **38**: 1267–1277.

Ryan MG, **Oren R**, **Waring RH. 2018**. Fruiting and sink competition. *Tree Physiology* **38**: 1261–1266.

Sala A, **Hopping K**, **McIntire EJB**, **Delzon S**, **Crone EE. 2012**. Masting in whitebark pine (*Pinus albicaulis*) depletes stored nutrients. *New Phytologist* **196**: 189–199.

Seleznyova AN, **Tustin DS**, **Thorp TG. 2008**. Apple dwarfing rootstocks and interstocks affect the type of growth units produced during the annual growth cycle: precocious transition to flowering affects the composition and vigour of annual shoots. *Annals of Botany* **101**: 679–687.

Sinclair TR. 1998. Historical changes in harvest index and crop nitrogen accumulation. *Crop Science* **38**: 638–643.

Spicer R, **Groover A. 2010**. Evolution of development of vascular cambia and secondary growth. *New Phytologist* **186**: 577–592.

Sprugel DG, **Hinckley TM**, **Schaap W. 1991**. The theory and practice of branch autonomy. *Annual Review of Ecology and Systematics* **22**: 309–334.

Stevenson MT, **Shackel KL. 1998**. Alternate bearing in pistachio as a masting phenomenon: constructuion cost of reporduction versus vegetative growth and storage. *Journal of the American Society for Horticultural Science* **123**: 1069–1075.

VIAS. 2005. *Time Table. Installation and instruction manual. Ver. 2.1*. Vienna: Vienna Institute of Archaeological Science.

Vitasse Y, **Schneider L**, **Rixen C**, **Christen D**, **Rebetez M. 2018**. Increase in the risk of exposure of forest and fruit trees to spring frosts at higher elevations in Switzerland over the last four decades. *Agricultural and Forest Meteorology* **248**: 60–69.

Wardlaw IF. 1990. Tansley Review No. 27 The control of carbon partitioning in plants. *New Phytologist* **116**: 341–381.

Webster AD. 1995. Rootstock and interstock effects on deciduous fruit tree vigour, precocity, and yield productivity. *New Zealand Journal of Crop and Horticultural Science* **23**: 373–382.

Żywiec M, **Zielonka T. 2013**. Does a heavy fruit crop reduce the tree ring increment? Results from a 12-year study in a subalpine zone. *Trees* **27**: 1365–1373.

Journal of Plant Growth Regulation
https://doi.org/10.1007/s00344-023-11052-6

Whole-Tree Storage of Non-structural Carbohydrates in Apple and Pear Trees on Size-Controlling Rootstocks

Plavcová Lenka[1] · Jupa Radek[1,4] · Mészáros Martin[2] · Hoch Günter[3]

Received: 28 October 2022 / Accepted: 26 May 2023

Abstract

Size-controlling rootstocks have been one of the major innovations facilitating high-efficiency fruit production; however, biological mechanisms responsible for their size-controlling effect remain unclear. In this study we investigated if apple and pear trees grafted on dwarfing and invigorating rootstocks differ in the size and dynamics of non-structural carbohydrate (NSC) storage pools. Seasonal dynamics in NSC concentrations were assessed in current-year shoots, coarse roots, trunks, and leaves. These measurements were then upscaled to whole-organ and whole-tree NSC pools and mutually compared. Because of the small variation in the relative biomass partitioning and generally similar organ-level NSC concentrations, the size of the NSC pools scaled tightly with the overall tree biomass with vigorous trees having greater absolute storage pools compared to dwarfing trees. The magnitudes of the seasonal fluctuation in NSC pools (i.e., November to May difference) were in the range from 0.55 to 3.93 kg per tree and 20 to 50 g per kg of tree's dry weight. In absolute terms, the seasonal fluctuations in NSC pools were higher in vigorously growing trees but in relative terms and also when scaled by the tree's biomass the differences between the low and high vigor trees became negligible, suggesting that the low and high vigor trees rely on their NSC reserves to a similar extent during their annual growth cycle. Thus, our results provide no support that the observed differences in growth vigor are driven by the availability of C-reserves.

Keywords Fruit trees · Reserves · Seasonal dynamics · Starch · Storage pools · Sugars · Wood

Introduction

The use of size-controlling rootstocks is one of the major innovations in modern horticulture contributing greatly to the increased efficiency of fruit production (Atkinson and Else 2003). While the exact biological mechanisms responsible for the size-controlling effect remain unclear, one hypothesis asserts that the dwarfing phenomena of some rootstocks might be related to their lower ability to store and/or mobilize carbohydrates (Basile and DeJong 2018). However, this potential mechanism of vigor control has not been extensively studied and is largely based on indirect evidence related to the differential growth seasonality, root anatomy, and stomatal conductance of dwarfing compared to invigorating rootstocks (Basile and DeJong 2018).

Non-structural carbohydrates (NSC) are the main carbon (C) storage resources in trees and their concentration in organs or tissues is often considered as an indicator of C balance (Körner 2003; Sala et al. 2012; Hoch 2015). Direct measurements of NSC concentrations in fruit trees on size-controlling rootstocks are scarce and the observed patterns are variable. Weibel et al. (2008) measured dormant season carbohydrate reserves in peach trees on six different size-controlling rootstocks and found the highest concentrations in the most vigorous rootstocks. In contrast, Foster et al. (2017) studied two dwarfing and one vigorous apple rootstocks and found that the dwarfing rootstocks accumulated

Handling Editor: Naeem Khan.

✉ Plavcová Lenka
lenka.plavcova@uhk.cz

[1] Department of Biology, Faculty of Science, University of Hradec Králové, Rokitanského 62, Hradec Králové CZ-500 03, Czech Republic

[2] Department of Technology, Research and Breeding Institute of Pomology, Holovousy 123, Hořice 508 01, Czech Republic

[3] Department of Environmental Sciences – Botany, University of Basel, Schönbeinstrasse 6, 4056 Basel, Switzerland

[4] Present Address: Department of Experimental Biology, Faculty of Science, Masaryk University, Kamenice 5, Brno CZ-625 00, Czech Republic

Published online: 08 June 2023

large amounts of starch, whereas their concentrations of soluble sugars were very low. Based on these observations they suggested that the dwarfing rootstocks behave as "super accumulators" that hold high starch reserves at the expense of vegetative growth. Olmstead et al. (2010) measured carbohydrate profiles in the graft union and adjacent rootstock and scion tissue in sweet cherry. They found that the starch concentrations were not consistently lower or higher in dwarfed vs. vigorous trees, but rather showed distinct seasonal patterns, leading to the suggestion that the NSC reserve accumulation and mobilization were perturbed by the higher resistance to NSC translocation at the graft union.

Measurements of NSC concentrations in plant organs and tissues provide a useful but incomplete assessment of carbohydrate reserves because the magnitude of NSC reserves depends on tree size and biomass partitioning between the different organs (Furze et al. 2019; Schoonmaker et al. 2021; Fermaniuk et al. 2021). Therefore, studies scaling-up NSC concentrations to the overall size of NSC pools allow for more meaningful quantitative considerations with respect to the tree's productivity (Bustan et al. 2011), ecological strategy (Barbaroux et al. 2003; Schoonmaker et al. 2021), or adaptation to climate (Fermaniuk et al. 2021). In addition, these studies help to assess the relative importance of different organs for storage. While roots are often believed to be the primary site for storage in trees (Loescher et al. 1990), the measurements of the whole-plant NSC pools highlighted the importance of above-ground stem and branch sapwood for C storage, mainly because of their large fraction within the total tree biomass (Bustan et al. 2011; Furze et al. 2019; Fermaniuk et al. 2021).

The whole-tree NSC pool and its dynamics are particularly important for understanding growth of dwarfed vs. invigorated trees because of their implicit difference in size. In addition, trees on size-controlling rootstocks may also differ in the relative biomass partitioning among their various organs. For instance, high relative proportions of roots, which are likely to contain high concentrations of carbohydrates, can make for a substantial contribution to the overall NSC budget. Similarly, greater allocation of biomass to leaves might be associated with higher photosynthetic gain which is the ultimate source of NSC. As in case of the measurements of NSC concentrations, biomass partitioning in trees on size-controlling rootstocks is currently poorly documented especially for large field-grown trees. Greater relative biomass allocation to roots has been found in peach trees on dwarfing rootstocks, likely as a compensation for the greater hydraulic resistance of their roots (Solari et al. 2006). In contrast, Tworkoski et al. (2016) reported greater relative biomass allocation to roots compared to leaves in vigorously growing apple trees grafted on MM.111 rootstock compared to the trees on semi-dwarfing M.9 rootstock. Vigorous apple trees on MM.106 rootstock also had fewer leaves per unit sapwood compared to trees on semi-dwarfing M.9 rootstock. Higher number of leaves per sapwood area resulted in a better water supply-to-water loss ratio in semi-dwarfing trees (Cohen and Naor 2002) but potentially also in a lower photosynthetic gain of those trees. Taken together, the differences in the overall tree size, differential biomass allocation, and NSC concentrations of individual organs or tissues all combine and affect the overall size of the NSC storage pool.

Another issue is if the entire NSC pool of a tree can indeed be remobilized and used as C source for metabolism and growth or if a proportion of NSC remain unused and become sequestered or utilized only in the case of an extreme event, such as severe defoliation or drought (Landhäusser and Lieffers 2012; Carbone et al. 2013; Richardson et al. 2015). Also, the adequacy of storage capacity needs to be evaluated relative to the overall growth. It is possible that dwarfing trees have smaller storage pools, but as they grow less, this capacity might be sufficient (Basile and DeJong 2018). To resolve these issues, quantifying seasonal fluctuations in the whole-tree NSC pool would be insightful, but, to the best of our knowledge, has not been done so far with respect to rootstock-induced control of growth vigor.

Thus, the aim of this study was to evaluate if apple trees on dwarfing rootstocks have lower NSC reserves and/or reduced capacity to mobilize NSC compared to trees on invigorating rootstocks (Basile and DeJong 2018). We address this question in terms of both organ-level NSC concentration as well as the size of the whole-tree NSC pool and its seasonal fluctuation.

Materials and Methods

Plant Material

All measurements were done on 29-year-old trees of *Malus* × *domestica* Borkh. var. 'Jonagold' and 27-year-old trees of *Pyrus communis* L. var. 'Williams' grafted onto rootstocks that induced either low or high growth vigor (Table 1). The low vigor rootstocks were J-TE-G for apple trees and S1 for pear trees. The high vigor rootstocks were J-TE-H for apple trees and pear seedling (PS) for pear trees. The trees were selected from a larger rootstock field trial so that they provided the greatest differences in growth vigor in the two studied species (Jupa et al. 2021). The trees were grown on the experimental fields of the Research and Breeding Institute of Pomology in Holovousy, the Czech Republic (50.37N, 15.57E; 283 m.a.s.l.). The site experiences a temperate climate with a mean annual temperature of 8.4 °C and a mean annual precipitation of 664 mm. The site is on a loamy brown soil (22.2% clay, 69.1% silt, and 8.7% sand) with neutral pH and a medium fertility. The trees

Table 1 Growth and yield characteristics of apple var. 'Jonagold' (J) and pear var. 'Williams' (W) grafted onto rootstocks inducing low (J-TE-G, S1) or high (J-TE-H, pear seedling) growth vigor

Scion	Rootstock	Abbrev	TCSA (cm^2)	Shoot length (cm)	Fruit yield (kg/tree)
Apple var. 'Jonagold'	Apple J-TE-G	J-low	113.9 ± 7.2	41.4 ± 2.3	41.2 ± 5.4
Apple var. 'Jonagold'	Apple J-TE-H	J-high	298.8 ± 10.6	62.2 ± 3.4	83.8 ± 18.3
Pear var. 'Williams'	Quince S1	W-low	159.5 ± 13.2	41.3 ± 2.1	10.9 ± 3
Pear var. 'Williams'	Pear seedling	W-high	277.4 ± 14.3	58.3 ± 3.1	11.3 ± 5.4

Trunk cross-sectional area (TCSA) and shoot length data were taken from Jupa et al. (2021)

Means ± SD ($n = 3$) are reported

were planted with a spacing of 4.5 × 2.3 m and 5.0 × 3.0 m for apple and pear trees, respectively. Trees were trained as freely growing hedgerows with a short stem height with the tip of the central leader being removed in the fifth year. Supplemental fertilization and pest management practices were applied according to local recommendations for commercial orchards. The weed control in 1.5-m-wide strips was maintained by herbicides and grass grown in inter-rows was periodically removed. No irrigation was supplied and no hand or chemical thinning of the fruits was conducted. For the measurements, three healthy individuals for each scion/rootstock combination were used.

Collection of Samples for NSC and Carbon Isotope Analyses

Sample for the NSC analyses were taken from coarse woody roots, trunks, 1-year-old shoots and leaves. The coarse woody roots (5–10 mm in diameter, 10–20 cm in length) were excavated from the soil depth of 15–50 cm and at the distance of 50 cm from the root collar. The trunk cores were extracted at the height of 30–50 cm, which was well above the graft union and well below the insertion of the lowest scaffold branches. A sharp increment borer (Mora Coretax, Switzerland) was used for the coring. The samples taken consisted of the outermost 3 cm of sapwood and the bark. The repeated coring throughout the season was conducted in a spiral fashion around the trunk to minimize the potential influence of the wounding caused by the previous sampling. The 1-year-old proleptic shoots (10–15 mm in diameter and 15–30 cm in length) were cut from a sun-lit part of the crown at the height of 1.5 m and the leaves were stripped from the woody axis. The sampling took place at the following five dates in 2019: 20th March (before bud break), 16th April (at bud break), 17th May (at full bloom), 19th July (at peak summer, approx. two weeks after the termination of shoot extension growth), and 4th November (beginning of winter dormancy). At each date, we collected six roots, six shoots (i.e., two specimens from each individual tree), and one trunk core per each tree. Immediately after the collection, the samples were transported to the laboratory where they were shortly microwaved (30 s at 600 W) to deactivate the NSC-modifying enzymes according to Popp et al. (1996). The samples were then oven dried at 80 °C for 5 days, homogenized using a centrifugal grounding mill (ZM 100, Retsch, Haan, Germany) and sent to the Plant Ecophysiology Laboratory at the University of Basel, Switzerland, for NSC analyses and to Stable Isotope Laboratory at the Crop Research Institute, the Czech Republic for the analysis of carbon isotopes.

NSC Analyses

Concentrations of NSC were analyzed using the enzymatic-photometric method described in Landhäusser et al. (2018). Briefly, low-molecular weight sugars were extracted from the plant powder with 80% ethanol at 90 °C for 10 min, the supernatant was collected, the pellet was washed three more times with ethanol, and the supernatants were mixed. After evaporation of the ethanol and resuspension of the extracts in deionized water, the total amount of glucose was determined photometrically after the enzymatic conversion of fructose and sucrose to glucose in a multiplate photometer (HR 700, Hamilton, Reno, NE, USA) at 340 nm by converting glucose-6-P to gluconate-6-P. To break down the starch in the remaining pellet, the pellet was resuspended in deionized water and first treated with α-amylase (from *Bacillus licheniformis*) for two hours at 85 °C. After centrifugation of the samples, an aliquot of the supernatant was treated with amyloglucosidase (from *Aspergillus niger*) at 55 °C for two hours for complete conversion of the starch to glucose. The total amount of glucose, corresponding to the initial amount of starch, was determined photometrically as given above. To control the reproducibility of the extraction, standard plant powder (Orchard leaves, Leco, St. Joseph, MI, USA) and pure starch, glucose, fructose, and sucrose solutions were included in the analysis. Glucose standard (1 mg mL^{-1}) was used to calculate the glucose concentrations of the extracts. All chemicals and enzymes were purchased from Sigma-Aldrich, St. Louis, MO, USA. NSC concentrations were expressed as % dry mass of starch and the

three quantitatively most important soluble sugars (glucose, fructose, and sucrose).

Carbon Isotope Analyses

Approximately 1 mg of powdered bulk sample of 1-year-old shoots and leaves was weighted into tin capsules and the isotopic ratio was measured using an elemental analyzer (Vario PYRO Cube, Elementar, Germany) coupled to an isotope mass spectrometer (Isoprime precision, Elementar, UK) at Crop Research Institute, Prague. The carbon isotopic composition ($\delta^{13}C$) was expressed relative to the international standard (Vienna Pee Dee Belemnite, VPDB) according to the following formula $\delta^{13}C = (R_{sample}/R_{VPDB} - 1)$, where R is the $^{13}C/^{12}C$ ratio of the sample or the VPDB standard.

Tree Harvesting and Biomass Estimation

The whole-tree biomass and the biomass of different tree parts including fruits, leaves, 1-year-old shoots, scaffold branches, trunk, stump, and coarse roots > 3 mm in diameter were assessed using destructive sampling at the end of the growing season. Fruits were manually picked, the leaves were stripped and the woody portions of the current-year shoots were clipped with a pair of hand pruners. Subsequently, the trees were felled with a chain saw and separated into trunks and scaffold branches. Tree stumps, including the root collar, the graft union, and the lowest 10 cm of the trunk, were then excavated with a mechanical digging machine. In place of the excavated stumps, we dug pits with the diameter of 2 m and a depth of 0.5 m (*M.* × *domestica*) and 0.8 m (*P. communis*) and sieved the soil to extract the coarse roots (> 3 mm in diameter). The dimensions of the pits were selected to represent the volume with the majority of root biomass. The fresh weight of all harvested tree parts was measured immediately using a portable scale with the accuracy of 0.01 kg. The measured fresh weights were converted to the dry weights (DW) using the conversion factor determined on smaller sub-samples. At least 20 sub-samples were measured for each tissue type.

Estimation of Whole-organ and Whole-tree NSC Pools

We used the dry weight biomass estimations and the measured NSC concentrations to calculate the size of NSC pools in different tree organs and in the whole trees. Considering the observed seasonal dynamics of NSC concentrations, the calculations were made for two contrasting periods of the growing season. First, we used May NSC data to characterize the situation when NSC reserves are at their minimums during the spring flush. This situation was contrasted with the conditions in November at the onset of winter dormancy, when the NSC reserves reached their maximal concentrations. The NSC concentrations and biomass DW for roots, shoots, and leaves were directly paired and multiplied, except that in May we reduced the biomass of shoots and leaves to 25% because the shoot extension growth and leaf unfolding were just at their beginning. For tree parts that were not directly monitored for NSC concentrations (e.g., scaffold branches, stumps) the NSC concentrations were calculated based on the measurements of the adjacent parts. Thus, we assumed that the NSC concentration of the stump was an average between the concentrations measured in the trunk and the roots. Similarly, the NSC concentrations of older scaffold branches were estimated as an average of the trunk and the current-year shoots. Furthermore, we assumed that heartwood contributes little to NSC storage pool due to the generally low NSC concentrations (Hoch et al. 2003). Therefore, we reduced the biomass of trunks, stumps, and scaffold branches by multiplying them with a factor of 0.7. The average sapwood depth in our trees was between 2 and 5 cm, which approximately correspond to a 70% of the total wood cross-sectional area, hence the factor 0.7. To obtain the estimation of the NSC pool for the whole tree, we summed the organ-level estimates of NSC contents.

Statistical Analyses

Differences in biomass ratios, sizes of the NSC pools, and seasonal fluctuation in NSC pools were analyzed with one-way ANOVA with scion/rootstock combination as the fixed factor. The means were then separated using Tukey HSD test. Differences in starch, soluble sugars, total NSC concentrations, and $\delta^{13}C$ were analyzed separately for each species and tissue type using a linear mixed-effects model. The models were fitted in R (R Development Core Team 2010) using lmer function from lme4 package (Bates et al. 2015). Homogeneity of variance and normality of the data were evaluated by visual inspection of model residuals. In these models, rootstock and sampling date (incl. the interaction term) were implemented as fixed factors and tree_id was included as random factor to account for the repeated sampling. The significance of the fixed effect factors was evaluated using F test with Satterthwaite approximation for the degrees of freedom implemented in the lmerTest package (Kuznetsova et al. 2017). For significant fixed effects, differences between pairs of means were evaluated using Tukey-adjusted pairwise comparisons. The results were considered significant at $\alpha = 0.05$.

Results

NSC Concentrations and Their Seasonal Dynamics

In both species, the NSC concentrations in all studied tissue types varied seasonally with the lowest values observed

during the May or July sampling and the highest values being reached in November (Figs. 1, 2). The trunk cores had the lowest total NSC concentrations of all measured organs, except for the leaves of pear trees that had NSC concentrations lower than 3% (d.w.) throughout the entire season. Despite broadly similar seasonal dynamics of NSC concentrations, there were some significant differences between the trees of contrasting vigor in both species. For instance, the roots of low vigor apple trees had significantly lower starch concentrations, but higher concentrations of soluble sugars early in the season than vigorously growing apple trees (Fig. 1a, e). At some sampling dates, the low vigor apple trees also showed significantly lower starch concentrations than high vigor apple trees in their shoots and leaves (Fig. 1c, d). In pear trees, low vigor trees had significantly higher starch and total NSC concentrations in trunks throughout the whole sampling period compared to vigorously growing trees (Fig. 2 b, j). Starch and total NSC concentrations were also higher in the roots of low vigor pear trees early in the growing season, but the opposite pattern was observed in November (Fig. 2 a, i). In November, low vigor pear trees also had significantly higher NSC concentrations in shoots than their high vigor counterparts (Fig. 2 c, k).

Tree Biomass Components

The difference in overall growth vigor for trees on size-controlling rootstocks was greater in apple trees than pear trees (Table 1, 2). In apple trees, trunk cross-sectional area (TCSA) of low vigor trees was 62% lower than TCSA in high vigor trees, while the difference was only 43% in pear trees (Table 1). Similarly, low vigor apple trees had about half the fruit yield in comparison with the high vigor rootstock-scion combination, while the difference in yield was minimal for pear trees (Table 1). The estimated mean total tree biomass (excluding fruits) was 27.7 kg in low vigor, 82.5 kg in high vigor apple trees, 39.6 kg in low vigor, and 78.9 kg in high vigor pear trees (Table 2). Thus, the low vigor trees had about 66% (in the case apple trees) and 50% (in the case of pear trees) less biomass

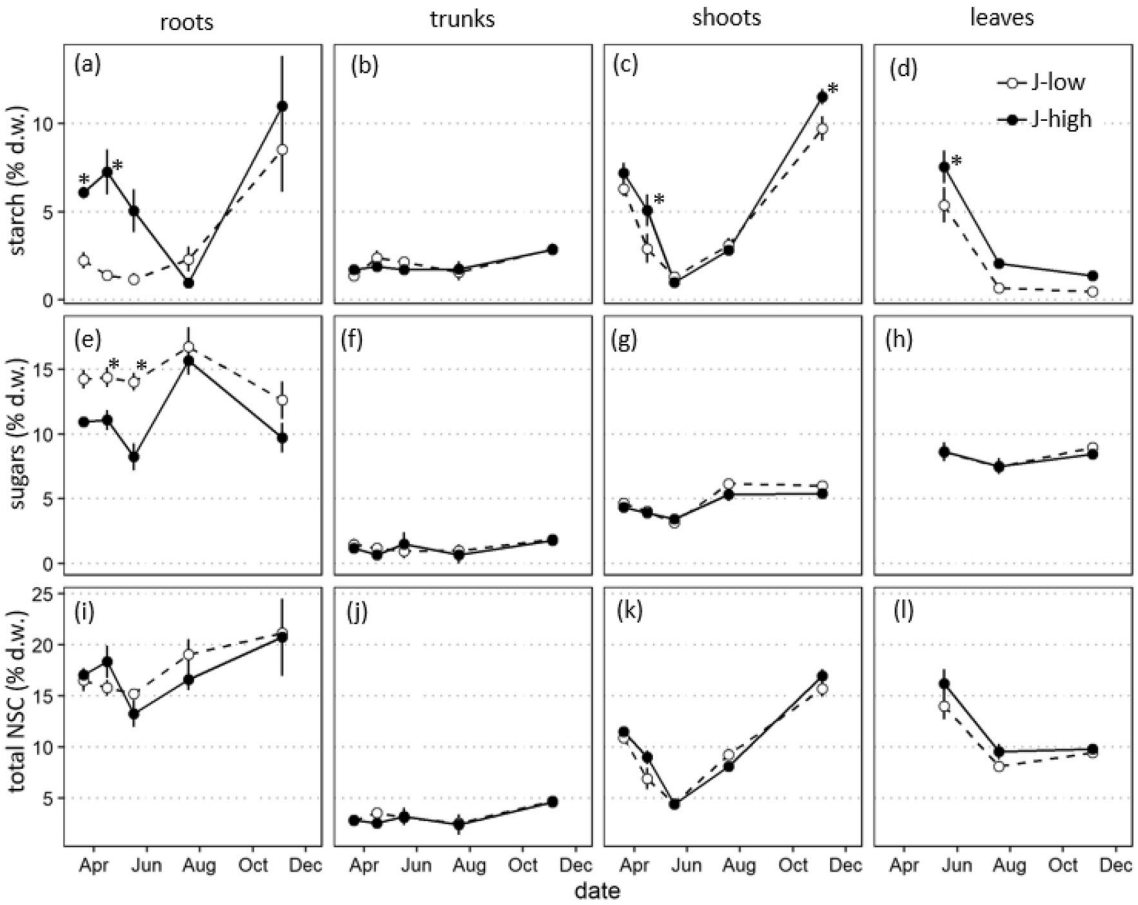

Fig. 1 Seasonal concentrations of starch, soluble sugars, and total NSC measured in coarse roots, trunk cores, 1-year-old shoots, and leaves of apple tree var. 'Jonagold' (J) grafted on rootstocks inducing low or high growth vigor. The data are means ± SE ($n = 3$ for trunk cores, $n = 6$ for other tree parts). The asterisk indicates significant differences between the rootstock means within the sampling date as evaluated with the Tukey-adjusted pairwise comparison

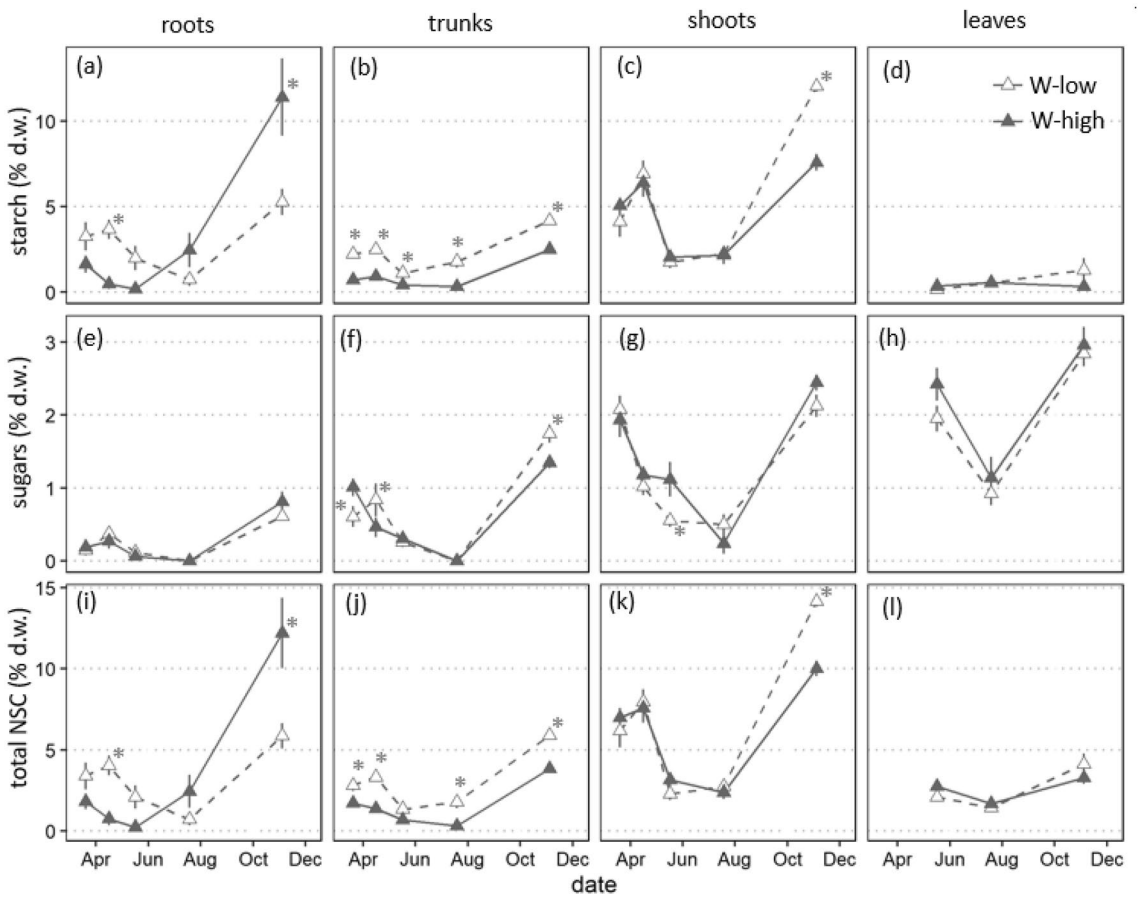

Fig. 2 Seasonal concentrations of starch, soluble sugars, and total NSC measured in woody roots, trunk cores, 1-year-old shoots, and leaves of pear var. 'Williams' (W) grafted on rootstocks inducing low or high growth vigor. The data are means ± SE ($n = 3$ for trunk cores, $n = 6$ for other tree parts). The asterisk indicates significant differences between the rootstock means within the sampling date as evaluated with the Tukey-adjusted pairwise comparison

Table 2 Estimated biomass dry weights (kg tree^{-1}) of various tree parts in apple tree var. 'Jonagold' (J) and pear tree var. 'Williams' (W) grafted onto rootstocks inducing low or high growth vigor

Organ	J-low	J-high	W-low	W-high
Roots	3.1 ± 0.7 (9.5%)	4.7 ± 0.9 (5%)	3.8 ± 0.1 (9.2%)	7.1 ± 1.1 (9.3%)
Stump	7.4 ± 0.8 (22.6%)	22.1 ± 5.3 (23.6%)	7.4 ± 0.6 (18.2%)	21 ± 5.7 (26%)
Trunk	9.6 ± 1.8 (29.2%)	37.6 ± 2 (40.7%)	12.7 ± 2.8 (31.2%)	24.8 ± 5.1 (31.1%)
Scaffold branches	6.1 ± 0.5 (18.7%)	12.7 ± 2.7 (13.7%)	11.9 ± 2.4 (29.1%)	17.9 ± 4.5 (22.1%)
1-year-old shoots	0.3 ± 0.1 (0.9%)	1.6 ± 0.5 (1.7%)	1.6 ± 0.4 (3.8%)	4.1 ± 2.2 (4.8%)
Leaves	1.3 ± 0.3 (3.9%)	3.8 ± 0.5 (4.1%)	2.2 ± 0.3 (5.3%)	4 ± 1.3 (4.9%)
Fruits	5 ± 0.7 (15.3%)	10.1 ± 2.2 (11.1%)	1.3 ± 0.4 (3.2%)	1.4 ± 0.7 (1.8%)
Total	32.7 ± 3 (100%)	92.6 ± 8.6 (100%)	40.9 ± 2.9 (100%)	80.3 ± 15.9 (100%)

The values in brackets refer to the percent fraction of a given tree part relative to the total tree biomass
Means ± SD ($n = 3$) are reported

than their high vigor counterparts. The majority of tree biomass consisted of older woody parts (trunk, scaffold branches, and stump). All together these tissues comprised 72–88% of total standing tree biomass. 1-year-old shoots and leaves represented between 4.8 and 9.7% of the total tree biomass. Across all trees, leaf biomass, and correspondingly the estimated leaf area (LA), scaled tightly with the TCSA ($r = 0.954$, $P < 10^{-4}$), resulting in a similar LA-to-TCSA ratio (Fig. 3a). Root biomass represented less than 10% of the total tree biomass. However, the fraction of below-ground biomass increased, if parts of the stump were considered as below-ground component. When half of the stump weight was attributed to the

below-ground biomass, while the second half was considered above-ground, estimated above- to below-ground biomass ratios ranged between 3:1 and 5:1 (Fig. 3b). Fruits accounted for 15.3 and 11.1% of total biomass in low and high vigor apple trees, while this fraction was much lower (between 1.8 and 3.2%) in pear trees. The ratios of reproductive to vegetative biomass were not significantly different between low vs. high vigor trees, but this ratio was higher for apple than pear trees (Fig. 3c). In contrast, pear trees had greater biomass of 1-year-old shoots than apple trees (4% vs 1.5% in pear vs apple trees, respectively).

Estimated NSC Storage Pools

The whole-tree NSC pools estimates excluding fruits were 1.89 kg for low vigor apple, 4.77 kg for high vigor apple, 0.64 kg for low vigor pear, and 0.75 kg for high vigor pear in May. For November, the whole-tree NSC pool estimates were 2.44 kg for low vigor apple, 6.54 kg for high vigor apple, 2.47 kg for low vigor pear, and 4.68 kg for high vigor pear (Table 3, Fig. 4a). Thus, in absolute terms high vigor apple trees had the greatest NSC pool size from all measured trees, while the low vigor pear trees had the smallest pool size. The seasonal fluctuations expressed as the absolute difference between the November and May pool size was highest (3.93 kg) in high vigor pear trees and lowest (0.55 kg) in low vigor apple trees (Fig. 4b). The difference in the seasonal fluctuation between trees on low vs. high vigor rootstocks was significant ($P < 0.05$) in pear trees, while the difference was even larger, but due to higher variation not statistically significant in apple trees. When expressed as a fraction of the November (i.e., maximal) pool size, the magnitude of the seasonal fluctuation accounted for 22.5% in low vigor apple, 27.1% in high vigor apple, 74.1% in low vigor pear, and 84% in high vigor pear. Finally, when scaled to the tree's biomass, the fluctuation was higher in pear trees than apple trees with no significant difference between low and high vigor trees (Fig. 4c).

Variation in $\delta^{13}C$

The $\delta^{13}C$ values of 1-year-old shoots and leaves varied between − 26 and − 30‰. In apple trees, no significant differences in $\delta^{13}C$ were found between low and high vigor trees, whereas in pear trees low vigor trees had significantly higher $\delta^{13}C$ values in shoots and leaves in at least some sampling dates (Fig. 5).

Discussion

The main aim of our study was to compare the size of NSC pools and NSC dynamics in trees grafted on low vs. high vigor rootstocks (Table 1), while considering differences in

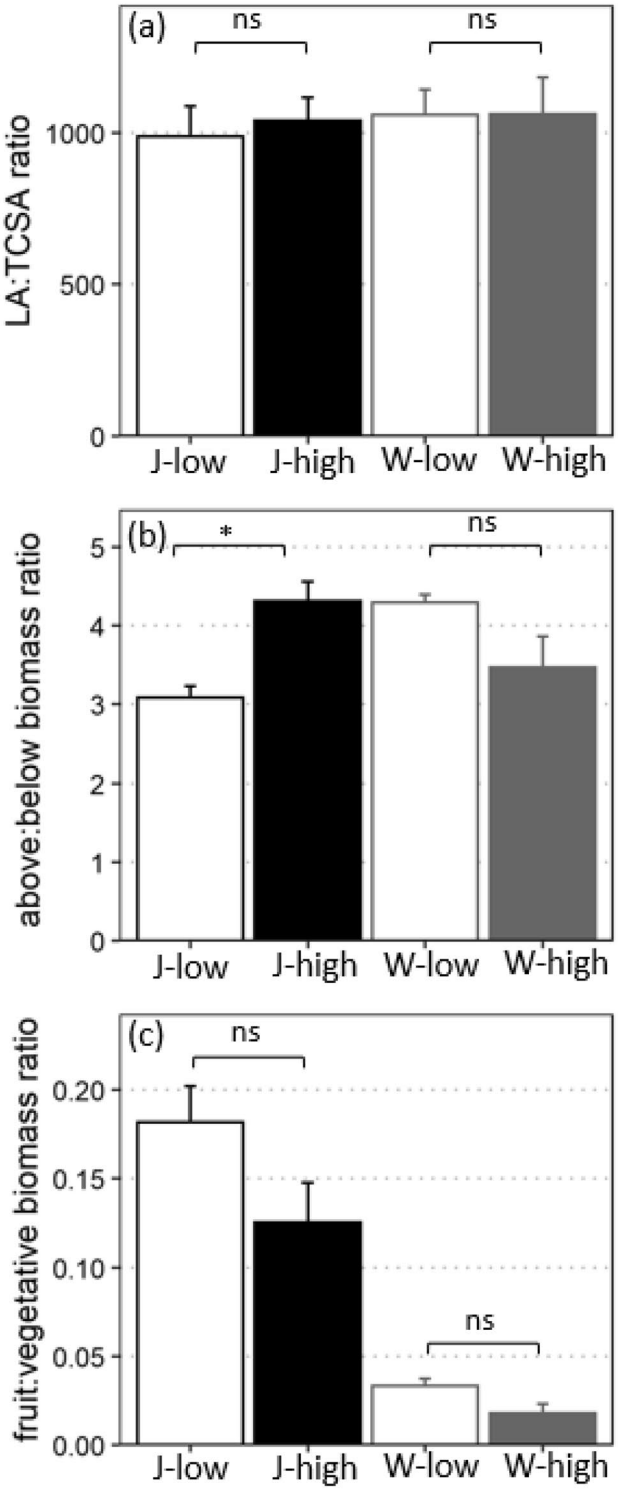

Fig. 3 **a** Ratio between leaf area (LA) and trunk cross-sectional area (TCSA), **b** ratio between above- and below-ground biomass, **c** ratio between reproductive (i.e., fruit) and vegetative biomass in apple tree var. 'Jonagold' (J) and pear tree var. 'Williams' (W) grafted onto rootstocks inducing low or high growth vigor. The bars represent means ± SE ($n = 3$). The results of Tukey-adjusted pairwise comparisons of means are labeled either with asterisk (significant differences at $\alpha = 0.05$) or "ns" (non-significant)

Table 3 Estimated NSC pool size (kg) in May (during spring flush) and November (the onset of winter dormancy) of various tree parts in apple tree var. 'Jonagold' (J) and pear tree var. 'Williams' (W) grafted onto rootstocks inducing low or high growth vigor

NSC pool in May (kg)				
Organ	J-low	J-high	W-low	W-high
Roots	0.48 ± 0.11 (25.1%)	0.63 ± 0.2 (13.3%)	0.08 ± 0.06 (12.4%)	0.02 ± 0.01 (2.4%)
Stump	0.82 ± 0.1 (43.5%)	2.24 ± 0.91 (46.9%)	0.13 ± 0.08 (20.8%)	0.09 ± 0.03 (11.3%)
Trunk	0.31 ± 0.13 (16.1%)	1.23 ± 0.61 (25.8%)	0.18 ± 0.08 (28%)	0.18 ± 0.09 (24.2%)
Scaffold branch	0.24 ± 0.03 (12.7%)	0.51 ± 0.07 (10.6%)	0.23 ± 0.08 (35.5%)	0.41 ± 0.07 (54.6%)
1-year-old shoots	0.004 ± 0.002 (0.2%)	0.02 ± 0.002 (0.4%)	0.009 ± 0.002 (1.4%)	0.03 ± 0.01 (4.1%)
Leaves	0.05 ± 0.02 (2.4%)	0.15 ± 0.01 (3.1%)	0.012 ± 0.004 (1.9%)	0.03 ± 0.004 (3.4%)
Total	1.89 ± 0.29 (100%)	4.77 ± 1.69 (100%)	0.64 ± 0.28 (100%)	0.75 ± 0.19 (100%)
NSC pool in November (kg)				
Organ	J-low	J-high	W-low	W-high
Roots	0.58 ± 0.23 (23.9%)	0.94 ± 0.22 (14.4%)	0.25 ± 0.06 (10.1%)	0.87 ± 0.06 (18.6%)
Stump	0.81 ± 0.24 (33.2%)	2.5 ± 0.54 (38.2%)	0.34 ± 0.11 (13.9%)	1.56 ± 0.43 (33.3%)
Trunk	0.32 ± 0.05 (12.9%)	1.22 ± 0.07 (18.6%)	0.53 ± 0.12 (21.4%)	0.66 ± 0.1 (14.2%)
Scaffold branch	0.57 ± 0.09 (23.2%)	1.24 ± 0.23 (18.9%)	1.04 ± 0.24 (42.1%)	1.05 ± 0.28 (22.5%)
1-year-old shoots	0.05 ± 0.01 (1.9%)	0.27 ± 0.07 (4.1%)	0.22 ± 0.07 (9%)	0.41 ± 0.24 (8.8%)
Leaves	0.12 ± 0.03 (4.9%)	0.37 ± 0.06 (5.7%)	0.09 ± 0.03 (3.5%)	0.12 ± 0.02 (2.6%)
Total	2.44 ± 0.57 (100%)	6.54 ± 0.83 (100%)	2.47 ± 0.38 (100%)	4.68 ± 0.94 (100%)

The values in brackets refer to the percent fraction of a given tree part relative to the total tree pool size.

Means ± SD ($n = 3$) are reported.

tree's overall size and biomass allocation into different tree parts. Because of the small variation in the relative biomass partitioning (Table 2) and generally similar organ-level NSC concentrations (Fig. 1, 2), we found that the size of the NSC pools scaled tightly with the overall plant biomass with vigorous trees having greater absolute storage pools compared to low vigor trees (Fig. 4a). The magnitudes of the seasonal fluctuation (i.e., the difference in NSC pool size between November and May) in the range from 0.55 to 3.93 kg were similar as those estimated for forest trees in the boreal zone (Schoonmaker et al. 2021; Fermaniuk et al. 2021). In the absolute terms, the seasonal fluctuation was higher in vigorously growing trees. However, in relative terms and also when scaled by the tree's biomass, the differences between the low and high vigor trees became negligible (Fig. 4c). This finding suggests that the low and high vigor trees rely on their NSC reserves to a similar extent during their annual growth cycle. In other words, the size of NSC storage pool and the NSC demands vary in accordance with each other in low and high vigor trees, which indicates that a mechanism other than the ability to accumulate or utilize NSC is driving growth differences observed in these rootstocks.

The relative magnitude of seasonal fluctuation of NSCs differed between apple and pear trees with apple trees showing smaller relative fluctuation. This was because the apple trees maintained high NSC pool in May (Fig. 4a), mainly due to high soluble sugar concentrations in their roots (Fig. 1e). The differences in the root NSC pool size between the two species could originate from their different root morphology and anatomy (Jupa et al. 2021). Apple trees have relatively shallow root systems and may need high concentrations of soluble sugars to adjust osmotically to frequently drying upper soil horizon (Davies and Lakso 1979). Also, apple tree roots have thick bark and abundant ray parenchyma accentuating their role in storage (Jupa et al. 2021). In contrast, pear trees have deep sinker roots, thin bark, and high vessel density on the root cross-sections, which has been related to their high water-conducting capacity (Jupa et al. 2021). Based on our estimates, roots and stump accounted for about a half of the total tree NSC pool in apple trees and high vigor pear trees (Table 3). Our estimates also indicate that the stump that consisted of the root crown, graft union, and the lowest portion of the trunk could be an important site for storage because of its large biomass and presumably high NSC concentrations at least in the root structures. On the other hand, the graft union and the associated outgrowth tissue can represent a severe restriction for the long-distance xylem and phloem transport (Soumelidou et al. 1994; Olmstead et al. 2010).

Based on our data, trunk and scaffold branches also harbor a substantial portion of the NSC reserves (Table 2), particularly in low vigor pear trees. The importance of above-ground woody tissue for NSC storage, which originates mainly from its large total biomass, agrees well with the previous results on forest trees (Hoch et al. 2003;

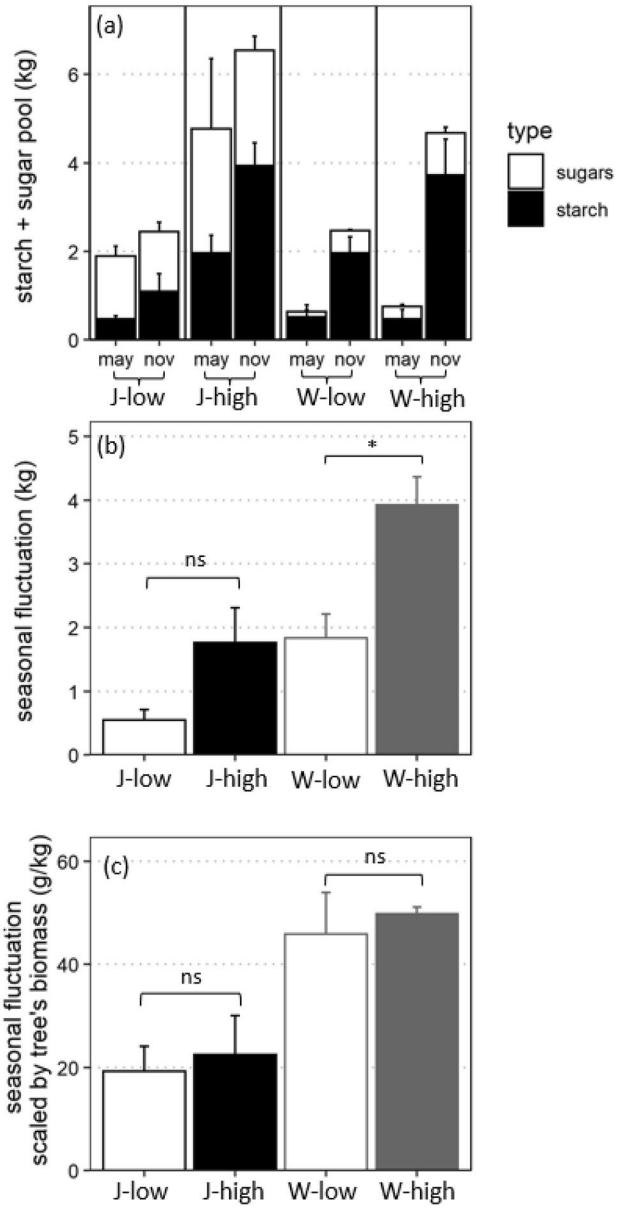

Fig. 4 **a** Mean estimated pool sizes of starch and soluble sugars in May (during spring flush) and November (during the onset of winter dormancy) in the whole trees of apple tree var. 'Jonagold' (J) and pear tree var. 'Williams' (W) grafted onto rootstocks inducing low or high growth vigor. **b** Difference in the estimated pool sizes between November and May in the four studied scion/rootstock combinations. **c** Difference in the estimated pool sizes scaled by the tree's biomass. The data are means ± SE ($n = 3$). The results of Tukey-adjusted pairwise comparisons of means are labeled either with asterisk (significant differences at $\alpha = 0.05$) or "ns" (non-significant)

Würth et al. 2005; Furze et al. 2019). In contrast to other measured organs, trunk tissue NSC concentrations were low (Fig. 1, 2) and not very dynamic suggesting that trunk sapwood is large but not a very active NSC pool (Carbone et al. 2013). Interestingly, the high vigor pear trees had consistently lower starch concentrations in their trunks compared to low vigor trees (Fig. 2b). This finding could indicate that NSC reserves were used to fuel rapid cambial growth or to support stem suckering which was quite intense in high vigor pear trees. Compared to the perennial woody organs, the biomass of current-year shoots, leaves, and fruit was relatively small, accounting for 11.5 to 20.1% of the total biomass (Table 2). The ratio of reproductive (i.e., fruit) to vegetative above-ground biomass was higher for apple trees than pear trees and did not differ significantly between low vs. high vigor trees (Fig. 3c), although the trend for higher yield efficiency in low vigor trees was apparent and consistent with the previous findings in this rootstock trial (Kosina 2004) as well as broader horticultural literature (Atkinson and Else 2003). If we consider that the fruit represents a major sink for carbohydrates (DeJong and Grossman 1995), it is likely that a higher yield efficiency related with lower leaf to fruit ratio may further compete with the vegetative growth.

Total leaf area is an important determinant of photosynthetic gain and overall growth (Watson 1958). Differences in the relative proportion of leaf area were anticipated between low versus high vigor trees as a consequence of architectural changes during canopy development. For instance, low vigor trees typically have shorter shoot internodes and different proportions of sympodial to monopodial branching (Seleznyova et al. 2008), which is in pome fruit closely related to different proportions between vegetative and reproductive wood (Costes et al. 2006). We found that leaf area scaled allometrically with TCSA with a common exponent which resulted in a similar leaf area-to-TCSA ratio across all studied trees (Fig. 3a). The scaling between leaf and sapwood cross-sectional area presumably reflects the functional balance between water loss, C gain, and water transport toward the leaf evaporating sites (Petit et al. 2018). Thus, our results indicate that, from the structural point of view, this balance was roughly the same for low and high vigor trees. However, the measurements of leaf and shoot carbon isotopic composition (Fig. 5) suggest that low vigor pear trees likely had lower stomatal conductance compared to high vigor pear trees and both scion/rootstock combinations of apple trees, which might have translated into lower photosynthetic gain and lower growth vigor. In agreement with our results, less negative ^{13}C values were associated with reduced vigor in 'Honeycrisp' apple tree scion grafted onto a series of size-controlling rootstocks (Casagrande Biasuz and Kalcsits 2022). Less-depleted $\delta^{13}C$ can also be caused by a greater contribution of stored carbohydrates relative to the current-year assimilates (Han et al. 2016). This interpretation would be supported by the less negative $\delta^{13}C$ values of spring compared to summer leaves. To disentangle these possibility measurements of compound-specific $\delta^{13}C$ or $\delta^{18}O$ composition or leaf gas exchange rates could be helpful (Hartmann and Trumbore 2016).

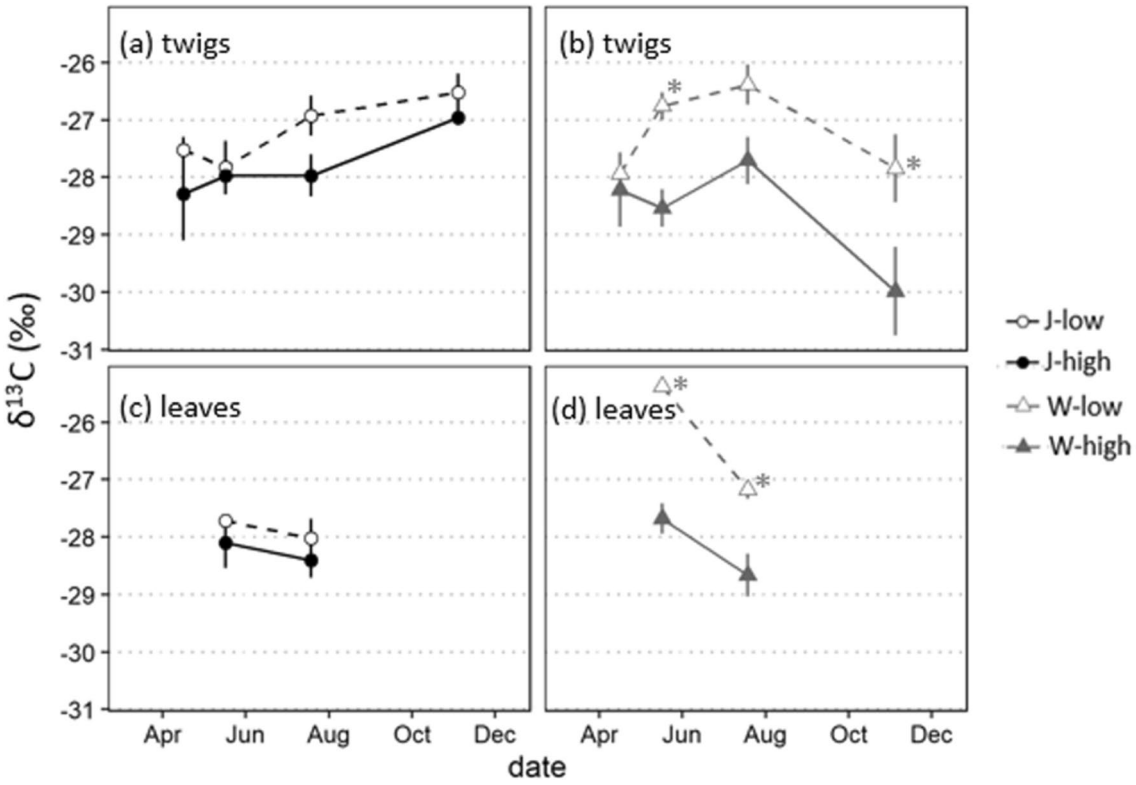

Fig. 5 Seasonal carbon isotope ($\delta^{13}C$) variation in 1-year-old shoots and leaves of apple tree var. 'Jonagold' (J) and pear tree var. 'Williams' (W) grafted onto rootstocks inducing low or high growth vigor. The data are means ± SE ($n = 3$). The asterisk indicates significant differences between the rootstock means within the sampling date (Tukey-adjusted pairwise comparison)

To the best of our knowledge, this is the first study that tested the carbohydrate reserve theory of rootstock-induced control of growth vigor (Basile and DeJong 2018) from the perspective of whole-tree NSC storage. We found that the size of the NSC storage pool as well as the magnitude of seasonal fluctuation varied proportionally with tree size. Thus, from the whole tree perspective, the trees seem to rely on NSC reserves to a similar extent and there was no evidence for a generally lower NSC storage capacity in low vigor trees compared to their high vigor counterparts. Nevertheless, there were some nuances in the dynamics of NSC concentrations across organs, indicating that NSC use and demands were locally perturbed by the different size-controlling rootstocks. It is unlikely that these small differences would be the ultimate cause of differential growth vigor. Instead, other mechanisms such as disturbed water, hormonal, or nutritional relations were likely to affect the trees' growth and subsequently C use.

Acknowledgements The project was supported by the Czech Science Foundation (Grant No. 18-19722Y). We thank Dr. Raimanová for carbon isotope measurements. Jana Fenclová, Lucy Boulton, Aneta Mahrová, and Dr. Pavel Svoboda are acknowledged for field assistance. We thank Amanda Schoonmaker for her feedback on an earlier draft of this paper.

Author Contributions LP: conceived the study, LP, RJ, and MM: carried out the field work and biomass measurements. GH: carried out the NSC analyses. LP: analysed the data and wrote the text of the manuscript with all co-authors contributing.

Funding This work was funded by Grantová Agentura České Republiky (Grant No. 18-19722Y).

Declarations

Conflict of interest On behalf of all authors, the corresponding author states that there is no conflict of interest.

References

Atkinson CJ, Else MA (2003) Enhancing harvest index in temperate fruit tree crops through the use of dwarfing rootstocks. In Proceedings of the International workshop on cocoa breeding for improved production systems, pp 118–131

Barbaroux C, Bréda N, Dufrêne E (2003) Distribution of above-ground and below-ground carbohydrate reserves in adult trees of two contrasting broad-leaved species (*Quercus petraea* and *Fagus sylvatica*). New Phytol 157:605–615. https://doi.org/10.1046/j.1469-8137.2003.00681.x

Basile B, DeJong TM (2018) Control of fruit tree vigor induced by dwarfing rootstocks. Hortic Rev 46:39–97. https://doi.org/10.1002/9781119521082.ch2

Bates D, Mächler M, Bolker B, Walker S (2015) Fitting linear mixed-effects models using lme4. J Stat Softw 67:1–48. https://doi.org/10.18637/jss.v067.i01

Bustan A, Avni A, Lavee S et al (2011) Role of carbohydrate reserves in yield production of intensively cultivated oil olive (*Olea europaea* L.) trees. Tree Physiol 31:519–530. https://doi.org/10.1093/treephys/tpr036

Carbone MS, Czimczik CI, Keenan TF et al (2013) Age, allocation and availability of nonstructural carbon in mature red maple trees. New Phytol 200:1145–1155. https://doi.org/10.1111/nph.12448

Casagrande Biasuz E, Kalcsits LA (2022) Apple rootstocks affect functional leaf traits with consequential effects on carbon isotope composition and vegetative vigour. AoB PLANTS 14:1–11. https://doi.org/10.1093/aobpla/plac020

Cohen S, Naor A (2002) The effect of three rootstocks on water use, canopy conductance and hydraulic parameters of apple trees and predicting canopy from hydraulic conductance: apple rootstocks influence canopy and hydraulic conductance. Plant Cell Environ 25:17–28. https://doi.org/10.1046/j.1365-3040.2002.00795.x

Costes E, Lauri PÉ, Regnard JL (2006) Analyzing fruit tree architecture: implication for tree management and fruit production. Hortic Rev 32:1–61

Davies FS, Lakso AN (1979) Diurnal and seasonal changes in leaf water potential components and elastic properties in response to water stress in apple trees. Physiol Plant 46:109–114

DeJong TM, Grossman YL (1995) Quantifying sink and source limitations on dry matter partitioning to fruit growth in peach trees. Physiol Plant 95:437–443

Fermaniuk C, Fleurial KG, Wiley E, Landhäusser SM (2021) Large seasonal fluctuations in whole-tree carbohydrate reserves: is storage more dynamic in boreal ecosystems? Ann Bot 128:943–957. https://doi.org/10.1093/aob/mcab099

Foster TM, McAtee PA, Waite CN et al (2017) Apple dwarfing rootstocks exhibit an imbalance in carbohydrate allocation and reduced cell growth and metabolism. Hortic Res 4:17009. https://doi.org/10.1038/hortres.2017.9

Furze ME, Huggett BA, Aubrecht DM et al (2019) Whole-tree nonstructural carbohydrate storage and seasonal dynamics in five temperate species. New Phytol 221:1466–1477. https://doi.org/10.1111/nph.15462

Han Q, Kagawa A, Kabeya D, Inagaki Y (2016) Reproduction-related variation in carbon allocation to woody tissues in *Fagus crenata* using a natural ^{13}C approach. Tree Physiol 36:1343–1352. https://doi.org/10.1093/treephys/tpw074

Hartmann H, Trumbore S (2016) Understanding the roles of nonstructural carbohydrates in forest trees – from what we can measure to what we want to know. New Phytol 211:386–403. https://doi.org/10.1111/nph.13955

Hoch G (2015) Carbon Reserves as indicators for carbon limitation in trees. In: Lüttge U, Beyschlag W (eds) Progress in Botany. Springer, Cham, pp 321–346

Hoch G, Richter A, Korner Ch (2003) Non-structural carbon compounds in temperate forest trees. Plant Cell Environ 26:1067–1081. https://doi.org/10.1046/j.0016-8025.2003.01032.x

Jupa R, Mészáros M, Plavcová L (2021) Linking wood anatomy with growth vigour and susceptibility to alternate bearing in composite apple and pear trees. Plant Biol 23:172–183. https://doi.org/10.1111/plb.13182

Körner C (2003) Carbon limitation in trees. J Ecol 91:4–17. https://doi.org/10.1046/j.1365-2745.2003.00742.x

Kosina J (2004) Growth and yield of apples on new Czech dwarfing rootstocks. Acta Hortic 663:945–948

Kuznetsova A, Brockhoff PB, Christensen RHB (2017) lmerTest Package: Tests in linear mixed effects models. J Stat Softw 82:1–26

Landhäusser SM, Chow PS, Dickman LT et al (2018) Standardized protocols and procedures can precisely and accurately quantify non-structural carbohydrates. Tree Physiol 38:1764–1778

Landhäusser SM, Lieffers VJ (2012) Defoliation increases risk of carbon starvation in root systems of mature aspen. Trees 26:653–661. https://doi.org/10.1007/s00468-011-0633-z

Loescher WH, McCamant T, Keller JD (1990) Carbohydrate reserves, translocation, and storage in woody plant roots. HortSci 25:274–281. https://doi.org/10.21273/HORTSCI.25.3.274

Olmstead MA, Lang NS, Lang GA (2010) Carbohydrate profiles in the graft union of young sweet cherry trees grown on dwarfing and vigorous rootstocks. Sci Hortic 124:78–82. https://doi.org/10.1016/j.scienta.2009.12.022

Petit G, von Arx G, Kiorapostolou N et al (2018) Tree differences in primary and secondary growth drive convergent scaling in leaf area to sapwood area across Europe. New Phytol 218:1383–1392. https://doi.org/10.1111/nph.15118

Popp M, Lied W, Meyer AJ et al (1996) Sample preservation for determination of organic compounds: microwave versus freeze-drying. J Exp Bot 47:1469–1473

R Development Core Team (2010) R: a language and environment for statistical computing. R Foundation for Statistical Computing, Vienna Austria, http://www.R-project.org.

Richardson AD, Carbone MS, Huggett BA et al (2015) Distribution and mixing of old and new nonstructural carbon in two temperate trees. New Phytol 206:590–597. https://doi.org/10.1111/nph.13273

Sala A, Woodruff DR, Meinzer FC (2012) Carbon dynamics in trees: feast or famine? Tree Physiol 32:764–775. https://doi.org/10.1093/treephys/tpr143

Schoonmaker AL, Hillabrand RM, Lieffers VJ et al (2021) Seasonal dynamics of non-structural carbon pools and their relationship to growth in two boreal conifer tree species. Tree Physiol 41:1563–1582. https://doi.org/10.1093/treephys/tpab013

Seleznyova AN, Tustin DS, Thorp TG (2008) Apple dwarfing rootstocks and interstocks affect the type of growth units produced during the annual growth cycle: precocious transition to flowering affects the composition and vigour of annual shoots. Ann Bot 101:679–687. https://doi.org/10.1093/aob/mcn007

Solari LI, Johnson S, DeJong TM (2006) Hydraulic conductance characteristics of peach (*Prunus persica*) trees on different rootstocks are related to biomass production and distribution. Tree Physiol 26:1343–1350. https://doi.org/10.1093/treephys/26.10.1343

Soumelidou K, Battey NH, John P, Barnett JR (1994) The anatomy of the developing bud union and its relationship to dwarfing in apple. Ann Bot 74:605–611

Tworkoski T, Fazio G, Glenn DM (2016) Apple rootstock resistance to drought. Sci Hortic 204:70–78. https://doi.org/10.1016/j.scienta.2016.01.047

Watson DJ (1958) The Dependence of net assimilation rate on leaf-area index. Ann Bot 22:37–54

Weibel A, Reighard G, Rajapakse N, DeJong T (2008) Dormant carbohydrate reserves of two peach cultivars grafted on different vigor rootstocks. In: IX International Symposium on Integrating Canopy, Rootstock and Environmental Physiology in Orchard Systems 903. pp 815–820

Würth MKR, Peláez-Riedl S, Wright SJ, Körner C (2005) Non-structural carbohydrate pools in a tropical forest. Oecologia 143:11–24. https://doi.org/10.1007/s00442-004-1773-2

Irrigation Science
https://doi.org/10.1007/s00271-022-00839-2

ORIGINAL PAPER

Yield and water relations of two apple cultivars under irrigation

Lenka Plavcová[1] · Martin Mészáros[2] · Radek Jupa[1,3] · Klára Scháňková[2] · Zuzana Kovalíková[1] · Jan Náměstek[2] · Aneta Mahrová[1]

Received: 24 June 2022 / Accepted: 21 December 2022

Abstract

Because of an increased incidence of drought, irrigation has become an important agricultural practice in formerly mesic regions. Efficient irrigation scheduling depends on a good knowledge of tree water relations. For three growing seasons, we monitored stem water potential (Ψ_{stem}) in two apple tree cultivars (*Malus*×*domestica cv.* 'Red Jonaprince' and 'Gala Brookfield') with and without irrigation. We also determined xylem potentials at 12% and 50% percent loss of conductivity (Ψ_{12}, Ψ_{50}) and vessel diameters in current-year shoots. To evaluate if trees are capable of osmotic adjustment, we measured turgor loss point (TLP), osmotic potential at full turgor, and the concentrations of organic osmolytes (proline, glucose, sucrose, and sorbitol) in leaves throughout the growing season. We found that Ψ_{stem} did not drop below − 1.6 MPa, which is well above the Ψ_{50} and TLP. Irrigated trees (ETc-100) had slightly higher Ψ_{stem} than trees without irrigation (ETc-0). The observed conditions in one of the 3 years resulted in similar yields but smaller fruit sizes of the non-irrigated trees. The triploid cultivar 'Red Jonaprince' had typically more negative Ψ_{stem} than the diploid cultivar 'Gala Brookfield', but 'Gala Brookfield' exhibited higher limitations in fruit growth during drought and shoot growth during wet periods. Concentrations of all measured osmolytes were higher in leaves of non-irrigated trees of 'Gala Brookfield' and increased during the season, while the pattern was more variable in 'Red Jonaprince'. In summary, our results indicate that 'Red Jonaprince' favours hydraulic efficiency against safety, while 'Gala Brookfield' adopts a more conservative growth strategy.

Introduction

Apple (*Malus* × *domestica* Borkh.) is one of the most important fruit trees growing in the temperate zone with a long tradition in cultivation. Currently, 86 million tons of apples are produced worldwide on a harvested area of about 4.6 million ha (FAO 2022). There are currently more than 10,000 named cultivars of apple trees, although only a few dozen of them are widely cultivated in commercial orchards (O'Rourke 2003). Among them, 'Gala Brookfield' and 'Red Jonaprince' are two highly popular cultivars. 'Gala Brookfield' is a moderately vigorous diploid, late summer cultivar originating as a cross of 'Kidd's Orange' and 'Golden Delicious'. This cultivar was bred in New Zealand and patented in 1973 (McKenzie 1973). 'Red Jonaprince' is a vigorous triploid invented in the Netherlands as a naturally occurring mutation of the unpatented cultivar 'Jonagold' from a cross of 'Golden Delicious' and 'Jonathan' (Princen and Princen 1999).

There are many differences between these two cultivars, such as pollination efficiency, fruit size, and growth vigour, which are related to the different number of chromosome sets. As for reproduction, triploids are not able to self-pollinate, and a high percentage of the triploid pollen is sterile (He et al. 2018). Triploid apple tree varieties typically have larger fruit sizes and more vigorous growth in comparison with diploids (Nikolaevich et al. 2015; Sedov et al. 2017). Beyond the yield and growth parameters, there are also differences in leaf size, leaf colouring, and the size of stomata and guard cells (He et al. 2018; Makarenko 2021). Polyploids are also generally thought to be more drought tolerant (Maherali et al. 2009; Hennig et al. 2015), although lower thresholds for the spread of drought-induced xylem

✉ Lenka Plavcová
lenka.plavcova@uhk.cz

[1] Department of Biology, Faculty of Science, University of Hradec Králové, Rokitanského 62, CZ-500 03 Hradec Králové, Czech Republic

[2] Research and Breeding Institute of Pomology, Holovousy 129, CZ-508 01 Hořice, Czech Republic

[3] Department of Experimental Biology, Faculty of Science, Masaryk University, Kamenice 5, CZ-625 00 Brno, Czech Republic

Published online: 05 January 2023

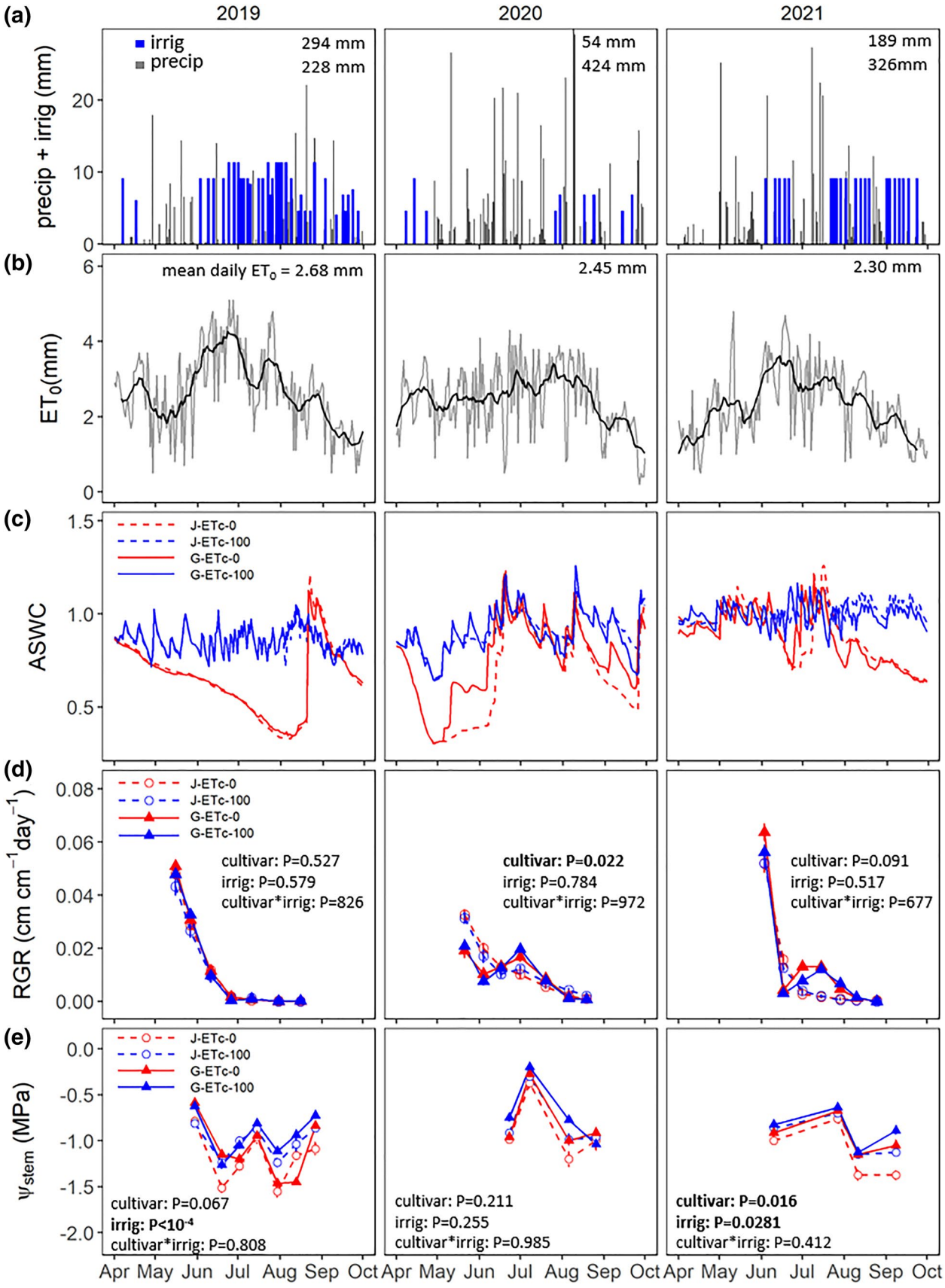
(a)
2019
2020
2021
irrig
precip
294 mm
228 mm
54 mm
424 mm
189 mm
326mm
precip + irrig (mm)
(b)
mean daily ET0 = 2.68 mm
2.45 mm
2.30 mm
ET0(mm)
(c)
J-ETc-0
J-ETc-100
G-ETc-0
G-ETc-100
ASWC
(d)
RGR (cm cm−1day−1)
cultivar: P=0.527
irrig: P=0.579
cultivar*irrig: P=826
cultivar: P=0.022
irrig: P=0.784
cultivar*irrig: P=972
cultivar: P=0.091
irrig: P=0.517
cultivar*irrig: P=677
(e)
ψstem (MPa)
cultivar: P=0.067
irrig: P<10-4
cultivar*irrig: P=0.808
cultivar: P=0.211
irrig: P=0.255
cultivar*irrig: P=0.985
cultivar: P=0.016
irrig: P=0.0281
cultivar*irrig: P=0.412
Apr May Jun Jul Aug Sep Oct

◂**Fig. 1** **a** Daily precipitation and irrigation, **b** reference evapotranspiration (ET_0) and **c** available soil water capacity (ASWC) under non-irrigated (ETc-0) and irrigated (ETc-100) apple trees of 'Red Jonaprince' (J) and 'Gala Brookfield' (G) cultivars in years 2019, 2020 and 2021. **d** Relative extension growth rates of shoots (RGR) and **e** midday stem water potential (Ψ_{stem}) for non-irrigated (ETc-0) and irrigated (ETc-100) trees of each cultivar are shown. Points and error bars represent means ± standard error; $n = 16–20$ for shoot RGR; $n = 4$ for Ψ_{stem}

embolism were recently found for tetraploid apple trees compared to their diploid predecessors (Baerdemaeker et al. 2018). Thus, there is a need for more data on hydraulic traits of apple trees of different ploidy, which would be helpful for the assessment of apple tree performance under drought.

Apple trees have been traditionally grown in temperate areas, but they are also cultivated in semi-arid regions such as Israel or Turkey (Webster 2005a). More recently, apple cultivation has been expanded even to the tropics. To achieve high yields and good marketable quality of fruits and to sustain the long-term health of trees, it is important to maintain favourable water balance of apple orchards. Irrigation is necessary to sustain apple fruit production in semi-arid regions with minimal summer precipitation and high evaporative demands. However, irrigation is now becoming increasingly important even in temperate zones because longer and more intense drought periods occur in many formerly mesic regions because of climate change (Tromp 2005; Brás et al. 2021).

To successfully manage orchard water balance and schedule irrigation efficiently, the knowledge of site conditions (climate, soil properties) and water requirements of planted trees is essential (Webster 2005a, b). Different cultivars have different native drought tolerance (Beikircher and Mayr 2017) and may respond differently to irrigation in terms of their vegetative and generative growth. In addition, tree water requirements may vary with the intensity of cropping with high crop loads resulting in increased water use (Naor et al. 2008). Irrigation scheduling is often based on evapotranspiration estimated from measured meteorological conditions (Allen and Pereira 2009; Dragoni and Lakso 2008), while various soil- and plant-based indicators are used to adjust irrigation to achieve desired water status of the orchard site or cultivated trees (Glenn 2010; Robinson et al. 2022).

Midday stem water potential (Ψ_{stem}) is one of the most widely used plant-based indicators for irrigation scheduling and a sensitive measure of plant water status (Shackel et al. 1997; Naor 1999; Ortuño et al. 2009). To use Ψ_{stem} as an irrigation indicator, it is necessary to determine a threshold value, i.e. the value when the drought stress starts to have negative impacts on the total fruit yield or fruit size (DeSwaef et al. 2009; Robinson et al. 2022). In addition, it is useful to put the stem water potential experienced under field conditions into a physiological context. There are a number of plant functional traits related to hydraulic safety and efficiency which have been linked to drought tolerance (Hacke and Sperry 2001). For instance, vulnerability to embolism and hydraulic conductivity, which are both closely linked to vessel diameter, are important features of xylem that are closely related to growth performance and drought resistance of trees (Gleason et al. 2012; Hacke et al. 2017). However, these parameters have not been widely studied across apple tree cultivars.

Soft living tissues, such as leaves, can increase their drought tolerance by lowering their turgor loss point in the process known as osmotic adjustment (Bartlett et al. 2014). Alternatively, the adjustment of cell wall properties can make leaf tissue more elastic allowing for the expansive growth and stomatal opening at lower turgor (Davies and Lakso 1979). Accumulation of osmotic compounds, e.g. proline, sorbitol or soluble sugars, is also involved in plant drought tolerance (Wang and Stutte 1992). The osmolytes reduce the osmotic potential of cells and help to maintain turgor which is essential for expansive growth and stomatal control (Rodriguez-Dominguez et al. 2016). Besides their role in osmotic adjustment and reduced water loss, the osmolytes may also serve as osmoprotectants that stabilize membranes and macromolecular compounds (Gomes et al. 2010).

In this study, we monitored yield, Ψ_{stem} and shoot growth in irrigated and non-irrigated apple trees of 'Red Jonaprice' and 'Gala Brookfield' cultivars during three consecutive growing seasons. The results of these measurements are interpreted in the context of important hydraulic traits, namely xylem vulnerability to embolism, vessel diameter, turgor loss point, and accumulation of compatible osmolytes (proline, sucrose, glucose, and sorbitol). We hypothesized that non-irrigated trees would have lower Ψ_{stem}, slower shoot growth, lower fruit yield and/or smaller fruits due to water deficit conditions. Also, the trees might acclimate to water deficit by increasing their embolism resistance, lowering their turgor loss point or increasing the concentration of compatible osmolytes.

Materials and methods

Experimental site and irrigation treatments

The experiment was conducted on seven-year-old apple trees of 'Red Jonaprince' and 'Gala Brookfield' grown at Research and Breeding Institute of Pomology Holovousy Ltd. (Czech Republic—15°34′48.031″E, 50°22′24.520″N) in the years 2019–2021. The local mean temperature and precipitation during the vegetation period were 16.7 °C and 228 mm, 15.9 °C and 424 mm, and 15.2 °C with 326 mm

for the years 2019, 2020, and 2021, respectively. For the detailed distribution of precipitation, irrigation and reference evapotranspiration (ET_0), see Fig 1a and b. The orchard was planted on silty loam brown soil (Loganathan 1987), characterized by 22.2 % clay, 69.1 % silt, and 8.7 % sand. The soil characteristics were evaluated by laboratory analyses with Kopeckého cylinders (Pospíšilová et al. 2016) and corresponded to 34.2 vol. % water content at field capacity and 15.9 vol. % at permanent wilting point according to the estimates published by Kaufmann and Cleveland (2008). The scions were grafted on M9 rootstock and planted at a spacing of 3.5 × 1.2 m for 'Red Jonaprince' and 3.5 × 1.0 m for 'Gala Brookfield'. The trees were trained as slender spindles combined with "Klik" pruning with a final height of 3.2 m. Crown volumes calculated by multiplying the crown widths and lengths were between 1.2 and 2.9 m^3 at the beginning of the irrigation study and increased to between 3.0 and 7.8 m^3 at the end of 2021. The fruit set was regulated by hand thinning at BBCH 72 (fruit diameter of 20 mm) using the equilifruit disc (Kon and Schupp 2013) after previous chemical thinning in the case of 'Gala Brookfield'. The chemical thinning was done by a mixture of benzyladenine and naphthalene-1-acetic acid applied at a fruit size of 10−15 mm. The plant protection and fertilization were carried out in accordance with the rules of integrated fruit production. Trees rows (1 m in width) were managed with herbicides combined with mechanical treating of the soil surface. The interrows were covered by periodically moved grass.

Irrigation treatment replacing 100% of the estimated crop evapotranspiration (ETc-100) was applied and contrasted to non-irrigated control (ETc-0) in each of the two cultivars. The trees were grown in neighbouring north-south oriented rows and the irrigation treatment was applied to a whole sector within each row that encompassed 17 trees. A subset of 10 trees was selected in each sector to obtain trees of similar vigour and flowering intensity at the beginning of the irrigation experiment, and these trees were used for the measurements. The irrigated sectors did not change between seasons; thus, the effect of irrigation would be compounded over the three years of experiment. The trees were drip-irrigated with emitters flow capacity 2.3 L h^{-1} placed in 0.5 m spacing. The dripline was fixed to a wire installed 0.5 m above the soil surface. The crop evapotranspiration was calculated according to the Penman-Monteith equation (Allen et al. 1998), including later updates described by Allen and Pereira (2009). For the calculation, data from the meteorological station including air temperature (DS18B20, Dallas Semiconductor) and humidity (HIH-4000, Honeywell) in 2 m above ground, wind direction and speed (W2, Tlusťák, Praha), solar radiation (SG002,5, Tlusťák, Praha), and rainfall (Small Rain Gauge 100.053, Pronamic) installed inside the orchard were used. The microclimatic data were further validated by the official meteorological data by the Czech Hydro-Meteorological Institute. The soil moisture in tree rows was measured continuously with Virrib sensors (Fiedler AMS, Czech Republic) installed in each treatment at a depth of 30 cm. The soil volumetric water content was further transformed to saturation proportion of the available soil water content (ASWC; Fig. 1c) calculated as the difference in soil water content between the field capacity and the wilting point. Irrigation was applied from 1st April to 30th September. The total irrigation volumes applied per vegetation season were 294 mm in 2019, 54 mm in 2020 and 189 mm in 2021(Fig. 1a). The irrigation management was set to maintain at least 0.7 ASWC in the root zone 30 cm deep, regularly applying water until full ASWC capacity. Thus, irrigation volume and frequency varied based on the ASWC criteria and was between 4 and 11 mm per dose, applied 2–3 times per week during drought periods (see Fig. 1a for more details on irrigation doses and scheduling).

Growth and fruit production

Apple trees of each cultivar and irrigation treatment (n = 7–10 for each cultivar irrigation treatment group; the variable n is due to the exclusion of trees with obvious signs of health problems) were measured for the following characteristics: total growth expressed as trunk cross section area (TCSA), the growth of extension shoots, flowering intensity, fruit yield, fruit number per unit TCSA and the proportion of the fruit in size categories. The fruits were categorized according to the fruit diameter size: (i) small: < 65 mm, (ii) medium: 65–70 mm, and (iii) large >70 mm, for 'Gala Brookfield' and (i) small <65 mm, (ii) medium: 65-75 mm, and (iii) large >75 mm, for 'Red Jonaprince'. The TCSA was calculated from the trunk circumference measured 10 cm under the first branching. The measurements of the shoot length were carried out in 14 days intervals from May to September. The flowering intensity was scaled by 1–9, where 1—almost no flowers along the shoots, and 9—the bearing shoots were fully covered by flower clusters. For a more detailed description of the flowering intensity scale, see Table S1 and Figure S1. The fruit yield was expressed in kg of fruits per tree. Shoot extension growth was expressed as the relative growth rates (RGR) of annual proleptic shoots, which was calculated according to the following formula:

$$RGR = \frac{\ln L_2 - \ln L_1}{t_2 - t_1}$$

where L_1 and L_2 are shoot lengths measured at two consecutive measuring dates and t_2–t_1 is the number of days between the two dates. Also, key phenological stages (including bud break, full bloom, fruits 20 mm in size, end of vegetative

growth, harvest, and leaf fall) were monitored using the extended BBCH scale by Meier 1997.

Midday stem water potential

To assess plant water status, midday stem water potential (Ψ_{stem}) was measured from June to September in 14 days intervals on four individual trees per cultivar and treatment. Prior to the measurements, fully expanded leaves on two current-year shoots per tree were covered with an aluminium bag and left to equilibrate for at least one hour. The covered leaves were excised between 11:00 and 13:00 hour solar time, and Ψ_{stem} was measured immediately using a portable pressure chamber (1505D-EXP, PMS Instrument Company, Albany, OR, USA). The average of the two measurements per individual tree was calculated and used in statistical analyses.

Xylem hydraulic traits

To provide physiological context for the measured Ψ_{stem} values, we assessed several structural and functional hydraulic traits on six individual trees per cultivar and irrigation treatment in growing season 2020. Supported leaf area and xylem cross-sectional area were measured in current-year shoots at a standard distance of 30 cm from the apex (Lechthaler et al. 2019). Furthermore, we measured vessel diameters in the current-year shoots. For these measurements, 30 µm thick cross sections were prepared at a standard distance of 30 cm from the shoot apex with a sliding microtome (GSL1, Swiss Federal Research Institute WSL, Birmensdorf, Switzerland). The sections were stained with toluidine blue for 2 min, mounted in glycerol and observed under a digital microscope (VHX-7000, Keyence, Japan) at 200× magnification. Vessel diameters were measured in the wedge-shaped region delimited by rays. At least 100 vessels were measured for each shoot cross section, excluding the smallest protoxylem vessels closest to the pith. Image analysis was carried out using ImageJ software (Schindelin et al. 2012).

The vulnerability of stem xylem to drought-induced embolism was assessed by generating vulnerability curves with the Cavitron device (Lauri et al. 2011). For these measurements, fully developed current-year shoots were sampled from five individuals per cultivar and irrigation treatment (one shoot per individual) in the early morning hours at the beginning of September 2020. The shoots were covered with a moist paper towel, inserted into a black plastic bag, and immediately transported to the University of Innsbruck (Austria) where they were stored in a cooling room and processed within 4 days after their collection. All lateral branches were removed underwater, and the cut surface was sealed with glue (Loctite 409; Loctite, Rocky Hill, USA). The segments were shortened from each side to 30 cm and perfused with degassed, ultrafiltered (0.23 µm) distilled water, enriched with Micropur Classic Liquid (0.005% v/v; Katadyn Products, Kemptthal, Switzerland) preventing microbial growth at 90 kPa for 30 min to completely remove embolism. Then, branches were trimmed several times from each side underwater to 27.4 cm using a sharp wood carving knife and inserted into a 28 cm rotor installed in a modified Sorvall RC-5 centrifuge (Thermo Fisher Scientific, Waltham, MA, USA). Since this technique may be sensitive to open vessel artefacts resulting in erroneous vulnerability curves (Martin-St. Paul et al. 2014), maximum vessel length was quantified in similar current-year shoots before the vulnerability measurements using the air injection technique. The longest vessels did not exceed 20 cm indicating that no open vessels were present in the branch segments.

For the Cavitron analyses, the same solution as for flushing of samples (see above) was used. The samples were first equilibrated for 10 min at low rpm, corresponding to xylem water potential (Ψ) above − 0.1 MPa. Then, rpm was increased to successively reduce Ψ by 0.5 or 1 MPa steps. Ψ was kept constant for 10 min before the flow rate through the sample was measured. Ψ was reduced until the hydraulic conductivity decreased by more than 95%.

During the measurement, the per cent loss of hydraulic conductivity (PLC; %) was calculated according to the following equation:

$$\mathrm{PLC} = 100(K_{\max} - K_{\mathrm{h}})/K_{\max}$$

where K_{max} corresponds to maximum hydraulic conductivity and K_h is the actual hydraulic conductivity measured at a given Ψ.

Sigmoid vulnerability curves (plot of PLC vs. Ψ) were observed in all tested species, and the data were fitted with an exponential sigmoid function following Pammenter and Vander Willigen (1998):

$$PLC = \frac{100}{1 + \exp a(\Psi - \Psi_{50})}$$

where a is a constant related to the curve slope, and Ψ_{50} corresponds to the Ψ at 50% loss of hydraulic conductivity.

In addition, Ψ at 12% loss of hydraulic conductivity (Ψ_{12} ~ initial point of runaway embolism) was calculated according to the following equations (see Domec and Gartner, 2001 for details):

$$\Psi_{12} = \frac{2}{a} + \Psi_{50}$$

Pressure–volume analyses

Pressure–volume curves were carried out to determine the turgor loss point (TLP) and osmotic potential at full turgor

(Π_O) of leaves (Bartlett et al 2014; Lenz et al. 2006). The pressure–volume measurements were done on six leaves taken from six trees for each cultivar and irrigation treatment during growing season 2021. For the measurements, current-year shoots were excised early in the morning before the leaves started to lose water due to transpiration. The bottom parts of the shoots were placed into a container with tap water. The shoots were covered with a black plastic bag and transported to the laboratory. One fully expanded leaf was then cut from each shoot, and its fresh weight and leaf water potential (Ψ_L) were measured at regular intervals while the leaf was left to dehydrate on a laboratory bench. At the end of the measurements, the leaves were oven-dried (80°C, 48 hours), and the relative water content (RWC) was calculated from their fresh (FW), saturated (SW), and dry weight (DW) at each desiccation point using the following formula:

$$RWC = \frac{FW - DW}{SW - DW} * 100$$

The reciprocal value of Ψ_L ($1/\Psi_L$) was then plotted against relative water loss (RWL = 100-RWC), and TLP and Π_O were derived separately for each measured leaf using a standard approach in which the TLP is at the transition of the linear and parabolic phases of the pressure–volume curve and Π_O is the intersection of the linear portion of the pressure–volume curve with the y-axis (Tyree and Hammel 1972; Bartlett et al. 2014).

Concentrations of glucose, sucrose, sorbitol, and proline

For the measurements of osmolytes concentrations, mature fully developed leaves were excised from the same shoots as those used for the pressure–volume curve measurements. An aliquot of fresh leaves was homogenized in 80% ethanol, heated at 80 °C for 20 min, and centrifuged at 4500 rpm for 10 min. The supernatant was collected in a clean tube, and the pellet was resuspended in 80% ethanol and reheated at 80 °C for 20 min. After centrifugation, the supernatants were pooled. This step was repeated once more with 50% ethanol.

The content of proline was determined using ninhydrin reaction method (Cross et al. 2006). The combined supernatant was mixed with acidified ninhydrin reagent (1% ninhydrin, 59% glacial acetic acid, 20% ethanol, 20% distilled water) and left incubated for 20 min at 95 °C. After rapid cooling to 25 °C, the absorbance was read at 520 nm (Cintra 101, Dandenong, Australia). Proline (Sigma-Aldrich, Darmstadt, Germany) was used as a standard.

The content of soluble sugars (glucose, sucrose) and sugar alcohol sorbitol in the combined supernatants was determined using UHPLC Infinity II 1290 system (Agilent Technologies, Santa Clara, CA, USA) using a 6470 Series Triple Quadrupole mass spectrometer (Agilent Technologies; electrospray ionization, negative polarity) as detector. The method used a BEH Amide column (2.1 mm × 150 mm, 2.6 µm, Waters, Milford, MA, USA). An isocratic elution program was used for chromatographic separation applying a mobile phase comprising 20% of the mixture of 0.05% formic acid in water and 80% of the mixture acetonitrile/methanol (in 8:2 ratio). The flow rate was 0.4 mL min^{-1}. Ion source parameters: gas temperature 150 °C, gas flow 6 L min^{-1}, nebulizer 40 psi, sheath gas temperature 300 °C, sheath gas flow 128 L min^{-1}, capillary voltage 2500 V, and nozzle voltage 0 V. The sample injection volume was 1 µL. All standards used were purchased from Sigma-Aldrich (Darmstadt, Germany).

Statistical analyses

The difference between cultivar and irrigation treatment was evaluated using two-way ANOVA after graphically checking the assumptions of normality and heteroscedasticity by exploring boxplots and residual plots. As discrete ordinal variable, the flowering intensity was analysed using an ordinal regression. The difference in the proportions of fruits divided in three fruit size categories was tested using Pearson's χ^2 test. In the case of variables measured repeatedly throughout the year (i.e. RGR, $\Psi_{stem,}$ TLP, Π_O, and the concentrations of osmolytes), we used mixed effect models with cultivar and irrigation as fixed factors and date as a random factor. For RGR and Ψ_{stem}, the models were fitted separately for each year. The models were fitted using *lmer* function from the lme4 package (Bates et al. 2015). All statistical analyses were performed in R (R Development Core Team 2010).

Results

Microclimatic conditions

Out of the three years, the growing season of 2019 was the driest and hottest, while the growing season of 2020 was the wettest, particularly during the peak summer (Fig. 1a, b). The mean daily reference evapotranspiration (ET_0) was 2.68 mm in 2019, 2.45 mm in 2020 2.30 in 2021 (Fig. 1b). Maximal daily ET_0 was 5.1 mm in 2019, 4.3 mm in 2020 and 4.8 mm in 2021, corresponding to vapour pressure deficit (VPD) between 1.51 and 2.17 kPa. Available soil water capacity (ASWC) was higher in irrigated (ETc-100) than in non-irrigated (ETc-0) plots (Fig. 1c). Two major periods of soil water deficit, when ASWC decreased below 0.5, could be detected during the first two studied growing seasons (Fig. 1c). In 2019, soil water availability decreased gradually in non-irrigated plots until early August, when substantial

rainfall finally occurred. Another short dry period occurred in April of 2020 but was followed by very wet May, June, and July. Low soil water availability was also observed in the late growing season of 2020 and 2021, but during these periods, ASWC did not drop much below 0.75 (Fig. 1c).

Phenology and shoot growth

The bud break occurred at the end of March or early April depending on year (Table 1). Full bloom occurred around 25th April in 2019 and 2020 and was delayed to around 15th May in 2021 (Table 1). Shoot expansion started in mid-May in all three years, but the dynamics of growth differed across years and cultivars (Fig. 1d). In 2019, the shoot elongation was rapid in May and June and the shoot growth was terminated relatively early at the beginning of July (Fig. 1d). In 2020 and 2021, the 'Gala Brookfield' cultivar showed a marked slowdown in shoot elongation in June followed by a more rapid expansion in July (Fig. 1d). The shoot relative growth rates did not differ significantly between irrigated and non-irrigated trees. The harvest dates varied between 9th and 24th September and leaf fall between 20th October and 10th November (Table 1).

Midday stem water potential

The measured values of Ψ_{stem} varied between − 0.2 and − 1.6 MPa across dates, cultivars, and irrigation treatments (Fig. 1e). In 2019 and 2021, Ψ_{stem} differed significantly between irrigation treatments, with irrigated trees having less negative Ψ_{stem} (Fig. 1e). The differences in Ψ_{stem} between the irrigation treatments generally appeared later in the season (i.e., in August). In 2019, the difference between irrigated and non-irrigated appeared already in June in 'Red Jonaprince' cultivar but not in 'Gala Brookfield'. The difference between cultivars was significant in 2021 and marginally significant ($P = 0.067$) in 2019, with 'Red Jonaprince' having more negative values of Ψ_{stem}. The lowest values of around -1.6 MPa were observed in 'Red Jonaprince' in mid-June and late July of 2019.

Fruit yield

Both cultivars showed high flowering intensity (ranging between 6.6 and 8.8) in 2019 and 2021 (Table 2). In 2020, the flowering intensity was only moderate (4.7–5.6) and low (2.5–2.6) in 'Gala Brookfield' and 'Red Jonaprince', respectively (Tables 2, 3). Total yield and number of fruits per TCSA were higher in 'Red Jonaprince' than 'Gala Brookfield' in 2019 and 2021, whereas the opposite trend was observed in 2020. The effect of irrigation on yield parameters was mostly non-significant (Table 3), but there were some differences in the fruit size distribution between irrigated and non-irrigated trees. In particular, the proportion of large fruits was significantly higher in irrigated than non-irrigated trees of both cultivars in 2019. In addition, non-irrigated trees of 'Gala Brookfield' also had a relatively high proportion (25%) of small fruits in 2019 (Tables 2, 3) than the non-irrigated 'Red Jonaprince'.

Xylem hydraulic traits

Hydraulic traits differed mainly between cultivars, but not between irrigation treatments. The supported leaf area scaled with xylem cross-sectional area in 'Gala Brookfield', whereas such a relationship was not found in 'Red Jonaprince' (Fig. 2). 'Red Jonaprince' had significantly greater vessel diameters than'Gala Brookfield' ($P = 0.002$), particularly in irrigated trees (Fig. 3a). The cultivars differed significantly in Ψ_{12} values, with 'Red Jonaprince' starting to lose hydraulic conductivity at less negative xylem water potentials than 'Gala Brookfield' (Fig. 3b). There was also a slight tendency for more negative Ψ_{12} values in irrigated than non-irrigated trees; however, the difference was not statistically significant ($P = 0.081$). Ψ_{50} was statistically different neither between cultivars nor between irrigation treatments (Fig. 3c).

Table 1 Main phenology stages for 'Red Jonaprince' (J) and 'Gala Brookfield' (G) cultivars in years 2019–2021

Year	Cultivar	Bud break (BBCH10/54)	Full bloom (BBCH65)	Fruits 20 mm in size (BBCH 34/72)	End of vegetative growth (BBCH91/81)	Harvest (BBCH 87)	Leaf fall (BBCH 95)
2019	J	27-Mar	23-Apr	27-May	31-Jul	23-Sep	25-Oct
	G	29-Mar	25-Apr	1-Jun	31-Jul	9-Sep	20-Oct
2020	J	1-Apr	23-Apr	2-Jun	30-Aug	24-Sep	10-Nov
	G	2-Apr	24-Apr	8-Jun	20-Aug	21-Sep	5-Nov
2021	J	12-Apr	14-May	11-Jun	25-Aug	24-Sep	4-Nov
	G	12-Apr	16-May	18-Jun	20-Aug	20-Sep	4-Nov

The phenology stages were assessed based on BBCH classification by Meier (1997)

Table 2 Number of measured trees (n), flowering intensity, annual fruit yield, number of fruits per trunk cross-sectional area (TCSA) and the proportion of fruit in three size categories (small, medium, and large) in control (ETc-0) and irrigated (ETc-100) trees of 'Red Jonaprince' (J) and 'Gala Brookfield' (G) cultivars in years 2019, 2020 and 2021

Year	Treatment	n	Flowering intensity	Yield (kg tree^{-1})	Fruit per TCSA (fruit cm^{-2})	Fruit size			PEARSON χ^2
						Small	Medium	Large	
2019	J-ETc-0	8	7.3 ± 1.5	38.2 ± 2.7	15.8 ± 1.7	0.083	0.528	0.389	χ^2 = 48.43, df = 2, pval = 3.052e^{-11}
	J-ETc-100	9	6.6 ± 1.7	35 ± 6.6	14.4 ± 2.2	0.09	0.42	0.49	
	G-ETc-0	10	8.3 ± 0.5	28 ± 4.7	16.7 ± 2.7	0.256	0.432	0.312	χ^2 = 273.04, df = 2, pval = 2.2e^{-16}
	G-ETc-100	10	7.8 ± 0.6	25.6 ± 5.4	16.3 ± 3.1	0.108	0.333	0.559	
2020	J-ETc-0	10	2.6 ± 2.2	10.8 ± 14.5	2.2 ± 3.5	0.013	0.139	0.848	χ^2 = 57.13, df = 2, pval = 3.936e^{-13}
	J-ETc-100	10	2.5 ± 1.7	7.4 ± 7.2	2.1 ± 3.5	0.129	0.213	0.657	
	G-ETc-0	10	4.7 ± 1.5	17 ± 4.8	6.4 ± 1.3	0.139	0.202	0.659	χ^2 = 20,33, df = 2, pval = 3.844e^{-05}
	G-ETc-100	10	5.6 ± 1.2	18.9 ± 3.1	9 ± 1.5	0.207	0.207	0.586	
2021	J-ETc-0	8	8.6 ± 0.5	40.2 ± 3.8	8.8 ± 1	0.046	0.285	0.669	χ^2 = 26,12, df = 2, pval = 2.134e^{-06}
	J-ETc-100	8	8.8 ± 0.5	40.3 ± 4	9.3 ± 2.2	0.076	0.329	0.595	
	G-ETc-0	7	8.1 ± 0.4	17.9 ± 3.8	6.3 ± 0.9	0.113	0.29	0.596	χ^2 = 6.89, df = 2, pval = 0.032
	G-ETc-100	8	8.1 ± 0.4	19.4 ± 2.5	8.5 ± 0.9	0.137	0.329	0.533	

Results are shown as mean ± standard deviation, n = 7–10

The results of the Pearson´s χ^2 testing for the difference between irrigation treatments within each cultivar are shown in the last column

Table 3 Summary of two-way ANOVA or ordinal regression in case of flowering intensity in which the effect of cultivar, irrigation and their interaction was tested at a level of significance α = 0.05

Year	Variable	Cultivar		Irrigation		Cultivar × irrigation	
		F/χ^2	*P-value*	*F*/χ^2	*P-value*	*F*/χ^2	*P-value*
2019	Flowering intensity	7.93	0.005	4.03	0.045	0.004	0.949
	Yield (kg tree^{-1})	33.02	< 0.001	2.8	0.104	0.06	0.803
	Fruit per TCSA (fruit cm^{-2})	3.00	0.093	1.1	0.309	0.34	0.567
	Number of small fruits	12.67	0.001	15.0	< 0.001	4.87	0.034
	Number of large fruits	2.22	0.146	6.7	0.014	0.08	0.781
2020	Flowering intensity	18.12	< 0.001	1.11	0.293	0.70	0.404
	Yield (kg tree^{-1})	10.54	0.003	0.1	0.794	0.97	0.332
	Fruit per TCSA (fruit cm^{-2})	42.43	< 0.001	2.1	0.156	2.70	0.109
	Number of small fruits	19.13	< 0.001	3.6	0.066	0.84	0.364
	Number of large fruits	16.95	< 0.001	0.3	0.609	0.90	0.35
2021	Flowering intensity	8.20	0.004	0.06	0.804	0.16	0.692
	Yield (kg tree^{-1})	285.44	< 0.001	0.4	0.542	0.31	0.58
	Fruit per TCSA (fruit cm^{-2})	9.61	0.004	6.8	0.015	3.20	0.085
	Number of small fruits	1.28	0.268	4.4	0.045	0.18	0.677
	Number of large fruits	131.15	< 0.001	0.6	0.461	0.40	0.533

F values for two-way ANOVA or χ^2 value for ordinal regression (for flowering intensity) are shown together with corresponding *P* values

Pressure–volume analyses

Turgor loss point (TLP) and osmotic potential at full turgor (Π_O) were not significantly different between cultivars and irrigation treatments (Fig. 4). Seasonally, TLP decreased by 0.6 MPa from − 2.8 MPa in June to -3.4 MPa in July and August (Fig. 4a). The seasonal decrease was also evident in Π_O for 'Gala Brookfield', whereas for 'Red Jonaprince', the Π_O decreased from June to July and then slightly increased from July to August (Fig. 4b).

Concentrations of proline, soluble sugars and sorbitol

'Gala Brookfield' had significantly higher concentrations of glucose, sucrose and sorbitol than'Red Jonaprince' (Fig. 5).

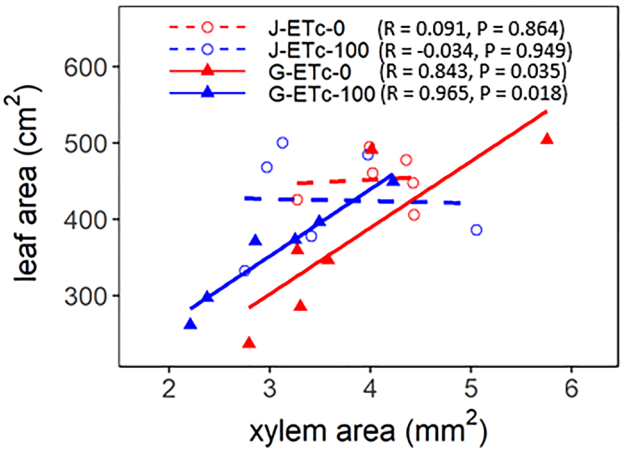

Fig. 2 Relationship between xylem cross-sectional area and supported leaf area of annual shoot of non-irrigated (ETc-0) and irrigated (ETc-100) apple trees of 'Red Jonaprince' (J) and 'Gala Brookfield' (G) cultivars. Data were fitted with linear functions. Results of the Pearson's correlation tests are shown

Moreover, the concentrations of glucose and sucrose were significantly higher in non-irrigated control trees of 'Gala Brookfield', while the opposite trend was observed in 'Red Jonaprince' (Fig. 5a, b). For sorbitol, the effects of irrigation and the interaction between cultivar and irrigation were non-significant (Fig. 5c). There was also no statistically significant difference in the concentrations of proline between cultivars and irrigation treatments, although the concentrations tended to be higher in non-irrigated trees (Fig. 5d). Also, the cultivars showed distinct seasonal patterns in proline concentrations. While the proline concentration increased linearly in 'Red Jonaprince', it increased from June to July and decreased slightly from July to August in 'Gala Brookfield'.

Discussion

Irrigation is an important management practice in apple tree orchards. Soil- and plant-based indicators are used for efficient irrigation scheduling, but their threshold values associated with the desired tree performance need to be determined. In this study, we monitored yield performance, shoot extension growth, and midday stem water potential in irrigated (ETc-100) and non-irrigated (ETc-0) apple trees of triploid 'Red Jonaprince' and diploid 'Gala Brookfield' cultivars during three consecutive growing seasons. The study was carried out in the mesic temperate orchard with substantial summer rainfall (Fig. 1a, b). Nevertheless, the soil profile can become water depleted during spring and summer and the site can experience periods of drought if rainfall is scarce (Fig. 1c, Jupa et al. 2022). From the three measured years, none of them was exceptionally dry,

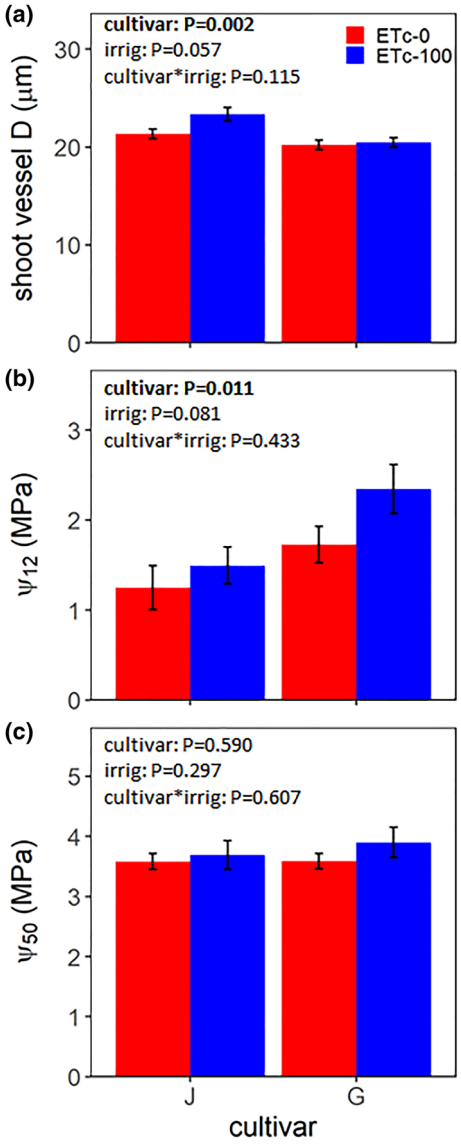

Fig. 3 **a** Mean shoot vessel diameter (D), **b** xylem potential at 12% and **c** 50% loss of hydraulic conductivity (Ψ_{12} and Ψ_{50}) in annual shoots of non-irrigated (ETc-0) and irrigated (ETc-100) apple trees of 'Red Jonaprince' (J) and 'Gala Brookfield' (G) cultivars. Columns and error bars represent means and standard errors, $n = 6$ for vessel diameter, $n = 5$ for Ψ_{12} and Ψ_{50}

although all of them were hotter than the long-term average (data by the Czech Hydrometeorological Institute, https://bit.ly/3qF6jcQ). The year 2019 was the driest of the three studied years, and the applied irrigation surpassed the natural rainfall. In contrast, the year 2020 was the wettest, and substantial rainfall occurred in June and early July, resulting in a low irrigation requirement of 54 mm. Despite clear differences in soil moisture between irrigated and non-irrigated plots (Fig. 1c), there was no major reduction in shoot extension growth between the irrigated and non-irrigated trees (Fig. 1d). As substantial drought can inhibit vegetative

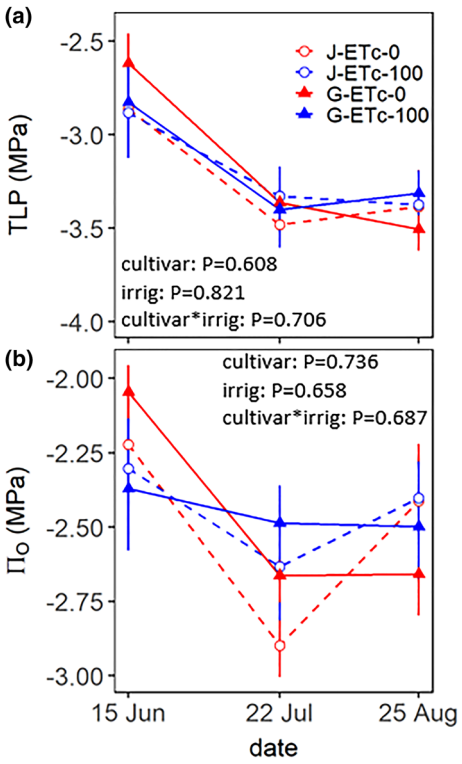

Fig. 4 Seasonal time course of **a** leaf turgor loss point (TLP) and **b** osmotic potential at full saturation (Π_O) in non-irrigated (ETc-0) and irrigated (ETc-100) apple trees of 'Red Jonaprince' (J) and 'Gala Brookfield' (G) cultivars. Points and error bars represent means and standard errors, n = 6

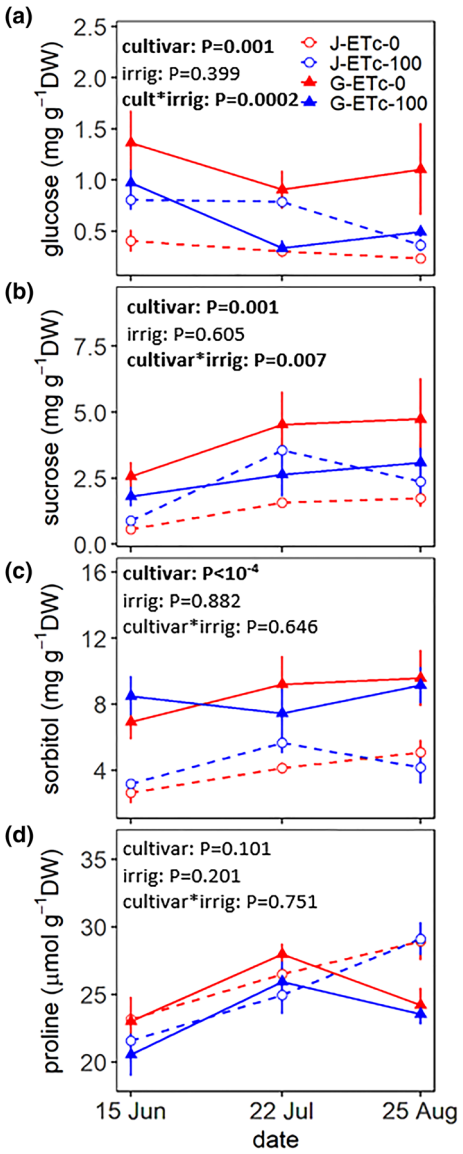

Fig. 5 Concentrations of glucose (**a**), sucrose (**b**) sorbitol (**c**) and proline (**d**) in leaves of non-irrigated (ETc-0) and irrigated (ETc-100) apple trees of 'Red Jonaprince' (J) and 'Gala Brookfield' (G) cultivars. Points and error bars represent means and standard errors, $n = 6$

growth (Ebel et al. 1995), it is likely that the wet periods in May provided enough water for shoot elongation. The bare impact of water shortage on the shoot growth during early July 2019 was associated with the early end of their extension growth. As suggested by the different growth dynamics among years, the shoot growth was responsive to environmental conditions with 'Gala Brookfield' showing possibly higher susceptibility for growth reduction under wet and cloudy weather (Fig. 1d).

We found significantly lower values of Ψ_{stem} in non-irrigated than irrigated trees in two out of the three studied growing seasons (Fig. 1e). The lower Ψ_{stem} in non-irrigated apple trees usually paralleled the decline in ASWC. The difference between irrigated and non-irrigated trees was not significant only during the wettest growing season 2020. As the Ψ_{stem} of − 1.6 was recently considered critical for apple fruit growth (DeSwaef et al. 2009; Robinson et al. 2022), non-irrigated trees of both cultivars could be deemed mildly drought-stressed during summer 2019. The effect of drought could be associated with their lower proportion of large fruit compared to the trees supported by irrigation (Tables 2, 3) as the drought period was approximately two month long and covered a significant part of the rapid fruit growth phase (Boland et al. 2002). Similar results showing a production of smaller fruits under water deficit conditions were reported for apple trees grown in semi-arid environment (Noar et al. 1995). The reduction of fruit size was more pronounced in the diploid 'Gala Brookfield' cultivar that exhibited a higher distance in the proportion of each class between the irrigated and non-irrigated trees (Table 2). As the diploid apple cultivars bear naturally fruit of smaller size (Nikolaevich et al. 2015; Sedov et al. 2017), they are more susceptible to water deficit for maintaining the appropriate calibre. The second drought period experienced in the spring 2020 seems to bring no effect on the yield of apple trees. This suggests

a lower susceptibility of apple tree yield parameters to a mild drought experienced during early phenological phases (i.e. bud break and flowering, Table 1). Previous research has also shown that yield parameters of apple trees were not negatively affected when water deficit occurred in late season (105–183 days after full bloom) (Mills et al. 1996). In addition, variation in yield, which was observed among the years and between the two cultivars (Table 2), could be associated with different water needs per tree. Higher crop load is usually associated with higher rates of leaf gas exchange (Palmer et al. 1997). On the other hand, trees with more fruits have lower leaf area (Wünsche et al. 2000) because generative and vegetative growth is usually negatively related (Forshey and Elfving 2011; Plavcová et al. 2022). Thus, these relationships should be jointly considered when devising deficit irrigation strategies for apple tree orchards.

'Red Jonaprince' tended to have lower Ψ_{stem} than 'Gala Brookfield' (Fig. 1e), with non-irrigated trees of this cultivar having the lowest seasonal Ψ_{stem} in all three measured growing seasons. 'Red Jonaprince' is a vigorously growing triploid (Princen and Princen 1999), and it is possible that the growth efficiency might compromise with drought safety. Hydraulic safety vs. efficiency trade-off is a well-established relationship in plant ecophysiology (Sperry et al. 2008; Gleason et al. 2016). Out of the two measures of hydraulic safety that we quantified in this study; the cultivars differed significantly only in Ψ_{12}, which relates to the onset of xylem embolism in the current-year shoots (Fig. 3b). This result is consistent with the findings of De Baerdemaeker et al. 2018 on tetraploid variant of 'Gala' compared to a diploid variant. The measured Ψ_{12} values, which were around −1.4 MPa in 'Red Jonaprince', correspond roughly with the seasonal minimum of Ψ_{stem}, suggesting that the level of drought stress experienced by the trees was rather low. Indeed, the Ψ_{50} values, which correspond to 50% loss of conductivity, were in a range of − 3.5 to − 3.9 MPa (Fig. 3c), far lower than the seasonal minimum of Ψ_{stem}. The Ψ_{50} values measured here are in good agreement with those measured by Beikircher et al. (2013) in three different apple cultivars grown in northern Italy. Similar Ψ_{50} values were also obtained in an apple progeny derived from a 'Starkrimson' × 'Granny Smith' cross (Lauri et al. 2011), although the range of variation was broader (from − 3.3 to 5.2 MPa) in this case. In general, the Ψ_{50} value of − 3.5 MPa is rather low for representatives of temperate angiosperm tree species and points to a high embolism resistance of apple trees.

Reduction of leaf area and stomatal closure, which limit the onset of runaway embolism, may provide other drought-coping mechanisms in apple trees (Lauri et al. 2016). We found that the leaf area of 'Red Jonaprince' shoots did not scale with the xylem cross-sectional area (Fig. 2), which might have resulted in a worse water supply to evaporating leaves (Petit et al. 2018). On the other hand, the shoot xylem of 'Red Jonaprince' cultivar had significantly larger vessel diameters (Fig. 3a) and hence, likely higher xylem-area-specific hydraulic conductivity compared to 'Gala Brookfield'. In addition, the non-irrigated trees had slightly lower vessel diameters ($P = 0.075$) than irrigated ones (Fig. 3a) in 'Red Jonaprince' but not in 'Gala Brookfield'. The adjustment of vessels diameter to the water supply is a well-known response in trees (Fichot et al. 2010; Plavcová and Hacke 2012; Jupa et al. 2021) and likely results in the optimization of water transport efficiency and safety against drought-induced embolism under given field conditions (Hacke et al. 2017).

Similarly, the turgor loss point (TLP) in the range of − 2.6 to − 3.5 MPa (Fig. 4a) is relatively low for a temperate angiosperm species as a comprehensive meta-analysis found a mean TLP value of − 1.6 MPa for this plant group (Bartlett et al. 2014). Both TLP and osmotic pressure at full saturation (Π_O) declined substantially from June to July, but then stayed about the same in August (Fig. 4). The shift in TLP from June to July was in the magnitude of -0.6 MPa, which is a slightly higher value than what was found across 283 wild and crop species globally (Bartlett et al. 2014). In contrast to the seasonal osmotic adjustment observed in our study, there were significant differences in neither TLP nor Π_O between cultivars and between irrigation treatments. The lack of TLP and Π_O shifts in trees without irrigation is somewhat surprising and indicates that the non-irrigated trees did not acclimate their wilting point towards greater soil water deficit. A possible explanation for this observation could be that the water deficit was not so strong even in non-irrigated trees to elicit changes in pressure–volume relations of leaves.

While we did not observe differences in TLP and Π_O between cultivars and irrigation treatments (Fig. 4), there were significant differences in the concentrations of some osmolytes (Fig. 5). The increase in concentrations of soluble sugars (Fig 5a, b), and to a lesser extent of proline (Fig. 5d), in non-irrigated trees was more apparent in 'Gala Brookfield' cultivar, while 'Red Jonaprince' showed slightly higher concentrations of osmolytes in irrigated trees (except for proline). This wide range of responses is perhaps not surprising given the numerous roles that these compounds fulfil in plants. The changes in water-soluble sugars and sugar alcohols, mostly glucose, sucrose, and sorbitol, can be a result of the regulation of sugar metabolism between storage and export. Here and in other studies (Yang et al. 2019; Šircelj et al. 2007), sorbitol was the main photosynthetic assimilation compound in apple leaves and showed a higher accumulation than the two analysed soluble sugars. Thus, sorbitol rather than sucrose is preferentially accumulated in drought-stressed plants and acts as storage of carbon (Yang et al. 2019). On the other hand, sucrose represents a more accessible form of sugar than sorbitol and can be easily degraded to hexose molecules to maintain sufficient turgor

(Yang et al. 2019). Moreover, sucrose may act as a signalling molecule and participate in the crosstalk between hormonal, oxidative, and defence signalling (Ruan 2014). The vast majority of studies focusing on the analysis of proline levels were carried out in greenhouses and in short-term artificially induced drought conditions. In these studies, drought significantly increased proline values, with this effect being more pronounced in drought-tolerant cultivars (Yang et al. 2019; Jiménez et al. 2013). The concentration of proline also increased with drier and hotter weather conditions in the field-grown apple trees (Nenko et al. 2018). On the contrary, proline levels were not significantly affected by irrigation in two-year-old orchard apple trees (Šircelj et al. 2007). The increase in proline content in our study may not only be directly related to its role as an osmolyte but may also reflect its role in balancing the cell redox status via stabilisation of cell membrane and proteins and scavenging of reactive oxygen species (Verbruggen and Hermans 2008).

While the measurements of yield, shoot growth and Ψ_{stem} were carried out during three consecutive seasons, the measurements of xylem hydraulic traits, pressure–volume analyses of leaves and the measurements of concentrations of osmolytes in leaves were carried out only during a single growing season, leaving a possibility that these traits may vary slightly as a result of phenotypic and/or developmental plasticity (Plavcová and Hacke 2012; Lauri et al. 2016; Sorek et al. 2021). Thus, repeated measurements of these traits would be useful to set more robust physiological boundaries to observed Ψ_{stem} values.

Conclusions

The results of our irrigation study carried out at the wetter edge of the moisture availability gradient indicate that yield parameters and shoot growth of the two apple tree cultivars were quite robust against mild water deficit. Only in one of the three studied years we identified a reduction in fruit size in non-irrigated trees. The triploid cultivar 'Red Jonaprince' favoured hydraulic efficiency against hydraulic safety, making it potentially more susceptible to hydraulic failure if the water deficit becomes more severe than what was observed in the current three years. The diploid cultivar 'Gala Brookfield' adopted a more conservative strategy with its growth and yield parameters being more responsive to environmental conditions.

Supplementary Information The online version contains supplementary material available at https://doi.org/10.1007/s00271-022-00839-2.

Acknowledgements The project was funded by the project QK1910165 Ministry of Agriculture, the Czech Republic. We thank Jana Fenclová and Vít Gloser for their technical assistance. Stefan Mayr is acknowledged for allowing access to the Cavitron device to measure the vulnerability curves. We thank two anonymous reviewers for their thoughtful comments on an earlier version of this paper.

Author contributions L.P., M.M., R.J., K.S., Z.K. and A.M. conducted the measurements. L.P. wrote the main manuscript text with all authors contributing.

Data availability The data of this study are available from the corresponding author upon request.

Declarations

Conflict of interest The authors declare no conflict of interest.

References

Allen RG, Pereira LS (2009) Estimating crop coefficients from fraction of ground cover and height. Irrig Sci 28:17–34.Bartlett MK, Scoffoni C, Sack L (2012) The determinants of leaf turgor loss point and prediction of drought tolerance of species and biomes: a global meta-analysis: drivers of plant drought tolerance. Ecol Lett 15:393–405

Bartlett MK, Zhang Y, Kreidler N et al (2014) Global analysis of plasticity in turgor loss point, a key drought tolerance trait. Ecol Lett 17:1580–1590

Bates D, Mächler M, Bolker B, Walker S (2015) Fitting linear mixed-effects models using lme4. J Stat Softw 67:1–48

Beikircher B, Mayr S (2017) Annual patterns of xylem embolism in high-yield apple cultivars. Funct Plant Biol 44:587–596

Beikircher B, De Cesare C, Mayr S (2013) Hydraulics of high-yield orchard trees: a case study of three *Malus domestica* cultivars. Tree Physiol 33:1296–1307

Brás TA, Seixas J, Carvalhais N, Jagermeyr J (2021) Severity of drought and heatwave crop losses tripled over the last five decades in Europe. Environ Res Lett 16:065012

Cross JM, von Korff M, Altmann T et al (2006) Variation of enzyme activities and metabolite levels in 24 Arabidopsis accessions growing in carbon-limited conditions. Plant Physiol 142:1574–1588

Davies FS, Lakso AN (1979) Diurnal and seasonal changes in leaf water potential components and elastic properties in response to water stress in apple trees. Physiol Plant 46:109–114

De Baerdemaeker NJF, Hias N, Van den Bulcke J et al (2018) The effect of polyploidization on tree hydraulic functioning. Am J Bot 105:161–171

De Swaef T, Steppe K, Lemeur R (2009) Determining reference values for stem water potential and maximum daily trunk shrinkage in young apple trees based on plant responses to water deficit. Agric Water Manag 96:541–550

Dragoni D, Lakso AN (2008) An apple-specific ET model. Acta Hortic 903:1175–1179

Ebel RC, Proebsting EL, Evans RG (1995) Deficit irrigation to control vegetative growth in apple and monitoring fruit growth to schedule irrigation. Hort Sci 30:1229–1232

FAO. (Crops and livestock products). License: CC BY-NC-SA 3.0 IGO. Extracted from: https://www.fao.org/faostat/en/#data/QCL. Accessed 9 Jun 2022.

Fichot R, Barigah TS, Chamaillard S et al (2010) Common trade-offs between xylem resistance to cavitation and other physiological traits do not hold among unrelated *Populus deltoides* ×*Populus nigra* hybrids. Plant Cell Environ 33:1553–1568

Forshey CG, Elfving DC (2011) The relationship between vegetative growth and fruiting in apple trees. In: Janick J (ed) Horticultural reviews. Wiley, Hoboken, pp 229–287

Gleason SM, Butler DW, Ziemińska K et al (2012) Stem xylem conductivity is key to plant water balance across Australian angiosperm species. Funct Ecol 26:343–352
Gleason SM, Westoby M, Jansen S et al (2016) Weak tradeoff between xylem safety and xylem-specific hydraulic efficiency across the world's woody plant species. New Phytol 209:123–136
Glenn DM (2010) Canopy gas exchange and water use efficiency of ´Empire´ apple in response to particle film, irrigation and microclimatic factors. J Am Soc of Hortic Sci 135:25–32
Gomes FP, Oliva MA, Mielke MS et al (2010) Osmotic adjustment, proline accumulation and cell membrane stability in leaves of *Cocos nucifera* submitted to drought stress. Sci Hortic 126:379–384
Hacke UG, Sperry JS (2001) Functional and ecological xylem anatomy. Perspect Plant Ecol Evol Syst 4:97–115
Hacke UG, Spicer R, Schreiber SG, Plavcová L (2017) An ecophysiological and developmental perspective on variation in vessel diameter: variation in xylem vessel diameter. Plant Cell Environ 40:831–845
He P, Li L, Cheng L, Wang H, Chang Y (2018) Variation in ploidy level and morphological traits in the progeny of the triploid apple variety Jonagold. Czech J Genet Plant Breed 54:135–142
Hennig A, Kleinschmit JRG, Schoneberg S, Löffler S, Janßen A, Polle A (2015) Water consumption and biomass production of protoplast fusion lines of poplar hybrids under drought stress. Front Plant Sci 6:1–14
Jiménez S, Dridi J, Gutiérrez D, Moret D, Irigoyen JJ, Moreno MA, Gogorcena Y (2013) Physiological, biochemical and molecular responses in four Prunus rootstocks submitted to drought stress. Tree Physiol 33:1061–1075
Jupa R, Krabičková D, Plichta R, Mayr S, Gloser V (2021) Do angiosperm tree species adjust intervessel lateral contact in response to soil drought? Physiol Plant 172:2048–2058
Jupa R, Mészáros M, Hoch G, Plavcová L (2022) Trunk radial growth, water and carbon relations of mature apple trees on two size-controlling rootstocks during severe summer drought. Tree Physiol 42:289–303
Lauri P-E, Gorza O, Cochard H et al (2011) Genetic determinism of anatomical and hydraulic traits within an apple progeny. Plant Cell Environ 34:1276–1290
Lauri P-E, Barigah TS, Lopez G et al (2016) Genetic variability and phenotypic plasticity of apple morphological responses to soil water restriction in relation with leaf functions and stem xylem conductivity. Trees 30:1893–1908
Lechthaler S, Turnbull TL, Gelmini Y et al (2019) A standardization method to disentangle environmental information from axial trends of xylem anatomical traits. Tree Physiol 39:495–502
Lenz TI, Wright IJ, Westoby M (2006) Interrelations among pressure–volume curve traits across species and water availability gradients. Physiol Plant 127:423–433
Loganathan P (1987) Soil quality considerations in the selection of sites for aquaculture
Maherali H, Walden AE, Husband BC (2009) Genome duplication and the evolution of physiological responses to water stress. New Phytol 184:721–731
Makarenko S (2021) Morphological markers with a triploid set of chromosomes by breeding of apple tree at the polyploid level. BIO Web Conf 38:78–88
McKenzie DW (1973) Apple tree. Plant Patent 3637, United States Patent PP03637. United States. Filled August 1, 1973, issued October 15, 1973. Access: https://www.freepatentsonline.com/PP03637.html. Accessed 4 Jan 2023
Meier U (1997) Growth stages of mono- and dicotyledonous plants. Blackwell Wissenschafts-Verlag, Berlin
Mills TM, Behboudian MH, Clothier BE (1996) Water relations, growth, and the composition of `Braeburn' apple fruit under deficit irrigation. J Amer Soc Hort Sci 121:286–291
Naor A (1999) Midday stem water potential as a plant water stress indicator for irrigation scheduling in fruit trees. Int Symp Irrig Hortic Crops 537:447–454
Naor A, Klein I, Doron I (1995) Stem Water Potential and Apple Size. J Amer Soc Hort Sci 120:577–582
Naor A, Naschitz S, Peres M, Gal Y (2008) Responses of apple fruit size to tree water status and crop load. Tree Physiol 28:1255–1261
Nenko NI, Sergeeva NN, Kiseleva GK, Sergeev YI, Yablonskaya EK, Yakuba YF (2018) Dynamic of proline, pigment contents, water fractions in apple (*Malus domestica* Borkh.) foliage under temperature drought stress and protection measures. Sel'skokhozyaĭstvennaya Biol 53:598–604
Nikolaevich SE, Alekseyevna SG, Mikhailovna SZ (2015) Yield regularity, fruit weight and consumer qualities of triploid apple cultivars developed at the All Russian Research Institute of Fruit Crop Breeding (VNIISPK). Am Pomol Soc 69:201–205
O'Rourke D (2003) World production, trade, consumption and economic outlook for apples. In: Ferree DC, Warrington IJ (eds) Apples: botany, production and uses. CABI Publishing, Oxfordshire, pp 15–29
Palmer JW, Giuliani R, Adams HM (1997) Effect of crop load on fruiting and leaf photosynthesis of 'Braeburn'/M.26 apple trees. Tree Physiol 17:741–746
Petit G, von Arx G, Kiorapostolou N et al (2018) Tree differences in primary and secondary growth drive convergent scaling in leaf area to sapwood area across Europe. New Phytol 218:1383–1392
Plavcová L, Hacke UG (2012) Phenotypic and developmental plasticity of xylem in hybrid poplar saplings subjected to experimental drought, nitrogen fertilization, and shading. J of Exp Bot 63:6481–6491
Plavcová L, Mészáros M, Šilhán K, Jupa R (2022) Relationships between trunk radial growth and fruit yield in apple and pear trees on size-controlling rootstocks. Ann Bot 130:477–489
Princen WJFA and Princen AFMJ (1999) Apple tree named ´Red Jonaprince´. Plant Patent 11,112, United States Patent US00PP11112P. Date of patent: November 2, 1999. Access: https://patentimages.storage.googleapis.com/f2/b6/27/24fe5d5ee6d592/USPP11112.pdf. Accessed 4 Jan 2023
R Development Core Team (2010) R: a language and environment for statistical computing. R Foundation for Statistical Computing, Vienna
Robinson TL, Lordan J, Francescatto P (2022) Irrigation of apple in humid climate in wet and dry years. Acta Hortic 1335:477–482
Rodriguez-Dominguez CM, Buckley TN, Egea G et al (2016) Most stomatal closure in woody species under moderate drought can be explained by stomatal responses to leaf turgor. Plant Cell Environ 39:2014–2026
Ruan YL (2014) Sucrose metabolism: gateway to diverse carbon use and sugar signaling. Annu Rev Plant Biol 65:33–67
Schindelin J, Arganda-Carreras I, Frise E et al (2012) Fiji - an open source platform for biological image analysis. Nat Methods 9:676–682
Sedov EN, Sedysheva GA, Makarkina MA, Serova ZM (2017) Development of triploid apple cultivars as a priority in selection. Russ J Genet Appl Res 7:773–780
Šircelj H, Tausz M, Grill D, Batič F (2007) Detecting different levels of drought stress in apple trees (Malus domestica Borkh.) with selected biochemical and physiological parameters. Sci Hortic 113:362–369
Sorek Y, Greenstein S, Netzer Y et al (2021) An increase in xylem embolism resistance of grapevine leaves during the growing season is coordinated with stomatal regulation, turgor loss point and intervessel pit membranes. New Phytol 229:1955–1969

Sperry JS, Meinzer FC, McCulloh KA (2008) Safety and efficiency conflicts in hydraulic architecture: scaling from tissues to trees. Plant Cell Environ 31:632–645

Tromp AD (2005) Water relations. In: Tromp J, Webster AD, Wertheim SJ (eds) Fundamentals of Temperate Zone tree fruit production. Backhuys, Cambridge, pp 26–38

Tyree MT, Hammel HT (1972) The measurement of the turgor pressure and the water relations of plants by the pressure-bomb technique. J Exp Bot 23:267–282

Verbruggen N, Hermans C (2008) Proline accumulation in plants: a review. Amino Acids 35:753–759

Wang Z, Stutte GW (1992) The role of carbohydrates in active osmotic adjustment in apple under water stress. J Amer Soc Hort Sci 117:816–823

Webster AD (2005) The origin, distribution and genetics diversity of temperate fruits. In: Webster AD, Wertheim SJ, Tromp J (eds) Fundamentals of Temperate Zone Tree Fruit Production. Backhuys, Cambridge, pp 1–11

Webster AD (2005b) Sites and soils for temperate tree-fruit production: their selection and amelioration. In: Webster AD, Wertheim SJ, Tromp J (eds) Fundamentals of Temperate Zone tree fruit production. Backhuys, Cambridge, pp 12–25

Wünsche JN, Palmer JW, Greer DH (2000) Effects of crop load on fruiting and gas-exchange characteristics of `Braeburn'/M.26 apple trees at full canopy. J Amer Soc Hort Sci 125:93–99

Yang J, Zhang J, Li C, Zhang Z, Ma F, Li M (2019) Response of sugar metabolism in apple leaves subjected to short-term drought stress. Plant Physiol Biochem 141:164–171